REMODELING OF CARDIAC PASSIVE ELECTRICAL PROPERTIES AND SUSCEPTIBILITY TO VENTRICULAR AND ATRIAL ARRHYTHMIAS

EDITED BY: George E. Billman

PUBLISHED IN: Frontiers in Physiology

frontiers Research Topics

frontiers

ISSN 1664-8714
ISBN 978-2-88919-647-0
DOI 10.3389/978-2-88919-647-0

About Frontiers

Frontiers is more than just an open-access publisher of scholarly articles: it is a pioneering approach to the world of academia, radically improving the way scholarly research is managed. The grand vision of Frontiers is a world where all people have an equal opportunity to seek, share and generate knowledge. Frontiers provides immediate and permanent online open access to all its publications, but this alone is not enough to realize our grand goals.

Frontiers Journal Series

The Frontiers Journal Series is a multi-tier and interdisciplinary set of open-access, online journals, promising a paradigm shift from the current review, selection and dissemination processes in academic publishing. All Frontiers journals are driven by researchers for researchers; therefore, they constitute a service to the scholarly community. At the same time, the Frontiers Journal Series operates on a revolutionary invention, the tiered publishing system, initially addressing specific communities of scholars, and gradually climbing up to broader public understanding, thus serving the interests of the lay society, too.

Dedication to Quality

Each Frontiers article is a landmark of the highest quality, thanks to genuinely collaborative interactions between authors and review editors, who include some of the world's best academicians. Research must be certified by peers before entering a stream of knowledge that may eventually reach the public - and shape society; therefore, Frontiers only applies the most rigorous and unbiased reviews.
Frontiers revolutionizes research publishing by freely delivering the most outstanding research, evaluated with no bias from both the academic and social point of view.
By applying the most advanced information technologies, Frontiers is catapulting scholarly publishing into a new generation.

What are Frontiers Research Topics?

Frontiers Research Topics are very popular trademarks of the Frontiers Journals Series: they are collections of at least ten articles, all centered on a particular subject. With their unique mix of varied contributions from Original Research to Review Articles, Frontiers Research Topics unify the most influential researchers, the latest key findings and historical advances in a hot research area! Find out more on how to host your own Frontiers Research Topic or contribute to one as an author by contacting the Frontiers Editorial Office: **researchtopics@frontiersin.org**

REMODELING OF CARDIAC PASSIVE ELECTRICAL PROPERTIES AND SUSCEPTIBILITY TO VENTRICULAR AND ATRIAL ARRHYTHMIAS

Topic Editor:
George E. Billman, The Ohio State University, USA

Image used with permission: https://commons.wikimedia.org/wiki/File:Lightning3.jpg#filelinks

The effective management of cardiac arrhythmias, either of atrial or of ventricular origin, remains a major challenge. Sudden cardiac death due to ventricular tachyarrhythmias remains the leading cause of death in industrialized countries while atrial fibrillation is the most common rhythm disorder; an arrhythmia that's prevalence is increasing and accounts for nearly one quarter of ischemic stokes the elderly population. Yet, despite the enormity of the problem, effective therapeutic interventions remain elusive. In fact, several initially promising antiarrhythmic agents were found to increase rather than decrease mortality in patients recovering from myocardial infarction. The question then is what went wrong, why have these interventions proven to be so ineffective? An obvious answer is the drugs were designed to attack the wrong therapeutic target. Clearly, targeting single ion channels (using either isolated ion channels or single myocytes preparations) has proven to be less than effective. What then is the appropriate target? It is well established that cardiac electrical properties can vary substantially between single cells and intact preparations. One obvious example is the observation that action potential duration is much longer in isolated cells as compared to multi-cellular preparations or intact hearts. Due

to the low electrical resistance between adjacent myocytes, the cells act in coordinated fashion producing "electrotonic interdependence" between neighboring cells. Myocardial infarction and/or acute ischemia provoke profound changes in the passive electrical properties of cardiac muscle. In particular, electrotonic uncoupling of the myocytes disrupts the coordinated activation and repolarization of cardiac tissue. The resulting compensatory changes in ionic currents decrease cardiac electrical stability increasing the risk for life-threatening changes in the cardiac rhythm. Thus, the electrical properties of myocardial cells must be considered as a unit rather than in isolation. It is the purpose of this Research Topic to evaluate the largely neglected relationship between changes in passive electrical properties of cardiac muscle and arrhythmia formation.

Citation: Billman, G. E., ed. (2015). Remodeling of Cardiac Passive Electrical Properties and Susceptibility to Ventricular and Atrial Arrhythmias. Lausanne: Frontiers Media. doi: 10.3389/978-2-88919-647-0

Table of Contents

frontiers in Physiology

EDITORIAL
published: 06 July 2015
doi: 10.3389/fphys.2015.00196

Editorial: Cardiac electronic remodeling and susceptibility to arrhythmias: an introduction and brief historical overview

George E. Billman[1]* *and Carlos L. del Rio*[2]

[1] Department of Physiology and Cell Biology, The Ohio State University, Columbus, OH, USA, [2] QTest Labs LLC, Columbus, OH, USA

Keywords: arrhythmias, cardiac, ventricular fibrillation, atrial fibrillation, gap junctions, electrotronic coupling, myocardial electrical properties, myocardial infarction

Edited and reviewed by:
Ruben Coronel, Academic Medical Center, Netherlands

***Correspondence:**
George E. Billman, george.billman@frontiersin.org

Specialty section:
This article was submitted to Cardiac Electrophysiology, a section of the journal Frontiers in Physiology

Received: *19 June 2015*
Accepted: *23 June 2015*
Published: *06 July 2015*

Citation:
Billman GE and del Rio CL (2015) Editorial: Cardiac electronic remodeling and susceptibility to arrhythmias: an introduction and brief historical overview. Front. Physiol. 6:196. doi: 10.3389/fphys.2015.00196

The effective management of cardiac arrhythmias, either of atrial or of ventricular origin, remains a major challenge. Sudden cardiac death due to ventricular tachyarrhythmias remains the leading cause of death in industrialized countries (Hayashi et al., 2015) while atrial fibrillation is the most common rhythm disorder, the prevalence of this arrhythmia is increasing and accounts for nearly one quarter of ischemic strokes in the elderly population (Chugh et al., 2015). Yet, despite the enormity of the problem, effective therapeutic interventions remain elusive. In fact, several initially promising antiarrhythmic agents were found to increase rather than decrease mortality in patients recovering from myocardial infarction (Behr and Roden, 2013). The question then is what went wrong, why have these pharmacological interventions proven to be so ineffective? An obvious answer that is the drugs were designed to attack the wrong therapeutic target. Clearly, targeting single ion channels (using either isolated ion channels or single myocyte preparations) has proven to be less than effective. What then is the appropriate target? It is well established that cardiac electrical properties can vary substantially between single cells and intact preparations. One obvious example is the observation that action potential duration is much longer in isolated cells as compared to multi-cellular preparations or intact hearts. Due to the low electrical resistance between adjacent myocytes, the cells act in coordinated fashion producing an "electrotonic interdependence" between neighboring cells that results in a more uniform (and shorter) action potential duration than would be recorded in single uncoupled cells.

Engelmann (1875) was perhaps the first to recognize that the cardiac myocytes work as coordinated unit. He proposed what he called a "healing over" principle (as referenced by Janse, 2003) to describe how myocytes were joined to work and to live together (forming what is now known as a functional syncytium). However, the electrophysiological basis for the cell-to-cell-coupling was not established until the 1950's when Dr. Silvio Weidmann laid the "engineering" foundations of modern cardiac electrophysiology. His work provided the quantitative basis to Engelmann's "healing over" concept (Niggli et al., 2006), recognizing the importance of passive myocardial electrical properties to cardiac excitation/conduction (Weidmann, 1952). Weidmann (1952) applied earlier theoretical principles (Hodgkin and Rushton, 1946) to model a cardiac (Purkinje) fiber as a core-conductor/cable, having "a well-conducting protoplasm and by a thin surface membrane having a high resistance (r_m) and a large capacity (c_m) per unit area." This "cable model" considers that the intracellular and extracellular potentials vary along the longitudinal axis only, and that both the cytoplasm and the extracellular spaces can be approximated as ideal ohmic conductors (with r_i and r_e respective resistances per unit length). Hence, propagating cardiac action potentials along a fiber can be described by the following second-order partial differential equation (PDE):

$$\left(\frac{1}{r_e + r_i}\right)\frac{\partial^2}{\partial x^2}V_m \;=\; c_m \cdot \frac{\partial}{\partial t}V_m \;+\; I_{ionic}\,(V, t) \qquad (1)$$

where I_{ionic} is the nonlinear membrane ionic current density ($\mu A/cm^2$), defined by the active/stochastic electrical properties of the cell. Alternatively, multiplying by r_m, Equation (1) can be re-written as

$$\lambda^2 \frac{\partial^2}{\partial x^2}V_m \;=\; \tau\frac{\partial}{\partial t}V_m \;+\; V_{ionic}\,(V, t) \qquad (2)$$

where $\lambda \;=\; \sqrt{\frac{r_m}{r_e + r_i}}$ is the length (and/or space) constant, a parameter that indicates how far a stationary current will "electrotonically" influence the voltage along the fiber, and $\tau = r_m c_m$ is the trans-membrane time-constant (e.g., Plonsey, 1969; Aidley, 1971).

Using this theoretical framework, Weidmann (1952) demonstrated that the electrical length/space constant was much larger than the cell length (defining the basis for the "electrotonic" modulation/homogenization of potentials across adjacent cells). He found that the internal longitudinal resistance (myoplasm in series with cell-to-cell contact) was much smaller than the membrane resistance. This result suggested the existence of low-resistance connections between neighboring cells, which Weidmann later demonstrated by studying and modeling (via the use of analog electrical circuits) the diffusion of potassium (Weidmann, 1960, 1966), showing that permeability of the intercalated disk to this ion was far greater than of the cell membrane. Subsequent investigations have identified the structural components (i. e., conforming proteins) of these intercellular junctional connections/channels, or "gap junctions" and have also confirmed their role in electrotonic coupling of the adjacent cells and in action potential propagation (for reviews see De Groot and Coronel, 2004; Wit and Peters, 2012; Dhein et al., 2014; Kleber and Saffitz, 2014). Alterations in these passive electrical properties can also lead to the generation of abnormal cardiac rhythms (both atrial and ventricular arrhythmias).

Myocardial infarction and/or acute ischemia provoke profound changes in the passive electrical properties of cardiac muscle (De Groot and Coronel, 2004). In particular, electrotonic uncoupling the myocytes disrupts the coordinated activation and repolarization of cardiac tissue. The resulting compensatory changes in ionic currents decrease cardiac electrical stability increasing the risk for life-threatening changes in the cardiac rhythm. Thus, the electrical properties of myocardial cells must be considered as a unit rather than in isolation. It is the purpose of this monograph to evaluate the largely neglected relationship between changes in passive electrical properties of cardiac muscle and arrhythmia formation. The book contains both state-of-the art reviews of the literature and original research articles that address various aspects of the effects of the passive electrical properties of the myocardium on cardiac rhythm. A brief summary of each chapter follow.

The role that changes in intrinsic properties of pacemaker cells (Yaniv et al., 2015), sinoatrial fibrosis (Csepe et al., 2015) and source sink (source—electrical charge for impulse generation; sink—the charge necessary to excite the surrounding tissue, impulse conduction) balance (Unudurthi et al., 2014) play in sinoatrial function and dysfunction are reviewed in chapters 2, 3 and 4, respectively. In a similar manner, the predominant role that gap junctions play in both normal and pathological changes in cardiac rhythm is reviewed in chapters 5–8. For example, Dhein et al. (2014) and Kleber and Saffitz (2014) review how electrotonic interactions, mediated both by junctional coupling proteins and geometrical/physiological factors, modulate source-sink phenomena in order to trigger/sustain normal cardiac rhythm and arrhythmogenesis (chapters 5 and 6). Kessler et al. (2014) further evaluate the contribution of heterogeneous gap junction remodeling to an increased risk for arrhythmias in several pathological conditions including hypertrophic, dilated, ischemic, and arrhythmic cardiomyopathies (chapter 7). Smit and Coronel (2014) next examine whether stem cells (implanted for stem cell replacement therapy) form functional electrotonic connections with cardiomyocytes and then evaluate the proarrhythmic risk that could result as a consequence of these connections (chapter 8). Trayanova et al. (2014) provide a state of the art assessment of computational modeling of atrial and ventricular arrhythmogenesis that result from disease induced changes in myocardial passive electrical properties (chapter 9), while Cabo (2014) uses similar computational approaches to analyze the effect on the dynamics of impulse propagation induced by simulated premature ventricular contractions in the infracted myocardium (structural heterogeneities caused by changes in gap junction conductance) (chapter 10). The functional significance of myofibroblast sodium currents on supraventricular arrhythmia formation is similarly investigated by Koivumäki et al. (2014) (chapter 11), while Walton et al. (2013) evaluate electrotonic modulation of repolarization using optical mapping techniques in species with large (pig) and small (rat) hearts (chapter 12). Despite the unequivocal mechanistic relationship(s) between passive electrical changes and arrhythmias, no study to date has directly assessed the ability of indices reflective of electrotonic coupling to stratify arrhythmic susceptibility *in vivo*. Therefore, del Rio et al. (2015) studied the effects of exercise-induced autonomic neural activation on electrotonic coupling as measured by myocardial electrical impedance in dogs know to be either susceptible or resistant to ischemically-induced ventricular fibrillation. They report that beta-adrenergic receptor activation enhances electrotonic coupling to a greater extent in susceptible as compared to dogs resistant to malignant arrhythmias and could thereby mask pro-arrhythmic repolarization abnormalities, an observation that may help explain false negative findings associated with exercise-stress testing in the clinic (chapter13).

The authors hope that this monograph will provide a better appreciation of the crucial role that myocardial passive electrical properties play in not only the maintenance of a normal cardiac rhythm but also how changes in these parameters can trigger atrial and ventricular arrhythmias. The application of this knowledge should facilitate the development of more effective anti-arrhythmic therapies.

References

Aidley, D. J. (1971). *The Physiology of Excitable Cells*. New York, NY: Cambridge University Press.

Behr, E. R., and Roden, D. (2013). Drug-induced arrhythmia: pharmacogenomics prescribing? *Eur. Heart J.* 34, 89–95. doi: 10.1093/eurheartj/ehs351

Cabo, C. (2014). Dynamics of propagation of premature impulses in structurally remodeled infarcted myocardium: a computational analysis. *Front. Physiol.* 5:483. doi: 10.3389/fphys.2014.00483

Chugh, S. S., Havmoeller, R., Narayanan, K., Singh, D., Rienstra, M., Benjamin, E. J., et al. (2015). Worldwide epidemiology of atrial fibrillation: a global burden of disease 2010 study. *Circulation* 129, 837–847. doi: 10.1161/CIRCULATIONAHA.113.005119

Csepe, T. A., Kalyanasundaram, A., Hansen, B. J., Zhao, J., and Fedorov, V. V. (2015). Fibrosis: a structural modulator of sinoatrial node physiology and dysfunction. *Front. Physiol.* 6:37. doi: 10.3389/fphys.2015.00037

De Groot, J. R., and Coronel, R. (2004). Acute ischemia-induced gap junctional uncoupling and arrhythmogenesis. *Cardiovasc. Res.* 62, 323–334. doi: 10.1016/j.cardiores.2004.01.033

del Rio, C. L., Clymer, B. D., and Billman, G. E. (2015). Myocardial electronic response to submaximal exercise in dogs with myocardial infarctions: evidence for β-adrenoceptor mediated enhanced coupling during exercise testing. *Front. Physiol.* 6:25. doi: 10.3389/fphys.2015.00025

Dhein, S., Seidel, T., Salameh, A., Jozwiak, J., Hagen, A., Kostelka, M., et al. (2014). Remodeling of cardiac passive electrical properties and susceptibility to ventricular and atrial arrhythmias. *Front. Physiol.* 5:424. doi: 10.3389/fphys.2014.00424

Engelmann, T. (1875). Über die Lietung der Erregung im Herzmuskel. *Pfluers Arch.* 11, 465–480. doi: 10.1007/BF01659313

Hayashi, M., Shimzu, W., and Albert, C. M. (2015). The spectrum of epidemiology underlying sudden cardiac death. *Circ. Res.* 116, 1887–1906. doi: 10.1161/CIRCRESAHA.116.304521

Hodgkin, A. L., and Rushton, W. A. (1946). The electrical constants of a crustacean nerve fibre. *Proc. R. Soc. Med.* 134, 444–479. doi: 10.1098/rspb.1946.0024

Janse, M. J. (2003). A brief history of sudden cardiac death and its therapy. *Pharmacol. Ther.* 100, 89–99. doi: 10.1016/S0163-7258(03)00104-9

Kessler, E. L., Boulaksil, M., van Rijen, H. V. M., Vos, M. A., and van Veen, T. A. B. (2014). Passive ventricular remodeling in cardiac disease: focus on heterogeneity. *Front. Physiol.* 5:482. doi: 10.3389/fphys.2014.00482

Kleber, A. G., and Saffitz, J. E. (2014). Role of the intercalated disc in cardiac propagation and arrhythmogenesis. *Front. Physiol.* 5:404. doi: 10.3389/fphys.2014.00404

Koivumäki, J. T., Clark, R. B., Belke, D., Kondo, C., Fedak, P. W. M., Maleckar, M. M. C., et al. (2014). Na^+ current expression in human atrial myofibroblasts: identity and functional roles. *Front. Physiol.* 5:275. doi: 10.3389/fphys.2014.00275

Niggli, E., Kléber, A., and Weingart, R. (2006). Founder of cardiac cellular electrophysiology: honouring Silvio Weidmann, 7 April 1921 – 11 July 2005. *J. Physiol.* 570, 431–432. doi: 10.1113/jphysiol.2005.101550

Plonsey, R. (1969). *Bioelectric Phenomena*. New York, NY: McGraw-Hill.

Smit, N. W., and Coronel, R. (2014). Stem cells can form gap junctions with cardiac myocytes and exert pro-arrhythmic effects. *Front. Physiol.* 5:419. doi: 10.3389/fphys.2014.00419

Trayanova, N. A., Boyle, P. M., Arevalo, H. J., and Zahid, S. (2014). Exploring susceptibility to atrial and ventricular arrhythmias resulting from remodeling of the passive electrical properties of the heart: a simulation approach. *Front. Physiol.* 5:435. doi: 10.3389/fphys.2014.00435

Unudurthi, S. D., Wolf, R. M., and Hund, T. J. (2014). Role of sinoatrial node architecture in maintaining a balanced source-sink relationship and synchronous cardiac pacemaking. *Front. Physiol.* 5:446. doi: 10.3389/fphys.2014.00446

Walton, R. D., Benson, A. P., Hardy, M. E. L., White, E., and Bernus, O. (2013). Electrophysiological and structural determinants of electronic modulation of repolarization by the activation sequence. *Front. Physiol.* 4:281. doi: 10.3389/fphys.2013.00281

Weidmann, S. (1952). The electrical constants of Purkinje fibres. *J. Physiol.* 118, 348–360. doi: 10.1113/jphysiol.1952.sp004799

Weidmann, S. (1960). Sheep heart; low resistance of intercalated discs to the movement of 42K. *J. Physiol.* 153, 32P.

Weidmann, S. (1966). The diffusion of radiopotassium across intercalated disks of mammalian cardiac muscle. *J. Physiol.* 187, 323–342. doi: 10.1113/jphysiol.1966.sp008092

Wit, A. L., and Peters, N. S. (2012). The role of gap junctions in the arrhythmias of ischemia nd infarction. *Heart Rhythm* 9, 308–311. doi: 10.1016/j.hrthm.2011.09.056

Yaniv, Y., Tsutsui, K., and Lakatta, E. G. (2015). Potential effects of intrinsic heart pacemaker cell mechanisms in dysrhythmic cardiac action potential firing. *Front. Physiol.* 6:47. doi: 10.3389/fphys.2015.00047

Conflict of Interest Statement: The authors declare that the research was conducted in the absence of any commercial or financial relationships that could be construed as a potential conflict of interest.

frontiers in
PHYSIOLOGY

PERSPECTIVE ARTICLE
published: 23 February 2015
doi: 10.3389/fphys.2015.00047

Potential effects of intrinsic heart pacemaker cell mechanisms on dysrhythmic cardiac action potential firing

Yael Yaniv[1]*, Kenta Tsutsui[2] and Edward G. Lakatta[2]*

[1] *Biomedical Engineering Faculty, Technion-Israel Institute of Technology, Haifa, Israel*
[2] *Laboratory of Cardiovascular Science, Biomedical Research Center, Intramural Research Program, National Institute on Aging, National Institutes of Health, Baltimore, MD, USA*

Edited by:
George E. Billman, The Ohio State University, USA

Reviewed by:
Vadim V. Fedorov, The Ohio State University, USA
Thomas Hund, The Ohio State University, USA

***Correspondence:**
Yael Yaniv, Biomedical Engineering Faculty, Technion-Israel Institute of Technology, 3200003 Haifa, Israel
e-mail: yaely@bm.technion.ac.il;
Edward G. Lakatta, Laboratory of Cardiovascular Science, Biomedical Research Center, Intramural Research Program, National Institute on Aging, NIH, 251 Bayview Blvd, Baltimore, 21224 MD, USA
e-mail: lakattae@grc.nia.nih.gov

The heart's regular electrical activity is initiated by specialized cardiac pacemaker cells residing in the sinoatrial node. The rate and rhythm of spontaneous action potential firing of sinoatrial node cells are regulated by stochastic mechanisms that determine the level of coupling of chemical to electrical clocks within cardiac pacemaker cells. This coupled-clock system is modulated by autonomic signaling from the brain via neurotransmitter release from the vagus and sympathetic nerves. Abnormalities in brain-heart clock connections or in any molecular clock activity within pacemaker cells lead to abnormalities in the beating rate and rhythm of the pacemaker tissue that initiates the cardiac impulse. Dysfunction of pacemaker tissue can lead to tachy-brady heart rate alternation or exit block that leads to long atrial pauses and increases susceptibility to other cardiac arrhythmia. Here we review evidence for the idea that disturbances in the intrinsic components of pacemaker cells may be implemented in arrhythmia induction in the heart.

Keywords: arrhythmias, atrial fibrillation, coupled-clock pacemaker system, heart rate variability, sinus node disease

INTRODUCTION

Normal cardiac impulse initiation and conduction are generated by specialized, self-excitable, pacemaker cells residing in the sinoatrial node (SAN). Defects in these cell-intrinsic capacities to elicit spontaneous action potentials (APs) can lead to disturbances of the rate and rhythm of heart beats, and can induce numerous clinical arrhythmia syndromes: (i) SAN dysfunction has been postulated to be a source of sinus nodal re-entry (i.e., reciprocal beats between SAN and atrium) tachyarrhythmia (Birchfield et al., 1957) which accounts for 2–17% of all arrhythmias (Cossu and Steinberg, 1998). While diagnosis of this arrhythmia is difficult, due to electrocardiographic similarity of the P-wave to the normal sinus rhythm (Gomes et al., 1995), microelectrode studies in isolated rabbit hearts (Han et al., 1968) and later in humans (Childers et al., 1973) indeed demonstrate that SAN is the source that induces re-entry. (ii) Sick sinus syndrome, characterized by symptomatic dysfunction of the SAN (reviewed in Dobrzynski et al., 2007), can be manifested as sinus bradycardia, sinus arrest, or SAN block, and in some cases supraventricular tachyarrhythmias ("tachy-brady" syndrome), atrial flutter or atrial fibrillation. In mice with an inducible phenotype that mimics sick sinus syndrome, heart beating intervals (BIs) were completely irregular both *in vivo* and in the isolated Langendroff perfused model (no brain-heart signaling) (Herrmann et al., 2007). Telemetric ECG recordings revealed a variety of arrhythmias: sino-atrial arrhythmia, sino-atrial pause and supraventricular or ventricular tachycardia. (iii) It has been suggested that abnormal stretch of the rat atria that accompanies many heart diseases (De Jong et al., 2013) and occurs even in transplanted human hearts (Slovut et al., 1998) (no brain-heart connection) induces respiratory sinus arrhythmia.

Here we review evidence for the idea that changes in the membrane and sarcoplasmic reticulum (SR) components of pacemaker cells may be implicated in arrhythmia induction in the heart.

INTRINSIC COUPLED-CLOCK MECHANISMS TO PACEMAKER CELLS CONTROL THE HEART RATE AND RHYTHM

To understand abnormal SAN function it is essential to first understand the normal function of intrinsic properties of pacemaker cells and their modulation by brain-heart signaling. Experimental and theoretical data over the past two decades indicate that pacemaker cells residing in the SAN entrain their AP BI variability (BIV) by regulation of intracellular electric and mechanical coupling (reviewed in Yaniv et al., 2013a).

The coupled-clock system (Yaniv et al., 2013b; Maltsev et al., 2014) that controls the pacemaker cell beating rate and rhythm consists of an intracellular "Ca^{2+} clock" and "M clock." The sarcoplasmic reticulum Ca^{2+} pump and ryanodine channels act as a "Ca^{2+} clock," discharging local Ca^{2+} releases (LCRs) close to the cell surface membrane; LCRs activate membrane electrogenic clock molecules ("M clock"), mainly the Na^{+}/Ca^{2+} exchanger. Na^{+}-Ca^{2+} exchange current, the f-channel current, and K^{+} channel current, other components of the M clock, concurrently drive the diastolic membrane depolarization to ignite the next AP. The Ca^{2+} and M clocks entrain each

other through electrical and chemical signaling: Ca^{2+} activation of calmodulin -adenylyl cyclase (AC)-dependent protein kinase A (PKA) and Ca^{2+}/calmodulin-dependent protein kinase II (CaMKII). Both of these signaling pathways affect phosphorylation of proteins of both clocks [i.e., phospholamban (PLB) and ryanodine receptors (Ca^{2+} clock) and L type and K^+ channels (M clock)]. Additionally, cAMP positively shifts the f-channel activation curve. Based on the coupled-clock theory, a change in the activity or in the quantity of every molecule within the M or the Ca^{2+} clock or a change in the chemical coupling signaling of both clocks will perturb the function of the other clock, and thus alter the degree of entrainment between them. For example, in rabbit pacemaker cells, reduction in I_f activity or in Ca^{2+} clock proteins leads to reduction in the coupled-clock phosphorylation activity and LCR signal (Yaniv et al., 2014b). Thus, a reduction of internal signaling within one clock can lead to a reduction in the degree of clock coupling and changes in the function of the other clock that change automaticity.

Even under normal conditions, spontaneous AP BIs of mammals including human pacemaker cells are not constant, but vary around the average AP BI, due to stochastic properties of intrinsic mechanisms of the coupled-clock system (Verheijck et al., 1998; Rocchetti et al., 2000; Zaza and Lombardi, 2001; Monfredi et al., 2013; Papaioannou et al., 2013; Yaniv et al., 2014b). The degree of AP BIV is related to variability in both the timing of LCR occurrence during the diastolic depolarization, and to the ensemble LCR Ca^{2+} signal: an increase in LCR variability is associated with a reduced ensemble LCR Ca^{2+} signal that occurs later in diastole (i.e., prolonging the next AP ignition). Based on the coupled-clock theory, the stochasticity of LCR periods (i.e., the times of LCR occurrences following the prior AP) not only depends upon stochasticity of spontaneous RyR activation, but also upon stochastic sarcolemmal ion channel openings and closings that regulate the cell Ca^{2+} balance. The amplitude and timing of LCR Ca^{2+} signals to M clock proteins report the efficiency of clock coupling, i.e., a weaker LCR signal to M clock proteins that occurs later in time reports less-efficient clock coupling. Consequently, changes in the steady-state AP BI and the BIV embody contributions of both clocks. Reduction in the degree of synchronization between the clocks disturbs the ability to maintain the basal average AP BI, leading not only to a reduction in the average AP BI, but also to an increase in variability around the prolonged average AP BI.

Autonomic neural input can entrain the rate and rhythm of electrical impulses that are generated by SAN tissue of mammals (Difrancesco, 1993; Boyett et al., 2000; Monfredi et al., 2014; Yaniv et al., 2014a). The balance between sympathetic to parasympathetic stimulation has a role in synchronizing intrinsic clock periods of individual pacemaker cells. β adrenergic receptor stimulation increases synchronization of intrinsic clock mechanisms leading to a decrease of both BI and BIV of pacemaker cells (**Figures 1B,C**). Moreover, β adrenergic receptor stimulation of a single pacemaker cell increases the probability that the beating intervals exhibit fractal-like behavior. Cholinergic receptor stimulation of pacemaker cells, on the other hand, decreases synchronization of intrinsic clock mechanisms, leading to an increase of both the average BI and BIV (**Figures 1B,C**).

SYNCHRONIZATION OF ACTIVITY ACROSS THE POPULATION OF CELLS CAN IMPACT ON THE HEART RATE AND RHYTHM

Although we have focused here upon synchronization of mechanisms intrinsic to pacemaker cells, cell-to-cell interactions (electrotonic and mechanical) of pacemaker cells residing in SAN tissue also entrain the rate and rhythm of electrical impulses that emanate from the SAN (Jalife, 1984; Watanabe et al., 1995). These interactions have a role in synchronizing the intrinsic clock periods of individual cells (Sheikh et al., 2013), because the average range of basal AP BI and AP BIV of single isolated pacemaker cells is well above their range when they reside in rabbit SAN tissue (Yaniv et al., 2014a) (**Figure 1A**). When pacemaker cells are embedded within SAN tissue, those with the shortest AP BI create a primary pacemaker area within the SAN, leading to the origin of an electrotonic force that spreads to other SAN cells, resulting in the emanation of an electric impulse that excites the rest of the heart (Anumonwo et al., 1991). This impulse controls the heart rate and rhythm. When rabbit pacemaker cells are isolated from SAN tissue, their beating interval entropy increases dramatically compared to that when these cells reside in SAN tissue (**Figure 1B**), and fractal-like behavior of AP BIs, a feature that characterizes AP BI of SAN tissue, is absent in isolated single pacemaker cells (Yaniv et al., 2014a).

CHANGES IN HEART RATE VARIABILITY INDEXES AND THE PRESENCE OF ARRHYTHMIA

An increase in pacemaker cells AP BIV, or in mathematical terms coupled-clock-system entropy, above a certain threshold leads to abnormal impulse generation by the SAN that is defined as arrhythmia. Two regimes of heart rate variability (HRV) are analyzed in patients with arrhythmogenic events: during the events when the entropy of the system increases (Costa et al., 2008), and before the occurrence of arrhythmia. The occurrence of major arrhythmic events in patients with right ventricular cardiomyopathy is associated with a reduced BIV (Battipaglia et al., 2012). Interestingly, heart rate variability indexes decrease just prior to an arrhythmogenic event (Postolache et al., 2011). As we summarized here, the degree of synchronization of intrinsic mechanisms to pacemaker cells and the degree of synchronization among pacemaker cells within the SAN are determinants of the heart rate and rhythm. Autonomic receptors on pacemaker cells respond to the imbalances of autonomic impulses associated with cardiac diseases. Specifically, autonomic receptor stimulation of single pacemaker cells alters their beat-to-beat variability. Thus, intrinsic pacemaker mechanisms may contribute to HRV *in vivo*. Although mechanisms of HRV may vary from one patient to another, documentation of the relationship between HRV and different arrhythmias in human patients (**Table 1**) is an important initial step to conceptually link intrinsic pacemaker mechanisms to arrhythmogenic events. Note, that this sort of evidence, however, does not prove that altered synchronization of pacemaker clock mechanisms residing within the SAN are the sole cause of all patient arrhythmias that may be linked to changes in HRV.

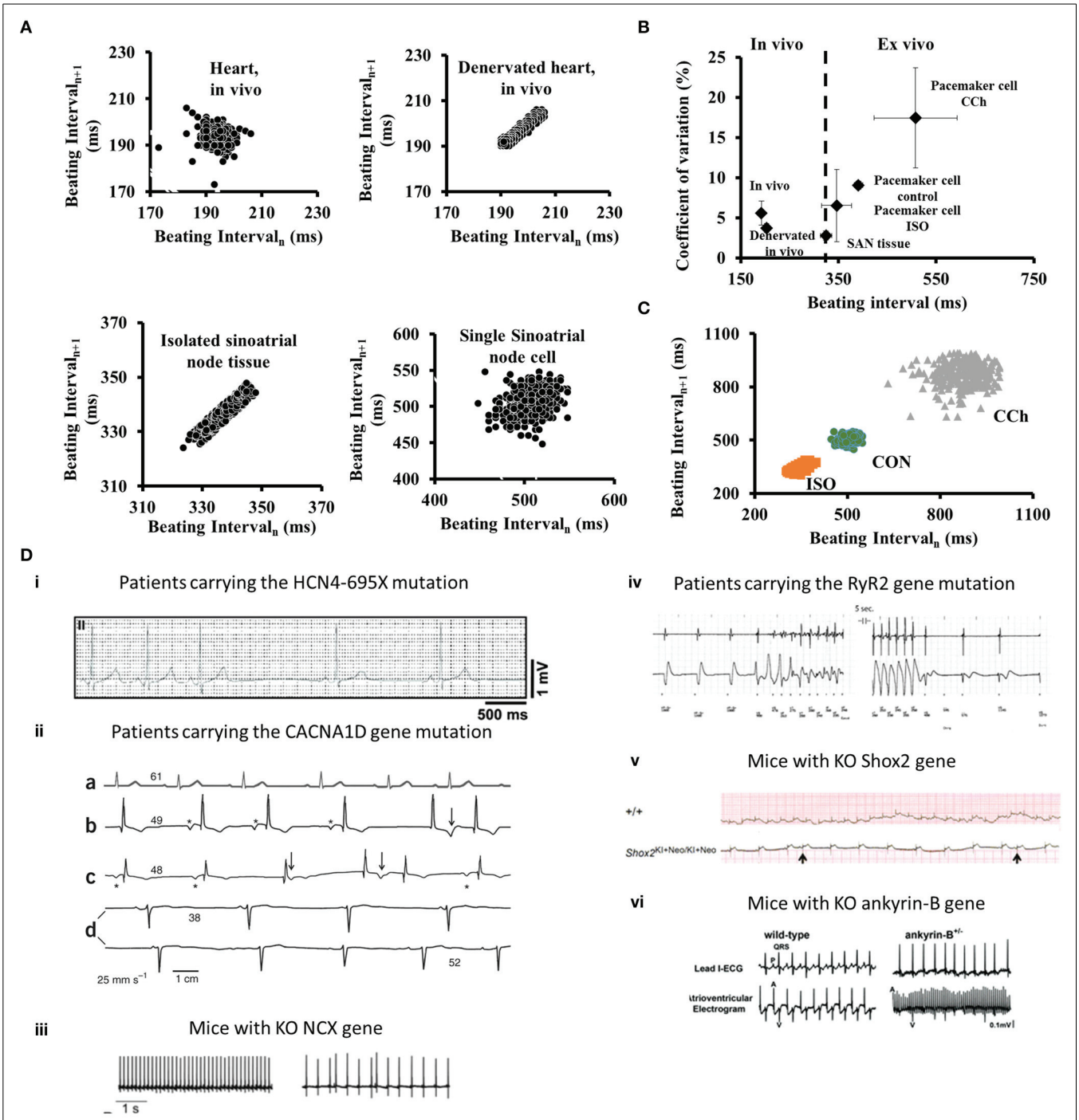

FIGURE 1 | (A) Poincaré plots of the beating interval at different levels of integration from the heart *in vivo* to single isolated pacemaker cells. (B) The relationship between beating intervals and coefficients of variation at different levels of integration from the heart *in vivo* to single pacemaker cells in isolation. **(C)** Poincaré plots of the beating interval variability in single SANC under control (CON), β-adrenergic receptor stimulation (ISO) or cholinergic receptor stimulation (CCh). Modified from Yaniv et al. (2014a). **(D)** Examples of arrhythmias associated with changes in intrinsic clock mechanisms recorded *in vivo*: (i) in patients carrying the HCN4-695X mutation (adapted from Schweizer et al., 2010); (ii) (a–d) ECG recordings from an unaffected person (a) and three individuals who are homozygous for the CACNA1D mutation (b–d) (adapted from Baig et al., 2011); (iii) Cardiac arrhythmias in freely moving NCX KO mice (adapted from Herrmann et al., 2013); (iv) A rapid and presumably polymorphic ventricular tachycardia in patents with mutation in RyR2 (adapted from Bhuiyan et al., 2007); (v) ECG recording demonstrate the occurrence of arrhythmia in Shox2 KO mice (adapted from Liu et al., 2011); (vi) ECG recording from ankyrin-B KO mice (adapted from Cunha et al., 2011).

Table 1 | Summary of primary studies assessing the changes of heart rate variability when arrhythmia occurs.

Type of arrhythmia	Number of patients	Findings	Study
AF	27	Decreased pNN50 was an independent predictor of AF relapse	Akyurek et al., 2003
AF	784	Impaired LF spectral component predicted new-onset AF	Perkiomaki et al., 2014
AF	83	Time and frequency indices attenuated when the treatments failed	Seaborn et al., 2014
PSVT	64	HR increased, HRV and HF power decreased after catheter ablation for PSVT	Kocovic et al., 1993
Sick sinus syndrome	30	Poincare plot often showed random-like pattern; Beta coefficient* of fractal increased toward 0 in sinoatrial node dysfunction	Bergfeldt and Haga, 2003
Sick sinus syndrome	181	Decreased SDNN and rMSSD after pulmonary vein isolation	Wang et al., 2013
VF	24	HRV indices consistently did not change before VF	Vybiral et al., 1993
VF	15	VF patients had lower DFA alpha (0.64 vs. 1.05) and fractal beta coefficient* (−1.63 vs. −1.31) than control	Makikallio et al., 1999
VT	40	All power spectra of HRV decreased before the onset of sustained VT compared to before nonsustained VT	Huikuri et al., 1993
VF/AVB	25	V-shaped trough appeared in the curve of ln(LF/HF) and ln(HF) prior to VF and AVB, respectively	Osaka et al., 2010
VF/AVB	292	Beta coefficient* < −1.5 was the most powerful predictor of VF	Gang et al., 2011
VT/VF	312 after myocardial infraction	Decreased SDNN, VLF, HF, DFA alpha1 predicted VT/VF	Huikuri et al., 2009
VT/VF	28	Decreased scattering in Poincare plot before arrhythmic event	Rozen et al., 2013

*PSVT, Paroxysmal supraventricular tachycardia; VF, Ventricular fibrillation; VT, Ventricular tachycardia; AF, atrial fibrillation; AVB, atrioventricular block; DFA, Detrended fluctuation analysis; pNN50, the number of pairs of successive beats that differ by more than 50 ms; SDNN, standard deviation of the average beating intervals; rMSSD, root mean square of successive differences; HF, high frequency; LF, low frequency; VLF, very low frequency. *Beta coefficient is the slope between power spectra and VLF in log-log scale.*

DIRECT PHARMACOLOGICAL INHIBITION OF COUPLED-CLOCK PROTEINS OF PACEMAKER CELLS CAUSES CHANGES IN RATE AND RHYTHM

Direct pharmacological inhibition of coupled-clock proteins can induce arrhythmias. For example: (i) caging of intracellular Ca^{2+} by NP-EGTA in isolated rabbit pacemaker cells induces an increase in LCR variability and AP BI bradycardia together with arrhythmic events (Yaniv et al., 2011). (ii) A sudden increase in stochastic ryanodine receptor open probability, elicited by caffeine spritz in isolated rabbit pacemaker cells, induces tachycardia, together with arrhythmic events (Yaniv et al., 2013d). (iii) Specific PKA inhibitors (Younes et al., 2008) or CaMKII inhibitors (Yaniv et al., 2013c) superfused onto isolated rabbit pacemaker cells induce AP BI bradycardia together with arrhythmic events. (iv) Perturbing clock coupling in rabbit pacemaker cells by directly inhibiting either the M (ivabradine, an I_f inhibitor) or Ca^{2+} clock (cyclopiazonic acid, a SR Ca^{2+} pump inhibitor) produces increases in AP BI and AP BIV that are related to increases in LCR period and LCR period variability (Yaniv et al., 2014b). These results provide evidence that supports the coupled-clock theory, demonstrating the ability of the LCR Ca^{2+} signal to report the degree of synchronization between the two clocks, and how changes in the degree of synchronization lead to changes in AP BI and AP BIV.

REDUCED EFFICIENCY OF INTRINSIC COUPLED-CLOCK PACEMAKER MECHANISMS AND ARRHYTHMIA

Similar to direct pharmacological inhibitors of coupled-clock proteins, mutation and genetically induced gene deletion of different components of the coupled-clock system are associated with arrhythmias *in vivo*.

HCN GENE

The hyperpolarization-activated channel (I_f) consists of three HCN members (HCN1, HCN2, and HCN4) (Ludwig et al., 1998). HCN4 comprises the major fraction (70–80%) of SAN I_f. Various mutations of human HCN4 channels are associated with arrhythmias, and with bradycardia in particular (Yeh et al., 2009; Schweizer et al., 2010; Duhme et al., 2013). Interestingly, the spontaneous cardiac beating rate of HCN4-knockout embryos is significantly slower than that of wild-type, but no arrhythmic events are observed. These results are in contrast to the conditional deletion of HCN4 in adult animals, where bradycardia is not evident but sinus pauses are detected (Stieber et al., 2004; Herrmann et al., 2007; Yeh et al., 2009) (**Figure 1D**). Other HCN transcripts that compose funny current channel in the mouse are HCN2, and a low level of HCN1. HCN2-deficient mice display mild cardiac dysrhythmia, both in the presence and absence of autonomic control of the heart rate (Stieber et al., 2004; Herrmann et al., 2007). Similarly, HCN1-deficient mice exhibit sinus dysrhythmia *in vivo* and in single isolated cells (Fenske et al., 2013). Interestingly, HCN1-deficient mice exhibit high beat-to-beat dispersion (quantified by Poincaré plots) that is typically observed in SAN dysfunction (Fenske et al., 2013). Therefore, HCN4 apparently is required to protect the heart from severe bradycardia and HCN2 and HCN1 are required to prevent arrhythmias.

Ivabradine is a specific I_f blocker that reduces the heart rate in patients, specifically patients with inappropriate sinus tachycardia to eliminate arrhythmia (Cappato et al., 2012). However, a recent study in isolated rabbit pacemaker cells demonstrated that ivabradine, even at a concentration that specifically inhibits I_f, but does not directly suppress L-type current, SR Ca^{2+} cycling and other surface membrane ion channels, indirectly suppresses intracellular Ca^{2+} cycling (Yaniv et al., 2012, 2013b). The reduction in arrhythmic events is therefore likely due to drug effect on synchronization of functions within the coupled-clock system, and not simply to I_f inhibition, *per se* (Yaniv and Lakatta, 2013).

$Ca_v1.3$

Voltage-gated Ca_v1 channels ($Ca_v1.2$ and $Ca_v1.3$) mediate L-type Ca^{2+} channels that play distinct roles in mediating Ca^{2+} balance in the pacemaker cell. Both $Ca_v1.2$ and $Ca_v1.3$ channels are expressed in SAN, and $Ca_v1.3$ expression in the atria and SAN cells is higher than in ventricular myocytes (Marger et al., 2011). $Ca_v1.3$ current is activated faster and at more negative voltages than $Ca_v1.2$ current and, therefore, in mice can contribute earlier during the diastolic depolarization (Christel et al., 2012). Bradycardia and arrhythmia are particularly prominent in $Ca_v1.3$ knockout mouse pacemaker cells (Mangoni et al., 2003). Loss of function of $Ca_v1.3$ both in mice and humans causes sick sinus syndrome (see above) and is characterized by severe bradycardia (Platzer et al., 2000; Baig et al., 2011). Moreover, patients with a mutation in the CACNA1D gene, which encodes the pore-forming α_1 subunit of $Ca_v1.3$, experience pronounced bradycardia in 12–24-h ECG recordings, and their HRV time-domain indices are increased (Baig et al., 2011) (**Figure 1D**). Note that functional significance of $Ca_v1.3$ in large mammals has yet to be demonstrated.

NCX1

The Na^+/Ca^{2+} exchanger has two important roles in pacemaker cells: it not only maintains the cell Ca^{2+} balance by matching Ca^{2+} efflux to Ca^{2+} influx through the L-type Ca^{2+} current, but also contributes to diastolic depolarization (Maltsev et al., 2014). Specific knockout of SAN Na^+/Ca^{2+} exchanger mice induces bradycardia and increases BIV in the proportion of mycoytes that express arrhythmic AP BI compared to control mice (Herrmann et al., 2013) (**Figure 1D**). Interestingly, numerical model simulations predict that only a reduction in Na^+/Ca^{2+} exchanger density to below a specific threshold is accompanied by arrhythmic AP BI (Maltsev et al., 2013).

TRPM4

TRPM4 is a monovalent nonselective cation channel permeable to Na^+, K^+, and Li^+, but not to Ca^{2+} (Launay et al., 2002). Activation of TRPM4 channels that exist in murine pacemaker cells is achieved by both membrane depolarization and by a rise in intracellular Ca^{2+} (Hof et al., 2013). Although TRPM4 KO mice have heart rates similar to those of their controls, they exhibit a higher incidence of sinus pauses (Hof et al., 2013).

RYANODINE CHANNELS

The stochasticity of spontaneous RyR activation determines the diastolic LCR Ca^{2+} signal and therefore the degree of synchronization of intracellular function of the coupled-clock system. A mutation in RyR, exon-3, in patients with catecholaminergic polymorphic ventricular tachycardia, is associated with arrhythmias (Bhuiyan et al., 2007) (**Figure 1D**). Isolated pacemaker cells from mice that express this mutation have a prolonged average AP BI with pauses between AP BIs together with an impaired chronotropic response to β adrenergic stimulation (Neco et al., 2012). Similarly, in inducible, heart tissue-specific RyR2 knockout mice, both *in vivo* ECG telemetry and *in vitro* isolated perfused heart, demonstrated bradycardic BI and arrhythmia (Bround et al., 2012).

Shox2 AND OTHER TRANSCRIPTION FACTORS

The Shox2 transcriptional factor has been identified as a key regulator in pacemaker formation and differentiation (Liu et al., 2011). Shox2 gene KO mice have a significantly reduced heart beat rate and increased number of arrhythmic events (Liu et al., 2011) (**Figure 1D**). Moreover, deficient Shox2 transcription factor during development may cause abnormal of mouse SAN development associated with severe arrhythmias (Hoffmann et al., 2013). Therefore, the Shox2 gene also appears to be critical for normal pacemaking function. Other transcription factors than Shox2 are involved in pacemaker function. In this regard, expression of Tbx18 in guinea pig has been shown as an essential gene whose expression can convert quiescent cardiomyocytes to pacemaker cells (Kapoor et al., 2013), therefore, increasing the pacemaker-induced spontaneous beating rate of the cells and decreasing their BIV. Interestingly, Tbx18 transduction to the guinea pig embryonic cell lineage inhibits Cx43 expression, leading to significant electrical uncoupling (Kapoor et al., 2011).

ANKYRIN-B

Ankyrins are adaptor proteins that are required for targeting channels and transporters in pacemaker cells to the membranes in which they function. Human patients with ankyrin-B-deficiency have highly penetrant sinus node dysfunction coupled with increased susceptibility to spontaneous and inducible atrial fibrillation (Le Scouarnec et al., 2008). Interestingly, ankyrin-B -deficient mice also have reduced expression of Na^+/Ca^{2+} exchanger and Na^+/K^+ ATPase (Le Scouarnec et al., 2008). Finally, cells isolated from ankyrin-B-deficient mice have increased BIV (Cunha et al., 2011) (**Figure 1D**). Thus, down regulation of ankyrin-B induces abnormal membrane organization that is implicated in a reduced efficiency of pacemaker clock coupling that causes abnormal electrical activity within SAN.

CELL-TO-CELL UNCOUPLING MECHANISMS

As described above, the BIs of pacemaker cells residing in the SAN become entrained by electrotonic and mechanical cell-to-cell interactions within the tissue (Jalife, 1984; Watanabe et al., 1995). Numerical model simulations predict that cardiac arrhythmias can occur when normal coupling between pacemaker cells in SAN tissue is perturbed (Ostborn et al., 2001). Cardiac diseases, and specifically sick sinus syndrome, are associated with reduction in cell-cell junctional proteins (Dobrzynski et al., 2007). ECG of mice with a cardiac conduction-specific knockout of desmoplakin, a protein that affects mechanical cell-to-cell interaction in

the cardiac conduction system, exhibits sinus arrhythmias characterized by a strikingly increased number of sinus pauses compared to wild-type mice (Sheikh et al., 2013).

PASSIVE MECHANISMS

Although connexin43 is absent in the center of the pacemaker tissue, it is expressed in the peripheral area. A reduction in connexin 43 in aged guinea pig SAN is associated with a reduction in heart rate and an increase in arrhythmogenic events (Jones et al., 2004). Moreover, pacemaker tissue contains functional gap junctions and connecting cardiac fibroblasts (Camelliti et al., 2004). Because an increase in fibroblasts expression can slow the generation of pacemaker excitability, it may be involved in bradycardia and sick sinus syndrome (for review see Kohl et al., 2005). A detailed review of the role of passive pacemaker tissue properties on its electrical conductance is present in this issue (Unudurthi et al., 2014).

REDUCED EFFICIENCY OF SYNCHRONIZATION OF ACTIVITY ACROSS POPULATIONS OF CELLS AND ARRHYTHMIA

High-resolution optical mapping of SAN tissue has helped to resolve how reduced synchronization of activity across populations of cells within the SAN can induce arrhythmia. In this regard, different intrinsic mechanisms can be involved in tachy-brady heart-rate alteration and exit block that leads to long sinus pauses and increases susceptibility to cardiac arrhythmias: (i) an increase in adenosine level in human SAN tissue, an endogenous metabolite of the heart, through adenosine A1 receptor upregulating, can lead to SAN dysfunction (Lou et al., 2013, 2014); (ii) an increase in B-type and C-type natriuretic peptides increase the mice SAN conduction velocity and shift the initial exit site (Azer et al., 2014). (iii) Mutation in Ca^{2+}-binding protein calsequestrin 2 is associated with different cardiac diseases. In calsequestrin knockout mice the SAN exhibits bradycardia, conduction abnormalities and increase beat-to-beat variability (Glukhov et al., 2013). (iv) Ganglion nerve plexi can stimulate the intrinsic cardiac nervous system. In mice pulmonary vein ganglia stimulation shifts the origin of SAN discharges and decreases the heart rate (Zarzoso et al., 2013). (v) Impaired SR function in canine failing hearts results in an impaired shift in the location of the pacemaker site in response to β-AR stimulation (Shinohara et al., 2010).

SUMMARY

Changes in heart rate and rhythm are harbingers of the appearance of arrhythmogenic events. Reduction in the degree of synchronization of any intrinsic clock functions of pacemaker cells or in the synchronization among pacemaker cells residing in the SAN can be associated with arrhythmia occurrence. The extent to which restoring normal synchronization of intrinsic clock periods within pacemaker cells and among pacemaker cells can prevent arrhythmogenic events awaits further elucidation. In our opinion, future work requires a focus on the connection between dysfunction of inherent intrinsic mechanisms associated with different cardiac diseases and cardiac arrhythmias. This connection can be explored in genetically manipulated mouse models, in animals like rabbit, dog and sheep with heart failure or atrial fibrillation, and in human-derived cardiomyocytes or human SAN. This knowledge will contribute greatly to our understanding of cardiac impulse initiation in health and in cardiac disease.

ACKNOWLEDGMENTS

This research was partially supported by the Intramural Research Program of the NIH, National Institute on Aging, by Technion VPR Fund –Krbling Biomedical Engineering Research Fund (YY) and by NSFC-ISF joint research program, No. 398/14 (YY).

REFERENCES

Akyurek, O., Diker, E., Guldal, M., and Oral, D. (2003). Predictive value of heart rate variability for the recurrence of chronic atrial fibrillation after electrical cardioversion. *Clin. Cardiol.* 26, 196–200. doi: 10.1002/clc.4960260411

Anumonwo, J. M., Delmar, M., Vinet, A., Michaels, D. C., and Jalife, J. (1991). Phase resetting and entrainment of pacemaker activity in single sinus nodal cells. *Circ. Res.* 68, 1138–1153. doi: 10.1161/01.RES.68.4.1138

Azer, J., Hua, R., Krishnaswamy, P. S., and Rose, R. A. (2014). Effects of natriuretic peptides on electrical conduction in the sinoatrial node and atrial myocardium of the heart. *J. Physiol.* 592, 1025–1045. doi: 10.1113/jphysiol.2013.265405

Baig, S. M., Koschak, A., Lieb, A., Gebhart, M., Dafinger, C., Nurnberg, G., et al. (2011). Loss of Ca(v)1.3 (CACNA1D) function in a human channelopathy with bradycardia and congenital deafness. *Nat. Neurosci.* 14, 77–84. doi: 10.1038/nn.2694

Battipaglia, I., Scalone, G., Macchione, A., Pinnacchio, G., Laurito, M., Milo, M., et al. (2012). Association of heart rate variability with arrhythmic events in patients with arrhythmogenic right ventricular cardiomyopathy/dysplasia. *Circ. J.* 76, 618–623. doi: 10.1253/circj.CJ-11-1052

Bergfeldt, L., and Haga, Y. (2003). Power spectral and Poincare plot characteristics in sinus node dysfunction. *J. Appl. Physiol. (1985).* 94, 2217–2224. doi: 10.1152/japplphysiol.01037.2002

Bhuiyan, Z. A., Van Den Berg, M. P., Van Tintelen, J. P., Bink-Boelkens, M. T., Wiesfeld, A. C., Alders, M., et al. (2007). Expanding spectrum of human RYR2-related disease: new electrocardiographic, structural, and genetic features. *Circulation* 116, 1569–1576. doi: 10.1161/CIRCULATIONAHA.107.711606

Birchfield, R. I., Menefee, E. E., and Bryant, G. D. (1957). Disease of the sinoatrial node associated with bradycardia, asystole, syncope, and paroxysmal atrial fibrillation. *Circulation* 16, 20–26. doi: 10.1161/01.CIR.16.1.20

Boyett, M. R., Honjo, H., and Kodama, I. (2000). The sinoatrial node, a heterogeneous pacemaker structure. *Cardiovasc. Res.* 47, 658–687. doi: 10.1016/S0008-6363(00)00135-8

Bround, M. J., Asghari, P., Wambolt, R. B., Bohunek, L., Smits, C., Philit, M., et al. (2012). Cardiac ryanodine receptors control heart rate and rhythmicity in adult mice. *Cardiovasc. Res.* 96, 372–380. doi: 10.1093/cvr/cvs260

Camelliti, P., Green, C. R., Legrice, I., and Kohl, P. (2004). Fibroblast network in rabbit sinoatrial node: structural and functional identification of homogeneous and heterogeneous cell coupling. *Circ. Res.* 94, 828–835. doi: 10.1161/01.RES.0000122382.19400.14

Cappato, R., Castelvecchio, S., Ricci, C., Bianco, E., Vitali-Serdoz, L., Gnecchi-Ruscone, T., et al. (2012). Clinical efficacy of ivabradine in patients with inappropriate sinus tachycardia: a prospective, randomized, placebo-controlled, double-blind, crossover evaluation. *J. Am. Coll. Cardiol.* 60, 1323–1329. doi: 10.1016/j.jacc.2012.06.031

Childers, R. W., Arnsdorf, M. F., De La Fuente, D. J., Gambetta, M., and Svenson, R. (1973). Sinus nodal echoes. Clinical case report and canine studies. *Am. J. Cardiol.* 31, 220–231. doi: 10.1016/0002-9149(73)91035-7

Christel, C. J., Cardona, N., Mesirca, P., Herrmann, S., Hofmann, F., Striessnig, J., et al. (2012). Distinct localization and modulation of Cav1.2 and Cav1.3 L-type Ca^{2+} channels in mouse sinoatrial node. *J. Physiol.* 590, 6327–6342. doi: 10.1113/jphysiol.2012.239954

Cossu, S. F., and Steinberg, J. S. (1998). Supraventricular tachyarrhythmias involving the sinus node: clinical and electrophysiologic characteristics. *Prog. Cardiovasc. Dis.* 41, 51–63. doi: 10.1016/S0033-0620(98)80022-4

Costa, M. D., Peng, C. K., and Goldberger, A. L. (2008). Multiscale analysis of heart rate dynamics: entropy and time irreversibility measures. *Cardiovasc. Eng.* 8, 88–93. doi: 10.1007/s10558-007-9049-1

Cunha, S. R., Hund, T. J., Hashemi, S., Voigt, N., Li, N., Wright, P., et al. (2011). Defects in ankyrin-based membrane protein targeting

pathways underlie atrial fibrillation. *Circulation* 124, 1212–1222. doi: 10.1161/CIRCULATIONAHA.111.023986

De Jong, A. M., Maass, A. H., Oberdorf-Maass, S. U., De Boer, R. A., Van Gilst, W. H., and Van Gelder, I. C. (2013). Cyclical stretch induces structural changes in atrial myocytes. *J. Cell. Mol. Med.* 17, 743–753. doi: 10.1111/jcmm.12064

Difrancesco, D. (1993). Pacemaker mechanisms in cardiac tissue. *Annu. Rev. Physiol.* 55, 455–472. doi: 10.1146/annurev.ph.55.030193.002323

Dobrzynski, H., Boyett, M. R., and Anderson, R. H. (2007). New insights into pacemaker activity: promoting understanding of sick sinus syndrome. *Circulation* 115, 1921–1932. doi: 10.1161/CIRCULATIONAHA.106.616011

Duhme, N., Schweizer, P. A., Thomas, D., Becker, R., Schroter, J., Barends, T. R., et al. (2013). Altered HCN4 channel C-linker interaction is associated with familial tachycardia-bradycardia syndrome and atrial fibrillation. *Eur. Heart J.* 34, 2768–2775. doi: 10.1093/eurheartj/ehs391

Fenske, S., Krause, S. C., Hassan, S. I., Becirovic, E., Auer, F., Bernard, R., et al. (2013). Sick sinus syndrome in HCN1-deficient mice. *Circulation* 128, 2585–2594. doi: 10.1161/CIRCULATIONAHA.113.003712

Gang, U. J., Jons, C., Jorgensen, R. M., Abildstrom, S. Z., Messier, M. D., Haarbo, J., et al. (2011). Risk markers of late high-degree atrioventricular block in patients with left ventricular dysfunction after an acute myocardial infarction: a CARISMA substudy. *Europace* 13, 1471–1477. doi: 10.1093/europace/eur165

Glukhov, A. V., Kalyanasundaram, A., Lou, Q., Hage, L. T., Hansen, B. J., Belevych, A. E., et al. (2013). Calsequestrin 2 deletion causes sinoatrial node dysfunction and atrial arrhythmias associated with altered sarcoplasmic reticulum calcium cycling and degenerative fibrosis within the mouse atrial pacemaker complex. *Eur. Heart J.* doi: 10.1093/eurheartj/eht452. [Epub ahead of print].

Gomes, J. A., Mehta, D., and Langan, M. N. (1995). Sinus node reentrant tachycardia. *Pacing Clin. Electrophysiol.* 18, 1045–1057. doi: 10.1111/j.1540-8159.1995.tb04747.x

Han, J., Malozzi, A. M., Moe, G. K. (1968). Sino-atrial reciprocation in the isolated rabbit heart. *Circ. Res.* 22, 355–362.

Herrmann, S., Lipp, P., Wiesen, K., Stieber, J., Nguyen, H., Kaiser, E., et al. (2013). The cardiac sodium-calcium exchanger NCX1 is a key player in the initiation and maintenance of a stable heart rhythm. *Cardiovasc. Res.* 99, 780–788. doi: 10.1093/cvr/cvt154

Herrmann, S., Stieber, J., Stockl, G., Hofmann, F., and Ludwig, A. (2007). HCN4 provides a 'depolarization reserve' and is not required for heart rate acceleration in mice. *EMBO J.* 26, 4423–4432. doi: 10.1038/sj.emboj.7601868

Hof, T., Simard, C., Rouet, R., Salle, L., and Guinamard, R. (2013). Implication of the TRPM4 nonselective cation channel in mammalian sinus rhythm. *Heart Rhythm* 10, 1683–1689. doi: 10.1016/j.hrthm.2013.08.014

Hoffmann, S., Berger, I. M., Glaser, A., Bacon, C., Li, L., Gretz, N., et al. (2013). Islet1 is a direct transcriptional target of the homeodomain transcription factor Shox2 and rescues the Shox2-mediated bradycardia. *Basic Res. Cardiol.* 108, 339. doi: 10.1007/s00395-013-0339-z

Huikuri, H. V., Raatikainen, M. J., Moerch-Joergensen, R., Hartikainen, J., Virtanen, V., Boland, J., et al. (2009). Prediction of fatal or near-fatal cardiac arrhythmia events in patients with depressed left ventricular function after an acute myocardial infarction. *Eur. Heart J.* 30, 689–698. doi: 10.1093/eurheartj/ehn537

Huikuri, H. V., Valkama, J. O., Airaksinen, K. E., Seppanen, T., Kessler, K. M., Takkunen, J. T., et al. (1993). Frequency domain measures of heart rate variability before the onset of nonsustained and sustained ventricular tachycardia in patients with coronary artery disease. *Circulation* 87, 1220–1228. doi: 10.1161/01.CIR.87.4.1220

Jalife, J. (1984). Mutual entrainment and electrical coupling as mechanisms for synchronous firing of rabbit sino-atrial pace-maker cells. *J. Physiol.* 356, 221–243. doi: 10.1113/jphysiol.1984.sp015461

Jones, S. A., Lancaster, M. K., and Boyett, M. R. (2004). Ageing-related changes of connexins and conduction within the sinoatrial node. *J. Physiol.* 560, 429–437. doi: 10.1113/jphysiol.2004.072108

Kapoor, N., Galang, G., Marban, E., and Cho, H. C. (2011). Transcriptional suppression of connexin43 by TBX18 undermines cell-cell electrical coupling in postnatal cardiomyocytes. *J. Biol. Chem.* 286, 14073–14079. doi: 10.1074/jbc.M110.185298

Kapoor, N., Liang, W., Marban, E., and Cho, H. C. (2013). Direct conversion of quiescent cardiomyocytes to pacemaker cells by expression of Tbx18. *Nat. Biotechnol.* 31, 54–62. doi: 10.1038/nbt.2465

Kocovic, D. Z., Harada, T., Shea, J. B., Soroff, D., and Friedman, P. L. (1993). Alterations of heart rate and of heart rate variability after radiofrequency catheter ablation of supraventricular tachycardia. Delineation of parasympathetic pathways in the human heart. *Circulation* 88, 1671–1681. doi: 10.1161/01.CIR.88.4.1671

Kohl, P., Camelliti, P., Burton, F. L., and Smith, G. L. (2005). Electrical coupling of fibroblasts and myocytes: relevance for cardiac propagation. *J. Electrocardiol.* 38, 45–50. doi: 10.1016/j.jelectrocard.2005.06.096

Launay, P., Fleig, A., Perraud, A. L., Scharenberg, A. M., Penner, R., and Kinet, J. P. (2002). TRPM4 is a Ca^{2+}-activated nonselective cation channel mediating cell membrane depolarization. *Cell* 109, 397–407. doi: 10.1016/S0092-8674(02)00719-5

Le Scouarnec, S., Bhasin, N., Vieyres, C., Hund, T. J., Cunha, S. R., Koval, O., et al. (2008). Dysfunction in ankyrin-B-dependent ion channel and transporter targeting causes human sinus node disease. *Proc. Natl. Acad. Sci. U.S.A.* 105, 15617–15622. doi: 10.1073/pnas.0805500105

Liu, H., Chen, C. H., Espinoza-Lewis, R. A., Jiao, Z., Sheu, I., Hu, X., et al. (2011). Functional redundancy between human SHOX and mouse Shox2 genes in the regulation of sinoatrial node formation and pacemaking function. *J. Biol. Chem.* 286, 17029–17038. doi: 10.1074/jbc.M111.234252

Lou, Q., Glukhov, A. V., Hansen, B., Hage, L., Vargas-Pinto, P., Billman, G. E., et al. (2013). Tachy-brady arrhythmias: the critical role of adenosine-induced sinoatrial conduction block in post-tachycardia pauses. *Heart Rhythm* 10, 110–118. doi: 10.1016/j.hrthm.2012.09.012

Lou, Q., Hansen, B. J., Fedorenko, O., Csepe, T. A., Kalyanasundaram, A., Li, N., et al. (2014). Upregulation of adenosine A1 receptors facilitates sinoatrial node dysfunction in chronic canine heart failure by exacerbating nodal conduction abnormalities revealed by novel dual-sided intramural optical mapping. *Circulation* 130, 315–324. doi: 10.1161/CIRCULATIONAHA.113.007086

Ludwig, A., Zong, X., Jeglitsch, M., Hofmann, F., and Biel, M. (1998). A family of hyperpolarization-activated mammalian cation channels. *Nature* 393, 587–591. doi: 10.1038/31255

Makikallio, T. H., Koistinen, J., Jordaens, L., Tulppo, M. P., Wood, N., Golosarsky, B., et al. (1999). Heart rate dynamics before spontaneous onset of ventricular fibrillation in patients with healed myocardial infarcts. *Am. J. Cardiol.* 83, 880–884. doi: 10.1016/S0002-9149(98)01068-6

Maltsev, A. V., Yaniv, Y., Stern, M. D., Lakatta, E. G., and Maltsev, V. A. (2013). RyR-NCX-SERCA local cross-talk ensures pacemaker cell function at rest and during the fight-or-flight reflex. *Circ. Res.* 113, e94–e100. doi: 10.1161/CIRCRESAHA.113.302465

Maltsev, V. A., Yaniv, Y., Maltsev, A. V., Stern, M. D., and Lakatta, E. G. (2014). Modern perspectives on numerical modeling of cardiac pacemaker cell. *J. Pharmacol. Sci.* 125, 6–38. doi: 10.1254/jphs.13R04CR

Mangoni, M. E., Couette, B., Bourinet, E., Platzer, J., Reimer, D., Striessnig, J., et al. (2003). Functional role of L-type Cav1.3 Ca^{2+} channels in cardiac pacemaker activity. *Proc. Natl. Acad. Sci. U.S.A.* 100, 5543–5548. doi: 10.1073/pnas.0935295100

Marger, L., Mesirca, P., Alig, J., Torrente, A., Dubel, S., Engeland, B., et al. (2011). Functional roles of Ca(v)1.3, Ca(v)3.1 and HCN channels in automaticity of mouse atrioventricular cells: insights into the atrioventricular pacemaker mechanism. *Channels (Austin)* 5, 251–261. doi: 10.4161/chan.5.3.15266

Monfredi, O., Lyashkov, A. E., Johnsen, A. B., Inada, S., Schneider, H., Wang, R., et al. (2014). Biophysical characterization of the underappreciated and important relationship between heart rate variability and heart rate. *Hypertension* 64, 1334–1343. doi: 10.1161/HYPERTENSIONAHA.114.03782

Monfredi, O., Maltseva, L. A., Spurgeon, H. A., Boyett, M. R., Lakatta, E. G., and Maltsev, V. A. (2013). Beat-to-beat variation in periodicity of local calcium releases contributes to intrinsic variations of spontaneous cycle length in isolated single sinoatrial node cells. *PLoS ONE* 8:e67247. doi: 10.1371/journal.pone.0067247

Neco, P., Torrente, A. G., Mesirca, P., Zorio, E., Liu, N., Priori, S. G., et al. (2012). Paradoxical effect of increased diastolic $Ca^{(2+)}$ release and decreased sinoatrial node activity in a mouse model of catecholaminergic polymorphic ventricular tachycardia. *Circulation* 126, 392–401. doi: 10.1161/CIRCULATIONAHA.111.075382

Osaka, M., Watanabe, E., Murata, H., Fuwamoto, Y., Nanba, S., Sakai, K., et al. (2010). V-shaped trough in autonomic activity is a possible precursor of life-threatening cardiac events. *Circ. J.* 74, 1906–1915. doi: 10.1253/circj.CJ-09-0935

Ostborn, P., Wohlfart, B., Ohlén, G. (2001). Arrhythmia as a result of poor intercellular coupling in the sinus node: a simulation study. *J. Theor. Biol.* 211, 201–217. doi: 10.1006/jtbi.2001.2339

Papaioannou, V. E., Verkerk, A. O., Amin, A. S., and De Bakker, J. M. (2013). Intracardiac origin of heart rate variability, pacemaker funny current and their possible association with critical illness. *Curr. Cardiol. Rev.* 9, 82–96. doi: 10.2174/157340313805076359

Perkiomaki, J., Ukkola, O., Kiviniemi, A., Tulppo, M., Ylitalo, A., Kesaniemi, Y. A., et al. (2014). Heart rate variability findings as a predictor of atrial fibrillation in middle-aged population. *J. Cardiovasc. Electrophysiol.* 25, 719–724. doi: 10.1111/jce.12402

Platzer, J., Engel, J., Schrott-Fischer, A., Stephan, K., Bova, S., Chen, H., et al. (2000). Congenital deafness and sinoatrial node dysfunction in mice lacking class D L-type Ca^{2+} channels. *Cell* 102, 89–97. doi: 10.1016/S0092-8674(00)00013-1

Postolache, G., Oliveira, M., Rocha, I., Girao, P. S., and Postolache, O. (2011). New insight into arrhythmia onset using HRV and BPV analysis. *Conf. Proc. IEEE Eng. Med. Biol. Soc.* 2011, 2691–2694. doi: 10.1109/IEMBS.2011.6090739

Rocchetti, M., Malfatto, G., Lombardi, F., and Zaza, A. (2000). Role of the input/output relation of sinoatrial myocytes in cholinergic modulation of heart rate variability. *J. Cardiovasc. Electrophysiol.* 11, 522–530. doi: 10.1111/j.1540-8167.2000.tb00005.x

Rozen, G., Kobo, R., Beinart, R., Feldman, S., Sapunar, M., Luria, D., et al. (2013). Multipole analysis of heart rate variability as a predictor of imminent ventricular arrhythmias in ICD patients. *Pacing Clin. Electrophysiol.* 36, 1342–1347. doi: 10.1111/pace.12180

Schweizer, P. A., Duhme, N., Thomas, D., Becker, R., Zehelein, J., Draguhn, A., et al. (2010). cAMP sensitivity of HCN pacemaker channels determines basal heart rate but is not critical for autonomic rate control. *Circ. Arrhythm. Electrophysiol.* 3, 542–552. doi: 10.1161/CIRCEP.110.949768

Seaborn, G. E., Todd, K., Michael, K. A., Baranchuk, A., Abdollah, H., Simpson, C. S., et al. (2014). Heart rate variability and procedural outcome in catheter ablation for atrial fibrillation. *Ann. Noninvasive Electrocardiol.* 19, 23–33. doi: 10.1111/anec.12098

Sheikh, F., Mezzano, V., Wright, A., Zanella, F., Lyon, R. S., Gu, Y., et al. (2013). A novel role for mechanical cell-cell junction proteins in sinus node function. *J. Mol. Cell. Cardiol.* 65.

Shinohara, T., Park, H. W., Han, S., Shen, M. J., Maruyama, M., Kim, D., et al. (2010). Ca^{2+} clock malfunction in a canine model of pacing-induced heart failure. *Am. J. Physiol. Heart Circ. Physiol.* 299, H1805–H1811. doi: 10.1152/ajpheart.00723.2010

Slovut, D. P., Wenstrom, J. C., Moeckel, R. B., Wilson, R. F., Osborn, J. W., and Abrams, J. H. (1998). Respiratory sinus dysrhythmia persists in transplanted human hearts following autonomic blockade. *Clin. Exp. Pharmacol. Physiol.* 25, 322–330. doi: 10.1111/j.1440-1681.1998.tb02358.x

Stieber, J., Hofmann, F., and Ludwig, A. (2004). Pacemaker channels and sinus node arrhythmia. *Trends Cardiovasc. Med.* 14, 23–28. doi: 10.1016/j.tcm.2003.09.006

Unudurthi, S. D., Wolf, R. M., and Hund, T. J. (2014). Role of sinoatrial node architecture in maintaining a balanced source-sink relationship and synchronous cardiac pacemaking. *Front. Physiol.* 5:446. doi: 10.3389/fphys.2014.00446

Verheijck, E. E., Wilders, R., Joyner, R. W., Golod, D. A., Kumar, R., Jongsma, H. J., et al. (1998). Pacemaker synchronization of electrically coupled rabbit sinoatrial node cells. *J. Gen. Physiol.* 111, 95–112. doi: 10.1085/jgp.111.1.95

Vybiral, T., Glaeser, D. H., Goldberger, A. L., Rigney, D. R., Hess, K. R., Mietus, J., et al. (1993). Conventional heart rate variability analysis of ambulatory electrocardiographic recordings fails to predict imminent ventricular fibrillation. *J. Am. Coll. Cardiol.* 22, 557–565. doi: 10.1016/0735-1097(93)90064-8

Wang, K., Chang, D., Chu, Z., Yang, Y., Gao, L., Zhang, S., et al. (2013). Denervation as a common mechanism underlying different pulmonary vein isolation strategies for paroxysmal atrial fibrillation: evidenced by heart rate variability after ablation. *Sci. World J.* 2013:569564. doi: 10.1155/2013/569564

Watanabe, E. I., Honjo, H., Anno, T., Boyett, M. R., Kodama, I., and Toyama, J. (1995). Modulation of pacemaker activity of sinoatrial node cells by electrical load imposed by an atrial cell model. *Am. J. Physiol.* 269, H1735–H1742.

Yaniv, Y., Ahmet, I., Liu, J., Lyashkov, A. E., Guiriba, T. R., Okamoto, Y., et al. (2014a). Synchronization of sinoatrial node pacemaker cell clocks and its autonomic modulation impart complexity to heart beating intervals. *Heart Rhythm* 11, 1210–1219. doi: 10.1016/j.hrthm.2014.03.049

Yaniv, Y., and Lakatta, E. G. (2013). Pacemaker gene mutations, bradycardia, arrhythmias and the coupled clock theory. *J. Cardiovasc. Electrophysiol.* 24, E28–E29. doi: 10.1111/jce.12236

Yaniv, Y., Lyashkov, A. E., and Lakatta, E. G. (2013a). The fractal-like complexity of heart rate variability beyond neurotransmitters and autonomic receptors: signaling intrinsic to sinoatrial node pacemaker cells. *Cardiovasc. Pharmacol.* 2:111. doi: 10.4172/2329-6607.1000111

Yaniv, Y., Lyashkov, A. E., Sirenko, S., Okamoto, Y., Guiriba, T. R., Ziman, B. D., et al. (2014b). Stochasticity intrinsic to coupled-clock mechanisms underlies beat-to-beat variability of spontaneous action potential firing in sinoatrial node pacemaker cells. *J. Mol. Cell. Cardiol.* 77, 1–10. doi: 10.1016/j.yjmcc.2014.09.008

Yaniv, Y., Maltsev, V. A., Escobar, A. L., Spurgeon, H. A., Ziman, B. D., Stern, M. D., et al. (2011). Beat-to-beat $Ca^{(2+)}$-dependent regulation of sinoatrial nodal pacemaker cell rate and rhythm. *J. Mol. Cell. Cardiol.* 51, 902–905. doi: 10.1016/j.yjmcc.2011.08.029

Yaniv, Y., Maltsev, V. A., Ziman, B. D., Spurgeon, H. A., and Lakatta, E. G. (2012). The "Funny" current inhibition by ivabradine at membrane potentials encompassing spontaneous depolarization in pacemaker cells. *Molecules* 17, 8241–8254. doi: 10.3390/molecules17078241

Yaniv, Y., Sirenko, S., Ziman, B. D., Spurgeon, H. A., Maltsev, V. A., and Lakatta, E. G. (2013b). New evidence for coupled clock regulation of the normal automaticity of sinoatrial nodal pacemaker cells: bradycardic effects of ivabradine are linked to suppression of intracellular $Ca^{(2)(+)}$ cycling. *J. Mol. Cell. Cardiol.* 62, 80–89. doi: 10.1016/j.yjmcc.2013.04.026

Yaniv, Y., Spurgeon, H. A., Ziman, B. D., and Lakatta, E. G. (2013c). $Ca^{(2)+}$/calmodulin-dependent protein kinase II (CaMKII) activity and sinoatrial nodal pacemaker cell energetics. *PLoS ONE* 8:e57079. doi: 10.1371/journal.pone.0057079

Yaniv, Y., Stern, M. D., Lakatta, E. G., and Maltsev, V. A. (2013d). Mechanisms of beat-to-beat regulation of cardiac pacemaker cell function by $Ca^{(2)(+)}$ cycling dynamics. *Biophys. J.* 105, 1551–1561. doi: 10.1016/j.bpj.2013.08.024

Yeh, Y. H., Burstein, B., Qi, X. Y., Sakabe, M., Chartier, D., Comtois, P., et al. (2009). Funny current downregulation and sinus node dysfunction associated with atrial tachyarrhythmia: a molecular basis for tachycardia-bradycardia syndrome. *Circulation* 119, 1576–1585. doi: 10.1161/CIRCULATIONAHA.108.789677

Younes, A., Lyashkov, A. E., Graham, D., Sheydina, A., Volkova, M. V., Mitsak, M., et al. (2008). $Ca^{(2+)}$ -stimulated basal adenylyl cyclase activity localization in membrane lipid microdomains of cardiac sinoatrial nodal pacemaker cells. *J. Biol. Chem.* 283, 14461–14468. doi: 10.1074/jbc.M707540200

Zarzoso, M., Rysevaite, K., Milstein, M. L., Calvo, C. J., Kean, A. C., Atienza, F., et al. (2013). Nerves projecting from the intrinsic cardiac ganglia of the pulmonary veins modulate sinoatrial node pacemaker function. *Cardiovasc. Res.* 99, 566–575. doi: 10.1093/cvr/cvt081

Zaza, A., and Lombardi, F. (2001). Autonomic indexes based on the analysis of heart rate variability: a view from the sinus node. *Cardiovasc. Res.* 50, 434–442. doi: 10.1016/S0008-6363(01)00240-1

Conflict of Interest Statement: The authors declare that the research was conducted in the absence of any commercial or financial relationships that could be construed as a potential conflict of interest.

Received: 15 November 2014; accepted: 03 February 2015; published online: 23 February 2015.

*Citation: Yaniv Y, Tsutsui K and Lakatta EG (2015) Potential effects of intrinsic heart pacemaker cell mechanisms on dysrhythmic cardiac action potential firing. Front. Physiol. **6**:47. doi: 10.3389/fphys.2015.00047*

This article was submitted to Cardiac Electrophysiology, a section of the journal Frontiers in Physiology.

frontiers in
PHYSIOLOGY

MINI REVIEW ARTICLE
published: 12 February 2015
doi: 10.3389/fphys.2015.00037

Fibrosis: a structural modulator of sinoatrial node physiology and dysfunction

Thomas A. Csepe[1], Anuradha Kalyanasundaram[1], Brian J. Hansen[1], Jichao Zhao[2] and Vadim V. Fedorov[1]*

[1] *Department of Physiology and Cell Biology, Davis Heart and Lung Research Institute, The Ohio State University Wexner Medical Center, Columbus, OH, USA*
[2] *Auckland Bioengineering Institute, The University of Auckland, Auckland, New Zealand*

Edited by:
Ruben Coronel, Academic Medical Center, Netherlands

Reviewed by:
Morten B. Thomsen, University of Copenhagen, Denmark
Gerard J. J. Boink, Academic Medical Center, Netherlands

***Correspondence:**
Vadim V. Fedorov, Department of Physiology and Cell Biology, The Ohio State University, Wexner Medical Center, 300A Hamilton Hall, 1645 Neil Avenue, Columbus, OH 43210-1218, USA
e-mail: vadim.fedorov@osumc.edu; fedorov.2@osu.edu

Heart rhythm is initialized and controlled by the Sinoatrial Node (SAN), the primary pacemaker of the heart. The SAN is a heterogeneous multi-compartment structure characterized by clusters of specialized cardiomyocytes enmeshed within strands of connective tissue or fibrosis. Intranodal fibrosis is emerging as an important modulator of structural and functional integrity of the SAN pacemaker complex. In adult human hearts, fatty tissue and fibrosis insulate the SAN from the hyperpolarizing effect of the surrounding atria while electrical communication between the SAN and right atrium is restricted to discrete SAN conduction pathways. The amount of fibrosis within the SAN is inversely correlated with heart rate, while age and heart size are positively correlated with fibrosis. Pathological upregulation of fibrosis within the SAN may lead to tachycardia-bradycardia arrhythmias and cardiac arrest, possibly due to SAN reentry and exit block, and is associated with atrial fibrillation, ventricular arrhythmias, heart failure and myocardial infarction. In this review, we will discuss current literature on the role of fibrosis in normal SAN structure and function, as well as the causes and consequences of SAN fibrosis upregulation in disease conditions.

Keywords: sinoatrial node, fibrosis, sinus node dysfunction, aging, exit block, sinoatrial reentry, atrial fibrillation, heart failure

INTRODUCTION

> "*We might mention also that, in some of the pathological hearts cut by us, sections of this region* (i.e., the sinoatrial node) *appeared to show a definite increase in the amount of fibrous tissue present-a fact of considerable importance...*"
>
> (Keith and Flack, 1907)

In the human heart, cardiac rhythm is initiated and regulated by the primary pacemaker of the heart, the Sinoatrial Node (SAN) (Keith and Flack, 1907; Lewis et al., 1910; James, 1961; Boineau et al., 1988; Opthof, 1988; Boyett et al., 2000; Chandler et al., 2009; Fedorov et al., 2010b). Initiation of heart rhythm occurs within specialized cardiomyocytes of the SAN and is propagated throughout the atria and ventricles by the cardiac conduction system. Sinus Node Dysfunction (SND), also referred to as Sick Sinus Syndrome (SSS), commonly translates into rhythm abnormalities manifested as brady-arrhythmias or tachycardia-bradycardia (tachy-brady) syndrome (Mangrum and DiMarco, 2000), which are frequently associated with cardiac diseases including atrial fibrillation (AF), malignant ventricular arrhythmias, heart failure (HF) and cardiac arrest (Luu et al., 1989; Sumitomo et al., 2007; Faggioni et al., 2013; Hjortshoj et al., 2013; Alonso et al., 2014; Jensen et al., 2014). With the aging population, it is projected that the annual incidence of SND cases in the US will increase from 78,000 in 2012 to 172,000 in 2060 (Jensen et al., 2014). SND is the predominant prognosis for electronic pacemaker implantation (Mangrum and DiMarco, 2000; Packer et al., 2009; Greenspon et al., 2012), emphasizing the important role that the SAN plays in maintaining normal cardiac rhythm and in human arrhythmic diseases.

Since the discovery of the SAN by Keith and Flack in 1907, significant strides in our understanding of SAN pacemaker function (Lakatta and DiFrancesco, 2009) have allowed for new and exciting therapeutic strategies to treat SAN disease, such as the development of Ivabradine as a selective drug against inappropriate SAN tachycardia (Cappato et al., 2012) and artificial biological pacemakers (Miake et al., 2002; Rosen et al., 2004; Rosen, 2014). The heterogeneous distribution of specialized ion channels, intracellular sodium/calcium handling proteins, gap junction channels and receptors within the SAN pacemaker complex are a few of the critical players shown to be involved in SAN pacemaking that have been addressed in recent reviews (Monfredi et al., 2010; Dobrzynski et al., 2013; Wu and Anderson, 2014). In addition to these molecular mechanisms, the passive, structural features of the SAN complex also contributes significantly to its normal functioning.

In contrast to the simplified SAN structure in many textbooks, studies in both human and canine hearts have revealed that the SAN is a complex multi-compartment structure (James, 1961; Opthof, 1988; Boineau et al., 1989; Beau et al., 1995; Boyett et al., 2000; Sanchez-Quintana et al., 2005; Chandler et al., 2009; Fedorov et al., 2009, 2010a). The SAN, in almost all mammalian hearts, is characterized by clusters of specialized cardiomyocytes,

enmeshed within strands of connective tissue or fibrosis, mostly a combination of collagen, elastin and fibroblasts (Lev, 1954; Hudson, 1960; Truex et al., 1967; Sanchez-Quintana et al., 2002). This fibrotic matrix provides mechanical protection (Alings et al., 1995) of the SAN and electrically insulates the SAN pacemaker cells from the surrounding atrial myocardium, thereby efficiently regulating normal sinus rhythm. This review will take a more in depth look at the role of fibrosis in normal SAN function, as well as factors involved in unfavorable fibrosis production observed in patients and animal models with cardiac diseases and SND (Liu et al., 2007; de Jong et al., 2011; Nakao et al., 2012; Glukhov et al., 2013, 2015; Alonso et al., 2014; Jensen et al., 2014; Morris and Kalman, 2014).

FIBROSIS IN NORMAL SAN FUNCTION

FIBROSIS DEFINES SAN STRUCTURE AND MAINTAINS FUNCTIONAL INTEGRITY OF THE PACEMAKER COMPLEX

The SAN is anatomically located at the junction of the superior vena cava and right atrium in the mammalian heart (**Figure 1A**). In the normal adult human heart, the SAN is 12–20 mm long and 2–6 mm wide, identified by its ellipsoidal shape that traverses intramurally. The superior part (head) lies about 1 mm beneath the epicardium, separated by a layer of connective tissue and fat (Keith and Flack, 1907; James, 1961; Truex et al., 1967; Matsuyama et al., 2004; Sanchez-Quintana et al., 2005). The SAN spreads from its head inferiorly for 10–20 mm remaining beneath the sulcus terminalis and just above the crista terminalis and has several extensions into the surrounding atrial myocardium, forming the specialized sinoatrial conduction pathways (SACPs) (Lev, 1954; Hudson, 1960; Demoulin and Kulbertus, 1978; Fedorov et al., 2010b) (**Figure 1A**). Importantly, the SAN consists of small clusters of pacemaker myocytes, arranged in parallel rows that frequently anastomose. Dense connective tissue, nerve fibers, and capillaries are interspersed with the SAN pacemaker clusters, creating the SAN pacemaker complex.

A century ago, Keith and Flack's pioneering studies described fibrotic insulation in the human SAN: "In the human heart the fibers (i.e., SAN pacemaker cell clusters) are striated, fusiform, with well-marked elongated nuclei, plexiform in arrangement, and embedded in *densely packed connective tissue*" (Keith and Flack, 1907). Since then, extensive investigations of the human SAN structure by many others (Lev, 1954; Hudson, 1960; James, 1961; Truex et al., 1967; Demoulin and Kulbertus, 1978; Matsuyama et al., 2004) have confirmed the extensive fibrotic pattern within the node. Fibrosis provides an encompassing, honeycomb-like, structural support composed of a network of collagen sheaths of endomysium (Sanchez-Quintana et al., 2002) (**Figure 1B**). These data show that interstitial fibrosis within the normal SAN builds scaffolding to "house" the sophisticated SAN myocytes and may be necessary to maximize electrical insulation and safe propagation in the SAN complex (Davies and Pomerance, 1972; Fedorov et al., 2010b, 2012) (**Figure 1B**). Furthermore, the human SAN is electrically insulated from the surrounding atria by fibrosis and fatty tissue (Lev, 1954; Sanchez-Quintana et al., 2005; Monfredi et al., 2010; Fedorov et al., 2010b) except for distinct SACPs, which electrically connect the SAN to

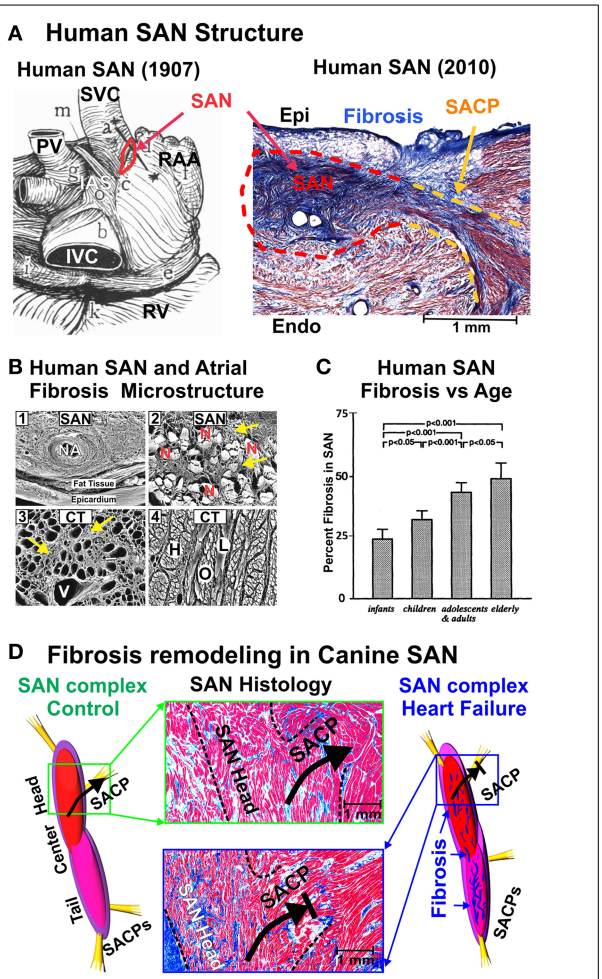

FIGURE 1 | (A) Left: Drawing of the posterior human atrial anatomy from (Keith and Flack, 1907), with SAN outlined in red. Right: Histological cross section of the SAN (red outline) connected to the atria by a SACP (yellow outline). The SAN is seen to be isolated from the atria by sup-epicardial fat and connective tissue. Modified from Fedorov et al. (2010b, 2012) with permission. **(B)** 1—Scanning electron micrograph of the SAN and nodal artery (NA) of a cross section through the CT after digestion of the nodal cells. The collagenous sheaths of endomysial fibrosis formed a complex network in the gaps between the nodal cells, whereas occasional perimysial septums were seen between them. 2—Scanning electron micrograph of non-macerated SAN cells (N), which are encased in dense and coarse endomysial sheaths (yellow arrows) in a specimen from a 75 year old. 3—Scanning electron micrograph of a cross section through the CT, after digestion, from a specimen of 70 years shows a diffuse notable excess of endomysial sheaths (yellow arrows) indicating focal interstitial reactive fibrosis. Vascular space (V) corresponds to a coronary vein. 4—Scanning electron micrograph of non-macerated cross section through the body of the CT shows mainly longitudinal fibers (H) with intermingling oblique (O) or lateral (L) fibers. From Sanchez-Quintana et al. (2002) with permission. **(C)** Graph showing percentage of fibrous connective tissue volume to the total SAN volume, mean value, and standard deviation. From Shiraishi et al. (1992); used with permission. **(D)** Fibrosis in the SAN is increased in HF vs. control dog. Left: A structural model of the control canine SAN complex and SACPs. Middle: histological sections showing upregulated fibrotic and fatty content in SAN complex (black outline) and SACP in HF (bottom, blue box) compared to control (top, green box). Right: A structural model of the heart failure SAN complex and SACPs,

(Continued)

FIGURE 1 | Continued
showing upregulated intranodal fibrosis (blue fibrotic strands). Modified from Lou et al. (2014) with permission. Abbreviations: CT, crista terminalis; Endo, endocardium; Epi, epicardium; HF, heart failure; IAS, interatrial septum; PV, pulmonary veins; RAA, right atrial appendage; RV, right ventricle; SACP, sinoatrial conduction pathway; SAN, sinoatrial node; SVC and IVC, superior and inferior vena cava.

the right atrium (Fedorov et al., 2012). Integral to SAN function, fibrotic and fatty insulation of the SAN prevents the depression of pacemaker automaticity from the hyperpolarizing electrical load of the atrial myocardium (Joyner and van Capelle, 1986).

SAN FIBROSIS INCREASES WITH HEART SIZE AND AGE

Considerable physiological and structural evidence support the generalization that large mammals (including human, dog, pig, yak, horse, etc.) have a more compact and distinct SAN structure than smaller mammals (Keith and Flack, 1907; James, 1961; Opthof et al., 1987; Fedorov et al., 2009, 2012; Duan et al., 2012; Lou et al., 2013, 2014; Glukhov et al., 2015). Histological studies clearly demonstrated that interstitial fibrosis is an inherent component of normal SAN structure and can be traced from newborn hearts (Lev, 1954; Shiraishi et al., 1992; Alings et al., 1995). The size of the heart, as well as its mechanical demands, increases dramatically throughout life and may have a major effect on SAN structure and function. In 1954, Lev published the first detailed study of structural changes of the SAN with age in 54 human SAN samples ranging from 4 months gestation to 90 years of age; this exhaustive investigation revealed that the SAN tissue was already clearly discernable from the atrial tissue at 5 months gestation, particularly due to the greater abundance of fibroblasts and distinctly higher number of collagen fibers (Lev, 1954). Collagen content in the human infant SAN is about 24% and this number climbs to about 70% fibrosis in the adult heart (Shiraishi et al., 1992; Alings et al., 1995) (**Figure 1C**). This natural correlation between aging and increased fibrotic content in the SAN has also been documented in animal models, for example SAN fibrosis in mouse rises from 12–17% at 3 months to 23–25% at 12 months (Hao et al., 2011; Glukhov et al., 2015). The age-induced increase of SAN fibrosis is strongly correlated with slowed intrinsic heart rate as well as slowed SAN conduction in human and mammalian hearts (Kuga et al., 1993; Sanders et al., 1994; Noujaim et al., 2004; Hao et al., 2011; Akoum et al., 2012). The SAN modeling study by Oren and Clancy (2010) is in agreement with a study by Fahrenbach et al. (2007): fibrosis correlates with slowed intrinsic conduction through two mechanisms: (1) heterocellular coupling enables the fibroblast to depolarize the cardiomyocytes (or act as a current sink), (2) fibroblasts physically separate the pacemaker cardiomyocytes, slowing SAN rhythm through a reduction in mutual entrainment (Jalife, 1984).

Apart from aging, a natural size-to-fibrotic content relationship is evidenced in the gradual increase in SAN percent fibrosis as the size of the species increases. The adult mouse SAN is composed of less fibrosis (Hao et al., 2011; Glukhov et al., 2015) than the adult cat SAN, which consists of 27% fibrosis (Alings et al., 1995). The healthy adult canine SAN has a range of 22–30% fibrosis (Glukhov et al., 2013; Lou et al., 2014), while the normal adult human SAN shows roughly 45% fibrosis (Alings et al., 1995). The contribution of increased intranodal fibrosis in large mammals to their functional demands is not completely clear, but as the atrial tissue increases in large vs. small hearts, more insulation around the SAN may be necessary to protect it from the electrical and mechanical load of the atria (Joyner and van Capelle, 1986). Universally, large mammals have slower heart rates vs. smaller animals as established by Noujaim et al.'s multi-species study (Noujaim et al., 2004). Based on the studies discussed above, we suggest that intranodal fibrosis is inversely correlated with intrinsic SAN rhythm and conduction, and directly correlated with age and heart size.

FIBROSIS PROVIDES MECHANICAL PROTECTION FOR THE SAN AND PREVENTS PATHOPHYSIOLOGICAL HEART RATE RESPONSES TO ATRIAL STRETCH AND PRESSURE

In addition to structural scaffolding and electrical insulation from the atria, interstitial fibrosis within the SAN can prevent it from increased interstitial volume changes due to stretch or compression. As the natural growth during the life span or size of the animal increases, the size and thickness of the atria also increases to meet contractile demands (Sanchez-Quintana et al., 2002). Mechanical stretch is a powerful myogenic modulator of SAN function (Brooks and Lange, 1977); in fact, possibly as a local regulator of heart rate, stretch and/or increased intra-atrial pressure can increase SAN rhythm, whereas compression and/or increased arterial pressure in the SAN artery may lead to slowing of SAN rhythm (James and Nadeau, 1962; Lange et al., 1966; Hashimoto et al., 1967). These local responses to stretch and pressure may be carried out through stretch-activated channels in pacemaker cells and SAN fibroblasts, which have been shown to electrically couple with SAN myocytes in some studies (Kohl et al., 1994; Kamkin et al., 2003; Cooper and Kohl, 2005; Fahrenbach et al., 2007; Oren and Clancy, 2010). By providing a relatively tough casing for the compact SAN, fibrosis could prevent the node from overstretching due to the mechanical pressures of the atrial myocardium (Alings et al., 1995).

FIBROSIS IN SAN DYSFUNCTION

INCREASING FIBROSIS WITHIN THE SAN PACEMAKER COMPLEX IS ASSOCIATED WITH SND AND ARRHYTHMIAS

SND is conceptualized as a spectrum of heart rhythm disturbances including bradycardia, sinus pauses/arrest, exit block, "inappropriate" sinus tachycardia and re-entrant arrhythmias, (Alonso et al., 2014; Jensen et al., 2014). It is largely a disease of the elderly and its incidence increases in an exponential manner with age (Mandel et al., 1999; Adan and Crown, 2003; Dobrzynski et al., 2007). Although human SND can be induced by a number of different pathophysiological mechanisms such as drug effects, autonomic imbalances, cardiomyopathy and electrophysiological alterations, SAN structural abnormalities have been commonly observed in these dysfunctions and are significantly associated with HF, SAN ischemia, and inflammatory conditions (Jordan et al., 1978; Adan and Crown, 2003; Sanders et al., 2004; Kottkamp, 2012). In 1907, Keith and Flack saw a "definite increase in the amount of fibrous tissue" present in the SAN from pathological hearts (Keith and Flack, 1907). Later, Hudson emphasized

the association of extensive fibrotic lesions in the human SAN with established arrhythmia, especially AF, and suggested that temporary arrhythmias may be associated with minor fibrotic lesions in the SAN (Hudson, 1960). Thery et al. demonstrated a direct correlation between SAN fibrosis and the occurrence of tachy-brady syndrome (Thery et al., 1977). Tachy-brady syndrome, or tachy-brady arrhythmias, have been explained as "the heart rate alternating between too fast and too slow," where termination of paroxysmal tachycardia "may be followed by long atrial pauses lasting several seconds, which can provoke another tachyarrhythmia paroxysm" (**Figure 2A**) (Moss and Davis, 1974; Lou et al., 2013, 2014). While the natural increase in SAN fibrosis observed with aging and heart size is not directly associated with SND, degenerative loss of SAN pacemaker cells and their replacement with fibrosis tissue is frequently evident upon pathologic examination of specimens from patients with SND (Birchfield et al., 1957; Davies and Pomerance, 1972; Thery et al., 1977; Hurle et al., 2006; Yeh et al., 2009).

EXCESSIVE FIBROSIS LEADS TO CONDUCTION BLOCKS AND REENTRY IN THE SAN PACEMAKER COMPLEX

Upregulated interstitial fibrosis may lead to disruption of the continuity of electrically coupled myocytes (Nguyen et al., 2014), which alters the delicate balance between depolarized cells (source) and the resting tissue ahead (sink), thereby disrupting SAN pacemakers' mutual entrainment (Jalife, 1984; Delmar et al., 1986; Michaels et al., 1987). As such, too much fibrosis slows activity of primary pacemaker clusters, as well as enhances beat-to-beat variability and atrial arrhythmias due to competition between multiple primary and subsidiary/latent pacemaker clusters within and outside the SAN pacemaker complex (Glukhov et al., 2013). Increased nodal fibrosis can cause slowed and decremental conduction within the SAN complex, especially in the SACPs (**Figure 1D**), leading to SAN exit block and long pauses, especially after tachycardia termination. Specifically, the atrial tachyarrhythmia or fast pacing depresses conduction/excitability in the structurally remodeled poorly coupled SACP (**Figure 1D**) which enhances source-sink mismatch and leads to exit block from the SAN after tachyarrhythmia termination, which can give rise to tachy-brady syndrome and cardiac arrest (Fedorov et al., 2010a; Glukhov et al., 2010, 2013; Hao et al., 2011; Swaminathan et al., 2011; Froese et al., 2012; Lou et al., 2014). Intramural optical mapping studies integrated with micro-structural analysis directly revealed that fibrosis could also lead to intranodal longitudinal and transverse conduction blocks and cause SAN micro- and macro-reentry (Glukhov et al., 2013; Lou et al., 2014) (**Figures 2B–D**). Interestingly, SAN macro-reentry (where signal travels from the one SACP to the atria and then back to the SAN through another SACP) will lead to tachycardia, but micro-reentry inside the SAN may lead to exit block in the

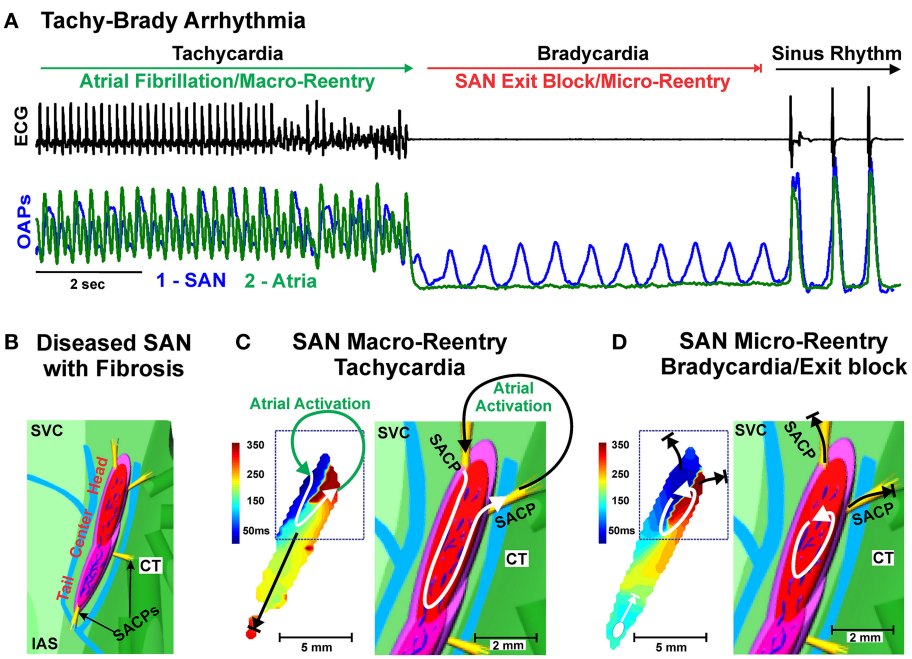

FIGURE 2 | (A) Example of Tachy-Brady arrhythmia often observed in structurally remodeled hearts with upregulated intranodal fibrosis. Atrial Fibrillation or Tachycardia leads to Bradycardia (long pauses) due to SAN exit block, followed by recovery of sinus rhythm or new Tachycardia event. ECG (black) and Optical Action Potentials (green and blue). Modified from Lou et al. (2013) with permission. **(B)** Enlarged epicardial view of 3D canine SAN model based on structural and functional data from optical mapping experiments. The SAN is demarcated from the atrium (green) by 3 bifurcating coronary arteries (light blue) and connective tissue (light purple). The yellow bundles show SACPs that electrically connect the SAN to the atrium. **(C)** Macro-reentry between the SAN and atria that occurred in the structurally remodeled canine heart after cessation of atrial tachypacing. Path of macro-reentry correlated with fibrotic strands within SAN. **(D)** SAN micro-reentry transformed from the previous macro-reentry is shown. Fibrosis strands were the structural substrates anchoring micro-reentry to this area. **(B–D)** modified from Glukhov et al. (2013) with permission. Abbreviations as seen in **Figure 1**.

SACP and severe bradycardia (Glukhov et al., 2013) (**Figure 2**). Histological analysis revealed that these arrhythmias required intranodal fibrotic strands not present in healthy hearts, indicating a critical role of intranodal fibrosis in creating structural substrates for SAN macro- and micro-reentry and atrial arrhythmias (Glukhov et al., 2013; Lou et al., 2014).

Importantly, disease-induced increases in interstitial fibrosis can abnormally insulate latent atrial pacemaker clusters thereby increasing their pacemaking properties (Boineau et al., 1988; Anderson et al., 2009; Atkinson et al., 2013; Dobrzynski et al., 2013). We recently demonstrated this novel mechanism in a mouse model of Calsequestrin 2 knockout, wherein increased pathological fibrosis indeed insulated latent atrial pacemaker clusters that competed with the SAN, causing heterogeneous conduction within the atria and subsequently AF and ventricular tachycardia (Glukhov et al., 2015). However, Verheule et al. found significant depression of atrial conduction and higher inducibility of AF in a mouse model of atria-specific TGF-β1 overexpression but no evidence of SAN dysfunction, indicating upregulation of atrial fibrosis alone may not be sufficient to cause SAN dysfunction (Verheule et al., 2004).

It is not always clear whether fibrosis upregulation always precedes SAN dysfunction, or if fibrosis is generated as a response to SAN dysfunction. However, in SND animal models and recent clinical late-gadolinium MRI studies (Akoum and Marrouche, 2014) where structural remodeling in the SAN was studied, upregulated fibrosis in the SAN pacemaker complex was found (Sakabe et al., 2005; Hao et al., 2011; Herrmann et al., 2011; Swaminathan et al., 2011; Froese et al., 2012; Nakao et al., 2012; Glukhov et al., 2013; Wolf et al., 2013; Lou et al., 2014).

DISEASE-INDUCED FIBROBLAST-MYOCYTE COUPLING

Additionally, some studies have suggested that fibroblast-myocyte coupling (Kohl et al., 1994; Camelliti et al., 2004) can increase during pathological structural remodeling (e.g., MI and HF) (Kamkin et al., 2001, 2002; Vasquez et al., 2010); however, the existence of these electrical connections is still up for debate (Kohl and Gourdie, 2014). Depending on membrane potential, coupling and distribution, the fibroblast-pacemaker cell connections can increase or decrease the source-sink mismatch, thus accelerating or decelerating the pacemaking of the SAN (Fahrenbach et al., 2007). Increased coupling with interspersed fibroblasts may create abnormal cell-to-cell interactions as well as interrupt electrical coupling between SAN myocytes (decreased mutual entrainment) within the SAN complex, which has been shown in modeling (Oren and Clancy, 2010) and cell culture (Fahrenbach et al., 2007) studies. Furthermore, excessive extracellular matrix protein deposition by fibroblasts within the node can increase stiffness, which could impede the normal myogenic response of the SAN to changes in either stretch or arterial pressure, as mentioned above.

MULTIPLE MECHANISMS UPREGULATE FIBROSIS IN THE SAN

Abnormal proliferation of fibroblasts and excessive secretion of ECM proteins have been shown to underlie cardiac fibrosis (Fan et al., 2012). The development of SAN arrhythmias have also been shown to occur in parallel with the loss of pacemaker cells (Hurle et al., 2006; Herrmann et al., 2011; Swaminathan et al., 2011; Wu and Anderson, 2014), leading to activated and reparative fibroblasts that replace dead cardiomyocytes and additional collagen deposition (Davies and Pomerance, 1972; Burstein and Nattel, 2008; Akoum et al., 2012). These deposits may form large, non-compliant areas of collagenous fibrosis devoid of cardiomyocytes, as in myocardial infarction(de Jong et al., 2011), or it may lead to increased intranodal fibrosis, as seen in HF (**Figure 1D**).

From the limited mechanistic studies on fibrosis within the SAN, there are multiple mechanisms believed to upregulate intranodal fibrosis. Myofibroblasts, the activated phenotype of fibroblasts, are known to underlie the excessive deposition of ECM proteins and are more mobile and contractile than fibroblasts (Davis and Molkentin, 2014). Overexpression of myocardial transforming growth factor β1 (TGF-β1) in mice has been shown to selectively increase fibrosis in the atria by causing a cellular transition from fibroblast to the activated myofibroblast phenotype (Nakajima et al., 2000; Vasquez et al., 2011). However, the presence of activated myofibroblasts is yet to be demonstrated in the SAN.

Another mechanism believed to be associated with increased fibrosis is the upregulation of Angiotensin II (Ang II). Circulating Ang II activates NADPH oxidase and increases oxidized calmodulin kinase II, leading to SAN cell apoptosis and fibrosis (Swaminathan et al., 2011). Ox-CaMKII-mediated loss of functional SAN cells contributes to SAN dysfunction and sudden cardiac death (Wu and Anderson, 2014). Recently, we demonstrated that fibrosis is increased within the SAN and could contribute to the slowed heart rate in a mouse model of catecholaminergic polymorphic ventricular tachycardia, a human arrhythmic disease (Glukhov et al., 2015). In this model of abnormal calcium (Ca^{2+}) leak via the ryanodine receptors from the sarcoplasmic reticulum, increased fibrosis could either be due to upregulation of CaMKII secondary to altered Ca^{2+} signaling and/or SAN cell death leading to replacement with connective tissue.

Given the significant role that fibrotic remodeling plays in SND, anti-fibrotic approaches may present therapeutic options for this disease. For example, the ACE inhibitor Enalapril has been shown to reduce SAN fibrosis and SND in a four-week canine model of atrial tachycardia (Sakabe et al., 2005). Corticosteroids have also been shown to reduce TGF-β1 and fibrosis in mouse lungs (Miller et al., 2006), and promising results in patients with complete AV block due to cardiac sarcoidosis have been observed (Selan et al., 2014). These results suggest that corticosteroids may prevent and/or restore fibrosis-induced SAN conduction impairment, but no study has specifically investigated if this approach is feasible.

FUTURE DIRECTIONS AND CONCLUSION

Even after one century of extensive research on the SAN, the lack of understanding of the human SAN complexity remains a critical barrier to the optimal treatment of heart rhythm disorders. Studies on explanted human SAN are necessary to determine its microstructure as well as structural and mechanistic role of fibrosis in normal as well as diseased hearts. Novel imaging techniques such as MRI or microCT (Akoum et al., 2012; Stephenson et al., 2012; Disertori et al., 2014) should be employed in addition to histological analyses to identify the intact structure

as well as the contribution of fibrosis to SAN function and dysfunction.

Heterogeneous distribution of fibrosis within and around the SAN pacemaker complex plays a crucial role in proper SAN function by providing (1) structural and functional integrity/stability of the SAN (2) electrical insulation of SAN myocyte clusters and the entire SAN complex, apart from SACPs, preventing depression of pacemaker automaticity from the hyperpolarizing effect of the surrounding atria (3) mechanical protection from pathophysiological heart rate changes due to stretch and pressure from the contractile force of the atria.

The protective role that fibrosis plays in healthy hearts is necessary for proper SAN function, but this role becomes pathophysiological when fibrosis is upregulated in cardiac diseases, leading to (1) slowed SAN rhythm due to fibrosis replacement of pacemaker cells (2) beat-to-beat variability and slowed intranodal conduction due to decreased electrical coupling between SAN myocytes and pacemaker cell clusters (3) long pauses due to source–sink mismatch causing exit block in the SACPs (4) SAN micro- and macro-reentry due to fibrosis-induced conduction dissociation in the SAN. All of these pathological conditions can lead to arrhythmias such as tachy-brady syndrome and AF. By continuing to expand our knowledge of the complex structure that makes up the SAN and exploring the multiple mechanisms involved in fibrosis upregulation, we will come closer to providing new and less invasive treatment options for a growing population of aging patients suffering from SND.

FUNDING

This work was supported by National Institute of Health HL115580 (to Vadim V. Fedorov), National Scientist Development Grant from the American Heart Association (to Anuradha Kalyanasundaram) and by the International Mobility Fund from Royal Society of New Zealand (to Jichao Zhao and Vadim V. Fedorov).

REFERENCES

Adan, V., and Crown, L. A. (2003). Diagnosis and treatment of sick sinus syndrome. *Am. Fam. Physician* 67, 1725–1732.

Akoum, N., and Marrouche, N. (2014). Assessment and impact of cardiac fibrosis on atrial fibrillation. *Curr. Cardiol. Rep.* 16:518. doi: 10.1007/s11886-014-0518-z

Akoum, N., McGann, C., Vergara, G., Badger, T., Ranjan, R., Mahnkopf, C., et al. (2012). Atrial fibrosis quantified using late gadolinium enhancement MRI is associated with sinus node dysfunction requiring pacemaker implant. *J. Cardiovasc. Electrophysiol.* 23, 44–50. doi: 10.1111/j.1540-8167.2011.02140.x

Alings, A. M., Abbas, R. F., and Bouman, L. N. (1995). Age-related changes in structure and relative collagen content of the human and feline sinoatrial node. A comparative study. *Eur. Heart J.* 16, 1655–1667.

Alonso, A., Jensen, P. N., Lopez, F. L., Chen, L. Y., Psaty, B. M., Folsom, A. R., et al. (2014). Association of sick sinus syndrome with incident cardiovascular disease and mortality: the atherosclerosis risk in communities study and cardiovascular health study. *PLoS ONE* 9:e109662. doi: 10.1371/journal.pone.0109662

Anderson, R. H., Yanni, J., Boyett, M. R., Chandler, N. J., and Dobrzynski, H. (2009). The anatomy of the cardiac conduction system. *Clin. Anat.* 22, 99–113. doi: 10.1002/ca.20700

Atkinson, A. J., Logantha, S. J., Hao, G., Yanni, J., Fedorenko, O., Sinha, A., et al. (2013). Functional, anatomical, and molecular investigation of the cardiac conduction system and arrhythmogenic atrioventricular ring tissue in the rat heart. *J. Am. Heart Assoc.* 2:e000246. doi: 10.1161/JAHA.113.000246

Beau, S. L., Hand, D. E., Schuessler, R. B., Bromberg, B. I., Kwon, B., Boineau, J. P., et al. (1995). Relative densities of muscarinic cholinergic and beta-adrenergic receptors in the canine sinoatrial node and their relation to sites of pacemaker activity. *Circ. Res.* 77, 957–963. doi: 10.1161/01.RES.77.5.957

Birchfield, R. I., Menefee, E. E., and Bryant, G. D. (1957). Disease of the sinoatrial node associated with bradycardia, asystole, syncope, and paroxysmal atrial fibrillation. *Circulation* 16, 20–26. doi: 10.1161/01.CIR.16.1.20

Boineau, J. P., Canavan, T. E., Schuessler, R. B., Cain, M. E., Corr, P. B., and Cox, J. L. (1988). Demonstration of a widely distributed atrial pacemaker complex in the human heart. *Circulation* 77, 1221–1237. doi: 10.1161/01.CIR.77.6.1221

Boineau, J. P., Schuessler, R. B., Canavan, T. E., Corr, P. B., Cain, M. E., and Cox, J. L. (1989). The human atrial pacemaker complex. *J. Electrocardiol.* 22(Suppl.), 189–197. doi: 10.1016/S0022-0736(07)80122-1

Boyett, M. R., Honjo, H., and Kodama, I. (2000). The sinoatrial node, a heterogeneous pacemaker structure. *Cardiovasc. Res.* 47, 658–687. doi: 10.1016/S0008-6363(00)00135-8

Brooks, C. M., and Lange, G. (1977). Interaction of myogenic and neurogenic mechanisms that control heart rate. *Proc. Natl. Acad. Sci. U.S.A.* 74, 1761–1762. doi: 10.1073/pnas.74.4.1761

Burstein, B., and Nattel, S. (2008). Atrial fibrosis: mechanisms and clinical relevance in atrial fibrillation. *J. Am. Coll. Cardiol.* 51, 802–809. doi: 10.1016/j.jacc.2007.09.064

Camelliti, P., Green, C. R., LeGrice, I., and Kohl, P. (2004). Fibroblast network in rabbit sinoatrial node: structural and functional identification of homogeneous and heterogeneous cell coupling. *Circ. Res.* 94, 828–835. doi: 10.1161/01.RES.0000122382.19400.14

Cappato, R., Castelvecchio, S., Ricci, C., Bianco, E., Vitali-Serdoz, L., Gnecchi-Ruscone, T., et al. (2012). Clinical efficacy of ivabradine in patients with inappropriate sinus tachycardia: a prospective, randomized, placebo-controlled, double-blind, crossover evaluation. *J. Am. Coll. Cardiol.* 60, 1323–1329. doi: 10.1016/j.jacc.2012.06.031

Chandler, N. J., Greener, I. D., Tellez, J. O., Inada, S., Musa, H., Molenaar, P., et al. (2009). Molecular architecture of the human sinus node: insights into the function of the cardiac pacemaker. *Circulation* 119, 1562–1575. doi: 10.1161/CIRCULATIONAHA.108.804369

Cooper, P. J., and Kohl, P. (2005). Species- and preparation-dependence of stretch effects on sino-atrial node pacemaking. *Ann. N.Y. Acad. Sci.* 1047, 324–335. doi: 10.1196/annals.1341.029

Davies, M. J., and Pomerance, A. (1972). Quantitative study of ageing changes in the human sinoatrial node and internodal tracts. *Br. Heart J.* 34, 150–152. doi: 10.1136/hrt.34.2.150

Davis, J., and Molkentin, J. D. (2014). Myofibroblasts: trust your heart and let fate decide. *J. Mol. Cell. Cardiol.* 70, 9–18. doi: 10.1016/j.yjmcc.2013.10.019

de Jong, S., van Veen, T. A., van Rijen, H. V., and de Bakker, J. M. (2011). Fibrosis and cardiac arrhythmias. *J. Cardiovasc. Pharmacol.* 57, 630–638. doi: 10.1097/FJC.0b013e318207a35f

Delmar, M., Jalife, J., and Michaels, D. C. (1986). Effects of changes in excitability and intercellular coupling on synchronization in the rabbit sino-atrial node. *J. Physiol.* 370, 127–150. doi: 10.1113/jphysiol.1986.sp015926

Demoulin, J. C., and Kulbertus, H. E. (1978). Histopathological correlates of sinoatrial disease. *Br. Heart J.* 40, 1384–1389. doi: 10.1136/hrt.40.12.1384

Disertori, M., Mase, M., Marini, M., Mazzola, S., Cristoforetti, A., Del, G. M., et al. (2014). Electroanatomic mapping and late gadolinium enhancement MRI in a genetic model of arrhythmogenic atrial cardiomyopathy. *J. Cardiovasc. Electrophysiol.* 25, 964–970. doi: 10.1111/jce.12440

Dobrzynski, H., Anderson, R. H., Atkinson, A., Borbas, Z., D'Souza, A., Fraser, J. F., et al. (2013). Structure, function and clinical relevance of the cardiac conduction system, including the atrioventricular ring and outflow tract tissues. *Pharmacol. Ther.* 139, 260–288. doi: 10.1016/j.pharmthera.2013.04.010

Dobrzynski, H., Boyett, M. R., and Anderson, R. H. (2007). New insights into pacemaker activity: promoting understanding of sick sinus syndrome. *Circulation* 115, 1921–1932. doi: 10.1161/CIRCULATIONAHA.106.616011

Duan, D., Yu, S., and Cui, Y. (2012). Morphological study of the sinus node and its artery in yak. *Anat. Rec. (Hoboken).* 295, 2045–2056. doi: 10.1002/ar.22591

Faggioni, M., Hwang, H. S., van der Werf, C., Nederend, I., Kannankeril, P. J., Wilde, A. A., et al. (2013). Accelerated sinus rhythm prevents catecholaminergic polymorphic ventricular tachycardia in mice and in patients. *Circ. Res.* 112, 689–697. doi: 10.1161/CIRCRESAHA.111.300076

Fahrenbach, J. P., Mejia-Alvarez, R., and Banach, K. (2007). The relevance of non-excitable cells for cardiac pacemaker function. *J. Physiol.* 585, 565–578. doi: 10.1113/jphysiol.2007.144121

Fan, D., Takawale, A., Lee, J., and Kassiri, Z. (2012). Cardiac fibroblasts, fibrosis and extracellular matrix remodeling in heart disease. *Fibrogenesis Tissue Repair* 5:15. doi: 10.1186/1755-1536-5-15

Fedorov, V. V., Chang, R., Glukhov, A. V., Kostecki, G., Janks, D., Schuessler, R. B., et al. (2010a). Complex interactions between the sinoatrial node and atrium during reentrant arrhythmias in the canine heart. *Circulation* 122, 782–789. doi: 10.1161/CIRCULATIONAHA.109.935288

Fedorov, V. V., Glukhov, A. V., and Chang, R. (2012). Conduction barriers and pathways of the sinoatrial pacemaker complex: their role in normal rhythm and atrial arrhythmias. *Am. J. Physiol. Heart Circ. Physiol.* 302, H1773–H1783. doi: 10.1152/ajpheart.00892.2011

Fedorov, V. V., Glukhov, A. V., Chang, R., Kostecki, G., Aferol, H., Hucker, W. J., et al. (2010b). Optical mapping of the isolated coronary-perfused human sinus node. *J. Am. Coll. Cardiol.* 56, 1386–1394. doi: 10.1016/j.jacc.2010.03.098

Fedorov, V. V., Schuessler, R. B., Hemphill, M., Ambrosi, C. M., Chang, R., Voloshina, A. S., et al. (2009). Structural and functional evidence for discrete exit pathways that connect the canine sinoatrial node and atria. *Circ. Res.* 104, 915–923. doi: 10.1161/CIRCRESAHA.108.193193

Froese, A., Breher, S. S., Waldeyer, C., Schindler, R. F., Nikolaev, V. O., Rinne, S., et al. (2012). Popeye domain containing proteins are essential for stress-mediated modulation of cardiac pacemaking in mice. *J. Clin. Invest.* 122, 1119–1130. doi: 10.1172/JCI59410

Glukhov, A. V., Fedorov, V. V., Anderson, M. E., Mohler, P. J., and Efimov, I. R. (2010). Functional anatomy of the murine sinus node: high-resolution optical mapping of ankyrin-B heterozygous mice. *Am. J. Physiol. Heart Circ. Physiol.* 299, H482–H491. doi: 10.1152/ajpheart.00756.2009

Glukhov, A. V., Hage, L. T., Hansen, B. J., Pedraza-Toscano, A., Vargas-Pinto, P., Hamlin, R. L., et al. (2013). Sinoatrial node reentry in a canine chronic left ventricular infarct model: the role of intranodal fibrosis and heterogeneity of refractoriness. *Circ. Arrhythm. Electrophysiol.* 6, 984–994. doi: 10.1161/CIRCEP.113.000404

Glukhov, A. V., Kalyanasundaram, A., Lou, Q., Hage, L. T., Hansen, B. J., Belevych, A. E., et al. (2015). Calsequestrin 2 deletion causes sinoatrial node dysfunction and atrial arrhythmias associated with altered sarcoplasmic reticulum calcium cycling and degenerative fibrosis within the mouse atrial pacemaker complex. *Eur. Heart J.* doi: 10.1093/eurheartj/eht452. [Epub ahead of print].

Greenspon, A. J., Patel, J. D., Lau, E., Ochoa, J. A., Frisch, D. R., Ho, R. T., et al. (2012). Trends in permanent pacemaker implantation in the United States from 1993 to 2009: increasing complexity of patients and procedures. *J. Am. Coll. Cardiol.* 60, 1540–1545. doi: 10.1016/j.jacc.2012.07.017

Hao, X., Zhang, Y., Zhang, X., Nirmalan, M., Davies, L., Konstantinou, D., et al. (2011). TGF-beta1-mediated fibrosis and ion channel remodeling are key mechanisms in producing the sinus node dysfunction associated with SCN5A deficiency and aging. *Circ. Arrhythm. Electrophysiol.* 4, 397–406. doi: 10.1161/CIRCEP.110.960807

Hashimoto, K., Tanaka, S., Hirata, M., and Chiba, S. (1967). Responses of the sinoatrial node to change in pressure in the sinus node artery. *Circ. Res.* 21, 297–304. doi: 10.1161/01.RES.21.3.297

Herrmann, S., Fabritz, L., Layh, B., Kirchhof, P., and Ludwig, A. (2011). Insights into sick sinus syndrome from an inducible mouse model. *Cardiovasc. Res.* 90, 38–48. doi: 10.1093/cvr/cvq390

Hjortshoj, S., Riahi, S., Nielsen, J. C., Skjoth, F., Lundbye-Christensen, S., and Andersen, H. R. (2013). Does atrial pacing lead to atrial fibrillation in patients with sick sinus syndrome? insights from the DANPACE trial. *Europace* 16, 241–245. doi: 10.1093/europace/eut306

Hudson, R. E. (1960). The human pacemaker and its pathology. *Br. Heart J.* 22, 153–167. doi: 10.1136/hrt.22.2.153

Hurle, A., Climent, V., and Sanchez-Quintana, D. (2006). Sinus node structural changes in patients with long-standing chronic atrial fibrillation. *J. Thorac. Cardiovasc. Surg.* 131, 1394–1395. doi: 10.1016/j.jtcvs.2006.01.031

Jalife, J. (1984). Mutual entrainment and electrical coupling as mechanisms for synchronous firing of rabbit sino-atrial pace-maker cells. *J. Physiol.* 356, 221–243. doi: 10.1113/jphysiol.1984.sp015461

James, T. N. (1961). Anatomy of the human sinus node. *Anat. Rec.* 141, 109–139. doi: 10.1002/ar.1091410205

James, T. N., and Nadeau, R. A. (1962). Direct perfusion of the sinus node: an experimental model for pharmacologic and electrophysiologic studies of the heart. *Henry Ford Hosp. Med. Bull.* 10, 21–25.

Jensen, P. N., Gronroos, N. N., Chen, L. Y., Folsom, A. R., deFilippi, C., Heckbert, S. R., et al. (2014). Incidence of and risk factors for sick sinus syndrome in the general population. *J. Am. Coll. Cardiol.* 64, 531–538. doi: 10.1016/j.jacc.2014.03.056

Jordan, J. L., Yamaguchi, I., and Mandel, W. J. (1978). "Function and dysfunction of the sinus node clinical studies in the evaluation of sinus node function," in *The Sinus Node*, ed F. I. Bonke (The Hague; Boston; London: Martinus Nijholff Medical Division). 3–22. doi: 10.1007/978-94-009-9715-8_1

Joyner, R. W., and van Capelle, F. J. (1986). Propagation through electrically coupled cells. How a small SA node drives a large atrium. *Biophys. J.* 50, 1157–1164. doi: 10.1016/S0006-3495(86)83559-7

Kamkin, A., Kiseleva, I., Wagner, K. D., Bohm, J., Theres, H., Gunther, J., et al. (2003). Characterization of stretch-activated ion currents in isolated atrial myocytes from human hearts. *Pflugers Arch.* 446, 339–346. doi: 10.1007/s00424-002-0948-0

Kamkin, A., Kiseleva, I., Wagner, K. D., Pylaev, A., Leiterer, K. P., Theres, H., et al. (2002). A possible role for atrial fibroblasts in postinfarction bradycardia. *Am. J. Physiol. Heart Circ. Physiol.* 282, H842–H849. doi: 10.1152/ajpheart.00240.2001

Kamkin, A., Kiseleva, I., Wagner, K. D., Scholz, H., Theres, H., Kazanski, V., et al. (2001). Mechanically induced potentials in rat atrial fibroblasts depend on actin and tubulin polymerisation. *Pflugers Arch.* 442, 487–497. doi: 10.1007/s004240100564

Keith, A., and Flack, M. (1907). The form and nature of the muscular connection between the primary divisions of the vertebrate heart. *J. Anat. Physiol.* 41, 172–189.

Kohl, P., and Gourdie, R. G. (2014). Fibroblast-myocyte electrotonic coupling: does it occur in native cardiac tissue? *J. Mol. Cell. Cardiol.* 70, 37–46. doi: 10.1016/j.yjmcc.2013.12.024

Kohl, P., Kamkin, A. G., Kiseleva, I. S., and Noble, D. (1994). Mechanosensitive fibroblasts in the sino-atrial node region of rat heart: interaction with cardiomyocytes and possible role. *Exp. Physiol.* 79, 943–956. doi: 10.1113/expphysiol.1994.sp003819

Kottkamp, H. (2012). Fibrotic atrial cardiomyopathy: a specific disease/syndrome supplying substrates for atrial fibrillation, atrial tachycardia, sinus node disease, AV node disease, and thromboembolic complications. *J. Cardiovasc. Electrophysiol.* 23, 797–799. doi: 10.1111/j.1540-8167.2012.02341.x

Kuga, K., Yamaguchi, I., and Sugishita, Y. (1993). Age-related changes of sinus node function and autonomic regulation in subjects without sinus node disease–assessment by pharmacologic autonomic blockade. *Jpn. Circ. J.* 57, 760–768. doi: 10.1253/jcj.57.760

Lakatta, E. G., and DiFrancesco, D. (2009). What keeps us ticking: a funny current, a calcium clock, or both? *J. Mol. Cell. Cardiol.* 47, 157–170. doi: 10.1016/j.yjmcc.2009.03.022

Lange, G., Lu, H. H., Chang, A., and Brooks, C. M. (1966). Effect of stretch on the isolated cat sinoatrial node. *Am. J. Physiol.* 211, 1192–1196.

Lev, M. (1954). Aging changes in the human sinoatrial node. *J. Gerontol.* 9, 1–9. doi: 10.1093/geronj/9.1.1

Lewis, T., Oppenheimer, A., and Oppenheimer, B. S. (1910). The site of origin of the mammalian heart beat: the pacemaker in the dog. *Heart* II, 147–169.

Liu, J., Dobrzynski, H., Yanni, J., Boyett, M. R., and Lei, M. (2007). Organisation of the mouse sinoatrial node: structure and expression of HCN channels. *Cardiovasc. Res.* 73, 729–738. doi: 10.1016/j.cardiores.2006.11.016

Lou, Q., Glukhov, A. V., Hansen, B., Hage, L., Vargos-Pinto, P., Billman, G. E., et al. (2013). Tachy-brady arrhythmias: the critical role of adenosine-induced sinoatrial conduction block in post-tachycardia pauses. *Heart Rhythm* 10, 110–118. doi: 10.1016/j.hrthm.2012.09.012

Lou, Q., Hansen, B. J., Fedorenko, O., Csepe, T. A., Kalyanasundaram, A., Li, N., et al. (2014). Upregulation of adenosine A1 receptors facilitates sinoatrial node dysfunction in chronic canine heart failure by exacerbating nodal conduction abnormalities revealed by novel dual-sided intramural optical mapping. *Circulation* 130, 315–324. doi: 10.1161/CIRCULATIONAHA.113.007086

Luu, M., Stevenson, W. G., Stevenson, L. W., Baron, K., and Walden, J. (1989). Diverse mechanisms of unexpected cardiac arrest in advanced heart failure. *Circulation* 80, 1675–1680. doi: 10.1161/01.CIR.80.6.1675

Mandel, W. J., Jordan, J. L., and Karagueuzian, H. S. (1999). Disorders of sinus function. *Curr. Treat. Options Cardiovasc. Med.* 1, 179–186. doi: 10.1007/s11936-999-0021-9

Mangrum, J. M., and DiMarco, J. P. (2000). The evaluation and management of bradycardia. *N. Engl. J. Med.* 342, 703–709. doi: 10.1056/NEJM200003093421006

Matsuyama, T. A., Inoue, S., Kobayashi, Y., Sakai, T., Saito, T., Katagiri, T., et al. (2004). Anatomical diversity and age-related histological changes in the human right atrial posterolateral wall. *Europace* 6, 307–315. doi: 10.1016/j.eupc.2004.03.011

Miake, J., Marban, E., and Nuss, H. B. (2002). Biological pacemaker created by gene transfer. *Nature* 419, 132–133. doi: 10.1038/419132b

Michaels, D. C., Matyas, E. P., and Jalife, J. (1987). Mechanisms of sinoatrial pacemaker synchronization: a new hypothesis. *Circ. Res.* 61, 704–714. doi: 10.1161/01.RES.61.5.704

Miller, M., Cho, J. Y., McElwain, K., McElwain, S., Shim, J. Y., Manni, M., et al. (2006). Corticosteroids prevent myofibroblast accumulation and airway remodeling in mice. *Am. J. Physiol. Lung Cell. Mol. Physiol.* 290, L162–L169. doi: 10.1152/ajplung.00252.2005

Monfredi, O., Dobrzynski, H., Mondal, T., Boyett, M. R., and Morris, G. M. (2010). The anatomy and physiology of the sinoatrial node–a contemporary review. *Pacing Clin. Electrophysiol.* 33, 1392–1406. doi: 10.1111/j.1540-8159.2010.02838.x

Morris, G. M., and Kalman, J. M. (2014). Fibrosis, electrics and genetics. perspectives in sinoatrial node disease. *Circ. J.* 78, 1272–1282. doi: 10.1253/circj.CJ-14-0419

Moss, A. J., and Davis, R. J. (1974). Brady-Tachy syndrome. *Prog. Cardiovasc. Dis.* 16, 439–454. doi: 10.1016/0033-0620(74)90005-X

Nakajima, H., Nakajima, H. O., Salcher, O., Dittie, A. S., Dembowsky, K., Jing, S., et al. (2000). Atrial but not ventricular fibrosis in mice expressing a mutant transforming growth factor-beta(1) transgene in the heart. *Circ. Res.* 86, 571–579. doi: 10.1161/01.RES.86.5.571

Nakao, S., Hirakawa, A., Fukushima, R., Kobayashi, M., and Machida, N. (2012). The anatomical basis of bradycardia-tachycardia syndrome in elderly dogs with chronic degenerative valvular disease. *J. Comp. Pathol.* 146, 175–182. doi: 10.1016/j.jcpa.2011.03.016

Nguyen, T. P., Qu, Z., and Weiss, J. N. (2014). Cardiac fibrosis and arrhythmogenesis: the road to repair is paved with perils. *J. Mol. Cell. Cardiol.* 70, 83–91. doi: 10.1016/j.yjmcc.2013.10.018

Noujaim, S. F., Lucca, E., Munoz, V., Persaud, D., Berenfeld, O., Meijler, F. L., et al. (2004). From mouse to whale: a universal scaling relation for the PR Interval of the electrocardiogram of mammals. *Circulation* 110, 2802–2808. doi: 10.1161/01.CIR.0000146785.15995.67

Opthof, T. (1988). The mammalian sinoatrial node. *Cardiovasc. Drugs Ther.* 1, 573–597. doi: 10.1007/BF02125744

Opthof, T., de Jonge, B., Jongsma, H. J., and Bouman, L. N. (1987). Functional morphology of the pig sinoatrial node. *J. Mol. Cell. Cardiol.* 19, 1221–1236. doi: 10.1016/S0022-2828(87)80532-1

Oren, R. V., and Clancy, C. E. (2010). Determinants of heterogeneity, excitation and conduction in the sinoatrial node: a model study. *PLoS Comput. Biol.* 6:e1001041. doi: 10.1371/journal.pcbi.1001041

Packer, D. L., Prutkin, J. M., Hellkamp, A. S., Mitchell, L. B., Bernstein, R. C., Wood, F., et al. (2009). Impact of implantable cardioverter-defibrillator, amiodarone, and placebo on the mode of death in stable patients with heart failure: analysis from the sudden cardiac death in heart failure trial. *Circulation* 120, 2170–2176. doi: 10.1161/CIRCULATIONAHA.109.853689

Rosen, M. R. (2014). Gene therapy and biological pacing. *N. Engl. J. Med.* 371, 1158–1159. doi: 10.1056/NEJMcibr1408897

Rosen, M. R., Brink, P. R., Cohen, I. S., and Robinson, R. B. (2004). Genes, stem cells and biological pacemakers. *Cardiovasc. Res.* 64, 12–23. doi: 10.1016/j.cardiores.2004.05.012

Sakabe, M., Fujiki, A., Nishida, K., Sugao, M., Nagasawa, H., Tsuneda, T., et al. (2005). Enalapril preserves sinus node function in a canine atrial fibrillation model induced by rapid atrial pacing. *J. Cardiovasc. Electrophysiol.* 16, 1209–1214. doi: 10.1111/j.1540-8167.2005.50100.x

Sanchez-Quintana, D., Anderson, R. H., Cabrera, J. A., Climent, V., Martin, R., Farre, J., et al. (2002). The terminal crest: morphological features relevant to electrophysiology. *Heart* 88, 406–411. doi: 10.1136/heart.88.4.406

Sanchez-Quintana, D., Cabrera, J. A., Farre, J., Climent, V., Anderson, R. H., and Ho, S. Y. (2005). Sinus node revisited in the era of electroanatomical mapping and catheter ablation. *Heart* 91, 189–194. doi: 10.1136/hrt.2003.031542

Sanders, P., Morton, J. B., Kistler, P. M., Spence, S. J., Davidson, N. C., Hussin, A., et al. (2004). Electrophysiological and electroanatomic characterization of the atria in sinus node disease: evidence of diffuse atrial remodeling. *Circulation* 109, 1514–1522. doi: 10.1161/01.CIR.0000121734.47409.AA

Sanders, W. E. J., Sorrentino, R. A., Greenfield, R. A., Shenasa, H., Hamer, M. E., and Wharton, J. M. (1994). Catheter ablation of sinoatrial node reentrant tachycardia. *J. Am. Coll. Cardiol.* 23, 926–934. doi: 10.1016/0735-1097(94)90639-4

Selan, J. C., Michaelson, M., Fanburg, B. L., and Estes, N. A. (2014). Evaluation and management of heart rhythm disturbances due to cardiac sarcoidosis. *Heart Lung Circ.* 23, 1100–1109. doi: 10.1016/j.hlc.2014.07.065

Shiraishi, I., Takamatsu, T., Minamikawa, T., Onouchi, Z., and Fujita, S. (1992). Quantitative histological analysis of the human sinoatrial node during growth and aging. *Circulation* 85, 2176–2184. doi: 10.1161/01.CIR.85.6.2176

Stephenson, R. S., Boyett, M. R., Hart, G., Nikolaidou, T., Cai, X., Corno, A. F., et al. (2012). Contrast enhanced micro-computed tomography resolves the 3-dimensional morphology of the cardiac conduction system in mammalian hearts. *PLoS ONE* 7:e35299. doi: 10.1371/journal.pone.0035299

Sumitomo, N., Sakurada, H., Taniguchi, K., Matsumura, M., Abe, O., Miyashita, M., et al. (2007). Association of atrial arrhythmia and sinus node dysfunction in patients with catecholaminergic polymorphic ventricular tachycardia. *Circ. J.* 71, 1606–1609. doi: 10.1253/circj.71.1606

Swaminathan, P. D., Purohit, A., Soni, S., Voigt, N., Singh, M. V., Glukhov, A. V., et al. (2011). Oxidized CaMKII causes cardiac sinus node dysfunction in mice. *J. Clin. Invest.* 121, 3277–3288. doi: 10.1172/JCI57833

Thery, C., Gosselin, B., Lekieffre, J., and Warembourg, H. (1977). Pathology of sinoatrial node. Correlations with electrocardiographic findings in 111 patients. *Am. Heart J.* 93, 735–740. doi: 10.1016/S0002-8703(77)80070-7

Truex, R. C., Smythe, M. Q., and Taylor, M. J. (1967). Reconstruction of the human sinoatrial node. *Anat. Rec.* 159, 371–378. doi: 10.1002/ar.1091590406

Vasquez, C., Benamer, N., and Morley, G. E. (2011). The cardiac fibroblast: functional and electrophysiological considerations in healthy and diseased hearts. *J. Cardiovasc. Pharmacol.* 57, 380–388. doi: 10.1097/FJC.0b013e31820cda19

Vasquez, C., Mohandas, P., Louie, K. L., Benamer, N., Bapat, A. C., and Morley, G. E. (2010). Enhanced fibroblast-myocyte interactions in response to cardiac injury. *Circ. Res.* 107, 1011–1020. doi: 10.1161/CIRCRESAHA.110.227421

Verheule, S., Sato, T., Everett, T., Engle, S. K., Otten, D., Rubart-von der, L. M., et al. (2004). Increased vulnerability to atrial fibrillation in transgenic mice with selective atrial fibrosis caused by overexpression of TGF-beta1. *Circ. Res.* 94, 1458–1465. doi: 10.1161/01.RES.0000129579.59664.9d

Wolf, R. M., Glynn, P., Hashemi, S., Zarei, K., Mitchell, C. C., Anderson, M. E., et al. (2013). Atrial fibrillation and sinus node dysfunction in human ankyrin-B syndrome: a computational analysis. *Am. J. Physiol. Heart Circ. Physiol.* 304, H1253–H1266. doi: 10.1152/ajpheart.00734.2012

Wu, Y., and Anderson, M. E. (2014). CaMKII in sinoatrial node physiology and dysfunction. *Front. Pharmacol.* 5:48. doi: 10.3389/fphar.2014.00048

Yeh, Y. H., Burstein, B., Qi, X. Y., Sakabe, M., Chartier, D., Comtois, P., et al. (2009). Funny current downregulation and sinus node dysfunction associated with atrial tachyarrhythmia: a molecular basis for tachycardia-bradycardia syndrome. *Circulation* 119, 1576–1585. doi: 10.1161/CIRCULATIONAHA.108.789677

Conflict of Interest Statement: The authors declare that the research was conducted in the absence of any commercial or financial relationships that could be construed as a potential conflict of interest.

Received: 07 December 2014; accepted: 24 January 2015; published online: 12 February 2015.

*Citation: Csepe TA, Kalyanasundaram A, Hansen BJ, Zhao J and Fedorov VV (2015) Fibrosis: a structural modulator of sinoatrial node physiology and dysfunction. Front. Physiol. **6**:37. doi: 10.3389/fphys.2015.00037*

This article was submitted to Cardiac Electrophysiology, a section of the journal Frontiers in Physiology.

frontiers in
PHYSIOLOGY

REVIEW ARTICLE
published: 26 November 2014
doi: 10.3389/fphys.2014.00446

Role of sinoatrial node architecture in maintaining a balanced source-sink relationship and synchronous cardiac pacemaking

Sathya D. Unudurthi[1,2], Roseanne M. Wolf[3] and Thomas J. Hund[1,2,4]*

[1] Department of Biomedical Engineering, College of Engineering, The Ohio State University, Columbus, OH, USA
[2] The Dorothy M. Davis Heart and Lung Research Institute, The Ohio State University Wexner Medical Center, Columbus, OH, USA
[3] Department of Mathematics, The University of Dubuque, Dubuque, IA, USA
[4] Division of Cardiovascular Medicine, Department of Internal Medicine, The Ohio State University Wexner Medical Center, Columbus, OH, USA

Edited by:
George E. Billman, The Ohio State University, USA

Reviewed by:
Raimond L. Winslow, The Johns Hopkins University, USA
Crystal M. Ripplinger, University of California, Davis, USA

***Correspondence:**
Thomas J. Hund, The Dorothy M. Davis Heart and Lung Research Institute, The Ohio State University Wexner Medical Center, 473 W. 12th Avenue, Columbus, OH 43210, USA
e-mail: thomas.hund@osumc.edu

Normal heart rhythm (sinus rhythm) depends on regular activity of the sinoatrial node (SAN), a heterogeneous collection of specialized myocytes in the right atrium. SAN cells, in general, possess a unique electrophysiological profile that promotes spontaneous electrical activity (automaticity). However, while automaticity is required for normal pacemaking, it is not necessarily sufficient. Less appreciated is the importance of the elaborate structure of the SAN complex for proper pacemaker function. Here, we review the important structural features of the SAN with a focus on how these elements help manage a precarious balance between electrical charge generated by the SAN ("source") and the charge needed to excite the surrounding atrial tissue ("sink"). We also discuss how compromised "source-sink" balance due, for example to fibrosis, may promote SAN dysfunction, characterized by slow and/or asynchronous pacemaker activity and even failure, in the setting of cardiovascular disease (e.g., heart failure, atrial fibrillation). Finally, we discuss implications of the "source-sink" balance in the SAN complex for cell and gene therapies aimed at creating a biological pacemaker as replacement or bridge to conventional electronic pacemakers.

Keywords: sinoatrial node, automaticity, pacemaking, source-sink relationship, intercellular coupling, sick sinus syndrome, arrhythmia

INTRODUCTION

The sinoatrial node (SAN), located in the right atrium, serves as the primary site for initiation of the normal heartbeat (sinus rhythm) (**Figure 1**). Together with the cardiac conduction system [the atrioventricular node (AVN) and the His–Purkinje system], the SAN is responsible for orchestrating the precise sequence of electrical events underlying the normal heart rhythm. This sequence begins with generation of the electrical impulse in the SAN, which then spreads rapidly through the atria and to the AVN. AVN conduction is slow, thereby introducing a delay between atrial and ventricular systole to facilitate filling of the ventricles before they contract. The AVN also serves as a secondary pacemaker in the event of SAN failure (e.g., due to aging, cardiovascular disease). After exiting the AVN, the impulse propagates rapidly through the His-Purkinje system, comprised of a common bundle (the bundle of His), and left and right bundle branches that give rise to a network of terminal Purkinje fibers which simultaneously communicate the impulse to the ventricular muscle at multiple discrete locations (Purkinje-muscle junctions). The His–Purkinje system supports rapid conduction with action potential (AP) propagation velocities up to ten-fold higher than in the ventricular mass to ensure synchronous activation of the ventricular muscle (Boyett, 2009). This sequence of electrical events is essential for normal heart function and depends on a number of distinguishing cell and tissue properties shared by each component of the pacemaker and conduction system. First and foremost, cells in the pacemaker and conduction system possess the defining characteristic of automaticity, an ability to generate an action potential in the absence of an external stimulus. Automaticity is required for cardiac pacemaking and depends on a unique ion channel expression profile conducive to spontaneous AP generation. Second, and the major focus of this review, aside from active cell membrane properties (e.g., voltage-gated ion channel activity), tissue structure and cell-to-cell communication are tightly controlled in these tissues to handle the unique energetic demands placed on them during the excitation cycle. Specifically, these tissues are designed to balance the supply of depolarizing current generated by activating cells ("sources") with the demand of downstream quiescent cells ("sinks"). Source-sink relationships are important throughout the heart, but tissues in the pacemaker and conduction system, in particular, have evolved elaborate structures/properties to facilitate activation of a large tissue mass by a relatively small number of cells (e.g., atrial activation by the sinoatrial node; ventricular activation by His-Purkinje fibers). The goal of this review is to discuss mechanisms important for regulation of cardiac pacemaking with a specific focus on the role of passive tissue properties.

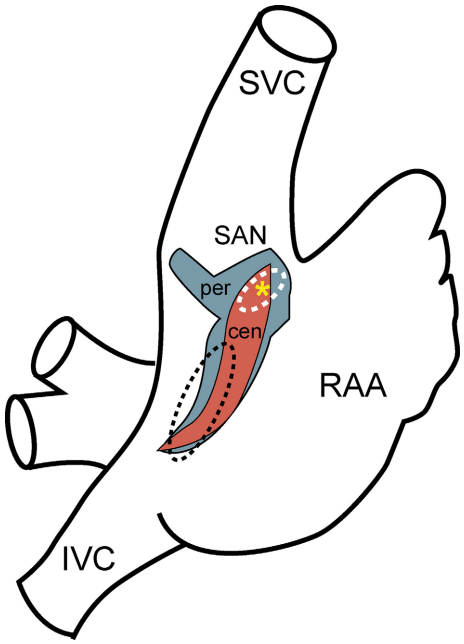

FIGURE 1 | Sinoatrial node anatomy. Schematic diagram of the right atrium showing approximate location and extent of rabbit sinoatrial node determined by computer three-dimensional reconstruction (red, central SAN region; blue, peripheral SAN region; yellow asterisk, leading pacemaker site) compared to previous estimates from the human based on anatomy and function (white dashed line, SAN; black dashed line, ectopic atrial region) (Talano et al., 1978; Dobrzynski et al., 2005). (SVC, superior vena cava; IVC, inferior vena cava; RAA, right atrial appendage).

THE SINOATRIAL NODE

SINOATRIAL NODE ANATOMY

The SAN was discovered over a century ago by Arthur Keith and Martin Flack as an anatomically defined tissue at the junction of the superior vena cava and right atria (Keith and Flack, 1907). For decades following this discovery, the SAN was defined as a compact unifocal region surrounded by secondary extranodal atrial pacemakers that could randomly compete with the leading pacemaker site in the SAN. Today, the SAN is recognized to be a distributed and heterogeneous complex adjacent to the crista terminalis with distinct regions defined by unique electrophysiological and structural properties (**Figure 1**) (Boineau et al., 1980, 1988; Dobrzynski et al., 2005, 2007; Fedorov et al., 2012). In larger animals, including the human, the node is functionally isolated with the exception of well-defined exit pathways that allow for communication between the SAN and atrial tissue (Fedorov et al., 2009, 2010, 2012; Nikolaidou et al., 2012). The anatomical basis of this insulation has been attributed to surrounding connective tissue, which insulates the pacemaker's automaticity from the hyperpolarizing electrical activity of the atrial myocardium. Other reports describe nodal/atrial interdigitations without a fibrous border that rely upon delicate spatial control of gap junction coupling (Ten Velde et al., 1995; Sanchez-Quintana et al., 2005). A distinguishing feature of SAN found in multiple species is the presence of a centrally located artery around which the SAN cells are organized (Sanchez-Quintana et al., 2005).

SINOATRIAL NODE CELL MORPHOLOGY

The sinoatrial node is a collection of weakly coupled, heterogeneous cells, including pacemaker cells as well as non-pacemaker cells such as atrial myocytes, adipocytes and fibroblasts. Within the node, pacemaker cells vary by size and electrophysiological properties and may be divided into three major classes: (1) "Elongated spindle shaped cells," which range up to 80 μm in length and have a faintly striated cell body with one or more nuclei; (2) "Spindle cells," which have a similar shape to that of elongated spindle cells, but are shorter in length, extending up to 40 μm and are predominantly mono-nucleated; and (3) "Spider cells" have irregularly shaped branches with blunt ends (Verheijck et al., 1998) (**Figure 2**). A gradual transition has been observed in AP properties from the central area toward the SAN periphery (Kodama and Boyett, 1985). One of the possible reasons for this transition has been attributed to the arrangement and distribution of nodal cells in SAN node, although there is some debate about the exact underlying cellular distribution (Zhang et al., 2001; Dobrzynski et al., 2005; Oren and Clancy, 2010) (**Figure 2**). Regardless, it is clear that heterogeneity is the rule as none of the described cell types have been found exclusively in a specific SAN area. In rabbit, for example, a uniform distribution of the three major pacemaker cell types has been observed in the central SAN area. In the crista terminalis region, atrial cells are the predominant cell type (63 ± 18%), with a subpopulation of pacemaker cells, most of which are elongated spindle nodal cells. The septal area of SAN is mostly composed of atrial cells (88 ± 19%) and all the four types of SAN cells have an almost uniform presence in this region (Verheijck et al., 1998). Despite the diversity in morphology and electrophysiology within the SAN region, there are important unifying active membrane properties of these cells that are essential for normal pacemaking.

SINOATRIAL NODE CELL ACTIVE MEMBRANE PROPERTIES

SAN cell automaticity depends on an electrophysiological profile that is distinct from that in atrial or ventricular cells (Mangoni and Nargeot, 2008). First and foremost, while APs from ventricular and atrial cells possess a stable rest potential, the SAN AP lacks a stable rest potential due in large part to lack of the inward rectifier K^+ channel I_{K1} (**Figure 3**). Instead the SAN AP reaches a maximum diastolic potential (∼-60 mV) followed by a spontaneous depolarization phase that eventually reaches threshold to generate another AP. Pacemaking depends on tight regulation of this spontaneous depolarization phase, which results from the coordinated effort of multiple ion channels/transporters/exchangers. Among the important currents contributing to diastolic depolarization is the hyperpolarization-activated "funny" current (I_f) (due primarily to *HCN4* in SAN cells), with permeability to both Na^+ and K^+ and biophysical properties that make it a depolarizing current during diastole. I_f activates as the membrane potential approaches its max diastolic value and helps to spontaneously depolarize the membrane. At the same time, a low level of Ca^{2+} release from sarcoplasmic reticulum ryanodine receptor Ca^{2+} release channels likely promotes a depolarizing

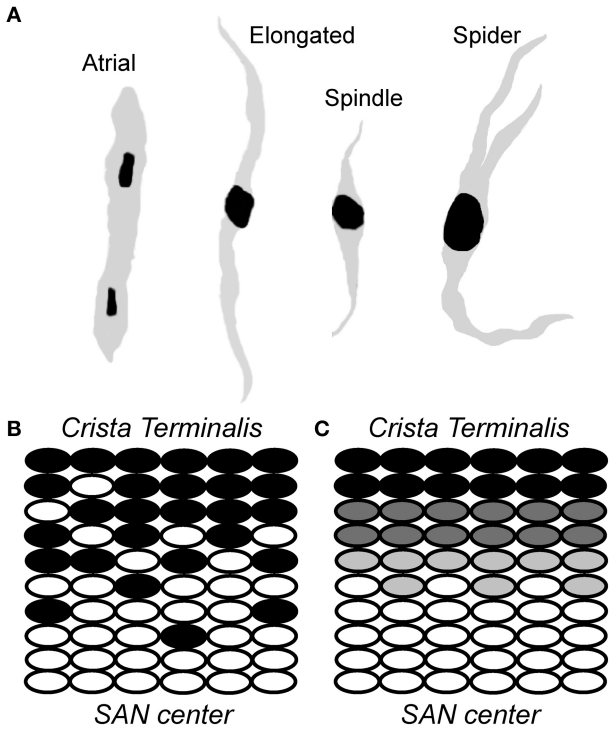

FIGURE 2 | Sinoatrial node is a heterogeneous collection of morphologically and electrophysiologically distinct myocytes. (A) A schematic representation of cells found in the sinoatrial node region, including relatively large "elongated" spindle shaped cells, "spindle" cells that are similar in shape to that of elongated spindle cells with a shorter length, and irregularly shaped "spider" cells. **(B,C)** Two different models have been proposed to account for transition from typical/central SAN (white ovals) to atrial (black ovals) cells: **(C)** a gradual transition of intermediate cells (gray) from SAN center to crista terminalis; and **(B)** "mosaic" model involving gradually decreasing ratio of SAN to atrial cell densities from SAN center to crista terminalis (Verheijck et al., 1998).

current via the Na^+/Ca^{2+} exchanger (Lakatta et al., 2010). Once the membrane potential reaches about −50 mV, transient or T-type Ca^{+2} channels (namely, $Ca_v3.1$, $Ca_v3.2$, and $Ca_v3.3$) open, allowing for Ca^{2+} entry into the cell and further depolarization of the cell membrane. As the membrane potential approaches −40 mV, L-type Ca^{2+} channels (first $Ca_v1.3$, then $Ca_v1.2$ at slightly less negative potentials) activate, giving rise to the SAN cell upstroke, which is much slower than that in atrial or ventricular myocytes due to the low levels of voltage-gated Na^+ channel (Na_v) expressed in SAN cells (orders or magnitude smaller than Na_v in ventricular myocytes). Although Na_v does not have the prominent role in the SAN AP upstroke, Na_v expression in SAN (and surrounding atrial) tissue is important for source-sink balance and pacemaking (discussed more below), such that Na_v deficiency is often associated with bradycardia and/or defects in the pacemaker and conduction system (Benson et al., 2003; Veldkamp et al., 2003; Makiyama et al., 2005). SAN AP repolarization is promoted by the activities of several classes of voltage-gated K^+ channels. The transient outward K^+ current (I_{to}), carried by $K_v1.4$, $K_v4.2$, and $K_v4.3$, is responsible for the early phase of SAN AP repolarization, while delayed-rectifier K^+ currents ultrarapid (I_{Kur}, $K_v1.5$), rapid (I_{Kr}, ERG), and slow (I_{Ks}, K_vLQT1) K^+ currents control late repolarization and the maximal diastolic potential (especially I_{Kr}). Other K^+ currents (e.g., $I_{K,ATP}$, $I_{K,Ach}$) are important for dynamic response of SAN excitability to parasympathetic, metabolic factors. While steady-state rest is never achieved in the normal SAN, the activities of these K^+ channels together with inactivation of L-type Ca^{2+} channels allows the membrane to reset for the next spontaneous action potential.

SOURCE-SINK RELATIONSHIPS IN HEART

While the ionic events described in the previous section are essential for SAN cell automaticity, cardiac pacemaking is, in fact, an emergent property of a heterogeneous, coupled system of both spontaneously active and quiescent cells (**Figure 3**). Therefore, a complete analysis of pacemaking accounts for not only events at the single cell level but also those tissue-level factors that will shape the emergent behavior. In particular, to understand the behavior of the intact SAN, it is helpful to reflect on the delicate electrical source-sink relationships that exist in the SAN region (Nikolaidou et al., 2012). Throughout the heart, successful propagation of the action potential depends on a cell first receiving electrical current from neighboring excited cells and then, once excited, sending current downstream to neighboring quiescent cells. Thus, every cell will both give charge to ("source") and take charge from ("sink") surrounding tissue at different times in their activation cycle. Propagation will be successful as long as the active sources can generate enough current to satisfy local sinks. Alternatively, if the sink overwhelms the source, propagation will fail. Tissue structure and electrical coupling have a huge influence on source-sink relationships, and can tip the balance for or against successful propagation at critical junctures (Joyner et al., 1991; Rohr et al., 1997; Shaw and Rudy, 1997). The concept of safety factor has been introduced to quantify the balance between sources and sinks in ventricular and atrial tissue (Delgado et al., 1990; Shaw and Rudy, 1997; Kleber and Rudy, 2004; Boyle and Vigmond, 2010). Briefly, safety factor is the ratio of how much charge a cell generates to the charge threshold for activation. A safety factor greater than one is indicative of safe conduction with an appropriate balance between source and sink, while a safety factor less than one is indicative of a source-sink mismatch with high susceptibility to conduction failure. Experimental and modeling studies have shown that safety factor tends to be low for propagation that occurs from a smaller cell to a larger cell and/or from a relatively small number of cells to a larger number of cells (Fast and Kleber, 1995; Rohr et al., 1997; Wang and Rudy, 2000), conditions that are highly relevant for the SAN complex. It is known that the atrium places a considerable electrical load on the SAN (Kirchhof et al., 1987). How, then, does the heart manage robust pacemaking under these unsafe conditions? The complete answer to this question cannot be understood without considering the SAN architecture itself.

SINOATRIAL NODE STRUCTURE AND SOURCE-SINK BALANCE

Perhaps the most important structural features for managing source-sink balance in SAN region are conduction barriers found

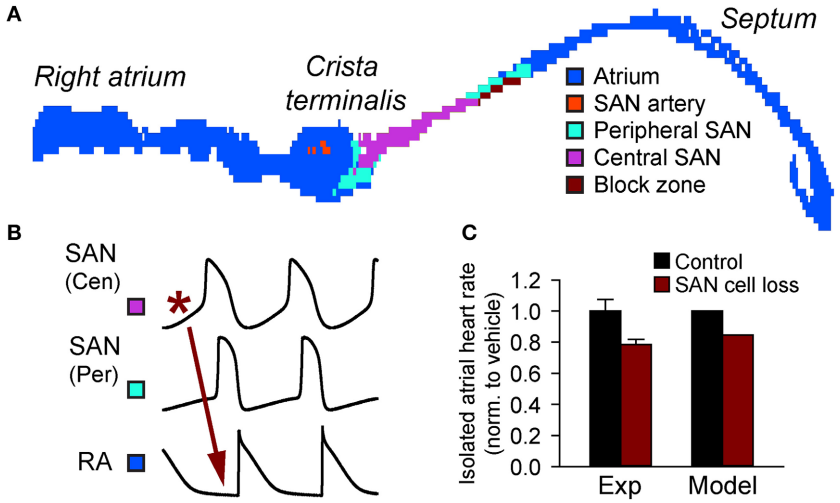

FIGURE 3 | Importance of source-sink balance in the intact sinoatrial node complex. (A) A two-dimensional histologically reconstructed mathematical model of the intact sinoatrial node based on immunohistological data (Dobrzynski et al., 2005; Butters et al., 2010) identifying the distribution of cells throughout the right atrium (adapted from Luo et al., 2013). **(B)** Normal activation initiates in the central SAN region, spreads through the SAN periphery, and finally to the right atrium. **(C)** Cell loss slows activation of the right atrium in both experiment (19% cell loss induced by streptozotocin (STZ) treatment and assessed by TUNEL staining) and computer simulations (Replacement of 19% of SAN cells with inexcitable elements) (Luo et al., 2013).

between the SAN and surrounding atrial tissue (Fedorov et al., 2012; Nikolaidou et al., 2012). In large animals (e.g., canine and human), where the SAN is embedded in a relatively thick, three-dimensional atrial wall, layers of connective tissue isolate much of the SAN from the atrial myocardium (Fedorov et al., 2012; Nikolaidou et al., 2012). In smaller animals, the atrial wall is much thinner (practically two-dimensional) reducing the load on the SAN. However, even in this environment, a discrete region of conduction block ("block zone") prevents direct activation of the interatrial septum and likely consists of fibrous, connective, and/or fatty tissue (Fedorov et al., 2012; Nikolaidou et al., 2012) (**Figure 3**). Thus, in both large and small animals well-defined non-conducting regions help reduce electrical loading of the SAN and preserve a sustainable source-sink balance.

Another important way source-sink balance is maintained in the SAN region is through electrical coupling between cells. Specifically, electrical coupling is poor in the SAN relative to that in the surrounding atrial myocardium due to preferential expression of gap junctions containing low conductance connexins (Connexin45) (Boyett et al., 2006; Dobrzynski et al., 2007). Modeling and experimental studies have demonstrated a somewhat counter-intuitive relationship between electrical coupling and safety factor, with uncoupling decreasing conduction velocity while increasing safety over a wide range (Shaw and Rudy, 1997; Rohr et al., 1998; Kleber and Saffitz, 2014). Partial uncoupling of SAN cells from neighboring cells prevents these cells from becoming overwhelmed by demand, in essence reducing the apparent size of the atrium (Joyner and Van Capelle, 1986; Watanabe et al., 1995). Importantly, experimental and modeling studies have shown that successful entrainment of atrial activation by the SAN requires only a low degree of coupling between SAN and atrial cells (Cai et al., 1994; Joyner et al., 1998). Once the electrical impulse emerges from the SAN, it can then propagate safely through the atria, into the AV node and eventually into the His-Purkinje system. Another region where a similar potential mismatch is observed is at the Purkinje muscle junction where the terminal Purkinje fibers couple to the ventricular mass. In fact, uncoupling has been shown to improve conduction across the Purkinje muscle junction (Morley et al., 2005). Aside from influencing safety for propagation, the degree of electrical coupling may also affect the dynamics of SAN cell spontaneous activation, with potential implications for synchronization of pacemaker activity (Glynn et al., 2014).

Finally, multiple experimental and modeling studies have demonstrated the importance of a gradient in membrane properties from the central to peripheral SAN region for normal pacemaking (Boyett et al., 2000; Zhang et al., 2007; Inada et al., 2014). Contributing to this gradient is the observed relationship between SAN cell size (or membrane capacitance) and densities of multiple ion currents, including voltage-gated Na^+ and Ca^{2+} currents, as well as transient outward K^+ current (I_{to}), rapid and slow delayed rectifier K^+ currents (I_{Kr}, I_{Ks}) and funny current (I_f). Mathematical modeling has shown that, in particular, increased expression of the voltage-gated Na^+ channel in the SAN periphery is necessary to support excitation of the atria by the SAN (Zhang et al., 2007).

Mounting experimental and modeling data support the notion that defects in SAN tissue architecture may tip the source-sink balance in a negative direction and promote sinus node dysfunction (Thery et al., 1977; Sanders et al., 2004; Dobrzynski et al., 2007; Fedorov et al., 2012; Nikolaidou et al., 2012). In fact, it has been known for almost 40 years that SAN structural changes (e.g., SAN cell loss and fibrosis) with aging is associated with sinus node dysfunction (Thery et al., 1977). Alterations in the normal gradient of electrophysiological properties in the SAN complex has been proposed as an additional mechanism for slowing of

pacemaking with aging (Alings and Bouman, 1993). Besides the normal aging process, cardiovascular disease (e.g., heart failure) has also been shown to produce dramatic electrophysiological and structural remodeling in the atrium (Sanders et al., 2004; Dobrzynski et al., 2007). Increased expression of adenosine receptors within the SAN region together with increased fibrosis have recently been linked to loss of synchrony and sinus node dysfunction in a canine heart failure model (Lou et al., 2014). At the same time, experimental and modeling work has found that chronic angiotensin infusion (heart failure condition) in the mouse results in CaMKII-induced apoptosis resulting in SAN cell loss, which disrupts the normal source-sink balance leading to sinoatrial node dysfunction (Swaminathan et al., 2011) (**Figure 3**). A similar relationship between cell loss and sinus node dysfunction has been observed in a mouse model of diabetes and in ankyrin-B syndrome (Luo et al., 2013; Wolf et al., 2013).

IMPLICATIONS OF SOURCE-SINK RELATIONSHIP FOR THERAPY

Studies from multiple groups have focused on development of a biological pacemaker as a replacement or bridge to traditional implantable electronic devices (reviewed in Cho and Marban, 2010; Rosen et al., 2011; Munshi and Olson, 2014; Rosen, 2014). These efforts are motivated by the limitations of electronic pacemakers, which include risk for infection (affecting ∼2% of patients Rosen, 2014), lead fracture, and/or lack of autonomic responsiveness. Approaches include gene- and cell-based therapies to induce pacemaker activity from cells/regions that normally are quiescent (Miake et al., 2002; Bucchi et al., 2006; Tse et al., 2006; Zhang et al., 2011; Boink et al., 2012; Hu et al., 2014). Results have been mixed with reports of successful induction of physiologic heart rate using biological pacemaker in large animal models (Boink et al., 2013; Hu et al., 2014). Important limitations to these studies include both the magnitude and duration of the response to the intervention. For example, a recent gene therapy study used the transcription factor T-box 18 to reprogram right ventricular myocytes into pacemaker cells in a porcine heart block model *in vivo* (Hu et al., 2014). While authors reported a restored heart rate between 75 and 80 bpm in the T-box 18 transduced animals, there is some question about the exact mechanism as the adenoviral vector alone (GFP) also partially rescued heart rate (∼65 bpm). Furthermore, heart rate effects in both the T-box 18 and GFP groups were transient and began to decline at time points greater than 11 days after injection (Hu et al., 2014; Rosen, 2014). While these biological approaches are compelling, the question is can we solve this challenging problem without considering the structure of the natural cardiac pacemaker? Is there a way to increase the efficacy of biological pacemakers by implanting/reprogramming them in supportive structures? Can we find a way to repair the natural pacemaker itself? New gene and cell-based therapies that address some of these questions may help fulfill the promise of an effective biological pacemaker.

CONCLUSIONS

The SAN is an intricately designed structure tailored to support robust pacemaking, from the molecular composition of SAN cells to their spatial arrangement and connectivity to other cells. While cardiac pacemaking depends on the automaticity of the individual myocyte, architectural factors at the tissue level are also essential for robust pacemaking. This architecture involves a distinct SAN anatomy, a unique pattern of intercellular coupling, and gradients in electrophysiological profiles that help manage a very delicate source-sink balance, due to a very small number of cells having responsibility for activating a much larger number of cells. Importantly, structural remodeling of the SAN pacemaker complex is commonly associated with sinus node dysfunction (e.g., with aging, atrial fibrillation or heart failure). A major challenge going forward is to determine whether/how we can tune SAN architecture and the associated source-sink relationship for therapeutic benefit.

ACKNOWLEDGMENTS

This work was supported by National Institutes of Health (NIH) (grant number HL114893 to Thomas J. Hund) and James S. McDonnell Foundation (to Thomas J. Hund).

REFERENCES

Alings, A. M., and Bouman, L. N. (1993). Electrophysiology of the ageing rabbit and cat sinoatrial node–a comparative study. *Eur. Heart J.* 14, 1278–1288. doi: 10.1093/eurheartj/14.9.1278

Benson, D. W., Wang, D. W., Dyment, M., Knilans, T. K., Fish, F. A., Strieper, M. J., et al. (2003). Congenital sick sinus syndrome caused by recessive mutations in the cardiac sodium channel gene (SCN5A). *J. Clin. Invest.* 112, 1019–1028. doi: 10.1172/JCI200318062

Boineau, J. P., Canavan, T. E., Schuessler, R. B., Cain, M. E., Corr, P. B., and Cox, J. L. (1988). Demonstration of a widely distributed atrial pacemaker complex in the human heart. *Circulation* 77, 1221–1237. doi: 10.1161/01.CIR.77.6.1221

Boineau, J. P., Schuessler, R. B., Hackel, D. B., Miller, C. B., Brockus, C. W., and Wylds, A. C. (1980). Widespread distribution and rate differentiation of the atrial pacemaker complex. *Am. J. Physiol.* 239, H406–H415.

Boink, G. J., Duan, L., Nearing, B. D., Shlapakova, I. N., Sosunov, E. A., Anyukhovsky, E. P., et al. (2013). HCN2/SkM1 gene transfer into canine left bundle branch induces stable, autonomically responsive biological pacing at physiological heart rates. *J. Am. Coll. Cardiol.* 61, 1192–1201. doi: 10.1016/j.jacc.2012.12.031

Boink, G. J., Nearing, B. D., Shlapakova, I. N., Duan, L., Kryukova, Y., Bobkov, Y., et al. (2012). Ca^{2+}-stimulated adenylyl cyclase AC1 generates efficient biological pacing as single gene therapy and in combination with HCN2. *Circulation* 126, 528–536. doi: 10.1161/CIRCULATIONAHA.111.083584

Boyett, M. R. (2009). "And the beat goes on." The cardiac conduction system: the wiring system of the heart. *Exp. Physiol.* 94, 1035–1049. doi: 10.1113/expphysiol.2009.046920

Boyett, M. R., Honjo, H., and Kodama, I. (2000). The sinoatrial node, a heterogeneous pacemaker structure. *Cardiovasc. Res.* 47, 658–687. doi: 10.1016/S0008-6363(00)00135-8

Boyett, M. R., Inada, S., Yoo, S., Li, J., Liu, J., Tellez, J., et al. (2006). Connexins in the sinoatrial and atrioventricular nodes. *Adv. Cardiol.* 42, 175–197. doi: 10.1159/000092569

Boyle, P. M., and Vigmond, E. J. (2010). An intuitive safety factor for cardiac propagation. *Biophys. J.* 98, L57–L59. doi: 10.1016/j.bpj.2010.03.018

Bucchi, A., Plotnikov, A. N., Shlapakova, I., Danilo, P. Jr., Kryukova, Y., Qu, J., et al. (2006). Wild-type and mutant HCN channels in a tandem biological-electronic cardiac pacemaker. *Circulation* 114, 992–999. doi: 10.1161/CIRCULATIONAHA.106.617613

Butters, T. D., Aslanidi, O. V., Inada, S., Boyett, M. R., Hancox, J. C., Lei, M., et al. (2010). Mechanistic links between Na+ channel (SCN5A) mutations and impaired cardiac pacemaking in sick sinus syndrome. *Circ. Res.* 107, 126–137. doi: 10.1161/CIRCRESAHA.110.219949

Cai, D., Winslow, R. L., and Noble, D. (1994). Effects of gap junction conductance on dynamics of sinoatrial node cells: two-cell and large-scale network models. *IEEE Trans. Biomed. Eng.* 41, 217–231. doi: 10.1109/10.284940

Cho, H. C., and Marban, E. (2010). Biological therapies for cardiac arrhythmias: can genes and cells replace drugs and devices? *Circ. Res.* 106, 674–685. doi: 10.1161/CIRCRESAHA.109.212936

Delgado, C., Steinhaus, B., Delmar, M., Chialvo, D. R., and Jalife, J. (1990). Directional differences in excitability and margin of safety for propagation in sheep ventricular epicardial muscle. *Circ. Res.* 67, 97–110. doi: 10.1161/01.RES.67.1.97

Dobrzynski, H., Boyett, M. R., and Anderson, R. H. (2007). New insights into pacemaker activity: promoting understanding of sick sinus syndrome. *Circulation* 115, 1921–1932. doi: 10.1161/CIRCULATIONAHA.106.616011

Dobrzynski, H., Li, J., Tellez, J., Greener, I. D., Nikolski, V. P., Wright, S. E., et al. (2005). Computer three-dimensional reconstruction of the sinoatrial node. *Circulation* 111, 846–854. doi: 10.1161/01.CIR.0000152100.04087.DB

Fast, V. G., and Kleber, A. G. (1995). Block of impulse propagation at an abrupt tissue expansion: evaluation of the critical strand diameter in 2- and 3-dimensional computer models. *Cardiovasc. Res.* 30, 449–459. doi: 10.1016/S0008-6363(95)00071-2

Fedorov, V. V., Glukhov, A. V., and Chang, R. (2012). Conduction barriers and pathways of the sinoatrial pacemaker complex: their role in normal rhythm and atrial arrhythmias. *Am. J. Physiol. Heart Circ. Physiol.* 302, H1773–H1783. doi: 10.1152/ajpheart.00892.2011

Fedorov, V. V., Glukhov, A. V., Chang, R., Kostecki, G., Aferol, H., Hucker, W. J., et al. (2010). Optical mapping of the isolated coronary-perfused human sinus node. *J. Am. Coll. Cardiol.* 56, 1386–1394. doi: 10.1016/j.jacc.2010.03.098

Fedorov, V. V., Schuessler, R. B., Hemphill, M., Ambrosi, C. M., Chang, R., Voloshina, A. S., et al. (2009). Structural and functional evidence for discrete exit pathways that connect the canine sinoatrial node and atria. *Circ. Res.* 104, 915–923. doi: 10.1161/CIRCRESAHA.108.193193

Glynn, P., Onal, B., and Hund, T. J. (2014). Cycle length restitution in sinoatrial node cells: a theory for understanding spontaneous action potential dynamics. *PLoS ONE* 9:e89049. doi: 10.1371/journal.pone.0089049

Hu, Y. F., Dawkins, J. F., Cho, H. C., Marban, E., and Cingolani, E. (2014). Biological pacemaker created by minimally invasive somatic reprogramming in pigs with complete heart block. *Sci. Transl. Med.* 6, 245ra294. doi: 10.1126/scitranslmed.3008681

Inada, S., Zhang, H., Tellez, J. O., Shibata, N., Nakazawa, K., Kamiya, K., et al. (2014). Importance of gradients in membrane properties and electrical coupling in sinoatrial node pacing. *PLoS ONE* 9:e94565. doi: 10.1371/journal.pone.0094565

Joyner, R. W., Kumar, R., Golod, D. A., Wilders, R., Jongsma, H. J., Verheijck, E. E., et al. (1998). Electrical interactions between a rabbit atrial cell and a nodal cell model. *Am. J. Physiol.* 274, H2152–H2162.

Joyner, R. W., Sugiura, H., and Tan, R. C. (1991). Unidirectional block between isolated rabbit ventricular cells coupled by a variable resistance. *Biophys. J.* 60, 1038–1045. doi: 10.1016/S0006-3495(91)82141-5

Joyner, R. W., and Van Capelle, F. J. (1986). Propagation through electrically coupled cells. How a small SA node drives a large atrium. *Biophys. J.* 50, 1157–1164. doi: 10.1016/S0006-3495(86)83559-7

Keith, A., and Flack, M. (1907). The form and nature of the muscular connections between the primary divisions of the vertebrate heart. *J. Anat. Physiol.* 41, 172–189.

Kirchhof, C. J., Bonke, F. I., Allessie, M. A., and Lammers, W. J. (1987). The influence of the atrial myocardium on impulse formation in the rabbit sinus node. *Pflugers Arch.* 410, 198–203. doi: 10.1007/BF00581916

Kleber, A. G., and Rudy, Y. (2004). Basic mechanisms of cardiac impulse propagation and associated arrhythmias. *Physiol. Rev.* 84, 431–488. doi: 10.1152/physrev.00025.2003

Kleber, A. G., and Saffitz, J. E. (2014). Role of the intercalated disc in cardiac propagation and arrhythmogenesis. *Front. Physiol.* 5:404. doi: 10.3389/fphys.2014.00404

Kodama, I., and Boyett, M. R. (1985). Regional differences in the electrical activity of the rabbit sinus node. *Pflugers Arch.* 404, 214–226. doi: 10.1007/BF00581242

Lakatta, E. G., Maltsev, V. A., and Vinogradova, T. M. (2010). A coupled SYSTEM of intracellular Ca^{2+} clocks and surface membrane voltage clocks controls the timekeeping mechanism of the heart's pacemaker. *Circ. Res.* 106, 659–673. doi: 10.1161/CIRCRESAHA.109.206078

Lou, Q., Hansen, B. J., Fedorenko, O., Csepe, T. A., Kalyanasundaram, A., Li, N., et al. (2014). Upregulation of adenosine A1 receptors facilitates sinoatrial node dysfunction in chronic canine heart failure by exacerbating nodal conduction abnormalities revealed by novel dual-sided intramural optical mapping. *Circulation* 130, 315–324. doi: 10.1161/CIRCULATIONAHA.113.007086

Luo, M., Guan, X., Di, L., Kutschke, W., Gao, Z., Yang, J., et al. (2013). Diabetes increases mortality after myocardial infarction by oxidizing CaMKII. *J. Clin. Invest.* 123, 1262–1274. doi: 10.1172/JCI65268

Makiyama, T., Akao, M., Tsuji, K., Doi, T., Ohno, S., Takenaka, K., et al. (2005). High risk for bradyarrhythmic complications in patients with Brugada syndrome caused by SCN5A gene mutations. *J. Am. Coll. Cardiol.* 46, 2100–2106. doi: 10.1016/j.jacc.2005.08.043

Mangoni, M. E., and Nargeot, J. (2008). Genesis and regulation of the heart automaticity. *Physiol. Rev.* 88, 919–982. doi: 10.1152/physrev.00018.2007

Miake, J., Marban, E., and Nuss, H. B. (2002). Biological pacemaker created by gene transfer. *Nature* 419, 132–133. doi: 10.1038/419132b

Morley, G. E., Danik, S. B., Bernstein, S., Sun, Y., Rosner, G., Gutstein, D. E., et al. (2005). Reduced intercellular coupling leads to paradoxical propagation across the Purkinje-ventricular junction and aberrant myocardial activation. *Proc. Natl. Acad. Sci. U.S.A.* 102, 4126–4129. doi: 10.1073/pnas.0500881102

Munshi, N. V., and Olson, E. N. (2014). Translational medicine. improving cardiac rhythm with a biological pacemaker. *Science* 345, 268–269. doi: 10.1126/science.1257976

Nikolaidou, T., Aslanidi, O. V., Zhang, H., and Efimov, I. R. (2012). Structure-function relationship in the sinus and atrioventricular nodes. *Pediatr. Cardiol.* 33, 890–899. doi: 10.1007/s00246-012-0249-0

Oren, R. V., and Clancy, C. E. (2010). Determinants of heterogeneity, excitation and conduction in the sinoatrial node: a model study. *PLoS Comput. Biol.* 6:e1001041. doi: 10.1371/journal.pcbi.1001041

Rohr, S., Kucera, J. P., Fast, V. G., and Kleber, A. G. (1997). Paradoxical improvement of impulse conduction in cardiac tissue by partial cellular uncoupling. *Science* 275, 841–844. doi: 10.1126/science.275.5301.841

Rohr, S., Kucera, J. P., and Kleber, A. G. (1998). Slow conduction in cardiac tissue, I: effects of a reduction of excitability versus a reduction of electrical coupling on microconduction. *Circ. Res.* 83, 781–794. doi: 10.1161/01.RES.83.8.781

Rosen, M. R. (2014). Gene therapy and biological pacing. *N. Engl. J. Med.* 371, 1158–1159. doi: 10.1056/NEJMcibr1408897

Rosen, M. R., Robinson, R. B., Brink, P. R., and Cohen, I. S. (2011). The road to biological pacing. *Nat. Rev. Cardiol.* 8, 656–666. doi: 10.1038/nrcardio.2011.120

Sanchez-Quintana, D., Cabrera, J. A., Farre, J., Climent, V., Anderson, R. H., and Ho, S. Y. (2005). Sinus node revisited in the era of electroanatomical mapping and catheter ablation. *Heart* 91, 189–194. doi: 10.1136/hrt.2003.031542

Sanders, P., Kistler, P. M., Morton, J. B., Spence, S. J., and Kalman, J. M. (2004). Remodeling of sinus node function in patients with congestive heart failure: reduction in sinus node reserve. *Circulation* 110, 897–903. doi: 10.1161/01.CIR.0000139336.69955.AB

Shaw, R. M., and Rudy, Y. (1997). Ionic mechanisms of propagation in cardiac tissue. Roles of the sodium and L-type calcium currents during reduced excitability and decreased gap junction coupling. *Circ. Res.* 81, 727–741. doi: 10.1161/01.RES.81.5.727

Swaminathan, P. D., Purohit, A., Soni, S., Voigt, N., Singh, M. V., Glukhov, A. V., et al. (2011). Oxidized CaMKII causes sinus node dysfunction in mice. *J. Clin. Invest.* 121, 3277–3288. doi: 10.1172/JCI57833

Talano, J. V., Euler, D., Randall, W. C., Eshaghy, B., Loeb, H. S., and Gunnar, R. M. (1978). Sinus node dysfunction. An overview with emphasis on autonomic and pharmacologic consideration. *Am. J. Med.* 64, 773–781. doi: 10.1016/0002-9343(78)90516-8

Ten Velde, I., De Jonge, B., Verheijck, E. E., Van Kempen, M. J., Analbers, L., Gros, D., et al. (1995). Spatial distribution of connexin43, the major cardiac gap junction protein, visualizes the cellular network for impulse propagation from sinoatrial node to atrium. *Circ. Res.* 76, 802–811. doi: 10.1161/01.RES.76.5.802

Thery, C., Gosselin, B., Lekieffre, J., and Warembourg, H. (1977). Pathology of sinoatrial node. Correlations with electrocardiographic findings in 111 patients. *Am. Heart J.* 93, 735–740. doi: 10.1016/S0002-8703(77)80070-7

Tse, H. F., Xue, T., Lau, C. P., Siu, C. W., Wang, K., Zhang, Q. Y., et al. (2006). Bioartificial sinus node constructed via *in vivo* gene transfer of an engineered pacemaker HCN Channel reduces the dependence on electronic

pacemaker in a sick-sinus syndrome model. *Circulation* 114, 1000–1011. doi: 10.1161/CIRCULATIONAHA.106.615385

Veldkamp, M. W., Wilders, R., Baartscheer, A., Zegers, J. G., Bezzina, C. R., and Wilde, A. A. (2003). Contribution of sodium channel mutations to bradycardia and sinus node dysfunction in LQT3 families. *Circ. Res.* 92, 976–983. doi: 10.1161/01.RES.0000069689.09869.A8

Verheijck, E. E., Wessels, A., Van Ginneken, A. C., Bourier, J., Markman, M. W., Vermeulen, J. L., et al. (1998). Distribution of atrial and nodal cells within the rabbit sinoatrial node: models of sinoatrial transition. *Circulation* 97, 1623–1631. doi: 10.1161/01.CIR.97.16.1623

Wang, Y., and Rudy, Y. (2000). Action potential propagation in inhomogeneous cardiac tissue: safety factor considerations and ionic mechanism. *Am. J. Physiol. Heart Circ. Physiol.* 278, H1019–H1029.

Watanabe, E. I., Honjo, H., Anno, T., Boyett, M. R., Kodama, I., and Toyama, J. (1995). Modulation of pacemaker activity of sinoatrial node cells by electrical load imposed by an atrial cell model. *Am. J. Physiol.* 269, H1735–H1742.

Wolf, R. M., Glynn, P., Hashemi, S., Zarei, K., Mitchell, C. C., Anderson, M. E., et al. (2013). Atrial fibrillation and sinus node dysfunction in human ankyrin-B syndrome: a computational analysis. *Am. J. Physiol. Heart Circ. Physiol.* H1253–H1266. doi: 10.1152/ajpheart.00734.2012

Zhang, H., Holden, A. V., and Boyett, M. R. (2001). Gradient model versus mosaic model of the sinoatrial node. *Circulation* 103, 584–588. doi: 10.1161/01.CIR.103.4.584

Zhang, H., Lau, D. H., Shlapakova, I. N., Zhao, X., Danilo, P., Robinson, R. B., et al. (2011). Implantation of sinoatrial node cells into canine right ventricle: biological pacing appears limited by the substrate. *Cell Transplant.* 20, 1907–1914. doi: 10.3727/096368911X565038

Zhang, H., Zhao, Y., Lei, M., Dobrzynski, H., Liu, J. H., Holden, A. V., et al. (2007). Computational evaluation of the roles of Na^+ current, I_{Na}, and cell death in cardiac pacemaking and driving. *Am. J. Physiol. Heart Circ. Physiol.* 292, H165–H174. doi: 10.1152/ajpheart.01101.2005

Conflict of Interest Statement: The Associate Editor George E. Billman declares that, despite having collaborated with author Thomas J. Hund, the review process was handled objectively and no conflict of interest exists. The authors declare that the research was conducted in the absence of any commercial or financial relationships that could be construed as a potential conflict of interest.

Received: 12 October 2014; accepted: 31 October 2014; published online: 26 November 2014.

Citation: Unudurthi SD, Wolf RM and Hund TJ (2014) Role of sinoatrial node architecture in maintaining a balanced source-sink relationship and synchronous cardiac pacemaking. Front. Physiol. ***5****:446. doi: 10.3389/fphys.2014.00446*

This article was submitted to Cardiac Electrophysiology, a section of the journal Frontiers in Physiology.

frontiers in PHYSIOLOGY

REVIEW ARTICLE
published: 03 November 2014
doi: 10.3389/fphys.2014.00424

Remodeling of cardiac passive electrical properties and susceptibility to ventricular and atrial arrhythmias

Stefan Dhein[1]*†, Thomas Seidel[2†], Aida Salameh[3], Joanna Jozwiak[4], Anja Hagen[5], Martin Kostelka[1], Gerd Hindricks[4] and Friedrich-Wilhelm Mohr[1]

[1] Clinic for Cardiac Surgery, Heart Center Leipzig, University Leipzig, Leipzig, Germany
[2] Nora Eccles Harrison Cardiovascular Research and Training Institute, University of Utah, Salt Lake City, UT, USA
[3] Clinic for Pediatric Cardiology, Heart Center Leipzig, University Leipzig, Leipzig, Germany
[4] Clinic for Cardiology, Heart Center Leipzig, University Leipzig, Leipzig, Germany
[5] Hospital for Children and Adolescents, University of Leipzig, Leipzig, Germany

Edited by:
George E. Billman, The Ohio State University, USA

Reviewed by:
Candido Cabo, City University of New York, USA
Hugh Clements-Jewery, West Virginia School of Osteopathic Medicine, USA

***Correspondence:**
Stefan Dhein, Clinic for Cardiac Surgery, Heart Center Leipzig, University of Leipzig, Struempellstr. 39, 04289 Leipzig, Germany
e-mail: stefan.dhein@medizin.uni-leipzig.de

† *These authors have contributed equally to this work.*

Coordinated electrical activation of the heart is essential for the maintenance of a regular cardiac rhythm and effective contractions. Action potentials spread from one cell to the next via gap junction channels. Because of the elongated shape of cardiomyocytes, longitudinal resistivity is lower than transverse resistivity causing electrical anisotropy. Moreover, non-uniformity is created by clustering of gap junction channels at cell poles and by non-excitable structures such as collagenous strands, vessels or fibroblasts. Structural changes in cardiac disease often affect passive electrical properties by increasing non-uniformity and altering anisotropy. This disturbs normal electrical impulse propagation and is, consequently, a substrate for arrhythmia. However, to investigate how these structural changes lead to arrhythmias remains a challenge. One important mechanism, which may both cause and prevent arrhythmia, is the mismatch between current sources and sinks. Propagation of the electrical impulse requires a sufficient source of depolarizing current. In the case of a mismatch, the activated tissue (source) is not able to deliver enough depolarizing current to trigger an action potential in the non-activated tissue (sink). This eventually leads to conduction block. It has been suggested that in this situation a balanced geometrical distribution of gap junctions and reduced gap junction conductance may allow successful propagation. In contrast, source-sink mismatch can prevent spontaneous arrhythmogenic activity in a small number of cells from spreading over the ventricle, especially if gap junction conductance is enhanced. Beside gap junctions, cell geometry and non-cellular structures strongly modulate arrhythmogenic mechanisms. The present review elucidates these and other implications of passive electrical properties for cardiac rhythm and arrhythmogenesis.

Keywords: electrical propagation, passive electrical properties, cardiac tissue, gap junction, connexin, anisotropy, inhomogeneity, cable theory

INTRODUCTION

Although the heart can be considered as a simple mechanical pump, this pump is a highly complex system involving mechanical, electrical, active, passive, and endocrine factors. Many of these factors are subject to remodeling processes in cardiac disease and, thus, are not necessarily constant. This review focuses on remodeling of the passive electrical properties of the heart and its importance for arrhythmogenesis.

Passive electrical properties of cardiac tissue comprise the specific resistance of intracellular and extracellular spaces as well as membrane capacitance. These are strongly influenced by tissue structure. This involves size, shape and arrangement of cardiac cells, including myocytes and non-myocytes, as well as connective tissue, extracellular and intracellular volume conductors and gap junctions. Moreover, anisotropy and inhomogeneities in the spatial (or in some cases temporal) distribution of these factors are of importance.

Electrical anisotropy in the heart refers to differing specific resistances in longitudinal and transverse fiber direction. The elongated shape of myocytes and intercellular coupling mainly at cell poles result in lower longitudinal than transverse resistance. This applies both to the extra- and intracellular space. Spatial inhomogeneities in cardiac tissue, e.g., zones with enhanced deposition of collagen, (fibrosis, which increases with age), lead to a spatial variation of these resistances, which is referred to as non-uniformity. In consequence, cardiac tissue can be considered as non-uniform and anisotropic.

A simple model of the electrical equivalent circuit of cardiac tissue is a cable formed by cells coupled in series via Ohmic resistors. Each cell in this cable represents a resistor with a parallel capacitor (for review see Weidmann, 1990). The change in voltage is a function of distance (x) according to $V_x = V_0 \exp(-x/\lambda)$ with the length constant $\lambda = \sqrt{(r_m/r_i)}$. The membrane resistance, r_m, is expressed in Ωcm, the intracellular longitudinal resistance,

r_i, in Ω/cm. The input resistance at $x = 0$ can be described as $r_{input} = V_0/I = r_i\lambda$. Due to the fiber geometry with radius a, the specific membrane resistance R_m equals $2\ \pi a r_m$ [Ωcm^2] and specific intracellular resistance $R_i = \pi a^2 r_i$ [Ωcm]. The specific membrane capacitance can be described as $C_m = \tau/R_m$ with the time constant τ. In a multicellular preparation with parallel running fibers the longitudinal resistance of the extracellular space r_o also has to be considered. For these conditions λ is reflected by $\lambda = \sqrt{(r_m/(r_i + r_o))}$ and the conduction velocity θ depends on $\theta = \sqrt{(1/(\tau_{foot} C_m (r_i + r_o))}$. This cable theory was originally formulated for nerve axons (Hodgkin and Rushton, 1946) and later on for Purkinje fibers (Weidmann, 1952). It holds true for a continuous cable (**Figure 1**).

However, this is oversimplifying, since the intracellular space of adjacent cells is connected via gap junction channels. A cluster of single gap junction channels forms a gap junction, which connects the cytoplasm of two adjacent cells by the resistance R_{GJ} (see **Figure 2**). The gap junction resistance is higher than the resistance of the cytoplasm. Furthermore, the resistance r_o of the extracellular space is not homogeneous. The resistance R_{cleft} of the extracellular cleft between two cells near intercalated disks (2–5 nm wide) can be assumed to differ significantly from the much wider clefts elsewhere (>20 nm) not only because of its small width, but also because it contains anchoring proteins and gap junction channels. Therefore, the cable necessarily becomes discontinuous (**Figure 2**).

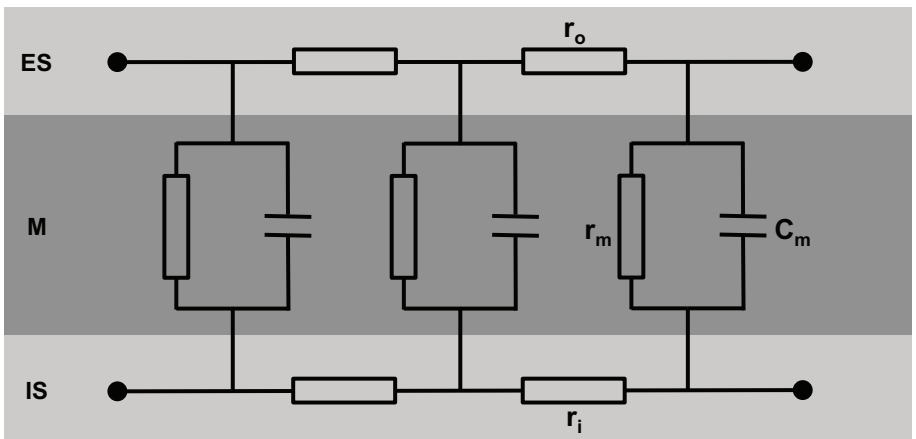

FIGURE 1 | Schematic view of cardiac tissue modeled as a simple cable consisting of intracellular (r_i) and extracellular (r_o) resistors and capacitors (C_m). ES, extracellular space; M, cell membrane; IS, intracellular space.

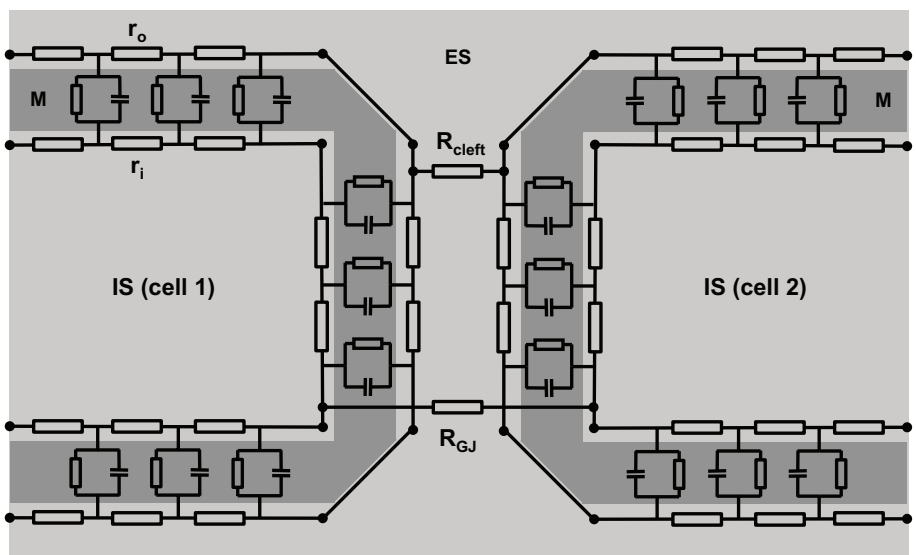

FIGURE 2 | A more realistic scheme of coupled cardiac cells considering discontinuous properties. The cell membrane (M) is represented by a series of resistor-capacitor circuits, connecting the extracellular space (ES) with the intracellular space (IS). They are interconnected within one cell via extracellular (r_o) and intracellular (r_i) resistors. Gap junction resistance (R_{GJ}) connects the intracellular spaces of adjacent cells, while extracellular coupling is realized via the resistance of the extracellular cleft (R_{cleft}).

Fast sodium channels are essential for impulse propagation. Opening of these channels at the beginning of an action potential generates a depolarizing current (I_{Na}), which is responsible for the fast voltage upstroke. Therefore, I_{Na} plays a key role in the propagation of action potentials from cell to cell. It has been shown that these sodium channels are clustered at cell-cell contact zones (Kucera et al., 2002; Maier et al., 2004). This further complicates a correct description of the electrophysiological behavior at cell poles. It also shows that modeling cardiac tissue as a continuum is only reasonable on a macroscopic scale.

Although the equivalent circuit of a discontinuous cable depicted in **Figure 2** is more complex than the simple cable, it remains an oversimplification because it does not reflect the geometrical properties of cells and tissue. Cardiomyocytes are typically not shaped like bricks or regular cylinders—as often assumed in mathematical tissue models—but, instead, are of irregular shape with branches interdigitating at the cell poles (Spach et al., 2000). Additionally, cell size shows some variation.

In this regard, it is important to consider the ratio between the cell surface A_m and the gap junction conductance g_{GJ} (Seidel et al., 2010): increased diameter of the cell can enhance longitudinal propagation velocity θ_L if g_{GJ} is enhanced proportionally to A_m. If g_{GJ} remains constant, however, increased diameter reduces θ_L. This becomes clear when considering that A_m is linearly related to the cell capacitance C_m. Thus, it is important to analyze the ratio of g_{GJ}/A_m in order to understand whether a change in cell size will enhance or reduce θ_L. Furthermore, transverse g_{GJ} may contribute to longitudinal propagation, which cannot be described by a one-dimensional model (Seidel et al., 2010).

Next, we need to consider the three-dimensional nature of the myocardium and the uneven distribution of fibrotic material, mostly collagen fibers, and fibroblasts. Initially, fibroblasts have been considered electrically silent, but research in the past two decades indicates that electrical propagation seems possible. It has been suggested that myofibroblasts can slow conduction (Rohr, 2004, 2012). Furthermore, it has been shown experimentally that impulse propagation along fibroblast inserts was successful over distances up to 300 μm (Gaudesius et al., 2003). However, it needs to be noted that these cells—although not capable of producing action potentials—were coupled via gap junction channels (see below), while HeLa cells without gap junctions did not enable propagation. Thus, it seems that communication-deficient zones will cause propagation failure.

HOW ARE CARDIAC CELLS COUPLED?

Since the discovery of cardiac gap junctions, which form intercellular channels connecting the cytoplasm of adjacent myocytes, it is established that they represent a low-resistance pathway for electrical propagation (Page and Shibata, 1981). However, gap junction resistance is still higher than the cytoplasmic resistance. Accordingly, impulse propagation along the membrane of one cell is faster than over the intercellular gap junction. The time delay at gap junctions is about 0.21–0.27 ms, and ∼0.05–0.1 ms at the cell membrane (Fast and Kléber, 1993; Hubbard et al., 2007).

COUPLING WITHOUT GAP JUNCTIONS

If one considers neighbored cells as closely packed capacitors, ephaptic coupling via electrical fields might be possible (Sperelakis, 1979). Electrical field coupling (Sperelakis and Mann, 1977) or ephaptic coupling (Copene and Keener, 2008) refers to the initiation of an action potential in a non-activated downstream cell by the electrical field caused by an activated upstream cell. This kind of impulse propagation does not require cytoplasmic connections via gap junctions. It might occur at the intercalated disks, where the membranes of adjacent cells are only 2–5 nm apart.

Accumulation of K^+ in the junctional extracellular cleft seems necessary to allow sodium channels at the intercalated disk of the upstream cell to fire some microseconds earlier than the channels in the remaining surface membrane. In a theoretical model, this was necessary for effective coupling (Sperelakis and Mann, 1977). However, at present it is unclear whether ephaptic coupling contributes to action potential propagation in normal tissue. Computer simulation studies indicate that, under certain conditions, ephaptic coupling may play a role, but strongly depends on parameters like sodium channel conductance and distribution, and the width of the extracellular cleft at the intercalated disk (Mori et al., 2008; Lin and Keener, 2010). Recent data show that in the perinexus Cx43 gap junctions interact with Na(v)1.5 channels (Rhett et al., 2012). The perinexus has therefore been suggested as the anatomical correlate for ephaptic coupling, the ephapse (Rhett et al., 2013; Veeraraghavan et al., 2014). Local accumulation and shifts of ions may alter local membrane potential. However, there is a lack of experimental evidence, because these local changes on a nanometer scale are difficult to measure. Hence, it remains unclear whether ephaptic coupling significantly contributes to cardiac impulse propagation, especially when considering that, according to the Guoy-Chapman theory, the electrical field near a charged membrane falls to zero within 2–3 nm (Carnie and McLaughlin, 1983).

Experimental evidence suggests that cells need to be coupled by gap junctions to allow the propagation of an electrical impulse: Weingart and Maurer (1988) showed that after manipulating two cells into intimate side-to-side contact, initially there was no transmission of electrotonic potentials or action potentials from one cell to the other. Action potential transfer became possible only after the cells had established new gap junctions. This experiment seems to rule out non-gap junctional mechanisms of intercellular action potential spreading. However, recent evidence was presented for another mechanism of electrical cell-to-cell coupling. Membrane-tunneling nanotubues were suggested as cytosolic bridges between cells (He et al., 2011). This theory, however, still needs further investigation.

CONNEXINS AND GAP JUNCTIONS

Cardiomyocytes and fibroblasts are homocellularly interconnected by gap junction channels (for review see Dhein, 1998, 2004). Heterocellular coupling between cardiomyocytes and fibroblasts, however, has only been shown in cell culture (Goshima and Tonomura, 1969; Gaudesius et al., 2003) or in the sinus node (Camelliti et al., 2004), but not in living ventricular myocardium. Cells can communicate via these gap junction

channels. Each channel is about 150 Å long. The membranes of the two cells are separated in this area by a gap of nearly 20 Å, which is spanned by the channel subunits (Beyer et al., 1995). Cardiomyocytes are connected by intercalated disks, which contain three main structures: the fascia adherens, the desmosome (sometimes called macula adherens), and the nexus. While the fascia adherens is composed of two lipid bilayers separated by 200–300 Å, the desmosome is an almost laminated structure formed by the two membranes. At the nexus both cells are in most intimate contact. This zone contains the gap junction channels, which typically are clustered (Gourdie et al., 1990). A gap junction channel comprises of two hemichannels, which are provided by either cell. Each hemichannel is composed of 6 protein subunits, the connexins. Thus, a gap junction channel is a dodecameric channel with a pore in the center (**Figure 3**). Connexins belong to a large protein family with at least 21 isoforms in humans. The connexin protein is a four-transmembrane domain protein with an intracellular N- and C-terminal, 2 extracellular loops, and one intracellular loop. For details see Makowski et al. (1977); Chen et al. (1989); Perkins et al. (1997). The most variant part is the C-terminus, which also serves as binding partner for a number of protein kinases, which can control connexin trafficking, assembly, dis-assembly and single channel conductance by phosphorylation. Connexins are characterized by their molecular weight. For instance, Cx43 refers to the connexin with a molecular weight of 43 kDa. The family of connexins is divided with regard to the amino acid sequences and C-terminal length into five subgroups, i.e., α, β, γ, δ, and ε. The genetic names are composed of a "GJ" followed by the family and a number. Thus, Gjα1 means Cx43 which was the first connexin being characterized from the α-group (see http://www.genenames.org/genefamily/gj.php for reference). For a detailed overview on connexins (see Nielsen et al., 2012).

In the heart the predominant connexin isoform is Cx43, which is found in ventricles and atria. Cx40 is mainly found in atrium and in the specific conduction system. Cx45 is mainly found in early developmental stages, in the conduction system, and between fibroblasts and cardiomyocytes. Connexins are synthesized in the rough endoplasmatic reticulum, folded and transported to the trans Golgi network, where they are oligomerized to hexameric hemichannels (connexons). These hexameres are then transported to the plasma membrane and inserted. It is assumed that they flow with lipid rafts within the membrane and accumulate in areas where N-cadherin and zonula occludens-1 protein (ZO-1) are present. At these sites they dock to other hexameres of the neighboring cell forming the gap junction channel. If the connexins are poly-phosphorylated at certain amino acids of the C-terminal, they can be ubiquitinylated and then degraded. Besides the classical proteosomal degradation lysosomal degradation also has been described.

Regulation of gap junction coupling can be realized by modulating the number of channels, i.e., by influencing synthesis, trafficking docking or degradation, or by changes of the single channel conductance. For a detailed review, see Dhein (2004); Salameh and Dhein (2005); Axelsen et al. (2013). Channel conductance depends on the connexin isoform, the phosphorylation state of the connexin, and on the connexin composition of the channel (e.g., homomeric, heteromeric) (Harris, 2001; Moreno, 2004). Interestingly, besides an open and a closed state a single channel can exhibit several conductance states (Harris, 2001; Bukauskas and Verselis, 2004). Moreover, heterotypic channels consisting of hemichannels of different connexin isoforms can show asymmetric voltage-dependent gating. Asymmetric gating refers to the observation that the conductance-to-voltage relationship depends on the polarity of the transjunctional voltage (see e.g., Bukauskas and Verselis, 2004; Schulte et al., 2008).

ANISOTROPY AND NON-UNIFORMITY (INHOMOGENEITY)

Anisotropy is defined as the property of being directionally dependent. With regard to cardiac tissue the term is mostly used

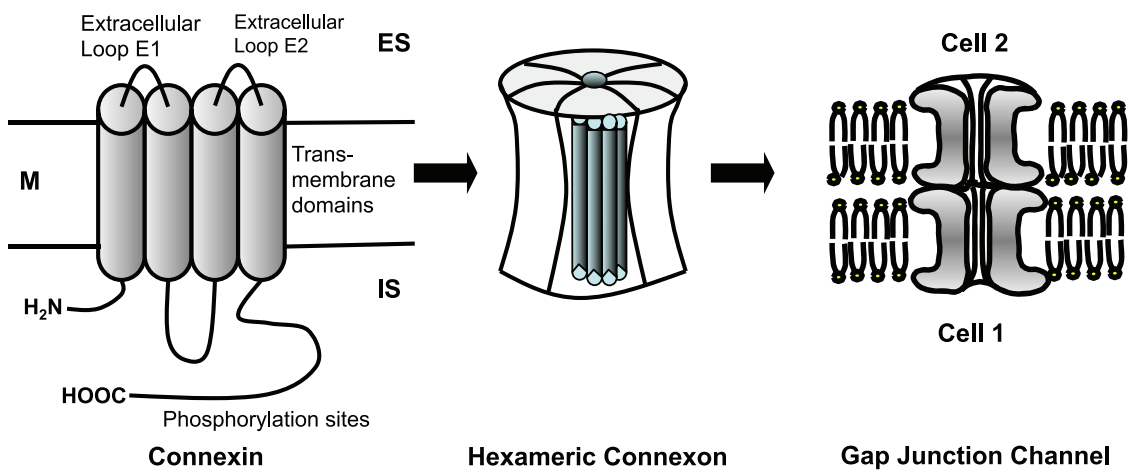

FIGURE 3 | Connexins are four-transmembrane proteins with two extracellular loops and one intracellular loop. They build hexameric connexons (hemichannels), which dock to a connexon of an adjacent cell forming a complete, dodecameric gap junction channel. M, cell membrane; ES, extracellular space; IS, intracellular space.

to describe that specific longitudinal resistivity is lower than transverse resistivity. However, anisotropy values for extracellular and intracellular resistivity differ significantly. Further properties to be taken into account are discontinuity, which means that the fibers are separated by intercalated disks (in contrast to a continuous cable), and non-uniformity, which describes the spatial variation of anisotropy. The latter is due to variations in cellular morphology, cell types (myocytes and non-myocytes) and fibrotic material (collagen) or other non-conducting structures like connective tissue, fat, vessels etc. The difference between uniform and non-uniform anisotropy has many consequences for the pathophysiology of arrhythmia (Spach and Dolber, 1990).

Intracellular resistivity is higher in transverse than in longitudinal direction. Thus, anisotropy in the intracellular space ranges from ∼5 to 10 (Clerc, 1976; Roberts and Scher, 1982; Stinstra et al., 2005) and mainly results from cardiomyocyte shape and cellular distribution of connexins. In many cardiac diseases the expression of connexins (Cx43, Cx40, Cx45) is altered. Enhanced levels of Cx43 have been found in cardiac hypertrophy, while in chronic infarction and severe heart failure Cx43 levels are reduced (Severs, 1994; Kostin et al., 2003; Severs et al., 2006). Alterations of Cx43 and Cx40 have been described in atrial fibrillation (Dupont et al., 2001; Polontchouk et al., 2001; Boldt et al., 2003). Since in atrial fibrillation both increased and decreased Cx43 levels have been found, it was suggested that the absolute level may depend not only on the type of arrhythmia but also on the concomitant cardiac pathology (Dhein et al., 2011). In many cardiac pathologies, e.g., chronic atrial fibrillation, cardiac hypertrophy, heart failure and after myocardial infarction, connexins were no longer restricted to cell poles but also expressed at the lateral cell membrane (Polontchouk et al., 2001; Kostin et al., 2002; Cabo et al., 2006). It remained unclear for years whether these lateral gap junctions are functional. In the case of atrial fibrillation, electrophysiological mapping together with immunohistology showed that the lateralization was accompanied by enhanced transverse conduction velocity θ_T (Dhein et al., 2011), suggesting that at least a fraction of these lateral gap junctions is functional.

The concept of electrical anisotropy also applies to resistivity of the extracellular space and, besides influencing impulse propagation, has a strong effect on the distribution of epicardial potentials (Roberts and Scher, 1982; Johnston et al., 2001; Stinstra et al., 2005; Schwab et al., 2013). Experimental and computational studies reported anisotropies in the extracellular space ranging from 1.5 to 3.5 (Clerc, 1976; Roberts et al., 1979; Stinstra et al., 2005; Hand et al., 2009). Schwab et al. (2013) distinguished between the two transverse directions (vertical or parallel to the epicardial surface) suggesting differences in anisotropy and pathological remodeling. Their results also indicate spatially non-uniform anisotropy in ventricular myocardium after infarction.

Evidence is growing that the extracellular space, including fibroblasts, plays an important role in cardiac disease and related electrophysiological changes for review see Pellman et al. (2010); Yue et al. (2011); Weber et al. (2013). This is also reflected in the use of bi-domain or multi-domain models for the simulation of cardiac impulse propagation, taking extracellular conductivity and fibroblasts into account (Jack et al., 1975; Peskoff, 1979; Geselowitz and Miller, 1983; Roberts et al., 2008; Sachse et al., 2009). The group of Veeraraghavan et al. (2012) suggested that the effect of gap junction conductance on impulse propagation is modulated by the fraction of extracellular space. They showed that the percentage of extracellular volume was inversely correlated to conduction velocity. This result is surprising because increased extracellular volume should result in lower extracellular resistivity and, according to cable theory, lead to faster propagation. They found that these effects were especially pronounced in transverse fiber direction. However, to increase extracellular volume they used mannitol, which also reduced cell width. A reduction in cell width, however, can strongly slow transverse velocity (Seidel et al., 2010; Toure and Cabo, 2010). Furthermore, with decreasing velocity the effect of gradual uncoupling (higher gap junction resistance) increases because of a switch from continuous to discontinuous propagation, preferably in transverse fiber direction (Seidel et al., 2010). These results show that effects of intra- and extracellular space on impulse propagation are complex and not easy to predict. It remains challenging to measure extracellular conductance and anisotropy in intact cardiac tissue because due to transmembrane channels the measured current between two electrodes will always contain an intracellular component.

As a result of non-uniformity and anisotropy in cardiac tissue fractionated waveforms develop. These have been interpreted as the reflection of discontinuous propagation where each of the multiple negative peaks represents the activation of a small group of fibers (Spach and Dolber, 1986, 1990). Interestingly, aging leads to a change in the tissue's biophysical properties and is associated with increased non-uniformity. This is due to the deposition of collagen fibers between the cells resulting in predominant uncoupling of side-to-side connections (Spach and Dolber, 1986, 1990; Dhein and Hammerath, 2001).

SOURCE-SINK PROBLEM

When an action potential propagates, the action potential upstroke velocity and amplitude are larger in the case of transverse propagation together with a shorter time constant of the foot potential τ_{foot}. From a theoretical point of view this could mean that longitudinal propagation is more vulnerable to conduction block because of its lower upstroke velocity and amplitude. The increase in upstroke velocity in transverse propagation results from higher resistivity and reduced space constant in this direction. Thus, less current is lost to the neighboring cells (Delmar et al., 1987).

In order to elicit an action potential in a cell, it must receive a depolarizing current from an adjacent, activated cell. The activated cell acts as current source, while the non-activated cell is a current sink with the voltage difference being the driving force for this current. The current transfer is mainly realized via gap junction channels and, to some extent, via the extracellular space. Whether enough current can be transferred to activate a cell is a complex and geometric problem: if a small source (e.g., a tiny strand of activated cardiomyocytes) meets a large sink (e.g., a large area of non-activated cardiomyocytes) the current will flow radially from the activated site to many non-activated sites. Hence, the source current is distributed to many neighboring cells

and in each of these the accumulated charge may be too low to trigger an action potential. This will cause conduction failure (Rohr et al., 1997; Rohr, 2004, 2012; Lee and Pogwizd, 2006). In this situation a paradoxical effect can occur: reducing gap junction conductance may preserve conduction by resolving the source-sink mismatch because less current is lost to adjacent sites (Rohr et al., 1997). This is, e.g., realized in the sinus node, where a small current source (sinus node) meets a large sink (atrium). At the sinus node/atrium border there is only little expression of connexins in interdigitating finger-like zones extending from the sinus node into the atrium (Joyner and van Capelle, 1986; Boyett et al., 2006). This reduces the sink because only a small current can flow to a small number of activation sites. In cable theory, this is represented by a smaller space constant leading to a lower capacitive load. On the other hand, if there is high gap junction coupling, the space constant increases leading to a high capacitive load (current sink) and a source-sink mismatch which can evoke conduction failure.

Shaw and Rudy (1997a,b) attempted to describe these phenomena mathematically by the safety factor (SF) of propagation as $SF = Q_c + Q_{out}/Q_{in}$ (=charge produced/charge consumed). If coupling is reduced gradually the safety factor first is enhanced as a result of the smaller space constant. However, if very low levels of coupling are reached, SF decreases until SF <1 and conduction failure occurs. This happens when gap junctions are almost closed or absent, because then not enough current can be transferred to an adjacent cell before the activated cell repolarizes. In contrast, if I_{Na} is reduced this will result in a progressive reduction of SF. However, propagation velocity will be reduced in both situations (Shaw and Rudy, 1997a,b).

Situations with source-sink problems generally occur when the curvature of the propagating wave front is high. Accordingly, they may be found at the end of Purkinje fibers, during propagation through small isthmuses, around obstacles, and during spiral wave re-entry. Furthermore, source-sink mismatch may occur at the border between normal cardiac tissue and an ischemic zone, when depolarizing current flows into the ischemic region. Since this region is usually non-excitable, it will act as a current sink and, consequently, reduce conduction velocity.

ARRHYTHMOGENESIS

Many definitions of arrhythmias are based on comparing a pathological with the normal heart rhythm. Bradyarrhythmia is a rhythm slower than normal, while tachyarrhythmia is faster than normal. Bradyarrhythmias are often caused by a block or delay of conduction within the specific conduction system, i.e., between sinus node and atrium, between atrioventricular node and bundle of His or within the bundles. If in these structures conduction is impaired, e.g., by a scar resulting from infarction, this will lead to delayed ventricular activation. However, the situation can be more complex involving source-sink problems. As described above, the propagation of an action potential from Purkinje fibers to the working myocardium represents a tissue expansion, which is generally prone to conduction block (Rohr et al., 1997). Both high sodium channel conductance and relatively low intercellular coupling increase conduction safety under these conditions. However, pathological changes like gap junction lateralization or cellular hypertrophy (increased sink), and reduced sodium channel availability (decreased source) can lead to unidirectional conduction block (Kléber and Rudy, 2004; Seidel et al., 2010). If unidirectional block occurs in a Purkinje fiber, this will slow ventricular activation and lead to an abnormal activation pattern. This is part of the reason why Purkinje fibers are considered key players in initiation and maintenance of ventricular arrhythmias (for review, see e.g., Boyden et al., 2010). Besides, unidirectional block can lead to reentry circles resulting in ventricular tachycardia or fibrillation. Thus, bradyarrhythmia can evolve into tachyarrhythmia.

REENTRANT ACTIVATION

Reentry happens when the electrical activation follows a circular trajectory and is able to re-activate itself at the point of origin. It is a main cause of tachyarrhythmia. Several mechanisms for reentry are known. One common model is explained as follows: if at a bifurcation of the conducting system (e.g., the bifurcation in the anterior and posterior bundle branch) one branch acts as a unidirectional block, allowing conduction only from the periphery backwards, then activation may propagate along branch 2, thereafter across the ventricular muscle, and finally backwards via branch 1. The unidirectional block in this traditional consideration is thought to be caused by a prolonged refractory period in this area. Another classical example describes reentry as a wave which encircles an electrically inactive obstacle, e.g., a scar. This central zone can also be a permanently refractive area, steadily depolarized by the circulating wave, the "leading circle" (Allessie et al., 1977).

Detachment of the reentry wavefront from the obstacle can lead to spiral wave initiation. In this case, a usually non-stationary rotating source moves along a two- or three-dimensional trajectory. The waves initiated from this source show a typical spiral shape (Cabo et al., 1998). It has been shown that the trajectory of the spiral wave core and whether the wave is stable or not, depends strongly on tissue properties like excitability and non-uniformity (Pertsov et al., 1993).

A certain type of reentrant arrhythmia can originate from a situation in which two closely neighbored obstacles, e.g., collagenous strands or infarct scars, are located transverse to the direction of propagation, with only a small gap of low excitability in between. This structure forces the activation wave to circumvent the obstacles laterally. Behind, the tissue will be activated from both sides causing wavefront collision near the gap. The collision reduces the current sink and increases the source now allowing the activation to propagate through the gap and reactivate the area in front of the obstacles. This kind of reentry has been called "figure-of-eight" reentry mechanisms for ventricular arrhythmias. It may occur in particular when conduction velocity is low (el-Sherif et al., 1987; Lazzara, 1988). See **Figure 4** for illustration.

These explanations illustrate very well the observed phenomena, although underlying mechanisms may be a bit more complicated (see below).

CALCIUM-INDUCED DEPOLARIZATIONS

Under certain pathological conditions like increased adrenergic stimulation or ischemia-reperfusion, cellular calcium overload occurs, leading to spontaneous diastolic calcium waves. These

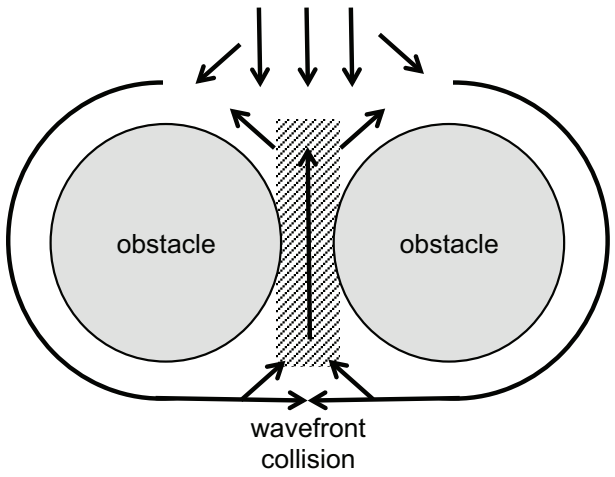

FIGURE 4 | Schematic illustration of a figure-of-eight reentry. A wavefront approaches two obstacles separated by a small gap of low excitability (gray area). Conduction is blocked in front of this gap, separating the wavefront. Behind the obstacles, wavefront collision occurs. This increases the current source while reducing the sink and, thus, allows activation of the area between the obstacles. If conduction is slow enough, this leads to reentry in front of the obstacles as shown by el-Sherif et al. (1987).

waves reflect spontaneous calcium release from the sarcoplasmic reticulum (Kimura et al., 1984; Marban et al., 1986). The sodium-calcium exchanger then operates in the forward mode generating a depolarizing current. The resulting increase of the membrane potential is often referred to as delayed afterdepolarization (DAD). DADs are considered as potential triggers for arrhythmia because, if big enough, they may initiate an action potential and, subsequently, arrhythmogenic ectopic extrasystoles (Lederer and Tsien, 1976; Xie et al., 2010). However, while it has been shown that a DAD can lead to an action potential in isolated cells (Capogrossi et al., 1987), it remains a matter of debate how a DAD in tissue can overcome the obvious source-sink mismatch (Xie et al., 2010; Tveito et al., 2012). A single cardiomyocyte is, on average, coupled to 4–6 adjacent cells. Under normal conditions, it is therefore impossible that an action potential is initiated. Here, the source-sink mismatch protects from arrhythmogenesis. To overcome the mismatch, there must be a reduced sink via uncoupling or an increased source via DAD synchronization between adjacent cells. Both mechanisms have been suggested to appear under conditions of gap-junctional remodeling (Morley et al., 2005) or adrenergic stimulation (Myles et al., 2012), respectively. Following this argumentation, enhanced coupling should increase the sink and may reduce the risk of arrhythmia. Interestingly, it was shown that the antiarrhythmic peptide AAP10 enhanced gap junction conductance and prevented from certain ventricular arrhythmia (Dhein et al., 1994; Müller et al., 1997; Jozwiak and Dhein, 2008; Hagen et al., 2009). This suggests that increasing gap junction conductance via drug therapy might be an effective strategy for certain forms of arrhythmia. Otherwise, closing of gap junctions could be a mechanism of cardiomyocytes to protect neighboring cells from further damage caused, e.g., by acidosis or calcium overload. It has been shown that gap-junction blockers like heptanol decrease the infarct size after myocardial ischemia (Miura et al., 2004). It is, therefore, surprising that the same effect was shown for gap junction openers like rotigaptide (Haugan et al., 2006), while other studies detected no influence on infarct size (Xing et al., 2003). Further research is required in this field to better understand these effects and to develop novel anti-arrhythmic drug therapies.

EFFECTS OF HYPERTROPHY

Cardiac hypertrophy is associated with electrophysiological remodeling and an elevated risk of severe arrhythmia (Tomaselli and Marbán, 1999; Kozhevnikov et al., 2002). This is partly due to changes in cellular electrophysiology like remodeling of potassium channels leading to increased action potential duration and elongated QT intervals (Beuckelmann et al., 1993; Swynghedauw et al., 2003). Whether isolated cellular hypertrophy has pro-arrhythmic effects is, therefore, hard to assess experimentally. However, mathematical models have shown that increased cell capacitance increases capacitive load and the discontinuity of action potential propagation. This steepens the relationship between gap-junction conductance and conduction velocity elevating the risk of conduction block both due to uncoupling and source-sink mismatch (Seidel et al., 2010). Furthermore, hypertrophy leads to increased length or diameter of cardiomyocytes, which has both been shown to influence conduction (McIntyre and Fry, 1997; Spach et al., 2000; Seidel et al., 2010). This suggests that hypertrophy itself, in addition to the associated cardiac disease, can be an arrhythmogenic substrate.

EFFECTS OF GAP JUNCTIONS—LATERALIZATION AND REMODELING

Remodeling of the geometrical distribution of gap junctions occurs in a variety of cardiac diseases (Polontchouk et al., 2001; Kostin et al., 2004; Cabo et al., 2006; Salameh et al., 2009). In most cases the fraction of lateral connexins increases. Provided that these connexins form functional channels, they could contribute to arrhythmogenic alterations in impulse propagation (Cabo et al., 2006; Seidel et al., 2010). However, it is discussed controversially since years whether lateral connexins form fully functional gap junction channels. They might as well form hemichannels, which are assumed to be closed in normal physiological situations, or represent a pool of connexins/hemichannels floating in the membrane until they find anchoring site where they form a complete channel with the hemichannel of a neighboring cell. Pathophysiological situations with lateralized gap junctions comprise atrial fibrillation (Polontchouk et al., 2001; Kostin et al., 2002) cardiomyopathy (Kostin et al., 2003, 2004; Severs et al., 2006; Salameh et al., 2009) or myocardial infarction (Cabo et al., 2006). A study investigating atrial tissue from patients suffering from chronic atrial fibrillation found connexin lateralization accompanied by enhanced transverse conduction velocity. Moreover, in the same study metoprolol treatment led to a lower degree of lateralization and lower transverse conduction velocity (Dhein et al., 2011). This provides evidence that at least parts of these connexins form functional lateral gap junctions, although electrode spacing of 1 mm did not allow to precisely link an activation propagation to a certain cell shape. Direct proof needs

(a) injection of dyes like Lucifer Yellow into cells within a vital layer of atrial tissue (metabolic coupling), and (b) microscopic mapping of electrical activation with a resolution $<10\,\mu m$. This should be complemented with connexin immunohistology and electron microscopy of the mapped area and exact superimposition. Theoretical studies have shown potential effects of gap junction lateralization on action potential propagation and possible arrhythmogenic mechanisms. High side-to-side coupling of cardiomyocytes may favor conduction block due to source-sink mismatches (Seidel et al., 2010), while low side-to-side coupling has been suggested to unmask inhomogeneities (Müller and Dhein, 1993; Seidel et al., 2010).

Non-uniformity and anisotropy in cardiac tissue can cause fractionated waveforms. This is increased by a reduction in gap junction protein expression resulting in progression of irregular activation patterns as shown by de Bakker and van Rijen (2006).

EFFECTS OF FIBROSIS AND ANISOTROPIC INHOMOGENEITY

Fibrosis is a very common process in cardiac remodeling. When cardiomyocytes are impaired by a pathological event and subsequently undergo apoptosis or necrosis, the remnants are eliminated in the context of an inflammatory process. Finally, the area formerly filled by cardiomyocytes is replaced with connective tissue. This includes fibroblasts and extracellular matrix, mainly collagen. This typical repair process helps to maintain cardiac shape and allows maintenance of intracardiac systolic pressures of about 120–150 mmHg. However, a disadvantage is that this replacement tissue is electrically silent, non-contractile and stiffer than normal myocardium. Fibrotic strands typically are between the cardiomyocytes, running parallel to their longitudinal axis (aligned to the fiber axis), thus separating laterally neighbored cardiomyocytes. Occasionally, there will be a remnant connection between cardiomyocytes, so that the activation pattern follows a zig-zag course with reduced transverse conduction velocity. In situations of a longitudinally propagating wavefront, this type of fibrosis will have only little effect. However, if the wavefronts travels transverse to the longitudinal axis, the fibrotic strand will form an obstacle causing "wavefront curvature" because the traveling wavefront will curve around this insulator (Fast and Kléber, 1997). A similar situation can occur at sudden changes in fiber direction (see "Texture of the Heart").

The biophysical properties of the fibrotic cardiac tissue can be described as strongly anisotropic (longitudinal resistance << transverse resistance), discontinuous (cells are separated from each other) and non-uniform (local changes in the anisotropic properties) (de Bakker et al., 1993, 1996). The typical ECG under these conditions of highly discontinuous anisotropic tissue exhibits fractionated QRS complexes with reduced amplitude in the case of reduced myocardial mass (Spear et al., 1979; de Bakker et al., 1988).

Fibroblasts, although non-excitable, may allow electrotonic spread of activation, but with considerable delay. Gaudesius et al. (2003) showed in a strand of cardiomyocytes with an interponate of some fibroblasts successful propagation of the action potential, but with a clear delay at the fibroblast site. They showed that the activation can be successfully transmitted over a distance of up to $300\,\mu m$ filled by fibroblasts. However, it needs to be mentioned that in pathophysiological situations these distances will not be filled with fibroblasts alone but also with a high fraction of collagen. Fibroblasts might couple via gap junctions to cardiomyocytes, which is presumably realized by Cx45 or Cx43, thereby connecting the low-resistance intracellular spaces of fibroblasts and cardiomyocytes. If there is a high fraction of collagen, however, continuous gap junction coupling between myocytes and fibroblasts over long distances becomes very unlikely. Additionally, the ohmic resistance of the extracellular space will be increased. This can lead to conduction failure. It is difficult to estimate the amount of collagenous tissue necessary for electrical isolation, but it will depend on the number of cells in relation to the mass of collagen. Furthermore, it remains unclear whether fibroblast-myocyte coupling occurs *in-vivo* (Kohl and Gourdie, 2014). So far, only one study provides convincing evidence for this possibility in the sinuatrial node (Camelliti et al., 2004), whereas other studies failed to identify heterocellular coupling in the ventricle (Baum et al., 2012).

Different types of fibrosis can be distinguished regarding the texture of collagen deposition: it may be diffuse with small, short, abundant collagenous strands or it may be patchy with larger areas of thick and long collagenous strands. It was shown that the latter type has a higher impact on activation propagation (Kawara et al., 2001). In a computer simulation, discontinuities could be minimized until they vanished when the fibrotic texture was progressively altered from a patchy type to a diffuse type (Pertsov, 1997).

TEXTURE OF THE HEART

Of note, myocardial fiber direction changes from the endocardium to the epicardium by nearly 90° (Greenbaum et al., 1981). In a normal, non-diseased heart this is a gradual change. However, in diseased hearts, e.g., in cardiomyopathy, myocyte disarray has been observed which leads to zones with a sudden change in fiber direction within a short distance. This can result in a sudden change in resistance since a wavefront traveling along the fiber axis suddenly encounters transverse myocyte strands, so that the electrical resistance for the wave changes. This will cause delay of propagation or wavefront curvatures or discontinuities or unidirectional block (Spach et al., 1982). Interestingly, a similar situation of sudden changes in fiber direction was observed in canine and human pulmonary veins. In this area atrial fibrillation is usually initiated, and this structural particularity may contribute to the arrhythmogeneity of this region (Hocini et al., 2002; Arora et al., 2003).

NON-EXCITABLE REGIONS

Beside myocardial fibers, non-excitable tissue components are present in the heart such as connective tissue (see above) or vessels or fat tissue. These non-excitable obstacles "may cause the formation of self-sustained vortices and uncontrolled high-frequency excitation in normal homogeneous myocardium" (Cabo et al., 1998). In this process the wavefront is thought to detach from the obstacle and form a vortex, i.e., spiral waves are initiated. This process of detachment and shedding of vortices is assumed to depend on wavefront curvature (Cabo et al., 1998).

However, there is another characteristic of non-excitable tissue regions: if a wavefront with low curvature propagates, current flows mainly along the potential gradient to the front. Hardly any current is lost to the sides or the area behind the wavefront, because there is no potential gradient. If the wave approaches a non-excitable, electrically insulated obstacle, current flowing to the front will decrease. Thus, in front of an obstacle less current is lost than during normal propagation. As a consequence, the action potential will be prolonged in this area due to the reduced current loss. In contrast, after the wave has surrounded the obstacle it meets unexcited tissue in front and lateral to the wavefront. Thus, current is lost to the sides and the front. As a result, action potential duration will be increased in front and shortened behind the obstacle. It has been shown by epicardial mapping around a coronary vessel that this is indeed the case (Gottwald et al., 1998). For illustration, see **Figure 5**. Interestingly, this study also showed that in ischemic tissue the difference in action potential duration before and behind an obstacle significantly increases due to slowed conduction. This is a consequence of the ischemic depolarization leading to reduced sodium channel availability, prolonging the time during which current can pass from the excited site to the non-excited sites. This will increase the current loss. Similarly, reduction in sodium channel conductance was shown to enhance local dispersion (variance in action potential duration) at zones of reduced gap junction coupling in a computer simulation (Müller and Dhein, 1993). It seems obvious that, in its extreme form, this phenomenon may lead to unidirectional block, which is a potential trigger of arrhythmia.

CHANGES OF THE BIOPHYSICAL PROPERTIES BY MECHANICAL FORCES

Mechanical stimuli will lead to local strain of cells, which means an alteration of cell length and length-to-width ratio. In computer simulations it has been shown that changes in cell geometry have an effect on conduction velocity (Spach et al., 2000; Seidel et al., 2010). A local stretch therefore can alter the local pathways of activation (Dhein et al., 2014). On the other hand, it has been shown that structural heterogeneities can affect stretch-induced ventricular arrhythmia (Seo et al., 2010). Wall thickness can be heterogeneously distributed over the ventricle, which will result in a regional modulation of a mechanical stimulus so that regional strain varies. This strain may activate stretch-activated ion channels thereby eliciting cardiac arrhythmia. It was recently shown that local left ventricular stretch leads to local delays in activation so that early and late activation occur closely beside each other (Dhein et al., 2014).

A sudden mechanical insult, an impact or blow by a small spheroid may induce ventricular fibrillation (Kalin et al., 2011). Such an insult is known as commotio cordis. The impact is thought to induce heterogeneity in repolarization within the wall together with a premature depolarization trigger.

IMPLICATIONS FOR THE CLINICS (AGE)

In the daily clinic we also see the importance of the passive electrical properties as, in particular, elderly patients suffer from cardiac arrhythmia. Age has been described to be associated with cardiac fibrosis (Gottwald et al., 1997) and with disturbances of cardiac conduction velocity and enhanced dispersion of action potential duration (Dhein and Hammerath, 2001). According to the latter study, fibrotic strands aligned to the cardiac myocytes result in reduced transverse propagation velocity and thereby enhanced anisotropy. The authors concluded that reduced lateral gap junction coupling may be a typical feature of aged hearts. In accordance with this assumption, they could show that reduction of gap junction coupling in young hearts could mimic the situation found in aged hearts. They also observed that the extracellular potentials were fractionated in areas where activation spread was particularly inhomogeneous. Thus, age-related fibrosis and the resulting disturbances in activation spreading and repolarization indicate that the biophysical passive properties of the tissue are changed and may help to explain why in elderly patients arrhythmia is more frequent than in the young.

Fibrosis is a key characteristic in atrial fibrillation (Boldt et al., 2004), which can be reduced by angiotensin-converting enzyme inhibitors (Boldt et al., 2006). Fibrosis is, among others, considered a major determinant for the development of atrial fibrillation

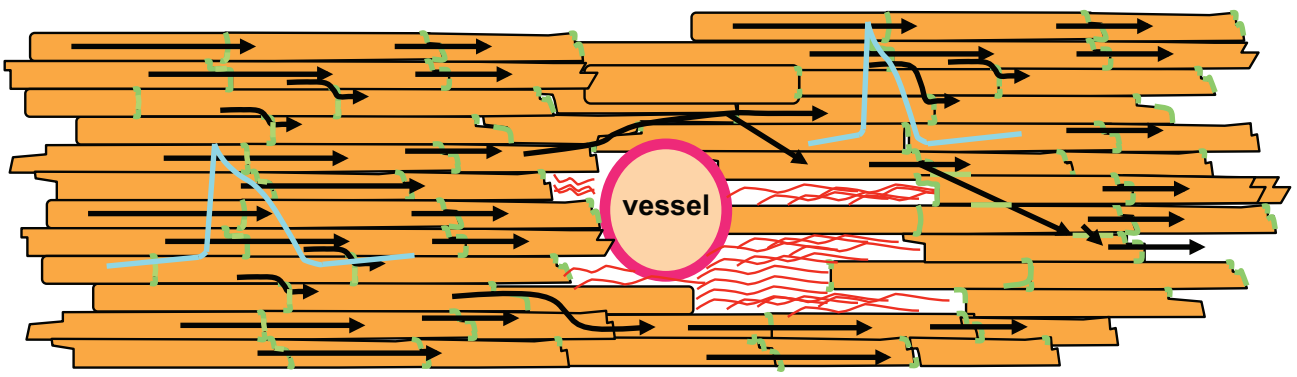

FIGURE 5 | Non-excitable regions like coronary vessels or connective tissue (shown as red strands around the vessel) lead to changes in action potential duration. In front of the non-excitable area, current sink decreases leading to longer action potential duration. In contrast, behind this area current sink is increased, which shortens the action potential. Action potential shapes are illustrated in blue, gap junctions in green, cardiomyocytes in orange. Black arrows indicate impulse propagation.

and may lead to structural uncoupling of fiber strands. Moreover, fibrosis enhances the complexity of atrial fibrillation (Verheule et al., 2013). Since according to the present knowledge fibrosis cannot be reversed, this marks a point of no return for atrial fibrillation. Clinical experience underlines that long-standing persistent atrial fibrillation with dilated atria and fibrotic tissue is unlikely to be successfully converted to sinus rhythm for a longer period.

Chronic pump failure leads to remodeling processes in the heart with hypertrophy of the fibers and lateralization of gap junctions. Clinically, it is known that patients suffering from heart failure, cardiomyopathy or cardiac hypertrophy often die from ventricular arrhythmia rather than from pump failure.

Passive electrical properties of cardiac tissue strongly influence myocardial activation, and thereby importantly contribute to the formation of arrhythmogenic substrates.

FINAL REMARK

There are numerous excellent studies on passive electrical properties, gap junctions, arrhythmia, mechano-electrical feedback and related issues. We seriously apologize to those authors who could not be cited.

REFERENCES

Allessie, M. A., Bonke, F. I., and Schopman, F. J. (1977). Circus movement in rabbit atrial muscle as a mechanism of tachycardia. III. The "leading circle" concept: a new model of circus movement in cardiac tissue without the involvement of an anatomical obstacle. *Circ. Res.* 41, 9–18. doi: 10.1161/01.RES.41.1.9

Arora, R., Verheule, S., Scott, L., Navarrete, A., Katari, V., Wilson, E., et al. (2003). Arrhythmogenic substrate of the pulmonary veins assessed by high-resolution optical mapping. *Circulation* 107, 1816–1821. doi: 10.1161/01.CIR.0000058461.86339.7E

Axelsen, L. N., Calloe, K., Holstein-Rathlou, N. H., and Nielsen, M. S. (2013). Managing the complexity of communication: regulation of gap junctions by post-translational modification. *Front. Pharmacol.* 4:130. doi: 10.3389/fphar.2013.00130

Baum, J. R., Long, B., Cabo, C., and Duffy, H. S. (2012). Myofibroblasts cause heterogeneous Cx43 reduction and are unlikely to be coupled to myocytes in the healing canine infarct. *Am. J. Physiol. Heart Circ. Physiol.* 302, H790–H800. doi: 10.1152/ajpheart.00498.2011

Beuckelmann, D. J., Näbauer, M., and Erdmann, E. (1993). Alterations of K^+ currents in isolated human ventricular myocytes from patients with terminal heart failure. *Circ. Res.* 73, 379–385. doi: 10.1161/01.RES.73.2.379

Beyer, E. C., Veenstra, R. D., Kanter, H. L., and Saffitz, J. E. (1995). "Molecular structure and patterns of expression of cardiac gap junction proteins," in *Cardiac Electrophysiology From cell to Bedside,* 2nd Edn., eds D. Zipes and J. Jalife (Philadelphia: WB Saunders), 31–38.

Boldt, A., Scholl, A., Garbade, J., Resetar, ME., Mohr, F. W., Gummert, J. F., et al. (2006). ACE-inhibitor treatment attenuates atrial structural remodeling in patients with lone chronic atrial fibrillation. *Basic Res. Cardiol.* 101, 261–267. doi: 10.1007/s00395-005-0571-2

Boldt, A., Wetzel, U., Lauschke, J., Weigl, J., Gummert, J., Hindricks, G., et al. (2004). Fibrosis in left atrial tissue of patients with atrial fibrillation with and without underlying mitral valve disease. *Heart* 90, 400–405. doi: 10.1136/hrt.2003.015347

Boldt, A., Wetzel, U., Weigl, J., Garbade, J., Lauschke, J., Hindricks, G., et al. (2003). Expression of angiotensin II receptors in human left and right atrial tissue in atrial fibrillation with and without underlying mitral valve disease. *J. Am. Coll. Cardiol.* 42, 1785–1792. doi: 10.1016/j.jacc.2003.07.014

Boyden, P. A., Hirose, M., and Dun, W. (2010). Cardiac Purkinje cells. *Heart Rhythm* 7, 127–135. doi: 10.1016/j.hrthm.2009.09.017

Boyett, M. R., Inada, S., Yoo, S., Li, J., Liu, J., Tellez, J., et al. (2006). Connexins in the sinoatrial and atrioventricular nodes. *Adv. Cardiol.* 42, 175–197. doi: 10.1159/000092569

Bukauskas, F. F., and Verselis, V. K. (2004). Gap junction channel gating. *Biochim. Biophys. Acta* 1662, 42–60. doi: 10.1016/j.bbamem.2004.01.008

Cabo, C., Pertsov, A. M., Davidenko, J. M., and Jalife, J. (1998). Electrical turbulence as a result of the critical curvature for propagation in cardiac tissue. *Chaos* 8, 116–126. doi: 10.1063/1.166292

Cabo, C., Yao, J., Boyden, P. A., Chen, S., Hussain, W., Duffy, H. S., et al. (2006). Heterogeneous gap junction remodeling in reentrant circuits in the epicardial border zone of the healing canine infarct. *Cardiovasc. Res.* 72, 241–249. doi: 10.1016/j.cardiores.2006.07.005

Camelliti, P., Green, C. R., LeGrice, I., and Kohl, P. (2004). Fibroblast network in rabbit sinoatrial node: structural and functional identification of homogeneous and heterogeneous cell coupling. *Circ. Res.* 94, 828–835. doi: 10.1161/01.RES.0000122382.19400.14

Capogrossi, M. C., Houser, S. R., Bahinski, A., and Lakatta, E. G. (1987). Synchronous occurrence of spontaneous localized calcium release from the sarcoplasmic reticulum generates action potentials in rat cardiac ventricular myocytes at normal resting membrane potential. *Circ. Res.* 61, 498–503. doi: 10.1161/01.RES.61.4.498

Carnie, S., and McLaughlin, S. (1983). Large divalent cations and electrostatic potentials adjacent to membranes. A theoretical calculation. *Biophys. J.* 44, 325–332. doi: 10.1016/S0006-3495(83)84306-9

Chen, L., Goings, G. E., Upshaw-Earley, J., and Page, E. (1989). Cardiac gap junctions and gap junction-associated vesicles: ultrastructural comparison of *in situ* negative staining with conventional positive staining. *Circ. Res.* 64, 501–514. doi: 10.1161/01.RES.64.3.501

Clerc, L. (1976). Directional differences of impulse spread in trabecular muscle from mammalian heart. *J. Physiol.* 255, 335–346.

Copene, E. D., and Keener, J. P. (2008). Ephaptic coupling of cardiac cells through the junctional electric potential. *J. Math. Biol.* 57, 265–284. doi: 10.1007/s00285-008-0157-3

de Bakker, J. M., van Capelle, F. J., Janse, M. J., Tasseron, S., Vermeulen, J. T., de Jonge, N., et al. (1993). Slow conduction in the infarcted human heart. 'Zigzag' course of activation. *Circulation* 88, 915–926. doi: 10.1161/01.CIR.88.3.915

de Bakker, J. M., van Capelle, F. J., Janse, M. J., Tasseron, S., Vermeulen, J. T., de Jonge, N., et al. (1996). Fractionated electrograms in dilated cardiomyopathy: origin and relation to abnormal conduction. *J. Am. Coll. Cardiol.* 27, 1071–1078. doi: 10.1016/0735-1097(95)00612-5

de Bakker, J. M., van Capelle, F. J., Janse, M. J., Wilde, A. A., Coronel, R., Becker, A. E., et al. (1988). Reentry as a cause of ventricular tachycardia in patients with chronic ischemic heart disease: electrophysiologic and anatomic correlation. *Circulation* 77, 589–606. doi: 10.1161/01.CIR.77.3.589

de Bakker, J. M., and van Rijen, H. M. (2006). Continuous and discontinuous propagation in heart muscle. *J. Cardiovasc. Electrophysiol.* 17, 567–573. doi: 10.1111/j.1540-8167.2006.00367.x

Delmar, M., Michaels, D. C., Johnson, T., and Jalife, J. (1987). Effects of increasing intercellular resistance on transverse and longitudinal propagation in sheep epicardial muscle. *Circ. Res.* 60, 780–785. doi: 10.1161/01.RES.60.5.780

Dhein, S. (1998). Gap junction channels in the cardiovascular system: pharmacological and physiological modulation. *Trends Pharmacol. Sci.* 19, 229–241. doi: 10.1016/S0165-6147(98)01192-4

Dhein, S. (2004). Pharmacology of gap junctions in the cardiovascular system. *Cardiovasc. Res.* 62, 287–298. doi: 10.1016/j.cardiores.2004.01.019

Dhein, S., Englert, C., Riethdorf, S., Kostelka, M., Dohmen, P. M., and Mohr, F. W. (2014). Arrhythmogenic effects by local left ventricular stretch: effects of flecainide and streptomycin. *Naunyn Schmiedebergs. Arch. Pharmacol.* 387, 763–775. doi: 10.1007/s00210-014-0988-y

Dhein, S., and Hammerath, S. B. (2001). Aspects of the intercellular communication in aged hearts: effects of the gap junction uncoupler palmitoleic acid. *Naunyn Schmiedebergs. Arch. Pharmacol.* 364, 397–408. doi: 10.1007/s002100100462

Dhein, S., Manicone, N., Müller, A., Gerwin, R., Ziskoven, U., Irankhahi, A., et al. (1994). A new synthetic antiarrhythmic peptide reduces dispersion of epicardial activation recovery interval and diminishes alterations of epicardial activation patterns induced by regional ischemia. A mapping study. *Naunyn Schmiedebergs Arch. Pharmacol.* 350, 174–184. doi: 10.1007/BF00241093

Dhein, S., Rothe, S., Busch, A., Rojas Gomez, D. M., Boldt, A., Reutemann, A., et al. (2011). Effects of metoprolol therapy on cardiac gap junction remodelling and conduction in human chronic atrial fibrillation. *Br. J. Pharmacol.* 164, 607–616. doi: 10.1111/j.1476-5381.2011.01460.x

Dupont, E., Ko, Y., Rothery, S., Coppen, S. R., Baghai, M., Haw, M., et al. (2001). The gap-junctional protein connexin40 is elevated in patients susceptible to postoperative atrial fibrillation. *Circulation* 103, 842–849. doi: 10.1161/01.CIR.103.6.842

el-Sherif, N., Gough, W. B., and Restivo, M. (1987). Reentrant ventricular arrhythmias in the late myocardial infarction period: 14. Mechanisms of resetting, entrainment, acceleration, or termination of reentrant tachycardia by programmed electrical stimulation. *Pacing Clin. Electrophysiol.* 10, 341–371. doi: 10.1111/j.1540-8159.1987.tb05974.x

Fast, V. G., and Kléber, A. G. (1993). Microscopic conduction in cultured strands of neonatal rat heart cells measured with voltage-sensitive dyes. *Circ. Res.* 73, 914–925. doi: 10.1161/01.RES.73.5.914

Fast, V. G., and Kléber, A. G. (1997). Role of wavefront curvature in propagation of cardiac impulse. *Cardiovasc. Res.* 33, 258–271. doi: 10.1016/S0008-6363(96)00216-7

Gaudesius, G., Miragoli, M., Thomas, S. P., and Rohr, S. (2003). Coupling of cardiac electrical activity over extended distances by fibroblasts of cardiac origin. *Circ. Res.* 93, 421–428. doi: 10.1161/01.RES.0000089258.40661.0C

Geselowitz, D. B., and Miller, W. T. (1983). A bidomain model for anisotropic cardiac muscle. *Ann. Biomed. Eng.* 11, 191–206. doi: 10.1007/BF02363286

Goshima, K., and Tonomura, Y. (1969). Synchronized beating of embryonic mouse myocardial cells mediated by FL cells in monolayer culture. *Exp. Cell. Res.* 56, 387–392. doi: 10.1016/0014-4827(69)90029-9

Gottwald, E., Gottwald, M., and Dhein, S. (1998). Enhanced dispersion of epicardial activation-recovery intervals at sites of histological inhomogeneity during regional cardiac ischaemia and reperfusion. *Heart* 79, 474–480.

Gottwald, M., Gottwald, E., and Dhein, S. (1997). Age-related electrophysiological and histological changes in rabbit hearts: age-related changes in electrophysiology. *Int. J. Cardiol.* 62, 97–106. doi: 10.1016/S0167-5273(97)00183-6

Gourdie, R. G., Harfst, E., Severs, N. J., and Green, C. R. (1990). Cardiac gap junctions in rat ventricle: localization using site-directed antibodies and laser scanning confocal microscopy. *Cardioscience* 1, 75–82.

Greenbaum, R. A., Ho, S. Y., Gibson, D. G., Becker, A. E., and Anderson, R. H. (1981). Left ventricular fibre architecture in man. *Br. Heart J.* 45, 248–263. doi: 10.1136/hrt.45.3.248

Hagen, A., Dietze, A., and Dhein, S. (2009). Human cardiac gap-junction coupling: effects of antiarrhythmic peptide AAP10. *Cardiovasc. Res.* 83, 405–415. doi: 10.1093/cvr/cvp028

Hand, P. E., Griffith, B. E., and Peskin, C. S. (2009). Deriving macroscopic myocardial conductivities by homogenization of microscopic models. *Bull. Math. Biol.* 71, 1707–1726. doi: 10.1007/s11538-009-9421-y

Harris, A. L. (2001). Emerging issues of connexin channels: biophysics fills the gap. *Q. Rev. Biophys.* 34, 325–472. doi: 10.1017/S0033583501003705

Haugan, K., Marcussen, N., Kjølbye, A. L., Nielsen, M. S., Hennan, J. K., and Petersen, J. S. (2006). Treatment with the gap junction modifier rotigaptide (ZP123) reduces infarct size in rats with chronic myocardial infarction. *J. Cardiovasc. Pharmacol.* 47, 236–242. doi: 10.1097/01.fjc.0000200990.31611.6e

He, K., Shi, X., Zhang, X., Dang, S., Ma, X., Liu, F., et al. (2011). Long-distance intercellular connectivity between cardiomyocytes and cardiofibroblasts mediated by membrane nanotubes. *Cardiovasc. Res.* 92, 39–47. doi: 10.1093/cvr/cvr189

Hocini, M., Ho, S. Y., Kawara, T., Linnenbank, A. C., Potse, M., Shah, D., et al. (2002). Electrical conduction in canine pulmonary veins: electrophysiological and anatomic correlation. *Circulation* 105, 2442–2448. doi: 10.1161/01.CIR.0000016062.80020.11

Hodgkin, A. L., and Rushton, W. A. (1946). The electrical constants of a crustacean nerve fibre. *Proc. R. Soc. Med.* 134, 444–479. doi: 10.1098/rspb.1946.0024

Hubbard, M. L., Ying, W., and Henriquez, C. S. (2007). Effect of gap junction distribution on impulse propagation in a monolayer of myocytes: a model study. *Europace* 9(Suppl. 6), vi20–vi28. doi: 10.1093/europace/eum203

Jack, J., Noble, D., and Tsien, R. (1975). *Electric Current Flow in Excitable Cells*. Oxford: Clarendon.

Johnston, P. R., Kilpatrick, D., and Li, C. Y. (2001). The importance of anisotropy in modeling ST segment shift in subendocardial ischaemia. *IEEE Trans. Biomed. Eng.* 48, 1366–1376. doi: 10.1109/10.966596

Joyner, R. W., and van Capelle, F. J. (1986). Propagation through electrically coupled cells. How a small SA node drives a large atrium. *Biophys. J.* 50, 1157–1164. doi: 10.1016/S0006-3495(86)83559-7

Jozwiak, J., and Dhein, S. (2008). Local effects and mechanisms of antiarrhythmic peptide AAP10 in acute regional myocardial ischemia: electrophysiological and molecular findings. *Naunyn Schmiedebergs. Arch. Pharmacol.* 378, 459–470. doi: 10.1007/s00210-008-0317-4

Kalin, J., Madias, C., Alsheikh-Ali, A. A., and Link, M. S. (2011). Reduced diameter spheres increases the risk of chest blow-induced ventricular fibrillation (commotio cordis). *Heart Rhythm* 8, 1578–1581. doi: 10.1016/j.hrthm.2011.05.009

Kawara, T., Derksen, R., de Groot, J. R., Coronel, R., Tasseron, S., Linnenbank, A. C., et al. (2001). Activation delay after premature stimulation in chronically diseased human myocardium relates to the architecture of interstitial fibrosis. *Circulation* 104, 3069–3075. doi: 10.1161/hc5001.100833

Kimura, S., Cameron, J. S., Kozlovskis, P. L., Bassett, A. L., and Myerburg, R. J. (1984). Delayed afterdepolarizations and triggered activity induced in feline Purkinje fibers by alpha-adrenergic stimulation in the presence of elevated calcium levels. *Circulation* 70, 1074–1082. doi: 10.1161/01.CIR.70.6.1074

Kléber, A. G., and Rudy, Y. (2004). Basic mechanisms of cardiac impulse propagation and associated arrhythmias. *Physiol. Rev.* 84, 431–488. doi: 10.1152/physrev.00025.2003

Kohl, P., and Gourdie, R. G. (2014). Fibroblast-myocyte electrotonic coupling: does it occur in native cardiac tissue? *J. Mol. Cell. Cardiol.* 70, 37–46. doi: 10.1016/j.yjmcc.2013.12.024

Kostin, S., Dammer, S., Hein, S., Klovekorn, W. P., Bauer, E. P., and Schaper, J. (2004). Connexin 43 expression and distribution in compensated and decompensated cardiac hypertrophy in patients with aortic stenosis. *Cardiovasc. Res.* 62, 426–436. doi: 10.1016/j.cardiores.2003.12.010

Kostin, S., Klein, G., Szalay, Z., Hein, S., Bauer, E. P., and Schaper, J. (2002). Structural correlate of atrial fibrillation in human patients. *Cardiovasc. Res.* 54, 361–379. doi: 10.1016/S0008-6363(02)00273-0

Kostin, S., Rieger, M., Dammer, S., Hein, S., Richter, M., Klövekorn, W. P., et al. (2003). Gap junction remodeling and altered connexin43 expression in the failing human heart. *Mol. Cell. Biochem.* 242, 135–144. doi: 10.1023/A:1021154115673

Kozhevnikov, D. O., Yamamoto, K., Robotis, D., Restivo, M., and El-Sherif, N. (2002). Electrophysiological mechanism of enhanced susceptibility of hypertrophied heart to acquired torsade de pointes arrhythmias: tridimensional mapping of activation and recovery patterns. *Circulation* 105, 1128–1134. doi: 10.1161/hc0902.104711

Kucera, J. P., Rohr, S., and Rudy, Y. (2002). Localization of sodium channels in intercalated disks modulates cardiac conduction. *Circ. Res.* 91, 1176–1182. doi: 10.1161/01.RES.0000046237.54156.0A

Lazzara, R. (1988). Electrophysiological mechanisms for ventricular arrhythmias. *Clin. Cardiol.* 11(3 Suppl. 2), II1–II4.

Lederer, W. J., and Tsien, R. W. (1976). Transient inward current underlying arrhythmogenic effects of cardiotonic steroids in Purkinje fibres. *J. Physiol.* 263, 73–100.

Lee, P. J., and Pogwizd, S. M. (2006). Micropatterns of propagation. *Adv. Cardiol.* 42, 86–106. doi: 10.1159/000092564

Lin, J., and Keener, J. P. (2010). Modeling electrical activity of myocardial cells incorporating the effects of ephaptic coupling. *Proc. Natl. Acad. Sci. U.S.A.* 107, 20935–20940. doi: 10.1073/pnas.1010154107

Maier, S. K., Westenbroek, R. E., McCormick, K. A., Curtis, R., Scheuer, T., and Catterall, W. A. (2004). Distinct subcellular localization of different sodium channel alpha and beta subunits in single ventricular myocytes from mouse heart. *Circulation* 109, 1421–1427. doi: 10.1161/01.CIR.0000121421.61896.24

Makowski, L., Caspar, D. L., Phillips, W. C., and Goodenough, D. A. (1977). Gap junction structures. II. Analysis of the x-ray diffraction data. *J. Cell. Biol.* 74, 629–645. doi: 10.1083/jcb.74.2.629

Marban, E., Robinson, S. W., and Wier, W. G. (1986). Mechanisms of arrhythmogenic delayed and early afterdepolarizations in ferret ventricular muscle. *J. Clin. Invest.* 78, 1185–1192. doi: 10.1172/JCI112701

McIntyre, H., and Fry, C. H. (1997). Abnormal action potential conduction in isolated human hypertrophied left ventricular myocardium. *J. Cardiovasc. Electrophysiol.* 8, 887–894. doi: 10.1111/j.1540-8167.1997.tb00850.x

Miura, T., Ohnuma, Y., Kuno, A., Tanno, M., Ichikawa, Y., Nakamura, Y., et al. (2004). Protective role of gap junctions in preconditioning against myocardial infarction. *Am. J. Physiol. Heart Circ. Physiol.* 286, H214–H221. doi: 10.1152/ajpheart.00441.2003

Moreno, A. P. (2004). Biophysical properties of homomeric and heteromultimeric channels formed by cardiac connexins. *Cardiovasc. Res.* 62, 276–286. doi: 10.1016/j.cardiores.2004.03.003

Mori, Y., Fishman, G. I., and Peskin, C. S. (2008). Ephaptic conduction in a cardiac strand model with 3D electrodiffusion. *Proc. Natl. Acad. Sci. U.S.A.* 105, 6463–6468. doi: 10.1073/pnas.0801089105

Morley, G. E., Danik, S. B., Bernstein, S., Sun, Y., Rosner, G., Gutstein, D. E., et al. (2005). Reduced intercellular coupling leads to paradoxical propagation across the Purkinje-ventricular junction and aberrant myocardial activation. *Proc. Natl. Acad. Sci. U.S.A.* 102, 4126–4129. doi: 10.1073/pnas.0500881102

Müller, A., and Dhein, S. (1993). Sodium channel blockade enhances dispersion of the cardiac action potential duration. A computer simulation study. *Basic Res. Cardiol.* 88, 11–22.

Müller, A., Gottwald, M., Tudyka, T., Linke, W., Klaus, W., and Dhein, S. (1997). Increase in gap junction conductance by an antiarrhythmic peptide. *Eur. J. Pharmacol.* 327, 65–72. doi: 10.1016/S0014-2999(97)89679-3

Myles, R. C., Wang, L., Kang, C., Bers, D. M., and Ripplinger, C. M. (2012). Local β-adrenergic stimulation overcomes source-sink mismatch to generate focal arrhythmia. *Circ. Res.* 110, 1454–1464. doi: 10.1161/CIRCRESAHA.111.262345

Nielsen, M. S., Axelsen, L. N., Sorgen, P. L., Verma, V., Delmar, M., and Holstein-Rathlou, N. H. (2012). Gap junctions. *Compr. Physiol.* 2, 1981–2035. doi: 10.1002/cphy.c110051

Page, E., and Shibata, Y. (1981). Permeable junctions between cardiac cells. *Annu. Rev. Physiol.* 43, 431–441. doi: 10.1146/annurev.ph.43.030181.002243

Pellman, J., Lyon, R. C., and Sheikh, F. (2010). Extracellular matrix remodeling in atrial fibrosis: mechanisms and implications in atrial fibrillation. *J. Mol. Cell. Cardiol.* 48, 461–467. doi: 10.1016/j.yjmcc.2009.09.001

Perkins, G., Goodenough, D., and Sosinsky, G. (1997). Three-dimensional structure of the gap junction connexon. *Biophys. J.* 72(2 Pt 1), 533–544. doi: 10.1016/S0006-3495(97)78693-4

Pertsov, A. (1997). "Scale of geometric structures responsible for discontinuous propagation in myocardial tissue," in *Discontinuous Conduction in the Heart*, eds P. Spooner, R. Joyner, and J. Jalife (New York, NY: Futura Publishing Company Inc.), 273–293.

Pertsov, A. M., Davidenko, J. M., Salomonsz, R., Baxter, W. T., and Jalife, J. (1993). Spiral waves of excitation underlie reentrant activity in isolated cardiac muscle. *Circ. Res.* 72, 631–650. doi: 10.1161/01.RES.72.3.631

Peskoff, A. (1979). Electric potential in three-dimensional electrically syncytial tissues. *Bull. Math. Biol.* 41, 163–181. doi: 10.1007/BF02460876

Polontchouk, L., Haefliger, J. A., Ebelt, B., Schaefer, T., Stuhlmann, D., Mehlhorn, U., et al. (2001). Effects of chronic atrial fibrillation on gap junction distribution in human and rat atria. *J. Am. Coll. Cardiol.* 38, 883–891. doi: 10.1016/S0735-1097(01)01443-7

Rhett, J. M., Ongstad, E. L., Jourdan, J., and Gourdie, R. G. (2012). Cx43 associates with Na(v)1.5 in the cardiomyocyte perinexus. *J. Membr. Biol.* 245, 411–422. doi: 10.1007/s00232-012-9465-z

Rhett, J. M., Veeraraghavan, R., Poelzing, S., and Gourdie, R. G. (2013). The perinexus: sign-post on the path to a new model of cardiac conduction? *Trends Cardiovasc. Med.* 23, 222–228. doi: 10.1016/j.tcm.2012.12.005

Roberts, D. E., Hersh, L. T., and Scher, A. M. (1979). Influence of cardiac fiber orientation on wavefront voltage, conduction velocity, and tissue resistivity in the dog. *Circ. Res.* 44, 701–712. doi: 10.1161/01.RES.44.5.701

Roberts, D. E., and Scher, A. M. (1982). Effect of tissue anisotropy on extracellular potential fields in canine myocardium *in situ*. *Circ. Res.* 50, 342–351. doi: 10.1161/01.RES.50.3.342

Roberts, S. F., Stinstra, J. G., and Henriquez, C. S. (2008). Effect of nonuniform interstitial space properties on impulse propagation: a discrete multidomain model. *Biophys. J.* 95, 3724–3737. doi: 10.1529/biophysj.108.137349

Rohr, S. (2004). Role of gap junctions in the propagation of the cardiac action potential. *Cardiovasc. Res.* 62, 309–322. doi: 10.1016/j.cardiores.2003.11.035

Rohr, S. (2012). Arrhythmogenic implications of fibroblast-myocyte interactions. *Circ. Arrhythm. Electrophysiol.* 5, 442–452. doi: 10.1161/CIRCEP.110.957647

Rohr, S., Kucera, J. P., Fast, V. G., and Kléber, A. G. (1997). Paradoxical improvement of impulse conduction in cardiac tissue by partial cellular uncoupling. *Science* 275, 841–844. doi: 10.1126/science.275.5301.841

Sachse, F. B., Moreno, A. P., Seemann, G., and Abildskov, J. A. (2009). A model of electrical conduction in cardiac tissue including fibroblasts. *Ann. Biomed. Eng.* 37, 874–889. doi: 10.1007/s10439-009-9667-4

Salameh, A., and Dhein, S. (2005). Pharmacology of gap junctions. New pharmacological targets for treatment of arrhythmia, seizure and cancer? *Biochim. Biophys. Acta* 1719, 36–58. doi: 10.1016/j.bbamem.2005.09.007

Salameh, A., Krautblatter, S., Karl, S., Blanke, K., Gomez, D. R., Dhein, S., et al. (2009). The signal transduction cascade regulating the expression of the gap junction protein connexin43 by beta-adrenoceptors. *Br. J. Pharmacol.* 158, 198–208. doi: 10.1111/j.1476-5381.2009.00344.x

Schulte, J. S., Scheffler, A., Rojas-Gomez, D., Mohr, F. W., and Dhein, S. (2008). Neonatal rat cardiomyocytes show characteristics of nonhomotypic gap junction channels. *Cell Commun. Adhes.* 15, 13–25. doi: 10.1080/15419060802014404

Schwab, B. C., Seemann, G., Lasher, R. A., Torres, N. S., Wulfers, E. M., Arp, M., et al. (2013). Quantitative analysis of cardiac tissue including fibroblasts using three-dimensional confocal microscopy and image reconstruction: towards a basis for electrophysiological modeling. *IEEE Trans. Med. Imaging* 32, 862–872. doi: 10.1109/TMI.2013.2240693

Seidel, T., Salameh, A., and Dhein, S. (2010). A simulation study of cellular hypertrophy and connexin lateralization in cardiac tissue. *Biophys. J.* 99, 2821–2830. doi: 10.1016/j.bpj.2010.09.010

Seo, K., Inagaki, M., Nishimura, S., Hidaka, I., Sugimachi, M., Hisada, T., et al. (2010). Structural heterogeneity in the ventricular wall plays a significant role in the initiation of stretch-induced arrhythmias in perfused rabbit right ventricular tissues and whole heart preparations. *Circ. Res.* 106, 176–184. doi: 10.1161/CIRCRESAHA.109.203828

Severs, N. J. (1994). Pathophysiology of gap junctions in heart disease. *J. Cardiovasc. Electrophysiol.* 5, 462–475. doi: 10.1111/j.1540-8167.1994.tb01185.x

Severs, N. J., Dupont, E., Thomas, N., Kaba, R., Rothery, S., Jain, R., et al. (2006). Alterations in cardiac connexin expression in cardiomyopathies. *Adv. Cardiol.* 42, 228–242. doi: 10.1159/000092572

Shaw, R. M., and Rudy, Y. (1997a). Electrophysiologic effects of acute myocardial ischemia. A mechanistic investigation of action potential conduction and conduction failure. *Circ. Res.* 80, 124–138. doi: 10.1161/01.RES.80.1.124

Shaw, R. M., and Rudy, Y. (1997b). Ionic mechanisms of propagation in cardiac tissue. Roles of the sodium and L-type calcium currents during reduced excitability and decreased gap junction coupling. *Circ. Res.* 81, 727–741. doi: 10.1161/01.RES.81.5.727

Spach, M., and Dolber, P. (1990). "Discontinuous anisotropic propagation," in *Cardiac Electrophysiology: A textbook*, eds M. Rosen, M. Janse, and A. Wit (Mount Kisco, NY: Futura Publishing Company Inc.), 517–534.

Spach, M. S., and Dolber, P. C. (1986). Relating extracellular potentials and their derivatives to anisotropic propagation at a microscopic level in human cardiac muscle. Evidence for electrical uncoupling of side-to-side fiber connections with increasing age. *Circ. Res.* 58, 356–371. doi: 10.1161/01.RES.58.3.356

Spach, M. S., Heidlage, J. F., Dolber, P. C., and Barr, R. C. (2000). Electrophysiological effects of remodeling cardiac gap junctions and cell size: experimental and model studies of normal cardiac growth. *Circ. Res.* 86, 302–311. doi: 10.1161/01.RES.86.3.302

Spach, M. S., Miller, W. T., Dolber, P. C., Kootsey, J. M., Sommer, J. R., and Mosher, C. E. (1982). The functional role of structural complexities in the propagation of depolarization in the atrium of the dog. Cardiac conduction disturbances due to discontinuities of effective axial resistivity. *Circ. Res.* 50, 175–191. doi: 10.1161/01.RES.50.2.175

Spear, J. F., Horowitz, L. N., Hodess, A. B., MacVaugh, H., and Moore, E. N. (1979). Cellular electrophysiology of human myocardial infarction. 1. Abnormalities of cellular activation. *Circulation* 59, 247–256. doi: 10.1161/01.CIR.59.2.247

Sperelakis, N. (1979). Propagation mechanisms in heart. *Annu. Rev. Physiol.* 41, 441–457. doi: 10.1146/annurev.ph.41.030179.002301

Sperelakis, N., and Mann, J. E. (1977). Evaluation of electric field changes in the cleft between excitable cells. *J. Theor. Biol.* 64, 71–96. doi: 10.1016/0022-5193(77)90114-X

Stinstra, J. G., Hopenfeld, B., and Macleod, R. S. (2005). On the passive cardiac conductivity. *Ann. Biomed. Eng.* 33, 1743–1751. doi: 10.1007/s10439-005-7257-7

Swynghedauw, B., Baillard, C., and Milliez, P. (2003). The long QT interval is not only inherited but is also linked to cardiac hypertrophy. *J. Mol. Med.* 81, 336–345. doi: 10.1007/s00109-003-0437-8

Tomaselli, G. F., and Marbán, E. (1999). Electrophysiological remodeling in hypertrophy and heart failure. *Cardiovasc. Res.* 42, 270–283. doi: 10.1016/S0008-6363(99)00017-6

Toure, A., and Cabo, C. (2010). Effect of cell geometry on conduction velocity in a subcellular model of myocardium. *IEEE Trans. Biomed. Eng.* 57, 2107–2114. doi: 10.1109/TBME.2010.2050064

Tveito, A., Lines, G. T., Edwards, A. G., Maleckar, M. M., Michailova, A., Hake, J., et al. (2012). Slow Calcium-Depolarization-Calcium waves may initiate fast local depolarization waves in ventricular tissue. *Prog. Biophys. Mol. Biol.* 110, 295–304. doi: 10.1016/j.pbiomolbio.2012.07.005

Veeraraghavan, R., Gourdie, R. G., and Poelzing, S. (2014). Mechanisms of cardiac conduction: a history of revisions. *Am. J. Physiol. Heart Circ. Physiol.* 306, H619–H627. doi: 10.1152/ajpheart.00760.2013

Veeraraghavan, R., Salama, M. E., and Poelzing, S. (2012). Interstitial volume modulates the conduction velocity-gap junction relationship. *Am. J. Physiol. Heart Circ. Physiol.* 302, H278–H286. doi: 10.1152/ajpheart.00868.2011

Verheule, S., Tuyls, E., Gharaviri, A., Hulsmans, S., van Hunnik, A., Kuiper, M., et al. (2013). Loss of continuity in the thin epicardial layer because of endomysial fibrosis increases the complexity of atrial fibrillatory conduction. *Circ. Arrhythm. Electrophysiol.* 6, 202–211. doi: 10.1161/CIRCEP.112.975144

Weber, K. T., Sun, Y., Bhattacharya, S. K., Ahokas, R. A., and Gerling, I. C. (2013). Myofibroblast-mediated mechanisms of pathological remodelling of the heart. *Nat. Rev. Cardiol.* 10, 15–26. doi: 10.1038/nrcardio.2012.158

Weidmann, S. (1952). The electrical constants of Purkinje fibres. *J. Physiol. (Lond).* 118, 348–360.

Weidmann, S. (1990). "Passive properties of cardiac fibers. A textbook," in *Cardiac Electrophysiology,* eds M. Rosen, M. Janse, and A. Wit (Mount Kisco, NY: Futura Publishing Company Inc.), 29–35.

Weingart, R., and Maurer, P. (1988). Action potential transfer in cell pairs isolated from adult rat and guinea pig ventricles. *Circ. Res.* 63, 72–80. doi: 10.1161/01.RES.63.1.72

Xie, Y., Sato, D., Garfinkel, A., Qu, Z., and Weiss, J. N. (2010). So little source, so much sink: requirements for afterdepolarizations to propagate in tissue. *Biophys. J.* 99, 1408–1415. doi: 10.1016/j.bpj.2010.06.042

Xing, D., Kjølbye, A. L., Nielsen, M. S., Petersen, J. S., Harlow, K. W., Holstein-Rathlou, N. H., et al. (2003). ZP123 increases gap junctional conductance and prevents reentrant ventricular tachycardia during myocardial ischemia in open chest dogs. *J. Cardiovasc. Electrophysiol.* 14, 510–520. doi: 10.1046/j.1540-8167.2003.02329.x

Yue, L., Xie, J., and Nattel, S. (2011). Molecular determinants of cardiac fibroblast electrical function and therapeutic implications for atrial fibrillation. *Cardiovasc. Res.* 89, 744–753. doi: 10.1093/cvr/cvq329

Conflict of Interest Statement: The authors declare that the research was conducted in the absence of any commercial or financial relationships that could be construed as a potential conflict of interest.

Received: 21 August 2014; accepted: 13 October 2014; published online: 03 November 2014.

Citation: Dhein S, Seidel T, Salameh A, Jozwiak J, Hagen A, Kostelka M, Hindricks G and Mohr F-W (2014) Remodeling of cardiac passive electrical properties and susceptibility to ventricular and atrial arrhythmias. Front. Physiol. ***5****:424. doi: 10.3389/fphys.2014.00424*

This article was submitted to Cardiac Electrophysiology, a section of the journal Frontiers in Physiology.

frontiers in
PHYSIOLOGY

REVIEW ARTICLE
published: 17 October 2014
doi: 10.3389/fphys.2014.00404

Role of the intercalated disc in cardiac propagation and arrhythmogenesis

Andre G. Kleber* and Jeffrey E. Saffitz

Department of Pathology, Beth Israel Medical Center, Harvard Medical School, Boston, MA, USA

Edited by:
George E. Billman, The Ohio State University, USA

Reviewed by:
Thomas Hund, The Ohio State University, USA
George E. Billman, The Ohio State University, USA

****Correspondence:***
Andre G. Kleber, Department of Pathology, Beth Israel Deaconess Medical Center, Harvard Medical School, Dana 752, 330 Brookline Avenue, Boston, MA 02215, USA
e-mail: akleber@bidmc.harvard.edu

This review article discusses mechanisms underlying impulse propagation in cardiac muscle with specific emphasis on the role of the cardiac cell-to-cell junction, called the "intercalated disc." The first part of this review deals with the role of gap junction channels, formed by connexin proteins, as a determinant of impulse propagation. It is shown that, depending on the underlying structure of the cellular network, decreasing the conductance of gap junction channels (so-called "electrical uncoupling") may either only slow, or additionally stabilize propagation and reverse unidirectional propagation block to bidirectional propagation. This is because the safety factor for propagation increases with decreasing intercellular electrical conductance. The role of heterogeneous connexin expression, which may be present in disease states, is also discussed. The hypothesis that so-called ephaptic impulse transmission plays a role in heart and can substitute for electrical coupling has been revived recently. Whereas ephaptic transmission can be demonstrated in theoretical simulations, direct experimental evidence has not yet been presented. The second part of this review deals with the interaction of three protein complexes at the intercalated disc: (1) desmosomal and adherens junction proteins, (2) ion channel proteins, and (3) gap junction channels consisting of connexins. Recent work has revealed multiple interactions between these three protein complexes which occur, at least in part, at the level of protein trafficking. Such interactions are likely to play an important role in the pathogenesis of arrhythmogenic cardiomyopathy, and may reveal new therapeutic concepts and targets.

Keywords: propagation velocity in heart, electrical-cell-to-cell coupling, intercalated disc, cardiac connexins, discontinuous propagation

INTRODUCTION

The observation that the heart is composed of billions of individual cardiac myocytes but functions as a highly coordinated syncytial structure has fascinated scientists since the nineteenth century (Engelmann, 1877). In 1952, Weidmann used classical electrical cable analysis and showed that electrical current injected into a single cell in a Purkinje strand spread along a distance considerably larger than the length of the cell itself, thus suggesting the free movement of electrical charge from one cell to another (Weidmann, 1952). This finding, implicating low resistance pathways between cardiac myocytes, was later confirmed in ventricular muscle (Weidmann, 1966). Since this pioneering work, gap junction channels bridging the cytoplasm of neighboring cells, and forming pathways for cell-to-cell flow of electrical current and small molecules, have been characterized in detail at the genetic, cell biological, and biophysical levels of organization and function (Harris, 2001; Valiunas et al., 2005).

With respect to the physiological role of the cardiac cell-cell interface, the "intercalated disc," the function and role of gap junctions, hosting channels composed of variety of connexins with regional specificity, has been the focus of many experimental and theoretical studies during the past decades (Kleber and Rudy, 2004). While the importance of gap junctions for cardiac function is not disputed, more recent work has shown that the intercalated disc also hosts a number of ion channels, including Na^+ channels and K^+ channels. Together with the proteins forming fascia adherens junctions and desmosomes (which interconnect actin filaments and intermediate filaments of adjacent cells), gap junction channels and ion channels form macromolecular protein complexes in the intercalated disc, each essential for cardiac function (Delmar and Liang, 2012; Delmar and Makita, 2012). Recent experimental studies suggest regulatory interactions between these functional complexes and their involvement in the pathogenesis of important cardiac diseases.

The goal of this review is to discuss (1) the role of gap junction channels and ion channels expressed in the intercalated disc in electrical propagation, and (2) interactions between these functional complexes and their role in disease.

THE CARDIAC CONNEXINS AND ELECTRICAL PROPAGATION

THE CARDIAC CONNEXINS Cx43, Cx40 AND Cx45

In atrial and ventricular myocardium, gap junction channels are formed by three connexins, connexin43 (Cx43), connexin40 (Cx40) and connexin45 (Cx45) (Kanter et al., 1992; Davis et al., 1994). A fourth connexin has been described in the atrioventricular node in mice and humans (Cx30.2 and Cx31.9, respectively)

(Bukauskas et al., 2006). Atrial myocardium gap junctions consist mainly of Cx43 and Cx40, ventricular myocardium of Cx43, and the specific ventricular conducting system of Cx40. Cx45 is present in the sinus and the atrio-ventricular nodes, and in small amounts in the atria and ventricles. Knowledge about the functional roles of Cx43, Cx40, and Cx45 in the cardiac intercalated disc has been derived mainly from experiments in heterologous cell systems and some questions remain unresolved. Common to all cardiac gap junction channels is the apposition and non-covalent binding of two juxtaposed connexons (each expressed in the intercalated disc by adjacent cells) to form a complete gap junction channel, and the composition of each connexon by six connexin molecules (Moreno, 2004; Cottrell and Burt, 2005). Pure homotypic and homomeric gap junction channels composed of Cx43 or Cx40 have relatively large electrical conductances (60–120 pS, and 175–210 pS, respectively) whereas Cx45 forms a small conductance channel of 30–40 pS (Moreno, 2004).

While it is often stated that the dominance of Cx43 in the ventricle and of Cx40 in the Purkinje system are responsible for the relatively high propagation velocities observed in these tissues, and that the presence of Cx45 contributes importantly to the low velocity in the atrio-ventricular node (for values see Kleber et al., 2011), the co-existence of Cx43 and Cx45 in the ventricles, and of Cx40, Cx43 and Cx45 in the atria, likely creates more complex biological interactions in which a connexin species present in relatively low amounts may have an important effect on conduction or modulate other aspects of cell-cell communication. For example, Cx45 has been shown to form heteromeric connexons with Cx43 (Moreno, 2004), and probably Cx40 (Desplantez et al., 2012) thereby reducing the unitary conductance of the channels. It has also been postulated that although Cx45 may not contribute much to intercellular electrical conductance by forming homomeric/homotypic channels, it could function as a modulator of gap junction size (Grikscheit et al., 2008).

In atrial myocardium Cx40 and Cx43 co-localize in the intercalated disc, but the role of mixed Cx43/Cx40 gap junction channels has not been clarified. In heterologous expression systems, it has been shown that Cx43 and Cx40 chemically aggregate, but the question of whether heteromeric connexons and heteromeric/heterotypic Cx43/Cx40 gap junction channels contribute significantly to intercellular current flow in heart remains disputed (Beyer et al., 2001; Cottrell and Burt, 2005). Another question of functional importance is whether expression and/or trafficking of Cx43 and Cx40 are coordinately regulated in atrial tissue. In human atrial tissue, for example, local expression levels of Cx43 and Cx40 affect local propagation velocity; high levels of Cx40 relative to Cx43 are inversely correlated with propagation velocity, whereas high levels of Cx43 relative to Cx40 correlate directly with local propagation velocity (Kanagaratnam et al., 2004). These results are in line with findings in cultured mouse atrial myocytes, in which genetic ablation of Cx40 is associated with *increased* propagation velocity and more Cx43 immmunosignal at the intercalated disc, whereas ablation of Cx43 leads to a decrease of propagation velocity and a concomitant reduction in Cx40 and Cx45 signal (Beauchamp et al., 2006; Desplantez et al., 2012). A further indication that atrial connexins are coordinately regulated comes from analysis of intercellular conductances in cells transfected with mutant Cx43 (Thibodeau et al., 2010). In this situation, co-expression of mutated Cx43 with wild type Cx43, or co-expression of mutated Cx43 with wild type Cx43 and wild type Cx40 produced a transdominant negative effect of the mutated Cx43 on intercellular conductance, indicating interactions between mutated Cx43 and wild type Cx43 and Cx40, possibly at the level of trafficking. Although basic mechanisms of connexin forward and retrograde trafficking have been defined recently (Smyth et al., 2010, 2012, 2014; Smyth and Shaw, 2012a,b), interactions between Cx43 and Cx40 and the resultant effects in cardiac disease remain largely unclarified.

THE EFFECT ON PROPAGATION OF CONNEXIN COMPARTMENTATION AT THE CELL SURFACE

Immediately after birth ventricular myocytes have a spindle-like shape and gap junction plaques are distributed at more or less regular intervals around the cell perimeter (Beauchamp et al., 2004). During development of the adult phenotype, gap junctions become concentrated at the cell border, and fewer junctions (∼30%) are located in the lateral cell membrane (Hoyt et al., 1989). In an elegant theoretical study specifically addressing the effect of gap junction distribution on propagation (Spach et al., 2000), the authors compared *two real cell types*, small neonatal canine ventricular myocytes with neonatal gap junction pattern and large adult canine ventricular myocytes with typical adult end-to-end gap junction distribution pattern, to *two virtual cell types*, small neonatal myocytes with the adult gap junction distribution pattern and large adult myocytes with the neonatal pattern. This approach enabled the authors to separate the effects of cell size from the effects of gap junction distribution on propagation. The surprising result was that the pattern of gap junction distribution exerts only a minor influence on propagation, while cell size (as expected) has a strong influence on propagation velocity.

THE PRINCIPLE OF ELECTRICAL CELL-TO-CELL COUPLING AND CARDIAC PROPAGATION

Insights into the roles of gap junctions and pathways of low electrical resistance between adjacent cells in propagation were derived originally from theories established in nerve (Hodgkin and Rushton, 1946). For propagation in a linear excitable structure with a homogeneous "intracellular electrical medium," the square root of propagation velocity is proportional to the electrical resistance of the intracellular medium (so-called "square root relationship") (Hodgkin, 1954; Tasaki and Hagiwara, 1957). In heart, the intracellular electrical medium is not homogeneous. Rather, the resistance of the cytoplasm is lower than the resistance of the gap junctions, and cytoplasmic propagation shows a finite conduction time (Fast and Kleber, 1993; Spach and Heidlage, 1995). Yet, for normal electrical coupling in heart and for small deviations thereof, the square root relationship is an approximate predictor of conduction behavior. At medium to high levels of electrical uncoupling, when the resistance of the intercellular barrier increases, the propagation behavior becomes discontinuous (Rudy and Quan, 1987). Discontinuous propagation in a linear strand of cells with uniform electrical uncoupling is resistant to propagation block, and a more than 100-fold increase in gap

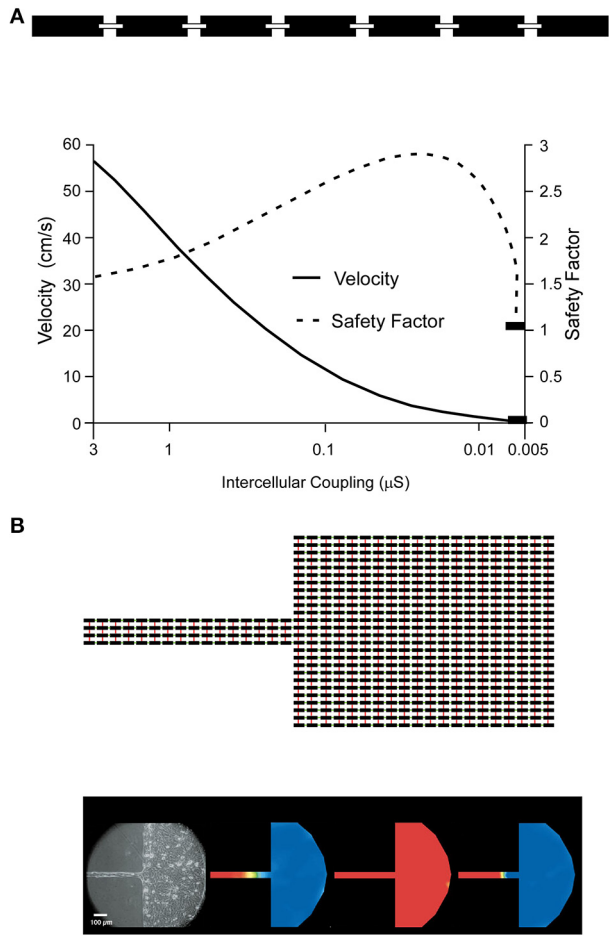

FIGURE 1 | Effect of cell-to-cell coupling on linear (A) vs. discontinuous (B) propagation: (A) depicts schematically a linearly conducting chain of cells coupled by resistors representing the gap junctions (top). The lower part shows the dependence of propagation velocity and safety factor of propagation on cell-to-cell coupling, expressed as conductance in nS. For explanation see text. Reproduced from Shaw and Rudy (1997) with permission. **(B)** The equivalent electrical circuit of a discontinuous tissue structure is illustrated on top. Black rectangles correspond to cells linked by resistors in the x-axis direction (green) and y-axis direction (red). The bottom (left most part) shows experimentally determined propagation in a engineered cell culture of the shape depicted on top (neonatal rat ventricular myocytes). Right of the cell culture picture three propagation maps are coded in color: activation (presence of action potential) is coded in red, resting cells are coded in blue. Normal propagation (left color map) from the strand to the bulk of cells is blocked in the strand, because of source-sink mismatch. Partial uncoupling of the cells restores propagation across the strand and into the bulk (middle color map), whereas as full gap junction uncoupling of the bulk cells produces block at the expansion (right color map). From Rohr et al. (1997) with permission.

junction resistance may be needed for block to occur (**Figure 1A**). This behavior, demonstrated in theoretical studies, was confirmed in engineered strands of neonatal rat ventricular myocytes uncoupled by palmitoleic acid (Rohr et al., 1998), and in strands with complete (i.e., germ-line) genetic ablation of Cx43, in which only a low degree of residual electrical coupling is present due to Cx45 (Beauchamp et al., 2004).

For simple multicellular structures represented, for instance, by a linear strand of cardiac myocytes, this behavior can be explained by the effect of the coupling resistance on the so-called safety factor of propagation (Shaw and Rudy, 1997). The safety factor (SF) can be defined as the ratio of the electrical charge produced by an excited cell and the charge needed to depolarize the same cell. As long as the charge produced by excitation is greater than the charge needed for excitation (SF $>$ 1), propagation is successful. The electrical charge produced by excitation (numerator in the SF formalism) must fulfill two functions which balance one another: it must change the charge at the membrane capacitance and thus produce the action potential, and it must drive the flow of electrical current across cell borders to excite cells downstream of the propagating wavefront. Importantly, increasing cell-to-cell electrical resistance homogeneously will slow propagation, but it will also enhance propagation safety (Shaw and Rudy, 1997) by limiting axial current being dissipated into the downstream cells. It will thus change the balance between the amount of charge flowing into the membrane capacitance and the amount of axial current flow, thereby promoting a higher and faster charge of the capacity and, accordingly, faster action potential upstroke (increase of dV/dt_{max} of the action potential). The fact that electrical uncoupling slows propagation (initially, as aforementioned with an increased propagation safety) is related to the decrease in axial current exciting the downstream cells. Initially this decrease causes slowing of the charge flowing into the membrane capacitance downstream and conduction slowing. Only when the degree of uncoupling becomes extreme does propagation safety decrease and block occurs (Shaw and Rudy, 1997).

While the safety factor principle, as defined by Shaw and Rudy, is very useful for understanding the general dependence of propagation on electrical coupling and the change in ion channel function (not discussed here) in linear structures, two further complexities warrant discussion: the discontinuous nature of cardiac architecture, and the effects of heterogeneity in expression of cardiac connexins with concomitant heterogeneity in electrical coupling.

THE INTERACTION BETWEEN THE MICRO-STRUCTURE OF THE MYOCARDIAL CELLULAR NETWORK AND PROPAGATION

Normal cardiac myocardium shows a laminar arrangement of myocardial "sheet-like" structures wrapped around the left ventricle and bridged by small trabeculae at regular intervals (Legrice et al., 1995; Pope et al., 2008). These structural discontinuities of the myocardial network occur at a scale similar to the wavelength of electrical excitation (approximately 1 mm) and are predicted to affect the behavior of the electrical waves. Moreover, additional structural changes, caused for instance by fibrosis in pathological settings or with aging (Dolber and Spach, 1987), may enhance this interaction. In the context of this review, it is important to discuss the role of cell-to-cell coupling as modulator of propagation at structural discontinuities, as shown by several theoretical and experimental studies. The ability to pattern 2-dimensional multicellular cardiac structures in culture to produce distinct and reproducible geometrical shapes offers the opportunity to study the effect of cellular network structure on propagation, and to unveil the biophysical behavior of such structures in theoretical

studies using equivalent simulated tissue shapes (Rohr et al., 1991).

A typical engineered structure is represented by a small fiber emerging from, or leading into, a large bulk of tissue (so-called "geometrical expansion"). The structural mismatch between the small fiber and the large bulk leads to a corresponding asymmetrical mismatch in electrical propagation. When the small fiber leads into a large bulk, axial current produced by the small amount of cells in the strand has to excite the large bulk. The expansion between the strand and the large mass causes axial electrical current to disperse (current sink), thus, causing current density to decrease. This dispersion causes a local delay in propagation and, in the extreme case, propagation block (Fast and Kleber, 1995a,b; Rohr et al., 1997). In the opposite direction, propagation remains safe, because the large bulk of tissue has only to excite the small mass of cells in the narrow fiber. Thus, the geometrical expansion causes propagation block to be unidirectional. Unidirectional block has been recognized as a prerequisite for initiation of circus movement and re-entry since the beginning of the last century (Mines, 1913). Similar phenomena occur at other types of structural discontinuities such as pivot points and isthmuses, and obey the same biophysical principles (Cabo et al., 1996, 1998; Fast et al., 1996; Kleber and Rudy, 2004).

Importantly, discontinuities in propagation, as described above, are very sensitive to the function of ion currents responsible for excitation and to the state of underlying electrical cell-to-cell coupling. Partial uncoupling of cells at a geometrical expansion produces resistance to dissipation of local current at this site and to a decrease in the current sink (**Figure 1B**). Reduced dispersion of axial current protects the impulse from being blocked at the expansion, a phenomenon that has been demonstrated in experimental and theoretical studies (Fast and Kleber, 1995a,b; Rohr et al., 1997). As a consequence, application of agents causing partial uncoupling of cells can reverse the unidirectional block and allow bidirectional propagation. In whole tissue this is predicted to decrease the probability of initiation of re-entry. In addition to the state of electrical cell-to-cell coupling, the state of the ion channels is an additional player affecting propagation at geometrical expansions, pivot points, and isthmuses. For example, the fact that impulses are delayed locally changes the contributions of the two charge carriers in excitation, the Na^+ inward current and the L-type Ca^{2+} inward current, to successful propagation. At a geometrical expansion the downstream cells are excited with a delay relative to the upstream cells. Accordingly the upstroke of the downstream action potential may occur at a time when the upstroke of the upstream action potential is nearly or fully complete. As a consequence the inward Na^+ current of the upstream cells is "too fast" to excite the downstream cells, and the excitatory charge is delivered instead by the slower L-type Ca^{2+} current. In other words, with increasing discontinuity the flow of L-type Ca^{2+} current becomes increasingly more important as the charge carrier for excitation (Shaw and Rudy, 1997). Proof of this behavior, which has been shown in several theoretical studies (Kleber and Rudy, 2004), is given by the observation, shown in **Figure 1**, that anterograde propagation across a geometrical expansion can be blocked by a Ca^{2+} channel blocker, depending on whether the source-to-sink mismatch is large enough and leads to a local delay >2 ms (Rohr and Kucera, 1997). This effect depends on the underlying state of cell-to-cell coupling, because partial uncoupling will decrease the degree of source-to-sink mismatch for a given structural discontinuity.

Taken together, these observations demonstrate that (1) microscopic tissue structure, (2) expression of ion channels and associated flow of depolarizing currents (Na^+ current and L-type Ca^{2+} current), and (3) cell-to-cell electrical coupling interact to affect local propagation and define local propagation and risk of unidirectional propagation block in tissues with a discontinuous structure such as occurs in the heart. Since microscopic cardiac structure may vary between individuals and may be affected by fibrosis associated with disease and age, it becomes difficult to accurately predict arrhythmogenesis and its prevention by drugs in any individual situation. Experimental and theoretical studies offer more of a general understanding, and the potential arrhythmogenic effect of changes in cell-to-cell coupling cannot be considered independently of changes in the other variables in this highly interactive system.

ELECTRICAL IMPULSE PROPAGATION IN PRESENCE OF VERY LOW AND HETEROGENEOUS CONNEXIN IMMUNOSIGNAL: DOES EPHAPTIC IMPULSE TRANSMISSION PLAY A ROLE?

Experiments involving conditional cardiac myocyte-specific knock-out of Cx43 in mice have shown that a marked decrease in Cx43 expression is necessary to produce ventricular arrhythmias. In the first such study (Gutstein et al., 2001a), in which genetic ablation of Cx43 by a Cre/loxP system decreased total myocardial Cx43 protein by 86–95% associated with a marked reduction in Cx43 immunosignal, electrical propagation velocity was reduced by only ∼50% and, in contrast to the situation with germ-line knock-out of Cx43, mortality was delayed by 15–30 days. In two subsequent studies, cardiac myocyte-specific genetic approaches were used to produce a progressive decrease in Cx43 expression with age (Danik et al., 2004) or to create a mosaic of ventricular tissues showing either normal or absent Cx43 expression (Gutstein et al., 2001b). In the first model, significant propagation slowing occurred only when the amount of Cx43 immunosignal decreased by $\geq$50%, and malignant ventricular arrhythmias were initiated if Cx43 immunosignal was $\leq$18%. In the second model, mosaic expression caused much more irregular electrical excitation patterns and marked arrhythmogenesis, suggesting that not only the average degree of ventricular Cx43 expression but also the distribution patterns and scale of heterogeneity might be important. In a subsequent study, intercellular conductance measured by dual whole cell voltage clamp in pairs of adult rat ventricular myocytes with genetic Cx43 ablation was dramatically reduced from 588 to 10 nS (Yao et al., 2003). Since impulse propagation was reduced by only 50% in tissue composed of the same cells (with conditional cardiac-specific Cx43 knockout associated with a marked decrease of Cx43 immunosignal), these observations raised the question of whether propagation of the cardiac impulse could occur in the absence of electrical cell-to-cell coupling. In fact, this phenomenon, so-called ephaptic impulse transmission, due to local circuit current at the intercalated disc, had been postulated in the 1960s (Sperelakis et al., 1960) and

proposed as an alternative to the role of gap junction channels (Weidmann, 1993).

Theoretical studies have investigated the possible role of ephaptic impulse transmission (also termed "field effect transmission") in myocardium using computer models that take into account the presence of Na^+ channels at the intercalated disc (Kucera et al., 2002; Mori et al., 2008; Veeraraghavan et al., 2014). The key difference in modeling an electrical equivalent circuit for ephaptic transmission relative to earlier models is the focus on the pool of Na^+ channels located within the intercalated disc, which in biophysical terms, represents a narrow cleft with an electrical resistance higher than the normal extracellular resistance. As a consequence, excitation of the upstream cell by inward flow of Na^+ current establishes a voltage gradient between the cleft space and the normal extracellular space, which acts to depolarize the cleft space and the Na^+ channels in the downstream cell facing the cleft. The excitatory effect on the downstream cell, which theoretically may occur in the absence of resistive coupling by gap junctions, depends critically on the cleft width (determining cleft resistance) and the extent to which Na^+ channels are clustered in the intercalated disc. These models also suggest that Na^+ ions accumulate with narrowing cleft width, a phenomenon that decreases the electrochemical gradient for Na^+ and is, therefore, expected to decrease Na^+ current (Kucera et al., 2002; Mori et al., 2008).

The hypothesis that ephaptic transmission occurs in the heart under conditions of marked cell-to-cell uncoupling was put forward as an alternative idea to explain why propagation velocity is only moderately reduced when Cx43 levels are apparently very low, such as occurs in mouse hearts following conditional cardiac myocyte-specific knockout of Cx43. However, its existence has never been proven experimentally. In pairs of cultured neonatal myocytes the existence of ephaptic transmission has been ruled out (Beauchamp et al., 2004). In pairs of ventricular myocytes with germline genetic ablation of Cx43 (i.e., not dependent on the action of Cre recombinase) there is residual electrical coupling (about 5% of normal) due to the presence of gap junction channels formed by Cx45. If these cells are chemically uncoupled, electrical impulse transfer is immediately and reversibly interrupted, while the cells remain excitable by field stimulation, demonstrating that in this setting ephaptic transmission cannot substitute for resistive coupling by gap junctions (Beauchamp et al., 2004).

An attempt to experimentally elucidate the mechanism of impulse propagation in ventricular tissue with inhomogeneous reduction in connexin distribution has been made by (1) quantifying the relationship between the amount of Cx43 at the intercalated disc (as measured by immunohistochemistry) and intercellular electrical conductance across the intercalated disc (McCain et al., 2012), and (2) engineering strands of neonatal mouse ventricular myocytes composed of fixed mixtures of wild type myocytes and cells with genetic Cx43 ablation (Beauchamp et al., 2012). Using this approach, it was first shown that the amount of Cx43 quantified immunohistochemically correlates linearly with electrical conductance, but low levels of conductance can be measured under conditions in which Cx43 signal is below the level of detection using conventional indirect immunofluorescence methods (McCain et al., 2012). In other words, the absence of detectable Cx43 immunosignal does not exclude residual electrical coupling and impulse transmission. In another study (Beauchamp et al., 2012), recently supported by theoretical work (Prudat and Kucera, 2014), it was shown that in tissue with heterogeneously distributed Cx43 expression, fast propagation can be maintained by meandering propagation involving cells with higher Cx43 levels (**Figure 2**). Marked propagation slowing is observed only when the proportion of Cx43-null cells falls below 50%. Moreover, the overall amount of apparent Cx43 immunosignal in such tissues markedly underestimates the percentage of cells expressing normal levels of Cx43 because no Cx43 immunofluorescence is detectable at boundaries between Cx43 expressing myocytes and cells with genetically ablated Cx43 expression (Beauchamp et al., 2012). In conclusion, the observation of relatively preserved propagation at low and inhomogeneous levels of Cx43 expression can be accounted for by cell-to-cell impulse transmission solely involving gap junction channels. The existence of ephaptic transmission as an additional modulator of cardiac impulse propagation has yet to be clearly demonstrated experimentally, although it can be simulated theoretically within narrow limits of specific variables. More sophisticated experimental studies will be required to clarify this point.

INTERACTIONS BETWEEN DESMOSOMAL PROTEINS, ION CHANNELS AND CONNEXINS AT THE INTERCALATED DISC

In the previous paragraphs, this review has focused on the role of gap junctions in impulse transmission and propagation. Ion channels were invoked in the discussion insofar as they might theoretically play a role in cell-to-cell transmission of the electrical impulse. Now, we will discuss mutual interactions between (i) desmosomal and fascia adherens proteins, (ii) connexins and (ii) ion channels expressed in the intercalated disc. New insights into such interactions have emerged recently, stimulated in large part by work to understand mechanisms in arrhythmogenic cardiomyopathy. It thus forms an interesting link to translational medicine and is an example how findings in translational science can feed back to the understanding of basic mechanisms of cardiac function. It mostly involves defining the effect of genetic ablation of components of one of these protein complexes or the use of cells transfected with mutant proteins implicated in human disease, and the subsequent association of the findings in animal models with the human phenotype.

An important principle underlying this work is that major classes of ion channels responsible for generating the cardiac action potential are partitioned in different membrane compartments such as the T-tubular invaginations, the (lateral) surface membrane and the intercalated discs (Cohen, 1996; Kucera et al., 2002; Maier et al., 2004; Petitprez et al., 2011; Milstein et al., 2012). The specificity of Na^+ channel partitioning has been further explained by observations that channels in specific locations are associated with specific regulatory proteins. This includes dystrophin in the case of Nav1.5 channels at the lateral membrane, and the MAGUK protein SAP97 for Nav1.5 at the intercalated disc (Petitprez et al., 2011). It has also been shown that SAP97, which has PDZ binding motifs for several ion channels, is an important

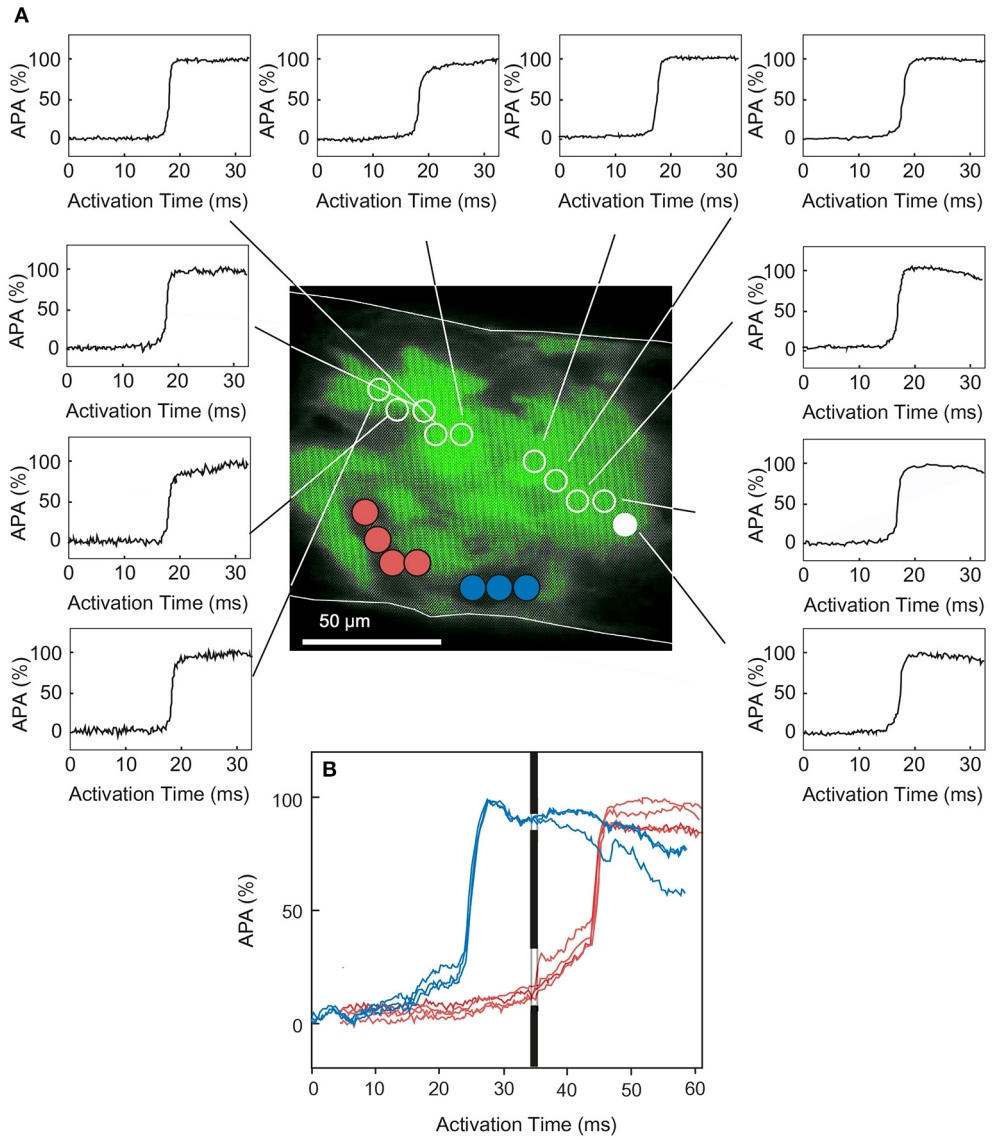

FIGURE 2 | Propagation in engineered cardiac tissue with heterogeneous expression of Cx43. (A) An engineered cardiac strand is produced by 50–50 mixtures of wild type cells (GFP-labeled) and cells with genetic ablation of Cx43 (no GFP-labeling). Electrical stimulation of this strand produces rapid meandering propagation across the Cx43 expressing cell cluster. The action potentials in **(B)** compare excitation of the area with Cx43 deletion (colored action potential) with the first and last action potentials of the Cx43 expressing cluster (which, at this time scale, appear to be nearly superimposed). This comparison illustrates a marked pre-delay and delay in excitation of the areas not expressing Cx43 with respect to the wild type cluster. However, all cells of the strands are eventually excited. From Beauchamp et al. (2012) with permission.

regulator of the intercalated disc fractions of Nav1.5 and Kir2.1 (Milstein et al., 2012). At the same time, recent studies involving knock-in of Nav1.5 channels lacking the PDZ binding motifs have implicated a more complex role for SAP97 involving localization of ion channels at the lateral membrane (Shy et al., 2014). Within the intercalated disc Nav1.5 channels have been shown to closely localize with Cx43 in a region around the gap junction plaque termed the perinexus (Rhett et al., 2012).

Recent studies have identified mechanistic links between proteins of the desmosome, Nav1.5 and Cx43. For example, silencing of plakophilin-2, an armadillo repeat protein contributing to the protein anchor of desmosomal cadherins, leads to a marked decrease in Na^+ inward current via Nav1.5 at the intercalated disc (Sato et al., 2009). Interactions between Cx43 and Nav1.5 expression at the intercalated disc are also suggested by observations that germline ablation of Cx43 in cultured neonatal rat atrial myoctes leads to a nearly 50% decrease in whole cell Na^+ current (Desplantez et al., 2012). Ankyrin-G, a polypeptide involved in surface expression and targeting of membrane channels, has been shown to affect plakophillin-2 and Nav1.5 expression at the intercalated disc (Sato et al., 2011; Makara et al., 2014). The role of ankyrin-G in the regulation of Cx43 is less clear. While silencing

of ankyrin-G decreased Cx43 and intercellular electrical conductance (Sato et al., 2011), no effect of cardiospecific knock-out of ankyrin-G on Cx43 was observed (Makara et al., 2014). Taken together, these observations highlight important, although as yet incompletely understood, interactions among regulatory proteins at the intercalated disc, desmosomal proteins, connexins and ion channels (Nav1.5 and probably others) at the intercalated disc which likely play a significant role in human heart disease.

Additional knowledge about these interactions has come from work defining the molecular pathology of arrhythmogenic cardiomyopathy, a disease in which approximately 60% of cases have (mainly dominant) mutations in desmosomal proteins (plakoglobin, desmoplakin, plakophilin-2, desmocollin-2 and desmoglein-2) (Saffitz et al., 2009; Sen-Chowdhry et al., 2010). For reasons not well understood, the majority of these cases are associated with a decrease in the amount of plakoglobin (γ-catenin) in the intercalated disc and a concomitant decrease in Cx43, raising the possibility that plakoglobin might play a central role in disease pathogenesis (Asimaki et al., 2009). Reductions in the levels of desmosomal plakoglobin and Cx43 at the intercalated disc apparently occur in the presence of normal cellular levels of these proteins, thus implicating a protein trafficking defect as an underlying mechanism. Arrhythmogenic cardiomyopathy is also associated with a marked decrease in Nav1.5 expression, as inferred from experiments involving cultures of neonatal rat ventricular myocytes transfected to express mutant forms of plakoglobin or plakophilin-2 known to cause the human disease. In both situations, a $\geq$50% decrease in Na^+ inward current has been observed (Asimaki et al., 2014).

A potentially important insight into the underlying molecular interactions came from discovery of a drug in a high throughput chemical screen in zebrafish. This small molecule, SB216763, annotated as an inhibitor of glycogen synthase kinase-3β (GSK-3β), prevents the development of cardiac failure in a fish model of arrhythmogenic cardiomyopathy and also prevents changes in the cardiac action potential and decreased currents flowing through Nav1.5 and Kir2.1 in isolated zebrafish ventricular myocytes. SB216763 also blocked expression of disease-related changes in cultured neonatal rat myocytes transfected to express known disease alleles (Asimaki et al., 2014). Furthermore, abnormal subcellular distribution of SAP97 is reversed by SB216763 in cardiac myocytes derived from pluripotent stem cells of 2 human probands carrying plakophilin-2 mutations. The exact role of GSK-3β and its inhibition in the disease phenotype is currently under investigation. Nevertheless, our current knowledge of disease mechanisms in arrhythmogenic cardiomyopathy suggests that expression of desmosomal proteins, connexins and at least two important ion channels (Nav1.5 and Kir2.1) are all regulated interactively at the level of trafficking.

SUMMARY: CELL-TO-CELL COUPLING, ARRHYTHMOGENESIS AND PROPAGATION

In the classical literature, the effects of changes in cell-to-cell coupling are mostly discussed using simple models of linear propagation. In such models, a decrease in cell-to-cell coupling will reduce propagation velocity and, accordingly, decrease the wavelength of excitation. As a consequence an increase in the likelihood of re-entry of circulating excitation is to be expected. This review attempts to summarize and discuss both the classical and contemporary literature which, taken together, reveals a much more complex role for cell-to-cell coupling in normal physiology and arrhythmogenesis. These complexities involve heterogeneous expression of connexins, the structure of the cellular network and expression of ion channels in the intercalated disc all being interactively affected by common regulators of expression. Moreover, disease phenotypes are likely to involve changes in multiple proteins affecting electrical propagation. This complexity of the arrhythmogenic substrate makes it difficult to exactly predict the exact impact of changes in cell-to-cell coupling as an event isolated from all other factors. At the extreme—as discussed in this review—electrical uncoupling may weaken the effect of a discontinuous structure and actually stabilize propagation. Theoretical simulation of these complex interactions including the multitude of variables is certainly a means to improve our understanding of the role in arrhythmogenesis.

The fact that a single disease may produce hundreds of changes at the level of functional proteins, which may be arrhythmogenic in concert, also casts doubt on the concept that targeting a single peripheral protein, as only one of the multitude of variables, will effectively reduce arrhythmogenesis. Instead so-called "upstream drugs" targeting an important common pathway of dysregulation and reversing a pathological phenotype are likely to be more effective. The discovery of an apparent GSK-3β inhibitor as a substance globally rescuing the arrhythmogenic cardiomyopathy phenotype supports this concept.

REFERENCES

Asimaki, A., Kapoor, S., Plovie, E., Karin Arndt, A., Adams, E., Liu, Z., et al. (2014). Identification of a new modulator of the intercalated disc in a zebrafish model of arrhythmogenic cardiomyopathy. *Sci. Transl. Med.* 6, 240–274. doi: 10.1126/scitranslmed.3008008

Asimaki, A., Tandri, H., Huang, H., Halushka, M. K., Gautam, S., Basso, C., et al. (2009). A new diagnostic test for arrhythmogenic right ventricular cardiomyopathy. *N. Engl. J. Med.* 360, 1075–1084. doi: 10.1056/NEJMoa0808138

Beauchamp, P., Choby, C., Desplantez, T., de Peyer, K., Green, K., Yamada, K. A., et al. (2004). Electrical propagation in synthetic ventricular myocyte strands from germline connexin43 knockout mice. *Circ. Res.* 95, 170–178. doi: 10.1161/01.RES.0000134923.05174.2f

Beauchamp, P., Desplantez, T., McCain, M. L., Li, W., Asimaki, A., Rigoli, G., et al. (2012). Electrical coupling and propagation in engineered ventricular myocardium with heterogeneous expression of connexin43. *Circ. Res.* 110, 1445–1453. doi: 10.1161/CIRCRESAHA.111.259705

Beauchamp, P., Yamada, K. A., Baertschi, A. J., Green, K., Kanter, E. M., Saffitz, J. E., et al. (2006). Relative contributions of connexins 40 and 43 to atrial impulse propagation in synthetic strands of neonatal and fetal murine cardiomyocytes. *Circ. Res.* 99, 1216–1224. doi: 10.1161/01.RES.0000250607.34498.b4

Beyer, E. C., Gemel, J., Martinez, A., Berthoud, V. M., Valiunas, V., Moreno, A. P., et al. (2001). Heteromeric mixing of connexins: compatibility of partners and functional consequences. *Cell Commun. Adhes.* 8, 199–204. doi: 10.3109/15419060109080723

Bukauskas, F. F., Kreuzberg, M. M., Rackauskas, M., Bukauskiene, A., Bennett, M. V., Verselis, V. K., et al. (2006). Properties of mouse connexin 30.2 and human connexin 31.9 hemichannels: implications for atrioventricular conduction in the heart. *Proc. Natl. Acad. Sci. U.S.A.* 103, 9726–9731. doi: 10.1073/pnas.0603372103

Cabo, C., Pertsov, A. M., Davidenko, J. M., Baxter, W. T., Gray, R. A., and Jalife, J. (1996). Vortex shedding as a precursor of turbulent electrical activity in cardiac muscle. *Biophys. J.* 70, 1105–1111. doi: 10.1016/S0006-3495(96)79691-1

Cabo, C., Pertsov, A. M., Davidenko, J. M., and Jalife, J. (1998). Electrical turbulence as a result of the critical curvature for propagation in cardiac tissue. *Chaos* 8, 116–126. doi: 10.1063/1.166292

Cohen, S. A. (1996). Immunocytochemical localization of rH1 sodium channel in adult rat heart atria and ventricle. Presence in terminal intercalated disks. *Circulation* 94, 3083–3086. doi: 10.1161/01.CIR.94.12.3083

Cottrell, G. T., and Burt, J. M. (2005). Functional consequences of heterogeneous gap junction channel formation and its influence in health and disease. *Biochim. Biophys. Acta* 1711, 126–141. doi: 10.1016/j.bbamem.2004.11.013

Danik, S. B., Liu, F., Zhang, J., Suk, H. J., Morley, G. E., Fishman, G. I., et al. (2004). Modulation of cardiac gap junction expression and arrhythmic susceptibility. *Circ. Res.* 95, 1035–1041. doi: 10.1161/01.RES.0000148664.33695.2a

Davis, L. M., Kanter, H. L., Beyer, E. C., and Saffitz, J. E. (1994). Distinct gap junction protein phenotypes in cardiac tissues with disparate conduction properties. *J. Am. Coll. Cardiol.* 24, 1124–1132. doi: 10.1016/0735-1097(94)90879-6

Delmar, M., and Liang, F. X. (2012). Connexin43 and the regulation of intercalated disc function. *Heart Rhythm* 9, 835–838. doi: 10.1016/j.hrthm.2011.10.028

Delmar, M., and Makita, N. (2012). Cardiac connexins, mutations and arrhythmias. *Curr. Opin. Cardiol.* 27, 236–241. doi: 10.1097/HCO.0b013e328352220e

Desplantez, T., McCain, M. L., Beauchamp, P., Rigoli, G., Rothen-Rutishauser, B., Parker, K. K., et al. (2012). Connexin43 ablation in foetal atrial myocytes decreases electrical coupling, partner connexins, and sodium current. *Cardiovasc. Res.* 94, 58–65. doi: 10.1093/cvr/cvs025

Dolber, P. C., and Spach, M. S. (1987). Thin collagenous septa in cardiac muscle. *Anat. Rec.* 218, 45–55. doi: 10.1002/ar.1092180109

Engelmann, T. (1877). Vergleichende Untersuchungen zur Lehre von den Muskel- und Nervenelektricitat. *Pfluegers Arch.* 15, 116–148. doi: 10.1007/BF01628342

Fast, V. G., Darrow, B. J., Saffitz, J. E., and Kleber, A. G. (1996). Anisotropic activation spread in heart cell monolayers assessed by high-resolution optical mapping. Role of tissue discontinuities. *Circ. Res.* 79, 115–127. doi: 10.1161/01.RES.79.1.115

Fast, V. G., and Kleber, A. G. (1993). Microscopic conduction in cultured strands of neonatal rat heart cells measured with voltage-sensitive dyes. *Circ. Res.* 73, 914–925. doi: 10.1161/01.RES.73.5.914

Fast, V. G., and Kleber, A. G. (1995a). Block of impulse propagation at an abrupt tissue expansion: evaluation of the critical strand diameter in 2- and 3-dimensional computer models. *Cardiovasc. Res.* 30, 449–459. doi: 10.1016/S0008-6363(95)00071-2

Fast, V. G., and Kleber, A. G. (1995b). Cardiac tissue geometry as a determinant of unidirectional conduction block: assessment of microscopic excitation spread by optical mapping in patterned cell cultures and in a computer model. *Cardiovasc. Res.* 29, 697–707. doi: 10.1016/S0008-6363(96)88643-3

Grikscheit, K., Thomas, N., Bruce, A. F., Rothery, S., Chan, J., Severs, N. J., et al. (2008). Coexpression of connexin 45 with connexin 43 decreases gap junction size. *Cell Commun. Adhes.* 15, 185–193. doi: 10.1080/15419060802013943

Gutstein, D. E., Morley, G. E., Tamaddon, H., Vaidya, D., Schneider, M. D., Chen, J., et al. (2001a). Conduction slowing and sudden arrhythmic death in mice with cardiac-restricted inactivation of connexin43. *Circ. Res.* 88, 333–339. doi: 10.1161/01.RES.88.3.333

Gutstein, D. E., Morley, G. E., Vaidya, D., Liu, F., Chen, F. L., Stuhlmann, H., et al. (2001b). Heterogeneous expression of Gap junction channels in the heart leads to conduction defects and ventricular dysfunction. *Circulation* 104, 1194–1199. doi: 10.1161/hc3601.093990

Harris, A. L. (2001). Emerging issues of connexin channels: biophysics fills the gap. *Q. Rev. Biophys.* 34, 325–472. doi: 10.1017/S0033583501003705

Hodgkin, A. L. (1954). A note on conduction velocity. *J. Physiol.* 125, 221–224.

Hodgkin, A. L., and Rushton, W. A. (1946). The electrical constants of a crustacean nerve fibre. *Proc. R. Soc. Med.* 134, 444–479. doi: 10.1098/rspb.1946.0024

Hoyt, R. H., Cohen, M. L., and Saffitz, J. E. (1989). Distribution and three-dimensional structure of intercellular junctions in canine myocardium. *Circ. Res.* 64, 563–574. doi: 10.1161/01.RES.64.3.563

Kanagaratnam, P., Cherian, A., Stanbridge, R. D., Glenville, B., Severs, N. J., and Peters, N. S. (2004). Relationship between connexins and atrial activation during human atrial fibrillation. *J. Cardiovasc. Electrophysiol.* 15, 206–216. doi: 10.1046/j.1540-8167.2004.03280.x

Kanter, H., Saffitz, J., and Beyer, E. (1992). Cardiac myocytes express multiple gap junction proteins. *Circ. Res.* 70, 438–444. doi: 10.1161/01.RES.70.2.438

Kleber, A. G., Janse, M. J., and Fast, V. G. (2011). "Normal and abnormal conduction in the heart," in *Handbook of Physiology, The Cardiovascular System, The Heart*, 455–530. doi: 10.1002/cphy.cp020112

Kleber, A. G., and Rudy, Y. (2004). Basic mechanisms of cardiac impulse propagation and associated arrhythmias. *Physiol. Rev.* 84, 431–488. doi: 10.1152/physrev.00025.2003

Kucera, J. P., Rohr, S., and Rudy, Y. (2002). Localization of sodium channels in intercalated disks modulates cardiac conduction. *Circ. Res.* 91, 1176–1182. doi: 10.1161/01.RES.0000046237.54156.0A

Legrice, I. J., Smaill, B. H., Chai, L. Z., Edgar, S. G., Gavin, J. B., and Hunter, P. J. (1995). Laminar structure of the heart: ventricular myocyte arrangement and connective tissue architecture in the dog. *Am. J. Physiol.* 269, H571–H582.

Maier, S. K., Westenbroek, R. E., McCormick, K. A., Curtis, R., Scheuer, T., and Catterall, W. A. (2004). Distinct subcellular localization of different sodium channel alpha and beta subunits in single ventricular myocytes from mouse heart. *Circulation* 109, 1421–1427. doi: 10.1161/01.CIR.0000121421.61896.24

Makara, M. A., Curran, J., Little, S., Musa, H., Polina, I., Smith, S. A., et al. (2014). Ankyrin-G coordinates intercalated disc signaling platform to regulate cardiac excitability *in vivo*. *Circ. Res.* doi: 10.1161/CIRCRESAHA.115.305154. [Epub ahead of print].

McCain, M. L., Desplantez, T., Geisse, N. A., Rothen-Rutishauser, B., Oberer, H., Parker, K. K., et al. (2012). Cell-to-cell coupling in engineered pairs of rat ventricular cardiomyocytes: relation between Cx43 immunofluorescence and intercellular electrical conductance. *Am. J. Physiol.* 302, H443–H450. doi: 10.1152/ajpheart.01218.2010

Milstein, M. L., Musa, H., Balbuena, D. P., Anumonwo, J. M., Auerbach, D. S., Furspan, P. B., et al. (2012). Dynamic reciprocity of sodium and potassium channel expression in a macromolecular complex controls cardiac excitability and arrhythmia. *Proc. Natl. Acad. Sci. U.S.A.* 109, E2134–E2143. doi: 10.1073/pnas.1109370109

Mines, G. R. (1913). On dynamic equilibrium in the heart. *J. Physiol.* 46, 349–383.

Moreno, A. P. (2004). Biophysical properties of homomeric and heteromultimeric channels formed by cardiac connexins. *Cardiovasc. Res.* 62, 276–286. doi: 10.1016/j.cardiores.2004.03.003

Mori, Y., Fishman, G. I., and Peskin, C. S. (2008). Ephaptic conduction in a cardiac strand model with 3D electrodiffusion. *Proc. Natl. Acad. Sci. U.S.A.* 105, 6463–6468. doi: 10.1073/pnas.0801089105

Petitprez, S., Zmoos, A. F., Ogrodnik, J., Balse, E., Raad, N., El-Haou, S., et al. (2011). SAP97 and dystrophin macromolecular complexes determine two pools of cardiac sodium channels Nav1.5 in cardiomyocytes. *Circ. Res.* 108, 294–304. doi: 10.1161/CIRCRESAHA.110.228312

Pope, A. J., Sands, G. B., Smaill, B. H., and Legrice, I. J. (2008). Three-dimensional transmural organization of perimysial collagen in the heart. *Am. J. Physiol. Heart Circ. Physiol.* 295, H1243–H1252. doi: 10.1152/ajpheart.00484.2008

Prudat, Y., and Kucera, J. P. (2014). Nonlinear behaviour of conduction and block in cardiac tissue with heterogeneous expression of connexin 43. *J. Mol. Cell. Cardiol.* 76C, 46–54. doi: 10.1016/j.yjmcc.2014.07.019

Rhett, J. M., Ongstad, E. L., Jourdan, J., and Gourdie, R. G. (2012). Cx43 associates with Na(v)1.5 in the cardiomyocyte perinexus. *J. Membr. Biol.* 245, 411–422. doi: 10.1007/s00232-012-9465-z

Rohr, S., and Kucera, J. P. (1997). Involvement of the calcium inward current in cardiac impulse propagation: induction of unidirectional conduction block by nifedipine and reversal by Bay K 8644. *Biophys. J.* 72, 754–766. doi: 10.1016/S0006-3495(97)78710-1

Rohr, S., Kucera, J. P., Fast, V. G., and Kleber, A. G. (1997). Paradoxical improvement of impulse conduction in cardiac tissue by partial cellular uncoupling. *Science* 275, 841–844. doi: 10.1126/science.275.5301.841

Rohr, S., Kucera, J. P., and Kleber, A. G. (1998). Slow conduction in cardiac tissue, I: effects of a reduction of excitability versus a reduction of electrical coupling on microconduction. *Circ. Res.* 83, 781–794. doi: 10.1161/01.RES.83.8.781

Rohr, S., Schölly, D. M., and Kleber, A. G. (1991). Patterned growth of neonatal rat heart cells in culture: morphological and electrophysiological characterization. *Circ. Res.* 68, 114–130. doi: 10.1161/01.RES.68.1.114

Rudy, Y., and Quan, W. L. (1987). A model study of the effects of the discrete cellular structure on electrical propagation in cardiac tissue. *Circ. Res.* 61, 815–823. doi: 10.1161/01.RES.61.6.815

Saffitz, J. E., Asimaki, A., and Huang, H. (2009). Arrhythmogenic right ventricular cardiomyopathy: new insights into disease mechanisms and diagnosis. *J. Investig. Med.* 57, 861–864. doi: 10.231/JIM.0b013e3181c5e631

Sato, P. Y., Coombs, W., Lin, X., Nekrasova, O., Green, K. J., Isom, L. L., et al. (2011). Interactions between ankyrin-G, Plakophilin-2, and Connexin43 at the cardiac intercalated disc. *Circ. Res.* 109, 193–201. doi: 10.1161/CIRCRESAHA.111.247023

Sato, P. Y., Musa, H., Coombs, W., Guerrero-Serna, G., Patino, G. A., Taffet, S. M., et al. (2009). Loss of plakophilin-2 expression leads to decreased sodium current and slower conduction velocity in cultured cardiac myocytes. *Circ. Res.* 105, 523–526. doi: 10.1161/CIRCRESAHA.109.201418

Sen-Chowdhry, S., Morgan, R. D., Chambers, J. C., and McKenna, W. J. (2010). Arrhythmogenic cardiomyopathy: etiology, diagnosis, and treatment. *Annu. Rev. Med.* 61, 233–253. doi: 10.1146/annurev.med.052208.130419

Shaw, R. M., and Rudy, Y. (1997). Ionic mechanisms of propagation in cardiac tissue. Roles of the sodium and L-type calcium currents during reduced excitability and decreased gap junction coupling. *Circ. Res.* 81, 727–741. doi: 10.1161/01.RES.81.5.727

Shy, D., Gillet, L., Ogrodnik, J., Albesa, M., Verkerk, A. O., Wolswinkel, R., et al. (2014). PDZ domain-binding motif regulates cardiomyocyte compartment-specific NaV1.5 channel expression and function. *Circulation* 130, 147–160. doi: 10.1161/CIRCULATIONAHA.113.007852

Smyth, J. W., Hong, T. T., Gao, D., Vogan, J. M., Jensen, B. C., Fong, T. S., et al. (2010). Limited forward trafficking of connexin 43 reduces cell-cell coupling in stressed human and mouse myocardium. *J. Clin. Invest.* 120, 266–279. doi: 10.1172/JCI39740

Smyth, J. W., and Shaw, R. M. (2012a). The gap junction life cycle. *Heart* 9, 151–153. doi: 10.1016/j.hrthm.2011.07.028

Smyth, J. W., and Shaw, R. M. (2012b). Visualizing cardiac ion channel trafficking pathways. *Methods Enzymol.* 505, 187–202. doi: 10.1016/B978-0-12-388448-0.00018-8

Smyth, J. W., Vogan, J. M., Buch, P. J., Zhang, S. S., Fong, T. S., Hong, T. T., et al. (2012). Actin cytoskeleton rest stops regulate anterograde traffic of connexin 43 vesicles to the plasma membrane. *Circ. Res.* 110, 978–989. doi: 10.1161/CIRCRESAHA.111.257964

Smyth, J. W., Zhang, S. S., Sanchez, J. M., Lamouille, S., Vogan, J. M., Hesketh, G. G., et al. (2014). A 14-3-3 mode-1 binding motif initiates gap junction internalization during acute cardiac ischemia. *Traffic* 15, 684–699. doi: 10.1111/tra.12169

Spach, M. S., and Heidlage, J. F. (1995). The stochastic nature of cardiac propagation at a microscopic level. Electrical description of myocardial architecture and its application to conduction. *Circ. Res.* 76, 366–380. doi: 10.1161/01.RES.76.3.366

Spach, M. S., Heidlage, J. F., Dolber, P. C., and Barr, R. C. (2000). Electrophysiological effects of remodeling cardiac gap junctions and cell size: experimental and model studies of normal cardiac growth. *Circ. Res.* 86, 302–311. doi: 10.1161/01.RES.86.3.302

Sperelakis, N., Hoshiko, T., and Berne, R. M. (1960). Nonsyncytial nature of cardiac muscle: membrane resistance of single cells. *Am. J. Physiol.* 198, 531–536.

Tasaki, I., and Hagiwara, S. (1957). Capacity of muscle fiber membrane. *Am. J. Physiol.* 188, 423–429.

Thibodeau, I. L., Xu, J., Li, Q., Liu, G., Lam, K., Veinot, J. P., et al. (2010). Paradigm of genetic mosaicism and lone atrial fibrillation: physiological characterization of a connexin 43-deletion mutant identified from atrial tissue. *Circulation* 122, 236–244. doi: 10.1161/CIRCULATIONAHA.110.961227

Valiunas, V., Polosina, Y. Y., Miller, H., Potapova, I. A., Valiuniene, L., Doronin, S., et al. (2005). Connexin-specific cell-to-cell transfer of short interfering RNA by gap junctions. *J. Physiol.* 568, 459–468. doi: 10.1113/jphysiol.2005.090985

Veeraraghavan, R., Poelzing, S., and Gourdie, R. G. (2014). Intercellular electrical communication in the heart: a new, active role for the intercalated disk. *Cell Commun. Adhes.* 21, 161–167. doi: 10.3109/15419061.2014.905932

Weidmann, S. (1952). The electrical constants of Purkinje fibres. *J. Physiol.* 118, 348–360.

Weidmann, S. (1966). The diffusion of radiopotassium across intercalated disks of mammalian cardiac muscle. *J. Physiol.* 187, 323–342.

Weidmann, S. (1993). Cardiac action potentials, membrane currents, and some personal reminiscences. *Annu. Rev. Physiol.* 55, 1–14. doi: 10.1146/annurev.ph.55.030193.000245

Yao, J. A., Gutstein, D. E., Liu, F., Fishman, G. I., and Wit, A. L. (2003). Cell coupling between ventricular myocyte pairs from connexin43-deficient murine hearts. *Circ. Res.* 93, 736–743. doi: 10.1161/01.RES.0000095977.66660.86

Conflict of Interest Statement: Kleber: Consultant, Schiller Inc., Baar, Switzerland. The authors declare that the research was conducted in the absence of any commercial or financial relationships that could be construed as a potential conflict of interest.

Received: 19 September 2014; paper pending published: 29 September 2014; accepted: 30 September 2014; published online: 17 October 2014.

*Citation: Kleber AG and Saffitz JE (2014) Role of the intercalated disc in cardiac propagation and arrhythmogenesis. Front. Physiol. **5**:404. doi: 10.3389/fphys.2014.00404*

This article was submitted to Cardiac Electrophysiology, a section of the journal Frontiers in Physiology.

frontiers in PHYSIOLOGY

REVIEW ARTICLE
published: 22 December 2014
doi: 10.3389/fphys.2014.00482

Passive ventricular remodeling in cardiac disease: focus on heterogeneity

Elise L. Kessler[1], Mohamed Boulaksil[1,2], Harold V. M. van Rijen[1], Marc A. Vos[1] and Toon A. B. van Veen[1]*

[1] *Division of Heart and Lungs, Department of Medical Physiology, University Medical Center Utrecht, Utrecht, Netherlands*
[2] *Department of Cardiology, Radboud University Medical Center, Nijmegen, Netherlands*

Edited by:
George E. Billman, The Ohio State University, USA

Reviewed by:
Jan Pavel Kucera, University of Bern, Switzerland
Crystal M. Ripplinger, University of California, Davis, USA

****Correspondence:***
Toon A. B. van Veen, University Medical Center Utrecht, Department of Medical Physiology, Division of Heart and Lungs, Yalelaan 50, Utrecht 3584 CM, Netherlands
e-mail: a.a.b.vanveen@umcutrecht.nl

Passive ventricular remodeling is defined by the process of molecular ventricular adaptation to different forms of cardiac pathophysiology. It includes changes in tissue architecture, such as hypertrophy, fiber disarray, alterations in cell size and fibrosis. Besides that, it also includes molecular remodeling of gap junctions, especially those composed by Connexin43 proteins (Cx43) in the ventricles that affect cell-to-cell propagation of the electrical impulse, and changes in the sodium channels that modify excitability. All those alterations appear mainly in a heterogeneous manner, creating irregular and inhomogeneous electrical and mechanical coupling throughout the heart. This can predispose to reentry arrhythmias and adds to a further deterioration into heart failure. In this review, passive ventricular remodeling is described in Hypertrophic Cardiomyopathy (HCM), Dilated Cardiomyopathy (DCM), Ischemic Cardiomyopathy (ICM), and Arrhythmogenic Cardiomyopathy (ACM), with a main focus on the heterogeneity of those alterations mentioned above.

Keywords: gap junction, sodium channel, fibrosis, arrhythmias, heterogeneity

INTRODUCTION

The lifelong purpose of the heart is maintenance of cardiac output and supply of all organs with an appropriate amount of oxygen and nutrients. At the same time it steers the controlled homeostasis of the blood via clearance of waste products, drugs and imbalanced levels of ions and proteins in the lungs, liver, and kidneys. To be able to fulfill this task, the heart has to adapt its workload to the needs of the body (Kemp and Conte, 2012). Many different diseases like coronary artery disease, myocardial infarction, hypertension, dysfunction of valves, congenital heart disease, lung diseases, diabetes, anemia, hyperthyroidism, and or arrhythmia/dysrhythmia can alter the performance of the heart (Lloyd-Jones et al., 2002; van Rijen et al., 2006; Roger et al., 2011). In order to preserve cardiac output under these conditions, the heart will start several compensatory mechanisms, like the Frank Starling mechanism, neurohumoral activation, and inflammational responses (Westerhof and O'Rourke, 1995; Lee and Tkacs, 2008). Moreover, the heart starts to modify the gene program that shapes the individual cells that compose the organ. This in an attempt to adapt chronically to the new requirements of its environment. These adaptations together will result in myocardial remodeling that most often has heterogeneous characteristics (Swynghedauw, 1999).

By nature, the heart itself is a rather heterogeneous organ: morphologically, the right and left side as well as atria and ventricles show various differences in cell constellations, hemodynamics and their respective electrical characteristics (Zimmer, 1994). The different resistances in peripheral and pulmonary circulation for instance are causative for the differences between left and right ventricle anatomy (right ventricular wall is much thinner than the left wall). Also with respect to molecular make-up and microarchitecture of the cardiac muscle significant differences exist. The way the fibers are orientated within the left and right ventricle is not comparable. Electrical impulse propagation faces differences in conduction velocity between left and right ventricles but also with the specialized conduction system. Part of that relies on differences in expression level and pattern of gap junction channels and the ion channels that underlie action potential generation.

The sodium channel protein Nav1.5, for instance, is heterogeneously distributed throughout the ventricles and the cardiac conduction system in healthy hearts (Remme et al., 2009). Besides that, two pools of Nav1.5 channels can be found in cardiomyocytes: a lateral pool and a pool in the intercalated disc that coexist and interact with different proteins (Petitprez et al., 2011). Also Cx43 is found in different densities within the healthy heart e.g., regarding the posterior and anterior wall of the ventricles (Strom et al., 2010).

Beyond the natural heterogeneity that is found under the normal physiological functioning of the heart, this review will focus on the heterogenic aspect that is involved in passive remodeling of the ventricles under pathophysiological conditions. Passive remodeling is defined as the chronic molecular and structural adaptations in ventricular cardiomyocytes and alterations in gene expression as induced by different forms of heart disease. Active remodeling, in contrast, is defined as phosphorylation processes that e.g., result from sympathic and parasympathic imbalance. This is exampled by the increase in heart rate that is facilitated

through alterations in phosphorylation of ion channels (e.g., L–type calcium channels) in the sinus node.

One of the most crucial and maladaptive factors of passive remodeling in the ventricles is heterogeneity in electrical and structural remodeling. In that perspective we will discuss factors associated with conduction and propagation of excitation, but not with respect to repolarization (e.g., potassium currents, heterogeneity in action potential duration), and contraction (e.g., calcium-handling and sarcomeric proteins). During remodeling, heterogeneous alterations in three factors contribute to increase the propensity to arrhythmias and to develop heart failure: (1) tissue architecture such as hypertrophy, fibrosis, fiber disarray, and cell size, (2) electrical coupling by means of gap junctions and especially those composed of Cx43, and (3) electrical excitability due to changes in sodium channels that are mainly composed of Nav1.5 (Kleber and Rudy, 2004; van Rijen et al., 2006; Bowers et al., 2010).

We will address remodeling of these factors during Dilated Cardiomyopathy (DCM), Hypertrophic Cardiomyopathy (HCM), Ischemic Cardiomyopathy (ICM) and Arrhythmogenic Cardiomyopathy (ACM), previously known as Arrhythmogenic Right Ventricular Cardiomyopathy/Dysplasia (ARVC/D). In general, DCM can be identified by cardiac chamber dilatation and reduced systolic function often leading to congestive heart failure. It is the most commonly occurring cardiomyopathy in adults and children and is associated with muscle dysfunction and/or volume overload. On the other hand, in children DCM is mostly caused by myocarditis and neurohumoral diseases (Towbin et al., 2006). DCM is defined as the presence of left ventricular fractional shortening (<25%) and/or LVEF < 45% and left ventricular end-diastolic dimensions (LVEDD) of >117% of the predicted value by the Henry formula (Mestroni et al., 1999). It can also be caused by a variety of genetic mutations that are uncovered upon analysis of family history and molecular genetic testing. These forms, however, are referred to as familial dilated cardiomyopathy (FDC) (Hershberger and Morales, 2013). HCM has been defined by the World Health Organization as the presence of left or biventricular hypertrophy, in absence of any cardiac or systemic cause (Richardson et al., 1996). When this definition is used, the general prevalence is about 1:500 (Maron, 2002). However, HCM can also be caused by mutations in genes encoding for cardiac sarcomeric and myofilament proteins; for the latter already more than 1400 mutations have been identified increasing the prevalence even more (Maron et al., 2012; Efthimiadis et al., 2014).

ICM results from myocardial ischemia and is characterized by remodeling due to myocardial infarction which eventually triggers loss of contractility, still being the leading cause of ventricular dysfunction worldwide (reviewed in Wu, 2007).

Finally, ACM is a non-ischemic progressive and predominantly heritable heart disease associated with cardiac arrhythmias and sudden cardiac death (Corrado et al., 2000). ACM is characterized through replacement of cardiomyocytes by fibro-fatty tissue (Thiene et al., 1988; Saffitz et al., 2009). About 60% of the cases have a hereditary basis and mutations causing ACM have been found in several desmosomal genes like desmoplakin (Rampazzo et al., 2002), plakoglobin (Asimaki et al., 2007), plakophilin2 (Gerull et al., 2004; van Tintelen et al., 2006), desmocollin2 (Heuser et al., 2006; Syrris et al., 2006), and desmoglein (Pilichou et al., 2006). Moreover, genes not related to the desmosome can be affected such as the transmembrane protein 43 (TMEM43), phospholamban (PLN), desmin and transforming growth factor beta3 (TGFβ3) (Beffagna et al., 2005; Merner et al., 2008; Otten et al., 2010; van der Zwaag et al., 2012).

In addition, a variety of mutations in several ion channels that add to action potential generation have been described to trigger pro-arrhythmic remodeling of the heart. This subset of arrhythmogenic cardiac diseases is, however, beyond the scope of this review.

TISSUE ARCHITECTURE

Several extrinsic and intrinsic factors can lead to alterations in cardiac workload. Those changes can trigger growth of individual myocytes leading to cardiac hypertrophy. An increased amount of hypertrophy is associated with a decreased conduction velocity of the electrical impulse (Winterton et al., 1994; Cooklin et al., 1997; McIntyre and Fry, 1997). Moreover, metaplasia of fibroblasts into myofibroblasts, a more contractile and collagen producing cell type can increase the deposition of the extracellular matrix (ECM) leading to fibrosis (Davis and Molketin, 2013). This is further supported by an increased rate of cell death—necrosis and apoptosis—and inflammatory processes such as the secretion of TNF-alpha or IL-6 (Gill et al., 2002; Nian et al., 2004). Besides that, also alterations in myocardial fiber orientation can importantly affect characteristics of cardiac impulse propagation (Vetter et al., 2005).

HYPERTROPHY AND CELL SIZE

The key feature of hypertrophy in general is an increased cell size that electrically can be measured as an increase in cell-capacitance. Hypertrophy and increased cell size counteract the increased wall tension as caused by changes in cardiac workload (Laplace's law). Therefore, hypertrophy is seen as a compensatory mechanism. However, cardiac impulse propagation as well as conduction velocity gradually decrease with increasing severity of hypertrophy (Winterton et al., 1994; Cooklin et al., 1997; McIntyre and Fry, 1997) leading to an elevated risk for heart failure and sudden cardiac death (Meyerburg et al., 1992).

In DCM mainly the cell length is increased and this is associated by dilation and systolic disturbances of predominantly the left ventricle. Also both ventricles can be impaired, but generally with normal left ventricular wall thickness (Richardson et al., 1996; DuPont et al., 2001). The effect of eccentric hypertrophy on electrical signaling has been addressed in several animal models. An increase in conduction velocity was shown in a rabbit model, where a combined pressure- and volume overload increased heart weight by about 100%, and both cell length and width were increased by about 30%. Delayed activation was indicated by an increase in QRS duration from 50 ms in control to 58 ms in rabbits with DCM. Parallel and transverse to fiber orientation, however, epicardial conduction velocity appeared increased by 18 and 16%, respectively while transmural conduction velocity was unchanged. The authors of this study concluded that the

increased cell size was responsible for the increase in longitudinal and transverse conduction velocity. Moreover, they concluded that the increased conduction velocity could not sufficiently compensate for the increased heart size, which was causative for the prolonged QRS durations (Wiegerinck et al., 2006). In a dog model of rapid pacing, it has been shown that QRS duration and cell length were increased, while cell width was reduced. Besides, transmural conduction velocity was reduced in both RV and LV, while Cx43 expression was reduced only in LV. As such, reduced cell width seems to play a dominant role in the reduced conduction velocity (Akar et al., 2004). In mice models, where DCM was induced by transverse aortic constriction (TAC), cell size, and the amount of hypertrophy was significantly increased after 6 weeks of TAC. This was leading to prolongations of PQ, QT, and QRS intervals, and slowing of right ventricular conduction velocity parallel to the fiber orientation (Boulaksil et al., 2010b). Data of a recent study with DCM patients showed elevated levels of myosin light-chain kinase and CRP that could possibly serve as diagnostic biomarkers for hypertrophy (Branishte et al., 2013).

In HCM, primarily cell width is increased (Formigli et al., 2003) leading to hypertrophy without dilation of the ventricles (Maron, 2002). This affects conduction of the electrical impulse as has been shown using computer modeling, where conduction velocity increased with cell size, and cell size was determined to be the dominant factor affecting conduction velocity (Spach et al., 2000). Also for HCM, several animal models have been described. In a rat model, where RV-HCM was induced by injections with monocrotaline (leading to pulmonary hypertension), increased cell width and lateralized Cx43 expression were found, while cell length was unaffected. Conduction velocity parallel to the fiber orientation was decreased, although perpendicular to the fiber orientation the conduction velocity was unchanged (Uzzaman et al., 2000). Similar results were obtained in another study that used the same rat model with monocrotaline induced pressure overload. In this study, RV cell width was increased, but again cell length remained unaffected. In the left ventricle, cell width and length were both decreased. Moreover, longer action potentials (at 90% repolarization), prolongation of the effective refractory period, and slowing of the longitudinal conduction velocity occurred (Hardziyenka et al., 2012). Besides the rat model, LV epicardial mapping was also performed in patients after chronic thromboembolic pulmonary hypertension. Comparable to the experimental model, these patients also showed prolongation of the effective refractory period and conduction slowing (Hardziyenka et al., 2012).

In ICM, cardiac hypertrophy can be found in the majority of patients (Kannel et al., 1961; Zaino and Tabor, 1963). In MRL (Murphy Roths Large) mice exhibiting an ICM phenotype, increased cell size and hypertrophy lead to a faster progression toward heart failure than in controls (Smiley et al., 2014). Moreover, electrocardiographic left ventricular hypertrophy embedded a predictive value for arrhythmias and mortality in ICM patients, making it an important factor to consider during diagnosis (Bender et al., 2012). In ACM no gross cardiac hypertrophy has been reported and the individual cell size is not increased either. Therefore, hypertrophy is not included as a parameter into the revised Task Force Criteria that are used to diagnose ACM (Marcus et al., 2010).

FIBROSIS AND MYOCARDIAL FIBER DISARRAY

In the healthy heart, cardiac myocytes are embedded in the ECM, a network of multiple molecules, proteins and thin intertwining strands of collagen fibers, synthesized by cardiac fibroblasts (Manabe et al., 2002). This network ensures tissue strength and allows cell-cell contact between neighboring cells (Weber et al., 1994). Cardiac fibrosis is the inappropriately high amount of collagen deposition in the heart during pathophysiological remodeling which hampers electrical conduction and enables the development of arrhythmias (Krenning et al., 2010). In addition, also cardiomyocyte fiber orientation plays an important role in the propagation of the electrical signal and fiber disarray can further facilitate the generation of ventricular arrhythmias (Brugada et al., 1991; Punske et al., 2005) This was recently shown in a study that combined data from neonatal rat cardiomyocytes and computer models (Kudryashova et al., 2014).

Fibrosis can be divided into replacement fibrosis (compact and patchy) and reactive fibrosis (interstitial and diffuse) (Swynghedauw, 1999). Typical examples of these four different forms we published before and are expressed in **Figure 1** of a review article by the de Jong et al. (2011). Replacement fibrosis occurs after clearance of dead myocytes, where cardiac cells will be replaced by collagen fibers facilitating the preservation of the structure of the myocardium as well as the clearance of debris (de Jong et al., 2011). This normally includes compact or patchy fibrosis that is generated after an infarct or in due to chronic pressure overload. These processes have been described both in patients and in experimental animal models (Xia et al., 2009). Compact fibrosis is created, when a whole area is replaced by fibrosis and no viable myocytes are left. Although this seems to be dramatic for the cardiac contractile performance, this form is the least arrhythmogenic (de Bakker et al., 1988). Patchy fibrosis describes areas, where fibrosis and myocardial cells are confounded. In this case, collagen fibers are long strands disturbing the electrical signal propagation (de Bakker et al., 1993). Reactive fibrosis describes the process when more collagen is produced than degraded without a loss of viable cardiomyocytes. This includes interstitial and diffuse fibrosis and can be caused by mutations and changes in gene expression, a phenotypical switch from fibroblasts into myofibroblasts, as well as due to aging (Biernacka and Frangogiannis, 2011). Interstitial fibrosis is localized in between the individual cells. High interstitial collagen content causes reduced compliance and electrical impairment (Rohr, 2009) possibly leading to arrhythmias and heart failure (Janicki and Brower, 2002). Diffuse fibrosis is comparable to patchy fibrosis, however, the collagen strands are short and this form is less arrhythmogenic (Kawara et al., 2001).

In murine animal models that can be followed and analyzed at different time points after the experimental intervention has been made, chronic pressure overload initially leads to reactive fibrosis and in later stages this may change into a heterogeneous deposition of replacement fibrosis. The switch is likely caused by the fact that at a certain time point proper nutrient supply to the cells fails

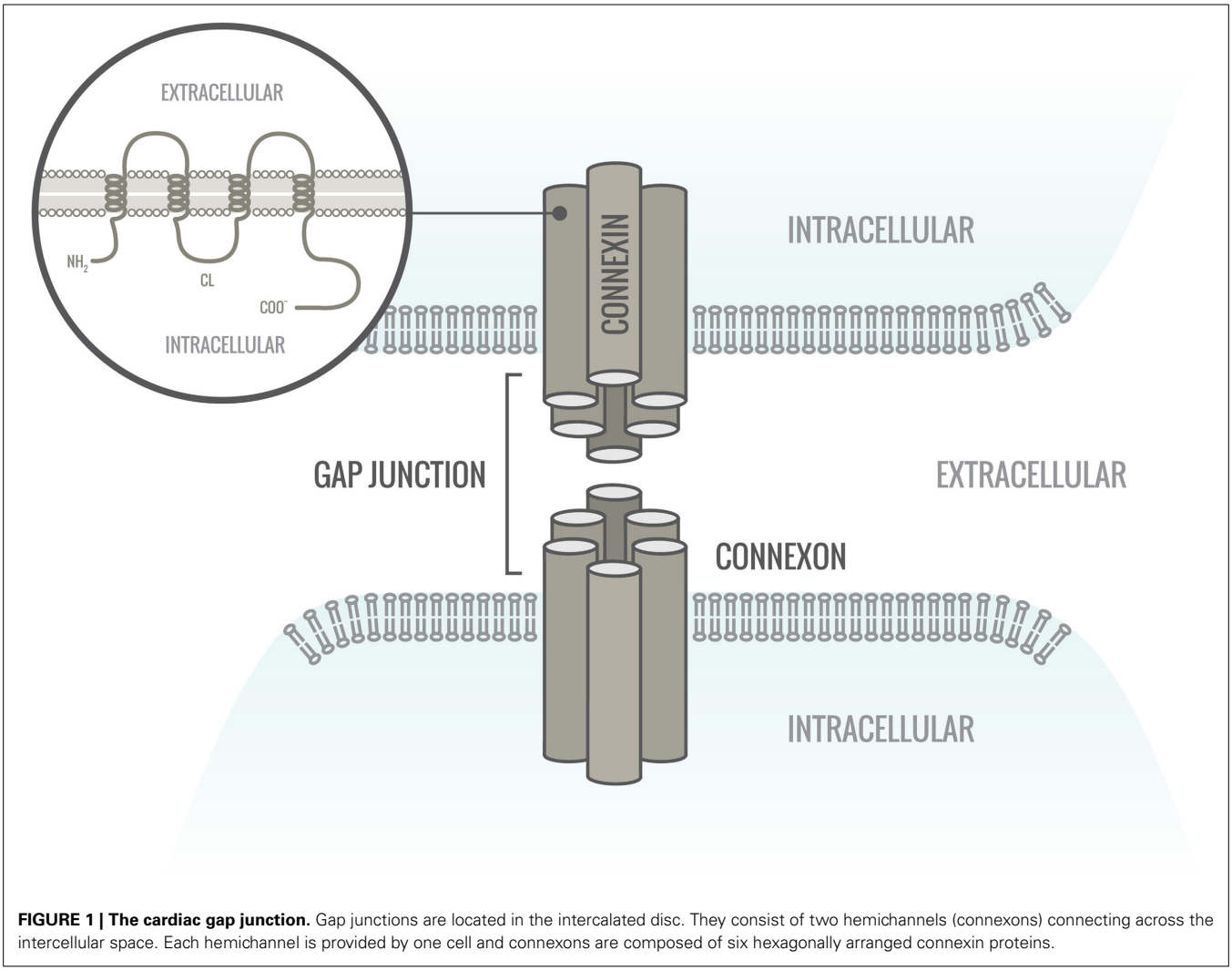

FIGURE 1 | The cardiac gap junction. Gap junctions are located in the intercalated disc. They consist of two hemichannels (connexons) connecting across the intercellular space. Each hemichannel is provided by one cell and connexons are composed of six hexagonally arranged connexin proteins.

to maintain a minimal level (Isoyama and Nitta-Komatsubara, 2002).

Myocardial fiber disarray is the result of altered fiber orientation after e.g., an infarct. Adjacent cardiomyocytes are then mostly aligned in a perpendicular way or obliquely to each other in or around the collagen (Hughes, 2004). Nowadays, predominantly computer models are used to simulate possible alterations and effects on electrical propagation caused by fiber disarray. Computer models are by definition artificial and similarly to genetic engineered animal models, care should be taken by extrapolating these results to the human heart. However, these mathematical models may provide valuable additive insight, since they allow studying the effects induced by individual alterations but also the summation of more than one altered factor can be studied systemically. With such models models, risk of cardiac death can be predicted in e.g., long QT patients and various factors can be implemented at the same time like cell size, wall thickness, action potential duration and fibrosis (Hoefen et al., 2012; Zhao et al., 2013).

In DCM predominantly patchy areas of interstitial and replacement fibrosis can be found, but also perivascular patterns have been described (Nakayama et al., 1987; Swynghedauw, 1999). In HCM patients, interstitial fibrosis predominates (Swynghedauw, 1999). In mice with chronic pressure overload, next to hypertrophy, increased levels of interstitial fibrosis have been reported in many cases (Xia et al., 2009; Boulaksil et al., 2010a,b). Moreover, myocardial disarray is one of the hallmarks of HCM (Hughes, 2004). Although it is also present in other cardiac diseases and even in physiologically aged hearts, through the presence in high quantities it is specific for HCM making it a highly sensitive and useful marker (Hughes and McKenna, 2005).

In ICM, infarcted myocytes are replaced predominantly by heterogeneously distributed replacement- and interstitial fibrosis creating islands of cardiomyocytes surrounded by scar tissue. This so-called "labyrinth" of viable strands of cardiomyocytes surrounded by insulating areas of fibrosis creates disconnection of myocytes that leads to excitation blocks and arrhythmias (Fenoglio et al., 1983; Weber et al., 2008). In murine infarct models, fiber disarray has been reported in the infarct border zone, although to a much lesser extent than in HCM (Smith et al., 1991).

ACM is characterized by degeneration of cardiomyocytes and fibro-fatty replacement (Thiene et al., 1988). One theory is that altered cell-cell adhesion due to mutations in genes encoding for structures of the intercalated disc, e.g., the desmosomes, causes injuries to myocytes. This promotes cell death and leads to replacement by fibro-fatty tissue (Saffitz et al., 2009). Histologically, analysis of fibrosis and fiber orientation can help to diagnose any of the above described diseases. Moreover, in all diseases, fibrosis leads to conduction blocks, which increases the propensity to develop reentry arrhythmias, or promotes the manifestation of ectopic impulse generation in relatively uncoupled clusters of cardiomyocytes due to disease-induced remodeling of the expressed ion channels.

ELECTRICAL COUPLING—GAP JUNCTIONS

Gap junctions in the heart are agglomerates of channels that connect the cytoplasm of two adjoining cells allowing electrical coupling between the cardiomyocytes as well as the exchange of certain small molecules, metabolites and ions up to a size of approximately 1 kDa (Elfgang et al., 1995; Noorman et al., 2009). One gap junction channel consists of two hemi-channels (connexons), each delivered by one of the two adjoining cells (**Figure 1**). The two connexons dock in the intercellular space to form a functional channel.

The connexons are composed of connexin proteins. In cardiomyocytes the three main isoforms that are expressed are Connexin 40 (Cx40), Connexin 45 (Cx45), and Connexin 43 (Cx43) with Cx43 being predominant in ventricular cardiomyocytes. Together with adherens junctions and desmosomes, gap junctions are localized in the intercalated disc (ICD), a step-like specialized membrane structure at the longitudinal cell edges between two cells (**Figure 2**). In those ICD's, gap junctions are normally present in the regions parallel (interplicate) to the longitudinal axis of the cardiomyocytes (Smith et al., 1991).

In patients of all four types of cardiac disease, a reduction in ventricular Cx43 localized at the ICD has been found (Peters et al., 1993; DuPont et al., 2001; Kaplan et al., 2004a). Using genetically engineered animal models, a plethora of data have been collected regarding to role of Cx43, using Cx43 knock out animal models. In 1995, the first Cx43 KO model revealed that these mice died perinatally due to major heart problems (malformation of the outflow tract) and cardiac failure (Reaume et al., 1995). Since then, conditional Cx43 KO mice and haploinsufficient animals have been generated. Nevertheless, results obtained from studies with heterozygous KO animals are contradicting. Mice showed reduced expression of Cx43 up to 50%, and in some studies this reduction resulted in reduced conduction velocity (Guerrero et al., 1997; Thomas et al., 1998; Eloff et al., 2001) while other

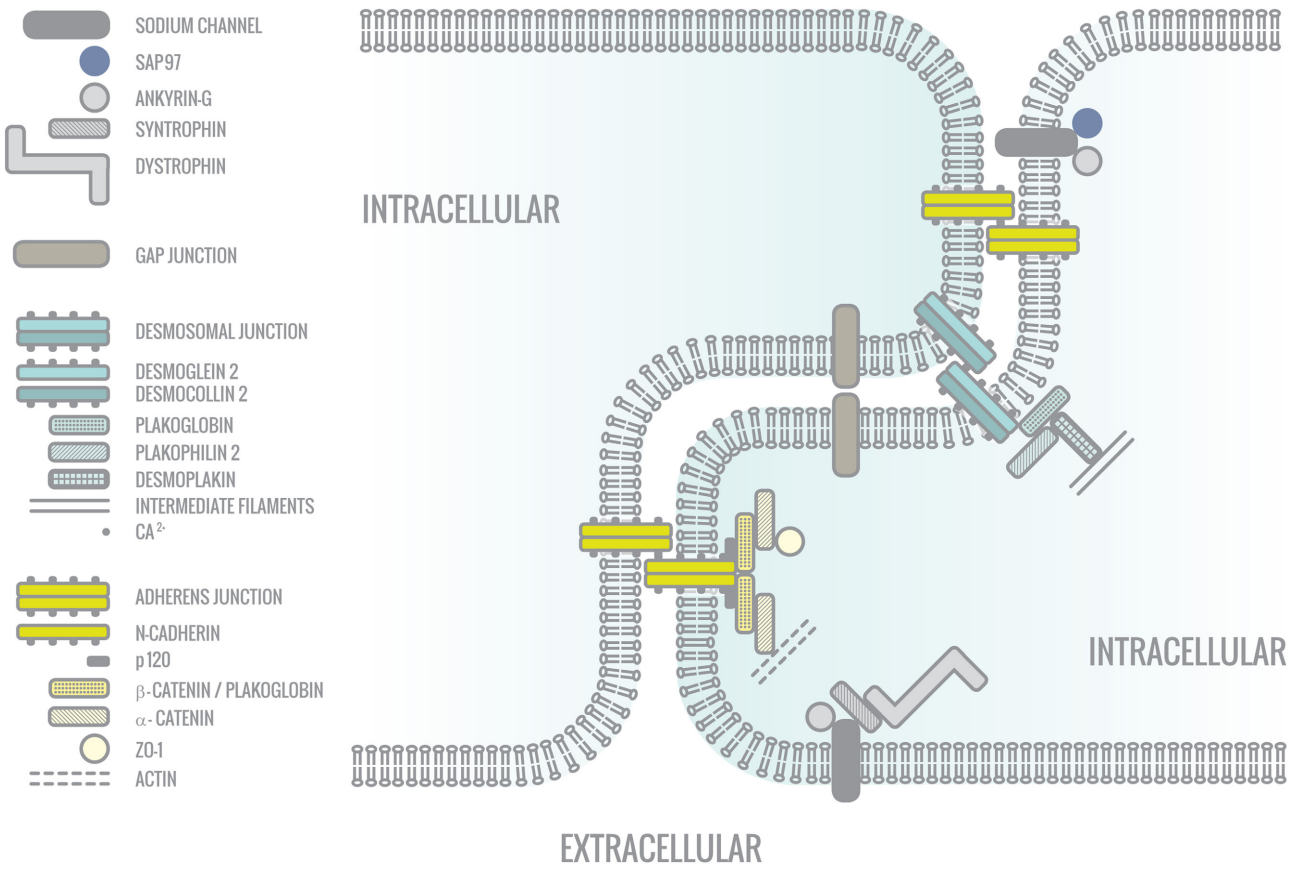

FIGURE 2 | The intercalated disc (ICD). The intercalated disc is the region between two cardiomyocytes, where different junctions are located: Gap junctions, adherens junctions, and desmosomal junctions as well as ion channels. They all form macromolecular protein complexes with different functions.

studies in which a similar reduction in Cx43 was achieved no alterations in conduction velocity were reported (Morley et al., 1999; van Rijen et al., 2004; Stein et al., 2009, 2011). These contradicting results triggered to invent a different approach to reduce Cx43 expression, and also to circumvent the problem of perinatal death in homozygous KO mice. This was achieved through generation of two conditional KO mice models (Orban et al., 1992).

In the first model, one coding region of the Cx43 gene was replaced by the fusion construct Cre-ER(t) and the other Cx43 allele was flanked by loxP (Feil et al., 1996) resulting in a 50% reduced expression of Cx43 under basic conditions ($Cx43^{CreER(t)/fl}$). Exposure to an agent activating the Cre recombinase (e.g., Tamoxifen) resulted in a further reduction of Cx43 expression up to maximally 95% (van Rijen et al., 2004). In the second model, the Cre gene was placed behind an alpha-myosin-heavy-chain (αMHC) promoter resulting in the deletion of the floxed Cx43 gene (αMHC-Cre/$Cx43^{fl/fl}$) once the promoter got activated (Gutstein et al., 2001). In this way, the Cx43 gene was knocked out around birth allowing those animals to develop normally during gestational stages. In both models, mice died due to arrhythmias. In the case of the αMHC-Cre/$Cx43^{fl/fl}$ mice death occurs around 1 or 2 months after birth (Gutstein et al., 2001) and in the case of the $Cx43^{CreER(t)/fl}$ mice within 1 month after induction of the deletion (Eckardt et al., 2004).

In cell cultures of neonatal mouse cardiomyocytes with genetically reduced levels of Cx43, no differences in action potential amplitude or minimum diastolic potential could be found compared to wild type cells. However, dV/dtmax and action potential duration was increased (Thomas et al., 2003). Also intercellular conductance was reduced and propagation was slower and highly discontinuous (Beauchamp et al., 2004). In tissue strands composed of these cells and wild type cells, propagation velocity decreased significantly, when the amount of wild type cells was less than 50%. Again, excitation between wild the two types of cells was highly discontinuous (Beauchamp et al., 2012).

In humans, DCM is linked to a reduced expression of Cx43, especially seen together with lateralization (Kitamura et al., 2002, 2003; Kostin et al., 2003; Salameh et al., 2009). In animal models this observation was confirmed repeatedly. In mice with forced retinoic acid signaling (Hall et al., 2000), Cx43 expression was reduced and lateralized, with in one study some upregulation of Cx40 in the ventricles (van Veen et al., 2002). This led to an increase in QRS duration, a reduction in conduction velocity and an increased spatial dispersion of conduction velocity (Hall et al., 2000; van Veen et al., 2002). Cx43 downregulation was also confirmed in mice with a knock-out of muscle LIM protein (an acronym of the three gene products Lin-11, Isl-1 and Mec-3) (Ehler et al., 2001), and in a guinea pig model of chronic pressure overload (Wang et al., 1999). However, in another mouse model with longstanding pressure overload, no reductions in total Cx43 could be observed, but 44% of the animals displayed arrhythmias (Boulaksil et al., 2010a). In a rabbit DCM model of a combined volume and pressure overload, reduced mid-myocardial Cx43 was reported, QRS duration was prolonged and arrhythmias were inducible (Wiegerinck et al., 2006). Besides this animal model, another DCM rabbit model induced by volume overload showed a reduction in Cx43 expression in different groups (Goldfine et al., 1999; Haugan et al., 2006). In a dog model of DCM (induced by RV pacing), lateralized Cx43 expression was described and immunofluorescent signals were decreased in the left ventricle, but not in the right. Moreover, arrhythmias could be induced and QRS duration was prolonged. This was associated with a reduced longitudinal and transversal conduction velocity in both LV and RV (Akar et al., 2007). It was also reported that downregulation of Cx43 triggered fibrosis formation after pressure overload thereby connecting the different passive changes in the heart (Jansen et al., 2012a). The latter study showed that the severity of fibrosis could directly be related to the amount of Cx43 downregulation.

In HCM patients, in an early stage of the disease, an initial increase in Cx43 expression was described together with extensive lateral staining. In later stages, Cx43 was reduced and heterogeneously distributed (Kostin et al., 2004). Other groups showed a reduction in Cx43 without lateralization, or even lateralization without changes in Cx43 expression levels (Peters et al., 1993; Sepp et al., 1996). Animal models confirm some of the observed changes in humans. As already described in the hypertrophy section, in a rat model where HCM was induced using monocrotaline, a decrease in Cx43 expression at the ICD with lateralization was shown (Uzzaman et al., 2000) resulting in a, reduced longitudinal conduction velocity. The transverse conduction velocity and also cell width were unaltered. The reduced longitudinal conduction velocity was probably not caused by the overall diminishing of Cx43, because normally mild changes in coupling do not affect conduction velocity. Moreover, increased lateral expression of Cx43 and hypertrophy did not sufficiently lower resistance perpendicular to the fiber orientation to alter transversal conduction velocity (Palka et al., 1997; Jongsma and Wilders, 2000; Gutstein et al., 2001; van Rijen et al., 2004). More likely the altered source/sink ratios due to the changed axial/perpendicular resistance ratio might have influenced the conduction velocity. In another rat model, where chronically elevated pulmonary pressure triggered development of HCM, the overall amount of Cx43 remained the same, but it was heterogeneously distributed (Sasano et al., 2007). In two different rabbit models of HCM (one with a mutation in troponin 1 and one with the beta-MyHC-Q403 mutation), a significant increase in total mid-myocardial expression of Cx43 has been described, including phosphorylated Cx43 (Sanbe et al., 2005; Ripplinger et al., 2007). In an UM-X7.1 cardiomyopathic hamster model of HCM (leading to loss of cytoskeletal delta-sarcoglycan protein and therefore to cardiac remodeling, failure, and mortality) hypertrophy, a decrease in Cx43 mRNA, increased amounts of fibrosis and arrhythmias were seen after 20 weeks (Ambra et al., 2002; Sato et al., 2008). Cardiac hypertrophy and heart failure can also be induced by overexpression of constitutively active form of cardiac calcineurin-A (CnA) in the mouse heart. Next to hypertrophy these mice develop rapidly after birth extensive amounts of fibrosis and show a high incidence of arrhythmias (Molkentin et al., 1998). In this model reduced Cx43 signals in the ICD's and decreased conduction velocity can be observed (Bierhuizen et al., 2008). In mice undergoing TAC, heterogeneous and partly

reduced signals of Cx43 have been reported leading to dispersed impulse conduction (Boulaksil et al., 2010a,b).

In ICM, ischemia reduces gap junction permeability (Dhein, 2006) and induces lateralization of Cx43 (Peters et al., 1993; Beardslee et al., 2000). The infarct border zone (the region bordering healthy and infarcted tissue) will, in that respect, be most at risk of remodeling. Already in 1991, Smith et al. reported gap junction remodeling in this zone, including reduced and lateralized Cx43 signals (Smith et al., 1991). This was also confirmed in dogs (Peters et al., 1997; Huang et al., 1999; Cabo et al., 2006), and patients (DuPont et al., 2001). In patients, alterations were even detected at areas distant from the border zone (Kostin et al., 2003). Moreover, an upregulation in Cx45 could be observed in the border zone, resulting in reduced gap junctional communication due to the intrinsic different properties of the Cx45 gap junction channels (Yamada et al., 2003). The observation of reduced and heterogeneously distributed Cx43 could also be confirmed in rabbit models (Tansey et al., 2006). However, in transgenic mice with 50% of the normal Cx43 expression level, the post-infarction area was smaller than in controls (Kanno et al., 2003). This would suggest that preservation of Cx43 is not *per se* beneficial for maintenance of function of the infarcted heart. Zhang et al. (2010) even proposed to be careful with increasing Cx43 expression in heart diseases until the meaning of alterations in expression of Cx43 upon myocardial infarction is fully understood. We have to keep in mind, however, that Cx43 gap junction channels not only are responsible for propagation of the electrical impulse in the heart, but also for metabolic coupling of the cardiomyocytes. In that respect, a smaller infarct size might rely on a reduced spreading of pro-apoptotic death signals due to a reduced level of intercellular coupling.

In ACM, reduced Cx43 expression has been reported in several studies. Theories are that Cx43 remodeling is triggered by abnormal mechanical coupling (Kaplan et al., 2004a) due to mutations in proteins composing junctions that support the structure of the cardiomyocytes. The different junctions in the intercalated disc assemble and form clusters. Therefore, dysfunction of one junction/protein influences the functioning of others (Agullo-Pascual et al., 2014). In human studies, heterogeneous disturbances in Cx43 signals, decreased presence in the intercalated disc, and lateralization of the signal has been reported in all different forms of ACM (Kaplan et al., 2004a; Noorman et al., 2013a). Although previously thought that this would predominantly be in the right ventricle, these changes are not exclusive and can also be found in the left ventricle and the septum (Noorman et al., 2013b). In general, this leads to scattered impulse conduction, which increases the susceptibility to arrhythmias (Boulaksil et al., 2010a). In the first attempts to investigate ACM in animal models, PKP2 mutations (the most abundant mutated desmosomal protein in humans) were used. In mice, homozygous null mutations in PKP2 are lethal whereas heterozygous mutations do not show any or only little phenotype (Ruiz et al., 1996; Grossman et al., 2004). Therefore, it is suggested that the abundant phenotypical presentation of ACM in patients is, on top of the genetic mutation, dependent on additional factors (e.g., inflammation, exercise). To study the familial cases, initially, two different familial forms of ACM have been studied with mutations in desmosomal genes different from PKP2: Naxos disease [mutation in plakoglobin (PKG)] (Protonotarios et al., 1986; McKoy et al., 2000; Protonotarios and Tsatsopoulou, 2004); and Carvajal-syndrome [desmoplakin (DPK)] (Carvajal-Huerta, 1998; Norgett et al., 2000). In patients, in both diseases, Cx43 is reduced in both ventricles in the early phase of the disease and an increase in non-phosphorylated Cx43 was detected that might be associated with accelerated down-regulation of the protein (Kaplan et al., 2004a,b). An *in vitro* model for Naxos disease using neonatal rat cardiomyocytes transfected with an adenovirus encoding the PKG 2057del2 mutation recapitulated all abnormalities seen in patients: reduced plakoglobin and Cx43 signal at the ICD's, increased apoptosis and secretion of inflammatory mediators (Asimaki et al., 2014). Moreover, a zebrafish model with the same mutation was used to screen for potential drugs to intervene with the development and progression of ACM (Asimaki et al., 2014). This latter study revealed promising results for future therapy since disease-causing targets could be identified and *in vitro* studies showed prevention and even regression of the disease when the intervention was applied in the early phases of cardiac remodeling.

EXCITABILITY

Proper contraction of the heart also results from a finely tuned impulse generation, which feeds propagation. In ventricular cardiomyocytes, action potential generation is initiated by the fast and robust depolarization as caused by the opening of the voltage-dependent Na^+ channels (Clancy and Kass, 2002). Already in 1921, Daly and Clark (1921) showed in frogs that rate, propagation velocity and force of the cardiac contraction were reduced in solutions containing a reduced (extra-cellular) sodium concentration.

The human sodium channel consists of one alpha and four beta subunits. The alpha subunit consists of four homologous domains connected by cytoplasmic linkers (**Figure 3**). Each of those domains consists in turn of six transmembrane sequences (Balser, 1999). In cardiomyocytes two different pools of Nav1.5 channels co-exist, namely at the lateral membranes where the channel interacts with the dystrophin-syntrophin complex and in the intercalated disc where it binds SAP97 (**Figure 2**) (Petitprez et al., 2011). Both pools are thought to interact with different proteins. At the ICD, it is envisioned that Nav1.5 can influence e.g., Cx43 in the gap junctions and *vice versa* (Delmar, 2012).

Initially, much work on excitability has been performed *in vitro* using neonatal rat cardiomyocytes. Lateron, *in vivo* experiments on reduced excitability have been performed in genetically engineered mice models. SCN5a haploinsufficient mice showed about a 50% reduction of sodium current, while having a normal survival rate (Papadatos et al., 2002). ECG analysis showed a prolonged RR interval, P-wave duration, PR interval, QRS duration, and QT interval together with an age related aggravation of the phenotype (Royer et al., 2005). In those SCN5a haploinsuffient mice, QRS prolongation and conduction slowing was observed. However, in young mice, epicardial conduction velocity was not reduced in the left ventricle and only mildly reduced in the right. The reduction in conduction velocity became more dominant in both ventricles in older mice (12–17 months) where it was

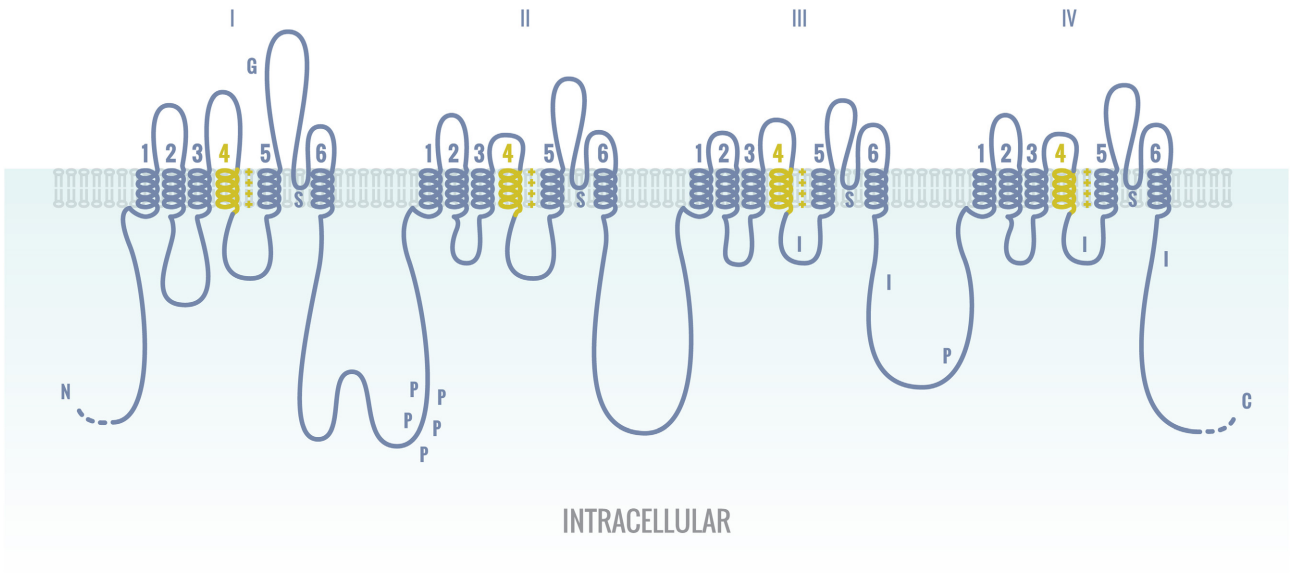

FIGURE 3 | The alpha subunit of the human sodium channel. The alpha subunit of the human sodium channel consists of four homologous domains connected by cytoplasmic linkers. Each domain is composed of six trans-membrane sequences. G, glycosylation; P, phosphorylation; S, ion selectivity; I, inactivation sites. Positive (+) charges in S4 are crucial for transmembrane voltage sensing.

associated with increased fibrosis and altered Cx43 expression (van Veen et al., 2005).

In patients with the 1795InsD mutation in the SCN5a gene, bradycardia, conduction delay, QT prolongation, and right precordial ST-elevation can be detected. To investigate the cause of sodium channel related diseases, and in particular the above mentioned one, Remme et al. created a 1798InsD mouse model (1798InsD is the mouse analog of 1795InsD in human), where indeed a single mutation leads to a phenotype of bradycardia, right ventricular conduction slowing, and QT prolongation (Remme et al., 2006). Given the enormous amount of sodium channel mutations leading to a pro-arrhythmic phenotype in patients, generation of such mouse models significantly has contributed to a better understanding of the underlying etiology. In a DCM dog model, in which disease was induced through RV pacing, neither sodium current density, nor upstroke velocity of the action potential in left ventricular endo- or epicardial myocytes differed from control individuals (Kaab et al., 1996; Akar et al., 2004). Similarly, in a DCM rabbit model, sodium current density did not differ from controls in left ventricular myocytes (Wiegerinck et al., 2006). Recent data from a Torsade de Pointes sensitive canine heart model after chronic AV block (CAVB) confirm that no changes in I_{Na} appear, although increased cell size was reported (Boulaksil et al., 2011).

HCM patients showed increased CaMKII phosphorylation of Nav1.5 channels, which is in general associated with a delayed inactivation of the current (Wagner et al., 2006; Coppini et al., 2013). Increased late sodium current leads to prolonged repolarization (and therefore an increased action potential duration) and arrhythmias as has been shown in patients and several animal models (Jelicks and Siri, 1995; Undrovinas et al., 1999; Gray et al., 2001; Mészáros et al., 2001; Coppini et al., 2013). Increased late sodium current also causes changes in calcium metabolism and homeostasis, influencing cell metabolism and contractile functioning of the cells. This in turn may lead to hypertrophy (Coppini et al., 2013). In mice with calcineurin-induced cardiac hypertrophy, reduced Nav1.5 protein and RNA amounts could be found in the ICD's (Bierhuizen et al., 2008).

ICM is also associated with increased late I_{Na} (Ju et al., 1996; Huang et al., 2001). Various causes can lead to an increase of intracellular sodium concentration in ischemic cardiomyocytes. First, ischemia seems to increase the amplitude of the late I_{Na} significantly (Hammarstrom and Gage, 2002). Anaerobic glycolysis, due to lack of sufficient oxygen supply to the cells, leads to a decrease of ATP and leaking of protons via the cardiac Na/H exchanger (NHE1). Because of that, more sodium enters the cell (Tani and Neely, 1989). Moreover, a reduction of Na^+/K^+ ATPase pump activity will cause an additional decrease of sodium extrusion (Xiao and Allen, 1999). Increased sodium levels will activate the Na/Ca exchanger. This, in turn, leads to an increased concentration of calcium in the cell and a reduction in intracellular pH. The altered ion concentrations will lead to drastic changes in cellular metabolism, signal transduction, electrophysiological characteristics and contractile properties, probably leading to cell damage and cell death (Silverman and Stern, 1994; Imahashi et al., 1999; Allen and Xiao, 2002).

In the early stages of hypoxia, an increase in intracellular sodium concentration was observed in rat hearts that returned back to pre-infarction levels, when ischemia was of short duration (Tani and Neely, 1989). When sodium is persistently elevated,

the subsequent increased calcium levels may be prevented by late sodium current inhibition through ranolazine (Soliman et al., 2012). Moreover, a NHE1 inhibitor has been reported to show cardio-protective effects after infarction in a rat model (Huber et al., 2012). Although controversial results have been published lateron about NHE1, it is still under investigation and thought to be one of the most effective post-infarct treatments (Karmazyn, 2013). Next to adherens-, gap- and desmosomal junctions, also ion channels are located in the ICD (Balse et al., 2012), and it becomes more and more clear that in ACM alterations in subcellular localization of sodium channels is importantly involved in the consequences of cardiac remodeling. In patients, a reduced localization of Nav1.5 in the ICD has been reported (Noorman et al., 2013a). In cultured cardiomyocytes, the reduced expression of PKP2, caused a subsequent reduction in the sodium current and a slower conduction velocity (Sato et al., 2009). Besides that, loss of expression of Ankyrin-G, an important protein that anchors the voltage-gated sodium channel, leads to disturbances in PKP2 and Cx43 expression. The other way around, loss of PKP2 causes a reduction in expression of Ankyrin-G as well as of Nav1.5 (Sato et al., 2011), thereby confirming the role of sodium channels in this disease. Besides that, in zebrafish and neonatal rat cardiomyocytes containing the mentioned 2057del2 plakoglobin (related to Naxos disease), a marked reduction in I_{Na} current density was observed (Asimaki et al., 2014). In these neonatal rat cardiomyocytes, the immunofluorescent Nav1.5 signal at the membrane was reduced, but total cell content appeared unchanged (Asimaki et al., 2014). This reduction in I_{Na} and consequently a reduced conduction velocity has also previously been shown in transgenic mice with a desmoglein-2 mutation (Rizzo et al., 2012). Moreover, reduced heterogeneous expression of Cx43 in conditional knockout mice caused decreased expression of Nav1.5, reduced sodium current and an increased vulnerability of those mice for arrhythmias (Jansen et al., 2012a). Similarly, PKP2 haploinsufficiency in mice resulted in a sodium current deficit and arrhythmogenesis when triggered with flecainide (Cerrone et al., 2012). The importance of these finding was reflected in a study of Cerrone et al. which showed that in patients with a mutation in PKP-2, provocation with flecainide triggered arrhythmias suggesting that also in these patients a concomitant sodium current deficit existed (Cerrone et al., 2014).

HETEROGENEITY

The natural mode of functional heterogeneity within the normal cardiac performance is also of importance during heart disease. Due to, e.g., pulmonary disease or aortic stenosis, different parts of the heart are affected prior to the other, leading to heterogenic alterations that conflict with the natural organization. In ACM, where disease-dependent changes often start in the right ventricle, the left ventricle can remain relatively unaffected in the early stages of disease. In an opposite fashion aortic stenosis will first remodel the left ventricle before right ventricular involvement manifests. Differently, right ventricular remodeling due to pulmonary hypertension might simultaneously trigger LV remodeling (atrophy) due to a reduced filling (Hardziyenka et al., 2012).

These different types of remodeling are part of various diseases and are by definition heterogeneous, since all of those diseases have different causes and therefore treatment options (Coronel et al., 2013).

Cardiac remodeling deteriorating into heart failure most likely depends on a combination of the mechanisms as described in this article, and it is characterized by heterogeneous remodeling of excitation-contraction coupling (Coronel et al., 2001; Lou et al., 2011). Pathophysiological heterogeneity in cardiac tissue sustains ventricular tachycardia, stabilizes reentry arrhythmias and provides substrate for sustained tachycardia (Pazo et al., 2004; Ripplinger et al., 2006).

Passive heterogeneous ventricular remodeling in the heart is one of the most destructive features of cardiac remodeling and every remodeling mechanism itself shows the worst outcome, when occurring heterogeneously. In this article, several mechanisms of passive remodeling have been described during DCM, HCM, ICM and ACM. Passive remodeling of tissue architecture was investigated focusing on fibrosis, alterations in cell size, hypertrophy and fiber disarray. Disturbances in electrical coupling were discussed by describing changes in the distribution of the gap junction protein Cx43. Remodeling of electrical excitability was studied using the sodium channel protein Nav1.5.

To summarize, different types of fibrosis occur in all of the four discussed heart diseases and act as modulators of impulse propagation ranging from conduction slowing, increased dispersion of conduction and even conduction block. Moreover, it can alter the structure of the heart, e.g., alterations in cellular dimensions, which is caused by modifications in molecular pathways that control normal cellular physiology. As a consequence this may lead to reductions in excitability and cell-to-cell conduction (Fenoglio et al., 1983; Kawara et al., 2001). Heterogeneously distributed fibrosis can even create a "labyrinth" in the heart facilitating reentry arrhythmias (Engelman et al., 2010). Therefore, this is considered to be worse than only local interstitial fibrosis since it would be more difficult for electrical signals to propagate though a labyrinth of fibrotic patches than only being obstructed by single fibers (Kawara et al., 2001; Tanaka et al., 2007). This idea was strengthened by a study where reduction of heterogeneous patchy fibrosis was one-on-one correlated to a reduction of arrhythmias (Stein et al., 2010).

Hypertrophy can be detected in HCM and ICM. Changes in cell size are the key features of HCM and DCM, whereby HCM is characterized by an increase in cell width and DCM by an increase in cell length. Myocardial fiber disarray mainly occurs in HCM, where it is even used as a biomarker. It can also be observed in ICM, but to a much lesser extend. Heterogeneously distributed hypertrophy, myocardial fiber disarray and changes in cell size can lead to alterations in impulse propagation and conduction velocity causing disturbed signaling, deregulated contractions, and eventually heart failure (Meyerburg et al., 1992; Winterton et al., 1994; Cooklin et al., 1997; McIntyre and Fry, 1997). Pathophysiological heterogeneity in the sense of right vs. left ventricles or atria can also worsen disease phenotype as is classically illustrated by the fact that progressive LV dysfunction eventually results in RV failure too with consequently, pulmonary remodeling and edema (Chen et al., 2012).

Heterogeneous distribution, de-phosphorylation and a reduction of Cx43 signals in the ICD are characteristics found in all four different heart diseases. They are one of the key features of ACM (Noorman et al., 2013a), but also occur in DCM, ICM, and late stages of HCM. This can lead to a reduction in longitudinal and an increase in transverse conduction (reducing the normal anisotropic mode of conduction) causing heterogeneous propagation (increased dispersion of conduction) and arrhythmogenesis. At these places signaling (mechanical or electrical) will be more difficult leading to de-regulated intercellular coupling (Boulaksil et al., 2010a). The heterogeneous distribution of the different proteins and structures can be sub-divided into macro and micro heterogeneity. Macro heterogeneity compares the different regions in the heart, whereas micro heterogeneity is a measure for local heterogeneity (Jansen et al., 2012a).

Changes in expression and distribution of the sodium channel protein Nav1.5 can also be seen in HCM, DCM, and ACM. Homogeneous distribution of Nav1.5 throughout different parts of the heart is crucial for normal conduction (Clancy and Kass, 2002) although functional expression levels differ between epicard, endocard, and conduction system (Remme et al., 2009). Heterogeneous distribution, caused by a local increase or decrease of sodium channels possibly facilitates arrhythmogenesis and therefore heart failure, since the sodium current will be hampered or fastened locally (Wagner et al., 2011; Shryock et al., 2013). Although these heterogeneous maladaptations can have effects when occurring alone, they are often found to trigger arrhythmias and eventually heart failure due to a combination of simultaneous alterations in different factors. Therefore, great care should be taken when investigating one single mechanism of remodeling, since a heterogeneous adaptation of one mechanism can also cause others to develop or are even linked to each other. This concept is illustrated by several studies, which report a simultaneous downregulation and de-phosphorylation of Cx43, and Nav1.5, (Stein et al., 2009; Jansen et al., 2012b; Noorman et al., 2013a) and even link this combination to an increased deposition of fibrotic materials (van Veen et al., 2005; Jansen et al., 2012a). These studies example the complexity of cardiac remodeling during pathophysiology in relation to the increase in propensity to develop arrhythmias.

Regarding the future perspective of cardiac research, one should focus on these connections between heterogeneous changes in single factors within the heart that lead to the total picture of heterogeneous remodeling. This might unravel currently unknown relationships between the various forms of maladaptation and help to improve the search for treatment options. In a study that was mentioned before, long term administration of the antihypertensive drugs eplerenone or losartan in a mouse model of extreme aging not only reduced the amount of interstitial- and patchy fibrosis, but also preserved a homogeneous pattern of gap junctional coupling. This preservation of the normal substrate for conduction resulted in a significantly reduced amount of arrhythmias (Stein et al., 2010). Beyond pharmacological interventions, pacing strategies (like cardiac resynchronization therapy) that aim to correct the abnormal sequence of activation, e.g., due to bundle branch block or electrical remodeling, will provide further future perspectives to improve performance of the remodeled heart.

ACKNOWLEDGMENTS

We acknowledge support from the Netherlands CardioVascular Research Initiative: the Dutch Heart Foundation, Dutch Federation of University Medical Centers, the Netherlands Organization for Health Research and Development, and the Royal Netherlands Academy of Sciences (CVON-PREDICT, Elise L. Kessler, Marc A. Vos, Toon A. B. van Veen).

REFERENCES

Agullo-Pascual, E., Cerrone, M., and Delmar, M. (2014). Arrhythmogenic cardiomyopathy and Brugada syndrome: diseases of the connexome. *FEBS Lett.* 588, 1322–1330. doi: 10.1016/j.febslet.2014.02.008

Akar, F. G., Nass, R. D., Hahn, S., Cingolani, E., Shah, M., Hesketh, G. G., et al. (2007). Dynamic changes in conduction velocity and gap junction properties during development of pacing-induced heart failure. *Am. J. Physiol. Heart Circ. Physiol.* 293, H1223–H1230. doi: 10.1152/ajpheart.00079.2007

Akar, F. G., Spragg, D. D., Tunin, R. S., Kass, D. A., and Tomaselli, G. F. (2004). Mechanisms underlying conduction slowing and arrhythmogenesis in nonischemic dilated cardiomyopathy. *Circ. Res.* 95, 717–725. doi: 10.1161/01.RES.0000144125.61927.1c

Allen, D. G., and Xiao, X. H. (2002). Role of the cardiac Na/H exchanger during ischemia and reperfusion. *Cardiovasc. Res.* 57, 934–941. doi: 10.1016/S0008-6363(02)00836-2

Ambra, R., Di Nardo, P., Fantini, C., Minieri, M., Canali, R., Natella, F., et al. (2002). Selective changes in DNA binding activity of transcription factors in UM-X7.1 cardiomyopathic hamsters. *Life Sci.* 71, 2369–2381. doi: 10.1016/S0024-3205(02)02020-9

Asimaki, A., et al. (2007). A novel dominant mutation in plakoglobin causes arrhythmogenic right ventricular cardiomyopathy. *Am. J. Hum. Genet.* 81, 964–973. doi: 10.1086/521633

Asimaki, A., Syrris, P., Wichter, T., Matthias, P., Saffitz, J. E., and McKenna, W. J. (2014). Identification of a new modulator of the intercalated disc in a zebrafish model of arrhythmogenic cardiomyopathy. *Sci. Transl. Med.* 6, 240ra74. doi: 10.1126/scitranslmed.3008008

Balse, E., Steele, D. F., Abriel, H., Coulombe, A., Fedida, D., and Hatem, S. N. (2012). Dynamic of ion channel expression at the plasma membrane of cardiomyocytes. *Physiol. Rev.* 92, 1317–1358. doi: 10.1152/physrev.00041.2011

Balser, J. R. (1999). Structure and function of the cardiac sodium channels. *Cardiovasc. Res.* 42, 327–338. doi: 10.1016/S0008-6363(99)00031-0

Beardslee, M. A., Lerner, D. L., Tadros, P. N., Laing, J. G., Beyer, E. C., Yamada, K. A., et al. (2000). Dephosphorylation and intracellular redistribution of ventricular connexin43 during electrical uncoupling induced by ischemia. *Circ. Res.* 87, 656–662. doi: 10.1161/01.RES.87.8.656

Beauchamp, P., Choby, C., Desplantez, T., de Peyer, K., Green, K., Yamada, K. A., et al. (2004). Electrical propagation in synthetic ventricular myocyte strands from germline connexin43 knockout mice. *Circ. Res.* 95, 170–178. doi: 10.1161/01.RES.0000134923.05174.2f

Beauchamp, P., Desplantez, T., McCain, M. L., Li, W., Asimaki, A., Rigoli, G., et al. (2012). Electrical coupling and propagation in engineered ventricular myocardium with heterogeneous expression of connexin43. *Circ. Res.* 110, 1445–1453. doi: 10.1161/CIRCRESAHA.111.259705

Beffagna, G., Occhi, G., Nava, A., Vitiello, L., Ditadi, A., Basso, C., et al. (2005). Regulatory mutations in transforming growth factor-beta3 gene cause arrhythmogenic right ventricular cardiomyopathy type 1. *Cardiovasc. Res.* 65, 366–373. doi: 10.1016/j.cardiores.2004.10.005

Bender, S. R., Friedman, D. J., Markowitz, S. M., Lerman, B. B., and Okin, P. M. (2012). Electrocardiographic left ventricular hypertrophy predicts arrhythmia and mortality in patients with ischemic cardiomyopathy. *J. Interv. Card. Electrophysiol.* 34, 237–245. doi: 10.1007/s10840-011-9661-2

Bierhuizen, M. F., Boulaksil, M., van Stuijvenberg, L., van der Nagel, R., Jansen, A. T., Mutsaers, N. A., et al. (2008). In calcineurin-induced cardiac hypertrophy expression of Nav1.5, Cx40 and Cx43 is reduced by different mechanisms. *J. Mol. Cell. Cardiol.* 45, 373–384. doi: 10.1016/j.yjmcc.2008.06.011

Biernacka, A., and Frangogiannis, N. G. (2011). Aging and cardiac fibrosis. *Aging Dis.* 2, 158–173.

Boulaksil, M., Jungschleger, J. G., Antoons, G., Houtman, M. J., de Boer, T. P., Wilders, R., et al. (2011). Drug-induced torsade de pointes arrhythmias in the chronic AV block dog are perpetuated by focal activity. *Circ. Arrhythm. Electrophysiol.* 4, 566–576. doi: 10.1161/CIRCEP.110.958991

Boulaksil, M., Noorman, M., Engelen, M. A., van Veen, T. A., Vos, M. A., de Bakker, J. M., et al. (2010b). Longitudinal arrhythmogenic remodelling in a mouse model of longstanding pressure overload. *Neth. Heart J.* 18, 509–515. doi: 10.1007/BF03091824

Boulaksil, M., Winckels, S. K., Engelen, M. A., Stein, M., van Veen, T. A., Jansen, J. A., et al. (2010a). Heterogeneous Connexin 43 distribution in heart failure is associated with dispersed conduction and enhanced susceptibility to ventricular arrhythmias. *Eur. J. Heart Fail.* 12, 913–921. doi: 10.1093/eurjhf/hfq092

Bowers, S. L., Borg, T. K., and Baudino, T. A. (2010). The dynamics of fibroblast-myocyte-capillary interactions in the heart. *Ann. N. Y. Acad. Sci.* 1188, 143–152. doi: 10.1111/j.1749-6632.2009.05094.x

Branishte, T., Jungschleger, J. G., Antoons, G., Houtman, M. J., de Boer, T. P., Wilders, R., et al. (2013). Aspects of molecular mechanisms in myocardial hypertrophy, particular morphological changes and cell bioenergetic characteristics in patients with dilated cardiomyopathy. *Rev. Med. Chir. Soc. Med. Nat. Iasi* 117, 851–856.

Brugada, J., Boersma, L., Kirchhof, C. J., Heynen, V. V., and Allessie, M. A. (1991). Reentrant excitation around a fixed obstacle in uniform anisotropic ventricular myocardium. *Circulation* 84, 1296–1306. doi: 10.1161/01.CIR.84.3.1296

Cabo, C., Yao, J., Boyden, P. A., Chen, S., Hussain, W., Duffy, H. S., et al. (2006). Heterogeneous gap junction remodeling in reentrant circuits in the epicardial border zone of the healing canine infarct. *Cardiovasc. Res.* 72, 241- 249. doi: 10.1016/j.cardiores.2006.07.005

Carvajal-Huerta, L. (1998). Epidermolytic palmoplantar keratoderma with woolly hair and dilated cardiomyopathy. *J. Am. Acad. Dermatol.* 39, 418–421. doi: 10.1016/S0190-9622(98)70317-2

Cerrone, M., Lin, X., Zhang, M., Agullo-Pascual, E., Pfenniger, A., Chkourko Gusky, H., et al. (2014). Missense mutations in plakophilin-2 cause sodium current deficit and associate with a brugada syndrome phenotype. *Circulation* 129, 1092–1103. doi: 10.1161/CIRCULATIONAHA.113.003077

Cerrone, M., Noorman, M., Lin, X., Chkourko, H., Liang, F. X., van der Nagel, R., et al. (2012). Sodium current deficit and arrhythmogenesis in a murine model of plakophilin-2 haploinsufficiency. *Cardiovasc. Res.* 95, 460–468. doi: 10.1093/cvr/cvs218

Chen, Y., Guo, H., Xu, D., Xu, X., Wang, H., Hu, X., et al. (2012). Left ventricular failure produces profound lung remodeling and pulmonary hypertension in mice: heart failure causes severe lung disease. *Hypertension* 59, 1170–1178. doi: 10.1161/HYPERTENSIONAHA.111.186072

Clancy, C. E., and Kass, R. S. (2002). Defective cardiac ion channels: from mutations to clinical syndromes. *J. Clin. Invest.* 110, 1075–1077. doi: 10.1172/JCI0216945

Cooklin, M., Wallis, W. R., Sheridan, D. J., and Fry, C. H. (1997). Changes in cell-to-cell electrical coupling associated with left ventricular hypertrophy. *Circ. Res.* 80, 765–771. doi: 10.1161/01.RES.80.6.765

Coppini, R., Ferrantini, C., Yao, L., Fan, P., Del Lungo, M., Stillitano, F., et al. (2013). Late sodium current inhibition reverses electromechanical dysfunction in human hypertrophic cardiomyopathy. *Circulation* 127, 575–584. doi: 10.1161/CIRCULATIONAHA.112.134932

Coronel, R., de Groot, J. R., and van Lieshout, J. J. (2001). Defining heart failure. *Cardiovasc. Res.* 50, 419–422. doi: 10.1016/S0008-6363(01)00284-X

Coronel, R., Wilders, R., Verkerk, A. O., Wiegerinck, R. F., Benoist, D., and Bernus, O. (2013). Electrophysiological changes in heart failure and their implications for arrhythmogenesis. *Biochim. Biophys. Acta* 1832, 2432–2441. doi: 10.1016/j.bbadis.2013.04.002

Corrado, D., Basso, C., and Thiene, G. (2000). Arrhythmogenic right ventricular cardiomyopathy: diagnosis, prognosis, and treatment. *Heart* 83, 588–595. doi: 10.1136/heart.83.5.588

Daly, I. B., and Clark, A. J. (1921). The action of ions upon the frog's heart. *J Physiol* 54, 367–383.

Davis, J., and Molketin, J. D. (2013). Myofibroblasts: trust your heart and let fate decide. *J. Mol. Cell Cardiol.* 70, 9–18. doi: 10.1016/j.yjmcc.2013.10.019

de Bakker, J. M., van Capelle, F. J., Janse, M. J., Tasseron, S., Vermeulen, J. T., de Jonge, N., et al. (1993). Slow conduction in the infarcted human heart. 'Zigzag' course of activation. *Circulation* 88, 915–926. doi: 10.1161/01.CIR.88.3.915

de Bakker, J. M., van Capelle, F. J., Janse, M. J., Wilde, A. A., Coronel, R., Becker, A. E., et al. (1988). Reentry as a cause of ventricular tachycardia in patients with chronic ischemic heart disease: electrophysiologic and anatomic correlation. *Circulation* 77, 589–606. doi: 10.1161/01.CIR.77.3.589

de Jong, S., Zwanenburg, J. J., Visser, F., der Nagel, R. V, van Rijen, H. V., Vos, M. A., et al. (2011). Direct detection of myocardial fibrosis by MRI. *J. Mol. Cell. Cardiol.* 51, 974–979. doi: 10.1016/j.yjmcc.2011.08.024

Delmar, M. (2012). Connexin43 regulates sodium current; ankyrin-G modulates gap junctions: the intercalated disc exchanger. *Cardiovasc. Res.* 93, 220–222. doi: 10.1093/cvr/cvr343

Dhein, S. (2006). Cardiac ischemia and uncoupling: gap junctions in ischemia and infarction. *Adv. Cardiol.* 42, 198–212. doi: 10.1159/000092570

DuPont, E., Matsushita, T., Kaba, R. A., Vozzi, C., Coppen, S. R., Khan, N., et al. (2001). Altered connexin expression in human congestive heart failure. *J. Mol. Cell. Cardiol.* 33, 359–371. doi: 10.1006/jmcc.2000.1308

Eckardt, D., Theis, M., Degen, J., Ott, T., van Rijen, H. V., Kirchhoff, S., et al. (2004). Functional role of connexin43 gap junction channels in adult mouse heart assessed by inducible gene deletion. *J. Mol. Cell. Cardiol.* 36, 101–110. doi: 10.1016/j.yjmcc.2003.10.006

Efthimiadis, G. K., Pagourelias, E. D., Gossios, T., and Zegkos, T. (2014). Hypertrophic cardiomyopathy in 2013, current speculations and future perspectives. *World J. Cardiol.* 6, 26–37. doi: 10.4330/wjc.v6.i2.26

Ehler, E., Horowits, R., Zuppinger, C., Price, R. L., Perriard, E., Leu, M., et al. (2001). Alterations at the intercalated disk associated with the absence of muscle LIM protein. *J. Cell Biol.* 153, 763–772. doi: 10.1083/jcb.153.4.763

Elfgang, C., Eckert, R., Lichtenberg-Fraté, H., Butterweck, A., Traub, O., Klein, R. A., et al. (1995). Specific permeability and selective formation of gap junction channels in connexin-transfected HeLa cells. *J. Cell Biol.* 129, 805–817. doi: 10.1083/jcb.129.3.805

Eloff, B. C., Lerner, D. L., Yamada, K. A., Schuessler, R. B., Saffitz, J. E., and Rosenbaum, D. S. (2001). High resolution optical mapping reveals conduction slowing in connexin43 deficient mice. *Cardiovasc. Res.* 51, 681–690. doi: 10.1016/S0008-6363(01)00341-8

Engelman, Z. J., Trew, M. L., and Smaill, B. H. (2010). Structural heterogeneity alone is a sufficient substrate for dynamic instability and altered restitution. *Circ. Arrhythm. Electrophysiol.* 3, 195–203. doi: 10.1161/CIRCEP.109.890459

Feil, R., Brocard, J., Mascrez, B., LeMeur, M., Metzger, D., and Chambon, P. (1996). Ligand-activated site-specific recombination in mice. *Proc. Natl. Acad. Sci. U.S.A.* 93, 10887–10890. doi: 10.1073/pnas.93.20.10887

Fenoglio, J. J., Ursell, P. C., Kellogg, C. F., Drusin, R. E., and Weiss, M. B. (1983). Diagnosis and classification of myocarditis by endomyocardial biopsy. *N. Engl. J. Med.* 308, 12–18. doi: 10.1056/NEJM198301063080103

Formigli, L., Ibba-Manneschi, L., Perna, A. M., Pacini, A., Polidori, L., Nediani, C., et al. (2003). Altered Cx43 expression during myocardial adaptation to acute and chronic volume overloading. *Histol. Histopathol.* 18, 359–369.

Gerull, B., Heuser, A., Wichter, T., Paul, M., Basson, C. T., McDermott, D. A., et al. (2004). Mutations in the desmosomal protein plakophilin-2 are common in arrhythmogenic right ventricular cardiomyopathy. *Nat. Genet.* 36, 1162–1164. doi: 10.1038/ng1461

Gill, C., Mestril, R., and Samali, A. (2002). Losing heart: the role of apoptosis in heart disease—a novel therapeutic target? *FASEB J.* 16, 135–146. doi: 10.1096/fj.01-0629com

Goldfine, S. M., Walcott, B., Brink, P. R., Magid, N. M., and Borer, J. S. (1999). Myocardial connexin43 expression in left ventricular hypertrophy resulting from aortic regurgitation. *Cardiovasc. Pathol.* 8, 1–6. doi: 10.1016/S1054-8807(98)00011-8

Gray, R. P., McIntyre, H., Sheridan, D. S., and Fry, C. H. (2001). Intracellular sodium and contractile function in hypertrophied human and guinea-pig myocardium. *Pflugers Arch.* 442, 117–123. doi: 10.1007/s004240000512

Grossman, K. S., Grund, C., Huelsken, J., Behrend, M., Erdmann, B., Franke, W. W., et al. (2004). Requirement of plakophilin 2 for heart morphogenesis and cardiac junction formation. *J. Cell Biol.* 167, 149–160. doi: 10.1083/jcb.200402096

Guerrero, P. A., Schuessler, R. B., Davis, L. M., Beyer, E. C., Johnson, C. M., Yamada, K. A., et al. (1997). Slow ventricular conduction in mice heterozygous for a connexin43 null mutation. *J. Clin. Invest.* 99, 1991–1998. doi: 10.1172/JCI119367

Gutstein, D. E., Liu, F. Y., Meyers, M. B., Choo, A., and Fishman, G. I. (2001). The organization of adherens junctions and desmosomes at the cardiac intercalated disc is independent of gap junctions. *J. Cell Sci.* 116, 875–885. doi: 10.1242/jcs.00258

Hall, D. G., Morley, G. E., Vaidya, D., Ard, M., Kimball, T. R., Witt, S. A., et al. (2000). Early onset heart failure in transgenic mice with dilated cardiomyopathy. *Pediatr. Res.* 48, 36–42. doi: 10.1203/00006450-200007000-00009

Hammarstrom, A. K., and Gage, P. W. (2002). Hypoxia and persistent sodium current. *Eur. Biophys.* 31, 323–333. doi: 10.1007/s00249-002-0218-2

Hardziyenka, M., Campian, M. E., Verkerk, A. O., Surie, S., van Ginneken, A. C., Hakim, S., et al. (2012). Electrophysiologic remodeling of the left ventricle in pressure overload-induced right ventricular failure. *J. Am. Coll. Cardiol.* 59, 2193–2202. doi: 10.1016/j.jacc.2012.01.063

Haugan, K., Miyamoto, T., Takeishi, Y., Kubota, I., Nakayama, J., Shimojo, H., et al. (2006). Rotigaptide (ZP123) improves atrial conduction slowing in chronic volume overload-induced dilated atria. *Basic Clin. Pharmacol. Toxicol.* 99, 71–79. doi: 10.1111/j.1742-7843.2006.pto_432.x

Hershberger, R. E., and Morales, A. (2013). "A dilated cardiomyopathy overview," in *GeneReviews®,* eds R. A. Pagon, M. P. Adam, H. H. Ardinger (Seattle, WA: University of Washington).

Heuser, A., Plovie, E. R., Ellinor, P. T., Grossmann, K. S., Shin, J. T., Wichter, T., et al. (2006). Mutant desmocollin-2 causes arrhythmogenic right ventricular cardiomyopathy. *Am. J. Hum. Genet.* 79, 1081–1018. doi: 10.1086/509044

Hoefen, R., Reumann, M., Goldenberg, I., Moss, A. J., O-Uchi, J., Gu, Y. et al. (2012). *In silico* cardiac risk assessment in patients with long QT syndrome: type 1: clinical predictability of cardiac models. *J. Am. Coll. Cardiol.* 60, 2182–2191. doi: 10.1016/j.jacc.2012.07.053

Huang, B., El-Sherif, T., Gidh-Jain, M., Qin, D., and El-Sherif, N. (2001). Alterations of sodium channel kinetics and gene expression in the postinfarction remodeled myocardium. *J. Cardiovasc. Electrophysiol.* 12, 218–225. doi: 10.1046/j.1540-8167.2001.00218.x

Huang, X. D., Sandusky, G. E., and Zipes, D. P. (1999). Heterogeneous loss of Connexin43 protein in ischemic dog hearts. *J. Cardiovasc. Electrophysiol.* 10, 79–91. doi: 10.1111/j.1540-8167.1999.tb00645.x

Huber, J. D., Bentzien, J., Boyer, S. J., Burke, J., De Lombaert, S., Eickmeier, C., et al. (2012). Identification of a potent sodium hydrogen exchanger isoform 1 (NHE1) inhibitor with a suitable profile for chronic dosing and demonstrated cardioprotective effects in a preclinical model of myocardial infarction in the rat. *J. Med. Chem.* 55, 7114–7140. doi: 10.1021/jm300601d

Hughes, S. E. (2004). The pathology of hypertrophic cardiomyopathy. *Histopathology* 44, 412–427. doi: 10.1111/j.1365-2559.2004.01835.x

Hughes, S. E., and McKenna, W. J. (2005). New insights into the pathology of inherited cardiomyopathy. *Heart* 91, 257–264. doi: 10.1136/hrt.2004.040337

Imahashi, K., Kusuoka, H., Hashimoto, K., Yoshioka, J., Yamaguchi, H., and Nishimura, T. (1999). Intracellular sodium accumulation during ischemia as the substrate for reperfusion injury. *Circ. Res.* 84, 1401–1406. doi: 10.1161/01.RES.84.12.1401

Isoyama, S., and Nitta-Komatsubara, Y. (2002). Acute and chronic adaptation to hemodynamic overload and ischemia in the aged heart. *Heart Fail. Rev.* 7, 63–69. doi: 10.1023/A:1013701923065

Janicki, J. S., and Brower, G. L. (2002). The role of myocardial fibrillar collagen in ventricular remodeling and function. *J. Card. Fail.* 8(6Suppl): 319–325. doi: 10.1054/jcaf.2002.129260

Jansen, J. A., Noorman, M., Musa, H., Stein, M., de Jong, S., van der Nagel, R., et al. (2012b). Reduced heterogeneous expression of Cx43 results in decreased Nav1.5 expression and reduced sodium current that accounts for arrhythmia vulnerability in conditional Cx43 knockout mice. *Heart Rhythm* 9, 600–607. doi: 10.1016/j.hrthm.2011.11.025

Jansen, J. A., van Veen, T. A., de Jong, S., van der Nagel, R., van Stuijvenberg, L., Driessen, H., et al. (2012a). Reduced Cx43 expression triggers increased fibrosis due to enhanced fibroblast activity. *Circ. Arrhythm. Electrophysiol.* 5, 380–390. doi: 10.1161/CIRCEP.111.966580

Jelicks, L. A., and Siri, F. M. (1995). Effects of hypertrophy and heart failure on $[Na^+]_i$ in pressure-overloaded guinea pig heart. *Am. J. Hypertens* 8, 934–943. doi: 10.1016/0895-7061(95)00219-F

Jongsma, H. J., and Wilders, R. (2000). Gap junctions in cardiovascular disease. *Circ. Res.* 86, 1193–1197. doi: 10.1161/01.RES.86.12.1193

Ju, Y. K., Saint, D. A., and Gage, P. W. (1996). Hypoxia increases persistent sodium current in rat ventricular myocytes. *J. Physiol.* 497, 337–347.

Kaab, S., Nuss, H. B., Chiamvimonvat, N., O'Rourke, B., Pak, P. H., Kass, D. A., et al. (1996). Ionic mechanism of action potential prolongation in ventricular myocytes from dogs with pacing-induced heart failure. *Circ. Res.* 78, 262–273. doi: 10.1161/01.RES.78.2.262

Kannel, W. B., Dawber, T. R., Kagan, A., Revotski, N., and Stokes, J. 3rd. (1961). Factors of risk in the development of coronary heart disease six-year follow-up experienee; the Framingham study. *Ann. Int. Med.* 55, 33–50. doi: 10.7326/0003-4819-55-1-33

Kanno, S., Kovacs, A., Yamada, K. A., and Saffitz, J. E. (2003). Connexin43 as a determinant of myocardial infarct sizefollowing coronary occlusion in mice. *J. Am. Coll. Cardiol.* 41, 681–686. doi: 10.1016/S0735-1097(02)02893-0

Kaplan, S. R., Gard, J. J., Carvajal-Huerta, L., Ruiz-Cabezas, J. C., Thiene, G., and Saffitz, J. E. (2004b). Structural and molecular pathology of the heart in Carvajal syndrome. *Cardiovasc. Pathol.* 13, 26–32. doi: 10.1016/S1054-8807(03)00107-8

Kaplan, S. R., Gard, J. J., Protonotarios, N., Tsatsopoulou, A., Spiliopoulou, C., Anastasakis, A., et al. (2004a). Remodeling of myocyte gap junctions in arrhythmogenic right ventricular cardiomyopathy due to a deletion in plakoglobin (Naxos disease). *Heart Rhythm* 1, 3–11. doi: 10.1016/j.hrthm.2004.01.001

Karmazyn, M. (2013). NHE-1: still a viable therapeutic target. *J. Mol. Cell. Cardiol.* 61, 77–82. doi: 10.1016/j.yjmcc.2013.02.006

Kawara, T., Derksen, R., de Groot, J. R., Coronel, R., Tasseron, S., Linnenbank, A. C., et al. (2001). Activation delay after premature stimulation in chronically diseased human myocardium relates to the architecture of interstitial fibrosis. *Circulation* 104, 3069–3075. doi: 10.1161/hc5001.100833

Kemp, C. D., and Conte, J. V. (2012). The pathophysiology of heart failure. *Cardiovasc. Pathol.* 21, 365–371. doi: 10.1016/j.carpath.2011.11.007

Kitamura, H., Ohnishi, Y., Yoshida, A., Okajima, K., Azumi, H., Ishida, A., et al. (2002). Heterogeneous loss of connexin43 protein in nonischemic dilated cardiomyopathy with ventricular tachycardia. *J. Cardiovasc. Electrophysiol.* 13, 865–870. doi: 10.1046/j.1540-8167.2002.00865.x

Kitamura, H., Yoshida, A., Ohnishi, Y., Okajima, K., Ishida, A., Galeano, E. J., et al. (2003). Correlation of connexin43 expression and late ventricular potentials in nonischemic dilated cardiomyopathy. *Circulation* 67, 1017–1021. doi: 10.1253/circj.67.1017

Kleber, A. G., and Rudy, Y. (2004). Basic mechanisms of cardiac impulse propagation and associated arrhythmias. *Physiol. Rev.* 84, 431–488. doi: 10.1152/physrev.00025.2003

Kostin, S., Dammer, S., Hein, S., Klovekorn, W. P., Bauer, E. P., and Schaper, J. (2004). Connexin 43 expression and distribution in compensated and decompensated cardiac hypertrophy in patients with aortic stenosis. *Cardiovasc. Res.* 62, 426–436. doi: 10.1016/j.cardiores.2003.12.010

Kostin, S., Rieger, M., Dammer, S., Hein, S., Richter, M., Klövekorn, W. P., et al. (2003). Gap junction remodeling and altered connexin43 expression in the failing human heart. *Mol. Cell. Biochem.* 242, 135–144. doi: 10.1023/A:1021154115673

Krenning, G., Zeisberg, E. M., and Kalluri, R. (2010). The origin of fibroblasts and mechanism of cardiac fibrosis. *J. Cell. Physiol.* 255, 631–637. doi: 10.1002/jcp.22322

Kudryashova, N. N., Teplenin, A. S., Orlova, Y. V., Selina, L. V., and Agladze, K. (2014). Arrhythmogenic role of the border between two areas of cardiac cell alignment. *J. Mol. Cell. Cardiol.* 76, 227–234. doi: 10.1016/j.yjmcc.2014.09.003

Lee, C. S., and Tkacs, N. C. (2008). Current concepts of neurohormonal activation in heart failure: mediators and mechanisms. *AACN Adv. Crit. Care* 19, 364–385. doi: 10.1097/01.AACN.0000340718.93742.c4

Lloyd-Jones, D. M., Larson, M. G., Leip, E. P., Beiser, A., D'Agostino, R. B., Kannel, W. B., et al. (2002). Lifetime risk for developing congestive heart failure: the framingham heart study. *Circulation* 106, 3068–3072. doi: 10.1161/01.CIR.0000039105.49749.6F

Lou, Q., Fedorov, V. V., Glukhov, A. V., Moazami, N., Fast, V. G., and Efimov, I. R. (2011). Transmural heterogeneity and remodeling of ventricular excitation-contraction coupling in human heart failure. *Circulation* 123, 1881–1890. doi: 10.1161/CIRCULATIONAHA.110.989707

Manabe, I., Shindo, T., and Nagai, R. (2002). Gene expression in fibroblasts and fibrosis: involvement in cardiac hypertrophy. *Circ. Res.* 91, 1103–1113. doi: 10.1161/01.RES.0000046452.67724.B8

Marcus, F. I., McKenna, W. J., Sherrill, D., Basso, C., Bauce, B., Bluemke, D. A., et al. (2010). Diagnosis of arrhythmogenic right ventricular cardiomyopathy/dysplasia - proposed modification of the task force criteria. *Circulation* 121, 1533–1541. doi: 10.1161/CIRCULATIONAHA.108.840827

Maron, B. J. (2002). Hypertrophic cardiomyopathy: a systematic review. *JAMA* 287, 1308–2130. doi: 10.1001/jama.287.10.1308

Maron, B. J., Maron, M. S., and Semsarian, C. (2012). Genetics of hypertrophic cardiomyopathy after 20 years. *J. Am. Coll. Cardiol.* 60, 705–715. doi: 10.1016/j.jacc.2012.02.068

McIntyre, H., and Fry, C. H. (1997). Abnormal action potential conduction in isolated human hypertrophied left ventricular myocardium. *J. Cardiovasc. Electrophysiol.* 8, 887–894. doi: 10.1111/j.1540-8167.1997.tb00850.x

McKoy, G., Protonotarios, N., Crosby, A., Tsatsopoulou, A., Anastasakis, A., Coonar, A., et al. (2000). Identification of a deletion in plakoglobin in arrhythmogenic right ventricular cardiomyopathy with palmoplantar keratoderma and woolly hair (Naxos disease). *Lancet* 355, 2119–2124. doi: 10.1016/S0140-6736(00)02379-5

Merner, N. D., Hodgkinson, K. A., Haywood, A. F., Connors, S., French, V. M., Drenckhahn, J. D., et al. (2008). Arrhythmogenic right ventricular cardiomyopathy type 5 is a fully penetrant, lethal arrhythmic disorder caused by a missense mutation in the TMEM43 gene. *Am. J. Hum. Genet.* 82, 809–821. doi: 10.1016/j.ajhg.2008.01.010

Mestroni, L., Rocco, C., Gregori, D., Sinagra, G., Di Lenarda, A., Miocic, S., et al. (1999). Familial dilated cardiomyopathy: evidence for genetic and phenotypic heterogeneity. Heart Muscle Disease Study Group. *J. Am. Coll. Cardiol.* 34, 181–190. doi: 10.1016/S0735-1097(99)00172-2

Mészáros, J., Khananshvili, D., and Hart, G. (2001). Mechanisms underlying delayed afterdepolarizations in hypertrophied left ventricular myocytes of rats. *Am. J. Physiol. Heart Circ. Physiol.* 281, H903–H914.

Meyerburg, R. J., Kessler, K. M., and Castellanos, A. (1992). Sudden cardiac death. Structure, function, and time-dependence of risk. *Circulation* 85(1 Suppl): I2–I10.

Molkentin, J. D., Lu, J. R., Antos, C. L., Markham, B., Richardson, J., Robbins, J., et al. (1998). A calcineurin-dependent transcriptional pathway for cardiac hypertrophy. *Cell* 93, 215–228. doi: 10.1016/S0092-8674(00)81573-1

Morley, G. E., Vaidya, D., Samie, F. H., Lo, C., Delmar, M., and Jalife, J. (1999). Characterization of conduction in the ventricles of normal and heterozygous Cx43 knockout mice using optical mapping. *J. Cardiovasc. Electrophysiol.* 10, 1361–1375. doi: 10.1111/j.1540-8167.1999.tb00192.x

Nakayama, Y., Shimizu, G., Hirota, Y., Saito, T., Kino, M., Kitaura, Y., et al. (1987). Functional and histopathologic correlation in patients with dilated cardiomyopathy: an integrated evaluation by multivariate analysis. *J. Am. Coll. Cardiol.* 10, 186–192.

Nian, M., Lee, P., Khaper, N., and Liu, P. (2004). Inflammatory cytokines and postmyocardial infarction remodeling. *Circ. Res.* 94, 1543–1553. doi: 10.1161/01.RES.0000130526.20854.fa

Noorman, M., Groeneweg, J. A., Asimaki, A., Rizzo, S., Papegaaij, M., van Stuijvenberg, L., et al. (2013b). End stage of arrhythmogenic cardiomyopathy with severe involvement of the interventricular septum. *Heart Rhythm* 10, 283–289. doi: 10.1016/j.hrthm.2012.10.029

Noorman, M., Hakim, S., Kessler, E., Groeneweg, J. A., Cox, M. G., Asimaki, A., et al. (2013a). Remodeling of the cardiac sodium channel, connexin43, and plakoglobin at the intercalated disk in patients with arrhythmogenic cardiomyopathy. *Heart Rhythm* 10, 412–419. doi: 10.1016/j.hrthm.2012.11.018

Noorman, M., van der Heyden, M. A., van Veen, T. A., Cox, M. G., Hauer, R. N., de Bakker, J. M., et al. (2009). Cardiac cell-cell junctions in health and disease: electrical versus mechanical coupling. *J. Mol. Cell. Cardiol.* 47, 23–31. doi: 10.1016/j.yjmcc.2009.03.016

Norgett, E. E., Hatsell, S. J., Carvajal-Huerta, L., Cabezas, J. C., Common, J., Purkis, P. E., et al. (2000). Recessive mutation in desmoplakin disrupts desmoplakin-intermediate filament interactions and causes dilated cardiomyopathy, woolly hair and keratoderma. *Hum. Mol. Genet.* 9, 2761–2766. doi: 10.1093/hmg/9.18.2761

Orban, P. C., Chui, D., and Marth, J. D. (1992). Tissue- and site-specific DNA recombination in transgenic mice. *Proc. Natl. Acad. Sci. U.S.A.* 89, 6861–6865. doi: 10.1073/pnas.89.15.6861

Otten, E., Asimaki, A., Maass, A., van Langen, I. M., van der Wal, A., de Jonge, N., et al. (2010). Desmin mutations as a cause of right ventricular heart failure affect the intercalated disks. *Heart Rhythm* 7, 1058–1064. doi: 10.1016/j.hrthm.2010.04.023

Palka, P., Lange, A., Fleming, A. D., Donnelly, J. E., Dutka, D. P., Starkey, I. R., et al. (1997). Differences in myocardial velocity gradient measured throughout the cardiac cycle in patients with hypertrophic cardiomyopathy, athletes and patients with left ventricular hypertrophy due to hypertension. *J. Am. Coll. Cardiol.* 30, 760–768. doi: 10.1016/S0735-1097(97)00231-3

Papadatos, G. A., Wallerstein, P. M., Head, C. E., Ratcliff, R., Brady, P. A., Benndorf, K., et al. (2002). Slowed conduction and ventricular tachycardia after targeted disruption of the cardiac sodium channel gene Scn5a. *Proc. Natl. Acad. Sci. U.S.A.* 99, 6210–6215. doi: 10.1073/pnas.082121299

Pazo, D., Kramer, L., Pumir, A., Kanani, S., Efimov, I., and Krinsky, V. (2004). Pinning force in active media. *Phys. Rev. Lett.* 93, 168303-1–168303-4. doi: 10.1103/PhysRevLett.93.168303

Peters, N. S., Coromilas, J., Severs, N. J., and Wit, A. L. (1997). Disturbed connexin43 gap junction distribution correlates with the location of reentrant circuits in the epicardial border zone of healing canine infarcts that cause ventricular tachycardia. *Circulation* 95, 988–996. doi: 10.1161/01.CIR.95.4.988

Peters, N. S., Green, C. R., Poole-Wilson, P. A., and Severs, N. J. (1993). Reduced content of connexin43 gap junctions in ventricular myocardium from hypertrophied and ischemic human hearts. *Circulation* 88, 864–875. doi: 10.1161/01.CIR.88.3.864

Petitprez, S., Zmoos, A. F., Ogrodnik, J., Balse, E., Raad, N., El-Haou, S., et al. (2011). SAP97 and dystrophin macromolecular complexes determine two pools of cardiac sodium channels Nav1.5 in cardiomyocytes. *Circ. Res.* 108, 294–304. doi: 10.1161/CIRCRESAHA.110.228312

Pilichou, K., Nava, A., Basso, C., Beffagna, G., Bauce, B., Lorenzon, A., et al. (2006). Mutations in desmoglein-2 gene are associated with arrhythmogenic right ventricular cardiomyopathy. *Circulation* 113, 1171–1179. doi: 10.1161/CIRCULATIONAHA.105.583674

Protonotarios, N., and Tsatsopoulou, A. (2004). Naxos disease and carvajal syndrome: cardiocutaneous disorders that highlight the pathogenesis and broaden the spectrum of arrhythmogenic right ventricular cardiomyopathy. *Cardiovasc. Pathol.* 13, 185–194. doi: 10.1016/j.carpath.2004.03.609

Protonotarios, N., Tsatsopoulou, A., Patsourakos, P., Alexopoulos, D., Gezerlis, P., Simitsis, S., et al. (1986). Cardiac abnormalities in familial palmoplantar keratosis. *Br. Heart J.* 56, 321–326. doi: 10.1136/hrt.56.4.321

Punske, B., Taccardi, B., Steadman, B., Ershler, P. R., England, A., Valencik, M. L., et al. (2005). Effect of fiber orientation on propagation: electrical mapping of genetically altered mouse hearts. *J. Electrocardiol.* 38, 40–44. doi: 10.1016/j.jelectrocard.2005.06.097

Rampazzo, A., Nava, A., Malacrida, S., Beffagna, G., Bauce, B., Rossi, V., et al. (2002). Mutation in human desmoplakin domain binding to plakoglobin causes a dominant form of arrhythmogenic right ventricular cardiomyopathy. *Am. J. Hum. Genet.* 71, 1200–1206. doi: 10.1086/344208

Reaume, A. G., de Sousa, P. A., Kulkarni, S., Langille, B. L., Zhu, D., Davies, T. C., et al. (1995). Cardiac malformation in neonatal mice lacking connexin 43. *Science* 267, 1831–1834. doi: 10.1126/science.7892609

Remme, C. A., Verkerk, A. O., Hoogaars, W. M., Aanhaanen, W. T., Scicluna, B. P., Annink, C., et al. (2009). The cardiac sodium channel displays differential distribution in the conduction system and transmural heterogeneity in the murine ventricular myocardium. *Basic Res. Cardiol.* 104, 511–522. doi: 10.1007/s00395-009-0012-8

Remme, C. A., Verkerk, A. O., Nuyens, D., van Ginneken, A. C., van Brunschot, S., Belterman, C. N., et al. (2006). Overlap syndrome of cardiac sodium channel disease in mice carrying the equivalent mutation of human SCN5A-1795insD. *Circulation* 114, 2584–2594. doi: 10.1161/CIRCULATIONAHA.106.653949

Richardson, P., McKenna, W., Bristow, M., Maisch, B., Mautner, B., O'Connell, J., et al. (1996). Report of the 1995 World Health Organization/International Society and Federation of Cardiology Task Force on the Definition and Classification of cardiomyopathies. *Circulation* 93, 841–842. doi: 10.1161/01.CIR.93.5.841

Ripplinger, C. M., Krinsky, V. I., Nikolski, V. P., and Efimov, I. R. (2006). Mechanisms of unpinning and termination of ventricular tachycardia. *Am. J. Physiol.* 291, H184–H192. doi: 10.1152/ajpheart.01300.2005

Ripplinger, C. M., Li, W., Hadley, J., Chen, J., Rothenberg, F., Lombardi, R., et al. (2007). Enhanced transmural fiber rotation and connexin 43 heterogeneity are associated with an increased upper limit of vulnerability in a transgenic rabbit

model of human hypertrophic cardiomyopathy. *Circ. Res.* 101, 1049–1057. doi: 10.1161/CIRCRESAHA.107.161240

Rizzo, S., Lodder, E. M., Verkerk, A. O., Wolswinkel, R., Beekman, L., Pilichou, K., et al. (2012). Intercalated disc abnormalities, reduced Na+ current density, and conduction slowing in desmoglein-2 mutant mice prior to cardiomyopathic changes. *Cardiovasc. Res.* 95, 409–418. doi: 10.1093/cvr/cvs219

Roger, V. L., Lloyd-Jones, D. M., Adams, R. J., Berry, J. D., Brown, T. M., Carnethon, M. R., et al. (2011). Heart disease and stroke statistics - update: a report fromthe American Heart Association. *Circulation* 123, e18–e209. doi: 10.1161/CIR.0b013e3182009701

Rohr, S. (2009). Myofibroblasts in diseased hearts: new players in cardiac arrhythmias. *Heart Rhythm* 6, 848–856. doi: 10.1016/j.hrthm.2009.02.038

Royer, A., van Veen, T. A., Le Bouter, S., Marionneau, C., Griol-Charhbili, V., Léoni, A. L., et al. (2005). Mouse model of SCN5A-linked hereditary Lenegre's disease: age-related conduction slowing and myocardial fibrosis. *Circulation* 111, 1738–1746. doi: 10.1161/01.CIR.0000160853.19867.61

Ruiz, P., Brinkmann, V., Ledermann, B., Behrend, M., Grund, C., Thalhammer, C., et al. (1996). Targeted mutation of plakoglobin in mice reveals essential functions of desmosomes in the embryonic heart. *J. Cell Biol.* 135, 215–225. doi: 10.1083/jcb.135.1.215

Saffitz, J., Asimaki, A., and Huang, H. (2009). Arrhythmogenic right ventricular cardiomyopathy: new insights into disease mechanisms and diagnosis. *J. Investig. Med.* 57, 861–864. doi: 10.231/JIM.0b013e3181c5e631

Salameh, A., Krautblatter, S., Karl, S., Blanke, K., Gomez, D. R., Dhein, S., et al. (2009). The signal transduction cascade regulating the expression of the gap junction protein connexin43 by beta-adrenoceptors. *Br. J. Pharmacol.* 158, 198–208. doi: 10.1111/j.1476-5381.2009.00344.x

Sanbe, A., James, J., Tuzcu, V., Nas, S., Martin, L., Gulick, J., et al. (2005). Transgenic rabbit model for human troponin I-based hypertrophic cardiomyopathy. *Circulation* 111, 2330–2338. doi: 10.1161/01.CIR.0000164234.24957.75

Sasano, C., Honjo, H., Takagishi, Y., Uzzaman, M., Emdad, L., Shimizu, A., et al. (2007). Internalization and dephosphorylation of connexin43 in hypertrophied right ventricles of rats with pulmonary hypertension. *Circulation* 71, 382–389. doi: 10.1253/circj.71.382

Sato, P. Y., Coombs, W., Lin, X., Nekrasova, O., Green, K. J., Isom, L. L., et al. (2011). Interactions between ankyrin-G, Plakophilin-2, and Connexin43 at the cardiac intercalated disc. *Circ. Res.* 109, 193–201. doi: 10.1161/CIRCRESAHA.111.247023

Sato, P. Y., Musa, H., Coombs, W., Guerrero-Serna, G., Patiño, G. A., Taffet, S. M., et al. (2009). Loss of plakophilin-2 expression leads to decreased sodium current and slower conduction velocity in cultured cardiac myocytes. *Circ. Res.* 105, 523–526. doi: 10.1161/CIRCRESAHA.109.201418

Sato, P. Y., Ohkusa, T., Honjo, H., Suzuki, S., Yoshida, M. A., Ishiguro, Y. S., et al. (2008). Altered expression of connexin43 contributes to the arrhythmogenic substrate during the development of heart failure in cardiomyopatic hamster. *Am. J. Physiol. Heart Circ.* 294, H1164–H1173. doi: 10.1152/ajpheart.00960.2007

Sepp, R., Severs, N. J., and Gourdie, R. G. (1996). Altered patterns of cardiac intercellular junction distribution in hypertrophic cardiomyopathy. *Heart* 76, 412–417. doi: 10.1136/hrt.76.5.412

Shryock, J. C., Song, Y., Rajamani, S., Antzelevitch, C., and Belardinelli, L. (2013). The arrhythmogenic consequences of increasing late INa in the cardiomyocyte. *Cardiovasc. Res.* 99, 600–611. doi: 10.1093/cvr/cvt145

Silverman, H. S., and Stern, M. D. (1994). Ionic basis of ischaemic cardiac injury: insights from cellular studies. *Cardiovasc. Res.* 28, 581–597. doi: 10.1093/cvr/28.5.581

Smiley, D., Smith, M. A., Carreira, V., Jiang, M., Koch, S. E., Kelley, M., et al. (2014). Increased fibrosis and progression to heart failure in MRL mice following ischemia/reperfusion injury. *Cardiovasc. Pathol.* 23, 327–334. doi: 10.1016/j.carpath.2014.06.001

Smith, J. H., Green, C. R., Peters, N. S., Rothery, S., and Severs, N. J. (1991). Altered patterns of gap junction distribution in ischemic heart disease. An immunohistochemical study of human myocardium using laser scanning confocal microscopy. *Am. J. Pathol.* 139, 801–821.

Soliman, D., Green, C. R., Peters, N. S., Rothery, S., and Severs, N. J. (2012). Late sodium current inhibition alone with ranolazine is sufficient to reduce ischemia- and cardiac glycoside-induced calcium overload and contractile dysfunction mediated by reverse-mode sodium/calcium exchange. *J. Pharmacol. Exp. Ther.* 343, 325–332. doi: 10.1124/jpet.112.196949

Spach, M. S., Heidlage, J. F., Dolber, P. C., and Barr, R. C. (2000). Electrophysiological effects of remodeling cardiac gap junctions and cell size experimental and model studies of normal cardiac growth. *Circ. Res.* 86, 302–311. doi: 10.1161/01.RES.86.3.302

Stein, M., Boulaksil, M., Jansen, J. A., Herold, E., Noorman, M., Joles, J. A., et al. (2010). Reduction of fibrosis-related arrhythmias by chronic renin-angiotensin-aldosterone system inhibitors in an aged mouse model. *Am. J. Physiol. Heart Circ. Physiol.* 299, 310–321. doi: 10.1152/ajpheart.01137.2009

Stein, M., van Veen, T. A., Hauer, R. N., de Bakker, J. M., and van Rijen, H. V. (2011). A 50% reduction of excitability but not of intercellular coupling affects conduction velocity restitution and activation delay in the mouse heart. *PLoS ONE* 6:e20310. doi: 10.1371/journal.pone.0020310

Stein, M., van Veen, T. A., Remme, C. A., Boulaksil, M., Noorman, M., van Stuijvenberg, L., et al. (2009). Combined reduction of intercellular coupling and membrane excitability differentially affects transverse and longitudinal cardiac conduction. *Cardiovasc. Res.* 83, 52–60. doi: 10.1093/cvr/cvp124

Strom, M., Wan, X., Poelzing, S., Ficker, E., and Rosenbaum, D. S. (2010). Gap junction heterogeneity as mechanism for electrophysiologically distinct properties across the ventricular wall. *Am. J. Physiol. Heart Circ. Physiol.* 298, 787–794. doi: 10.1152/ajpheart.00887.2009

Swynghedauw, B. (1999). Molecular mechanisms of myocardial remodeling. *Physiol. Rev.* 79, 215–262.

Syrris, P., Ward, D., Evans, A., Asimaki, A., Gandjbakhch, E., Sen-Chowdhry, S., et al. (2006). Arrhythmogenic right ventricular dysplasia/cardiomyopathy associated with mutations in the desmosomal gene desmocollin-2. *Am. J. Hum. Genet.* 79, 978–984. doi: 10.1086/509122

Tanaka, K., Zlochiver, S., Vikstrom, K. L., Yamazaki, M., Moreno, J., Klos, M., et al. (2007). Spatial distribution of fibrosis governs fibrillation wave dynamics in the posterior left atrium during heart failure. *Circ. Res.* 101, 839–847. doi: 10.1161/CIRCRESAHA.107.153858

Tani, M., and Neely, J. R. (1989). Role of intracellular Na^+ and Ca^{2+} overload and depressed recovery of ventricular function of reperfused ischemic rat hearts. Possible involvement of H^+-Na^+ and Na^+-Ca^{2+} exchange. *Circ. Res.* 65, 1045–1056. doi: 10.1161/01.RES.65.4.1045

Tansey, E. E., Kwaku, K. F., Hammer, P. E., Cowan, D. B., Federman, M., Levitsky, S., et al. (2006). Reduction and redistribution of gap and adherens junction proteins after ischemia and reperfusion. *Ann. Thorac. Surg.* 82, 1472–1479. doi: 10.1016/j.athoracsur.2006.04.061

Thiene, G., Nava, A., Corrado, D., Rossi, L., and Pennelli, N. (1988). Right ventricular cardiomyopathy and sudden death in young people. *N. Engl. J. Med.* 318, 129–133. doi: 10.1056/NEJM198801213180301

Thomas, S. A., Schuessler, R. B., Berul, C. I., Beardslee, M. A., Beyer, E. C., Mendelsohn, M. E., et al. (1998). Disparate effects of deficient expression of Connexin43 on atrial and ventricular conduction: evidence for chamber-specific molecular determinants of conduction. *Circulation* 97, 686–691. doi: 10.1161/01.CIR.97.7.686

Thomas, S. P., Kucera, J. P., Bircher-Lehmann, L., Rudy, Y., Saffitz, J. E., and Kléber, A. G. (2003). Impulse propagation in synthetic strands of neonatal cardiac myocytes with genetically reduced levels of connexin43. *Circ. Res.* 92, 1209–1216. doi: 10.1161/01.RES.0000074916.41221.EA

Towbin, J. A., Lowe, A. M., Colan, S. D., Sleeper, L. A., Orav, E. J., Clunie, S., et al. (2006). Incidence, causes, and outcomes of dilated cardiomyopathy in children. *JAMA* 296, 1867–1876. doi: 10.1001/jama.296.15.1867

Undrovinas, A. I., Maltsev, V. A., and Sabbah, H. N. (1999). Repolarization abnormalities in cardiomyocytes of dogs with chronic heart failure: role of sustained inward current. *Cell Mol. Life Sci.* 55, 494–505. doi: 10.1007/s000180050306

Uzzaman, M., Honjo, H., Takagishi, Y., Emdad, L., Magee, A. I., Severs, N. J., et al. (2000). Remodeling of gap junctional coupling in hypertrophied right ventricles of rats with monocrotaline-induced pulmonary hypertension. *Circ. Res.* 86, 871–878. doi: 10.1161/01.RES.86.8.871

van der Zwaag, P. A., van Rijsingen, I. A., Asimaki, A., Jongbloed, J. D., van Veldhuisen, D. J., Wiesfeld, A. C., et al. (2012). Phospholamban R14del mutation in patients diagnosed with dilated cardiomyopathy or arrhythmogenic right ventricular cardiomyopathy: evidence supporting the concept of arrhythmogenic cardiomyopathy. *Eur. J. Heart Fail.* 14, 1199–1207. doi: 10.1093/eurjhf/hfs119

van Rijen, H. V., Eckardt, D., Degen, J., Theis, M., Ott, T., Willecke, K., et al. (2004). Slow conduction and enhanced anisotropy increase the propensity for ventricular tachyarrhythmias in adult mice with induced deletion of connexin43. *Circulation* 109, 1048–1055. doi: 10.1161/01.CIR.0000117402.70689.75

van Rijen, H. V., van Veen, T. A., Gros, D., Wilders, R., and de Bakker, J. M. (2006). Connexins and cardiac arrhythmias. *Adv. Cardiol.* 42, 150–160. doi: 10.1159/000092567

van Tintelen, J. P., Entius, M. M., Bhuiyan, Z. A., Jongbloed, R., Wiesfeld, A. C., Wilde, A. A., et al. (2006). Plakophilin-2 mutations are the major determinant of familial arrhythmogenic right ventricular dysplasia/cardiomyopathy. *Circulation* 113, 1650–1658. doi: 10.1161/CIRCULATIONAHA.105.609719

van Veen, T. A., Stein, M., Royer, A., Le Quang, K., Charpentier, F., Colledge, W. H., et al. (2005). Impaired impulse propagation in Scn5a-knockout mice combined contribution of excitability, connexin expression, and tissue architecture in relation to aging. *Circ* 112, 1927–1935. doi: 10.1161/CIRCULATIONAHA.105.539072

van Veen, T. A., van Rijen, H. V., Wiegerinck, R. F., Opthof, T., Colbert, M. C., Clement, S., et al. (2002). Remodeling of gap junctions in mouse hearts hypertrophied by forced retinoic acid signaling. *J. Mol. Cell. Cardiol.* 34, 1411–1423. doi: 10.1006/jmcc.2002.2102

Vetter, F. J., Simons, S. B., Mironov, S., Hyatt, C. J., and Pertsov, A. M. (2005). Epicardial fiber organization in swine right ventricle and its impact on propagation. *Circ. Res.* 96, 244–251. doi: 10.1161/01.RES.0000153979.71859.e7

Wagner, S., Dybkova, N., Rasenack, E. C., Jacobshagen, C., Fabritz, L., Kirchhof, P., et al. (2006). Ca2+/calmodulin-dependent protein kinase II regulates cardiac Na+ channels. *J. Clin. Invest.* 116, 3127–3138. doi: 10.1172/JCI26620

Wagner, S., Ruff, H. M., Weber, S. L., Bellmann, S., Sowa, T., Schulte, T., et al. (2011). Reactive oxygen species-activated Ca/calmodulin kinase IIδ is required for late I(Na) augmentation leading to cellular Na and Ca overload. *Circ. Res.* 108, 555–565. doi: 10.1161/CIRCRESAHA.110.221911

Wang, X., Li, F., Campbell, S. E., and Gerdes, A. M. (1999). Chronic pressure overload cardiac hypertrophy and failure in guinea pigs: II. Cytoskeletal remodeling. *J. Mol. Cell. Cardiol.* 31, 319–331. doi: 10.1006/jmcc.1998.0885

Weber, K. T., Sun, Y., and Díez, J. (2008). Fibrosis: a living tissue and the infarcted heart. *J. Am. Coll. Cardiol.* 52, 2029–2031. doi: 10.1016/j.jacc.2008.09.012

Weber, K. T., Sun, Y., Tyagi, S. C., and Cleutjens, J. P. (1994). Collagen network of the myocardium: function, structural remodeling and regulatory mechanisms. *J. Mol. Cell. Cardiol.* 26, 279–292. doi: 10.1006/jmcc.1994.1036

Westerhof, N., and O'Rourke, M. F. (1995). Haemodynamic basis for the development of left ventricular failure. *J. Hypertens.* 13, 943–952.

Wiegerinck, R. F., Verkerk, A. O., Belterman, C. N., van Veen, T. A., Baartscheer, A., Opthof, T., et al. (2006). Larger cell size in rabbits with heart failure increases myocardial conduction velocity and QRS duration. *Circulation* 113, 806–813. doi: 10.1161/CIRCULATIONAHA.105.565804

Winterton, S. J., Turner, M. A., O'Gorman, D. J., Flores, N. A., and Sheridan, D. J. (1994). Hypertrophy causes delayed conduction in human and guinea pig myocardium: accentuation during ischaemic perfusion. *Cardiovasc. Res* 28, 47–54. doi: 10.1093/cvr/28.1.47

Wu, A. H. (2007). Management of patients with non−ischaemic cardiomyopathy. *Heart* 93, 403–408. doi: 10.1136/hrt.2005.085761

Xia, Y., Lee, K., Li, N., Corbett, D., Mendoza, L., and Frangogiannis, N. G. (2009). Characterization of the inflammatory and fibrotic response in a mouse model of cardiac pressure overload. *Histochem. Cell Biol.* 131, 471–481. doi: 10.1007/s00418-008-0541-5

Xiao, X. H., and Allen, D. G. (1999). Role of Na^+/H^+ exchanger during ischemia and preconditioning in the isolated rat heart. *Circ. Res.* 85, 723–730. doi: 10.1161/01.RES.85.8.723

Yamada, K. A., Rogers, J. G., Sundset, R., Steinberg, T. H., and Saffitz, J. (2003). Up-regulation of connexin45 in heart failure. *J. Cardiovasc. Electrophysiol.* 14, 1205–1212. doi: 10.1046/j.1540-8167.2003.03276.x

Zaino, E. C., and Tabor, S. H. (1963). Cardiac hypertrophy in acute myocardial infarction a study based on 100 autopsied cases. *Circulation* 28, 1081–1083. doi: 10.1161/01.CIR.28.6.1081

Zhang, Y., Wang, H., Kovacs, A., Kanter, E. M., and Yamada, K. A. (2010). Reduced expression of Cx43 attenuates ventricular remodeling after myocardial infarction via impaired TGF-beta signaling. *Am. J. Physiol. Heart Circ. Physiol.* 298, H477–H487. doi: 10.1152/ajpheart.00806.2009

Zhao, J., Stephenson, R. S., Sands, G. B., LeGrice, I. J., Zhang, H., Jarvis, J. C., et al. (2013). Atrial fibrosis and atrial fibrillation: a computer simulation in the posterior left atrium. *FIMH LNCS* 7945, 400–408. doi: 10.1007/978-3-642-38899-6_47

Zimmer, H. G. (1994). Some aspects of cardiac heterogeneity. *Basic Res. Cardiol.* 89, 101–117.

Conflict of Interest Statement: The authors declare that the research was conducted in the absence of any commercial or financial relationships that could be construed as a potential conflict of interest.

Received: 26 September 2014; accepted: 24 November 2014; published online: 22 December 2014.

*Citation: Kessler EL, Boulaksil M, van Rijen HVM, Vos MA and van Veen TAB (2014) Passive ventricular remodeling in cardiac disease: focus on heterogeneity. Front. Physiol. **5**:482. doi: 10.3389/fphys.2014.00482*

This article was submitted to Cardiac Electrophysiology, a section of the journal Frontiers in Physiology.

frontiers in PHYSIOLOGY

REVIEW ARTICLE
published: 29 October 2014
doi: 10.3389/fphys.2014.00419

Stem cells can form gap junctions with cardiac myocytes and exert pro-arrhythmic effects

Nicoline W. Smit[1]* and Ruben Coronel[1,2]

[1] Department of Clinical and Experimental Cardiology, Heart Centre, Academic Medical Centre, University of Amsterdam, Amsterdam, Netherlands
[2] L'Institut de RYthmologie et modélisation Cardiaque, Université Bordeaux Segalen, Bordeaux, France

Edited by:
George E. Billman, The Ohio State University, USA

Reviewed by:
Carmen Valenzuela, Consejo Superior de Investigaciones Científicas-Autonomous University of Madrid, Spain
Todd Joseph Herron, University of Michigan-Ann Arbor, USA

***Correspondence:**
Nicoline W. Smit, Heart Center, Department of Experimental Cardiology, Academic Medical Center, University of Amsterdam, K2-113, Meibergdreef 9, 1105 AZ Amsterdam, Netherlands
e-mail: n.w.smit@amc.uva.nl

Stem cell therapy has been suggested to be a promising option for regeneration of injured myocardium, for example following a myocardial infarction. For clinical use cell-based therapies have to be safe and applicable and are aimed to renovate the architecture of the heart. Yet for functional and coordinated activity synchronized with the host myocardium stem cells have to be capable of forming electrical connections with resident cardiomyocytes. In this paper we discuss whether stem cells are capable of establishing functional electrotonic connections with cardiomyocytes and whether these may generate a risk for arrhythmias. Application of stem cells in the clinical setting with outcomes concerning arrhythmogenic safety and future perspectives will also briefly be touched upon.

Keywords: stem cells, cardiomyocytes, electrotonic connections, arrhythmias, clinical trials

INTRODUCTION

Electrical remodeling and loss of working myocardium after a myocardial infarction (MI) remains a major health challenge (McMurray and Pfeffer, 2005). Both processes disrupt the coordinated activation and repolarization of the heart. A theoretical remedy would be to replace the injured tissue with new cardiomyocytes (CM) that are capable of integrating and forming a functional network with the resident cardiomyocytes.

Stem cells have an unlimited proliferation ability and are capable of differentiating into multiple cell types (Wagers and Weissman, 2004). These two properties explain why so much time and energy has been put in making cell therapy effective for regeneration of the myocardium. Yet for proper functional integration within the host's myocardium there are several prerequisites including safety (the absence of adverse effects), a suitable delivery mode and proper timing of delivery. Although many questions concerning stem cells and their mechanism of actions remain, numerous clinical trials have been performed, with varying results.

The Myoblast Autologous Grafting in Ischemic Cardiomyopathy (MAGIC) trial, a multicenter randomized double blind and placebo-controlled study, was the first human trial concerning regenerative stem cell therapy involving skeletal myoblasts. Patients ($n = 90$) with prior MI, left ventricular dysfunction [left ventricular ejection fraction (LVEF) $< 35\%$] and indications for coronary surgery received intra-myocardial injections of autologous myoblasts (low dose: 4×10^8 or high dose: 8×10^8) or placebo solutions. No changes were seen at 6 months in either global or regional left ventricular (LV) function between placebo treated patients and those treated with autologous skeletal myoblast (Eisen, 2008; Menasche et al., 2008). Arrhythmias were documented throughout the 6 months, although there was a higher occurrence in the pooled treatment group this was not significantly different from the control group, most likely owing to the small number of subjects.

In the CADUCEUS trial, cardio-sphere derived stem cells (CDC) were used, which were infused (low dose: 12.5×10^6 or high dose: 25×10^6) into the coronary artery of patients with LV dysfunction at 1.5–3 months post MI. The study was designed to assess safety. At 6 and 12 months follow-up period, despite the reduction in scar size and increase in viable myocardium in the group receiving CDC, no differences in ejection fraction were seen between the control and intervention groups (Makkar et al., 2012; Pompilio et al., 2012). Similar to the MAGIC trial non-sustained ventricular tachycardia (VT) occurred numerically more often in the CDC treated group. However, this was not statistically significant, again due to the small number of patients (17 patients in CDC group, 8 control patients).

The investigators of the SCIPIO and BOOST trials used C-kit$^+$ cardiac derived stem cells and autologous bone marrow stem cells, respectively, and did show functional improvements (Wollert et al., 2004; Bolli et al., 2011). The SCIPIO trial enrolled and randomized post MI patients with left ventricular dysfunction (LVEF $\leq 40\%$) before coronary artery bypass surgery into either the treatment (16 patients) or control group (7 patients) (Bolli et al., 2011). At 4 months post-surgery 16 patients received intracoronary infusion of stem cells (1×10^6). At 6 months post infusion, global improvement in left ventricular ejection fraction (LVEF) by approximately 8.2 ± 2.0 LVEF units was seen. LVEF increased by 12.3 ± 2.0 LVEF units at 1 year post treatment

(Bolli et al., 2011). In the BOOST trial, patients who had undergone successful percutaneous coronary intervention for (acute) ST-segment elevation MI were randomly assigned to the intracoronary bone-marrow transfer (30 patients) or to the control infusion (30 control patients). Patients showed increased global LVEF (about 6%) at 6 months post intracoronary infusion, which is similar to the SCIPIO trial. The effects observed in the BOOST trial, however, were not long-lasting and at 18 months and 5 years follow-up no difference was detected between the cell treated and non-cell treated groups. At 12 months post treatment the positive hemodynamic effects of the SCIPIO trial were maintained. However, that was the last follow-up point and hence it remains unknown whether the positive effects are long lasting or are only maintained up to 12 months post treatment as was seen in the BOOST trial. The SCIPIO trial investigators reported no occurrence of adverse arrhythmogenic events due to cell therapy such as (ventricular) arrhythmias but did not provide a definition of ventricular arrhythmias (Chugh et al., 2012). The BOOST trial reported that there was no difference in occurrence of adverse event, including arrhythmias, between treatment group and control group. However, also in this trial report, arrhythmias were not defined (e.g., duration of VT) and only mentioned as occurrence of VT (Meyer et al., 2006). In addition, similar to the MAGIC and CADUCEUS trial a limited number of patients were involved.

The clinical trials show that delivery of stem cells (either by intracoronary or intra-myocardial injection) is feasible and safe. However, whether the applied stem cells did differentiate and contribute to long-term functional improvements and safety remains questionable. The main reasons for this uncertainty are methodological differences between the trials and the low number of patients involved. Moreover, electrophysiological safety has not been extensively addressed and the electrophysiological variables investigated vary per study. This makes comparison between the studies difficult (Bursac et al., 2010).

Recently two meta-analyzes on stem cell based therapies in (i) chronic ischemic heart disease and congestive heart failure (Fisher et al., 2014) and (ii) acute MI (de Jong et al., 2014) were published. Each study included more than 20 randomized clinical trials adding up to more than 1200 patients. In the first meta-analysis concerning heart failure patients (without MI) there is moderate evidence that stem cells improve LVEF and that it has potential beneficial clinical outcome in terms of performance status (at least 1 year) and mortality (Fisher et al., 2014). The authors do underline the fact that the conclusions are still of low quality as the studies used are small and aimed at safety and feasibility. The second meta-analysis involving cell based therapies in patients with acute MI noted that there was a reasonable improvement in LVEF, which were explained by reduction in scar size and sustained LV end systole volume. Unlike the meta-analysis on heart failure no effects on clinical outcomes were found (de Jong et al., 2014). Similar to the other meta-analysis is that the studies included were only targeted at feasibility and safety.

Not only must cell therapy be delivered in a safe manner and at the right time, the cells should also be capable of making electrotonic connections with CM so that they can integrate and be properly functional within the host's myocardium. Currently, a number of different stem cell types are known, and although these are believed to behave differently from each other, this paper will evaluate studies that have used cardiomyocytes and stem cells, without focusing on one specific type/regardless of the type. The following questions will be addressed: (i) Are stem cells capable of forming functional intercellular connections with cardiomyocytes? and (ii) can pro-arrhythmic effects results from the interaction between stem cells and cardiomyocytes?

INTERCELLULAR CONNECTIONS

Gap junctions are specialized intercellular channels found in the membranes of neighboring cardiomyocytes, and allow exchange of ions and small molecules between cells (Kanno and Saffitz, 2001). These specialized regions are composed of two hexameric hemichannels, one in each neighboring CM. Each hemichannel, or connexon, in turn consists of 6 subunits called connexins (Kanno and Saffitz, 2001; Dhein, 2004). The gap junctional channels allow propagation of the action potential from one cell to the next. In normal healthy cardiomyocytes gap junctions are predominantly found at the intercalated disks, allowing the action potential to spread predominantly along the fiber's axis, resulting in faster conduction along the fiber than across the fiber direction (anisotropy) (Kanno and Saffitz, 2001).

The properties of these gap junctions play an important role in the determination of conduction velocity, and the electrical activation of the heart. Several cardiac connexin isoforms have been identified, each with a different channel conductance; the most predominantly expressed gap junction in ventricular myocytes is connexin43 (Cx43) (van Kempen et al., 1995). The lack of or loss of Cx43 is associated with diminished electrical coupling and formation of arrhythmias (de Groot et al., 2003; de Diego et al., 2008; Procida et al., 2009). Heart failure models show that decreased Cx43 coupling leads to an increase in conduction heterogeneity and to an increase in the inducibility of arrhythmias (Wiegerinck et al., 2008). The relation between uncoupling and conduction velocity is non-linear implying that a relatively large degree of loss of gap junctions is required to cause conduction slowing (Jongsma and Wilders, 2000). Furthermore, reduced intercellular coupling causes increased heterogeneity of repolarization and can contribute to a pro-arrhythmic substrate (Wiegerinck et al., 2008).

Because gap junctions are of crucial importance for the electrical activation and repolarization of the heart, alteration in gap junctions can lead to fundamental changes in the electrical activity of the heart. Stem cells must therefore be not only capable of coupling with CM but also do this with a sufficiently high gap junctional conductance.

ELECTROTONIC INTERACTIONS BETWEEN STEM CELLS AND CARDIOMYOCYTES

IN VITRO STUDIES

Various *in vitro* studies employing immunofluorescence staining have shown that gap junctions containing Cx43 exist between mesenchymal stem cells (MSC) and neonatal rat cardiomyocytes (NRCM) (Beeres et al., 2005; Chang et al., 2006; Pijnappels et al., 2006). Beeres et al. and Chang et al. additionally have proved, through the use of dye transfer, that these gap junctions were functional (Beeres et al., 2005; Chang et al., 2006).

The question therefore remains whether the gap junctions between MSC and cardiomyocytes also have (adverse) electrophysiological consequences. Electrophysiological functionality can be confirmed in *in vitro* studies with uncoupling substances such as gap junction blockers. Intercellular uncoupling or blocking of the formation of electrotonic connections can be used to detect both potential pro-arrhythmic as anti- arrhythmic consequences of the interconnections between the cell types. Using Tetrodotoxin in an *in vitro* co-culture of NRCM and human MSC, Askar et al. demonstrated that hetero-cellular coupling was the predominant mechanism for the observed conduction slowing in these preparations (Askar et al., 2013). Beeres et al. showed that electrotonic coupling with human MSC was needed to join two asynchronously beating fields of cardiomyocytes (Beeres et al., 2005). When carbenoxolene, a potent gap junctional uncoupling agent (de Groot et al., 2003), was added to these cultures the synchronized beating of the two fields was lost (Beeres et al., 2005; Pijnappels et al., 2006).

Another approach to establish functionality of connections between CM and stem cells is via genetic modification. In the *in vitro* model used by Beeres and Pijnappels, Cx43 knockdown in human MSC led to failure of synchronization of two asynchronously beating cardiomyocyte fields (Pijnappels et al., 2006). Co-cultures of skeletal myoblasts and NRCM demonstrated a decrease in conduction velocity and easily inducible re-entry, both of which could be attenuated when skeletal myoblasts were modified to overexpress Cx43 (Abraham et al., 2005; Tolmachov et al., 2006; Roell et al., 2007). More efficient coupling therefore appears to be beneficial whereas incomplete coupling is potentially arrhythmogenic.

IN VIVO STUDIES

Demonstrating functional coupling between stem cells and resident cardiomyocytes in *in vivo* studies is challenging. The implanted cells are usually not directly accessible and the lack of high-resolution functional measurements in a beating heart hampers direct assessment of functional coupling between stem cells and endogenous cardiomyocytes. Post mortem histological analyses may demonstrate successful engraftment of stem cells but not functional coupling.

Autologous stem cells engraftment has also been established in various studies through labeling stem cells with a cross-linkable membrane dye (Dye IL) (Price et al., 2006), transfection with GFP labeled lenti-virus (Valina et al., 2007; Mazo et al., 2011), or transfected *E. Coli* lac Z encoding B-gal (Rigol et al., 2010). Species-specific antibodies can determine the engraftment when xenografted cells are applied (Chong et al., 2014). However, in histological sections the electrophysiological interaction due to functional gap junctions cannot be demonstrated.

Alternative techniques to establish functional coupling *in vivo* is through calcium transients. Rubart et al. transplanted GFP expressing fetal cardiomyocytes into adult mice hearts (Rubart et al., 2003). Imaging of calcium transients in the intact heart of both host and donor cells showed that they were identical, encouraging the concept that cells can functionally couple to host cells (Rubart et al., 2003). Recently, this same concept was used to confirm functional coupling of human embryonic stem cell derived cardiomyocytes in a non-human primate myocardium (Chong et al., 2014). This last study convincingly supported the idea that stem cells can form a functional and synchronized network with the host myocardium. It has to be noted though that the cells used in this study are cardiomyocytes created from embryonic stem cells. This is where stem cell derived cardiomyocytes are purified and cryopreserved before application.

Kehat et al. performed *in vitro* electrophysiological analysis of hES that had formed spontaneous beating embryoid bodies. He demonstrated that hES had both structural and electrical features that resembled those of CM (Kehat et al., 2001). These hES were not grown together with myocytes and therefore it is not possible to state whether electrical coupling would form. Nevertheless, the fact that these cells obtained structural features specific for cardiomyocytes is attractive, because for proper integration within the myocardium the current generated in the host cell must not only pass through gap junctions to depolarize the transplanted cell, these cells must also have the appropriate excitation-contraction coupling properties.

PRO-ARRHYTHMIC EFFECTS OF ELECTROTONIC CONNECTIONS

Although engraftment of stem cells may occur, it does not imply that the engrafted cells are functionally and electrically coupled to resident cardiomyocytes. In addition, if these cells do couple electrically it is not self-evident that these interactions can contribute to the synchronized network of endogenous cardiomyocytes without any risks or side effects. It has been suggested that stem cells are capable of influencing the electrophysiological properties of cardiomyocytes, resulting in the formation of a pro-arrhythmic substrate (Chang et al., 2006; Askar et al., 2013). Proposed mechanisms including depolarization, anatomical block, abnormal automaticity and triggered activity are discussed and are schematically shown in **Figure 1**.

DEPOLARIZATION AND REFRACTORY PERIOD

The membrane potential of MSC has been shown to be around −35 mV (Heubach et al., 2004; Valiunas et al., 2004; Sundelacruz et al., 2008). After electrical coupling, depolarization of the resting membrane of CM is anticipated (Xie et al., 2009). The magnitude of depolarization depends on the membrane potential of the connected stem cell, but also to the extent of the intercellular coupling between the two cells (the coupling resistance) and the size of the cells (Tan and Joyner, 1990; Henriquez et al., 2001).

If depolarization of the resting membrane is severe (by more than 30 mV) the excitability of the cells is reduced; the voltage gated sodium channels are inactivated, resulting in reduction in upstroke velocity and conduction velocity (Shaw and Rudy, 1997; Kléber and Rudy, 2004; Hubbard et al., 2007). Also, the plateau phase is expected to be shorter while the action potential duration is expected to be prolonged **Figure 1A**. Action potential prolongation can lead to (unidirectional) block at tissue level and may facilitate re-entrant arrhythmias (de Bakker et al., 1993; Coronel et al., 2013).

Electrotonic connections between stem cells and cardiomyocytes can also lead to the "current sink" or "current

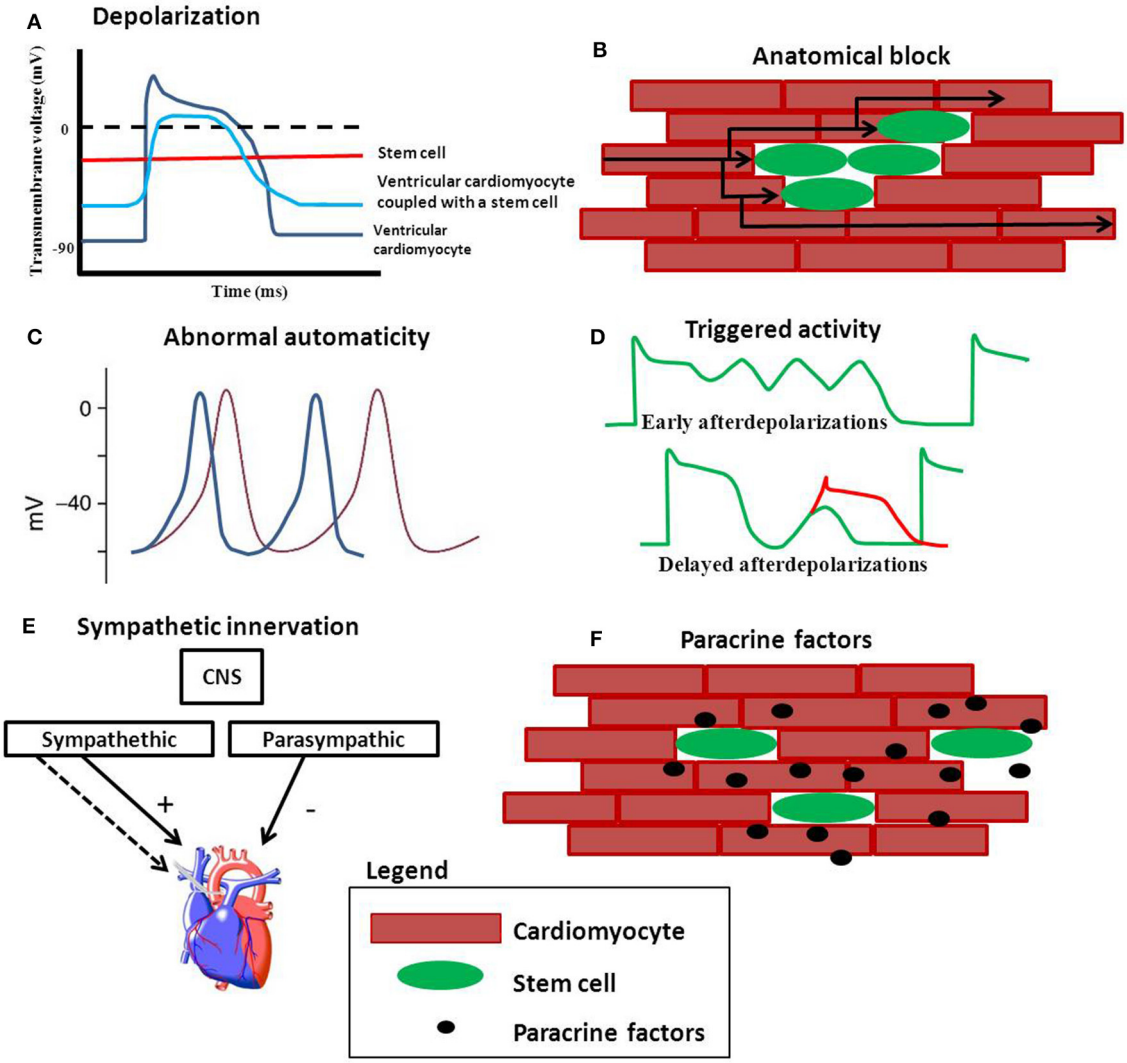

FIGURE 1 | Possible mechanisms of stem cell induced arrhythmias. **(A)** Depolarization of cardiomyocytes reduces the upstroke velocity and conduction velocity. **(B)** Clusters of stem cells can create an anatomical block and force the electrical pathway to find a different (and longer) route. **(C)** Stem cells can be spontaneously beating and may compete with the hosts own automaticity when engrafted. Stem cells may also be capable of inducing arrhythmias via triggered activity **(D)**. **(E)** Increased sympathetic innervation induced by stem cells can give an unbalance in the sympathetic and parasympathetic equilibrium. **(F)** Paracrine factors released by stem cells may effect electrophysiology of cardiomyocytes.

source" phenomenon (Rohr, 2004). This occurs when the load of an excited region supplying the depolarization current is not matched to the amount of current needed to excite the region ahead; current to load mismatch (Rohr, 2004). Stem cells depolarize cardiomyocytes, suggesting that the regions where stem cells are applied are more depolarized and that the depolarizing current coming from these hetero-cellular areas is not enough to excite the regions, consisting of endogenous cardiomyocytes, around it.

Depolarization of cardiomyocytes can thus lead to a reduction in upstroke velocity and conduction velocity but also affect the duration and shape of an action potential. These properties are all related to refractoriness and restitution properties (Hondeghem et al., 2001). Alterations in restitution properties and the effective refractory period (ERP) may lead to arrhythmias (Qu et al., 1999; Tran et al., 2007). The ERP plays an important role, together with conduction slowing and unidirectional block, in facilitating re-entry arrhythmias at a multicellular level. In a porcine MI model administration of MSC shortened ERP and resulted in steeper ERP restitution curves (Price et al., 2006), both indicators of electrical instability.

ANATOMICAL BLOCK

Cells used for cell-based regenerative therapies do not necessarily have to couple functionally to generate potential threatening situations for the formations of arrhythmias. Cells injected into the myocardium can integrate in such a way that they nestle themselves between CM causing resident CM to uncouple or

prevent the coupling of CM (Duffy, 2008). Islands of uncoupled cells can cause anatomical block, forcing the electrical wave front to find an alternative route, resulting in a possible increased activation time over a specific region (de Bakker et al., 1993) (Figure 2A). If this results in heterogeneous conduction slowing it could facilitate unidirectional block and re-entrant arrhythmias (Lammers et al., 1990; de Bakker et al., 1993). In infarcted rat myocardium the transplanted myoblasts were functionally isolated from the resident cardiomyocytes (Leobon et al., 2003). Although intracellular recordings in the heart were obtained and the action potentials evoked in the myotubes were accompanied by (local) contractions, these did not spread out over the myocardium (Leobon et al., 2003). Information on conduction heterogeneity and local (fractionated) electrograms were not present in this publication. Both factors could have indicated discontinuous conduction (de Bakker et al., 1993; de Bakker and Wittkampf, 2010) a potential indicator for arrhythmogenesis.

ABNORMAL AUTOMATICITY

Abnormal automaticity is yet another mechanism that can evoke arrhythmias. The normal regular spontaneous sinus rhythm can be lost because other excitable cells have a higher spontaneous activity than the original endogenous pacemaker cells (**Figure 1C**). This could hold true for human embryonic stem cells that form embryoid bodies of spontaneously beating cardiomyocytes. Kehat et al. transplanted clusters of spontaneously beating cardiomyocytes (derived from hES) into a swine with complete atrio-ventricular block (Kehat et al., 2004). They demonstrated that the ventricular ectopic rhythm that followed the transplantation was localized at the site of cell transplantation. The observation that the transplanted cells were able to pace the entire heart at first glance appears to be positive, especially for bio-pace making purposes (Rosen et al., 2007; Li, 2012). However, the pacing rhythm of the transplanted cells may interfere with the animal's own sinus rhythm. In a recent paper published by Chong et al. human embryonic stem cell derived cardiomyocytes were injected into a non-human primate model of myocardial ischemia and reperfusion. The animals showed an usual high number of non-lethal arrhythmias (Chong et al., 2014). Compared to small animal models (Laflamme et al., 2007; Shiba et al., 2012), in which the same human embryonic cells were also used, the high number of non-lethal arrhythmias seen in the non-primate model may be explained by graft automaticity. These animals have lower heart rates compared to the smaller animals (mice and rats) used prior (Chong et al., 2014).

TRIGGERED ACTIVITY

Triggered activity initiated by (delayed or early) after depolarizations, may also be involved in arrhythmogenesis caused by stem cell therapy (**Figure 1D**).

Although a scarce number of studies concerning human embryonic stem cell derived CM (Jonsson et al., 2011) and induced pluripotent stem cell derived CM (Knollmann, 2013) have been performed to look at pro-arrhythmic potential, no conclusion can be drawn yet to associated stem cells directly with early after depolarizations or delayed after depolarizations.

SYMPATHETIC HYPER-INNERVATION

Stimulation of sympathetic nerve sprouting is an alternative mechanism of stem cells that promote arrhythmogenesis (Pak et al., 2003; Kim et al., 2010). Although this process does not require the formation of gap junctions it is important to keep in mind when evaluating the safety of stem cells. The heart is innervated by both the parasympathetic and sympathetic nervous system (**Figure 1E**), whereby the latter has a higher density in de sub-epicardium and central conduction system (Kawano et al., 2003). Sympathetic stimulation leads to acceleration of the heart rate, contractility and can improve cardiac output. However, it has also been shown that disturbed innervation can cause lethal arrhythmias (Cao et al., 2000). Pak et al. stated that MSC induce cardiac nerve sprouting in a large animal model of MI (Pak et al., 2003). One month post MI induction, swines received injections of either a mixture of MSC and bone marrow cells, bone marrow cells alone or only the culture medium. One month later the animals were killed and immunofluorescence staining was performed on tissue samples. Samples were stained for nerve sprouting (growth-associated protein; GAP-43), sympathetic nerves (tyrosine hydroxylase; TH) and for tenascin expression. Animals receiving the combination treatment showed more GAP43-positive nerves, higher density of sympathetic nerves and higher tenascin expression (Pak et al., 2003) suggesting an increase in cardiac (sympathetic) nerve sprouting.

Kim et al. saw similar results when MSCs were injected in the myocardium of canines. In addition, he demonstrated the pro-arrhythmic risk of this hyper-innervation (Kim et al., 2010). Occurrence of ventricular fibrillation was 0% in the sham group and 33.3% in the group who received MSC. Hyper-innervation may therefore be an important mechanism for the pro-arrhythmic potential of stem cells.

PARACRINE FACTORS

An additional mechanism through which stem cells can be pro-arrhythmic is the influence of secreted paracrine factors or factors released once these cells are connected to cardiomyocytes (**Figure 1F**). Although the "paracrine hypothesis" (Gnecchi et al., 2008) is suggested to be an indirect mechanism behind improvement in left ventricular (LV) function, changes in scar properties, angiogenesis induction and/or improvement in survival of endogenous cardiomyocytes, several studies have documented pro-arrhythmic effects of paracrine factors (Pedrotty et al., 2009; Askar et al., 2013). However, the actual factor(s) and mechanism behind these observed results still need to be identified.

CONCLUSION

After nearly two decades of research in stem cell based therapies for cardiac regeneration the search for the "perfect" stem cell—based therapy for cardiac tissue regeneration continues as there are still many questions left that remain unanswered.

Stem cells have the ability to couple electrically to cardiomyocytes via gap junctions. Formations of functional intercellular connections influence the electrical properties of cardiomyocytes and are associated with pro-arrhythmic effects. Depolarization of resting membrane, heterogeneous conduction slowing, and electrical instability are factors that can occur after electrotonic

connections between stem cells and cardiomyocytes are formed. Depending on the magnitude of effect these factors can contribute to the formation of arrhythmias.

Future studies should not only be aimed at efficacy and long-term effects but also in making clinical trials similar so that factors (e.g., different in/exclusion criteria, cells dose/type, timing, and route of cell infusion) contributing to conflicting data can be limited and a provide solid framework for the safe application of stem cells without arrhythmogenic side effects.

FUNDING

The financial contributions of ICARUS of the BioMedical Materials program (project-P5.01) and the LeDucq (SHAPEHEART network) are gratefully acknowledged.

ACKNOWLEDGMENTS

We would like to thank Veronique M. F. Meijborg for her valuable input and suggestions.

REFERENCES

Abraham, M. R., Henrikson, C. A., Tung, L., Chang, M. G., Aon, M., Xue, T., et al. (2005). Antiarrhythmic engineering of skeletal myoblasts for cardiac transplantation. *Circ. Res.* 97, 159–167. doi: 10.1161/01.RES.0000174794.22491.a0

Askar, S. F., Ramkisoensing, A. A., Atsma, D. E., Schalij, M. J., de Vries, A. A., and Pijnappels, D. A. (2013). Engraftment patterns of human adult mesenchymal stem cells expose electrotonic and paracrine proarrhythmic mechanisms in myocardial cell cultures. *Circ. Arrhythm. Electrophysiol.* 6, 380–391. doi: 10.1161/CIRCEP.111.000215

Beeres, S. L., Atsma, D. E., van der Laarse, A., Pijnappels, D. A., van Tuyn, J., Fibbe, W. E., et al. (2005). Human adult bone marrow mesenchymal stem cells repair experimental conduction block in rat cardiomyocyte cultures. *J. Am. Coll. Cardiol.* 46, 1943–1952. doi: 10.1016/j.jacc.2005.07.055

Bolli, R., Chugh, A. R., D'Amario, D., Loughran, J. H., Stoddard, M. F., Ikram, S., et al. (2011). Cardiac stem cells in patients with ischaemic cardiomyopathy (SCIPIO): initial results of a randomised phase 1 trial. *Lancet* 378, 1847–1857. doi: 10.1016/S0140-6736(11)61590-0

Bursac, N., Kirkton, R. D., McSpadden, L. C., and Liau, B. (2010). Characterizing functional stem cell-cardiomyocyte interactions. *Regen. Med.* 5, 87–105. doi: 10.2217/rme.09.69

Cao, J. M., Chen, L. S., Kenknight, B. H., Ohara, T., Lee, M. H., Tsai, J., et al. (2000). Nerve sprouting and sudden cardiac death. *Circ. Res.* 86, 816–821. doi: 10.1161/01.RES.86.7.816

Chang, M. G., Tung, L., Sekar, R. B., Chang, C. Y., Cysyk, J., Dong, P., et al. (2006). Proarrhythmic potential of mesenchymal stem cell transplantation revealed in an *in vitro* coculture model. *Circulation* 113, 1832–1841. doi: 10.1161/CIRCULATIONAHA.105.593038

Chong, J. J., Yang, X., Don, C. W., Minami, E., Liu, Y. W., Weyers, J. J., et al. (2014). Human embryonic-stem-cell-derived cardiomyocytes regenerate non-human primate hearts. *Nature* 510, 273–277. doi: 10.1038/nature13233

Chugh, A. R., Beache, G. M., Loughran, J. H., Mewton, N., Elmore, J. B., Kajstura, J., et al. (2012). Administration of cardiac stem cells in patients with ischemic cardiomyopathy: the SCIPIO trial: surgical aspects and interim analysis of myocardial function and viability by magnetic resonance. *Circulation* 126(11 Suppl. 1), S54–S64. doi: 10.1161/CIRCULATIONAHA.112.092627

Coronel, R., Wilders, R., Verkerk, A. O., Wiegerinck, R. F., Benoist, D., and Bernus, O. (2013). Electrophysiological changes in heart failure and their implications for arrhythmogenesis. *Biochim. Biophys. Acta* 1832, 2432–2441. doi: 10.1016/j.bbadis.2013.04.002

de Bakker, J. M., van Capelle, F. J., Janse, M. J., Tasseron, S., Vermeulen, J. T., de Jonge, N., et al. (1993). Slow conduction in the infarcted human heart. 'Zigzag' course of activation. *Circulation* 88, 915–926. doi: 10.1161/01.CIR.88.3.915

de Bakker, J. M., and Wittkampf, F. H. (2010). The pathophysiologic basis of fractionated and complex electrograms and the impact of recording techniques on their detection and interpretation. *Circ. Arrhythm. Electrophysiol.* 3, 204–213. doi: 10.1161/CIRCEP.109.904763

de Diego, C., Pai, R. K., Chen, F., Xie, L. H., De, L. J., Weiss, J. N., et al. (2008). Electrophysiological consequences of acute regional ischemia/reperfusion in neonatal rat ventricular myocyte monolayers. *Circulation* 118, 2330–2337. doi: 10.1161/CIRCULATIONAHA.108.789149

de Groot, J. R., Veenstra, T., Verkerk, A. O., Wilders, R., Smits, J. P., Wilms-Schopman, F. J., et al. (2003). Conduction slowing by the gap junctional uncoupler carbenoxolone. *Cardiovasc. Res.* 60, 288–297. doi: 10.1016/j.cardiores.2003.07.004

de Jong, R., Houtgraaf, J. H., Samiei, S., Boersma, E., and Duckers, H. J. (2014). Intracoronary stem cell infusion after acute myocardial infarction: a meta-analysis and update on clinical trials. *Circ. Cardiovasc. Interv.* 7, 156–167. doi: 10.1161/CIRCINTERVENTIONS.113.001009

Dhein, S. (2004). Pharmacology of gap junctions in the cardiovascular system. *Cardiovasc. Res.* 62, 287–298. doi: 10.1016/j.cardiores.2004.01.019

Duffy, H. S. (2008). Cardiac connections–the antiarrhythmic solution? *N. Engl. J. Med.* 358, 1397–1398. doi: 10.1056/NEJMcibr0708922

Eisen, H. J. (2008). Skeletal myoblast transplantation: no MAGIC bullet for ischemic cardiomyopathy. *Nat. Clin. Pract. Cardiovasc. Med.* 5, 520–521. doi: 10.1038/ncpcardio1299

Fisher, S. A., Brunskill, S. J., Doree, C., Mathur, A., Taggart, D. P., and Martin-Rendon, E. (2014). Stem cell therapy for chronic ischaemic heart disease and congestive heart failure. *Cochrane Database Syst. Rev.* 4:CD007888. doi: 10.1002/14651858.CD007888

Gnecchi, M., Zhang, Z., Ni, A., and Dzau, V. J. (2008). Paracrine mechanisms in adult stem cell signaling and therapy. *Circ. Res.* 103, 1204–1219. doi: 10.1161/CIRCRESAHA.108.176826

Henriquez, A. P., Vogel, R., Muller-Borer, B. J., Henriquez, C. S., Weingart, R., and Cascio, W. E. (2001). Influence of dynamic gap junction resistance on impulse propagation in ventricular myocardium: a computer simulation study. *Biophys. J.* 81, 2112–2121. doi: 10.1016/S0006-3495(01)75859-6

Heubach, J. F., Graf, E. M., Leutheuser, J., Bock, M., Balana, B., Zahanich, I., et al. (2004). Electrophysiological properties of human mesenchymal stem cells. *J. Physiol.* 554(Pt 3), 659–672. doi: 10.1113/jphysiol.2003.055806

Hondeghem, L. M., Carlsson, L., and Duker, G. (2001). Instability and triangulation of the action potential predict serious proarrhythmia, but action potential duration prolongation is antiarrhythmic. *Circulation* 103, 2004–2013. doi: 10.1161/01.CIR.103.15.2004

Hubbard, M. L., Ying, W., and Henriquez, C. S. (2007). Effect of gap junction distribution on impulse propagation in a monolayer of myocytes: a model study. *Europace* 9 Suppl. 6, vi20-vi28. doi: 10.1093/europace/eum203

Jongsma, H. J., and Wilders, R. (2000). Gap junctions in cardiovascular disease. *Circ. Res.* 86, 1193–1197. doi: 10.1161/01.RES.86.12.1193

Jonsson, M. K., Wang, Q. D., and Becker, B. (2011). Impedance-based detection of beating rhythm and proarrhythmic effects of compounds on stem cell-derived cardiomyocytes. *Assay Drug Dev. Technol.* 9, 589–599. doi: 10.1089/adt.2011.0396

Kanno, S., and Saffitz, J. E. (2001). The role of myocardial gap junctions in electrical conduction and arrhythmogenesis. *Cardiovasc. Pathol.* 10, 169–177. doi: 10.1016/S1054-8807(01)00078-3

Kawano, H., Okada, R., and Yano, K. (2003). Histological study on the distribution of autonomic nerves in the human heart. *Heart Vessels* 18, 32–39. doi: 10.1007/s003800300005

Kehat, I., Kenyagin-Karsenti, D., Snir, M., Segev, H., Amit, M., Gepstein, A., et al. (2001). Human embryonic stem cells can differentiate into myocytes with structural and functional properties of cardiomyocytes. *J. Clin. Invest.* 108, 407–414. doi: 10.1172/JCI200112131

Kehat, I., Khimovich, L., Caspi, O., Gepstein, A., Shofti, R., Arbel, G., et al. (2004). Electromechanical integration of cardiomyocytes derived from human embryonic stem cells. *Nat. Biotechnol.* 22, 1282–1289. doi: 10.1038/nbt1014

Kim, S. K., Pak, H. N., Park, J. H., Fang, Y. F., Kim, G. I., Park, Y. D., et al. (2010). Cardiac cell therapy with mesenchymal stem cell induces cardiac

nerve sprouting, angiogenesis, and reduced connexin43-positive gap junctions, but concomitant electrical pacing increases connexin43-positive gap junctions in canine heart. *Cardiol. Young* 20, 308–317. doi: 10.1017/S1047951110000132

Kléber, A. G., and Rudy, Y. (2004). Basic mechanisms of cardiac impulse propagation and associated arrhythmias. *Physiol. Rev.* 84, 431–488. doi: 10.1152/physrev.00025.2003

Knollmann, B. C. (2013). Induced pluripotent stem cell-derived cardiomyocytes: boutique science or valuable arrhythmia model? *Circ. Res.* 112, 969–976. doi: 10.1161/CIRCRESAHA.112.300567

Laflamme, M. A., Chen, K. Y., Naumova, A. V., Muskheli, V., Fugate, J. A., Dupras, S. K., et al. (2007). Cardiomyocytes derived from human embryonic stem cells in pro-survival factors enhance function of infarcted rat hearts. *Nat. Biotechnol.* 25, 1015–1024. doi: 10.1038/nbt1327

Lammers, W. J., Schalij, M. J., Kirchhof, C. J., and Allessie, M. A. (1990). Quantification of spatial inhomogeneity in conduction and initiation of reentrant atrial arrhythmias. *Am. J. Physiol.* 259(4 Pt 2), H1254–H1263.

Leobon, B., Garcin, I., Menasche, P., Vilquin, J. T., Audinat, E., and Charpak, S. (2003). Myoblasts transplanted into rat infarcted myocardium are functionally isolated from their host. *Proc. Natl. Acad. Sci. U.S.A.* 100, 7808–7811. doi: 10.1073/pnas.1232447100

Li, R. A. (2012). Gene- and cell-based bio-artificial pacemaker: what basic and translational lessons have we learned? *Gene Ther.* 19, 588–595. doi: 10.1038/gt.2012.33

Makkar, R. R., Smith, R. R., Cheng, K., Malliaras, K., Thomson, L. E., Berman, D., et al. (2012). Intracoronary cardiosphere-derived cells for heart regeneration after myocardial infarction (CADUCEUS): a prospective, randomised phase 1 trial. *Lancet* 379, 895–904. doi: 10.1016/S0140-6736(12)60195-0

Mazo, M., Gavira, J. J., Pelacho, B., and Prosper, F. (2011). Adipose-derived stem cells for myocardial infarction. *J. Cardiovasc. Transl. Res.* 4, 145–153. doi: 10.1007/s12265-010-9246-y

McMurray, J. J., and Pfeffer, M. A. (2005). Heart failure. *Lancet* 365, 1877–1889. doi: 10.1016/S0140-6736(05)66621-4

Menasche, P., Alfieri, O., Janssens, S., McKenna, W., Reichenspurner, H., Trinquart, L., et al. (2008). The Myoblast Autologous Grafting in Ischemic Cardiomyopathy (MAGIC) trial: first randomized placebo-controlled study of myoblast transplantation. *Circulation* 117, 1189–1200. doi: 10.1161/CIRCULATIONAHA.107.734103

Meyer, G. P., Wollert, K. C., Lotz, J., Steffens, J., Lippolt, P., Fichtner, S., et al. (2006). Intracoronary bone marrow cell transfer after myocardial infarction: eighteen months' follow-up data from the randomized, controlled BOOST (BOne marrOw transfer to enhance ST-elevation infarct regeneration) trial. *Circulation* 113, 1287–1294. doi: 10.1161/CIRCULATIONAHA.105.575118

Pak, H. N., Qayyum, M., Kim, D. T., Hamabe, A., Miyauchi, Y., Lill, M. C., et al. (2003). Mesenchymal stem cell injection induces cardiac nerve sprouting and increased tenascin expression in a Swine model of myocardial infarction. *J. Cardiovasc. Electrophysiol.* 14, 841–848. doi: 10.1046/j.1540-8167.2003.03124.x

Pedrotty, D. M., Klinger, R. Y., Kirkton, R. D., and Bursac, N. (2009). Cardiac fibroblast paracrine factors alter impulse conduction and ion channel expression of neonatal rat cardiomyocytes. *Cardiovasc. Res.* 83, 688–697. doi: 10.1093/cvr/cvp164

Pijnappels, D. A., Schalij, M. J., van Tuyn, J., Ypey, D. L., de Vries, A. A., van der Wall, E. E., et al. (2006). Progressive increase in conduction velocity across human mesenchymal stem cells is mediated by enhanced electrical coupling. *Cardiovasc. Res.* 72, 282–291. doi: 10.1016/j.cardiores.2006.07.016

Pompilio, G., Capogrossi, M. C., Leone, A. M., and Crea, F. (2012). The SCIPIO and CADUCEUS studies. *G. Ital. Cardiol. (Rome).* 13, 777–782. doi: 10.1714/1188.13160

Price, M. J., Chou, C. C., Frantzen, M., Miyamoto, T., Kar, S., Lee, S., et al. (2006). Intravenous mesenchymal stem cell therapy early after reperfused acute myocardial infarction improves left ventricular function and alters electrophysiologic properties. *Int. J. Cardiol.* 111, 231–239. doi: 10.1016/j.ijcard.2005.07.036

Procida, K., Jorgensen, L., Schmitt, N., Delmar, M., Taffet, S. M., Holstein-Rathlou, N. H., et al. (2009). Phosphorylation of connexin43 on serine 306 regulates electrical coupling. *Heart Rhythm* 6, 1632–1638. doi: 10.1016/j.hrthm.2009.07.043

Qu, Z., Weiss, J. N., and Garfinkel, A. (1999). Cardiac electrical restitution properties and stability of reentrant spiral waves: a simulation study. *Am. J. Physiol.* 276(1 Pt 2), H269–H283.

Rigol, M., Solanes, N., Farre, J., Roura, S., Roque, M., Berruezo, A., et al. (2010). Effects of adipose tissue-derived stem cell therapy after myocardial infarction: impact of the route of administration. *J. Card. Fail.* 16, 357–366. doi: 10.1016/j.cardfail.2009.12.006

Roell, W., Lewalter, T., Sasse, P., Tallini, Y. N., Choi, B. R., Breitbach, M., et al. (2007). Engraftment of connexin 43-expressing cells prevents post-infarct arrhythmia. *Nature* 450, 819–824. doi: 10.1038/nature06321

Rohr, S. (2004). Role of gap junctions in the propagation of the cardiac action potential. *Cardiovasc. Res.* 62, 309–322. doi: 10.1016/j.cardiores.2003.11.035

Rosen, M. R., Brink, P. R., Cohen, I. S., and Robinson, R. B. (2007). Biological pacemakers based on I(f). *Med. Biol. Eng. Comput.* 45, 157–166. doi: 10.1007/s11517-006-0060-2

Rubart, M., Pasumarthi, K. B., Nakajima, H., Soonpaa, M. H., Nakajima, H. O., and Field, L. J. (2003). Physiological coupling of donor and host cardiomyocytes after cellular transplantation. *Circ. Res.* 92, 1217–1224. doi: 10.1161/01.RES.0000075089.39335.8C

Shaw, R. M., and Rudy, Y. (1997). Electrophysiologic effects of acute myocardial ischemia. A mechanistic investigation of action potential conduction and conduction failure. *Circ. Res.* 80, 124–138. doi: 10.1161/01.RES.80.1.124

Shiba, Y., Fernandes, S., Zhu, W. Z., Filice, D., Muskheli, V., Kim, J., et al. (2012). Human ES-cell-derived cardiomyocytes electrically couple and suppress arrhythmias in injured hearts. *Nature* 489, 322–325. doi: 10.1038/nature11317

Sundelacruz, S., Levin, M., and Kaplan, D. L. (2008). Membrane potential controls adipogenic and osteogenic differentiation of mesenchymal stem cells. *PLoS ONE* 3:e3737. doi: 10.1371/journal.pone.0003737

Tan, R. C., and Joyner, R. W. (1990). Electrotonic influences on action potentials from isolated ventricular cells. *Circ. Res.* 67, 1071–1081. doi: 10.1161/01.RES.67.5.1071

Tolmachov, O., Ma, Y. L., Themis, M., Patel, P., Spohr, H., MacLeod, K. T., et al. (2006). Overexpression of connexin 43 using a retroviral vector improves electrical coupling of skeletal myoblasts with cardiac myocytes *in vitro*. *BMC Cardiovasc. Disord.* 6:25. doi: 10.1186/1471-2261-6-25

Tran, D. X., Yang, M. J., Weiss, J. N., Garfinkel, A., and Qu, Z. (2007). Vulnerability to re-entry in simulated two-dimensional cardiac tissue: effects of electrical restitution and stimulation sequence. *Chaos* 17:043115. doi: 10.1063/1.2784387

Valina, C., Pinkernell, K., Song, Y. H., Bai, X., Sadat, S., Campeau, R. J., et al. (2007). Intracoronary administration of autologous adipose tissue-derived stem cells improves left ventricular function, perfusion, and remodelling after acute myocardial infarction. *Eur. Heart J.* 28, 2667–2677. doi: 10.1093/eurheartj/ehm426

Valiunas, V., Doronin, S., Valiuniene, L., Potapova, I., Zuckerman, J., Walcott, B., et al. (2004). Human mesenchymal stem cells make cardiac connexins and form functional gap junctions. *J. Physiol.* 555(Pt 3), 617–626. doi: 10.1113/jphysiol.2003.058719

van Kempen, M. J., ten Velde, I., Wessels, A., Oosthoek, P. W., Gros, D., Jongsma, H. J., et al. (1995). Differential connexin distribution accommodates cardiac function in different species. *Microsc. Res. Tech.* 31, 420–436. doi: 10.1002/jemt.1070310511

Wagers, A. J., and Weissman, I. L. (2004). Plasticity of adult stem cells. *Cell* 116, 639–648. doi: 10.1016/S0092-8674(04)00208-9

Wiegerinck, R. F., van Veen, T. A., Belterman, C. N., Schumacher, C. A., Noorman, M., de Bakker, J. M., et al. (2008). Transmural dispersion of refractoriness and conduction velocity is associated with heterogeneously reduced connexin43 in a rabbit model of heart failure. *Heart Rhythm* 5, 1178–1185. doi: 10.1016/j.hrthm.2008.04.026

Wollert, K. C., Meyer, G. P., Lotz, J., Ringes-Lichtenberg, S., Lippolt, P., Breidenbach, C., et al. (2004). Intracoronary autologous bone-marrow cell transfer after myocardial infarction: the BOOST randomised controlled clinical trial. *Lancet* 364, 141–148. doi: 10.1016/S0140-6736(04)16626-9

Xie, Y., Garfinkel, A., Camelliti, P., Kohl, P., Weiss, J. N., and Qu, Z. (2009). Effects of fibroblast-myocyte coupling on cardiac conduction and vulnerability to reentry: a computational study. *Heart Rhythm* 6, 1641–1649. doi: 10.1016/j.hrthm.2009.08.003

Conflict of Interest Statement: The authors declare that the research was conducted in the absence of any commercial or financial relationships that could be construed as a potential conflict of interest.

Received: 09 September 2014; accepted: 10 October 2014; published online: 29 October 2014.

*Citation: Smit NW and Coronel R (2014) Stem cells can form gap junctions with cardiac myocytes and exert pro-arrhythmic effects. Front. Physiol. **5**:419. doi: 10.3389/fphys.2014.00419*

This article was submitted to Cardiac Electrophysiology, a section of the journal Frontiers in Physiology.

frontiers in
PHYSIOLOGY

REVIEW ARTICLE
published: 12 November 2014
doi: 10.3389/fphys.2014.00435

Exploring susceptibility to atrial and ventricular arrhythmias resulting from remodeling of the passive electrical properties in the heart: a simulation approach

Natalia A. Trayanova*, Patrick M. Boyle, Hermenegild J. Arevalo and Sohail Zahid

Department of Biomedical Engineering, Institute for Computational Medicine, Johns Hopkins University, Baltimore, MD, USA

Edited by:
George E. Billman, The Ohio State University, USA

Reviewed by:
Colleen E. Clancy, University of California, Davis, USA
Vadim V. Fedorov, The Ohio State University, USA

****Correspondence:***
Natalia A. Trayanova, Department of Biomedical Engineering, Institute for Computational Medicine, Johns Hopkins University, 3400 N Charles St., 316 Hackerman Hall, Baltimore, MD 21218, USA
e-mail: ntrayanova@jhu.edu

Under diseased conditions, remodeling of the cardiac tissue properties ("passive properties") takes place; these are aspects of electrophysiological behavior that are not associated with active ion transport across cell membranes. Remodeling of the passive electrophysiological properties most often results from structural remodeling, such as gap junction down-regulation and lateralization, fibrotic growth infiltrating the myocardium, or the development of an infarct scar. Such structural remodeling renders atrial or ventricular tissue as a major substrate for arrhythmias. The current review focuses on these aspects of cardiac arrhythmogenesis. Due to the inherent complexity of cardiac arrhythmias, computer simulations have provided means to elucidate interactions pertinent to this spatial scale. Here we review the current state-of-the-art in modeling atrial and ventricular arrhythmogenesis as arising from the disease-induced changes in the passive tissue properties, as well as the contributions these modeling studies have made to our understanding of the mechanisms of arrhythmias in the heart. Because of the rapid advance of structural imaging methodologies in cardiac electrophysiology, we chose to present studies that have used such imaging methodologies to construct geometrically realistic models of cardiac tissue, or the organ itself, where the regional remodeling properties of the myocardium can be represented in a realistic way. We emphasize how the acquired knowledge can be used to pave the way for clinical applications of cardiac organ modeling under the conditions of structural remodeling.

Keywords: arrhythmia, computer modeling, structural remodeling, fibrosis, infarct

INTRODUCTION

Computer modeling has emerged as a powerful platform for the investigation of lethal heart rhythm disorders. Biophysically detailed simulations can explain experimental observations and help reveal how organ-scale arrhythmogenic phenomena (ectopic heartbeats, conduction failure, electrical turbulence, etc.) emerge from pathological effects at the tissue, cell, and protein levels. The development of this extensive "virtual heart" methodology (Noble, 2002; Vigmond et al., 2009; Gurev et al., 2011; Trayanova, 2011; Winslow et al., 2012) builds upon a strong foundation of research that seeks to use experiments and simulation to quantitatively characterize the action potential response of cardiac cells to electrical stimuli. Recent advancements in single-cell action potential modeling have produced building blocks for constructing models of the atria (Courtemanche et al., 1998; Nygren et al., 1998; Grandi et al., 2011), the ventricles (Ten Tusscher and Panfilov, 2006; Fink et al., 2008; Grandi et al., 2010; O'Hara et al., 2011), and the cardiac conduction system (Stewart et al., 2009; Aslanidi et al., 2010; Sampson et al., 2010; Li and Rudy, 2011; Vaidyanathan et al., 2013) with unprecedented levels of biophysical detail and accuracy. Such developments have helped to fuel the exciting progress made in simulating cardiac electrical behavior at the organ level (Moreno et al., 2011; Tandri et al., 2011; Trayanova et al., 2012; Boyle et al., 2013, 2014; Hu et al., 2014; Trayanova and Boyle, 2014; Clayton and Bishop, in press). Emergent, integrative behaviors in the heart result not only from complex interactions within a specific level but also from feed-forward and feedback interactions that connect a broad range of hierarchical levels of biological organization.

Several recent reviews have been written on our current understanding the mechanisms of atrial and ventricular mechanisms from an integrative interactions perspective (Janse, 2004; Rubart and Zipes, 2005; Jacquemet et al., 2008; Rudy et al., 2008; Plank et al., 2008b; Fishman et al., 2010; Dossel et al., 2012; John et al., 2012; Trayanova, 2012, 2014; Chen et al., 2014; Heijman et al., 2014), often derived from computer simulations, however, most of these focus on how remodeling in the active electrophysiological properties of the diseased heart contributes to the increased propensity to arrhythmias. One aspect of cardiac tissue behavior that has received less attention is the contribution, to the initiation and maintenance of arrhythmias, of the changes in the "passive" tissue properties that take place in the diseased heart. Under "passive" we refer to the aspects of electrophysiological behavior that are not associated with active ion transport across cell membranes; these include current flow in the intra- and extracellular domains of cardiac tissue and the aspects of tissue

composition and structure that determine the direction and magnitude of these currents. Under diseased conditions, remodeling of the passive tissue properties takes place, most often resulting from structural remodeling such as gap junction down-regulation and lateralization, fibrotic growth infiltrating the myocardium, or the development of an infarct scar. Such structural remodeling renders atrial, or ventricular tissue as a major substrate for arrhythmias. The current review focuses on these aspects of cardiac arrhythmogenesis.

However, because of this inherent complexity of cardiac arrhythmias, it is often difficult to dissect the contributions of individual players, and to elucidate interactions at a particular spatial scale. Computer simulations of cardiac electrophysiology have provided this ability. In this article, we review the current state-of-the-art in modeling atrial and ventricular arrhythmogenesis as arising from the disease-induced changes in the passive tissue properties, as well as the contributions these modeling studies have made to our understanding of the mechanisms of arrhythmias in the heart. Because of the rapid advance of structural imaging methodologies in cardiac electrophysiology, we chose to present studies that have used such imaging methodologies to construct geometrically realistic structural models of cardiac tissue, or the organ itself, where the regional remodeling properties of the myocardium can be represented also in a realistic way. We emphasize how the acquired knowledge can be used to pave the way for clinical applications of cardiac organ modeling under the conditions of structural changes. This review does not intend to be exhaustive on the subject, but to provide examples of how computer modeling could be instrumental in understanding arrhythmogenesis as it arises from disease remodeling at the various levels of biological and structural organization of the heart.

OVERVIEW OF METHODOLOGY FOR SIMULATING ARRHYTHMOGENESIS AND REPRESENTING THE REMODELING IN THE PASSIVE PROPERTIES OF THE MYOCARDIUM

Computer modeling of arrhythmogenesis has made enormous progress over the last decade, enabling the simulation of electrical function in cardiac tissue as well as in the entire organ. A schematic of the current state-of-the-art general approach to 3D multi-scale (from the molecule to the organ) arrhythmia modeling (atrial or ventricular) is shown in **Figure 1A**. Ionic exchanges across cell membranes, via ionic channels, pumps, and exchangers, represented by an action potential ionic model comprising of numerous ordinary differential and algebraic equations, drive current flow in the tissue. In the multi-scale atrial or ventricular model, propagation of the wave of action potential is simulated by solving (Vigmond et al., 2002, 2003; Plank et al., 2008b) a reaction-diffusion partial differential equation describing current flow through tissue composed of myocytes that are electrically connected via low-resistance gap junctions. Cardiac tissue has orthotropic passive electrical conductivities that arise from the cellular organization of the myocardium (cardiac muscle) into fibers and laminar sheets. Global conductivity values in the atrial or ventricular model are obtained by combining fiber and sheet organization with myocyte-specific local conductivity values.

Local fiber directions are typically mapped based on histological sectioning information (Nielsen et al., 1991; Vetter and McCulloch, 1998), or on diffusion tensor (DT) magnetic resonance imaging (MRI) (Helm et al., 2005), sometimes using an atlas heart (Vadakkumpadan et al., 2012). **Figure 1B**, left panel presents fiber orientation, as reconstructed from DTMR images, in the canine ventricles shown in **Figure 1A**. In cases where neither histological nor DTMR imaging information is available, rule-based approaches have been used to assign fiber orientation consistent with measurements, either manually or using a semi-automatic rule-based approach (Krueger et al., 2011; Bayer et al., 2012; Dossel et al., 2012). This particularly applies to atrial fiber orientation (**Figure 1B**, right panel) since DT imaging of the thin atrial walls does not provide reliable information about atrial fiber architecture.

The passive electrical properties of the myocardium (**Figure 1A**) can be regionally remodeled in disease, with the regional change originating from several major sources: (1) changes in gap junction resistance between cells resulting in changes in conductivity values; (2) deposition of collagen forming either local resistive barriers between fibers or replacing myocytes (interstitial or replacement fibrosis; in the atria, it is a hallmark of the aging tissue); (3) formation of an infarction scar in the ventricles as a result of ischemic cardiac disease; and (4) abnormal proliferation, under diseased conditions, of non-myocyte cells, such as myofibroblasts, which may or may not interact with the cardiomyocytes electrically.

Multi-scale models of arrhythmias are typically modular, allowing the use of any cellular ionic models, of different species and with different levels of biophysical detail. Furthermore, solutions are executed on user-specified organ geometries, which can be idealized, or anatomically-accurate, the latter either representing averaged geometries obtained from histological sectioning (Nielsen et al., 1991; Vetter and McCulloch, 1998), or individual hearts' (atria and/or ventricles) geometry, and structure (Bishop et al., 2010; Vadakkumpadan et al., 2010). Using MRI data for model geometry is essential in represent individual hearts' structural remodeling in the passive tissue properties, such as ventricular infarction or atrial fibrosis. **Figure 2A** presents the generation of the geometry/ structure of a whole-heart model of canine infarction from high-resolution *ex-vivo* MRI scans, where a level set method was applied to the MRI image stack to separate the myocardium from the surrounding suspension media. The infarct was segmented out into the two infarct zones, scar and the electrically-remodeled border zone, also termed gray zone (GZ) based on it appearance in the MRI scans; to do so the combined information from both the DTMRI, and the structural MRI scans was used (via the calculation of fractional anisotropy, **Figure 2A**). The resulting infarct segmentation revealed strands of GZ tissue penetrating the electrically inert scar tissue (segmentation panel, **Figure 2A**). The reconstructed whole heart canine model is shown in **Figure 2A** with the locations of different remodeling regions combined with the organ geometry information.

Clinical MRI scans with a contrast agent (late gadolinum enhancement, LGE, MRI) can also be used to visualize the structural remodeling in atria and ventricles (Nazarian et al., 2005; Assomull et al., 2006; Oakes et al., 2009; Roes et al., 2009;

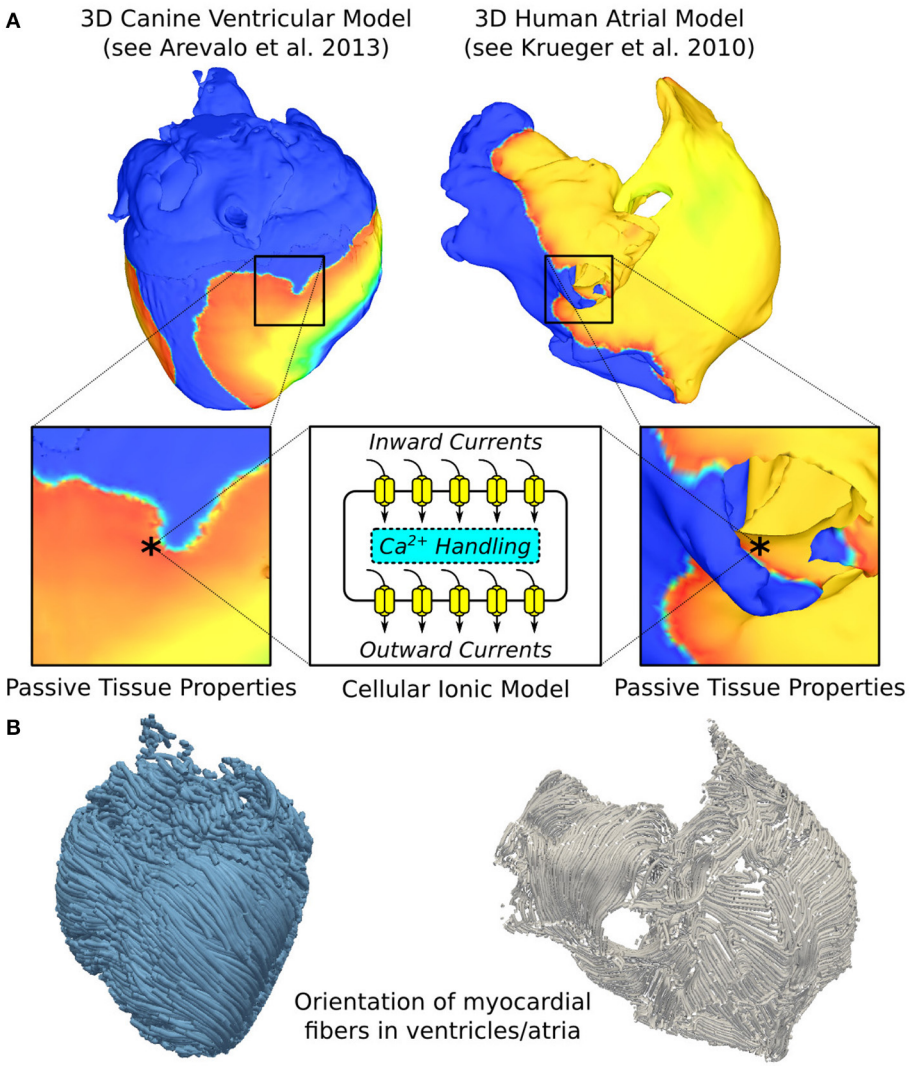

FIGURE 1 | Overall approach to image-based modeling of cardiac electrophysiology. (A) The multiscale aspect of cardiac electrophysiological models. Passive electrical coupling of cardiac cells mediates the tissue-scale propagation of bioelectric impulses that originate at the membrane level (action potentials). *indicates representative points in ventricular and atrial tissue models. 3D geometrical models are reconstructed from images of a canine heart (left), as in Arevalo et al. (2013), and human patient atria (right), as in Krueger et al. (2011). **(B)** Schematics showing the orientation of myocardial fibers in the ventricular and atrial models. Left panel modified with permission from Arevalo et al. (2013).

Akoum et al., 2011). **Figure 2B** presents ventricular model generation from clinical LGE-MRI images, as described in a recent paper (Prakosa et al., 2014). Finally, **Figure 2C** illustrates structural changes in a patient atrium, as reconstructed from clinical LGE-MRI scans, and described in detail in the original papers (McDowell et al., 2012, 2013) It has to be noted, however, that the segmentation of the LGE MRI fibrotic regions and even segmentation of the geometry of the thin atria from clinical MRI is fraught with uncertainty and an area of intense image-processing research.

Figure 2B, right-most panel, demonstrates how the images can be used to examine susceptibility to arrhythmias of the substrate and specifically, the role of structural remodeling (and thus remodeling in the passive electrical properties). It shows the generation of a reentrant arrhythmia in the infracted patient ventricles. Numerical approaches for simulating the electrical behavior of the heart have been described in detail in previous publications, some of which offer comprehensive reviews on the subject (Rodriguez and Trayanova, 2003; Jacquemet et al., 2008; Plank et al., 2008b; Trayanova, 2011; Dossel et al., 2012).

FIBROTIC REMODELING IN THE ATRIA AND ITS CONTRIBUTION TO ATRIAL FIBRILLATION

Structural remodeling, and specifically fibrosis, has been associated with the persistent/permanent version of atrial fibrillation (AF) (Burstein and Nattel, 2008; Yue et al., 2011). Fibrotic remodeling of atrial tissue involves processes that occur in parallel across multiple scales: at the membrane level, gap junction

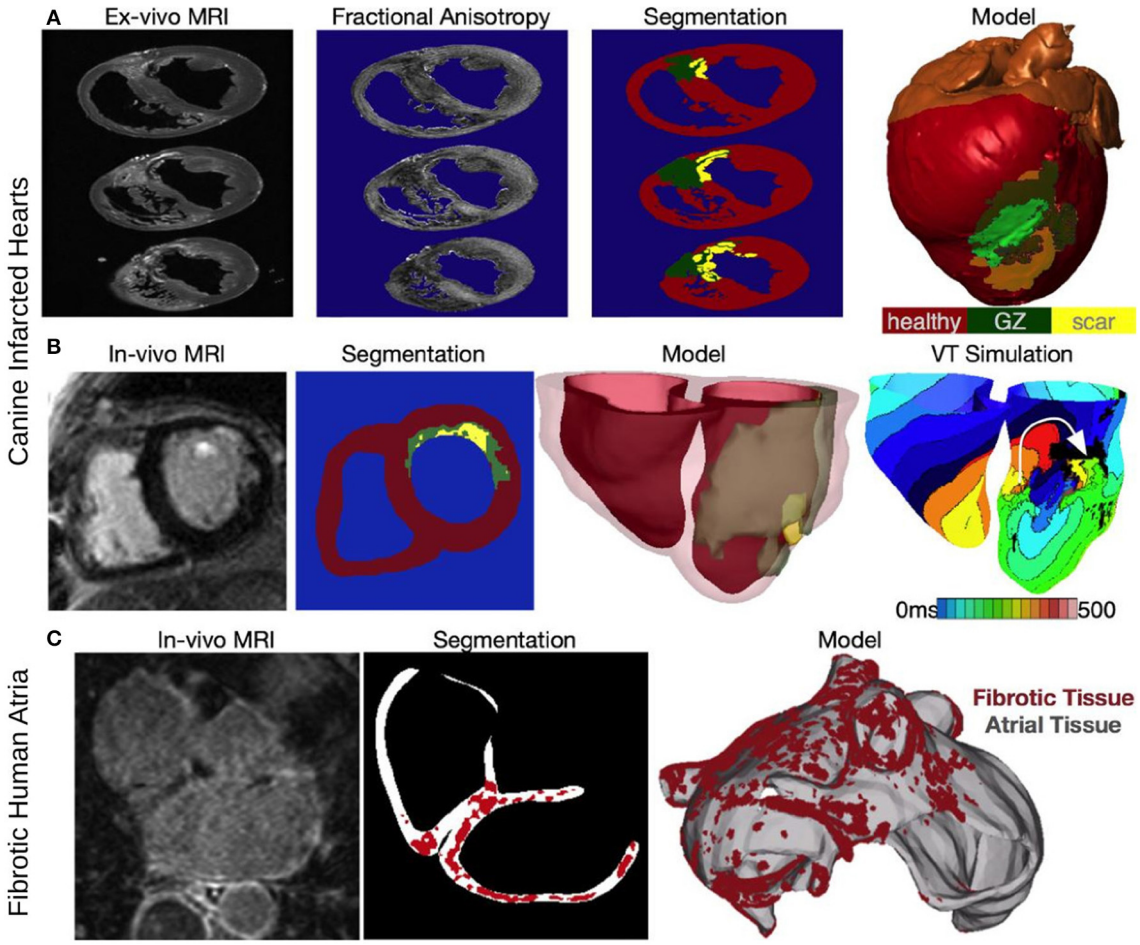

FIGURE 2 | Constructing image-based models of the ventricles from an infarcted canine heart (A,B) and the fibrotic atria of a human patient with AF. (A) Reconstruction from an *ex-vivo* MRI scan of an infarcted canine heart. Fractional anisotropy (FA) maps as calculated from the DT-MRI, brighter color corresponds with higher FA value. The images are segmented into healthy myocardium, gray zone (GZ), and scar, to reconstruct an image-based model of the infracted canine heart (right-most panel). Modified with permission from Arevalo et al. (2013). **(B)** Construction of a patient-specific ventricular model of arrhythmia from a clinical MR scan. Shown are images of an infarcted patient heart before ablation (treatment) and the corresponding segmentation: healthy (red), GZ (green), or scar (yellow). An image of the three-dimensional geometric model of the patient heart rendered with the epicardium and the infarct border zone semitransparent is shown in the third panel. The right-most panel presents *in silico* activation map of arrhythmia, revealing reentry on the left ventricular endocardium. The color code in the bottom right shows electrical activation time. Modified with permission from Winslow et al. (2012). **(C)** A model of the fibrotic human atria generated from a patient LGE-MRI scan (top left) following segmentation (top right) into normal and fibrotic tissue (fibrotic lesions in red). With permission from McDowell et al. (2012).

remodeling due to connexin 43 (Cx43) protein downregulation/hypophosphorylation, and lateralization (Kostin et al., 2002; Burstein et al., 2009), at the cellular level, fibroblast proliferation and phenotype switching (Rohr, 2009; Yue et al., 2011), and at the tissue level, the deposition of excess collagen (Xu et al., 2004; Burstein and Nattel, 2008), both from reactive interstitial fibrosis separating muscle bundles, and from reparative fibrosis replacing dead cardiomyocytes, both interfering with electric continuity and slowing conduction (Xu et al., 2004; Iwasaki et al., 2011). Thus, structural remodeling, combined with remodeling at the ion channel level, gives rise to complex interactions at the organ level, setting the stage for AF initiation and maintenance in the fibrotic atria.

Models of the fibrotic atria have accounted for different aspects of fibrotic remodeling, in an attempt to elucidate the mechanisms leading to altered conduction and those responsible for the drivers and organization of permanent AF. The simplest model representation of atrial structural remodeling was based on the assumption that a component of structural remodeling, gap junction remodeling (Cx43 downregulation/hypophosphorylation, and lateralization), occurs throughout the atria in a uniform fashion. Two such studies have been conducted thus far: one assumed that the coupling strength between computational cells was decreased (Cx43 downregulation/hypophosphorylation only) (Krogh-Madsen et al., 2012), while the other modeled increased anisotropy throughout the LA (representing both aspects of Cx43 remodeling) (Plank et al.,

2008a). One of these simulation studies showed (Krogh-Madsen et al., 2012) that decreasing the coupling between cells slowed conduction and decreased the wavelength, further perpetuating AF. The other study (Plank et al., 2008a) demonstrated that increased anisotropy throughout the fibrotic human LV was an additional mechanism for the breakup of PV ectopic waves into multiple reentrant circuits; higher anisotropy ratios resulted in sustained reentrant activity even though the ectopic focus was no longer present. Similar conclusions were obtained from a human atrial model (Krueger et al., 2014) where the locations of the fibrotic (i.e., high-anisotropy-ratio) regions were implemented from patient MRI-LGE scans.

The next component of fibrosis, collagen deposition, has been represented in models as insulating barriers, and in several ways: (i) by removing randomly the electrical connections between two 2D layers of atrial tissue, the endocardial and the epicardial, in order to model an increased level of dissociation between these two layers (a form of reactive interstitial fibrosis), mimicking experimental observations in goats (Eckstein et al., 2011); (ii) by introducing a set of random collagenous septa disconnecting cardiac fibers in the transverse direction (Jacquemet and Henriquez, 2009) (reactive interstitial fibrosis again); and (iii) by incorporating non-conductive regions of various sizes throughout the tissue (Tanaka et al., 2007; Burstein et al., 2009; Comtois and Nattel, 2011) (reparative fibrosis), either randomly throughout the atria, or based on imaging data. Endo-epicardial dissociation resulted (Eckstein et al., 2011) in a number of AF reentrant waves that was significantly higher than that in the case without dissociation, exacerbating AF complexity. The increase in collagen content in the interstitial spaces between fibers was not found to affect longitudinal conduction, (Burstein et al., 2009; McDowell et al., 2012, 2013) but caused slowed propagation in transverse direction, with the degree of slowing dependent of the length of the collagenous septa (Jacquemet and Henriquez, 2009).

Atrial models incorporating transverse collagen deposition (Tanaka et al., 2007; Burstein et al., 2009; Comtois and Nattel, 2011) (as in reparative fibrosis) have highlighted the significant interruption and disarray in atrial conduction patterns caused by it. Importantly, collagen deposition rather than connexin-43 (Cx43) remodeling was found to be the major factor in atrial conduction disturbances under HF conditions (Burstein et al., 2009) (**Figure 3A**). Furthermore, it was established that not only the total amount, but also the specific spatial distribution of collagen deposition (e.g., as generated by a stochastic algorithm) governed the occurrences of conduction block (Comtois and Nattel, 2011). To evaluate the consequences of HF remodeling (ionic and structural) on AF dynamics in the posterior left atrium (LA), Tanaka et al. (Tanaka et al., 2007) used 2D models of transmural posterior LA sections generated from histological data; patchy distributions of collagen were also reconstructed from that data. Simulations demonstrated that whether the mechanism sustaining AF was reentrant or focal, fibrous patches of large size were the major factor responsible for the different dynamics of AF waves in failing vs. control hearts; they anchored reentrant circuits and impaired wave propagation to generate delays and signal fractionation (**Figure 3B**).

The third major component of fibrotic remodeling, fibroblast proliferation and phenotype switching, has also been represented in computational models of the atria, particularly in view of the fact that fibroblasts, in addition to being part of the structural remodeling of the atria, can also exert electrophysiological influences on neighboring myocytes, possibly either through electrical coupling (Camelliti et al., 2004), or via paracrine effects (Pedrotty et al., 2009). The first study to explicitly incorporate fibroblast presence as a representation of fibrotic remodeling was the 2D atrial model by Ashihara et al. (2012). Within the fibrotic region, coupling of fibroblasts (kinetics governed by a fibroblast ionic model) to atrial myocytes caused shorter action potential duration (APD), slower conduction, and lower excitability as well as spiral wave breakups. This effect was exacerbated when fibroblast density increased (**Figure 4A**). Interestingly, when fibroblasts were substituted by collagen in the model, wave breakups were not observed.

All three elements of fibrotic remodeling (gap-junction remodeling, collagen deposition, and myofibroblast proliferation), were combined together in the LA model generated from MRI-LGE data of a patient with permanent AF (McDowell et al., 2012, 2013), capturing accurately both the atrial geometry and the distribution of fibrotic lesions. The model was used to examine the mechanisms for AF initiation by pulmonary vein (PV) ectopic stimulation. The study found that for fibrotic lesions typical of human remodeled atria under the conditions of persistent AF, gap junction remodeling in the fibrotic lesions was a necessary but not sufficient condition for the development of AF following a PV ectopic beat. The sufficient condition was myofibroblast proliferation in these lesions, where myofibroblasts exerted either electrotonic, or paracrine influences on myocytes within the lesions. Deposition of collagen in the lesions assisted the myofibroblasts' paracrine, or electrotonic effects by additionally shortening APD there (**Figure 4B**). The electrophysiological representation of fibrotic remodeling in the human atrial models remains, however, controversial because of the lack of sufficient experimental data.

ISCHEMIC CARDIOMYOPATHY REMODELING IN THE VENTRICLES AND ITS CONTRIBUTION TO VENTRICULAR TACHYCARDIA

Understanding ventricular arrhythmia mechanisms for a variety of diseases involving regional changes in the passive electrical properties has been aided, to a significant degree, by models and simulations. For instance, models representing regional ischemia (Tice et al., 2007; Jie et al., 2008, 2010; Jie and Trayanova, 2010) characterized the substrate for ischemia phase 1B arrhythmias by examining how the interplay between different degrees of hyperkalemia in the surviving layers, and the level of cellular uncoupling between these and the mid-myocardium layers (i.e., change in the passive properties of the myocardium) combine with the specific geometry of the ischemic zone in the ventricles to result in reentrant arrhythmias.

Ischemic cardiomyopathy (i.e., infarct-related) VT is the most frequent clinical ventricular arrhythmia, present in 64% of patients with ventricular rhythm disorder and in 89% of patients with sudden cardiac death (Stevenson et al., 1985). Recently, the

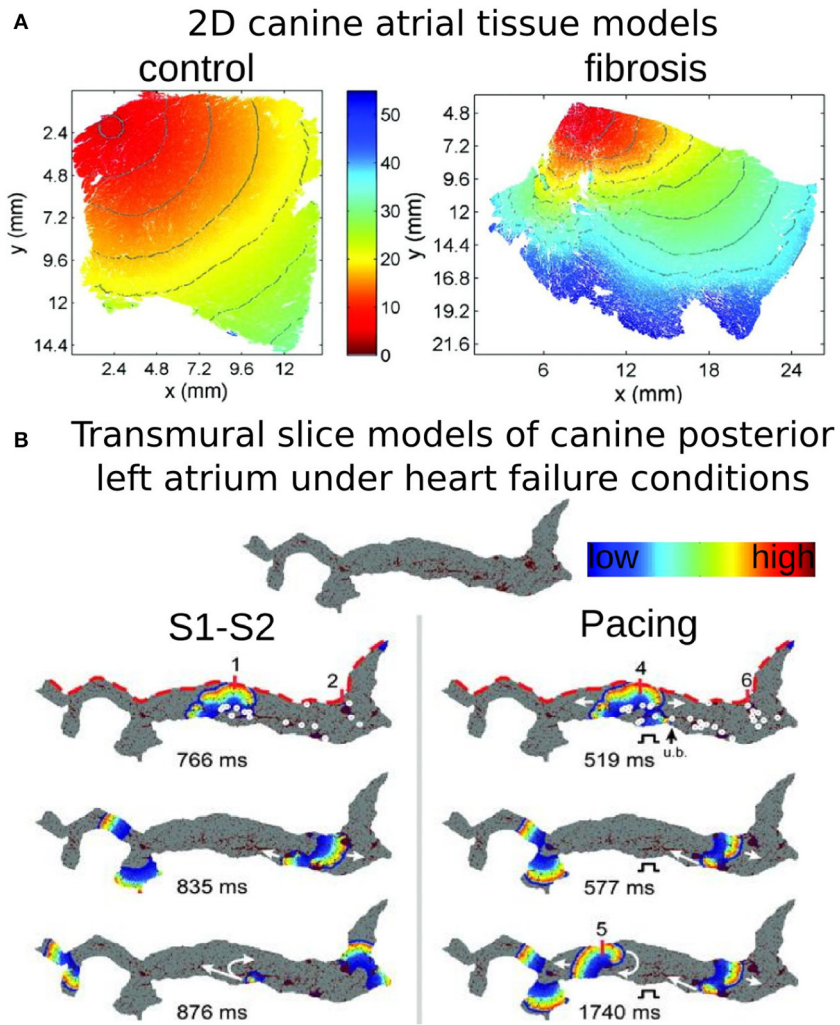

FIGURE 3 | Modeling fibrosis as regions of collagen presence. Collagen is represented as an insulator. **(A)** Simulations of propagation in models of 2D tissue sections of canine atrium (control, left, and fibrosis, right). With permission from Burstein et al. (2009). **(B)** Simulations in models of a transmural slice of canine posterior LA under HF conditions; the top of the slice (red dashed lines) corresponds to the epicardial surface. Snapshots at several timeframes for cross-field stimulation (left), and pacing at a frequency of 6 Hz (right), as well as endocardial time-space plots. Colors indicate transmembrane voltage from low (blue) to high (red). The site of unidirectional block (ub). is indicated by a black arrow. White circles on the upper voltage maps indicate sites of wavebreak. With permission from Tanaka et al. (2007).

peri-infarct (border) zone surrounding the necrotic scar, also known as GZs, as indicated above, based on its appearance as a region of intermediate intensity in the LGE-MRI scans, has been shown to correlate with post-MI mortality (Yan et al., 2006), clinical VT (Roes et al., 2009), and VT inducibility (Schmidt et al., 2007). Histological studies have shown these GZ regions to be a heterogeneous mix of viable myocardium and necrotic scar (Arheden et al., 2000). Animal experimental evidence has implicated the GZ as the arrhythmogenic substrate in myocardial infarction (MI) (Estner et al., 2011); Ashikaga et al. demonstrated that in infarcted swine hearts, reentrant circuits were anchored to strands of viable myocardium positioned over intramural scars (Ashikaga et al., 2007).

A recent swine heart study (Ng et al., 2012) demonstrated the feasibility of using simulations to predict the existence of VT circuits. In another study (Pop et al., 2011), a correspondence between *in vivo* electroanatomical and *in silico* voltage maps was demonstrated using a model of infarcted pig ventricles reconstructed from *ex vivo* MRI, and DTMRI data. Their simulations in two infarcted hearts successfully predicted the VT-inducibility consistent with the *in vivo* electrophysiological studies.

A clinically significant question is how infarct-related VTs relate to the specific GZ distribution and size in the ventricles. Addressing this question would provide an impetus to the development of improved criteria for stratifying arrhythmia risk in post-MI patients. A recent study (Arevalo et al., 2013) took this concept further and examined the role of infarct-related GZ extent in arrhythmogenesis, establishing that a minimum volume of remodeled tissue is needed for VT maintenance and demonstrating that the organizing center of infarct-related VT is located

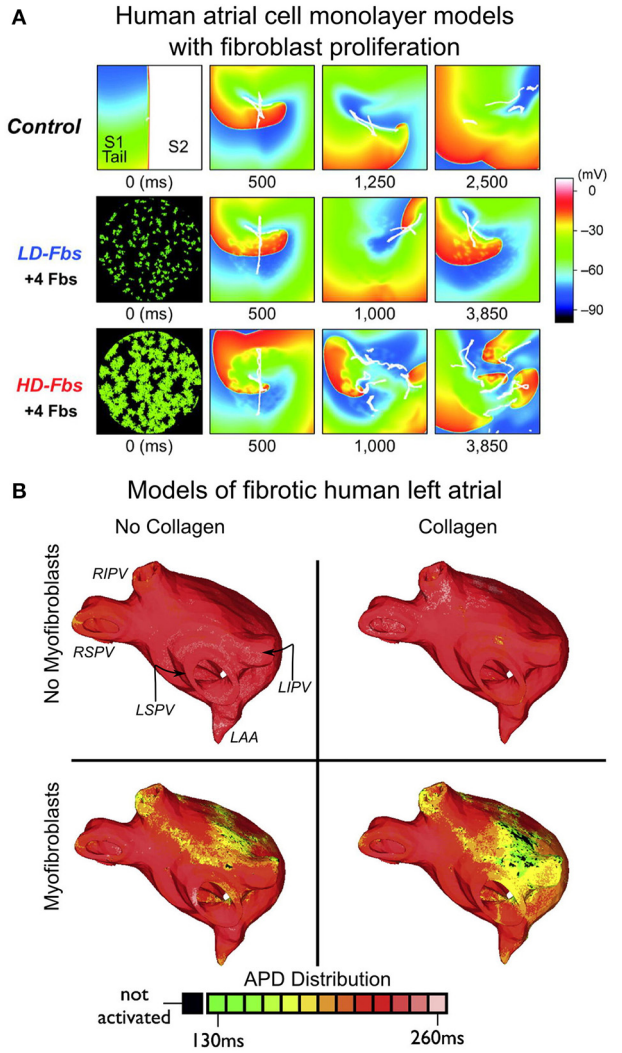

FIGURE 4 | Modeling fibroblast proliferation in the regions of fibrosis. **(A)** Effect of myocyte-fibroblast coupling (modeled as in Maleckar et al., 2009a) on spiral wave behavior in a human atrial cell monolayer model of size 4.5 × 4.5 cm. Top, control case without fibroblasts. Middle and bottom, models of low-density and high-density fibroblast proliferation (LD-Fbs and HD-Fbs) in a central circular region of the sheet. In the LD-Fbs, and HD-Fbs models, atrial myocytes (100 pF), each connecting to 4 fibroblasts (6.3 pF) within the Fb-Area, account for 12.5% and 50.0% of that area, respectively. With permission from Ashihara et al. (2012). **(B)** Maps of action potential duration (APD) in four human atrial models (same atrial geometry). Fibrotic lesions are modeled with (bottom row), and without (top row) myofibroblast infiltration (and coupling to myocytes), as well as with (right column), and without (left column) diffuse collagen deposition for both sets of maps. Myofibroblasts in the fibrotic regions were coupled to atrial myocytes as described in Maleckar et al. (2009a) and Maleckar et al. (2009b). Anatomical landmarks in upper-left sub-panel: right inferior, right superior, left inferior, and left superior pulmonary veins (RIPV, RSPV, LIPV, LSPV, respectively); left atrial appendage (LAA). With permission from McDowell et al. (2013).

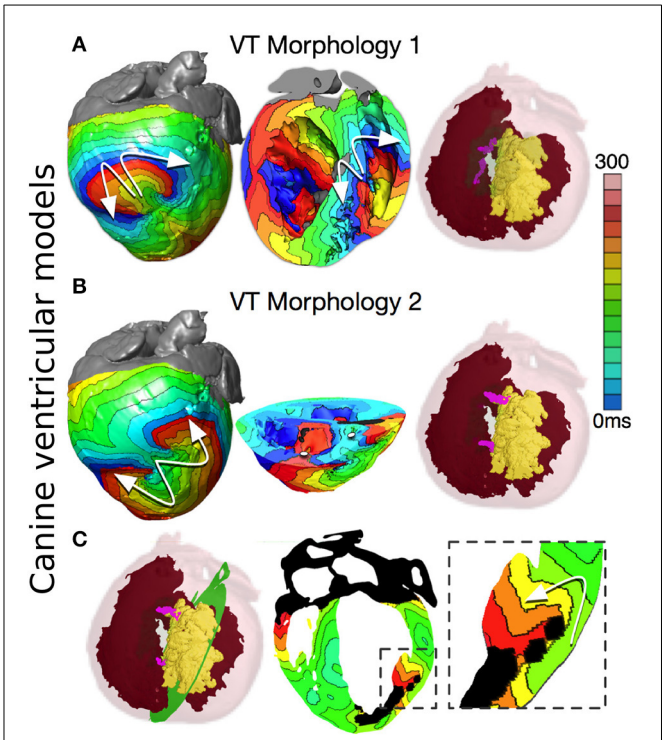

FIGURE 5 | Reentry morphologies during post-infarction ventricular tachycardia (VT) in a canine cardiac model. (A) VT morphology 1: Activation maps on the epicardium and in a long-axis cross-section of the ventricles, revealing figure-of-eight reentries on the epicardium, and on the right ventricular (RV) endocardium. VT is sustained by two I-type filaments (pink lines) located within the GZ with endpoints on the epicardium and RV endocardium. (Red: endocardial and epicardial surfaces, Yellow: scar surface, semi-transparent green: GZ) **(B)** VT morphology 2: Activation maps on the epicardium and in a short-axis cross-section of the ventricles, revealing figure-of-eight reentry on the epicardium, and two breakthroughs on endocardium (white dots). Reentry was organized around two I-type filaments with endpoints on the epicardium and scar (pink lines). **(C)** Activation map showing an apparent reentry around a scar distal from filaments. The overall VT morphology is similar to VT morphology 2 in Panel **B**. With permission from Arevalo et al. (2013).

within the border zone, regardless of the pacing site from which VT is induced. An example of simulations of infarct-related VT using an MRI-based canine heart model (see **Figure 1**) is presented in **Figure 5**; the model incorporated experimental data on electrophysiological remodeling in GZ. Programmed stimulation from the endocardial surface in this model revealed conduction slowing in the GZ, giving rise to VT inducibility, and reentrant circuit morphology consistent with experimental data. There are two distinct VT morphologies in this infracted canine heart. The first VT morphology was a figure-of-eight pattern on the epicardium and right ventricular (RV) endocardium (**Figure 5A**). For this VT morphology, the reentry revolved around two I-type filaments (organizing centers of reentrant activity) with endpoints at the epicardium and RV endocardium (**Figure 5A**, pink lines). The filaments were fully contained within the GZ and the endpoints remained in the same locations for the duration of the VT. The second VT morphology was a figure-of-eight reentry on the epicardium, had a direction of rotation (chirality) opposite to that of the first VT morphology, and was manifested as breakthroughs on the LV, and RV endocardial surfaces (**Figure 5B**). This was due to the reentrant activity being organized around

two I-type filaments with endpoints at the epicardium and the infarct scar (**Figure 5B**, pink lines). Since the filaments did not extend to the endocardium, no rotational activity was observed there. Both filaments were stably located within the GZ throughout the duration of the simulation. The intramural behavior of the reentrant circuits associated with the second VT morphology is presented in **Figure 5C**. Overall, the simulation results demonstrated that the organizing center of infarct-related VT is located within the GZ, regardless of the pacing site from which VT is induced. This result has important implications for ablation of infarct-related VT; it indicates that patient-specific simulations of VT could provide guidance for VT ablation in patients. Such simulation guidance could have a major clinical impact in predicting the optimal targets for catheter ablation of infarct-related VT in individual patient hearts.

Another recent study (Ashikaga et al., 2013) was the first attempt to take this concept to the clinic. **Figure 6A** presents a schematic how computer simulation prediction of the optimal VT ablation targets could be used in lieu of invasive electroanatomical mapping of the ventricles. **Figure 6B** presents comparisons between simulation-guided and standard electrophysiological approaches for identifying ablation targets in two patients with

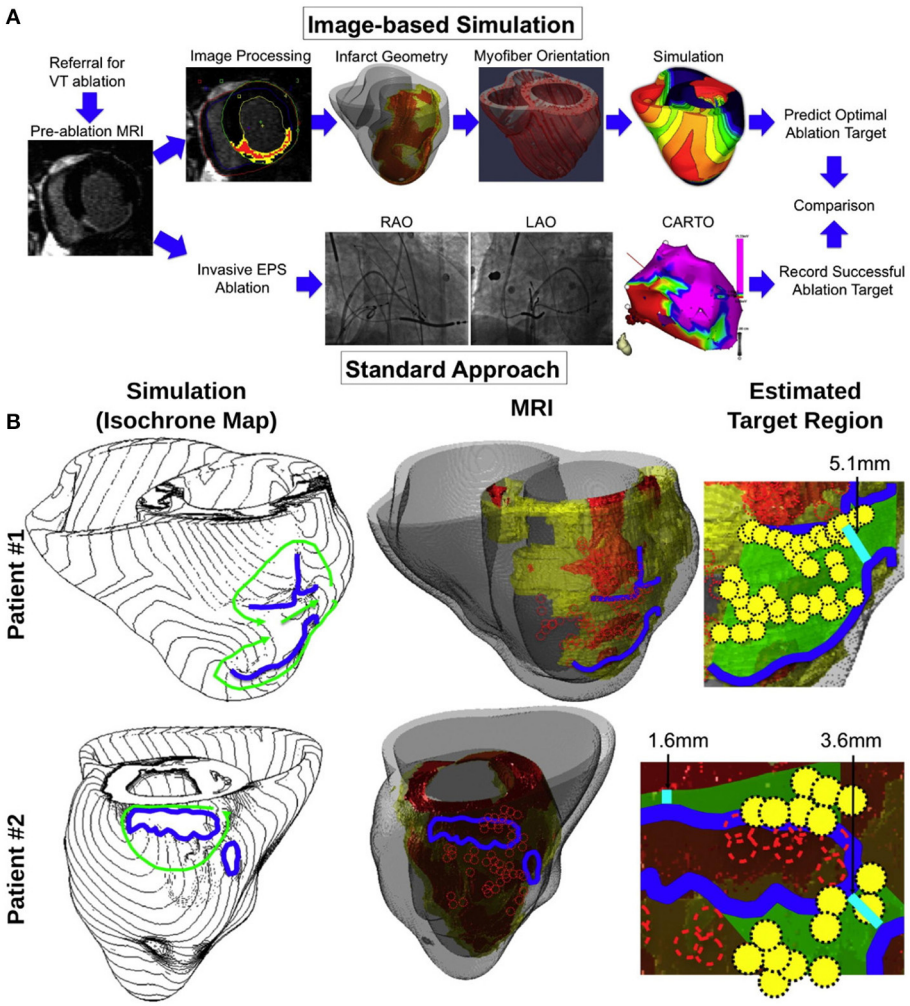

FIGURE 6 | (A) Proposed simulation-guided approach for determining the ablation targets of infarct-related ventricular tachycardia. The patients referred for ventricular tachycardia (VT) ablation undergo pre-ablation MRI, which was processed to provide the heart and infarct geometry (scar: red; GZ: yellow). These geometrical data were incorporated into a model of VT to estimate potential target regions. This method is alternative to an invasive electrophysiology study (EPS), and ablation ["Standard Approach"; by using biplane X-ray fluoroscopy and electroanatomical mapping (CARTO)]. LAO—left anterior oblique; RAO—right anterior oblique. **(B)** Comparison between simulation-guided and standard electrophysiological approaches for identifying endocardial ablation targets in two patients with infarct-related ventricular tachycardias (VTs). Left column: propagation pathways (green) and lines of conduction block (blue) are overlaid over VT activation maps simulated in image-based patient heart models. Middle column: preablation infarct geometry (infarct scar: orange, border zone: yellow, and non-infarcted: gray) along with ablation lesions delivered by the standard approach (red circles), and conduction block lines as calculated from ventricular simulations. Right column: optimal ablation zones (green shading) predicted by simulations, with narrowest isthmuses indicated (cyan); in both cases, only a fraction of the ablation sites from the standard approach were within the predicted optimal LV endocardial ablation zone (yellow circles). Modified with permission from Ashikaga et al. (2013).

infarct-related VTs. The results of the study demonstrated that that non-invasive simulation prediction of optimal targets for ablation of infarct-related VT could result in lesions that are much smaller than those executed in the clinic that successfully terminated VT (**Figure 6B**, right columns).

Simulation studies of ventricular arrhythmogenesis have recently begun to incorporate the role of cells other than myocytes in creating the arrhythmogenic substrate. Similar to the conditions under atrial fibrosis, differentiating fibroblasts, called myofibroblasts, have been reported to possibly play a role in the electrophysiological behavior of the scar, and GZ. Coupling to myofibroblasts in the region of infarct could affect cardiomyocyte electrophysiology, as demonstrated by simulation results (Maleckar et al., 2009a; Ashihara et al., 2012). A later study (McDowell et al., 2011) employed a high-resolution MRI-based computational model of the chronically infarcted rabbit ventricles, which was previously used (Rantner et al., 2012) to explore the role of infarct-related structural remodeling in vulnerability to electric shocks. The ventricular model was used to characterize the arrhythmogenic substrate resulting from myofibroblast infiltration (McDowell et al., 2011). It was found that myofibroblasts at low densities do not alter arrhythmia propensity, while at intermediate densities, myofibroblasts cause APD shortening, and exacerbate arrhythmia propensity. Interestingly, at high densities, myofibroblasts were found to protect against arrhythmia by causing resting depolarization, and blocking propagation. This study clearly indicated that non-myocyte cells could potentially have an important role in the altered passive electrophysiological properties of the myocardium.

CONCLUDING COMMENTS

The mechanisms that govern arrhythmia initiation and persistence in the heart, in both atria and ventricles, are highly complex, of dynamic nature, and involve interactions across multiple temporal and spatial scales, often leading to unpredictable outcomes and emergent phenomena. Electrophysiological experimental investigations in cells, tissues and the whole animal, and the human patient (Packer, 2004; Nattel et al., 2008; Iwasaki et al., 2011; Jalife, 2011; Schotten et al., 2011; Atienza et al., 2012) have led to a rapid increase in the body of knowledge regarding the mechanisms underlying arrhythmias. However, because of this inherent complexity, it is often difficult to dissect the contributions of individual players, and to elucidate interactions at a particular spatial scale. Computer simulations of cardiac electrophysiology have provided this ability, and this review article focuses, although not exhaustively and via examples from only a few simulation studies, on how remodeling in the "passive" electrical properties of the myocardium secondary to disease can render the organ susceptible to arrhythmias.

A lot remains to be uncovered, as remodeling of the electrical properties of the myocardium in disease, both passive and active, remains an intense area of research. As this review demonstrates, uncovering the integrative behavior of the heart resulting from such remodeling through simulation of atrial and ventricular function will continue to be strongly dependent on developments in experimental methodologies, which provide data to constrain, enrich, and validate the models. Of particular importance will be to fully characterize the complex remodeling that occurs in disease. Better understanding of the specific electrophysiological characteristics of remodeled tissue (i.e., GZ) surrounding the infarct in ischemic cardiomyopathy patients will enable more detailed mechanistic models of arrhythmia initiation, maintenance, and termination. Likewise, as experimental research addresses further the properties of the fibrotic myocardium, and in particular the electrophysiological aspects of the interaction between myocytes, and fibroblasts in the fibrotic lesions in the atria, atrial models are expected to provide a comprehensive view of the factors that drive arrhythmogenesis and influence arrhythmia dynamics in AF patients. Additionally, both atrial and ventricular modeling approaches could be improved by developing better capabilities to resolve the pathophysiological structure of the heart at high spatial resolution (isotropic voxel size of 1 mm or smaller); in particular, sensitive cardiac-specific tractography, and connectivity mapping techniques could provide a wealth of information valuable for constructing models of improved structural detail. Finally, present understanding of how atrial and ventricular myocardial fibers are oriented within the 3D volume of the heart is derived primarily from DT-MRI scans conducted on a handful of hearts *ex vivo*; imaging techniques capable of acquiring patient-specific maps of fiber orientation *in vivo* could be used to validate atlas-based approximations and incorporate disease-related changes in fibrous structure.

Clearly, we are poised at an exciting moment in cardiovascular medicine. The findings of molecular biology of the heart, the emergence of new technologies for measuring the properties of cells, tissues, and organ function, and the impact of Moore's law on computational modeling are coming together to drive the creation of new, quantitative, model-based approaches to understanding the function of the heart in disease, and to cardiovascular medicine of the future.

ACKNOWLEDGMENTS

Dr. Trayanova gratefully acknowledges support from the NIH Director's Pioneer Award DP1-HL123271, as well as support from NIH grants R01-HL103428 and R01-HL105216 and NSF grants CBET-0933029 and IOS-1124804.

REFERENCES

Akoum, N., Daccarett, M., McGann, C., Segerson, N., Vergara, G., Kuppahally, S., et al. (2011). Atrial fibrosis helps select the appropriate patient and strategy in catheter ablation of atrial fibrillation: a DE-MRI guided approach. *J. Cardiovasc. Electrophysiol.* 22, 16–22. doi: 10.1111/j.1540-8167.2010.01876.x

Arevalo, H., Plank, G., Helm, P., Halperin, H., and Trayanova, N. (2013). Tachycardia in post-infarction hearts: insights from 3D image-based ventricular models. *PLoS ONE* 8:e68872. doi: 10.1371/journal.pone.0068872

Arheden, H. K., Saeed, M., Higgins, C. B., Gao, D.-W., Ursell, P. C., Bremerich, J., et al. (2000). Reperfused rat myocardium subjected to various durations of ischemia: estimation of the distribution volume of contrast material with echo-planar MR imaging 1. *Radiology* 215, 520–528. doi: 10.1148/radiology.215.2.r00ma38520

Ashihara, T., Haraguchi, R., Nakazawa, K., Namba, T., Ikeda, T., Nakazawa, Y., et al. (2012). The role of fibroblasts in complex fractionated electrograms during persistent/permanent atrial fibrillation: implications for electrogram-based catheter ablation. *Circ. Res.* 110, 275–284. doi: 10.1161/CIRCRESAHA.111.255026

Ashikaga, H., Arevalo, H., Vadakkumpadan, F., Blake, R. C. 3rd., Bayer, J. D., Nazarian, S., et al. (2013). Feasibility of image-based simulation to estimate

ablation target in human ventricular arrhythmia. *Heart Rhythm* 10, 1109–1116. doi: 10.1016/j.hrthm.2013.04.015

Ashikaga, H., Sasano, T., Dong, J., Zviman, M. M., Evers, R., Hopenfeld, B., et al. (2007). Magnetic resonance–based anatomical analysis of scar-related ventricular tachycardia implications for catheter ablation. *Circ. Res.* 101, 939–947. doi: 10.1161/CIRCRESAHA.107.158980

Aslanidi, O. V., Sleiman, R. N., Boyett, M. R., Hancox, J. C., and Zhang, H. (2010). Ionic mechanisms for electrical heterogeneity between rabbit Purkinje fiber and ventricular cells. *Biophys. J.* 98, 2420–2431. doi: 10.1016/j.bpj.2010.02.033

Assomull, R. G., Prasad, S. K., Lyne, J., Smith, G., Burman, E. D., Khan, M., et al. (2006). Cardiovascular magnetic resonance, fibrosis, and prognosis in dilated cardiomyopathy. *J. Am. Coll. Cardiol.* 48, 1977–1985. doi: 10.1016/j.jacc.2006.07.049

Atienza, F., Martins, R. P., and Jalife, J. (2012). Translational research in atrial fibrillation: a quest for mechanistically based diagnosis and therapy. *Circ. Arrhythm. Electrophysiol.* 5, 1207–1215. doi: 10.1161/CIRCEP.111.970335

Bayer, J., Blake, R., Plank, G., and Trayanova, N. (2012). A novel rule-based algorithm for assigning myocardial fiber orientation to computational heart models. *Ann. Biomed. Eng.* 40, 2243–2254. doi: 10.1007/s10439-012-0593-5

Bishop, M. J., Plank, G., Burton, R. A., Schneider, J. E., Gavaghan, D. J., Grau, V., et al. (2010). Development of an anatomically detailed MRI-derived rabbit ventricular model and assessment of its impact on simulations of electrophysiological function. *Am. J. Physiol. Heart Circ. Physiol.* 298, H699–H718. doi: 10.1152/ajpheart.00606.2009

Boyle, P. M., Park, C. J., Arevalo, H. J., Vigmond, E. J., and Trayanova, N. A. (2014). Sodium current reduction unmasks a structure-dependent substrate for arrhythmogenesis in the normal ventricles. *PLoS ONE* 9:e86947. doi: 10.1371/journal.pone.0086947

Boyle, P. M., Williams, J. C., Ambrosi, C. M., Entcheva, E., and Trayanova, N. A. (2013). A comprehensive multiscale framework for simulating optogenetics in the heart. *Nat. Commun.* 4, 2370. doi: 10.1038/ncomms3370

Burstein, B., Comtois, P., Michael, G., Nishida, K., Villeneuve, L., Yeh, Y. H., et al. (2009). Changes in connexin expression and the atrial fibrillation substrate in congestive heart failure. *Circ. Res.* 105, 1213–1222. doi: 10.1161/CIRCRESAHA.108.183400

Burstein, B., and Nattel, S. (2008). Atrial fibrosis: mechanisms and clinical relevance in atrial fibrillation. *J. Am. Coll. Cardiol.* 51, 802–809. doi: 10.1016/j.jacc.2007.09.064

Camelliti, P., Green, C. R., Legrice, I., and Kohl, P. (2004). Fibroblast network in rabbit sinoatrial node: structural and functional identification of homogeneous and heterogeneous cell coupling. *Circ. Res.* 94, 828–835. doi: 10.1161/01.RES.0000122382.19400.14

Chen, P.-S., Chen, L. S., Fishbein, M. C., Lin, S.-F., and Nattel, S. (2014). Role of the autonomic nervous system in atrial fibrillation pathophysiology and therapy. *Circ. Res.* 114, 1500–1515. doi: 10.1161/CIRCRESAHA.114.303772

Clayton, R., and Bishop, M. (in press). Computational models of ventricular arrhythmia mechanisms: recent developments and future prospects. *Drug Discov. Today*. doi: 10.1016/j.ddmod.2014.04.002

Comtois, P., and Nattel, S. (2011). Interactions between cardiac fibrosis spatial pattern and ionic remodeling on electrical wave propagation. *Conf. Proc. IEEE Eng. Med. Biol. Soc.* 2011, 4669–4672. doi: 10.1109/IEMBS.2011.6091156

Courtemanche, M., Ramirez, R. J., and Nattel, S. (1998). Ionic mechanisms underlying human atrial action potential properties: insights from a mathematical model. *Am. J. Physiol.* 275, H301–H321.

Dossel, O., Krueger, M. W., Weber, F. M., Wilhelms, M., and Seemann, G. (2012). Computational modeling of the human atrial anatomy and electrophysiology. *Med. Biol. Eng. Comput.* 50, 773–799. doi: 10.1007/s11517-012-0924-6

Eckstein, J., Maesen, B., Linz, D., Zeemering, S., Van Hunnik, A., Verheule, S., et al. (2011). Time course and mechanisms of endo-epicardial electrical dissociation during atrial fibrillation in the goat. *Cardiovasc. Res.* 89, 816–824. doi: 10.1093/cvr/cvq336

Estner, H. L., Zviman, M. M., Herzka, D., Miller, F., Castro, V., Nazarian, S., et al. (2011). The critical isthmus sites of ischemic ventricular tachycardia are in zones of tissue heterogeneity, visualized by magnetic resonance imaging. *Heart Rhythm* 8, 1942–1949. doi: 10.1016/j.hrthm.2011.07.027

Fink, M., Noble, D., Virag, L., Varro, A., and Giles, W. R. (2008). Contributions of HERG K+ current to repolarization of the human ventricular action potential. *Prog. Biophys. Mol. Biol.* 96, 357–376. doi: 10.1016/j.pbiomolbio.2007.07.011

Fishman, G. I., Chugh, S. S., Dimarco, J. P., Albert, C. M., Anderson, M. E., Bonow, R. O., et al. (2010). Sudden cardiac death prediction and prevention: report from a National Heart, Lung, and Blood Institute and Heart Rhythm Society Workshop. *Circulation* 122, 2335–2348. doi: 10.1161/CIRCULATIONAHA.110.976092

Grandi, E., Pandit, S. V., Voigt, N., Workman, A. J., Dobrev, D., Jalife, J., et al. (2011). Human atrial action potential and Ca2+ model: sinus rhythm and chronic atrial fibrillation. *Circ. Res.* 109, 1055–1066. doi: 10.1161/CIRCRESAHA.111.253955

Grandi, E., Pasqualini, F. S., and Bers, D. M. (2010). A novel computational model of the human ventricular action potential and Ca transient. *J. Mol. Cell. Cardiol.* 48, 112–121. doi: 10.1016/j.yjmcc.2009.09.019

Gurev, V., Lee, T., Constantino, J., Arevalo, H., and Trayanova, N. A. (2011). Models of cardiac electromechanics based on individual hearts imaging data: image-based electromechanical models of the heart. *Biomech. Model. Mechanobiol.* 10, 295–306. doi: 10.1007/s10237-010-0235-5

Heijman, J., Voigt, N., Nattel, S., and Dobrev, D. (2014). Cellular and molecular electrophysiology of atrial fibrillation initiation, maintenance, and progression. *Circ. Res.* 114, 1483–1499. doi: 10.1161/CIRCRESAHA.114.302226

Helm, P. A., Tseng, H. J., Younes, L., McVeigh, E. R., and Winslow, R. L. (2005). *Ex vivo* 3D diffusion tensor imaging and quantification of cardiac laminar structure. *Magn. Reson. Med.* 54, 850–859. doi: 10.1002/mrm.20622

Hu, Y., Gurev, V., Constantino, J., and Trayanova, N. (2014). Optimizing cardiac resynchronization therapy to minimize ATP consumption heterogeneity throughout the left ventricle: a simulation analysis using a canine heart failure model. *Heart Rhythm* 11, 1063–1069. doi: 10.1016/j.hrthm.2014.03.021

Iwasaki, Y. K., Nishida, K., Kato, T., and Nattel, S. (2011). Atrial fibrillation pathophysiology: implications for management. *Circulation* 124, 2264–2274. doi: 10.1161/CIRCULATIONAHA.111.019893

Jacquemet, V., and Henriquez, C. S. (2009). Genesis of complex fractionated atrial electrograms in zones of slow conduction: a computer model of microfibrosis. *Heart Rhythm* 6, 803–810. doi: 10.1016/j.hrthm.2009.02.026

Jacquemet, V., Kappenberger, L., and Henriquez, C. S. (2008). Modeling atrial arrhythmias: impact on clinical diagnosis and therapies. *IEEE Rev. Biomed. Eng.* 1, 94–114. doi: 10.1109/RBME.2008.2008242

Jalife, J. (2011). Deja vu in the theories of atrial fibrillation dynamics. *Cardiovasc. Res.* 89, 766–775. doi: 10.1093/cvr/cvq364

Janse, M. J. (2004). Electrophysiological changes in heart failure and their relationship to arrhythmogenesis. *Cardiovasc. Res.* 61, 208–217. doi: 10.1016/j.cardiores.2003.11.018

Jie, X., Gurev, V., and Trayanova, N. (2010). Mechanisms of mechanically induced spontaneous arrhythmias in acute regional ischemia. *Circ. Res.* 106, 185–192. doi: 10.1161/CIRCRESAHA.109.210864

Jie, X., Rodriguez, B., De Groot, J. R., Coronel, R., and Trayanova, N. (2008). Reentry in survived subepicardium coupled to depolarized and inexcitable midmyocardium: insights into arrhythmogenesis in ischemia phase 1B. *Heart Rhythm* 5, 1036–1044. doi: 10.1016/j.hrthm.2008.03.025

Jie, X., and Trayanova, N. A. (2010). Mechanisms for initiation of reentry in acute regional ischemia phase 1B. *Heart Rhythm* 7, 379–386. doi: 10.1016/j.hrthm.2009.11.014

John, R. M., Tedrow, U. B., Koplan, B. A., Albert, C. M., Epstein, L. M., Sweeney, M. O., et al. (2012). Ventricular arrhythmias and sudden cardiac death. *Lancet* 380, 1520–1529. doi: 10.1016/S0140-6736(12)61413-5

Kostin, S., Klein, G., Szalay, Z., Hein, S., Bauer, E. P., and Schaper, J. (2002). Structural correlate of atrial fibrillation in human patients. *Cardiovasc. Res.* 54, 361–379. doi: 10.1016/S0008-6363(02)00273-0

Krogh-Madsen, T., Abbott, G. W., and Christini, D. J. (2012). Effects of electrical and structural remodeling on atrial fibrillation maintenance: a simulation study. *PLoS Comput. Biol.* 8:1002390. doi: 10.1371/journal.pcbi.1002390

Krueger, M. W., Rhode, K. S., O'Neill, M. D., Rinaldi, C. A., Gill, J., Razavi, R., et al. (2014). Patient-specific modeling of atrial fibrosis increases the accuracy of sinus rhythm simulations and may explain maintenance of atrial fibrillation. *J. Electrocardiol.* 47, 324–328. doi: 10.1016/j.jelectrocard.2013.11.003

Krueger, M. W., Schmidt, V., Tobón, C., Weber, F. M., Lorenz, C., Keller, D. U., et al. (2011). "Modeling atrial fiber orientation in patient-specific geometries: a semi-automatic rule-based approach," in *Functional Imaging and Modeling of the Heart*, eds D. N. Metaxas and L. Axel (Berlin; Heidelberg: Springer), 223–232.

Li, P., and Rudy, Y. (2011). A model of canine Purkinje cell electrophysiology and Ca(2+) cycling: rate dependence, triggered activity, and comparison to ventricular myocytes. *Circ. Res.* 109, 71–79. doi: 10.1161/CIRCRESAHA.111.246512

Maleckar, M. M., Greenstein, J. L., Giles, W. R., and Trayanova, N. A. (2009a). Electrotonic coupling between human atrial myocytes and fibroblasts alters myocyte excitability and repolarization. *Biophys. J.* 97, 2179–2190. doi: 10.1016/j.bpj.2009.07.054

Maleckar, M. M., Greenstein, J. L., Giles, W. R., and Trayanova, N. A. (2009b). K+ current changes account for the rate dependence of the action potential in the human atrial myocyte. *Am. J. Physiol. Heart Circ. Physiol.* 297, H1398–H1410. doi: 10.1152/ajpheart.00411.2009

McDowell, K. S., Arevalo, H. J., Maleckar, M. M., and Trayanova, N. A. (2011). Susceptibility to arrhythmia in the infarcted heart depends on myofibroblast density. *Biophys. J.* 101, 1307–1315. doi: 10.1016/j.bpj.2011.08.009

McDowell, K. S., Vadakkumpadan, F., Blake, R., Blauer, J., Plank, G., Macleod, R. S., et al. (2012). Methodology for patient-specific modeling of atrial fibrosis as a substrate for atrial fibrillation. *J. Electrocardiol.* 45, 640–645. doi: 10.1016/j.jelectrocard.2012.08.005

McDowell, K. S., Vadakkumpadan, F., Blake, R., Blauer, J., Plank, G., Macleod, R. S., et al. (2013). Mechanistic inquiry into the role of tissue remodeling in fibrotic lesions in human atrial fibrillation. *Biophys. J.* 104, 2764–2773. doi: 10.1016/j.bpj.2013.05.025

Moreno, J. D., Zhu, Z. I., Yang, P.-C., Bankston, J. R., Jeng, M.-T., Kang, C., et al. (2011). A computational model to predict the effects of class I anti-arrhythmic drugs on ventricular rhythms. *Sci. Transl. Med.* 3, 98ra83. doi: 10.1126/scitranslmed.3002588

Nattel, S., Burstein, B., and Dobrev, D. (2008). Atrial remodeling and atrial fibrillation: mechanisms and implications. *Circ. Arrhythm. Electrophysiol.* 1, 62–73. doi: 10.1161/CIRCEP.107.754564

Nazarian, S., Bluemke, D. A., Lardo, A. C., Zviman, M. M., Watkins, S. P., Dickfeld, T. L., et al. (2005). Magnetic resonance assessment of the substrate for inducible ventricular tachycardia in nonischemic cardiomyopathy. *Circulation* 112, 2821–2825. doi: 10.1161/CIRCULATIONAHA.105.549659

Ng, J., Jacobson, J. T., Ng, J. K., Gordon, D., Lee, D. C., Carr, J. C., et al. (2012). Virtual electrophysiological study in a 3-dimensional cardiac magnetic resonance imaging model of porcine myocardial infarction. *J. Am. Coll. Cardiol.* 60, 423–430. doi: 10.1016/j.jacc.2012.03.029

Nielsen, P. M., Le Grice, I. J., Smaill, B. H., and Hunter, P. J. (1991). Mathematical model of geometry and fibrous structure of the heart. *Am. J. Physiol.* 260, H1365–H1378.

Noble, D. (2002). Modeling the heart–from genes to cells to the whole organ. *Science* 295, 1678–1682. doi: 10.1126/science.1069881

Nygren, A., Fiset, C., Firek, L., Clark, J. W., Lindblad, D. S., Clark, R. B., et al. (1998). Mathematical model of an adult human atrial cell: the role of K+ currents in repolarization. *Circ. Res.* 82, 63–81. doi: 10.1161/01.RES.82.1.63

Oakes, R. S., Badger, T. J., Kholmovski, E. G., Akoum, N., Burgon, N. S., Fish, E. N., et al. (2009). Detection and quantification of left atrial structural remodeling with delayed-enhancement magnetic resonance imaging in patients with atrial fibrillation. *Circulation* 119, 1758–1767. doi: 10.1161/CIRCULATIONAHA.108.811877

O'Hara, T., Virag, L., Varro, A., and Rudy, Y. (2011). Simulation of the undiseased human cardiac ventricular action potential: model formulation and experimental validation. *PLoS Comput. Biol.* 7:e1002061. doi: 10.1371/journal.pcbi.1002061

Packer, D. L. (2004). Evolution of mapping and anatomic imaging of cardiac arrhythmias. *J. Cardiovasc. Electrophysiol.* 15, 839–854. doi: 10.1046/j.1540-8167.2004.04275.x

Pedrotty, D. M., Klinger, R. Y., Kirkton, R. D., and Bursac, N. (2009). Cardiac fibroblast paracrine factors alter impulse conduction and ion channel expression of neonatal rat cardiomyocytes. *Cardiovasc. Res.* 83, 688–697. doi: 10.1093/cvr/cvp164

Plank, G., Prassl, A. J., Wang, J. I., Seeman, G., Scherr, D., Sanchez-Quintana, D., et al. (2008a). Atrial fibrosis promotes the transition of pulmonary vein ectopy into reentrant arrhythmias. *Heart Rhythm*. 5(Suppl. 5), S162.

Plank, G., Zhou, L., Greenstein, J. L., Cortassa, S., Winslow, R. L., O'Rourke, B., et al. (2008b). From mitochondrial ion channels to arrhythmias in the heart: computational techniques to bridge the spatio-temporal scales. *Philos. Trans. A Math. Phys. Eng. Sci.* 366, 3381–3409. doi: 10.1098/rsta.2008.0112

Pop, M., Sermesant, M., Mansi, T., Crystal, E., Ghate, S., Peyrat, J. M., et al. (2011). Correspondence between simple 3-D MRI-based computer models and *in-vivo* EP measurements in swine with chronic infarctions. *IEEE Trans. Biomed. Eng.* 58, 3483–3486. doi: 10.1109/TBME.2011.2168395

Prakosa, A., Malamas, P., Zhang, S., Pashakhanloo, F., Arevalo, H., Herzka, D. A., et al. (2014). Methodology for image-based reconstruction of ventricular geometry for patient-specific modeling of cardiac electrophysiology. *Prog. Biophys. Mol. Biol.* 115, 226–234. doi: 10.1016/j.pbiomolbio.2014.08.009

Rantner, L. J., Arevalo, H. J., Constantino, J. L., Efimov, I. R., Plank, G., and Trayanova, N. A. (2012). Three-dimensional mechanisms of increased vulnerability to electric shocks in myocardial infarction: altered virtual electrode polarizations and conduction delay in the peri-infarct zone. *J. Physiol.* 590, 4537–4551. doi: 10.1113/jphysiol.2012.229088

Rodriguez, B., and Trayanova, N. (2003). Upper limit of vulnerability in a defibrillation model of the rabbit ventricles. *J. Electrocardiol.* 36(Suppl.), 51–56. doi: 10.1016/j.jelectrocard.2003.09.066

Roes, S. D., Borleffs, C. J. W., Van Der Geest, R. J., Westenberg, J. J., Marsan, N. A., Kaandorp, T. A., et al. (2009). Infarct tissue heterogeneity assessed with contrast-enhanced MRI predicts spontaneous ventricular arrhythmia in patients with ischemic cardiomyopathy and implantable cardioverter-defibrillator. *Circulation* 2, 183–190. doi: 10.1161/CIRCIMAGING.108.826529

Rohr, S. (2009). Myofibroblasts in diseased hearts: new players in cardiac arrhythmias? *Heart Rhythm* 6, 848–856. doi: 10.1016/j.hrthm.2009.02.038

Rubart, M., and Zipes, D. P. (2005). Mechanisms of sudden cardiac death. *J. Clin. Invest.* 115, 2305–2315. doi: 10.1172/JCI26381

Rudy, Y., Ackerman, M. J., Bers, D. M., Clancy, C. E., Houser, S. R., London, B., et al. (2008). Systems approach to understanding electromechanical activity in the human heart: a national heart, lung, and blood institute workshop summary. *Circulation* 118, 1202–1211. doi: 10.1161/CIRCULATIONAHA.108.772715

Sampson, K. J., Iyer, V., Marks, A. R., and Kass, R. S. (2010). A computational model of Purkinje fibre single cell electrophysiology: implications for the long QT syndrome. *J. Physiol.* 588, 2643–2655. doi: 10.1113/jphysiol.2010.187328

Schmidt, A., Azevedo, C. F., Cheng, A., Gupta, S. N., Bluemke, D. A., Foo, T. K., et al. (2007). Infarct tissue heterogeneity by magnetic resonance imaging identifies enhanced cardiac arrhythmia susceptibility in patients with left ventricular dysfunction. *Circulation* 115, 2006–2014. doi: 10.1161/CIRCULATIONAHA.106.653568

Schotten, U., Verheule, S., Kirchhof, P., and Goette, A. (2011). Pathophysiological mechanisms of atrial fibrillation: a translational appraisal. *Physiol. Rev.* 91, 265–325. doi: 10.1152/physrev.00031.2009

Stevenson, W. G., Brugada, P., Waldecker, B., Zehender, M., and Wellens, H. J. (1985). Clinical, angiographic, and electrophysiologic findings in patients with aborted sudden death as compared with patients with sustained ventricular tachycardia after myocardial infarction. *Circulation* 71, 1146–1152. doi: 10.1161/01.CIR.71.6.1146

Stewart, P., Aslanidi, O. V., Noble, D., Noble, P. J., Boyett, M. R., and Zhang, H. (2009). Mathematical models of the electrical action potential of Purkinje fibre cells. *Philos. Trans. A Math. Phys. Eng. Sci.* 367, 2225–2255. doi: 10.1098/rsta.2008.0283

Tanaka, K., Zlochiver, S., Vikstrom, K. L., Yamazaki, M., Moreno, J., Klos, M., et al. (2007). Spatial distribution of fibrosis governs fibrillation wave dynamics in the posterior left atrium during heart failure. *Circ. Res.* 101, 839–847. doi: 10.1161/CIRCRESAHA.107.153858

Tandri, H., Weinberg, S. H., Chang, K. C., Zhu, R., Trayanova, N. A., Tung, L., et al. (2011). Reversible cardiac conduction block and defibrillation with high-frequency electric field. *Sci. Transl. Med.* 3, 102ra196-102ra196. doi: 10.1126/scitranslmed.3002445

Ten Tusscher, K. H., and Panfilov, A. V. (2006). Alternans and spiral breakup in a human ventricular tissue model. *Am. J. Physiol. Heart Circ. Physiol.* 291, H1088–H1100. doi: 10.1152/ajpheart.00109.2006

Tice, B. M., Rodríguez, B., Eason, J., and Trayanova, N. (2007). Mechanistic investigation into the arrhythmogenic role of transmural heterogeneities in regional ischaemia phase 1A. *Europace* 9, vi46-vi58. doi: 10.1093/europace/eum204

Trayanova, N. A. (2011). Whole-heart modeling: applications to cardiac electrophysiology and electromechanics. *Circ. Res.* 108, 113–128. doi: 10.1161/CIRCRESAHA.110.223610

Trayanova, N. A. (2012). Computational cardiology: the heart of the matter. *ISRN Cardiol.* 2012, 269680. doi: 10.5402/2012/269680

Trayanova, N. A. (2014). Mathematical approaches to understanding and imaging atrial fibrillation significance for mechanisms and management. *Circ. Res.* 114, 1516–1531. doi: 10.1161/CIRCRESAHA.114.302240

Trayanova, N. A., and Boyle, P. M. (2014). Advances in modeling ventricular arrhythmias: from mechanisms to the clinic. *Wiley Interdiscip. Rev. Syst. Biol. Med.* 6, 209–224. doi: 10.1002/wsbm.1256

Trayanova, N. A., O'Hara, T., Bayer, J. D., Boyle, P. M., McDowell, K. S., Constantino, J., et al. (2012). Computational cardiology: how computer simulations could be used to develop new therapies and advance existing ones. *Europace* 14(Suppl. 5), v82–v89. doi: 10.1093/europace/eus277

Vadakkumpadan, F., Arevalo, H., Ceritoglu, C., Miller, M., and Trayanova, N. (2012). Image-based estimation of ventricular fiber orientations for personalized modeling of cardiac electrophysiology. *IEEE Trans. Med. Imaging* 31, 1051–1060. doi: 10.1109/TMI.2012.2184799

Vadakkumpadan, F., Arevalo, H., Prassl, A. J., Chen, J., Kickinger, F., Kohl, P., et al. (2010). Image-based models of cardiac structure in health and disease. *Wiley Interdiscip. Rev. Syst. Biol. Med.* 2, 489–506. doi: 10.1002/wsbm.76

Vaidyanathan, R., O'Connell, R. P., Deo, M., Milstein, M. L., Furspan, P., Herron, T. J., et al. (2013). The ionic bases of the action potential in isolated mouse cardiac Purkinje cell. *Heart Rhythm* 10, 80–87. doi: 10.1016/j.hrthm.2012.10.002

Vetter, F. J., and McCulloch, A. D. (1998). Three-dimensional analysis of regional cardiac function: a model of rabbit ventricular anatomy. *Prog. Biophys. Mol. Biol.* 69, 157–183. doi: 10.1016/S0079-6107(98)00006-6

Vigmond, E. J., Aguel, F., and Trayanova, N. A. (2002). Computational techniques for solving the bidomain equations in three dimensions. *IEEE Trans. Biomed. Eng.* 49, 1260–1269. doi: 10.1109/TBME.2002.804597

Vigmond, E. J., Hughes, M., Plank, G., and Leon, L. J. (2003). Computational tools for modeling electrical activity in cardiac tissue. *J. Electrocardiol.* 36, 69–74. doi: 10.1016/j.jelectrocard.2003.09.017

Vigmond, E., Vadakkumpadan, F., Gurev, V., Arevalo, H., Deo, M., Plank, G., et al. (2009). Towards predictive modelling of the electrophysiology of the heart. *Exp. Physiol.* 94, 563–577. doi: 10.1113/expphysiol.2008.044073

Winslow, R. L., Trayanova, N., Geman, D., and Miller, M. I. (2012). Computational medicine: translating models to clinical care. *Sci. Transl. Med.* 4, 158rv111. doi: 10.1126/scitranslmed.3003528

Xu, J., Cui, G., Esmailian, F., Plunkett, M., Marelli, D., Ardehali, A., et al. (2004). Atrial extracellular matrix remodeling and the maintenance of atrial fibrillation. *Circulation* 109, 363–368. doi: 10.1161/01.CIR.0000109495.02213.52

Yan, A. T., Shayne, A. J., Brown, K. A., Gupta, S. N., Chan, C. W., Luu, T. M., et al. (2006). Characterization of the peri-infarct zone by contrast-enhanced cardiac magnetic resonance imaging is a powerful predictor of post–myocardial infarction mortality. *Circulation* 114, 32–39. doi: 10.1161/CIRCULATIONAHA.106.613414

Yue, L., Xie, J., and Nattel, S. (2011). Molecular determinants of cardiac fibroblast electrical function and therapeutic implications for atrial fibrillation. *Cardiovasc. Res.* 89, 744–753. doi: 10.1093/cvr/cvq329

Conflict of Interest Statement: The authors declare that the research was conducted in the absence of any commercial or financial relationships that could be construed as a potential conflict of interest.

Received: 01 October 2014; paper pending published: 13 October 2014; accepted: 24 October 2014; published online: 12 November 2014.

*Citation: Trayanova NA, Boyle PM, Arevalo HJ and Zahid S (2014) Exploring susceptibility to atrial and ventricular arrhythmias resulting from remodeling of the passive electrical properties in the heart: a simulation approach. Front. Physiol. **5**:435. doi: 10.3389/fphys.2014.00435*

This article was submitted to Cardiac Electrophysiology, a section of the journal Frontiers in Physiology.

frontiers in PHYSIOLOGY

ORIGINAL RESEARCH ARTICLE
published: 16 December 2014
doi: 10.3389/fphys.2014.00483

Dynamics of propagation of premature impulses in structurally remodeled infarcted myocardium: a computational analysis

Candido Cabo[1,2]*

[1] Department of Computer Systems, New York City College of Technology, City University of New York, New York, NY, USA
[2] Doctoral Program in Computer Science, Graduate Center, City University of New York, New York, NY, USA

Edited by:
George E. Billman, The Ohio State University, USA

Reviewed by:
Ruben Coronel, Academic Medical Center, Amsterdam, Netherlands
Andre Georges Kleber, Harvard Medical School, USA

***Correspondence:**
Candido Cabo, Department of Computer Systems, New York City College of Technology, City University of New York, 300 Jay Street, Brooklyn, New York, NY 11201, USA
e-mail: ccabo@citytech.cuny.edu

Initiation of cardiac arrhythmias typically follows one or more premature impulses either occurring spontaneously or applied externally. In this study, we characterize the dynamics of propagation of single (S2) and double premature impulses (S3), and the mechanisms of block of premature impulses at structural heterogeneities caused by remodeling of gap junctional conductance (*Gj*) in infarcted myocardium. Using a sub-cellular computer model of infarcted tissue, we found that $|I_{Na,max}|$, prematurity (coupling interval with the previous impulse), and conduction velocity (CV) of premature impulses change dynamically as they propagate away from the site of initiation. There are fundamental differences between the dynamics of propagation of S2 and S3 premature impulses: for S2 impulses $|I_{Na,max}|$ recovers fast, prematurity decreases and CV increases as propagation proceeds; for S3 impulses low values of $|I_{Na,max}|$ persist, prematurity could increase, and CV could decrease as impulses propagate away from the site of initiation. As a consequence it is more likely that S3 impulses block at sites of structural heterogeneities causing source/sink mismatch than S2 impulses block. Whether premature impulses block at *Gj* heterogeneities or not is also determined by the values of *Gj* (and the space constant λ) in the regions proximal and distal to the heterogeneity: when λ in the direction of propagation increases >40%, premature impulses could block. The maximum slope of CV restitution curves for S2 impulses is larger than for S3 impulses. In conclusion: (1) The dynamics of propagation of premature impulses make more likely that S3 impulses block at sites of structural heterogeneities than S2 impulses block; (2) Structural heterogeneities causing an increase in λ (or CV) of >40% could result in block of premature impulses; (3) A decrease in the maximum slope of CV restitution curves of propagating premature impulses is indicative of an increased potential for block at structural heterogeneities.

Keywords: premature impulses, cell-to-cell conductance, structural remodeling, conduction velocity restitution curve, infarction, computer model

INTRODUCTION

Many cardiac arrhythmias have a reentrant mechanism, a pattern of excitation in which a wave rotates around an anatomical or functional obstacle (Wit and Janse, 1993). It is well-established that reentrant arrhythmias require a "trigger," which, in combination with a suitable "substrate," creates the conditions for initiation of a reentrant wave (i.e., a wave break) (Wit and Janse, 1993). One of the conditions for initiation of reentrant arrhythmias is the creation of a region of unidirectional block, which, by allowing propagation of the impulse in some directions but not in others, leads to the creation of wave breaks (Kleber and Rudy, 2004). Unidirectional block can occur in homogeneous tissue (Frazier et al., 1989; Quan and Rudy, 1990), in tissues with spatial heterogeneities in cell properties (refractory period, membrane excitability) (Janse and Kleber, 1981; Gough et al., 1985; Coronel, 1994) or in tissues with discontinuities in the microstructure (cell size, gap junction conductance) (Toure and Cabo, 2012) or the macrostructure (muscle bundle branches, narrow isthmuses, pivot points, tissue expansions) (Joyner, 1981; Spach et al., 1982; Cabo et al., 1994, 1996; Fast and Kleber, 1995).

In experimental and clinical cardiac electrophysiology, the conditions for unidirectional block are created by external electrical stimulation using sequences of closely coupled (i.e., premature) impulses (the "trigger"). Premature impulses can also occur spontaneously in healthy and diseased hearts as a result of reentry, abnormal automaticity or triggered activity (Peters et al., 2000). In healthy hearts, premature impulses are often benign (i.e., do not result in unidirectional block and arrhythmias) but, the structural and/or membrane remodeling caused by heart disease may lead to the creation of a suitable "substrate" such that premature impulses may result in unidirectional block and the initiation of arrhythmias (Nattel et al., 2007).

Structural remodeling following heart disease can cause local heterogeneities in the tissue microstructure, like an increase in

cell size (hypertrophy) (Nattel et al., 2007) and remodeling of connexin43 (Cx43) (Severs et al., 2008). Myocardial infarction results in a reduction of the amount of Cx43 with the consequent decrease in gap junction conductance and conduction velocity (Cabo et al., 2006). Regions of heterogeneous Cx43 expression and gap junction conductance have been described in infarcted (Cabo et al., 2006) and failing hearts (Poelzing and Rosenbaum, 2004; Akar et al., 2007). In an earlier computational study, we showed that, under conditions of uniform reduced excitability, heterogeneities in gap junction conductance could result in unidirectional block of non-premature impulses (Toure and Cabo, 2012). However, in cardiac patients, the areas of unidirectional block that lead to arrhythmias likely result from the interaction of spontaneously generated premature impulses and a substrate created by the remodeling of cell membrane properties and/or tissue structure (Baba et al., 2005; Cabo et al., 2006). In particular, the mechanisms of conduction and block of premature impulses in regions of heterogeneous gap junction conductance have not been fully characterized.

Our objective is to characterize the dynamics of propagation of premature impulses in the healing infarcted heart, and how those dynamics may result in unidirectional block in structurally remodeled myocardium with heterogeneities in gap junction conductance. To simulate the remodeling in cell membrane properties occurring after myocardial infarction, we use a previously developed ionic model of the action potential of cells from the canine epicardial border zone (Cabo and Boyden, 2003). To study the dynamics of propagation of the action potential, we use a sub-cellular computer model (Spach and Heidlage, 1995), which provides a realistic representation of the tissue microstructure including the natural variability in cell morphology and electrical connections through gap junctions. Sub-cellular models have been used to investigate the effect of cell size, gap junction remodeling, and myofibroblast proliferation on cardiac wave propagation (Hubbard et al., 2007; Cabo and Boyden, 2009; Toure and Cabo, 2010, 2012; Baum et al., 2012).

METHODS

NUMERICAL METHODS

We performed all simulations in a 2D monodomain model with governing equation: $\nabla \cdot ((1/(S_v R_i C_m))\nabla V_m) = (I_{ion}/C_m) + \partial V_m/\partial t$, where V_m is the transmembrane potential (in mV), I_{ion} is the ionic current ($\mu A/cm^2$), R_i is the resistivity of the intracellular space, S_v is the surface to volume ratio ($2000\,cm^{-1}$), and C_m is the specific capacitance ($1\,\mu F/cm^2$). Neumann (non-flow) boundary conditions were used. Membrane dynamics (I_{ion}) were formulated by an ionic model of the action potential of canine epicardial infarcted border zone cell (IZ cell dynamics) (Cabo and Boyden, 2003). The density and kinetics of several ionic currents of IZ cells are markedly different from cells from non-infarcted canine epicardium (Cabo and Boyden, 2003). Earlier results indicate that I_{Na} density is a major determinant of propagation (or block) at sites of microstructural discontinuities (Toure and Cabo, 2012). When compared to cells from normal epicardium, IZ cells have a reduced I_{Na} density that results in a slower conduction velocity and a delayed recovery from inactivation of the Na channel that results in post-repolarization refractoriness.

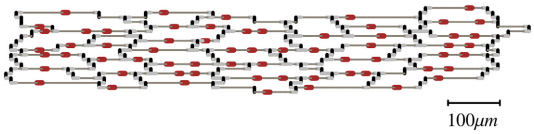

FIGURE 1 | Basic unit of the tissue architecture showing natural variability in cell size and shape as well as the location of gap junctions (Spach and Heidlage, 1995). Different types of gap junctions are shown on the cell membrane: plicate (black), interplicate (gray), and combined plicate (red).

We used the tissue architecture in **Figure 1** as the basis to create other architectures with different cell-to-cell gap junctional conductance (*Gj*) (Spach and Heidlage, 1995). The basic unit in **Figure 1** was replicated to create preparations of any size. That tissue architecture is a realistic representation of the natural variability in cell size and shape as well as the location of gap junctions. Each myocyte was electrically connected to neighboring myocytes only at the gap junctions. Three different types of gap junctions were simulated in the model: plicate (0.5 μS), interplicate (0.33 μS) and combined plicate gap junctions (0.062 μS) (**Figure 1**) (Spach and Heidlage, 1995). Plicate gap junctions, which are located in the plicate region of the intercalated disks, were simulated by resistors connecting cells electrically in the direction of the fiber orientation (longitudinally). Interplicate gap junctions, which are located in the interplicate region of the intercalated disks, were simulated by resistors connecting cells electrically in the direction transverse to the fiber orientation. Combined plicate gap junctions, which represent small intercalated disks located on the lateral membrane, between the larger intercalated disks containing the plicate and interplicate gap junctions, were simulated by resistors connecting cells electrically in the direction transverse to the fiber orientation. To study the effect of *Gj* heterogeneities on propagation, we used the basic tissue architecture, with different regions having different cell-to-cell *Gj* while the location of gap junctions was preserved. The regions with different cell-to-cell *Gj* were created by modifying the original conductance of the three types of gap junctions in the same proportion. The resistivity of the cytoplasm was 150 Ω *cm*. Cells were discretized with a space step of 10 μm in both longitudinal and transverse directions. Each discretized cell element consisted of two square membrane surfaces, each one having a surface area of 100 μm^2, separated by a depth of 10 μm, with a volume of 1000 μm^3. Those values result in a surface to volume ratio (S_v) of 0.2 μm^{-1} (= 2000 cm^{-1}). In all simulations S_v was kept constant. The governing equation was integrated using the semi-implicit Crank-Nicholson method with a time step of 5 μs.

SIMULATION PROTOCOLS

We studied the dynamics of propagation of premature impulses in uniform preparations having the same average cell-to-cell *Gj* and in preparations with a structural discontinuity having different average cell-to-cell *Gj* in the region proximal to the discontinuity and in the region distal to the discontinuity. Flat wave fronts

were initiated at the boundary of the proximal region of the preparation by an externally applied stimulus current (2x diastolic threshold). Propagation in all simulations was longitudinal, i.e., in the direction of the fiber orientation. The basic stimulation train consisted of 10 stimuli (S1) with a basic cycle length (BCL or S1S1) of 250 ms, after which single (S2), and double premature (S3) impulses with different coupling intervals were applied. The size of the preparations was 10 mm × 2.5 mm, and 7.5 mm × 2.5 mm, obtained by replication of the basic unit in **Figure 1** to the appropriate size.

We also calculated λ for tissue architectures with different cell-to-cell *Gj*. λ was calculated from the spatial decay of V_m, five membrane time constants (40 ms) after one end of the preparation was clamped at $-65\,mV$.

RESULTS

PROPAGATION OF SINGLE PREMATURE IMPULSES (S2) IN THE INFARCTED HEART

It is well-known that the conduction velocity (CV) of premature impulses decreases with the coupling interval between the premature impulse and the last impulse of the basic train (S1S2). **Figure 2A** shows the CV restitution curve for single premature impulses after a basic train with a S1S1 coupling interval of 250 ms in a computer model of the infarcted heart with average cell-to-cell coupling $Gj = 0.41\,\mu S$. The average CV of the most premature impulse that propagates (S1S2 = 198 ms) is 0.30 m/s, while the average CV of the basic impulse (S1S1 = 250 ms) is 0.48 m/s.

The CV of single premature impulses is not constant but it increases as the premature impulse propagates away from the stimulation site. **Figure 2B** shows the local CVs of premature impulses with S1S2 coupling intervals ranging from 198 ms (the shortest coupling interval that elicits a propagated response) to 250 ms. For S1S2 = 198 ms, CV varies from 0.12 m/s close to the stimulation site ($x = 0$ mm in **Figure 2B**) to 0.45 m/s 10 mm away from the stimulation site ($x = 10$ mm in **Figure 2B**). As the coupling interval of the premature impulses increases the changes in CV during propagation decrease. For example for the basic impulse in the train (S1S1 = 250 ms; thick black line in **Figure 2B**), CV close to the stimulation site is 0.47 m/s, and CV 10 mm away from the stimulation site is 0.49 m/s.

The changes in CV of premature impulses are caused by the dynamics of recovery from inactivation of the sodium channel. **Figure 3** shows how the absolute value of the peak I_{Na} current changes ($|I_{Na,max}|$), along a line in the center of the preparation, as the premature impulse propagates away from the stimulation site ($x = 0$ mm in **Figure 3**) for different coupling intervals. For S1S2 = 198 ms, $|I_{Na,max}|$ first decreases to reach a minimum of about 36 pA/pF about 2.5 mm (∼2.5 λ) away from the stimulation site and then increases steadily as the premature impulse propagates. This minimum identifies the location where the premature impulse is more vulnerable to block. The fact that the minimum $|I_{Na,max}|$ occurs about 2.5 λ from the stimulation site will have some implications for the conditions for block at sites of structural remodeling (see below). The steady increase in $|I_{Na,max}|$ (after having reached a minimum) correlates well with the increase in local CV as propagation proceeds shown in **Figure 2B**. Note in **Figure 3** that the boundaries of the preparation have an effect on the value of $|I_{Na,max}|$: the initiation of a propagating impulse by an external electrical stimulus affects the values of $|I_{Na,max}|$ within ∼0.5 mm of the site of initiation ($x = 0$ mm); the rapid decrease of $|I_{Na,max}|$ at the end of the preparation ($x = 10$ mm) is a consequence of the rapid increase in V_m caused by the collision of the propagating wave with the sealed boundary preventing I_{Na} from full activation (Spach and Kootsey, 1985).

An important consequence of the dynamics of propagation of single premature impulses shown in **Figures 2**, **3** is that as single premature impulses propagate away from the site of initiation, they become less and less premature. **Figure 4** shows the coupling interval of premature impulses with respect to the last impulse of the basic train (V1V2) as propagation proceeds away from the stimulation site ($x = 0$ mm). For example, a premature impulse initiated with a coupling interval of S1S2 = 200 ms at the simulation site, will have a V1V2 coupling interval of 206 ms at a distance of 5 mm from the stimulation site, and 208 ms at a distance of 10 mm from the stimulation site. This is a consequence of the difference in CV between the premature and the last basic impulse (**Figure 2**). Note also that premature impulses initiated

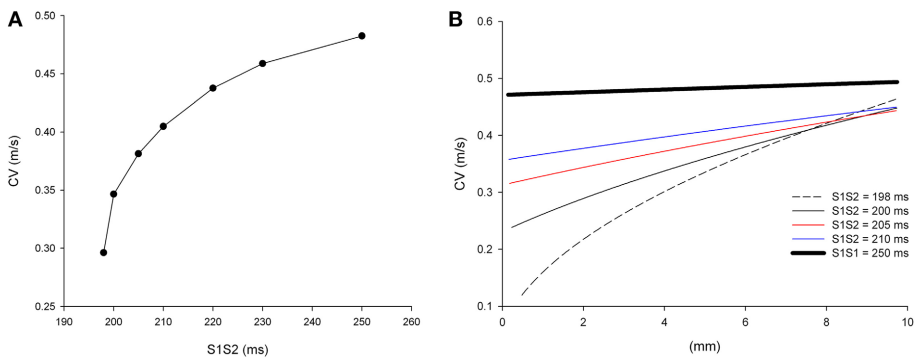

FIGURE 2 | Longitudinal conduction velocity (CV) of single premature impulses with different coupling intervals (S1S2) in a uniform infarcted myocardium preparation with average cell-to-cell coupling $Gj = 0.41\,\mu S$. **(A)** Average longitudinal CV in the preparation for different coupling intervals. **(B)** Local longitudinal CV as the impulse propagates away from the stimulation site ($x = 0$ mm). Size of the preparation: 10 × 2.5 mm.

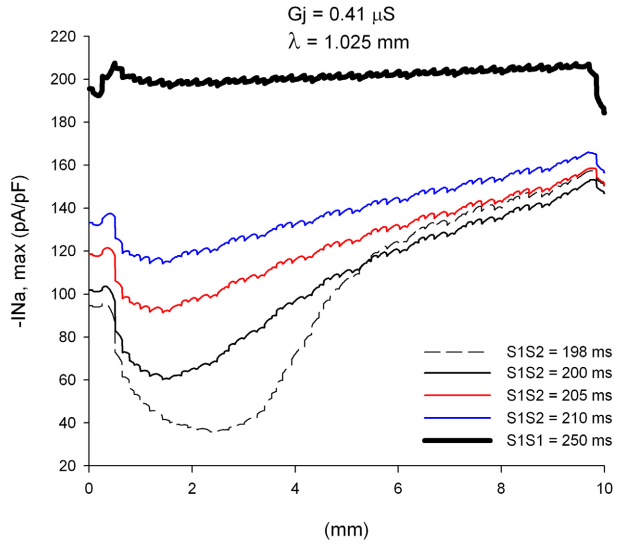

FIGURE 3 | Changes in I_{Na} current peak for single premature impulses, with different coupling intervals (S1S2), as the impulses propagate away from the stimulation site ($x = 0$ mm), in a uniform preparation with average cell-to-cell coupling $Gj = 0.41$ μS. The dashed plot (S1S2 = 198 ms) is the shortest coupling that resulted in a propagated response. Size of the preparation: 10 × 2.5 mm.

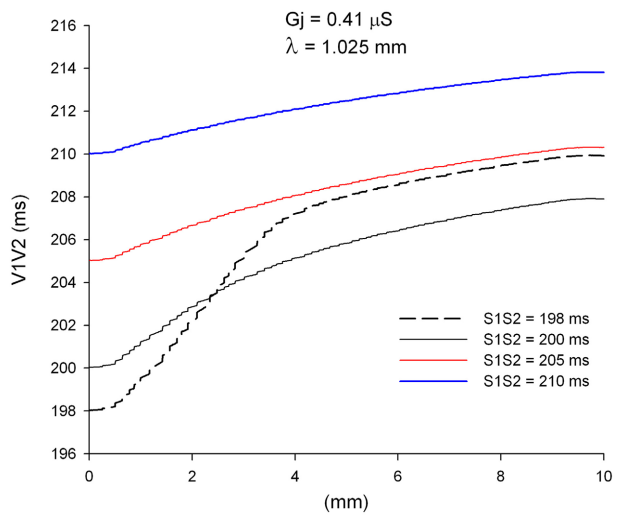

FIGURE 4 | Change in coupling interval between single premature impulses and the last impulse of the basic train (V1V2), for different coupling intervals (S1S2), as premature impulses propagate away from the stimulation site ($x = 0$ mm). The dashed plot (S1S2 = 198 ms) is the shortest coupling that resulted in a propagated response. Uniform preparation with average cell-to-cell coupling $Gj = 0.41$ μS. Size of the preparation: 10 × 2.5 mm.

with a very short coupling interval (S1S2 = 198 ms in **Figure 4**) can result in a longer V1V2 coupling interval far away from the stimulation site (compare V1V2 for S1S2 = 198 ms and S1S2 = 200 ms).

EFFECT OF STRUCTURAL REMODELING ON PROPAGATION OF SINGLE PREMATURE IMPULSES (S2)

We have reported earlier that, in normal myocardium, under conditions of reduced excitability (70% reduction in maximum sodium channel conductance), propagation of action potentials blocks at sites where the space constant in the direction of propagation increases by >40% (Toure and Cabo, 2012). Therefore, we analyzed the dynamics of propagation of premature impulses through heterogeneities in gap junctional conductance which result in increases of space constant of more than 40% in the direction of propagation. **Figure 5** shows $|I_{Na,max}|$ during propagation of premature impulses through a heterogeneity in gap junctional conductance ($\lambda_{distal}/\lambda_{proximal} = 1.49$ or an increase of 49% in the direction of propagation) which is identified in **Figure 5A** by the vertical dashed line. The refractory period is 197 ms (a premature with S1S2 = 197 ms fails to propagate in the proximal side of the heterogeneity). Note in **Figures 5A,B** that all premature impulses (S2) that propagate in the proximal side (S1S2 ≥ 198 ms), also propagate through the heterogeneity (propagation initiated at $x = 0$ mm). The effect of the heterogeneity is to reduce $|I_{Na,max}|$ by ∼30 pA/pF for the more premature impulses and by ∼20 pA/pF for the basic impulse of the stimulating train (S1S1 = 250 ms). At the interface, as the downstream impedance decreases in tissue with higher cell-to-cell coupling, the stimulatory efficacy of the wave front head decreases due to current dissipation, a phenomenon known as source/sink mismatch. The drop in the absolute value of peak I_{Na} caused by the heterogeneity is not sufficient to bring $|I_{Na,max}|$ below the value that is necessary to block propagation, and that is why all premature impulses propagate through the heterogeneity. For example, for S1S2 = 198 ms, after the premature impulses reaches a minimum $|I_{Na,max}|$ of 34 pA/pF 2.5 mm away from the stimulation site, $|I_{Na,max}|$ increases to ∼ 86 pA/pF as the premature impulse propagates, which is reduced by the source/sink mismatch at the heterogeneity to ∼ 58 pA/pF, a value which is still sufficient to sustain propagation.

If the initiation of premature impulses occurs closer to the heterogeneity, premature impulses block for a range of coupling intervals (**Figure 6**). In **Figure 6** initiation of premature impulses occurs 2.5 mm (∼ 2.5 λ) away from the same heterogeneity in gap junction conductance shown in **Figure 5**. Premature impulses initiated with coupling intervals S1S2 of 198–200 ms block at the heterogeneity (the window of vulnerability to block is 2–3 ms) (**Figures 6A,B**). Note that premature impulses at those same coupling intervals do not block when the premature impulses are initiated 5 mm (∼ 5 λ) away from the heterogeneity (**Figure 5**). The mechanism of block relates to the dynamics of propagation of premature impulses shown in **Figure 3**. Premature impulses show a minimum $|I_{Na,max}|$, and are more susceptible to block, at a distance ∼ 2 mm from the stimulation site (**Figures 3**, **5**); as propagation proceeds, $|I_{Na,max}|$ increases. The heterogeneity in gap junction conductance that results in a sudden increase in space constant in the direction of propagation causes a drop in $|I_{Na,max}|$ (**Figure 5A**). If that drop occurs when the premature impulse is more vulnerable, the value of $|I_{Na,max}|$ may decrease below the value that is necessary to sustain propagation,

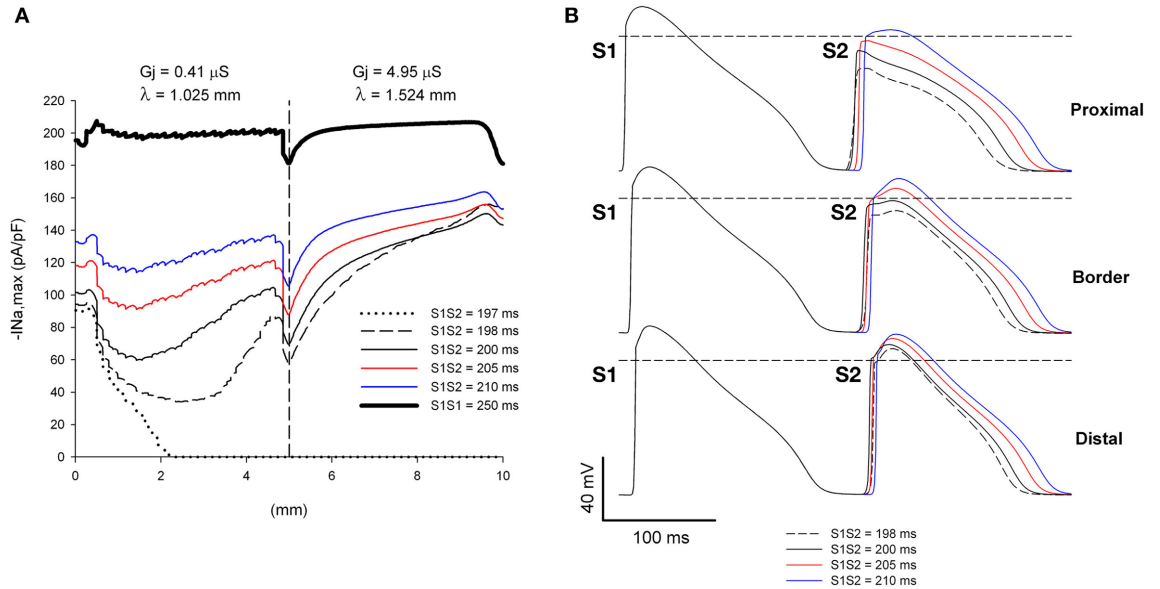

FIGURE 5 | Single premature impulses propagate through a structural heterogeneity when initiated far (5 mm away) from the heterogeneity. **(A)** Changes in I_{Na} current peak for single premature impulses, with different coupling intervals (S1S2), as the impulses propagate away from the stimulation site ($x = 0$ mm), in a preparation with a structural heterogeneity with average cell-to-cell coupling $Gj = 0.41\,\mu$S in the proximal side and $Gj = 4.95\,\mu$S in the distal side. The dashed vertical line indicates the location of the heterogeneity. **(B)** Action potentials calculated in the proximal side (2.5 mm from the border), at the border and in the distal side (2.5 mm from the border). Horizontal dashed line indicates a transmembrane potential of 0 mV. The dashed plot (S1S2 = 198 ms) is the shortest coupling that resulted in a propagated response. Size of the preparation: 10 × 2.5 mm (proximal side: 5 mm; distal side: 5 mm). Note that all single premature impulses propagate through the structural heterogeneity.

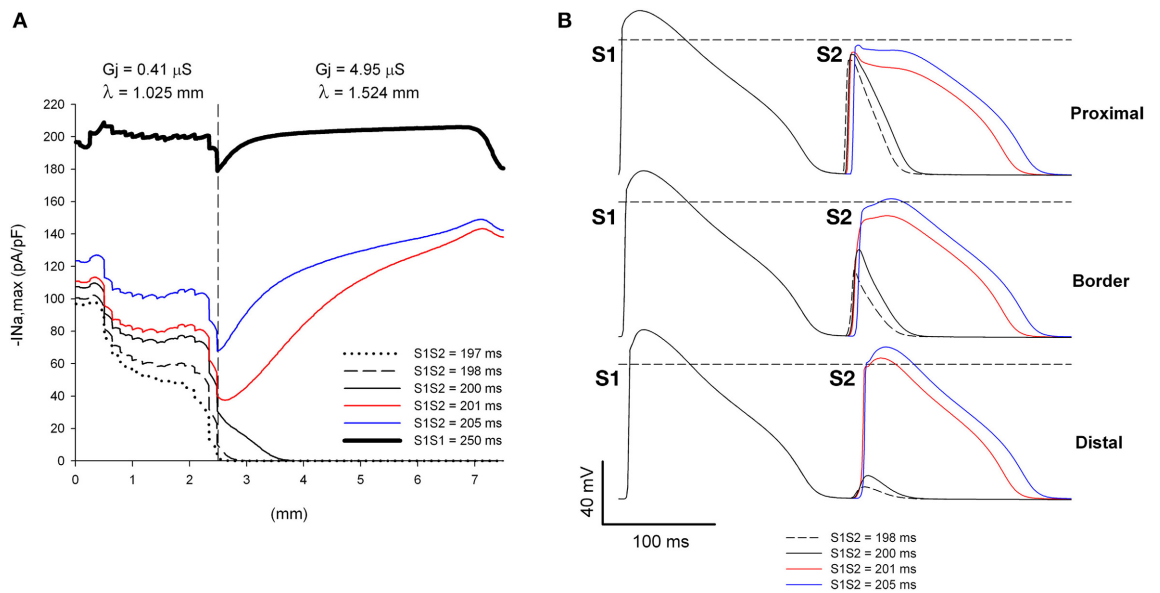

FIGURE 6 | Single premature impulses may block at a structural heterogeneity when initiated close (2.5 mm away) to the heterogeneity. **(A)** Changes in I_{Na} current peak for single premature impulses, with different coupling intervals (S1S2), as the impulses propagate away from the stimulation site ($x = 0$ mm), in a preparation with a structural heterogeneity with average cell-to-cell coupling $Gj = 0.41\,\mu$S in the proximal side and $Gj = 4.95\,\mu$S in the distal side. The dashed vertical line indicates the location of the heterogeneity. **(B)** Action potentials calculated in the proximal side (1.5 mm from the border), at the border and in the distal side (2.5 mm from the border). Horizontal dashed line indicates a transmembrane potential of 0 mV. The dashed plot (S1S2 = 198 ms) is the shortest coupling that resulted in a propagated response (in the proximal side). Size of the preparation: 7.5 × 2.5 mm (proximal side: 2.5 mm; distal side: 5 mm). Note that single premature impulses with S1S2 = 198–200 ms block at the structural heterogeneity.

and the premature impulse may block (S1S2 = 198–200 ms in **Figure 6A**). The critical value of $|I_{Na,max}|$ for propagation is ∼ 40 pA/pF (the minimum for S1S2 = 201 ms in **Figure 6A**). If the drop occurs when $|I_{Na,max}|$ has partially recovered from its minimum, the drop is not sufficient to bring $|I_{Na,max}|$ below the critical value for propagation, and the premature impulse propagates through the heterogeneity (S1S2 = 198 ms and 200 ms in **Figure 5A**).

The window of vulnerability to block increases when the difference in *Gj* between the distal and proximal sides of the heterogeneity (and consequently the ratio of the space constants) increases. **Figure 7** shows the dynamics of propagation of premature impulses through a heterogeneity with $\lambda_{distal}/\lambda_{proximal}$ = 1.62. The increase in the source/sink mismatch results in a larger drop in $|I_{Na,max}|$ at the heterogeneity (compare **Figure 7A** with **Figure 6A**). Premature impulses with coupling intervals S1S2 = 198–202 ms block at the heterogeneity increasing the window of vulnerability to block to 4–5 ms (which is larger than in **Figure 6**). Note the latency in the recovery of $|I_{Na,max}|$ for S1S2 = 203 ms, which indicates that the premature impulse hovers around the threshold of $|I_{Na,max}|$ necessary for propagation in the distal side (∼ 24 pA/pF). For the *Gj* heterogeneity in **Figure 7**, when initiation of premature impulses occurred 5 mm away from the heterogeneity, similarly to what occurred in **Figure 5**, all premature impulses propagated through the heterogeneity (not shown).

PROPAGATION OF DOUBLE PREMATURE IMPULSES (S3) IN THE INFARCTED HEART

Figure 8A shows the CV of double premature impulses (S3) initiated after a first premature (S2) with a coupling interval S1S2 = 200 ms with different S2S3 coupling intervals. As expected, and similarly to what occurred for single premature impulses (**Figure 2A**), average CV decreases with S2S3 coupling interval. **Figure 8B** shows the local CV as the S3 impulse propagate away from the stimulation site. CVs change less as the S3 premature propagates (**Figure 8B**) than when S2 impulses propagate (**Figure 2B**). Compare for example the changes in CV occurring when the S2 impulse with coupling interval S1S2 = 200 ms propagates (thick black line in **Figure 8B**) with the changes occurring when a S3 impulse with a coupling interval S2S3 = 166 ms propagates (black dashed line in **Figure 8B**). In contrast to what occurred during propagation of single premature impulses that show a monotonic increase in CV with propagation, during propagation of double premature impulses (S3) CV can decrease as the wave front propagates (coupling interval S2S3 = 180 ms in **Figure 8B**). For comparison purposes, **Figure 8C** shows both the CV restitution curves for single (S2) and double (S3) premature impulses. The maximum slope of the CV restitution curve for S3 is smaller than for S2, and for all diastolic intervals (DI), the CV for S3 premature impulses is smaller than for S2 premature impulses. However, the CV of a S3 impulse with a big DI is larger than the CV of a S2 impulse with a small DI (see below). For

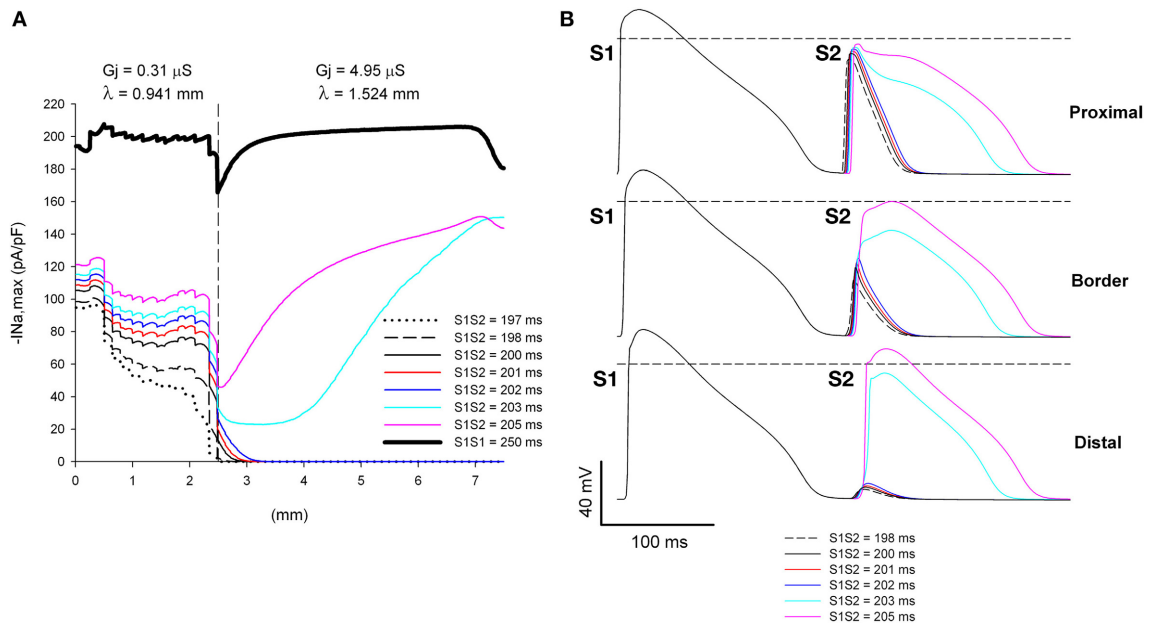

FIGURE 7 | Increasing the discontinuity in *Gj* at the heterogeneity increases the range of coupling intervals for which single premature impulses block at a structural heterogeneity when initiated close (2.5 mm away) to the heterogeneity. (A) Changes in I_{Na} current peak for single premature impulses, with different coupling intervals (S1S2), as the impulses propagate away from the stimulation site ($x = 0$ mm), in a preparation with a structural heterogeneity with average cell-to-cell coupling $Gj = 0.31\,\mu S$ in the proximal side and $Gj = 4.95\,\mu S$ in the distal side. The dashed vertical line indicates the location of the heterogeneity. **(B)** Action potentials calculated in the proximal side (1.5 mm from the border), at the border and in the distal side (2.5 mm from the border). Horizontal dashed line indicates a transmembrane potential of 0 mV. The dashed plot (S1S2 = 198 ms) is the shortest coupling that resulted in a propagated response (in the proximal side). Size of the preparation: 7.5 × 2.5 mm (proximal side: 2.5 mm; distal side: 5 mm). Note that single premature impulses with S1S2 = 198–202 ms block at the structural heterogeneity.

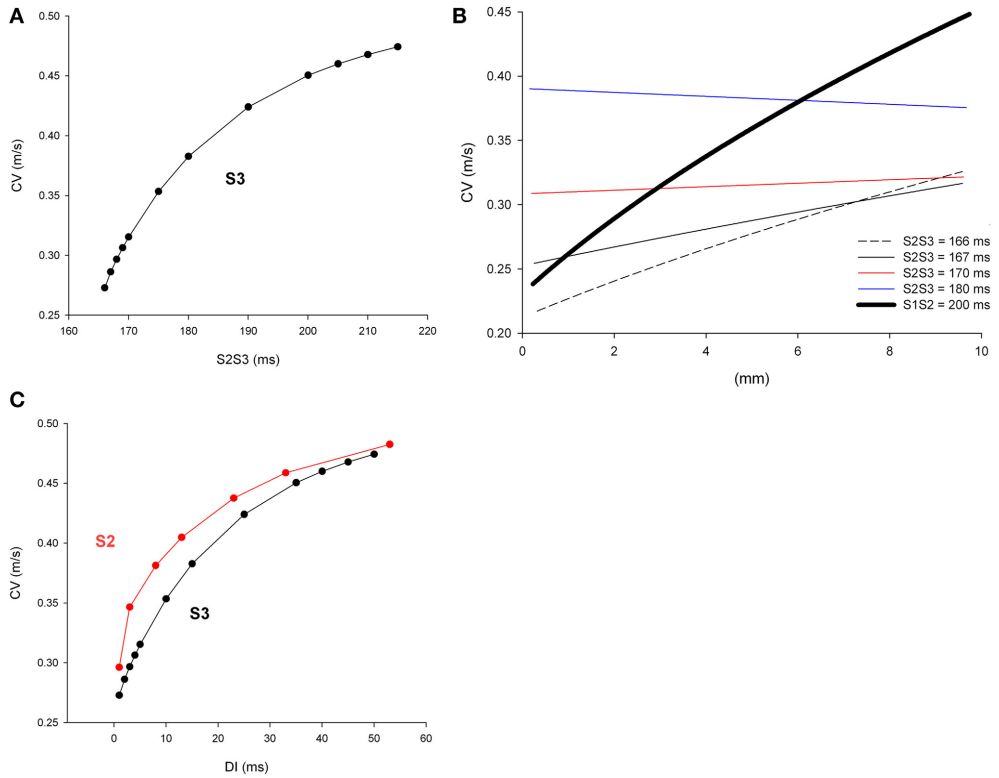

FIGURE 8 | Longitudinal conduction velocity (CV) of double premature impulses with different coupling intervals (S2S3), after a single premature with a coupling interval S1S2 = 200 ms, in a uniform infarcted myocardium preparation with average cell-to-cell coupling $Gj = 0.41\,\mu S$. (A) Average longitudinal CV in the preparation for different coupling intervals. **(B)** Local longitudinal CV as the impulse propagates away from the stimulation site ($x = 0$ mm). **(C)** Comparison of longitudinal CV restitution curves for single (S2) and double (S3) premature impulses. The diastolic interval (DI) is defined as (S1S2—Refractory period of S1) for S2 and (S2S3—Refractory period of S2) for S3 impulses. Size of the preparation: 10×2.5 mm.

example the CV of S3 with $DI = 25$ ms is 0.42 m/s while the CV of S2 with $DI = 3$ ms is 0.35 m/s.

We have shown earlier that single premature impulses become less premature as the impulse propagates away from the stimulation site (**Figure 4**) because the CV of single premature impulses (S2) is slower than the CV of the last basic impulse of the train (S1) (see CV restitution curve in **Figure 2A**). However, this is not necessarily the case for propagation of double premature impulses. **Figure 9** shows the coupling interval of double premature impulses (V2V3) as the impulse propagates away from the stimulation site. For S2S3 = 180 ms, the coupling interval of the double premature impulse (V2V3) decreases as the distance from the stimulation site increases (in contrast to what happened for single premature impulses in **Figure 4**). This is a consequence of the fact that the CV of the double premature impulse (S2S3 = 180 ms) is faster than the CV of the single premature impulse (S1S2 = 200 ms) (**Figures 8A,B**). The average CV for the single premature (S1S2 = 200 ms; $DI =$ 3 ms in S2 plot in **Figure 8B**) is ∼0.35 m/s, and the average CV for the double premature (S2S3 = 180 ms; $DI = 15$ ms in S3 plot in **Figure 8B**) is ∼0.38 m/s. Note also the differences in CV for single and double premature impulses in **Figure 8B**. Only for double premature impulses with a small S2S3 coupling interval (and small DI) the premature impulse becomes less premature as the distance from the stimulation site increases. For example, for S2S3 = 166 ms (black dashed line in **Figure 9**), the coupling interval of the double premature impulse 10 mm away from the stimulation site is V2V3 = 172 ms; this is a consequence of the fact that the CV of the double premature impulse is less than the CV of the single premature (**Figure 8B**).

We have shown earlier that single premature impulses reach a minimum $|I_{Na,max}|$ about 2 mm (2λ) from the stimulation site and then recover as propagation proceeds (**Figure 3**). For double premature impulses, $|I_{Na,max}|$ does not recover as fast as for single premature impulses and low values of $|I_{Na,max}|$ persist further away from the stimulation site (**Figure 10**). For double premature impulses, there is not a marked minimum from which $|I_{Na,max}|$ recovers quickly. For S2S3 = 166 ms ($DI = 1$ ms), low values of $|I_{Na,max}|$ persist 6 mm away from the stimulation site, and its recovery is very slow. Compare with the dynamics of recovery of S1S2 = 200 ms ($DI = 3$ ms), which is also shown for reference in **Figure 10** (thick black line). For S2S3 = 167, 170, and 180 ms there is no evidence of recovery of $|I_{Na,max}|$ with distance from the stimulation site except when the impulses reach the boundary of the preparation ($x = 10$ mm). In fact, for S2S3 = 170 and 180 ms, $|I_{Na,max}|$ decreases as the impulse propagates away of the simulation site.

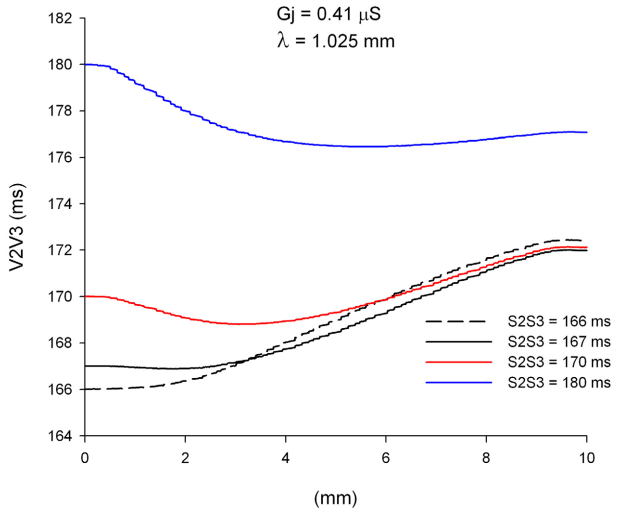

FIGURE 9 | Change in coupling interval between double premature impulses and a single premature with S1S2 = 200 ms (V2V3), for different coupling intervals (S2S3), as double premature impulses propagate away from the stimulation site ($x = 0$ mm). Uniform preparation with average cell-to-cell coupling $Gj = 0.41$ μS. Size of the preparation: 10 × 2.5 mm.

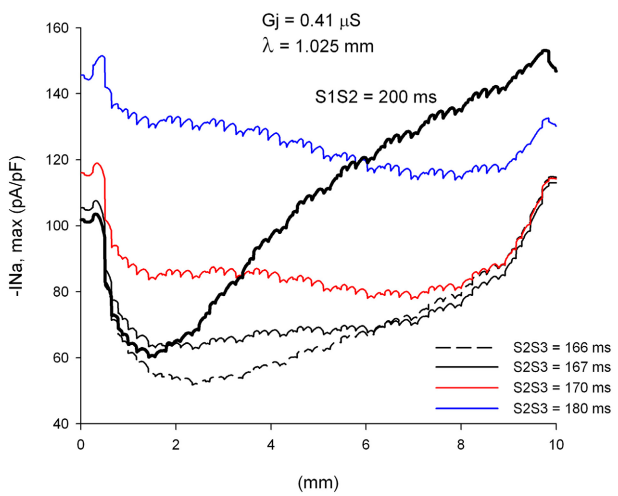

FIGURE 10 | Changes in I_{Na} current peak for double premature impulses with different coupling intervals (S2S3), initiated after a single premature with S1S2 = 200 ms, as the impulses propagate away from the stimulation site ($x = 0$ mm), in a uniform preparation with average cell-to-cell coupling $Gj = 0.41$ μS. Also shown for comparison are the changes in I_{Na} current peak for the single premature impulse (S1S2 = 200 ms; thick black line; also shown in **Figure 3**). Size of the preparation: 10 × 2.5 mm.

EFFECT OF STRUCTURAL REMODELING ON PROPAGATION OF DOUBLE PREMATURE IMPULSES (S3)

We have shown earlier that, for a heterogeneity with $\lambda_{distal}/\lambda_{proximal} = 1.49$ (or an increase of 49% in the direction of propagation), single premature impulses with the shortest coupling interval propagate through the heterogeneity when they are initiated far away (5 mm) from the heterogeneity (**Figure 5**). This is a consequence of the recovery of $|I_{Na,max}|$ of single premature impulses as they propagate away from the site of initiation. However, propagating double premature impulses do not show such a recovery in $|I_{Na,max}|$, and low values of $|I_{Na,max}|$ persist far way form the stimulation site (**Figure 10**). As a result, and in contrast to what occur with single premature impulses, double premature impulses initiated 5 mm away from a heterogeneity with $\lambda_{distal}/\lambda_{proximal} = 1.49$ block for a range of S2S3 coupling intervals from 170 to 173 ms (window of vulnerability is 4–5 ms) (**Figure 11**). The mechanism of block is the drop in $|I_{Na,max}|$ caused by the source/sink mismatch at the heterogeneity. For single premature impulses (thick black line in **Figure 11**), the drop occurs after $|I_{Na,max}|$ had recovered and the drop is not sufficient to reduce it below a value that cannot sustain propagation. In contrast, for double premature impulses (with short coupling intervals), $|I_{Na,max}|$ does not recover sufficiently with propagation and the drop in $|I_{Na,max}|$ at the heterogeneity decreases it to a value that cannot sustain propagation.

The window of vulnerability to block decreases when the difference in cell-to-cell Gj between the proximal and the distal side decreases. For $\lambda_{distal}/\lambda_{proximal} = 1.40$, the window of vulnerability decreases to 2–3 ms (**Figure 12A**), and for $\lambda_{distal}/\lambda_{proximal} = 1.3$ there is no block at the heterogeneity for any coupling interval (**Figure 12B**). As the difference in Gj between the proximal and distal side decreases, so does the drop in $|I_{Na,max}|$ caused by the Gj heterogeneity (**Figures 11**, **12**).

DISCUSSION

We have shown that $|I_{Na,max}|$, prematurity (i.e., coupling interval with the previous impulse), and CV of premature impulses change dynamically as they propagate away from the site of initiation, and that there are fundamental differences between the dynamics of propagation of single (S2) and double premature impulses (S3). Single premature impulses become less premature, recover their excitability ($|I_{Na,max}|$ increases) and CV increase as propagation proceeds. As a consequence it is unlikely that single premature impulses will block at structural heterogeneities causing source/sink mismatch unless the site of origin of the impulse is close (within 2.5 λ) to the site of the heterogeneity or a transition between thin and thick fibers. In contrast, double premature impulses could become more premature, they do not recover their excitability (low values of $|I_{Na,max}|$ persist far away from the site of initiation) and their CV could decrease as propagation proceeds. Those dynamics make it more likely that double premature impulses block at sites of structural heterogeneities than single premature impulses. While experimental and clinical electrophysiologists have reported for many years that the use of multiple premature impulses during programmed electrical stimulation increases the chances of initiation of ventricular tachycardia (Wit and Janse, 1993), our study provides novel insights into the dynamics of propagation of premature impulses and a mechanistic explanation of the conditions for block at sites of microstructural heterogeneities. The dynamic changes in CV of premature impulses as propagation proceeds away from the site of initiation implies

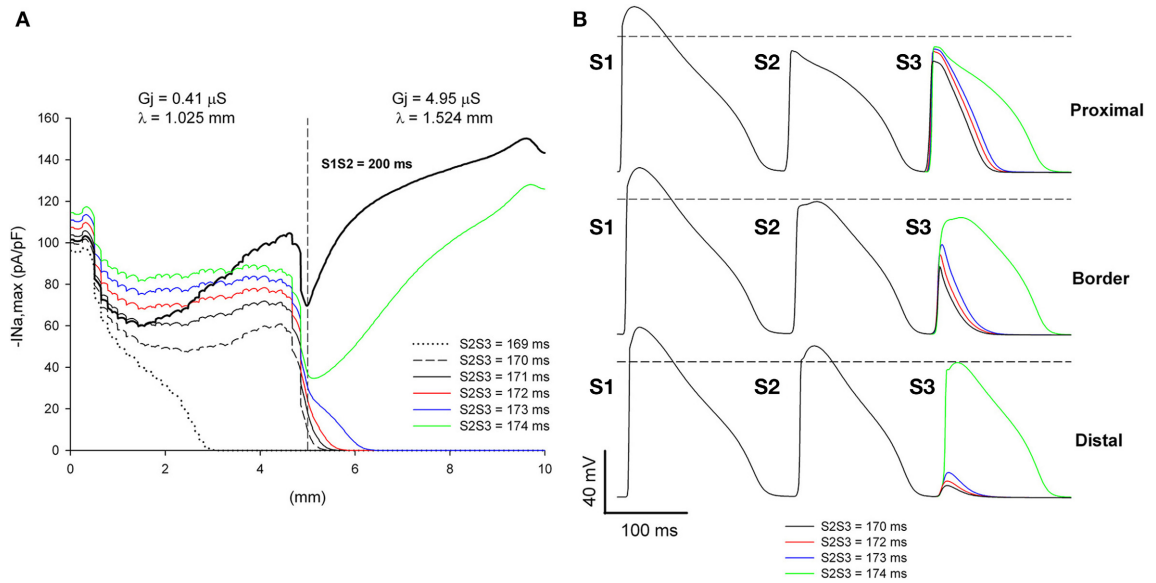

FIGURE 11 | Double premature impulses block at a structural heterogeneity even when initiated far (5 mm away) from the heterogeneity. (A) Changes in I_{Na} current peak for double premature impulses, with different coupling intervals (S2S3), as the impulses propagate away from the stimulation site ($x = 0$ mm), in a preparation with a structural heterogeneity with average cell-to-cell coupling $Gj = 0.41$ μS in the proximal side and $Gj = 4.95$ μS in the distal side. Also shown, for reference, are the changes in I_{Na} current peak for the single premature impulse (S1S2 = 200 ms) initiated before the double premature impulses. The dashed vertical line indicates the location of the heterogeneity. **(B)** Action potentials calculated in the proximal side (2.5 mm from the border), at the border and in the distal side (2.5 mm from the border). Horizontal dashed line indicates a transmembrane potential of 0 mV. The dashed plot (S2S3 = 170 ms) is the shortest coupling that resulted in a propagated response in the proximal side. Size of the preparation: 10 × 2.5 mm (proximal side: 5 mm; distal side: 5 mm). Note that double premature impulses with coupling intervals S2S3 = 170–173 ms block at the structural heterogeneity.

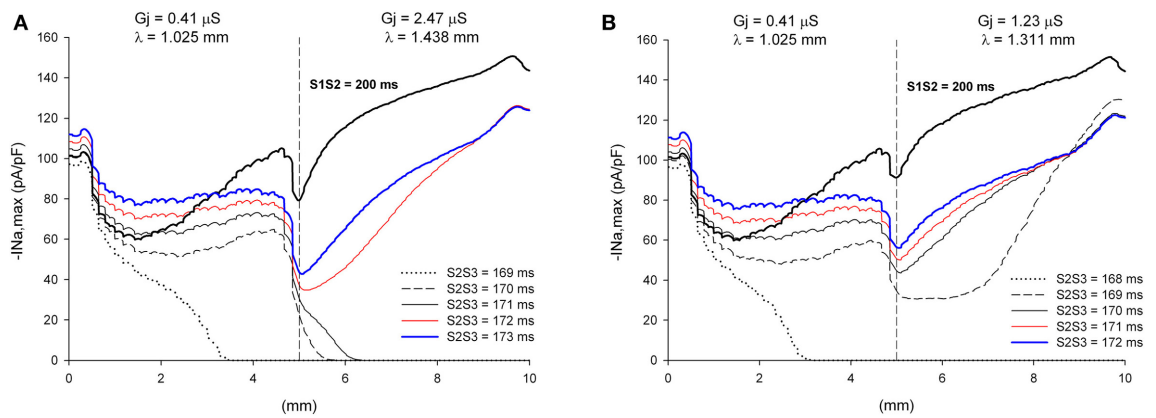

FIGURE 12 | Block at a structural heterogeneity depends on the difference in *Gj* between the proximal and the distal sides of the heterogeneity. Changes in I_{Na} current peak for double premature impulses, with different coupling intervals (S2S3), as the impulses propagate away from the stimulation site ($x = 0$ mm), in a preparation with a structural heterogeneity with average cell-to-cell coupling $Gj = 0.41$ μS in the proximal side and $Gj = 2.47$ μS in the distal side ($\lambda_{distal}/\lambda_{proximal} = 1.40$, **A**) and $Gj = 0.41$ μS in the proximal side and $Gj = 1.23$ μS in the distal side ($\lambda_{distal}/\lambda_{proximal} = 1.3$, **B**). Also shown, for reference, are the changes in I_{Na} current peak for the single premature impulse (S1S2 = 200 ms) initiated before the double premature impulses. The dashed vertical line indicates the location of the heterogeneity. Note that when $\lambda_{distal}/\lambda_{proximal} = 1.4$ the window of vulnerability is 2–3 ms (S2S3 = 170–171 ms, **A**) and that when $\lambda_{distal}/\lambda_{proximal} = 1.3$ there is no block at the heterogeneity for any S2S3 coupling interval **(B)**.

that measurement techniques that provide local CVs would be more suitable to quantify propagation of premature impulses than techniques that provide global CVs (Linnenbank et al., 2014).

INITIATION OF ARRHYTHMIAS BY EXTERNAL PREMATURE STIMULATION

Regions of heterogeneous Cx43 expression and gap junction conductance have been described in infarcted and failing hearts

(Poelzing and Rosenbaum, 2004; Cabo et al., 2006; Akar et al., 2007), can lead to source/sink mismatch and block of propagation (Kleber and Rudy, 2004), and are likely to provide the "substrate" that leads to initiation of cardiac arrhythmias in diseased hearts. Ventricular tachycardia (VT) can be initiated in clinical electrophysiology laboratories in ∼90% of the patients who suffer spontaneous episodes of VT (Wit and Janse, 1993). Several clinical studies (Wit and Janse, 1993) have shown that premature stimulation with a single premature stimulus can induce VT in 20–30% of the patients; two premature stimuli can increase that number by 55%, and the use of three premature impulses can further increase the number by 20%. All in all clinical evidence shows that the use of multiple premature impulses facilitates the initiation of VT. The failure of single premature impulses to initiate arrhythmias is generally explained by their inability to reach the site of the origin of the arrhythmia (Wit and Janse, 1993). Our results explain those experimental and clinical observations by the different dynamics of propagation of S2 and S3 premature impulses. S2 premature impulses may not be able to reach the site of origin of the arrhythmia (possibly a region with heterogeneous cell-to-cell *Gj*) because they recover their excitability relatively close to the stimulation site and they may not be sufficiently premature (**Figure 5**). In contrast, S3 premature impulses do not recover their excitability as fast as S2 impulses, and may be able to reach the site of origin of the arrhythmia with low values of $|I_{Na,max}|$ (**Figure 11**).

The site(s) where premature stimuli are applied during an electrophysiological study may determine whether clinical VTs are initiated or not. It has been reported that one or two premature stimuli initiated on the right ventricle may not induce all clinical VTs (Robertson et al., 1981; Morady et al., 1984). The yield of clinical VTs increases (more clinical VTs induced) when the same protocol is applied to the left ventricle (Robertson et al., 1981; Morady et al., 1984). It is possible that premature impulses are initiated closer to an area with structural heart disease during left ventricular stimulation than during right ventricular stimulation. That would be consistent with the results above demonstrating that single premature impulses may block at structural heterogeneities when the site of origin of the impulse is close to the heterogeneity (**Figures 6**, **7**) but not when the site of origin is far away (**Figure 5**).

SPONTANEOUS INITIATION OF ARRHYTHMIAS BY PREMATURE IMPULSES

The patterns of spontaneous initiation of sustained VT in post-myocardial infarction patients can be classified according to the morphology and coupling interval of the premature impulse(s) that precedes the tachycardia (Berger et al., 1988; Roelke et al., 1994). In the first pattern, the premature impulses have a morphology that is similar to that of the VT and a long coupling interval with the last sinus beat. Given the long coupling interval of premature impulses and their morphological similarity to the tachycardia, it has been speculated that those premature impulses could be sinus beats entering an infarcted region, conducting slowly in that region and exiting it before the next sinus beat arrives to excite the rest of the ventricle. In the second pattern, the premature impulses have a morphology that is different from that of the VT and a shorter coupling interval with the last sinus beat.

The success of single premature impulses in spontaneously initiating VT depends on the pattern of initiation. For the first pattern (similar morphology, long coupling), ∼70% of VT are initiated by single premature impulses. For the second pattern (different morphology, shorter coupling), only ∼16% of VT are initiated by single premature impulses and the rest by double or multiple premature impulses. While, for the first pattern, premature impulses are considered premature because they excite the ventricle prematurely (i.e., before the next sinus beat arrives), the long coupling intervals are much longer than the ventricular refractory period, and the dynamics of propagation of premature impulses described in this study most likely do not apply. However, for the second pattern, the shorter coupling intervals are likely closer to the refractory period, and the dynamics of propagation of premature impulses shown above explain why single premature impulses alone may not be successful in initiating VT, and two or more premature impulses could be necessary.

Microstructural heterogeneities caused by fibrosis can lead to abnormal propagation as a result of source/sink impedance mismatch in explanted hearts from patients with Brugada syndrome (Coronel et al., 2005; Hoogendijk et al., 2010). Even though the cellular mechanism of the heterogeneity in this study (cell-to-cell *Gj* remodeling) is not fibrosis, it is possible that the dynamics of propagation of premature impulses described here may play a role in the initiation of arrhythmias in Brugada syndrome patients.

CELLULAR MECHANISMS OF PROPAGATION AND BLOCK AT SITES OF MICROSTRUCTURAL HETEROGENEITIES CAUSING SOURCE/SINK IMPEDANCE MISMATCH

In an earlier computational study, we found that, in a model of healthy canine epicardium under conditions of reduced excitability (uniform 70% reduction of maximum I_{Na} conductance), heterogeneities in gap junction conductance or cell size (both parameters of the cellular microstructure contribute to λ) cause unidirectional block when λ in the direction of propagation increases by at least 40% (Toure and Cabo, 2012). We have also shown that heterogeneities in myofibroblast density, whose paracrine effect results in heterogeneities in *Gj*, may also create a substrate leading to unidirectional block (Baum et al., 2012). In particular, block of premature impulses occurred at a heterogeneity between an area with a high (50%) density of myofibroblasts ($\lambda \sim 1.02$ mm) and an area without myofibroblasts ($\lambda \sim 1.32$ mm) (Baum et al., 2012). The results presented here are quantitatively consistent with those earlier results (**Figures 11**, **12**), indicating that a sharp increase in λ by more than 30–40% in the direction of propagation may lead to block during premature stimulation or under conditions of reduced excitability. It seems that the threshold for block is independent of the cellular mechanism causing the change in space constant (gap junction conductance, cell size, myofibroblast density), and may apply to other situations in which cellular and/or tissue remodeling results in a change of λ. For instance, it may explain the conditions for block at the border between two regions with different fiber alignments (Kudryashova et al., 2014). Block would

be expected at a transition from a region where propagation occurs in the direction transverse to the fiber orientation (λ in the direction of propagation $= \lambda_{Trans}$) to a region where propagation occurs in the direction longitudinal to the fiber orientation (λ in the direction of propagation $= \lambda_{Long}$), if $\lambda_{Long}/\lambda_{Trans} > 1.40$.

The density and kinetics of ionic currents are also important determinants of propagation of the action potential at sites of microstructural heterogeneities. Our results show that source/sink impedance mismatch at the site of the heterogeneity causes a decrease in I_{Na} (**Figures 6**, **7**, **11**, **12**). When the value of I_{Na} at the site of the heterogeneity is close to the value necessary to sustain propagation, the L-type Ca current may determine whether propagation succeeds or not (Joyner et al., 1996; Rohr and Kucera, 1997; Rohr et al., 1997; Shaw and Rudy, 1997; Cabo et al., 2000). Consequently, we expect that modulation of the L-type Ca current will play a crucial role in determining successful propagation of premature impulses through microstructural heterogeneities caused by *Gj* remodeling in infarcted myocardium (Cabo et al., 2000).

RESTITUTION OF THE CONDUCTION VELOCITY OF PREMATURE IMPULSES

The difference in the dynamics of propagation of single (S2) and double premature (S3) impulses is reflected in their CV restitution curves (**Figure 8C**). The pronounced maximum slope of the CV restitution curve for S2 indicates a faster recovery of excitability with diastolic interval and propagation. The smaller maximum slope of the restitution curve for S3 indicates a slower recovery of excitability with diastolic interval and propagation. The cumulative experimental and clinical evidence, as well as the computations presented here, indicate that double premature impulses are more pro-arrhythmic than single premature impulses. Therefore, we can argue that a decrease in the maximum slope in the CV restitution curve of a propagating impulse is indicative of an increased potential for block at structural heterogeneities. This is consistent with other reports demonstrating that less steep CV restitution curves were more likely to cause spiral break up (Qu et al., 1999), and that steep CV restitution curves prevent block in heterogeneous tissues (Sampson and Henriquez, 2001).

REFERENCES

Akar, F. G., Nass, R. D., Hahn, S., Cingolani, E., Shah, M., Hesketh, G. G., et al. (2007). Dynamic changes in conduction velocity and gap junction properties during development of pacing-induced heart failure. *Am. J. Physiol. Heart Circ. Physiol.* 293, H1223–H1230. doi: 10.1152/ajpheart.00079.2007

Baba, S., Dun, W., Cabo, C., and Boyden, P. A. (2005). Remodeling in cells from different regions of the reentrant circuit during ventricular tachycardia. *Circulation* 112, 2386–2396. doi: 10.1161/CIRCULATIONAHA.105.534784

Baum, J., Long, B., Cabo, C., and Duffy, H. S. (2012). Myofibroblasts cause heterogeneous Cx43 reduction and are unlikely to be coupled to myocytes in the healing canine infarct. *Am. J. Physiol. Heart Circ. Physiol.* 302, H790–H800. doi: 10.1152/ajpheart.00498.2011

Berger, M. D., Waxman, H. L., Buxton, A. E., Marchlinski, F. E., and Josephson, M. E. (1988). Spontaneous compared with induced onset of sustained ventricular tachycardia. *Circulation* 78, 885–892. doi: 10.1161/01.CIR.78.4.885

Cabo, C., and Boyden, P. A. (2003). Electrical remodeling of the epicardial border zone in the canine infarcted heart: a computational analysis. *Am. J. Physiol. Heart Circ. Physiol.* 284, H372–H384. doi: 10.1152/ajpheart.00512.2002

Cabo, C., and Boyden, P. A. (2009). Extracellular space attenuates the effect of gap junctional remodeling on wave propagation: a computational study. *Biophys. J.* 96, 3092–3101. doi: 10.1016/j.bpj.2009.01.014

Cabo, C., Pertsov, A. M., Baxter, W. T., Davidenko, J. M., Gray, R. A., and Jalife, J. (1994). Wave-front curvature as a cause of slow conduction and block in isolated cardiac muscle. *Circ. Res.* 75, 1014–1028. doi: 10.1161/01.RES.75.6.1014

Cabo, C., Pertsov, A. M., Davidenko, J. M., Baxter, W. T., Gray, R. A., and Jalife, J. (1996). Vortex shedding as a precursor of turbulent electrical activity in cardiac muscle. *Biophys. J.* 70, 1105–1111. doi: 10.1016/S0006-3495(96)79691-1

Cabo, C., Schmitt, H., and Wit, A. L. (2000). New mechanism of antiarrhythmic drug action: increasing the L-type calcium current prevents reentrant arrhythmias in the infarcted canine heart. *Circulation* 102, 2417–2425. doi: 10.1161/01.CIR.102.19.2417

Cabo, C., Yao, J., Boyden, P. A., Chen, S., Hussain, W., Duffy, H. S., et al. (2006). Heterogeneous gap junction remodeling in reentrant circuits in the epicardial border zone of the healing canine infarct. *Cardiovasc. Res.* 72, 241–249. doi: 10.1016/j.cardiores.2006.07.005

Coronel, R. (1994). Heterogeneity in extracellular potassium concentration during early myocardial ischaemia and reperfusion: implications for arrhythmogenesis. *Cardiovasc. Res.* 28, 770–777. doi: 10.1093/cvr/28.6.770

Coronel, R., Casini, S., Koopmann, T. T., Wilms-Schopman, F. J., Verkerk, A. O., de Groot, J. R., et al. (2005). Right ventricular fibrosis and conduction delay in a patient with clinical signs of Brugada syndrome: a combined electrophysiological, genetic, histopathologic, and computational study. *Circulation* 112, 2769–2777. doi: 10.1161/CIRCULATIONAHA.105.532614

Fast, V. G., and Kleber, A. G. (1995). Cardiac tissue geometry as a determinant of unidirectional conduction block: assessment of microscopic excitation spread by optical mapping in patterned cell cultures and in a computer model. *Cardiovasc. Res.* 29, 697–707. doi: 10.1016/S0008-6363(96)88643-3

Frazier, D. W., Wolf, P. D., Wharton, J. M., Tang, A. S. L., Smith, W. M., and Ideker, R. E. (1989). Stimulus induced critical point. mechanism for electrical initiation of reentry in normal canine myocardium. *J. Clin. Invest.* 83, 1039–1052. doi: 10.1172/JCI113945

Gough, W. B., Mehra, R., Restivo, M., Zeiler, R. H., and el-Sherif, N. (1985). Reentrant ventricular arrhythmias in the late myocardial infarction period in the dog. 13. Correlation of activation and refractory maps. *Circ. Res.* 57, 432–442. doi: 10.1161/01.RES.57.3.432

Hoogendijk, M. G., Potse, M., Linnenbank, A. C., Verkerk, A. O., den Ruijter, H. M., van Amersfoorth, S. C., et al. (2010). Mechanism of right precordial ST-segment elevation in structural heart disease: excitation failure by current-to-load mismatch. *Heart Rhythm* 7, 238–248. doi: 10.1016/j.hrthm.2009.10.007

Hubbard, M. L., Ying, W., and Henriquez, C. S. (2007). Effect of gap junction distribution on impulse propagation in a monolayer of myocytes: a model study. *Europace* 9, Suppl. 6, vi20–vi28. doi: 10.1093/europace/eum203

Janse, M. J., and Kleber, A. G. (1981). Electrophysiological changes and ventricular arrhythmias in the early phase of regional myocardial ischemia. *Circ. Res.* 49, 1069–1081. doi: 10.1161/01.RES.49.5.1069

Joyner, R. W. (1981). Mechanisms of unidirectional block in cardiac tissues. *Biophys. J.* 35, 113–125. doi: 10.1016/S0006-3495(81)84778-9

Joyner, R. W., Kumar, R., Wilders, R., Jongsma, H. J., Verheijck, E., Golod, D. A., et al. (1996). Modulating L-type calcium current affects discontinuous cardiac action potential conduction. *Biophys. J.* 71, 237–245. doi: 10.1016/S0006-3495(96)79220-2

Kleber, A. G., and Rudy, Y. (2004). Basic mechanisms of cardiac impulse propagation and associated arrhythmias. *Physiol. Rev.* 84, 431–488. doi: 10.1152/physrev.00025.2003

Kudryashova, N. N., Teplenin, A. S., Orlova, Y. V., Selina, L. V., and Agladze, K. (2014). Arrhythmogenic role of the border between two areas of cardiac cell alignment. *J. Mol. Cell. Cardiol.* 76, 227–234. doi: 10.1016/j.yjmcc.2014.09.003

Linnenbank, A. C., deBakker, J. M. T., and Coronel, R. (2014). How to measure propagation velocity in cardiac tissue: asimulation study. *Front. Physiol.* 5:267. doi: 10.3389/fphys.2014.00267

Morady, F., DiCarlo, L., Winston, S., Davis, J. C., and Scheinman, M. M. (1984). A prospective comparison of triple extrastimuli and left ventricular stimulation in studies of ventricular tachycardia induction. *Circulation* 70, 52–27. doi: 10.1161/01.CIR.70.1.52

Nattel, S., Maguy, A., Bouter, S. L., and Yeh, Y.-H. (2007). Arrhythmogenic ion-channel remodeling in the heart: heart failure, myocardial infarction, and atrial fibrillation. *Physiol. Rev.* 87, 425–456. doi: 10.1152/physrev.00014.2006

Peters, N., Cabo, C., and Wit, A. L. (2000). "Arrhythmogenic mechanisms: automaticity, triggered activity and reentry," in *Cardiac Electrophysiology: from Cell to Bedside*, eds D. Zipes and J. Jalife (Philadelphia, PA: W. B. Saunders Company), 345–356.

Poelzing, S., and Rosenbaum, D. S. (2004). Altered connexin43 expression produces arrhythmia substrate in heart failure. *Am. J. Physiol. Heart Circ. Physiol.* 287, H1762–H1770. doi: 10.1152/ajpheart.00346.2004

Qu, Z., Weiss, J. N. and Garfinkel, A. (1999). Cardiac electrical restitution properties and stability of reentrant waves: a simulation study. *Am. J. Physiol. Heart Circ. Physiol.* 276, H269–H283.

Quan, W., and Rudy, Y. (1990). Unidirectional block and reentry of cardiac excitation: a model study. *Circ. Res.* 66, 367–382. doi: 10.1161/01.RES.66.2.367

Robertson, J. F., Cain, M. E., Horowitz, L. N., Spielman, S. R., Greenspan, A. M., Waxman, H. L., et al. (1981). Anatomic and electrophysiologic correlates of ventricular tachycardia requiring left ventricular stimulation. *Am. J. Cardiol.* 48, 263–268. doi: 10.1016/0002-9149(81)90606-8

Roelke, M., Garan, H., McGovern, B. A., and Ruskin, J. N. (1994). Analysis of the initiation of spontaneous monomorphic ventricular tachycardia by stored intracardiac electrograms. *J. Am. Coll. Cardiol.* 23, 117–122. doi: 10.1016/0735-1097(94)90509-6

Rohr, S., and Kucera, J. P. (1997). Involvement of the calcium inward current in cardiac impulse propagation: induction of unidirectional conduction block by nifedipine and reversal by Bay K 8644. *Biophys. J.* 72, 754–766 doi: 10.1016/S0006-3495(97)78710-1

Rohr, S., Kucera, J. P., Fast, V. G., and Kleber, A. G. (1997). Paradoxical improvement of impulse conduction in cardiac tissue by partial cellular uncoupling. *Science* 275, 841–844. doi: 10.1126/science.275.5301.841

Sampson, K. J., and Henriquez, C. S. (2001). Simulation and prediction of functional block in the presence of structural and ionic heterogeneity. *Am. J. Physiol. Heart Circ. Physiol.* 281, H2597–H2603.

Severs, N. J., Bruce, A. F., Dupont, E., and Rothery, S. (2008). Remodelling of gap junctions and connexin expression in diseased myocardium. *Cardiovasc. Res.* 80, 9–19. doi: 10.1093/cvr/cvn133

Shaw, R. M., and Rudy, Y. (1997). Ionic mechanisms of propagation in cardiac tissue: roles of the sodium and L-type calcium currents during reduced excitability and decreased gap junction coupling. *Circ. Res.* 81, 727–741. doi: 10.1161/01.RES.81.5.727

Spach, M. S., and Heidlage, J. F. (1995). The stochastic nature of cardiac propagation at a microscopic level. Electrical description of myocardial architecture and its application to conduction. *Circ. Res.* 76, 366–380. doi: 10.1161/01.RES.76.3.366

Spach, M. S., and Kootsey, J. M. (1985). Relating the sodium current and conductance to the shape of transmembrane and extracellular potentials by simulation: effects of propagation boundaries. *IEEE Trans. Biomed. Eng.* 32, 743–755. doi: 10.1109/TBME.1985.325489

Spach, M. S., Miller, W. T., Dolber, P. C., Kootsey, J. M., Sommer, J. R., and Mosher, C. E. (1982). The functional role of structural complexities in the propagation of depolarization in the atrium of the dog. Cardiac conduction disturbances due to discontinuities of effective axial resistivity. *Circ. Res.* 50, 175–191. doi: 10.1161/01.RES.50.2.175

Toure, A., and Cabo, C. (2010). Effect of cell geometry on conduction velocity in a subcellular model of myocardium. *IEEE Trans. Biomed. Eng.* 57, 2107–2114. doi: 10.1109/TBME.2010.2050064

Toure, A., and Cabo, C. (2012). Effect of heterogeneities in the cellular microstructure on propagation of the cardiac action potential. *Med. Biol. Eng. Comput.* 50, 813–825. doi: 10.1007/s11517-012-0934-4

Wit, A. L., and Janse, M. J. (1993). *The Ventricular Arrhythmias of Ischemia and Infarction: Electrophysiological Mechanisms*. Mount Kisco, NY: Futura Publishing Company.

Conflict of Interest Statement: The author declares that the research was conducted in the absence of any commercial or financial relationships that could be construed as a potential conflict of interest.

Received: 05 October 2014; accepted: 25 November 2014; published online: 16 December 2014.

Citation: Cabo C (2014) Dynamics of propagation of premature impulses in structurally remodeled infarcted myocardium: a computational analysis. Front. Physiol. ***5****:483. doi: 10.3389/fphys.2014.00483*

This article was submitted to Cardiac Electrophysiology, a section of the journal Frontiers in Physiology.

frontiers in PHYSIOLOGY

ORIGINAL RESEARCH ARTICLE
published: 07 August 2014
doi: 10.3389/fphys.2014.00275

Na^+ current expression in human atrial myofibroblasts: identity and functional roles

Jussi T. Koivumäki[1], Robert B. Clark[2], Darrell Belke[2], Colleen Kondo[2], Paul W. M. Fedak[3], Mary M. C. Maleckar[1] and Wayne R. Giles[2]*

[1] *Simula Research Laboratory, Center for Biomedical Computing and Center for Cardiological Innovation, Oslo, Norway*
[2] *Faculty of Kinesiology, University of Calgary, Calgary, AB, Canada*
[3] *Division of Cardiothoracic Surgery, Department of Cardiac Sciences, University of Calgary, Calgary, AB, Canada*

Edited by:
George E. Billman, The Ohio State University, USA

Reviewed by:
Ruben Coronel, Academic Medical Center, Netherlands
George E. Billman, The Ohio State University, USA

****Correspondence:***
Wayne R. Giles, Faculty of Kinesiology, University of Calgary, 2500 University Drive NW, Calgary, AB T2N 1N4, Canada
e-mail: wgiles@ucalgary.ca

In the mammalian heart fibroblasts have important functional roles in both healthy conditions and diseased states. During pathophysiological challenges, a closely related myofibroblast cell population emerges, and can have distinct, significant roles. Recently, it has been reported that human atrial myofibroblasts can express a Na^+ current, I_{Na}. Some of the biophysical properties and molecular features suggest that this I_{Na} is due to expression of Na_v 1.5, the same Na^+ channel α subunit that generates the predominant I_{Na} in myocytes from adult mammalian heart. In principle, expression of Na_v 1.5 could give rise to regenerative action potentials in the fibroblasts/myofibroblasts. This would suggest an active as opposed to passive role for fibroblasts/myofibroblasts in both the "trigger" and the "substrate" components of cardiac rhythm disturbances. Our goals in this preliminary study were: (i) to confirm and extend the electrophysiological characterization of I_{Na} in a human atrial fibroblast/myofibroblast cell population maintained in conventional 2-D tissue culture; (ii) to identify key molecular properties of the α and β subunits of these Na^+ channel(s); (iii) to define the biophysical and pharmacological properties of this I_{Na}; (iv) to integrate the available multi-disciplinary data, and attempt to illustrate its functional consequences, using a mathematical model in which the human atrial myocyte is coupled via connexins to fixed numbers of fibroblasts/myofibroblasts in a syncytial arrangement. Our experimental findings confirm that a significant fraction (approximately 40–50%) of these human atrial myofibroblasts can express I_{Na}. However, our data suggest that I_{Na} may be generated by a combination of Na_v 1.9, Na_v 1.2, and Na_v 1.5. Our results, when complemented with mathematical modeling, provide a background for re-evaluating pharmacological management of supraventricular rhythm disorders, e.g., persistent atrial fibrillation.

Keywords: Na^+ current, atrial arrhythmias, mathematical models, fibroblast, myofibroblast

INTRODUCTION

Within approximately the last 10 years, experimental results and clinical data have established that both fibroblast and myofibroblast cell populations in the mammalian heart (including the adult human) can play very important functional roles in physiological and pathophysiological settings, respectively (Nattel, 2002; Baudino et al., 2006; Munoz et al., 2008; Porter and Turner, 2009; Baum and Duffy, 2011; Biernacka and Frangogiannis, 2011). The fibroblast population, when judged in terms of cell numbers, is predominant in all adult mammalian hearts (cf. Baudino et al., 2006). Until quite recently, these fibroblasts were considered to be passive. That is, they were thought to have few, if any primary electrophysiological roles. Rather, both fibroblasts and myofibroblasts were believed to function predominantly in the synthesis, and degradation (homeostasis) of the extracellular matrix, largely as a consequence of their roles in collagen production/breakdown (Weber et al., 1993). However, this view changed after publication of data demonstrating that both fibroblasts and myofibroblasts have the capability of communicating (cell-to-cell) electrically and metabolically through conventional connexins within gap junctions. This connexin-mediated electrotonic communication may also include functional interactions of these fibroblasts/myofibroblasts with adjacent myocytes (Gaudesius et al., 2003; Chilton et al., 2007; Zlochiver et al., 2008; Kakkar and Lee, 2010). It is now apparent that both the fibroblast and the myofibroblast cell populations can serve as a significant source of paracrine substances that, when secreted, act on adjacent cells (Powell et al., 1999; Pedrotty et al., 2009; Rohr, 2011). Both fibroblasts and myofibroblasts can also be regulated by neurotransmitters, co-transmitters, peptides, and circulating hormones (Brilla et al., 1995; Rose et al., 2007; cf. Rose and Giles, 2008). Important early work on isolated fibroblasts also drew attention to the fact that the electrophysiological properties of these cells can be modulated significantly by mechanical perturbations, including both stretch and shear forces. Abramochkin et al. (2014) have recently reviewed this data.

Experimental work, based mainly on co-culture methods, combined with simulations using mathematical models of, e.g., human atrial myocytes and fibroblasts, have drawn attention to the possibility that the fibroblast cell population could significantly modulate the electrophysiological substrate in a number of cardiac tissues. Papers that deal specifically with these interactions in the atria include: (Maleckar et al., 2009a; Ashihara et al., 2012; McDowell et al., 2013) and ventricles (MacCannell et al., 2007; Sachse et al., 2008; McDowell et al., 2011) of the human heart. However, in all cases, these interactions have been assumed to be passive; that is, to not involve any regenerative or propagated responses that originate in the fibroblast/myofibroblast cell population (Gaudesius et al., 2003; Maleckar et al., 2009a; McDowell et al., 2011, 2013).

Important early work on atrial rhythm disturbances by Spach and his colleagues (Spach and Boineau, 1997) drew attention to the ability of "microfibrosis" to alter the electrical substrate in the atrium and thus promote arrhythmias. Spach et al. (2007) also recognized that in the human atrium an important consequence of aging was an increased incidence of supraventricular rhythm disturbances with some fibrosis. Enhanced fibrosis in the setting of healthy aging is now a well-known contributor to atrial flutter/fibrillation (Nattel, 2002; Biernacka and Frangogiannis, 2011; Diness et al., 2011; Guzadhur et al., 2012).

Recently, it has been reported that myofibroblasts derived from explanted human right atrial tissue (the right atrial appendage) can express measurable (and potentially functionally important) Na^+currents. Specifically, Chatelier et al. (2012) have reported that approximately 75% of the myofibroblasts that are isolated from the human right atrial appendage express Na^+ current after being maintained in a primary 2-D cell culture 8–12 days. They observed that 100% of these cells expressed Na^+ current after 13–17 days in culture. These investigators have also provided evidence that this Na^+ current is generated by the same Na^+ channel α subunit, Na_v 1.5 that produces the Na^+ current in the atria and ventricles of the adult human heart.

After the properties of this Na^+-selective integral membrane protein in fibroblasts/myofibroblasts are understood more completely, a paradigm shift concerning the functional properties of human cardiac syncytium in both health and disease may be required. As an example, the expression of Na_v 1.5 in this cell population raises the possibility that the myofibroblast cell population could be the source of ectopic foci. That is, this Na^+ current could provide a significant source of regenerative inward current. In principle, the resulting depolarization could serve both as the trigger and the substrate for supraventricular rhythm disturbances originating in the fibroblast/myofibroblast cell population.

The main focus of our study was to complement and extend the Chatelier et al. (2012) findings by addressing four separate, but related, objectives:

(i) To carry out whole-cell voltage clamp experiments and obtain the additional data that is needed for determining the probability that measurable Na^+ currents, I_{Na}, in fact can be recorded in single myofibroblasts from the human right atrial appendage, in situations where these cells are isolated, purified, and maintained in conventional 2-D culture.

(ii) To further define the functional roles of I_{Na} based on its fundamental biophysical properties, e.g., voltage-dependence of activation and inactivation.

(iii) To make PCR measurements aimed at identifying mammalian Na^+ channel α and β subunits in this myofibroblast cell population.

(iv) To integrate and illustrate the consequences of the Chatelier et al. (2012) findings and compare them with our results, through implementation of current mathematical models of the human atrial myocyte action potential coupled to a defined fibroblast/myofibroblast electrophysiological parameter set, and then to study these interactions *in silico* in selected ratios (myocytes/myofibroblasts) and coupling configurations.

Here, we report our preliminary findings based on conventional whole-cell voltage-clamp measurements of the electrophysiological properties of single myofibroblasts that were isolated from the human right atrial appendage and then placed in conventional 2-D tissue culture for approximately 6 days (2–4 passages). PCR analyses of the expression of a number of α and β subunits of mammalian Na^+ channels are also presented. Our results are compared and contrasted with those in the original paper on this topic (Chatelier et al., 2012). Mathematical models of the human atrial myocyte and/or the fibroblast/myofibroblast are used to explore and illustrate plausible functional consequences of Na^+ current expression in the myofibroblast population.

Taken together, this experimental and theoretical work contributes to ongoing discussions regarding possible functional roles for Na^+ current in human atrial myofibroblasts. These findings also raise interesting possibilities and questions concerning novel molecular targets in the compromised human atrium, e.g., during persistent atrial fibrillation (Benito et al., 2008; Biernacka and Frangogiannis, 2011; Aguilar-Shardonofsky et al., 2012). This class of rhythm disturbance is of importance due to its increased incidence during the healthy aging process (Benito et al., 2008; Aguilar-Shardonofsky et al., 2012; Guzadhur et al., 2012); and because persistent atrial fibrillation can increase the incidence of transient ischemic attack and/or stroke (cf. Bersohn et al., 2012).

METHODS

HUMAN RIGHT ATRIAL APPENDAGE TISSUE

Excised human atrial appendage specimens were obtained after written consent from patients undergoing coronary artery bypass graft surgeries at Foothills Medical Centre. Administrative approval was granted to the Fedak Laboratory by the University of Calgary Conjoint Health Ethics Board. After being transported to the Fedak Laboratory, each preparation was subjected to enzymatic treatment resulting in release of atrial fibroblasts, as described in previous papers from the Fedak Group (cf. Fedak et al., 2012).

CELL CULTURE METHODS

At selected times, (2 days to 2 weeks), populations of these myofibroblasts were transferred to the Giles Laboratory where they

were maintained in conventional 2-D culture for an additional 1–2 days. As required, cells were released by enzymatic treatment (trypsinization) and then used for electrophysiological studies on that same day.

ISOLATION OF MYOFIBROBLAST RNA AND TARGETED PCR ANALYSES

Messenger RNA was isolated from these cultured human atrial fibroblasts using a Qiagen RNeasy kit, and transformed into cDNA using Qiagen Quantitect reverse transcriptase kit according to the manufactures protocol. Real time-PCR analysis was performed using Quantitect SYBR Green Master Mix and primer pairs on a BioRad iCycler. Gene expression levels were calculated using the delta-delta CT method with 18s RNA serving as the housekeeping gene. Values represent the mean ± s.e.m. of three individual cell cultures performed in duplicate measurements. The primers for the analysis of human alpha and beta sodium channel subunits were generated at the University of Calgary DNA lab and BLASTed against the human genome to ensure 100% specificity against the targeted genes. To assess the possibility that expression of neonatal isoforms of the cardiac Na^+ channel were upregulated, SCN5A, or $Na_v1.5$, mRNA expression measurements were separated into primers recognizing splice variants 1 and 2, and primers recognizing variants 3 through 6 (see **Table 1**).

ELECTROPHYSIOLOGICAL METHODS

A small piece of coverslip with adherent cells was placed in a 200 µL recording chamber on the stage of an inverted microscope, where it was superfused with a HEPES-buffered solution (see below) at a rate of about 1 ml/min. The temperature was maintained at 20–22°C.

Membrane currents were measured in single human atrial myofibroblasts using whole-cell "patch clamp" techniques. Cells that were isolated from their neighbors, and lacked obvious connections to surrounding cells, were chosen for patch clamp recordings. Patch pipettes were pulled from borosilicate capillaries, and had a d.c. resistance of 4–9 MΩ when filled with pipette solution. Recordings of membrane current were made with a Multi-Clamp 700A amplifier (Molecular Devices; Sunnyvale, CA, USA). At least 75% series resistance compensation was used (series resistance <5 MΩ). When recording Na^+ currents in the absence of K^+ currents, a P/4 subtraction protocol was used to remove leak currents and reduce uncompensated capacity transient currents. Signals were digitized with a 1322A Digi-Data acquisition system (Molecular Devices), stored on a microcomputer and analyzed offline with pClamp v.8. Plots and statistical analysis were done with "Sigmaplot" (Systat Software; San Jose, CA, USA or "Prism" Graphpad Software, La Jolla, CA, USA).

Current-voltage relations for the global transmembrane ionic current expressed in single human atrial myofibroblasts were obtained using a series of 200 ms voltage clamp steps from −120 to +100 mV (see **Figure 1**). For Na^+ currents, a series of 100 ms steps from −50 to +40 mV (see **Figure 2**) were applied at 0.1 Hz. Steady-state inactivation of Na^+ current was determined with a two-step protocol consisting of a 500 ms "conditioning"

Table 1 | Primer sequences for PCR analyses of human atrial myofibroblast Na^+ channel complex transcripts.

Channel	Gene	Forward	Reverse
Na_V 1.1	SCN1A	ctccccacaccagtctttgt	tggtctgactcaggttgctg
Na_V 1.2	SCN2A	gccagcttatcaatcccaaa	tcttctgcaatgcgttgttc
Na_V 1.3	SCN3A	gtagtggtgcattggccttt	gcaccgagttctgagtagcc
Na_V 1.4	SCN4A	ttcacaggcatcttcacagc	ggaaggagcgtagcacagac
Na_V 1.5	SCN5A Var 1,2	cttcaccgccatttacacct	tgcgtaaggctgagacattg
Na_V 1.5	SCN5A Var 3,4,5,6	cttcaccgccatttacacct	aagttcgaagagccgacaaa
Na_V 1.6	SCN8A	tggacatccttttgccttc	ctgcaggaccactgcagata
Na_V 1.7	SCN9A	ccacttcatccaccacctct	actgcactgccttcgagaat
Na_V 1.8	SCN10A	tctttgcagcttcttcagca	acccacacagtcggattagc
Na_V 1.9	SCN11A	cccagcagctgttaaaggag	ctgggacagtcgtttggttt
$Na_V\beta$ 1	SCN1B	tgcgctatgagaatgaggtg	atcttcttgacgacgctggt
$Na_V\beta$ 2	SCN2B	tgacccactctcttccatcc	caccaggtcctctctgaagc
$Na_V\beta$ 3	SCN3B	ccacacacccagacttcctt	tcctgcaaagatgcagtgac
$Na_V\beta$ 4	SCN4B	cccccacagtcttccaagta	gagagcagaggagcaggcta

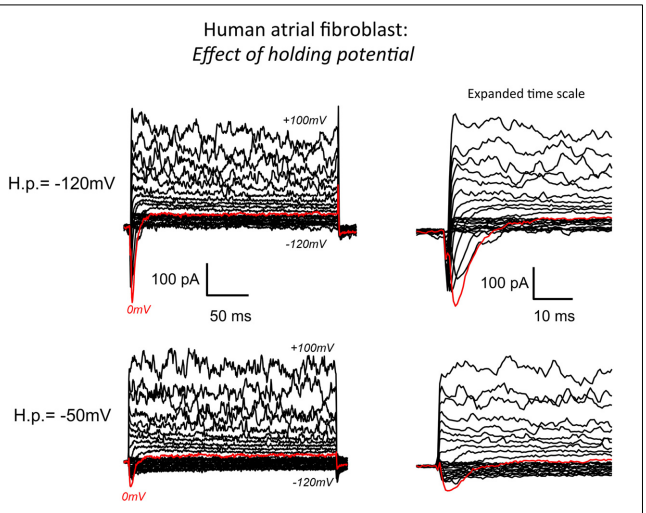

FIGURE 1 | Whole cell patch clamp records of the predominant transmembrane ionic currents recorded from an isolated human atrial myofibroblast using our standard superfusion solution at 22–23°C. The pipette solution in this experiment was "K^+-rich." (See Methods for details of solutions and voltage-clamp protocols). The superimposed current records in the bottom left panel are typical of the data recorded when the voltage clamp "holding potential" (−50 mV) was set near the presumed resting membrane potential of the myofibroblast (approximately −40 mV). As shown, membrane depolarizations in the voltage range from about +20 to 100 mV resulted in a large "noisy" outward current that is likely generated by Ca^{2+}-activated K^+ channels. In this and most other recordings, hyperpolarization from HP −50 mV produced only very small current changes (see Chilton et al., 2007). Note, however, that depolarizing steps did elicit (red trace) a small but distinct transient inward current. The same records at an expanded time scale are shown on the right. The data in the top panel were obtained in response to the same levels of step depolarizations applied from a holding potential of −120 mV. As expected from the fundamental biophysical properties of a voltage-dependent Na^+ (or Ca^{2+}) current this hyperpolarized HP "unmasked" a much more prominent transient inward current (see Results).

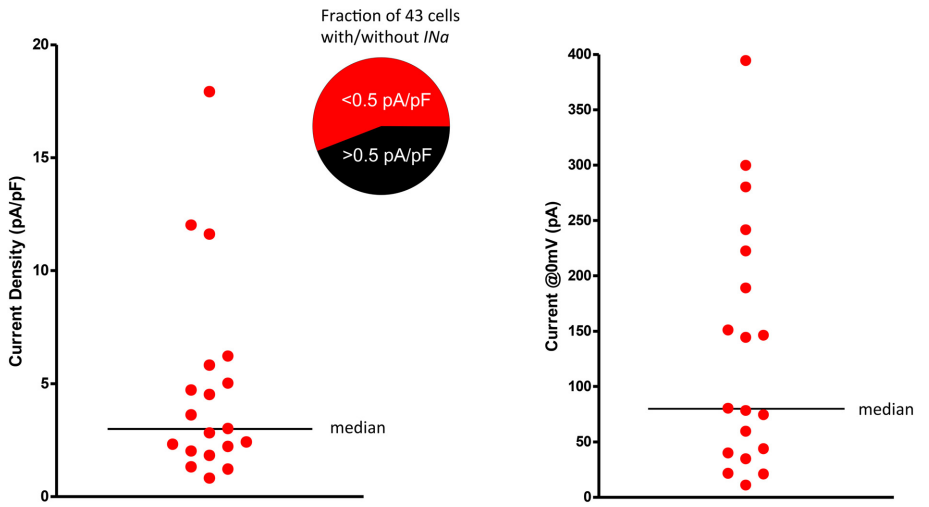

FIGURE 2 | Scatter plots illustrating the significant range of values of functional Na^+ current expression in isolated human atrial myofibroblasts ($n = 19$ cells). The data in the left panel summarizes these findings as current densities, i.e., by expressing I_{Na} values (recorded in response to depolarization to 0 mV) normalized for cell (myofibroblast) capacitance (mean ± s.e.m.; 30.8 ± 4.9 pF). The same data set is presented in the right panel as peak I_{Na} at 0 mV. Horizontal bars in both plots indicate the median value of each distribution.

clamp step to −120 mV, followed by a "test" step to −10 mV. Cell capacitance was obtained from the displacement current transient produced by a +10 mV step from the holding potential (HP) −40 mV, which was close to the apparent resting membrane potential of these cells (see Discussion).

Analar grade chemicals (Sigma-Aldrich) were used to make all solutions. "Standard" external solution consisted of (mM): NaCl, 140; KCl, 5; $CaCl_2$, 2; $MgCl_2$, 1; HEPES, 10; glucose, 5.5; mannitol, 15. pH was adjusted to 7.4 with NaOH. K^+-rich "internal" (pipette) solution consisted of (mM): K-aspartate, 100; KCl, 20; $MgCl_2$, 1; Na2ATP, 4; $CaCl_2$, 0.85; EGTA, 5; HEPES, 10. pH was adjusted to 7.2 with KOH. The approximate pCa of the solution was 7.9. Cs^+-rich pipette solution, used to isolate Na^+ currents, consisted of Cs-aspartate, 100; CsCl, 30; $MgCl_2$, 1; Na2ATP, 4; $CaCl_2$, 0.85; EGTA, 5; HEPES, 10. pH was adjusted to 7.2 with CsOH.

MATHEMATICAL MODELING OF THE HUMAN ATRIAL ACTION POTENTIAL AND MYOFIBROBLAST/MYOCYTE INTERACTIONS

Mathematical modeling was done using a combination of (i) the Koivumäki et al. model (2011) of the human atrial action potential and intracellular $[Ca^{2+}]_i$ changes, and (ii) the "active" model of the human atrial myofibroblast described in detail in Maleckar et al. (2009a,b). For our simulations, the mathematical expression for the inwardly rectifying background K^+ current, I_{K1}, in the fibroblast originally developed by MacCannell et al. (2007) was modified. This was done so that this important non-linear background current, and its contribution to the fibroblast resting potential could be simulated more accurately. Specifically, the equation for I_{K1} in Nygren et al. (Nygren and Giles, 2000) was used, and I_{K1} current density was scaled for the size (capacitance) of the fibroblast. This adjustment required a directly related small change in the size of the Na^+/K^+ pump current.

Three variants of this myofibroblast/atrial myocyte model were used in the simulations shown in **Figures 6–8**:

- V_o: the original model developed by Maleckar et al. (2009a) with I_{K1} modified as described.
- V_1: V_o with the addition of a Na^+ current based on the electrophysiological data shown in **Figures 1–4**.
- V_2: V_o after Na^+ current was parameterized based on the *in vitro* data published by Chatelier et al. (2012), as opposed to our data.

The illustrations in **Figures 6–9** were generated by using these myocyte/myofibroblast models, assuming connexin-mediated electrotonic cell-to-cell communication with an assumed gap junctional conductance of 0.5 nS. This value corresponds to the lower end of those measured between fibroblast-myocyte pairs *in vitro* (Maleckar et al., 2009a,b).

In addition to a 1:1 myocyte-myofibroblast coupling scheme, two slightly more complex sets of starting conditions were explored in these simulations. Either 3 or 9 myofibroblasts were connected in series to 1 myocyte. Based on our findings that only approximately 30–50% of the isolated myofibroblasts express a measurable Na^+ current, only approximately one third of these myofibroblasts models were programmed to express a Na^+ current with the properties in **Figures 1–4** (model variant V_1).

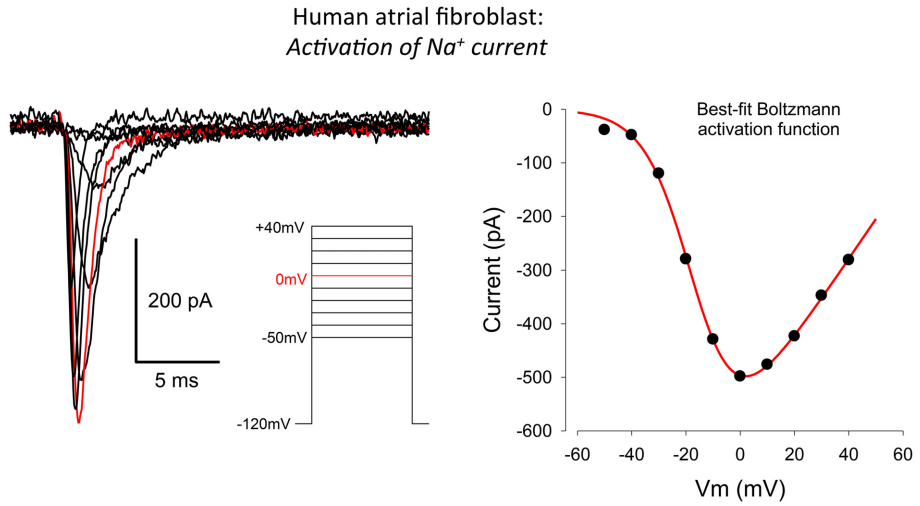

FIGURE 3 | Whole-cell voltage clamp records illustrating the activation of the transient inward Na^+ current in human atrial myofibroblasts. Raw data (10 superimposed current records) elicited by 100 ms depolarizing clamp steps from −50 to +40 mV are shown; the red trace indicates the current elicited at 0 mV. The voltage clamp protocol is shown in the inset. The plot in the right-hand panel is an I–V curve. It was constructed by plotting the peak inward current at each selected voltage clamp depolarization level. The patch pipette solution in this experiment was Cs^+-rich (Methods), to block the large and rapidly activating I_{K-Ca}, which obscured I_{Na} at potentials positive to about +30 mV (see **Figure 1** and text in Results).

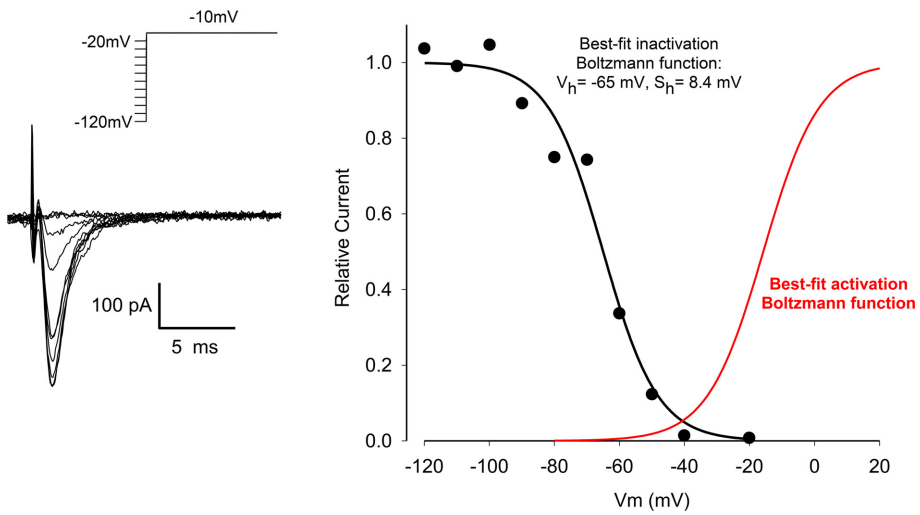

FIGURE 4 | Steady-state voltage-dependence of inactivation of I_{Na} in a human atrial myofibroblast (same cell as in Figure 3). The superimposed current records in the left panel were obtained in response to the conventional two-step voltage clamp protocol that is illustrated in the inset (500 ms "conditioning" step from −120 mV, "test" step to −20 mV). Peak inward I_{Na} values are plotted in the right-hand panel (continuous black curve) vs. the conditioning or prepulse potential. These results reveal a conventional inactivation relationship for I_{Na} in an adult mammalian myocyte with the half-inactivation membrane potential and maximum slope at $V_{1/2}$being −65 and 8.4 mV, respectively. The relationship shown in red—a derived voltage-dependent activation curve—is based on the data in **Figure 2**. See Results for further, more detailed description.

RESULTS

A conventional whole-cell patch clamp method was used to characterize the predominant transmembrane ionic currents in these single isolated human atrial myofibroblasts. Representative families of membrane currents are shown in **Figure 1**. In this myofibroblast and in the majority of others that were studied, voltage clamp depolarizations resulted in rapid activation of a small outward current. Larger depolarizations (in the +60 to +100 mV range) consistently gave rise to large "noisy" transmembrane records, that are characteristic of Ca^{2+}-activated K^+

currents. In contrast, hyperpolarizing clamp steps from the holding potential produced much smaller changes in transmembrane current, similar to the pattern that has been reported in rat ventricular fibroblasts/myofibroblasts (Chilton et al., 2005).

A main focus of this study was to determine whether transient inward Na^+ currents could be detected in these myofibroblasts. For this reason, families of transmembrane currents were generated from two different holding potentials. After each cell was voltage clamped near the resting potential, the holding potential was set to −50 mV, and step depolarizations lasting 100 ms were applied in 10 mV increments covering the range of membrane potentials −120 mV to +100 mV. As shown in the bottom row of **Figure 1**, this protocol produced small but measurable transient inward currents (indicated by the red traces). To enhance the likelihood of detecting Na^+ current, and to attempt to record the maximum transient inward Na^+ current that could be generated by each individual myofibroblast, the holding potential was then set to −120 mV. Transmembrane currents, in response to the same levels of depolarization, were elicited. These families of currents are shown in the top row of **Figure 1**. As expected (as a consequence of the more hyperpolarized holding potential removing inactivation), this maneuver resulted in significantly larger transient inward currents (see red traces). This type of protocol was applied to 40 myofibroblasts in total: the data indicate that approximately 50% of these isolated myofibroblasts express a measurable transient inward current, when the holding potential was −120 mV (see Discussion).

In this series of experiments, it became apparent that there was considerable variability in the expression levels of these Na^+ currents. The scatterplots in **Figure 2** illustrate and summarize this variability. Note that when the transient inward Na^+ current is measured, either in terms of current density (left) in response to a depolarization to 0 mV or plotted as peak current, (right) there is very significant heterogeneity or scatter. The average current density at 0 mV was approximately 3 pA/pF when the holding potential was −120 mV.

The raw data (left) and current-voltage relationship (right) in **Figure 3** provide useful information concerning the peak size, as well as the activation and inactivation kinetics, and the voltage-dependence of this peak inward current in the human atrial myofibroblast, respectively. The family of currents shown in the left panel of **Figure 3** was obtained by applying rectangular voltage clamp depolarizations from a holding potential of −120 mV, as illustrated in the inset. The peak current in response to this step-depolarization to 0 mV is highlighted in red. This current trace provides a point of reference for the summarized data described in **Figure 2**.

A representative peak inward current-voltage relationship is shown in the right panel of **Figure 3**. Note that this inward current first activates at a membrane potential near −50 mV, and that it is maximal near 0 mV. The positive limb of this I–V curve could not be obtained in its entirety due to the rapid activation of a substantial and noisy outward current (see **Figure 1**) at membrane potentials positive to approximately +50 mV. Overall, this pattern of current changes closely resembles families of currents and peak current-voltage relationships that have been published for Na^+ current in cardiac myocytes. This includes myocytes from human atrium (Baba et al., 2006), and data based on heterologous expression, when the α subunit of the cardiac Na^+ channel, Na_v 1.5 is overexpressed in mammalian cell lines, and then studied with conventional patch clamp methods.

The raw data and corresponding analysis shown in **Figure 4** summarize our experimental measurements of the steady-state inactivation characteristics of the Na^+ current in these human atrial myofibroblasts. A conventional two-step voltage clamp protocol was used to progressively inactivate this Na^+ current. From a holding potential of −120 mV, a relatively long "inactivating" prepulse (500 ms) was applied, and this was followed immediately by a second step-depolarization to −10 mV. As expected and as illustrated in the superimposed currents in the left panel, when the prepulse voltage depolarized the cell beyond approximately −40 mV, peak Na^+ current decreased progressively. This voltage-dependent inactivation was characterized over the entire physiological range of membrane potentials, as shown in the plot in the right panel of this Figure. The best-fit parameters for this steady-state inactivation relationship were: membrane potential for half an activation or V_h −65 mV, and maximum slope factor 8.4 mV. In this panel of **Figure 4**, the sigmoid relationship shown in red is a derived relationship depicting voltage-dependent activation for the Na^+ currents shown in **Figure 3** (right).

These electrophysiological findings are somewhat similar to those in the original paper on this topic (Chatelier et al., 2012). Certainly, both data sets reveal the functional expression of Na^+ channels in tissue cultured human atrial myofibroblasts.

Additional molecular evidence for the expression of Na^+ channels in these human atrial myofibroblasts is presented in **Figure 5**. These histograms are based on our PCR analyses of the relative expression levels of a range of human Na^+ channel (SCN-5) α and β subunits. From panel A note the two strongest α subunit signals are for the "nerve" Na^+ channels SCN9A and SCN2A, respectively. However, the predominant (TTX-insensitive) mammalian heart α subunit was also be detected. **Figure 5B** presents analogous PCR data directed toward Na^+ channel β subunits. Here, the β_1 subunit represents the predominant signal (see Discussion).

Our data (**Figures 1–5**) and the Chatelier et al. publication (2012) that first reported functional expression of Na^+ current in human atrial myofibroblasts suggest the possibility that these cells may be able to exhibit regenerative, action potential-like responses when appropriate depolarizing stimuli are applied. **Figures 6–8** illustrate the results of *in silico* tests of this possibility.

For these simulations, two quite different starting conditions were chosen: (i) the myofibroblast was assumed to have a resting membrane potential E_m of −35 mV, and (ii) the myofibroblast E_m values were set at −60 mV. This was done in recognition of the uncertainty of the fibroblast resting potential *in situ* (see Discussion), and because the Na^+ current is inactivated almost completely at −35 mV. In both cases, selected 16 ms de- and hyperpolarizing stimuli were applied intracellularly, as diagrammed in **Figure 6A**.

The results in **Figures 6B,C** illustrate the responses when the myofibroblast was stimulated from a steady membrane

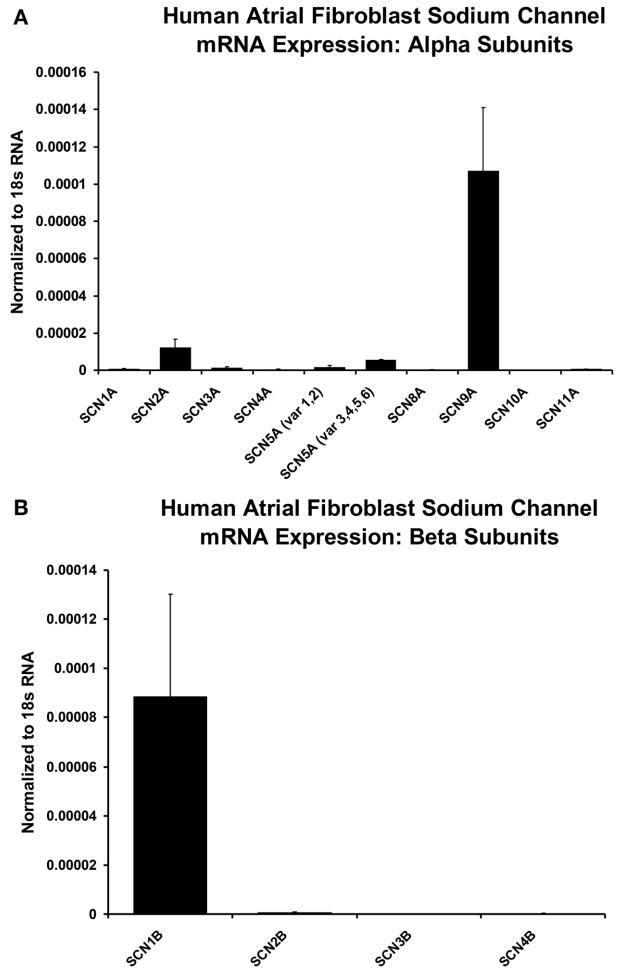

FIGURE 5 | Histograms of normalized data from PCR measurements of relative levels of Na^+ channel α and β subunits, based on RNA derived from populations of isolated human atrial myofibroblasts maintained in 2-D tissue culture. Note from panel **(A)** the predominant α subunits are SCN9A and SCN2A; Panel **(B)** shows that the strongest β subunit signal is for β_1. However, the cardiac isoform of Na^+ current α subunit, SCN5A, also can be detected (see Discussion). Sample size for mRNA measurements are from $n = 3$ individual samples for plated and collagen treated fbs (only plated values are shown). The statistical analysis was based on the difference between plated and collagen treated cells, with a simple unpaired *t*-test to compare gene expression under the two conditions.

potential of −35 mV, and no I_{Na} was introduced/expressed. As expected, the myofibroblast membrane potential responds to small rectangular stimuli with a quasi-exponential electrotonic de- or hyperpolarization, having characteristic time-courses governed approximately by the product of the mean input resistance (3–5 Gigohms) and single cell capacitance (6–10 pF). Note that the original mathematical model of the myofibroblast employed in these simulations (MacCannell et al., 2007) includes a rapidly activating delayed rectifier K^+ current, in accordance with experimental data from rat ventricular myofibroblasts. This K^+ current is activated when E_m depolarizes positive to approximately −30 mV. Indeed, the myofibroblast exhibits a partial repolarization (top trace, panel B) at positive membrane voltages (approximately 0 mV). In addition, a post-stimulus hyperpolarization due to the subsequent deactivation of this K^+ current was observed. The results in **Figure 6D,E** were obtained using the same 4 constant current stimuli (panel A) after the Na^+ current (identified in our study; **Figures 1–4**) was introduced. Note (panel **E**) that there is a tendency for regenerative depolarization in the voltage responses corresponding to all 3 depolarizing stimuli when E_m is set at −65 mV. The data in panels **F** and **G** is analogous to that in panels **D** and **E**, except that in these simulations I_{Na} equations that replicate the Na^+ current described by Chatelier et al. (2012) have been "introduced" into the myofibroblast.

In the next two sets of computational studies, a mathematical model of the human atrial myocyte was combined with the modified mammalian myofibroblast model that is described in Methods. Three sets of computations were done: (i) a fixed number of *in silico* myofibroblasts were coupled to a single human atrial myocyte through a linear resistance corresponding to a conductance of 0.5 nS. These results are shown in the left column, panels **B**,**E**,**H** of **Figure 7**. (ii) In the second set of computations, Na^+ current consistent with the biophysical properties depicted in **Figures 1–4** in this paper was introduced into the myofibroblast cell population. These results are shown in the middle column, or panels **C**, **F**, and **I** of **Figure 7**. (iii) Finally, an analogous set of computations was done, this time using the Na^+ current having the biophysical properties reported by Chatelier et al. (2012). In **Figure 7**, these computations are shown in the third column, or panels **D**,**G**,**J**. For a reference and starting point, panel **A** shows the atrial myocyte resting potential and action potential waveform (red); and also illustrates the assigned myofibroblast resting potential when these two types of cells are *not* coupled. Overall, this pattern of responses was *not* particularly revealing with respect to Na^+-current dependent patterns of action potential waveforms or the electrotonic responses in the myofibroblast population. Specifically, the expression of Na^+ current in the myofibroblast appeared to have *no* significant effects on the electrotonic waveform.

Note, however, that an important variable was that the myofibroblast resting membrane potential was initially set to that reported for these isolated cells, namely approximately −35 mV. After coupling in the 1:1 (panels **B–D**) and 1:3 (panels **E–G**) cases the fibroblast hyperpolarized and experienced a significant electrotonic depolarization and repolarization driven by the myocyte action potential. In the case of 1:9 ratio coupling (panels **H–J**) the atrial myocyte depolarized significantly and exhibited only a weak regenerative response, which resulted in a small electrotonic depolarization in the myofibroblast(s). We note that when the resting potential in either the myocyte or the fibroblasts is positive to approximately −60 mV, I_{Na} would be strongly inactivated (see **Figure 4**), and thus would not contribute to the membrane voltage profile in the myofibroblast or the immediately adjacent myocyte.

After recognizing that the resting membrane potential of the myofibroblast was a critically important determinant of the size of the peak inward Na^+ current, a second set of computations was carried out with the membrane potential of the myofibroblast set to approximately −65 mV, rather than −35 mV. In **Figure 8**,

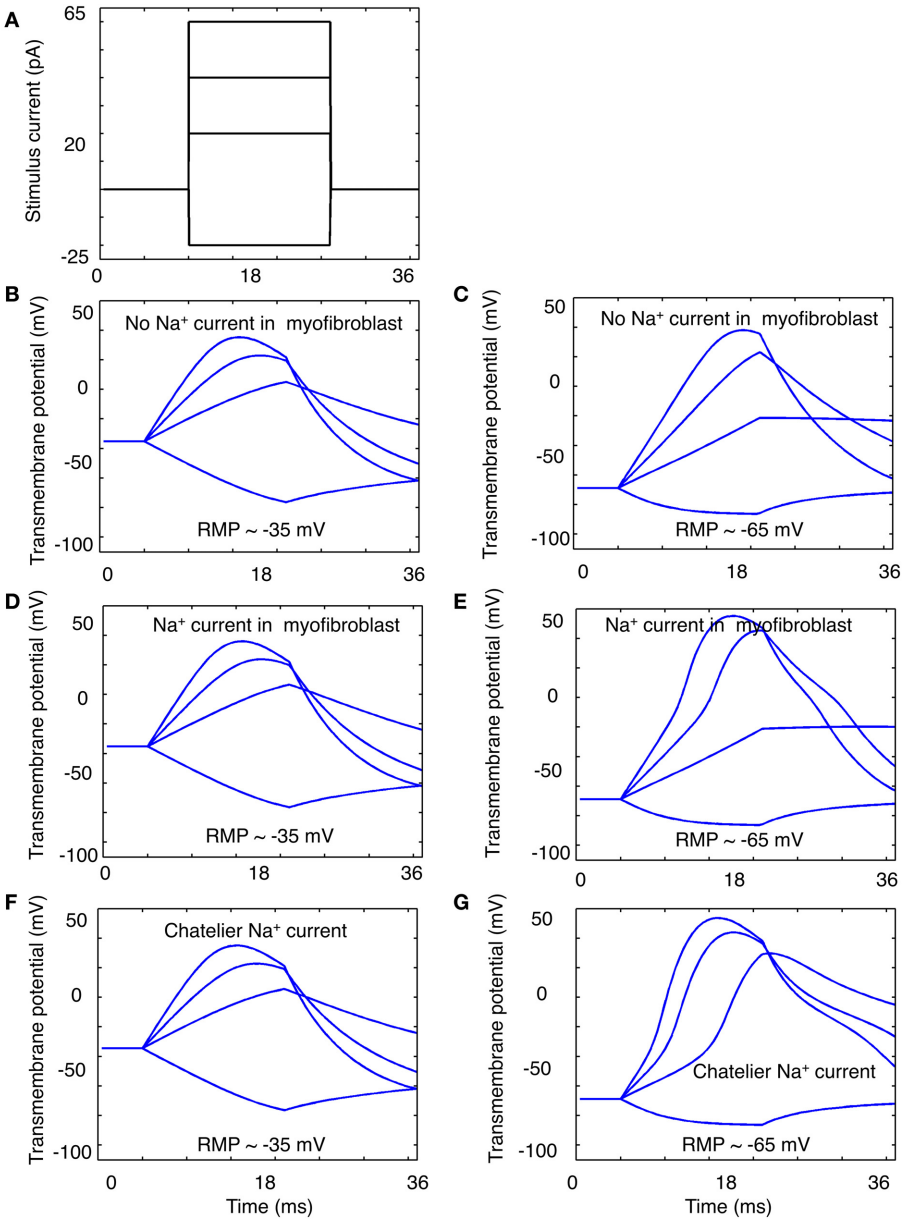

FIGURE 6 | Illustration of "electrotonic" responses in an *in silico* human atrial myofibroblast produced by 16 ms constant current stimuli that progressively depolarize or hyperpolarize the myofibroblast model. The stimulus protocol is shown in panel **(A)**. The superimposed responses in **(B,C)** were obtained using a modified (see Methods) MacCannell et al. (2007) model of an atrial myofibroblast with no Na^+ current added. The families of responses in **(D,E)** were obtained when this model also included equations for the Na^+ current in this paper; or the Na^+ current in the Chatelier et al. paper (2012) **(F,G)**. Note when Na^+ current is included, most of the depolarizing stimuli produce a biphasic response. This may suggest a contribution of Na^+ current activation to the stimulus-induced depolarization (see Discussion).

the presentation of the data is the same as that of data **Figure 7**. Thus, the panels in column 1 (**B**,**D**,**E**,**H**) were based on computations done with no Na^+ current in the myofibroblast cell population, and with coupling ratios of myocyte to myofibroblasts of 1:1, 1:3, and 1:9, respectively. As expected from our previous papers (MacCannell et al., 2007; Maleckar et al., 2009a), the myocyte membrane potential dominates that of the myofibroblast at low myofibroblast/myocyte ratios. In distinction, to when the myofibroblast resting membrane potential is much more depolarized (−35 mV), when the coupling ratio is 1:3 or 1:9, both the myofibroblasts and the myocytes have well-polarized resting membrane potentials. Partly for this reason, the waveform of the voltage change in the myofibroblast also differs substantially. This arises from the fact that more hyperpolarized resting membrane potential removes inactivation from the Na^+ channels. This effect would be expected to be strongly manifested in the computations shown in panels **C**,**F**,**I**—as well a **D**,**G**,**I**, since the voltage dependence for inactivation of the Na^+ current falls

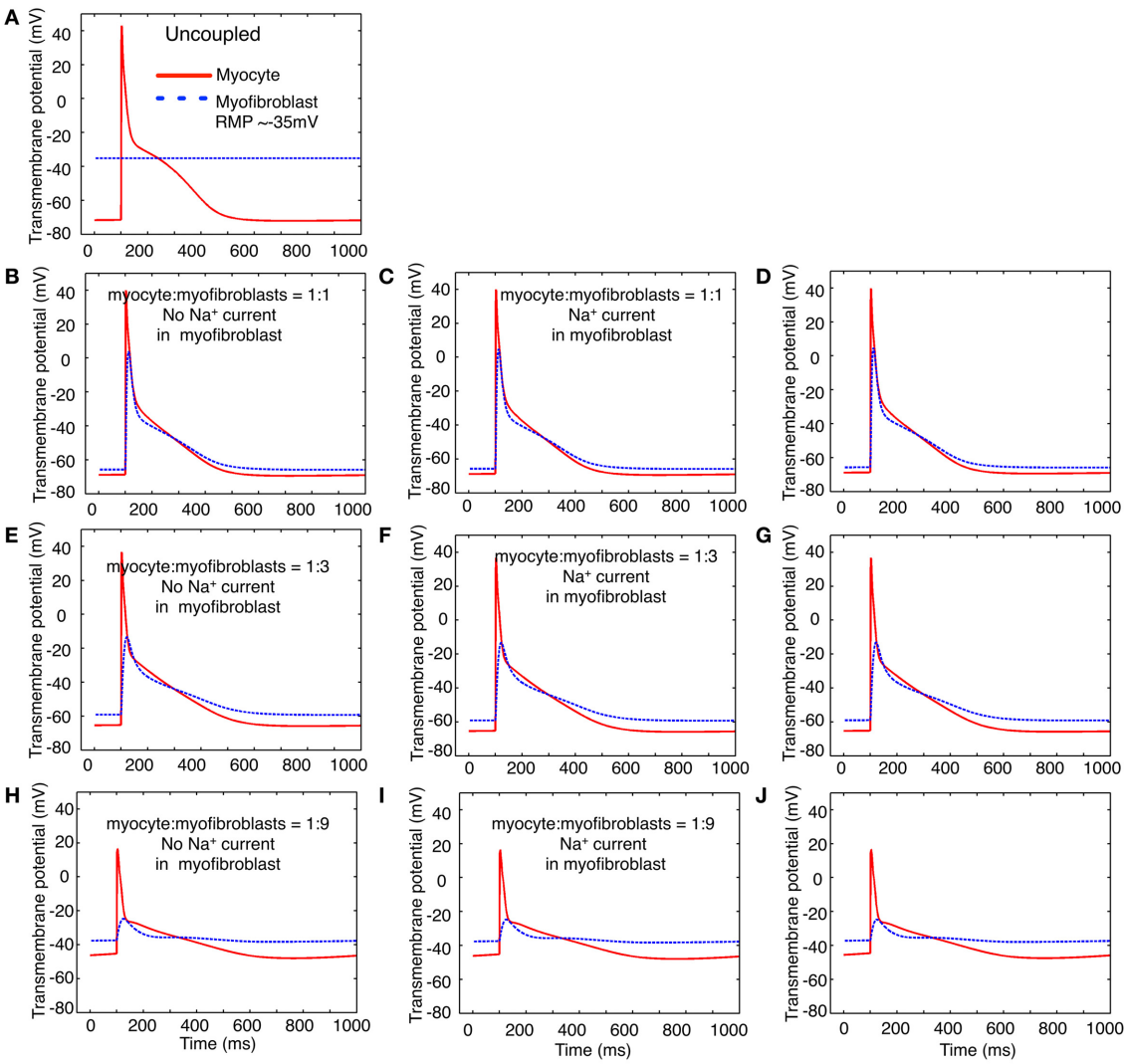

FIGURE 7 | Illustration of the effects of coupling selected numbers of myofibroblasts to 1 human atrial myocyte using an *in silico* hybrid mathematical model similar to the one first described by Maleckar et al. (2009a) when assuming a myofibroblast resting potential of −35 or −65 mV. Panel **(A)** shows the human atrial myocyte action potential (red) and the myofibroblast at a resting potential of −35 mV, prior to these cells being coupled through a linear intercellular conductance of 0.5 nS. The remainder of this Figure is arranged in three rows. Panels **(B–D)** illustrate responses obtained when the myocyte to myofibroblast ratio is 1:1, panels **(E–G)** were computed based on a myocyte to myofibroblast ratio of 1:3; and panels **(H–J)** show responses when myocyte to myofibroblast ratio was 1:9. The arrangement of the vertical columns allow a direct comparison of the electrophysiological effects of (a) there being no Na^+ current in any myofibroblast (left column, panels **B,E,H**); (b) the Na^+ current identified in our laboratory and described in the paper being introduced (panels **C,F,I**); or (c) the Na^+ current reported by Chatelier et al. (2012) being added to each myofibroblast **(D,G,J)**. Note that the myocyte action potential causes a significant electrotonic waveform in each myofibroblast at ratios of 1:1 and 1:3. At a coupling ratio of 1:9, the myofibroblasts exert a pronounced depolarizing influence of the myocyte resting potential in these assumed conditions (see Discussion).

well within the range of the resting membrane potential of the myofibroblast.

Careful inspection of some of the computational results in **Figures 7**, **8** may suggest that activation of I_{Na} in the myofibroblast influences the overall "substrate" electrophysiological profile. Thus, in some cases, the membrane potential in the myofibroblast(s) depolarizes, when the atrial myocyte is repolarizing.

The computational results shown in **Figure 9** provide some further insight into this intriguing possibility. All of these computations were done using a 1 myocyte to 1 myofibroblast ratio. Two different values of coupling (intercellular) resistance, either 0.5 nS (top row) or 8 nS (bottom row) were selected for study. As expected, when intercellular resistance is very small, the myocyte action potential produces an electrotonic response in the myofibroblast that is essentially unattenuated.

Note that at both these values of intercellular resistance (panels **C**,**D**), the current flowing between the "cells" is dominated by the net inward (depolarizing) and outward (repolarizing)

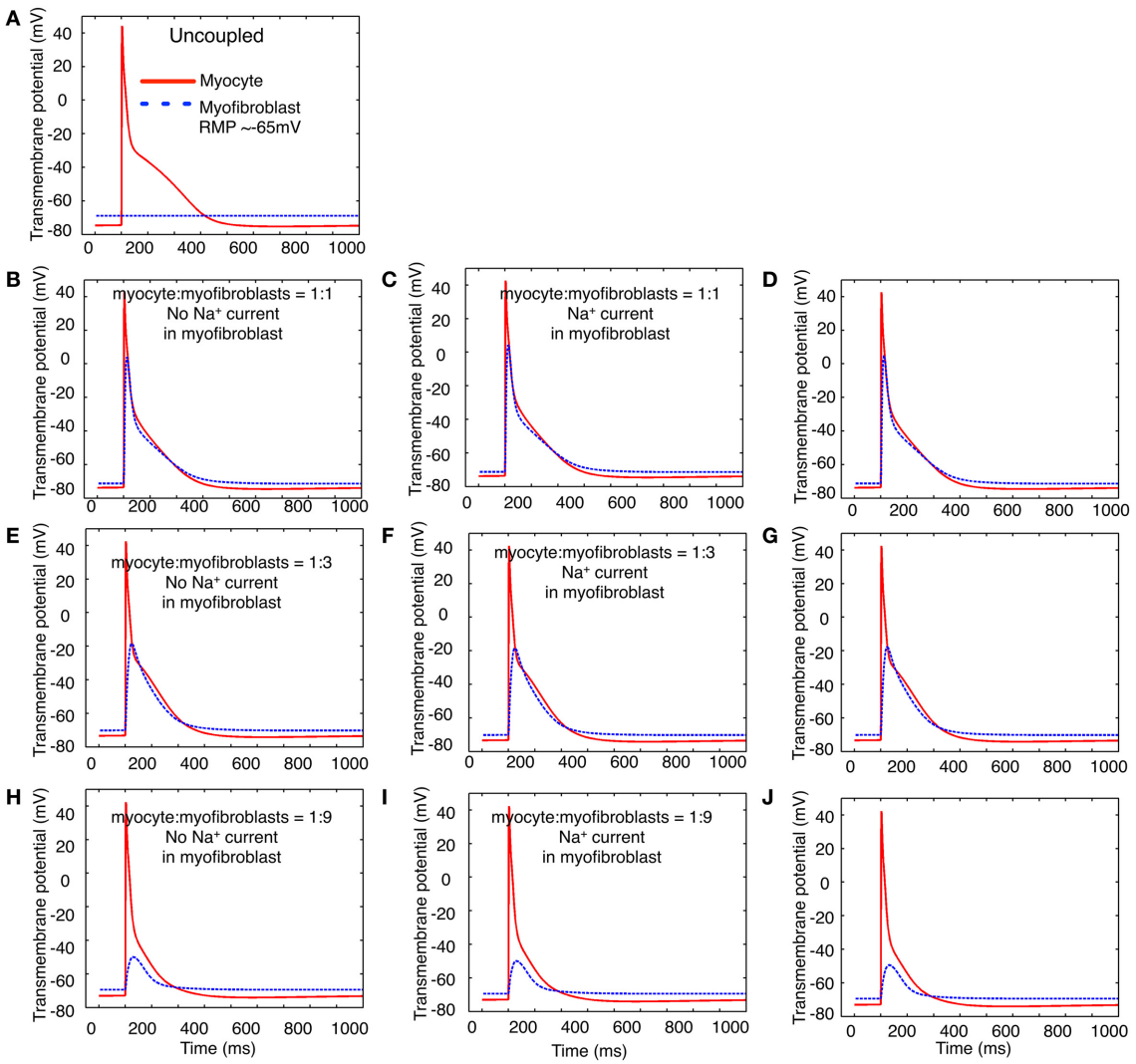

FIGURE 8 | Illustration of the effects of coupling selected numbers of myofibroblasts to 1 human atrial myocyte using an *in silico* hybrid model similar to the one first described by Maleckar et al. (2009a), assuming a myofibroblast resting potential of −65 mV. The layout of this Figure is the same as that of **Figure 7**. Note that two potentially important differences in the patterns of *in silico* responses were obtained: (1) in all situations, the myofibroblast electrotonic responses are larger, (2) the myofibroblasts exert only a minimal depolarizing influence on the resting potential of the atrial myocyte.

currents generated by the *atrial* myocyte. Panels **E** and **F** show the net transmembrane current in the myofibroblast population. Again, the inward, depolarizing current appears to be contributed mainly by the activation of I_{Na} in the *atrial* myocyte(s), as opposed to the myofibroblast(s) (see Discussion).

DISCUSSION

MAIN FINDINGS

The whole-cell voltage clamp measurements shown in **Figures 1–4** confirm that when human atrial fibroblasts are isolated and then placed in conventional 2-D culture, a sizeable fraction (approximately 50%) of these cells (myofibroblasts) express a measurable Na^+ current. A number of electrophysiological and biophysical features of this current are noteworthy. (i) Its peak amplitude (in the range: 0.8–17.9 pA/pF) is sufficient to suggest that the myofibroblast may exhibit a regenerative action potential. (ii) The steady-state voltage dependence of inactivation, and the derived relationship that depicts quasi steady-state voltage dependence of activation, both strongly resemble the analogous biophysical parameters for the Na^+ current recorded in adult human atrial myocytes (Baba et al., 2006). (iii) These findings, in conjunction with the PCR data in **Figure 5**, provide initial evidence that this current is similar to the Na^+ current in an adult human atrial myocyte, as was originally reported by Chatelier et al. (2012). However, we note that our PCR analysis yielded data that identifies two nerve Na^+ channel α subunits, $Na_v1.9$ and $Na_v1.2$, as the predominant transcripts. The cardiac Na^+ channel α subunit was detectable

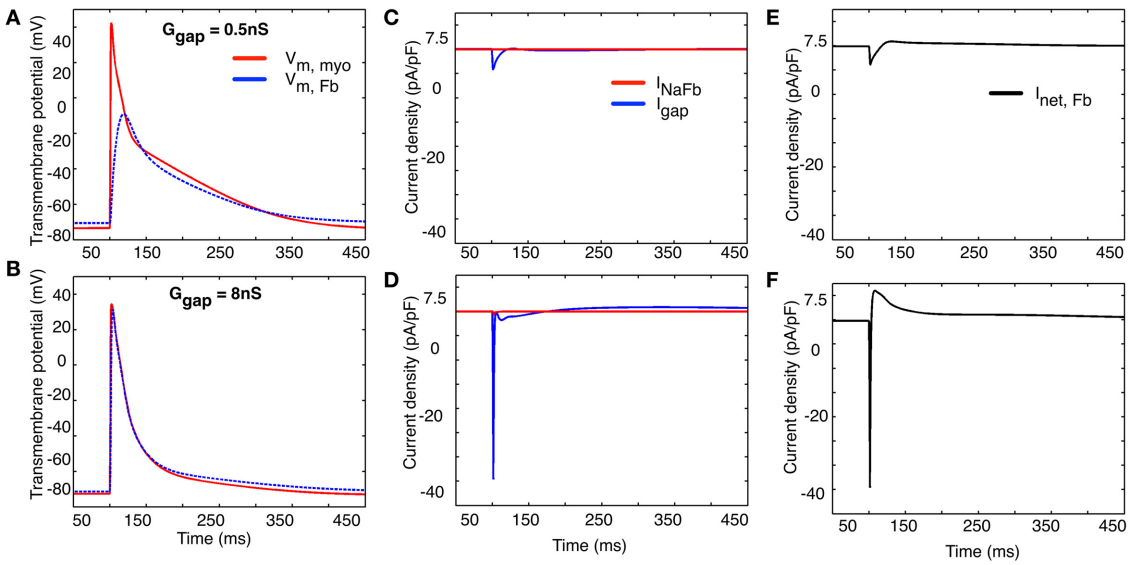

FIGURE 9 | Illustration of two selected values of the effects of coupling resistance on the electrotonic membrane potential (panels A,B), "gap current" and current flow between the two cell populations (1 myocyte: 1 myofibroblast, panels C,D) and the net transmembrane current in the collective myofibroblast population (panels E,F). See text in Results for further explanation.

in our myofibroblast preparation, but was less prominent than either $Na_v1.9$ or $Na_v1.2$.

Some of our findings differ from those in the original paper (Chatelier et al., 2012) that first identified Na^+ current in human atrial myofibroblasts. One of their most striking findings was that this Na^+ current exhibited a very hyperpolarized range of membrane potentials for activation and inactivation (see Figures 2B, 3A, in Chatelier et al., 2012). The reasons for these important differences may be due to the fact that some of the experimental conditions in the two studies differ. In the Chatelier et al. work (2012), the pH of the "internal solution" was 7.4; and perhaps more importantly, CsF rather than CsCl was used in the pipette-filling solution. It is well-known that F^- in the internal solution can cause a pronounced hyperpolarizing shift in Na^+ current gating parameters (Chandler and Meves, 1970). An important consequence of the gating variables for the Na^+ current being shifted in the hyperpolarizing direction in the Chatelier et al. paper (2012) is that the myofibroblast resting potential would need to be negative to −60 mV before this current could be activated. Second, in principle, there could be a substantial non-inactivating or "background/steady" Na^+ influx, when the myofibroblast membrane potential is in the voltage range approximately −90 to −40 mV. This would depolarize the myofibroblast and tend to increase $[Na^+]_i$ and have significant secondary consequences on $[Ca^{2+}]_i$, and $[pH]_i$ homeostasis.

These considerations raise the very important question: what is the resting potential of the human atrial fibroblast/myofibroblast? Values in the range −30 to −50 mV are often reported for isolated single cell mammalian fibroblast/myofibroblast preparations. However, accurate measurement of membrane potential in these small cells is very challenging (Dubois, 2000), especially under conditions, in which a background inwardly rectifying K^+ current is expressed (Wilson et al., 2011). This is the case in cardiac fibroblasts/myofibroblasts (Chilton et al., 2007), since an inwardly rectifying background current is expressed. It is also useful to recall that, as it is in fibroblasts, the classical experiments of the Kiseleva Group (Kiseleva et al., 1998; Kamkin et al., 2002; cf. Kohl, 2003) show that the mechano-sensitivity of cardiac fibroblasts can significantly change membrane potential (Abramochkin et al., 2014). It is likely that fibroblast membrane potential may vary with the mechanoelectric activity of the heart.

As mentioned, the data from our PCR measurements differ from the original findings (Chatelier et al., 2012) concerning the molecular identity of the Na^+ current α subunit(s) in human atrial myofibroblasts (see **Figure 6**). Thus, we suggest that the major α subunits are $Na_v1.9$ and Na_v 1.2, as opposed to Na_v 1.5. Of the four known Na^+ channel β subunits that could, in principle, contribute to the Na^+ channel complex (Abriel and Kass, 2005), the β_1 subunit predominates in the human atrial myofibroblasts in the mammalian heart, as is the case in the corresponding adult myocyte. At present, we cannot explain the significant difference in the pattern of Na^+ channel α subunit expression. However, it is possible that our cell culture preparation is less uniform than that of Chatelier et al. (2012). Our PCR analysis was done using a preparation that had been plated on coverslips only 24–48 h before being studied. However, these myofibroblasts had been passaged a number of times (2–6) before they were "released and plated." In contrast, Chatelier et al. studied myofibroblasts after some 3 weeks in culture, corresponding to approximately passage 9. This difference is an important issue that can only be resolved by a separate, much more extensive study.

Our study did not focus on the molecular pharmacology of the Na^+ currents in the myofibroblast. However, the original paper (Chatelier et al., 2012) reported (**Figure 5**) that tetrodotoxin (TTX) did block this current. In these experiments, the effective

concentrations of TTX were in the 10–100 μM range. This further supports its identity as a cardiac myocyte-like Na^+ current, generated by the complex of Na_v 1.5 and the β_1 subunit.

COMPUTATIONAL WORK

It is somewhat surprising that introduction of Na^+ current into the modified MacCannell model of the mammalian fibroblast (MacCannell et al., 2007) did *not* result in any convincing action potential-like regenerative responses (**Figures 6**, **7**). With respect to the results shown in **Figure 6**, this may be due to the fact that the relatively depolarized "assigned" resting potential (−35 or −65 mV) of the fibroblasts/myofibroblasts resulted in very significant inactivation of I_{Na}. A second contributing factor may be the incomplete information concerning the kinetics of activation and inactivation of I_{Na} in the human atrial myofibroblast. The high input resistance of these cells (5–10 Gigohms) results in a large intrinsic membrane time constant; and this may contribute to Na^+ current "accommodation"—inactivation developing at a rate similar to activation at membrane potential near the normal firing threshold for I_{Na}.

At this stage of its development, the hybrid modeling illustrated in **Figures 7**, **8** does not independently reveal significant new information. Perhaps the most realistic myocyte to myofibroblast ratios that we have explored is the 1:3 case. In this defined starting condition, we confirm that the myocyte action potential produces a significant electrotonic waveform in the connexin-coupled myofibroblasts (MacCannell et al., 2007; Maleckar et al., 2009a). In addition, when large differences in the resting potential of the myofibroblast vs. the myocyte are assumed/assigned, the myofibroblast can significantly depolarize the atrial myocyte. This depolarization would be expected to reduce myocyte excitability and conduction velocity; and may significantly change diastolic Ca^{2+} levels. It is worth noting that these effects could be anticipated to be spatially heterogeneous within the human atrial substrate.

TRANSLATIONAL PERSPECTIVES

The expression of Na^+ current (more specifically the detection of essential components of the Na^+ channel complex) in the myofibroblast, may be important for reasons quite different than the well-known ability of this integral membrane protein to give rise to a transient inward current and thus promote cell and/or substrate excitability. The so-called "non-conducting functions" of the Na^+ channel complex (Kaczmarek, 2006; Brackenbury and Isom, 2011) are gaining increasing attention, for example, in the setting of the metastatic phase of the progression of a number of different solid tumor cancers. During metastasis of solid tumors and during nerve "sprouting," it is very likely that the expression of Na^+ channels result in mechanical stability of the cells in which they are expressed, rather than, or in addition to, a conventional electrophysiological function (Chioni et al., 2009; Fraser et al., 2010). Some Na^+ channel β subunits can covalently link with well-known adhesion molecules. This suggests the possibility that expression of the β subunit, and by implication the entire Na^+ complex (Abriel and Kass, 2005), may have an important adhesion function. It is interesting that Watanabe et al. (2009) have reported alterations in the β1 and β2 subunits of the Na^+ channel in tissue taken from atria that had exhibited persistent fibrillation, a condition often associated with enhanced fibrosis and perhaps with altered cell-matrix dynamics.

It is also known that one aspect of an acute inflammatory response involves binding of emigrated neutrophils to the Na^+ channel complex, and a resulting (very significant) Na^+ influx, due to a "late" Na^+ current. This arises from Na^+ channels opening but then inactivating very slowly (Poon et al., 2001; Ward et al., 2006). Thus, provided that the membrane potential of the myofibroblast is sufficiently negative that even a small fraction of the Na^+ channels could open (see **Figure 2**), the pathophysiological chain events involving substantial leak of Na^+ into the cell through non-inactivating Na^+ channels followed by Ca^{2+} overload may need to be considered in the setting of cytokine or inflammation-induced apoptosis or necrosis.

Quite recently, the so-called "re-programmed" fibroblast has been advanced as the preparation of choice for heterologous introduction into the compromised myocardium or other end-organs in the context of Regenerative Medicine approaches to Chronic Disease Management (Leri and Kajstura, 2012; Palpant and Murry, 2012; Qian et al., 2012; Song et al., 2012; Srivastava and Ieda, 2012; Miki et al., 2013). The fundamental principles of fibroblast isolation and reprogramming appear now to be well understood. However, in the cases of cardiac and vascular pathophysiology, an essential requirement is that these implanted cells must have a stable, quiescent electrophysiological phenotype. For this reason, the expression of Na^+ current in myofibroblast that is the focus of this study needs to be understood fully and perhaps avoided or suppressed. Similar considerations are likely to apply to more preliminary attempts to use reprogrammed fibroblasts in the context of cardiac rhythm control (Yankelson et al., 2008; Cho and Marbán, 2010).

LIMITATIONS

A major limitation of the experimental work presented in this paper is that, as judged by both electrophysiological and PCR methodology, expression of Na^+ channels could be detected only a considerable time period *after seeding* of what were originally human atrial fibroblasts in 2-D tissue culture. This raises the possibility (both with respect to the Chatelier paper and our work) that Na^+ channel expression could be tissue culture specific. Such an epi-phenomenon would have little if any physiological or pathophysiological significance. Perhaps the strongest argument against this possibility is that, although ion channel expression is known to change in tissue culture, under most circumstances the expression levels are *reduced* (Banyasz et al., 2008). In addition, and as noted in Methods, although the enzymatic isolation of fibroblasts from the human atrial right appendage was somewhat similar in these two studies, in fact, post-isolation treatment of the resulting fibroblast/myofibroblast cell populations differed quite significantly. In our work [consistent with the previous work and ongoing investigations in the Fedak Laboratory (Fedak et al., 2012)], these cells are maintained and held in a 3D-substrate for most of the post-isolation period, i.e., to being released for study by conventional electrophysiological or PCR methods.

The results based on mathematical modeling (**Figures 6–9**) are preliminary, in part because the experimental data is incomplete. This part of this paper is limited by a lack of information with

respect to (i) the extent of the electrotonic coupling between myofibroblasts, and/or (ii) among single or multi-cellular groups of myofibroblasts and the immediately adjacent human atrial myocytes. It would seem implausible that this coupling ratio could be 1:1. Other, more likely possibilities are illustrated in the computations in **Figures 7** and **8**. It is clear, however, that more extensive and detailed experimental data and more refined computations are needed to further evaluate myocyte/fibroblast electrotonic interactions in defined starting conditions that are directed toward a defined myocyte/fibroblast ratio.

In addition, future work will need to consider the influence of tonic effects of autonomic transmitters and/or paracrine substances. Success based on these improvements may provide the possibility that within the extracellular matrix of the atrium, a "double hit" approach can be developed to modulate Na^+ channel activity, and thus achieve improved anti-arrhythmic therapy (Maingret et al., 2008).

AUTHOR CONTRIBUTIONS

Doctors Robert Clark and Darrell Belke were responsible for the experimental work shown in **Figures 1–4** and **5**, respectively. Doctors Jussi Koivumäki and Mary Maleckar produced the simulation results in **Figures 6–9**. Doctor Wayne Giles planned and wrote draft #1 of this manuscript. All authors read and provided comments on the original and revised manuscripts.

ACKNOWLEDGMENTS

An Alberta Innovates—Health Solutions Scientist Award (WRG), an AI-HS Starter Grant, the Canadian Institutes of Health Research, and the Heart and Stroke Foundation of Alberta supported the experimental work and mathematical model development in the Giles Laboratory. Jussi T. Koivumäki and Mary M. C. Maleckar gratefully acknowledge support via partnership in the Center for Cardiological Innovation at Oslo University Hospital and by a Center of Excellence grant from the Research Council of Norway to the Center for Biomedical Computing at Simula Research Laboratory. We are grateful to the Fedak Laboratory and Division of Cardiothoracic Surgery at the University of Calgary for supply of right atrial appendage tissue. Ms. Colleen Kondo prepared and maintained the tissue cultures and was responsible for project management.

REFERENCES

Abramochkin, D. V., Lozinsky, I. T., and Kamkin, A. (2014). Influence of mechanical stress on fibroblast-myocyte interactions in mammalian heart. *J. Mol. Cell. Cardiol.* 70C, 27–36. doi: 10.1016/j.yjmcc.2013.12.020

Abriel, H., and Kass, R. S. (2005). Regulation of the voltage-gated cardiac sodium channel Nav 1.5 by interacting proteins. *Trends Cardiovasc. Med.* 15, 35–40. doi: 10.1016/j.tcm.2005.01.001

Aguilar-Shardonofsky, M., Vigmond, E. J., Nattel, S., and Comtois, P. (2012). *In silico* optimization of atrial fibrillation—selective sodium channel blocker pharmacodynamics. *Biophys. J.* 102, 951–960. doi: 10.1016/j.bpj.2012.01.032

Ashihara, T., Haraguchi, R., Nakazawa, K., Namba, T., Ikeda, T., Nakazawa, Y., et al. (2012). The role of fibroblasts in complex fractionated electrograms during persistent/permanent atrial fibrillation: implications for electrogram-based catheter ablation. *Circ. Res.* 110, 275–284. doi: 10.1161/CIRCRESAHA.111.255026

Baba, S., Dun, W., Hirose, M., and Boyden, P. A. (2006). Sodium current function in adult and aged canine atrial cells. *Am. J. Physiol. Heart Circ. Physiol.* 291, H756–H761. doi: 10.1152/ajpheart.00063.2006

Banyasz, T., Lozinskiy, I., Payne, C. E., Edelmann, S., Norton, B., Chen, B., et al. (2008). Transformation of adult rat cardiac myocytes in primary culture. *Exp. Physiol.* 93, 370–382. doi: 10.1113/expphysiol.2007.040659

Baudino, T. A., Carver, W., Giles, W., and Borg, T. K. (2006). Cardiac fibroblasts: friend or foe? *Am. J. Physiol. Heart Circ. Physiol.* 291, H1015–H1026. doi: 10.1152/ajpheart.00023.2006

Baum, J., and Duffy, H. S. (2011). Fibroblasts and myofibroblasts: what are we talking about? *J. Cardiovasc. Pharmacol.* 57, 376–379. doi: 10.1097/FJC.0b013e3182116e39

Benito, B., Brugada, R., Perich, R. M., Lizotte, E., Cinca, J., Mont, L., et al. (2008). A mutation in the sodium channel is responsible for the association of long QT syndrome and familial atrial fibrillation. *Heart Rhythm* 5, 1434–1440. doi: 10.1016/j.hrthm.2008.07.013

Bersohn, M. M., Waldo, A. L., and Halperin, J. L. (2012). Subclinical atrial fibrillation and the risk of stroke. *N. Engl. J. Med.* 366, 1352.

Biernacka, A., and Frangogiannis, N. G. (2011). Aging and cardiac fibrosis. *Aging Disease* 2, 158–173.

Brackenbury, W. J., and Isom, L. L. (2011). Na channel beta subunits: overachievers of the ion channel family. *Front. Pharmacol.* 2:53. doi: 10.3389/fphar.2011.00053

Brilla, C., Maisch, B., Zhou, G., and Weber, K. (1995). Hormonal regulation of cardiac fibroblast function. *Eur. Heart J.* 16, 45–50. doi: 10.1093/eurheartj/16.suppl_C.45

Chandler, W. K., and Meves, H. (1970). Slow changes in membrane permeability and long-lasting action potentials in axons perfused with fluoride solutions. *J. Physiol.* 211, 707–728.

Chatelier, A., Mercier, A., Tremblier, B., Thériault, O., Moubarak, M., Benamer, N., et al. (2012). A distinct de novo expression of Nav1. 5 sodium channels in human atrial fibroblasts differentiated into myofibroblasts. *J. Physiol.* 590, 4307–4319. doi: 10.1113/jphysiol.2012.233593

Chilton, L., Giles, W. R., and Smith, G. L. (2007). Evidence of intercellular coupling between co-cultured adult rabbit ventricular myocytes and myofibroblasts. *J. Physiol.* 583, 225–236. doi: 10.1113/jphysiol.2007.135038

Chilton, L., Ohya, S., Freed, D., George, E., Drobic, V., Shibukawa, Y., et al. (2005). K+ currents regulate the resting membrane potential, proliferation, and contractile responses in ventricular fibroblasts and myofibroblasts. *Am. J. Physiol. Heart Circ. Physiol.* 288, H2931–H2939. doi: 10.1152/ajpheart.01220.2004

Chioni, A. M., Brackenbury, W. J., Calhoun, J. D., Isom, L. L., and Djamgoz, M. B. (2009). A novel adhesion molecule in human breast cancer cells: voltage-gated Na+ channel beta1 subunit. *Int. J. Biochem. Cell Biol.* 41, 1216–1227. doi: 10.1016/j.biocel.2008.11.001

Cho, H. C., and Marbán, E. (2010). Biological therapies for cardiac arrhythmias: can genes and cells replace drugs and devices? *Circ. Res.* 106, 674–685. doi: 10.1161/CIRCRESAHA.109.212936

Diness, J. G., Skibsbye, L., Jespersen, T., Bartels, E. D., Sørensen, U. S., Hansen, R. S., et al. (2011). Effects on atrial fibrillation in aged hypertensive rats by Ca2+-activated K+ channel inhibition. *Hypertension* 57, 1129–1135. doi: 10.1161/HYPERTENSIONAHA.111.170613

Dubois, J.-M. (2000). What is the true resting potential of small cells? *Gen. Physiol. Biophys.* 19, 3–7.

Fedak, P. W. M., Bai, L. P., Turnbull, J., Ngu, J., Narine, K., and Duff, H. J. (2012). Cell therapy limits myofibroblast differentiation and structural cardiac remodeling: basic fibroblast growth factor-mediated paracrine mechanism. *Circulation Heart Fail.* 5, 349–356. doi: 10.1161/CIRCHEARTFAILURE.111.965889

Fraser, S. P., Ozerlat-Gunduz, I., Onkal, R., Diss, J. K., Latchman, D. S., and Djamgoz, M. B. (2010). Estrogen and non-genomic upregulation of voltage-gated Na(+) channel activity in MDA-MB-231 human breast cancer cells: role in adhesion. *J. Cell. Physiol.* 224, 527–539. doi: 10.1002/jcp.22154

Gaudesius, G., Miragoli, M., Thomas, S. P., and Rohr, S. (2003). Coupling of cardiac electrical activity over extended distances by fibroblasts of cardiac origin. *Circ. Res.* 93, 421–428. doi: 10.1161/01.RES.0000089258.40661.0C

Guzadhur, L., Jiang, W., Pearcey, S. M., Jeevaratnam, K., Duehmke, R. M., Grace, A. A., et al. (2012). The age-dependence of atrial arrhythmogenicity in Scn5a+/- murine hearts reflects alterations in action potential propagation and recovery. *Clin. Exp. Pharmacol. Physiol.* 39, 518–527. doi: 10.1111/j.1440-1681.2012.05706.x

Kaczmarek, L. K. (2006). Non-conducting functions of voltage-gated ion channels. *Nat. Rev. Neurosci.* 7, 761–771. doi: 10.1038/nrn1988

Kakkar, R., and Lee, R. T. (2010). Intramyocardial fibroblast myocyte communication. *Circ. Res.* 106, 47–57. doi: 10.1161/CIRCRESAHA.109.207456

Kamkin, A., Kiseleva, I., Wagner, K.-D., Pylaev, A., Leiterer, K. P., Theres, H., et al. (2002). A possible role for atrial fibroblasts in postinfarction bradycardia. *Am. J. Physiol. Heart Circ. Physiol.* 282, H842–H849.

Kiseleva, I., Kamkin, A., Pylaev, A., Kondratjev, D., Leiterer, K. P., Theres, H., et al. (1998). Electrophysiological properties of mechanosensitive atrial fibroblasts from chronic infarcted rat heart. *J. Mol. Cell. Cardiol.* 30, 1083–1093. doi: 10.1006/jmcc.1998.0673

Kohl, P. (2003). Heterogeneous cell coupling in the heart: an electrophysiological role for fibroblasts. *Circ. Res.* 93, 381–383. doi: 10.1161/01.RES.0000091364.90121.0C

Koivumäki, J. T., Korhonen, T., and Tavi, P. (2011). Impact of sarcoplasmic reticulum calcium release on calcium dynamics and action potential morphology in human atrial myocytes: a computational study. *PLoS Comput. Biol.* 7:e1001067. doi: 10.1371/journal.pcbi.1001067

Leri, A., and Kajstura, J. (2012). Created equal? The many facets of cell reprogramming. *Circ. Res.* 111, 152–155. doi: 10.1161/CIRCRESAHA.112.272526

MacCannell, K. A., Bazzazi, H., Chilton, L., Shibukawa, Y., Clark, R. B., and Giles, W. R. (2007). A mathematical model of electrotonic interactions between ventricular myocytes and fibroblasts. *Biophys. J.* 92, 4121–4132. doi: 10.1529/biophysj.106.101410

Maingret, F., Coste, B., Padilla, F., Clerc, N., Crest, M., Korogod, S. M., et al. (2008). Inflammatory mediators increase Nav1.9 current and excitability in nociceptors through a coincident detection mechanism. *J. Gen. Physiol.* 131, 211–225. doi: 10.1085/jgp.200709935

Maleckar, M. M., Greenstein, J. L., Giles, W. R., and Trayanova, N. A. (2009a). Electrotonic coupling between human atrial myocytes and fibroblasts alters myocyte excitability and repolarization. *Biophys. J.* 97, 2179–2190. doi: 10.1016/j.bpj.2009.07.054

Maleckar, M. M., Greenstein, J. L., Giles, W. R., and Trayanova, N. A. (2009b). K+ current changes account for the rate dependence of the action potential in the human atrial myocyte. *Am. J. Physiol. Heart Circ. Physiol.* 297, H1398–H1410. doi: 10.1152/ajpheart.00411.2009

McDowell, K. S., Arevalo, H. J., Maleckar, M. M., and Trayanova, N. A. (2011). Susceptibility to arrhythmia in the infarcted heart depends on myofibroblast density. *Biophys. J.* 101, 1307–1315. doi: 10.1016/j.bpj.2011.08.009

McDowell, K. S., Vadakkumpadan, F., Blake, R., Blauer, J., Plank, G., MacLeod, R. S., et al. (2013). Mechanistic inquiry into the role of tissue remodeling in fibrotic lesions in human atrial fibrillation. *Biophys. J.* 104, 2764–2773. doi: 10.1016/j.bpj.2013.05.025

Miki, K., Yoshida, Y., and Yamanaka, S. (2013). Making steady progress on direct cardiac reprogramming toward clinical application. *Circ. Res.* 113, 13–15. doi: 10.1161/CIRCRESAHA.113.301788

Munoz, V., Campbell, K., and Shibayama, J. (2008). Fibroblasts: modulating the rhythm of the heart. *J. Physiol.* 586, 2423–2424. doi: 10.1113/jphysiol.2008.153387

Nattel, S. (2002). New ideas about atrial fibrillation 50 years on. *Nature* 415, 219–226. doi: 10.1038/415219a

Nygren, A., and Giles, W. R. (2000). Mathematical simulation of slowing of cardiac conduction velocity by elevated extracellular $[K^+]$ in a human atrial strand. *Ann. Biomed. Eng.* 28, 951–957. doi: 10.1114/1.1308489

Palpant, N. J., and Murry, C. E. (2012). Regenerative medicine: reprogramming the injured heart. *Nature* 485, 585–586. doi: 10.1038/485585a

Pedrotty, D. M., Klinger, R. Y., Kirkton, R. D., and Bursac, N. (2009). Cardiac fibroblast paracrine factors alter impulse conduction and ion channel expression of neonatal rat cardiomyocytes. *Cardiovasc. Res.* 83, 688–697. doi: 10.1093/cvr/cvp164

Poon, B. Y., Ward, C. A., Cooper, C. B., Giles, W. R., Burns, A. R., and Kubes, P. (2001). α4-Integrin mediates neutrophil-induced free radical injury to cardiac myocytes. *J. Cell Biol.* 152, 857–866. doi: 10.1083/jcb.152.5.857

Porter, K. E., and Turner, N. A. (2009). Cardiac fibroblasts: at the heart of myocardial remodeling. *Pharmacol. Ther.* 123, 255–278. doi: 10.1016/j.pharmthera.2009.05.002

Powell, D., Mifflin, R., Valentich, J., Crowe, S., Saada, J., and West, A. (1999). Myofibroblasts. I. Paracrine cells important in health and disease. *Am. J. Physiol. Cell Physiol.* 277, C1–C19. doi: 10.1111/j.1469-7793.1999.001af.x

Qian, L., Huang, Y., Spencer, C. I., Foley, A., Vedantham, V., Liu, L., et al. (2012). *In vivo* reprogramming of murine cardiac fibroblasts into induced cardiomyocytes. *Nature* 485, 593–598. doi: 10.1038/nature11044

Rohr, S. (2011). Cardiac fibroblasts in cell culture systems: myofibroblasts all along? *J. Cardiovasc. Pharmacol.* 57, 389–399. doi: 10.1097/FJC.0b013e3182137e17

Rose, R., Hatano, N., Ohya, S., Imaizumi, Y., and Giles, W. (2007). C-type natriuretic peptide activates a non-selective cation current in acutely isolated rat cardiac fibroblasts via natriuretic peptide C receptor-mediated signalling. *J. Physiol.* 580, 255–274. doi: 10.1113/jphysiol.2006.120832

Rose, R. A., and Giles, W. R. (2008). Natriuretic peptide C receptor signalling in the heart and vasculature. *J. Physiol.* 586, 353–366. doi: 10.1113/jphysiol.2007.144253

Sachse, F. B., Moreno, A. P., and Abildskov, J. A. (2008). Electrophysiological modeling of fibroblasts and their interaction with myocytes. *Ann. Biomed. Eng.* 36, 41–56. doi: 10.1007/s10439-007-9405-8

Song, K., Nam, Y.-J., Luo, X., Qi, X., Tan, W., Huang, G. N., et al. (2012). Heart repair by reprogramming non-myocytes with cardiac transcription factors. *Nature* 485, 599–604. doi: 10.1038/nature11139

Spach, M. S., and Boineau, J. P. (1997). Microfibrosis produces electrical load variations due to loss of side−to−side cell connections; a major mechanism of structural heart disease arrhythmias. *Pacing Clin. Electrophysiol.* 20, 397–413. doi: 10.1111/j.1540-8159.1997.tb06199.x

Spach, M. S., Heidlage, J. F., Dolber, P. C., and Barr, R. C. (2007). Mechanism of origin of conduction disturbances in aging human atrial bundles: experimental and model study. *Heart Rhythm* 4, 175–185. doi: 10.1016/j.hrthm.2006.10.023

Srivastava, D., and Ieda, M. (2012). Critical factors for cardiac reprogramming. *Circ. Res.* 111, 5–8. doi: 10.1161/CIRCRESAHA.112.271452

Ward, C. A., Bazzazi, H., Clark, R. B., Nygren, A., and Giles, W. R. (2006). Actions of emigrated neutrophils on Na(+) and K(+) currents in rat ventricular myocytes. *Prog. Biophys. Mol. Biol.* 90, 249–269. doi: 10.1016/j.pbiomolbio.2005.07.003

Watanabe, H., Darbar, D., Kaiser, D. W., Jiramongkolchai, K., Chopra, S., Donahue, B. S., et al. (2009). Mutations in sodium channel β1-and β2-subunits associated with atrial fibrillation. *Circulation* 2, 268–275. doi: 10.1161/CIRCEP.108.779181

Weber, K. T., Brilla, C. G., and Janicki, J. S. (1993). Myocardial fibrosis: functional significance and regulatory factors. *Cardiovasc. Res.* 27, 341–348. doi: 10.1093/cvr/27.3.341

Wilson, J. R., Clark, R. B., Banderali, U., and Giles, W. R. (2011). Measurement of the membrane potential in small cells using patch clamp methods. *Channels (Austin)* 5, 530–537. doi: 10.4161/chan.5.6.17484

Yankelson, L., Feld, Y., Bressler-Stramer, T., Itzhaki, I., Huber, I., Gepstein, A., et al. (2008). Cell therapy for modification of the myocardial electrophysiological substrate. *Circulation* 117, 720–731. doi: 10.1161/CIRCULATIONAHA.106.671776

Zlochiver, S., Munoz, V., Vikstrom, K. L., Taffet, S. M., Berenfeld, O., and Jalife, J. (2008). Electrotonic myofibroblast-to-myocyte coupling increases propensity to reentrant arrhythmias in two-dimensional cardiac monolayers. *Biophys. J.* 95, 4469–4480. doi: 10.1529/biophysj.108.136473

Conflict of Interest Statement: Gilead Sciences provided an unrestricted Grant to Dr. W. Giles. These funds supported part of this study.

Received: 31 January 2014; accepted: 07 July 2014; published online: 07 August 2014.
Citation: Koivumäki JT, Clark RB, Belke D, Kondo C, Fedak PWM, Maleckar MMC and Giles WR (2014) Na^+ current expression in human atrial myofibroblasts: identity and functional roles. Front. Physiol. ***5****:275. doi: 10.3389/fphys.2014.00275*
This article was submitted to Cardiac Electrophysiology, a section of the journal Frontiers in Physiology.

frontiers in PHYSIOLOGY

ORIGINAL RESEARCH ARTICLE
published: 08 October 2013
doi: 10.3389/fphys.2013.00281

Electrophysiological and structural determinants of electrotonic modulation of repolarization by the activation sequence

Richard D. Walton[1,2,3], Alan P. Benson[1], Matthew E. L. Hardy[1], Ed White[1] and Olivier Bernus[1,2,3]*

[1] Faculty of Biological Sciences, Multidisciplinary Cardiovascular Research Centre, School of Biomedical Sciences, Institute of Membrane and Systems Biology, University of Leeds, Leeds, UK
[2] Unité Inserm 1045, Centre de Recherche Cardio-Thoracique, Université Bordeaux Segalen, Bordeaux, France
[3] L'Institut de Rythmologie et Modélisation Cardiaque, Université de Bordeaux, Bordeaux, France

Edited by:
Zhilin Qu, University of California, Los Angeles, USA

Reviewed by:
Zhilin Qu, University of California, Los Angeles, USA
Flavio H. Fenton, Cornell University, USA

***Correspondence:**
Olivier Bernus, Inserm 1045, Centre de Recherche Cardio-Thoracique Unité, L'Institut de Rythmologie et Modélisation Cardiaque, Université Bordeaux Segalen, PTIB - Campus Xavier Arnozan, 144 rue Léo Saignat, Avenue du Haut Lévêque, 33600 Bordeaux, France
e-mail: olivier.bernus@u-bordeaux2.fr

Spatial dispersion of repolarization is known to play an important role in arrhythmogenesis. Electrotonic modulation of repolarization by the activation sequence has been observed in some species and tissue preparations, but to varying extents. Our study sought to determine the mechanisms underlying species- and tissue-dependent electrotonic modulation of repolarization in ventricles. Epi-fluorescence optical imaging of whole rat hearts and pig left ventricular wedges were used to assess epicardial spatial activation and repolarization characteristics. Experiments were supported by computer simulations using realistic geometries. Tight coupling between activation times (AT) and action potential duration (APD) were observed in rat experiments but not in pig. Linear correlation analysis found slopes of -1.03 ± 0.59 and -0.26 ± 0.13 for rat and pig, respectively ($p < 0.0001$). In rat, maximal dispersion of APD was 11.0 ± 3.1 ms but dispersion of repolarization time (RT) was relatively homogeneous (8.2 ± 2.7, $p < 0.0001$). However, in pig no such difference was observed between the dispersion of APD and RT (17.8 ± 6.1 vs. 17.7 ± 6.5, respectively). Localized elevations of APD ($12.9 \pm 8.3\%$) were identified at ventricular insertion sites of rat hearts both in experiments and simulations. Tissue geometry and action potential (AP) morphology contributed significantly to determining influence of electrotonic modulation. Simulations of a rat AP in a pig geometry decreased the slope of AT and APD relationships by 70.6% whereas slopes were increased by 75.0% when implementing a pig AP in a rat geometry. A modified pig AP, shortened to match the rat APD, showed little coupling between AT and APD with greatly reduced slope compared to the rat AP. Electrotonic modulation of repolarization by the activation sequence is especially pronounced in small hearts with murine-like APs. Tissue architecture and AP morphology play an important role in electrotonic modulation of repolarization.

Keywords: action potential duration, heterogeneity, ventricular repolarization, electrotonic current, cardiac electrophysiology

INTRODUCTION

Regional variations of the action potential duration (APD) are perhaps the best characterized form of electrophysiological heterogeneity in the heart. It has been reported in a wide range of species that spatial gradients of APD exist from base to apex and in the transmural plane of healthy myocardium (Wan et al., 2000; Antzelevitch, 2005). Such variations in APD serve to co-ordinate repolarization time (RT) of tissue to maintain normal functioning of the heart and are determined at a cellular level by the density of transmembrane ionic currents in various regions of the heart (Nerbonne and Kass, 2005).

At tissue level, intrinsic APD heterogeneity can be modulated by electrotonic interactions between cells (Laurita et al., 1996). Furthermore, such electrotonic interactions can lead to acute modulation of APD gradients depending on the activation sequence, leading to inverse linear relationships between activation time (AT) and APD (Franz et al., 1987; Laurita et al., 1997; Yuan et al., 2001; Banville and Gray, 2002; Yue et al., 2005; Chauhan et al., 2006; Hanson et al., 2009; Myles et al., 2010). The dynamic nature of this modulation has been attributed, in part, to the spatial gradient in membrane potential occurring during the repolarization phase of a propagating AP. Each cell is influenced by electrotonic load from its neighbors such that, cells repolarizing later generate an inward electrotonic current to their earlier repolarizing neighbors. In homogeneous tissue, this effectively prolongs the APD of the earlier activated cells and generates gradually decreasing APDs away from the pacing site. These APD gradients are the most pronounced at the pacing site, at the tissue

Abbreviations: 3D, Three-dimensional; AP, Action potential; APD, Action potential duration; APD_{80}, Action potential duration at 80% of repolarization; AT, Activation Time; DT-MRI, Diffusion Tensor Magnetic Resonance Imaging; LV, Left ventricle; P_g, Pig geometry; P_k, Pig kinetics; R_g, Rat geometry; R_k, Rat kinetics; RT, Repolarization time; RT_{max}, Maximum repolarization time; RT_{min}, Minimum repolarization time.

boundaries and in directions of slow propagation (Zubair et al., 1994).

Several computational studies have investigated the effects of electrotonic currents on repolarization in cardiac tissue. Sampson and Henriquez (2005) for example, observed that electrotonic interactions could completely mask the intrinsic transmural APD gradient in the small mouse heart, but not in the larger rabbit heart. A more recent computational study by Cherry and Fenton (2011) found that boundaries act as a sink and shorten APD in otherwise homogeneous tissues. Moreover, APD was abbreviated where APs collide, or significantly increased where APs travel around sharp cusps in tissue geometry, such as occurring at the insertion site of the septum with the ventricular wall. In experiments, electrotonic modulation of repolarization by activation sequence has been observed to various extents in myocardium of different species, including humans, and various tissue preparations (Franz et al., 1987; Laurita et al., 1997; Yuan et al., 2001; Banville and Gray, 2002; Yue et al., 2005; Chauhan et al., 2006; Hanson et al., 2009; Walton et al., 2010). However, the species-to-species variability and the effects of tissue geometry have not yet been shown nor elucidated experimentally.

In the present study we aimed to determine the mechanisms underlying species- and tissue-dependent electrotonic modulation of repolarization in ventricles. Therefore, we investigated acute electrotonic APD modulation by activation sequence in two distinct species, the rat and the pig, and two different tissue preparations, the intact heart (rat) and the left ventricular wedge preparation (pig). The rat is used extensively in cardiac electrophysiology studies (Macchi et al., 2004; Rossi et al., 2008; Wasserstrom et al., 2009), while the pig is more closely related to human in terms of cardiac electrophysiology (Yuan et al., 2001). We used an epi-fluorescence optical mapping technique that provides high spatio-temporal resolution of electrical activity (Walton et al., 2010) to relate epicardial AT to APD and RT. We also utilized detailed computational models of electrical propagation in realistic tissue geometries obtained by diffusion tensor magnetic resonance imaging (DT-MRI) to investigate the relative roles of AP morphology and tissue geometry on electrotonic modulation of repolarization.

METHODS

TISSUE PREPARATION

All experimental protocols conformed to the Animals (Scientific Procedures) Act 1986. Male Wistar rats ($N = 8$) weighing 220–250 g were euthanized by stunning and cervical dislocation and hearts rapidly excised. Hearts were submersed in cold (4°C) cardioplegic solution containing (in mmol/L): glucose, 277.5; KCl, 30; $NaHCO_3$, 25; mannitol, 34.3, pH 7.4. The aorta was cannulated and perfused at 7 ml/min with bicarbonate buffered saline solution containing (mmol/L): NaCl, 130; $NaHCO_3$, 24; NaH_2PO_4, 1.2; $MgCl_2$, 1; glucose, 5.6; KCl, 4; $CaCl_2$, 1.8; oxygenated with 95% O_2/5% CO_2, pH 7.4, 37°C. Female pigs (24–26 Kg, $N = 9$) were euthanized by intraperitoneal injection with sodium pentobarbital (35 mg/Kg) and the hearts were quickly excised. The aorta was cannulated and perfused with cold cardioplegic solution supplemented with heparin (5 U/ml). The left ventricular wall was dissected and the left anterior descending coronary artery was cannulated and perfused with bicarbonate buffered saline solution at 20 ml/min. In all experiments, the perfusate was supplemented with 10 μM blebbistatin for mechanical uncoupling of the myocardium.

OPTICAL MAPPING PROTOCOL AND SETUP

The tissue was stained with potentiometric dye DI-4-ANEPPS (50 μg/ml bicarbonate buffered saline solution) via the perfusate at the beginning of the experiment (Walton et al., 2010). Bipolar electrodes were used to stimulate the ventricles over a range of basic cycle lengths from 160 to 83 ms for rats and 1000–256 ms for pigs. Optical recordings were acquired through a high-frame-rate charge-coupled device video camera (SciMeasure Analytical systems, GA, USA) mounted with a lens (focal length 12 mm, 1:0.8 aperture ratio; Computar, London, UK). Excitation light from monochromatic LEDs, 530 nm, (Cairn Research Ltd, Kent, UK) illuminated the epicardial surface. Emission light from DI-4-ANEPPS was filtered through a broadband 700DF50 filter. Images (80 × 80 pixels) with pixel dimensions of 0.25 × 0.25 mm for rats and 0.4 × 0.4 mm for pigs were acquired at 1000 frames per s. Background fluorescence was subtracted from each frame to obtain the voltage-dependent optical signal. Optical APs acquired over 10 s were ensemble averaged and underwent temporal (3 ms kernel) and spatial (1.25 mm kernel) filtration.

DIFFUSION TENSOR MRI

We determined tissue geometry and architecture using DT MRI. Following optical mapping experiments, hearts, and ventricular wedge preparations were perfused with 4% formalin. Fixed hearts were immersed in the perfluoropolyether Fomblin (Sigma-Aldrich, St. Louis, USA) to reduce noise and enhance image contrast. High resolution (200 μm isotropic) imaging of the fiber orientation was performed with a 9.4 T NMR instrument (Bruker BioSpin, Ettlingen, Germany). Diffusion of protons was measured throughout the tissue in a set of 12 optimized directions (Papadakis et al., 1999) using a 3D diffusion-weighted spin-echo sequence with reduced encoding at 20°C (500 ms repetition time; 15 ms echo time; diffusion gradients with 2 ms duration and 7 ms separation; $b = 1000\ \mathrm{s\ mm^{-2}}$). Diffusion tensors, and the eigenvectors and eigenvalues of these tensors, were calculated from the diffusion measurements at each voxel throughout the tissue using in-house software. No smoothing or interpolation of the diffusion measurements was necessary: see Benson et al. (2011b) for examples of the calculated fiber directions in rat hearts.

COMPUTER SIMULATIONS

As in previous studies we used a monodomain approach to simulate AP wave propagation in cardiac tissue (Walton et al., 2010). Realistic geometry and fiber orientation (represented in the models by the electrical diffusion tensor $\mathbf{D}$) were obtained from DT-MRI (see above):

$\mathbf{D}$ at a particular point in space is given by

$$\mathbf{D} = D_1\mathbf{I} + (D_1 - D_2)\mathbf{e}_1\mathbf{e}_1^{\mathrm{T}}$$

where D_1 and D_2 are electrical diffusions along and across the fiber, respectively (both in $\mathrm{mm^2 ms^{-1}}$), $\mathbf{I}$ is the identity matrix, $\mathbf{e}_1$

is the primary eigenvector from DT-MRI, and the superscript T denotes vector transpose. We set D_1 to 0.095 mm^2ms^{-1} in the pig model and 0.17 mm^2ms^{-1} in the rat model, which gave conduction velocities of 0.6 ms^{-1} in the fiber direction in both cases. For anisotropic propagation, we used a 1/4 diffusion ratio (i.e., $D_2 = D_1/4$) in rat and 1/9 diffusion ratio in pig, which gave conduction velocities of 0.3 and 0.15 ms^{-1}, respectively, in the cross-fiber direction to match conduction velocity ratios measured by optical mapping. Electrical excitation at a particular point in the heart is then given by

$$\frac{\partial V}{\partial t} = \nabla(\mathbf{D}\nabla V) - I_{\text{ion}}$$

where V is membrane potential (mV), t is time (ms), ∇ is a spatial gradient operator, and I_{ion} is total membrane ionic current density (μA/μ F). For I_{ion} in the rat, we used the model of Pandit et al. (2001) with constant ion concentrations, Q_{10} modifications for temperature as in Noujaim et al. (2007). In addition, $G_{\text{Ca,L}}$ was increased by 75% and G_{to} decreased by 25% so that the model APD matched experimentally-recorded APDs. For I_{ion} in the pig, we used the Luo-Rudy dynamic guinea pig model (Faber and Rudy, 2000) (as no model for the pig is currently available), also with constant ion concentrations, and with $G_{\text{Ca,L}}$ increased by 25% and G_{Kr} and G_{Ks} both decreased by 30%, so that the model APD matched experimentally-recorded pig APD. For a subset of simulations we increased G_{Kr} and G_{Ks} by a factor of 28.5 to match the pig APD to the rat APD. In the rat left ventricle a linear transmural gradient in selected ion channel densities was implemented as in Pandit et al. (2001), Walton et al. (2010). For rat right ventricular tissue, the epicardial model conductances were scaled according to the values in Benoist et al. (2011). For the pig model, a transmural gradient was introduced by assuming the default model (Faber and Rudy, 2000) was epicardial, increasing G_{Na} by 33% and reducing G_{to} by 64% for the endocardial model, then linearly scaling these parameters as a function of transmural distance. In all cases, pacing was via a twice-diastolic threshold stimulus current for 10 beats (500 and 167 ms basic cycle lengths for the pig model or rat model, respectively). The models were coded in C, and solved using a forward-time center-space method (Press et al., 2007) and an operator splitting and adaptive time step technique (Qu and Garfinkel, 1999), with a fixed space step of 0.2 mm (as determined by the DT-MRI resolution), a minimum time step of $\Delta t_{\text{min}} = 0.01$ ms, and a maximum time step of $\Delta T = 0.25$ ms. No-flux boundary conditions were imposed by setting electrical diffusion along the vector normal to the local tissue surface to zero, a standard approach for finite difference models. See (Benson et al., 2008, 2011a) for further details.

DATA ANALYSIS AND STATISTICS

AT was measured at the level of the maximal time derivative of the AP upstroke in experiments and simulations. APDs were measured from the AT to 80% of repolarization (APD_{80}). RT was measured at the time of 80% of repolarization (RT = APD_{80} + AT). Linear correlation analysis was used to determine the relationship between AT and APD_{80} by comparing gradients of fits. Dispersion of APD_{80} and RT were measured as the difference between their respective 5 and 95% confidence intervals of normal sample distributions. Pixels incorporated in the measurement of dispersion were restricted to those with AT $\leq$ 10 ms. Statistical analyses using paired and unpaired t-tests determined significance when $p < 0.05$.

RESULTS

THE DISTRIBUTION OF THE ACTION POTENTIAL DURATION

Optical images from the epicardial surface of the rat ventricles and the pig left ventricular myocardium were obtained to investigate the relationship between the activation sequence and the spatial distribution of APD_{80}. **Figure 1** shows activation and APD_{80} maps for epicardial stimulation of the rat and pig tissues at 160 and 496 ms basic cycle lengths, respectively. **Figure 1A** (left panel) shows the activation map across the rat left ventricle following stimulation at the anterior insertion site (isochrones are shown every 1 ms). A total AT of 14.5 ms was found across the left ventricle. The corresponding spatial distribution of APD_{80} was heterogeneous (middle panel). The longest APD_{80} of 58.4 ms was observed at the pacing location and the shortest of 35.7 ms lay close to the site of the latest AT. The steepest mean spatial gradient of APD (1.6 ± 1.1 ms/mm) was found to lie along the direction of slowest AP propagation. Optical APs along the 10 ms isochrone, one from the base and another from the apex, were compared with an AP from an early (4 ms) activation site and aligned by the maximal derivative of the upstroke (right panel). APs from early activated regions were associated with slowed rates of repolarization relative to APs from late activated regions. **Figure 1B** shows activation and APD_{80} maps obtained from the simulations using the rat heart model. As in experiments, regions of early activation were associated with the longest APD_{80} (57.7 ms) that became gradually shorter with AT. Spatial gradients of APD_{80} were greatest in the directions of slowest propagation, consistent with experiments. APs extracted from voxels with early and late ATs were aligned by AT and superimposed to illustrate the difference in APD (right). As in experiments, relative prolongation of APDs associated with early ATs could be observed.

Figure 1C (left panel) shows the activation map from a coronary-perfused pig left ventricle that was stimulated from the anterior apical region. Smooth anisotropic propagation was observed across the tissue preparation with a total epicardial AT of 44.4 ms (isochrones are shown every 5 ms). Although a heterogeneous pattern of APD_{80} was found in the pig ventricle (middle panel), dispersion of APD_{80} did not seem to correlate with AT. The longest APD_{80} was observed at the mid-level of the left ventricular wall (276.7 ms) whereas the shortest was found close to the pacing site (237.7 ms). This is further confirmed by examination of individual optical APs obtained at various ATs as shown on the right panel. Interestingly, simulations showed some degree of APD_{80} modulation by the activation sequence with the longest APD_{80} (238.3 ms) near the pacing site (**Figure 1D**). Yet, this effect was small compared to the simulations and experiments in rat intact hearts. It should be noted that in both rat and pig simulations, base-to-apex gradients of APD were to incorporated in to the ionic models, or moreover a Purkinje fiber network. This will,

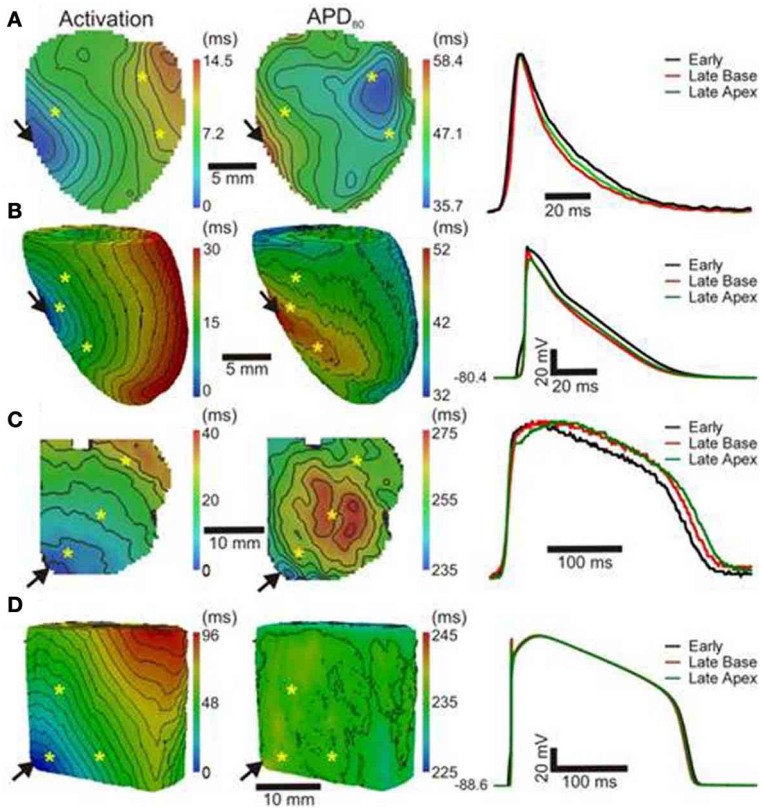

FIGURE 1 | AT and APD maps from rat and pig myocardium. Rat ventricles were paced from the anterior insertion sites (arrows) in experiments **(A)** and simulations **(B)**. Pig left ventricular wedge preparations were paced from the apex in experiments **(C)** and simulations **(D)**. Panels (from left to right) are AT, corresponding APD maps and AP traces acquired from pixels indicated by*. Isochrones are 1 and 5 ms spacing for rat and pig experiments and 2 and 5 ms for the corresponding simulations. AP traces are aligned by activation times.

in part, account for differences in the dispersion of APD and total AT observed between experiments and simulations.

In order to further establish the role of activation sequence we investigated APD_{80} distributions from secondary pacing locations in all experiments and simulations. **Figure 2** shows activation and APD_{80} maps from the same experiments as in **Figure 1** but when pacing the mid-free wall of the left ventricle. **Figure 2A** indicates that the region of longest APD_{80} in the rat heart was shifted to the new pacing location (compare with **Figure 1A**). APD_{80} became progressively shorter away from this site, predominantly in the direction of slow conduction (optical APs shown in right panel). A shift in APD_{80} to the site of earliest activation was consistently observed in simulations (**Figure 2B**). Conversely, changing the pacing location in the pig myocardium did not significantly alter the distribution of APD_{80} in experiments (**Figure 2C**). Although a region of long APD_{80} was evident at the pacing location in simulations (**Figure 2D**), the spatial gradient of APD_{80} across the epicardial surface was very shallow relative to that observed in the rat.

RELATIONSHIP BETWEEN ACTION POTENTIAL DURATION AND THE ACTIVATION SEQUENCE

The relationship between AT and APD_{80} at each pixel of the imaged surface was quantified by linear regression analysis. Representative data for rat and pig experiments are shown in **Figures 3A,B**, respectively. For all AT-APD plots, the relative APD_{80} from the maximum APD_{80} is shown by the secondary y-axes. These plots correspond to the activation and APD_{80} maps shown in **Figure 1** whereby tissue was paced from the mid-anterior insertion site in rat and apical region of LV in pig. A clear decreasing trend of APD_{80} with AT was revealed in the rat (slope $= -0.84$, $R = 0.65$) compared with a relatively shallow relationship and poor correlation in the pig wedge preparation (slope $= -0.05$, $R = 0.06$). Mean $\pm$ SD of R values of linear regression were significantly less in pig than rat (0.25 ± 0.22 vs. 0.66 ± 0.18, $p = 0.0002$). Relative to the maximum APD_{80} observed on the imaged surface, APD_{80} was decreased by as much as 38.9% in rat but only 16.0% in pig. Linear regression analyses of AT and APD_{80} relationships in rat (**Figure 3C**) and pig (**Figure 3D**) simulations were qualitatively similar to experiments. We further show that upon changing the location of pacing of the tissue to the mid-LV free wall, the steep AT, and APD relationship of rat simulations (**Figure 3E**) and shallow relationship of pig simulations (**Figure 3F**) were conserved. This data is further supported by statistical comparison of APD_{80} from early (4 ms) and late (10 ms) ATs. Across all rat hearts and stimulation sites (**Figure 3I**), a significant decrease in APD_{80} (13.8%) was found between early and late activated

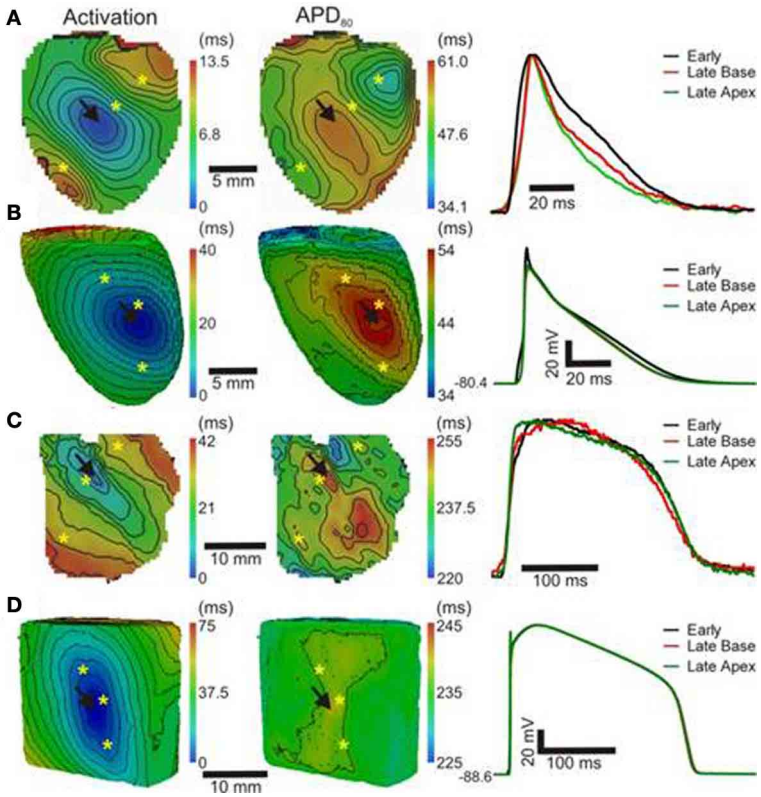

FIGURE 2 | APD distributions for alternative activation sequences in rat and pig myocardium. Rat experiments **(A)** and simulations **(B)**; and pig experiments **(C)** and simulations **(D)** with pacing from the mid free left ventricular wall (arrows). Panels (from left to right) are AT, corresponding APD maps and AP traces acquired from pixels indicated by *. Isochrones are as in **Figure 1**. AP traces are aligned by activation times.

zones ($p < 0.0001$), while no significant difference was observed in the pig wedge (**Figure 3J**). Correlations between AT and APD_{80} for rat and pig experiments were further assessed by comparison between slopes of the linear relationship between APD_{80} and AT. **Figure 3K** shows that AT-APD_{80} relationships across all experiments were significantly steeper in rats compared to pigs ($p < 0.0001$). In simulations, AT and APD_{80} values were extracted from the epicardial surface of the LV free wall in accordance with the imaging plane of experiments. We found a significant decrease in APD with AT in both the rat and pig model. However, over a 6 ms interval in AT when pacing the mid-LV fee wall, APD decreased by 7.57% in rat and by only 0.4% in pig (**Figures 3L,M**). The slope of AT and APD_{80} relationship in pig was only 11.6% of that observed in rat (**Figure 3N**). For comparison, we report that when pacing the mid-anterior insertion site in rat and apical region of the LV in pig, similar differences of Mean ± *SD* APD_{80} between 4 and 10 ms isochrones were identified as for the aforementioned pacing location (7.1 and 0.3%). Accordingly, a difference in the slope of AT and APD_{80} relationships between rat and pig was observed (29.6%).

THE DISPERSION OF REPOLARIZATION TIME

Since local RT depends on local APD, it is to be expected that modulation of APD by the activation sequence affects RT dispersion. **Figure 4A** shows that, in rat, progressive shortening of the APD throughout the activation sequence plays an important role in homogenizing the spatial dispersion of RT. However, for the pig, a lack of association between APD and AT resulted in RT to follow the sequence of activation and intrinsic heterogeneities of APD (**Figure 4B**). As total AT of the rat LV is typically <15 ms, the dispersion of RT was calculated from pixels corresponding to the earliest 10 ms of AT. The dispersion of RT ($RT_{95\%}$–$RT_{5\%}$) was 7 and 14 ms for the rat and pig shown in **Figures 4A,B**, respectively. Simulations were in accordance with experiments as seen by relatively homogeneous epicardial RT maps in rat whereas the reverse was seen for pig (**Figures 4C,D**). Similarly using the secondary pacing location, RT was relatively homogeneous in rat compared to pig. The dispersion of RT was seemingly consistent in rat at 8 (**Figure 4E**) and 16 ms in pig (**Figure 4F**). Simulations of the secondary pacing locations were again consistent with experiments (**Figures 4G,H**).

Comparisons of Mean ± *SD* (pooled from each pacing location) APD_{80} dispersion and RT dispersion for rat and pig experiments are shown in **Figures 4I,J**. The dispersion of RT is less than APD_{80} by 25.3% ($p < 0.0001$) in rat (**Figure 4I**) whereas no significant difference was observed in pig (**Figure 4J**). In simulations pacing at the mid-LV free wall the percentage change of APD_{80} dispersion

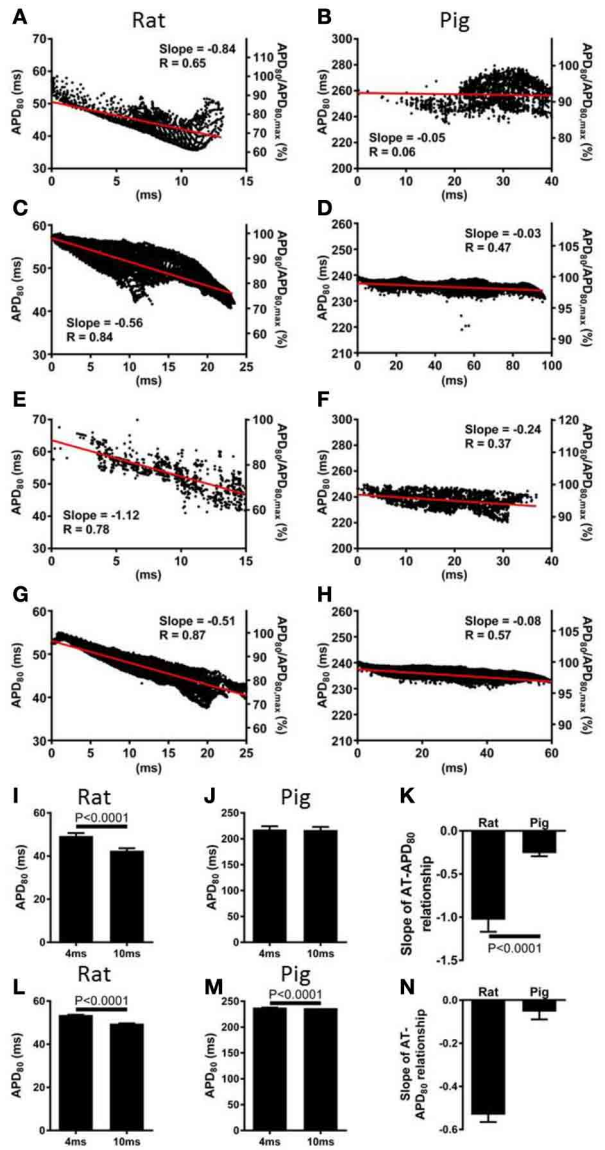

FIGURE 3 | Correlations between AT and APD in rat and pig myocardium. AT and APD plots corresponding to maps shown in **Figure 1** for rat **(A)** and pig **(B)** experiments. Slopes for linear correlation analyses are indicated. AT and APD plots of corresponding simulations are shown for rat **(C)** and pig **(D)**. Similarly, AT and APD plots from an alternative pacing location, as in **Figure 2**, are shown for rat **(E)** and pig **(F)** experiments and rat **(G)** and pig **(H)** simulations. Panels **(A–H)** are also expressed as a percentage of the maximum APD_{80}. Mean ± *SD* APD corresponding to 4 and 10 ms activation isochrones across all experiments and pooled from each pacing location in rat **(I)** and pig **(J)**. **(K)** Equally, slopes of linear correlations between AT and APD were quantified for all experiments and pacing locations and expressed as Mean ± *SD*. Similarly to experiments, early vs. late activation times were compared for rat **(L)** and pig **(M)** simulations shown in **Figure 2**. **(N)** Slopes from linear correlations of corresponding AT and APD data are compared. All mean differences were compared using *t*-tests. Significant differences are indicated if $P < 0.05$.

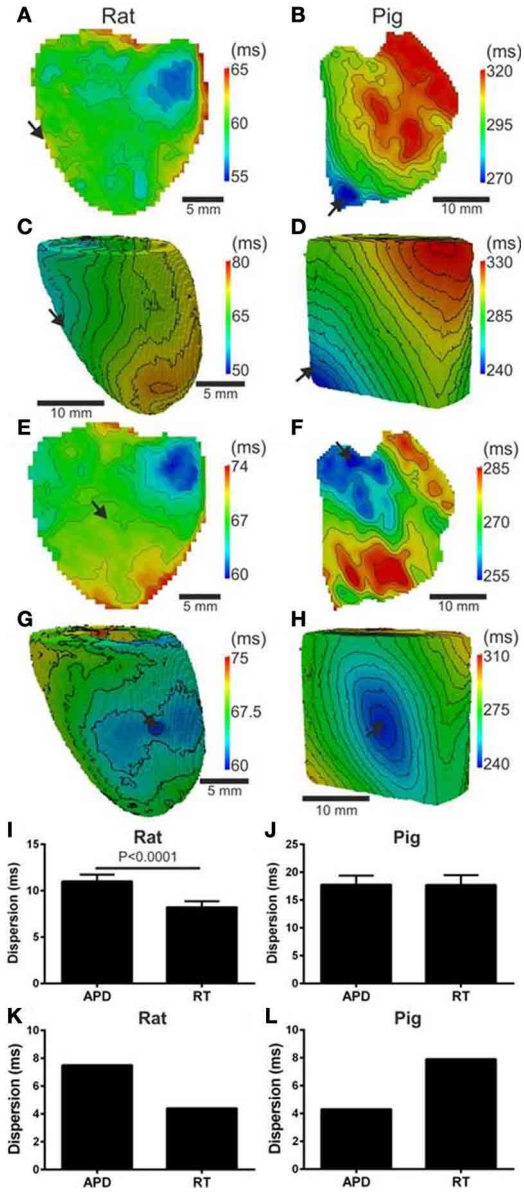

FIGURE 4 | Left ventricular dispersion of RT in rat and pig myocardium. RT maps corresponding to maps shown in **Figure 1** for rat **(A)** and pig **(B)** experiments and rat **(C)** and pig **(D)** simulations. Similarly, RT maps for an alternative pacing location, as in **Figure 2**, are shown for rat **(E)** and pig **(F)** and repeated for rat **(G)** and pig **(H)** simulations. Stimulation sites are indicated by arrows. Mean ± *SD* dispersion of APD and RT pooled from each pacing location are compared across all experiments in rat **(I)** and pig **(J)**. All mean differences from experiments were compared using paired *t*-tests. Significant differences are indicated if $P < 0.05$. Similarly to experiments, dispersion of APD and RT were compared for rat **(K)** and pig **(L)** simulations shown in **Figure 2**.

to RT dispersion supported experimental findings showing reduced RT dispersion in rat (41.3%, **Figure 4K**) but a relative and robust gain of RT dispersion in pig (83.7%, **Figure 4L**).

MODULATION OF ACTION POTENTIAL DURATION AND REPOLARIZATION TIME BY TISSUE ARCHITECTURE

In our rat heart experiments we found that the insertion sites of the two ventricles were the only regions where the AT-APD_{80} relationship could significantly be altered. **Figure 5A** shows a wave front propagating from a left ventricular mid-free wall pacing site to the right ventricle (left panels). In these experiments anterior and posterior activity was acquired simultaneously. The corresponding APD_{80} and RT distributions are shown in the middle and right panels, respectively. The longest and shortest APD_{80} were still located at the pacing site and the region of latest activation, respectively. **Figure 5B** shows APD_{80} profiles obtained from the maps in **Figure 5A** (dashed line). The profile was chosen through the pacing location and the site of shortest APD_{80}. On the anterior side, a region coinciding with the boundary between the left and right ventricle showed a local maximum in APD_{80} (31.9 ms). This had a significant effect on the local RT with a local increase of as much as 4.1 ms (**Figure 5C**). Computer simulations in the 3D model of the rat ventricle allow investigation of this phenomenon in more detail. **Figure 5D** shows transmural activation and APD_{80} maps in the model. The AP propagated anisotropically from the left ventricle into the septum and right free wall (left panel). The APD_{80} map reveals a region of enhanced APD_{80}, and consequently RT, localized to the septal-ventricular branching site (black box). Furthermore, the site of wave front collisions in the RV and septum were associated with significantly decreased APD_{80}, RT and enhanced mean gradients of APD_{80} shortening compared to those observed in the LV free wall (1.4 vs. 0.2 ms/mm). **Figures 5E,F** further illustrates these findings by plotting APD_{80} and RT, respectively, along the transmural profiles indicated in **Figure 5C** (dashed line).

RATE-DEPENDENCY OF ELECTROTONIC MODULATION OF REPOLARIZATION

In our experiments a strong relationship between APD_{80} and AT was preserved at different pacing frequencies in rat but not in pig. APs from short and long pacing cycle lengths are shown for rat (**Figure 6A**) and pig (**Figure 6B**) experiments. **Figure 6C** shows APD_{80} restitution curves from locations corresponding to relatively early (4 ms) and relatively late AT (10 ms) isochrones. Throughout the range of pacing cycle lengths applied in rat, ranging from 83 to 167 ms, the largest mean difference in APD_{80} between early and late AT data were found at longer pacing cycle lengths. At shorter pacing cycle lengths restitution curves tended toward convergence as indicated by a reduction in statistical power (although still significant). Convergence of APD_{80} restitution data at short cycle lengths was attributed to variation in the maximum slope of the restitution profile between early and late regions of AT. The maximal slope of APD_{80} data restitution was larger at regions of early AT compared with late AT

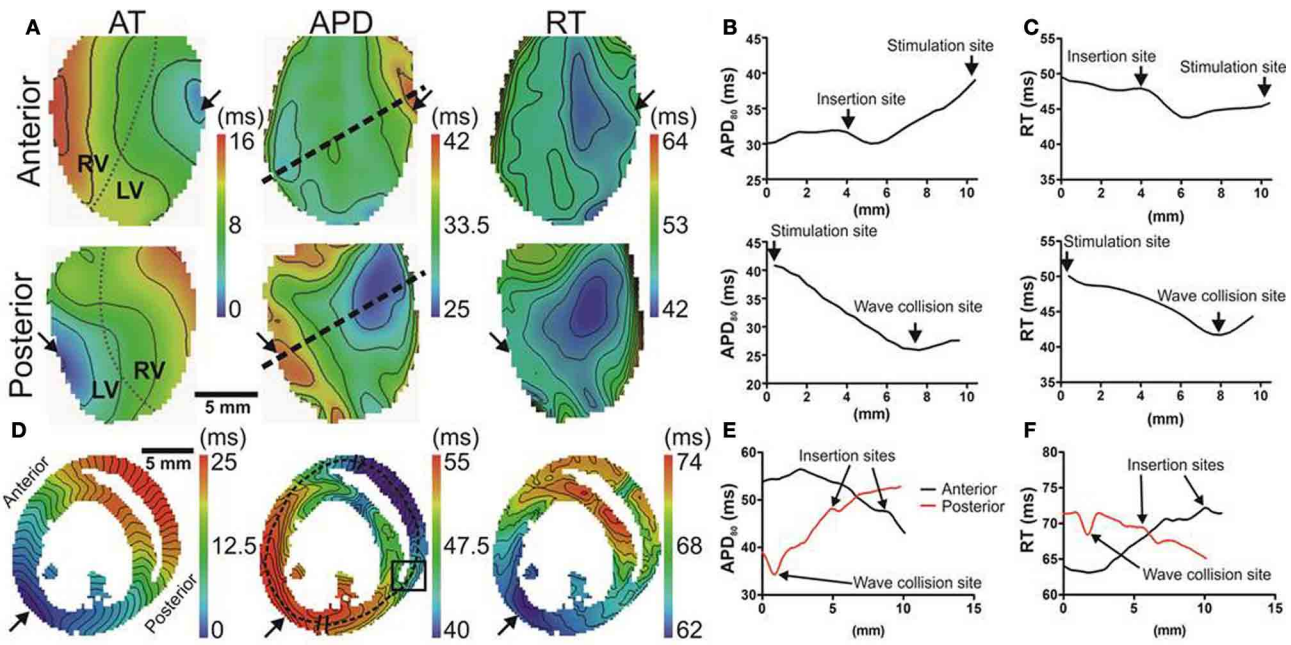

FIGURE 5 | Local modulation of APD in rat hearts by tissue architecture. (A) Hearts were simultaneously imaged from anterior (upper panels) and posterior (lower panels) views. Panels (from left to right) are AT and APD maps from ventricles paced at the mid left ventricular free wall (arrows). Insertion sites of left and right ventricular free walls are indicated by dotted lines in AT maps. Isochrones are spaced 2 ms. Linear profiles of APD **(B)** and RT **(C)** measured from anterior (upper panel) and posterior (lower panel) surfaces. APD values were taken along linear profiles intersecting the longest and shortest APD from each imaged surface (dashed lines in Panel **A**). Regions corresponding to pacing sites, insertion of ventricles and convergence of anterior and posterior wave fronts are indicated. **(D)** AT and APD maps in simulations are shown in the transverse plane. Isochrones are spaced 1 ms apart. A region of long APD was identified at the insertion site (box). Transmural profiles of APD **(E)** and RT **(F)** are plotted from pixels along dashed lines shown in **(D)**.

(0.21 vs. 0.08). In pig experiments, APD_{80} restitution was largely unaffected by AT between pacing cycle lengths ranging from 256 to 1000 ms (**Figure 6D**). Significant differences of APD_{80} were observed between early and late AT at 288 and 336 ms only. Despite modest differences in mean APD_{80} at specific cycle lengths, the maximal slope of restitution was equal (0.63) between early and late AT.

To determine the rate-dependency of electrotonic modulation of repolarization, the slope of linear correlations of the AT-APD_{80} relationship were quantified across all pacing cycle lengths in rat and pig experiments. **Figure 6E** shows the lack of dependence of the AT-APD_{80} slope on pacing cycle length. The mean of the slope was preserved between a range of −0.57 and −0.82. One-way analysis of variance determined no statistical variation within the sampled pacing cycle lengths ($P > 0.05$). Similarly for pig, slopes of AT-APD_{80} relationships were unaffected by pacing cycle length (**Figure 6F**). However, slopes were consistently less steep than for rat, ranging from −0.25 to −0.4 with no statistically significant variation for different pacing cycle lengths ($P > 0.05$).

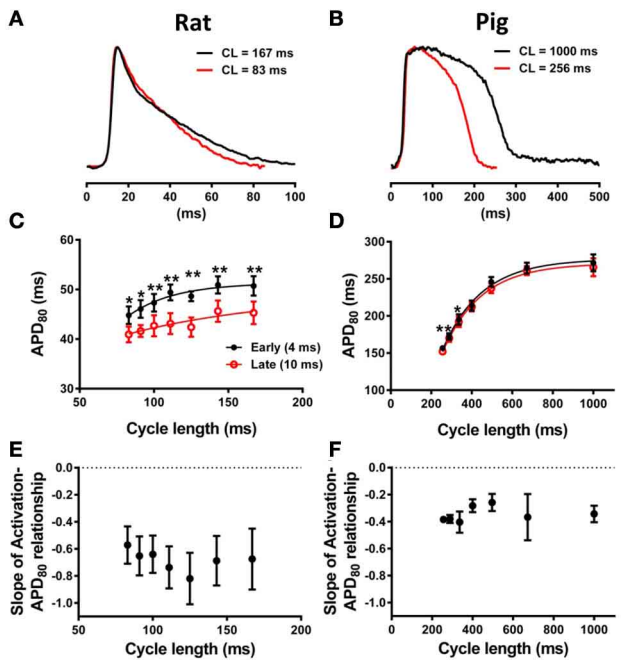

FIGURE 6 | Restitution properties of APD_{80} and its dependence on AT. (A) Representative optical AP traces extracted from the same pixel location during pacing with cycle lengths, CL, of 167 and 83ms in rat. **(B)** Similarly, optical AP traces from pig paced at 1000 and 256 ms cycle lengths are superimposed. Mean ± *SD* APD_{80} from 4 and 10 ms isochrones were plotted against pacing cycle length for rat **(C)** and pig **(D)** ($N = 7$and $N = 5$, respectively). Statistical differences between APD across all pacing frequencies were determined by paired *t*-tests (*$P < 0.05$; **$P < 0.01$). For comparison of the steepness of restitution, data were fitted with one-phase decay exponential curves. Mean ± *SD* of slopes of linear relationships between AT and APD_{80} were plotted against pacing cycle length for rat **(E)** and pig **(F)**. One-way ANOVA was used to determine statistical data variance across pacing cycle lengths tested ($P < 0.05$). No statistical deviations between means of slopes were observed for rat or pig.

DETERMINANTS OF ELECTROTONIC LOAD

The computational models allow investigation of the relative roles of AP shape (or kinetics), tissue size and tissue geometry on the electrotonic modulation of repolarization. This was first assessed by interchanging rat and pig AP kinetics (R_k and P_k, respectively) from simulations in rat and pig tissue geometries (R_g and P_g, respectively). In **Figure 7** R_kP_g and P_kR_g simulations were paced at the mid LV free wall, consistent with **Figure 2**. **Figures 7A,B** show AT and APD_{80} maps for the R_kP_g and P_kR_g simulations, respectively. The regions of longest APD_{80} was observed close to sites of stimulation in each simulation. In **Figure 7C** APD_{80} is plotted against AT for the R_kP_g (left panel) and P_kR_g (right panel) simulations. Maximal spatial in plane dispersion of APD_{80} was as much as 48.9% of the maximal epicardial APD_{80} in R_kP_g simulations, but only 4.1% in P_kR_g. The slope of the AT-APD_{80} relationship became less negative by 54.9 and 58.6% when comparing R_kR_g to P_kR_g and R_kP_g, respectively. Conversely, the steepness of this relationship became more pronounced by 66.3and 52.5% when comparing P_kP_g with P_kR_g and R_kP_g. The computational models were further used to assess the effects of tissue size alone on electrotonic modulation of repolarization by either increasing or decreasing the tissue dimensions by a factor of two in the rat geometry (R_{gx2})

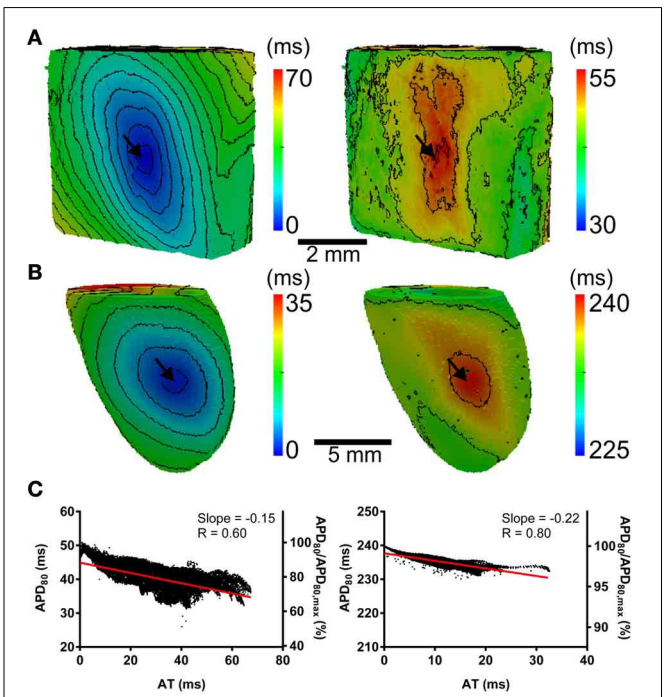

FIGURE 7 | The influence of electrophysiological kinetics and tissue geometry on the dispersion of APD. Electrophysiological kinetics for rat (R_k) and pig (P_k) simulations was interchanged between geometries (R_g and P_g, respectively). Ventricles were paced at the mid LV free wall (arrows). Panels are maps of AT (left panels) and APD_{80} (right panels) derived from simulations in the following configurations: R_kP_g **(A)** P_kR_g **(B)**. Isochrones are 4ms for all maps. **(C)** AT-APD plots for R_kP_g (left panel) and P_kR_g (right panel) simulations. Slopes of linear correlation analyses are indicated. Secondary *y*-axes show APD_{80} expressed as a percentage of maximum APD_{80}.

(**Figure 8A**) and pig wedge ($P_{gx0.5}$) (**Figure 8B**). In **Figure 8C** APD_{80} is plotted against AT for R_kR_{gx2} and $P_kP_{gx0.5}$ simulations, respectively. We find that by comparison to **Figure 3**, the slope of the AT-APD_{80} relationship becomes less negative by enlargement of rat heart simulations (−0.19 vs. −0.56). The converse was observed in the pig wedge of reduced dimensions, where an increased association between AT and APD_{80} is observed relative to simulations of true dimensions (−0.1 vs. −0.03 AT-APD_{80} slope). To ascertain the effects of AP morphology alone on electrotonic modulation of repolarization, we compared a modified pig kinetics model with an equivalent APD_{80} to the rat model. **Figure 9A** shows that the modified pig model retained a spike and dome-like AP with a considerably shortened plateau phase when compared to the unmodified pig AP (**Figures 1**, **2**) and an increased rate of repolarization during phase 3, relative to the rat AP. Despite APD_{80} being similar, epicardial APD_{80} in the $P_{k,short}R_g$ simulation showed little dependence on AT (**Figure 9B**). The slope of AT-APD relationship was less by as much as 92.0% compared to R_kR_g simulation (shown in **Figure 3G**).

For comparison to anisotropic simulations, isotropic (no fibers) simulations in rat heart and pig wedge geometries were performed. Here the uniform spread of excitation in rat was associated with near uniform gradients of APD_{80} away from the site of stimulus (**Figure 10A**). APD_{80} was found to change near 1:1 with AT shown by a change of 6 ms of AT, from 4 to 10 ms isochrones, modulated APD_{80} from a Mean ± *SD* of 57.5 ± 0.5 ms to 52.5 ± 1.3 ms. Therefore, a near simultaneous repolarization time was observed in the left ventricle of the isotropic rat simulation. Simulations in isotropic wedges also revealed a strengthening, although modest, of the relationship between AT and APD using the pig model compared to anisotropic wedges (**Figure 10B**). Despite this, early vs. late AT modulated APD_{80} from a Mean ± *SD* of 238.9 ± 0.3 ms to only 237.1 ± 0.3 ms. Consequently, significant dispersion of RT was still observed, and followed the activation sequence. **Figure 11** summarizes the slopes from linear correlations of APD_{80} plotted against AT for the simulations in **Figures 2**, **7–10**.

TRANSMURAL DISPERSION OF ACTION POTENTIAL DURATION

Finally, the influence of tissue geometry in the transmural plane on electrotonic modulation of repolarization was investigated. AT and APD_{80} values were extracted from transmural slices corresponding to the level of the pacing site for both rat (R_kR_g) and pig (P_kP_g) models. AT-APD_{80} relationships for rat and pig revealed clear descending linear distributions of APD_{80} with AT (**Figures 12A,B**, respectively). For the R_kR_g simulation, the shortest APD_{80} was observed at the latest AT with an APD_{80} that was 44.6% shorter than the maximal APD_{80} within the transmural plane. Percentage shortening of APD_{80}

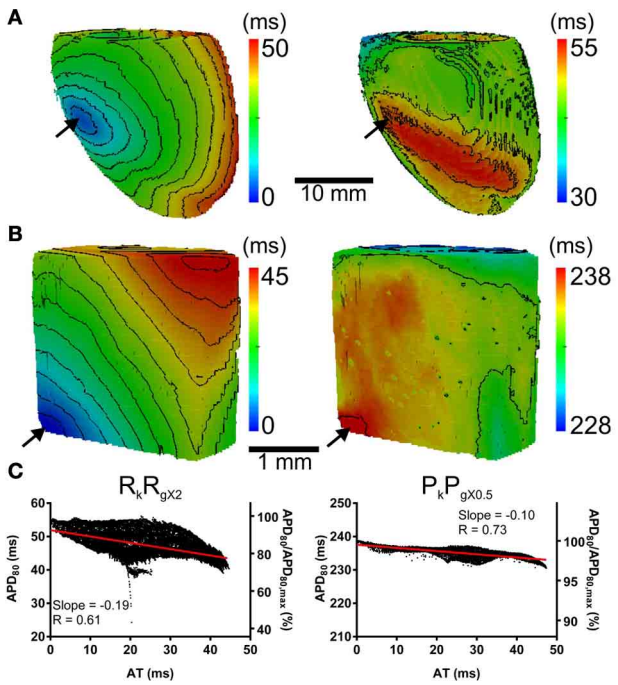

FIGURE 8 | The influence of tissue geometry on the dispersion of APD. Ventricles were paced at the mid-anterior insertion site of rat and apex of pig geometries (arrows). Panels are maps of AT (left panels) and APD (right panels). **(A)** Dimensions of rat geometries were increased by a factor of two (R_kR_{gX2}). **(B)** Pig kinetics were simulated in a pig geometry with dimensions scaled by half ($P_kP_{gX0.5}$). Isochrones are 4 ms for all maps. **(C)** AT-APD plots for R_kR_{gX2} (left panel) and $P_kP_{gX0.5}$ (right panel) simulations. Slopes of linear correlation analyses are indicated. Secondary *y*-axes show APD_{80} expressed as a percentage of maximum APD_{80}.

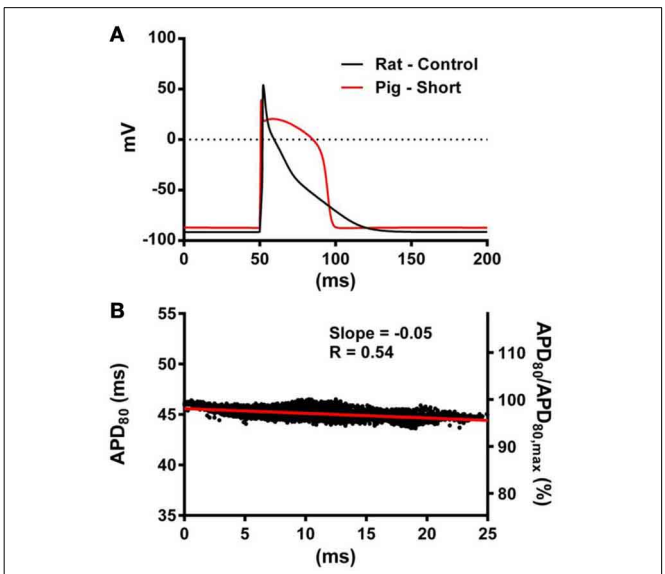

FIGURE 9 | The influence of AP morphology on coupling of AT and APD. In the rat geometry simulations of rat kinetics were compared to a modified pig kinetics model ($P_{k,short}R_g$) whereby G_{Ks} and G_{Ks} were increased by a factor of 28.5 to match the APD_{80} of the rat model. **(A)** Single cell AP traces comparing the rat and modified pig kinetics. Whole rat ventricle simulations were paced at the mid LV free wall. **(B)** AT-APD plot shown for $P_{k,short}R_g$ simulation. The comparative AT-APD plot for an R_kR_g simulation is shown in **Figure 3G**. Slope of linear correlation analyses is indicated. Secondary *y*-axes show APD_{80} expressed as a percentage of maximum APD_{80}.

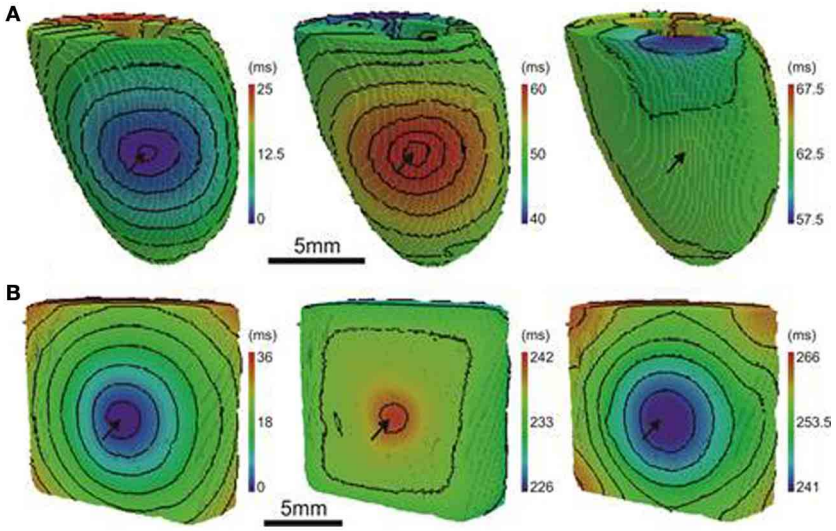

FIGURE 10 | AT, APD, and RT maps for isotropic simulations. In rat **(A)** and pig **(B)** simulations, the activation sequences (left panels) show no preferential direction of propagation. Sites of stimulation are indicated by arrows. The distribution of APD (middle panels) is tightly coupled to the activation sequence in rat simulations but to a much lesser extent in the pig. A decreasing trend of APD away from the pacing site was observed uniformly in all directions across the epicardial surface. A similar pattern of APD was observed in the pig simulations however the range of APD values were much smaller. The RT map was relatively homogeneous in the rat simulations compared to the pig (right panels). The RT pattern in pig closely followed the activation sequence. Isochrones are spaced 2 and 4 ms apart for rat and pig, respectively.

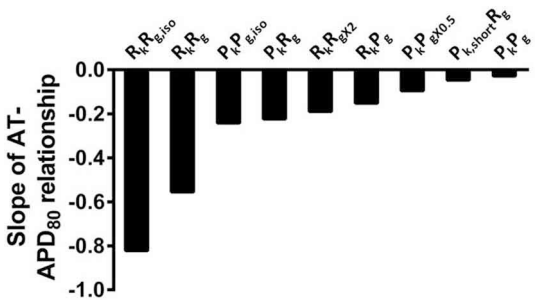

FIGURE 11 | The influence of anisotropy, AP morphology, and tissue geometry on the correlation between activation and APD in simulations. Comparison between slopes of linear correlations for each simulation in **Figures 2**, **7–10**.

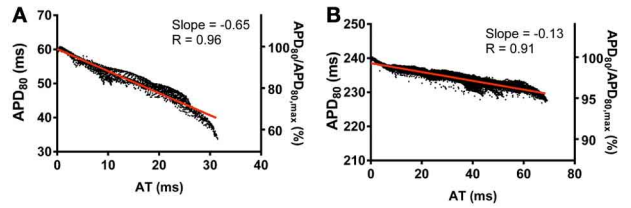

FIGURE 12 | Correlations between AT and APD in the transmural plane of rat (A) and pig (B) myocardium. AT and APD_{80} plots corresponding to the horizontal transmural plane at the level of the pacing site in simulations from **Figure 2**. Slopes for linear correlation analyses are indicated. Secondary *y*-axes show APD_{80} expressed as a percentage of maximum APD_{80}.

in P_kP_g was substantially less at 5.6%. The steepness of these relationships was −0.65 and −0.13 for rat and pig, which corresponds to increases of 27.5 and 62.5% in the transmural plane compared to the epicardial relationships, respectively. Similarly, AT-APD_{80} relationships were associated with augmented *R* values in both rat (0.96 vs. 0.87) and pig (0.91 vs. 0.57) models.

DISCUSSION

GENERAL DISCUSSION

The focus of the present study was to characterize the dynamic interplay between APD and the activation sequence in the myocardium with an aim to identify the mechanisms underlying acute electrotonic modulation of repolarization. Such mechanisms were investigated experimentally and computationally by comparing two species, rat, and pig, with distinct electrophysiological properties and two different tissue geometries, the whole heart and the ventricular slab. Using epifluorescence optical imaging we found a strong relationship between APD and AT in healthy rat hearts, leading to a large dispersion of APD, but relatively homogeneous RTs. This effect was especially pronounced in directions of slow conduction (**Figures 1**, **2**, **4**). In pig left ventricular wedge preparations however, spatial distributions of APD showed a relatively poor dependence on the activation sequence, consistent with previous studies (Lacroix et al., 1999; Kongstad et al., 2002; Liang et al., 2005). These results were consistent from two different pacing locations tested in each experimental model and simulations.

Our experimental results are in agreement with earlier computational studies that predicted an important role for the shape of the cardiac AP (Sampson and Henriquez, 2005; Cherry and Fenton, 2011). The electrotonic current is proportional to the membrane potential difference between neighboring cells and depends on the dynamic membrane resistance during repolarization (Sampson and Henriquez, 2005). In pig, due to the plateau phase, regions of tissue activated early in the activation sequence remain in relatively depolarized states long after all tissue has been activated. This significantly reduces the overall spatial gradient of the transmembrane potential during repolarization and consequently dampens its electrotonic modulation. Furthermore, the late phase 3 repolarization is strongly dominated by outward potassium currents and relatively small membrane resistance and therefore less sensitive to external currents. Conversely, the rat AP shape provides relatively constant membrane potential gradients throughout the whole repolarization duration. The late repolarization phase in the rat heart is also occurring at relatively slow rates, indicating a delicate balance between outward and inward currents, and is thus more susceptible to be affected by electrotonic currents (Vigmond et al., 2009). Our study is the first to investigate in detail and highlight the differences in electrotonic modulation of repolarization between two different mammalian species experimentally.

The rate dependency of the AT-APD relationship was investigated experimentally in both rat and pig ventricles. Reducing the pacing cycle length of tissue leads to AP shortening in both rat and pig myocardium. In our experiments, the shape of the AP, in terms of the rate of phase 3 repolarization, was largely preserved across all pacing cycle lengths for each species, as can be observed in **Figures 6A,B**. We did not observe a significant deviation of the slope of AT-APD relationship across pacing cycle lengths in either rat or pig experiments. Thus, it appears that irrespective of APD and pacing cycle length, the shape of the AP (triangular vs. spike-and-dome) is a main determinant of electrotonic modulation of repolarization. This is further supported by simulations shown in **Figure 9** that showed that shortening the pig APD (by abbreviation of the plateau phase whilst retaining a spike and dome AP) to match the rat APD, did not improve the relationship between AT and APD_{80}. These results show clearly that AP morphology plays a crucial role in electrotonic modulation of repolarization whereby the triangulated AP of the rat has significantly greater coupling between AT and APD than a spike-and-dome AP, as in pig. Hanson et al. (2009) using, S1S2 stimulation from the endocardium in human ventricles, observed that AT and activation-recovery interval (analogous to APD) reduced the steepness of linear correlations at S1S2 coupling intervals close to the shortest effective coupling interval. This study utilized noncontact balloon electrodes and therefore could not report on the AP morphology. However, S1S2 stimulation protocol may impose differential effects on AP morphology compared with dynamic stimulation since it is well established that the maximal slope of APD restitution is significantly enhanced by the S1S2 pacing protocol (Osadchii, 2012).

The role of tissue geometry on electrotonic modulation of repolarization has previously been investigated in theoretical models of cardiac propagation. Wang and Rudy (2000) used simulations of single ventricular muscle fibers that expand to multiple fibers, thus enhancing the number of neighboring cells at the site of the expansion, and found localized changes to APD at the sites of branching due to enhanced electrotonic load from fiber branches. More recently, Cherry and Fenton (2011) predicted a similar effect occurring at the insertions site of the left and right ventricle, and the septum, in homogeneous but anisotropic two-dimensional simulations of an axial slice of dog heart. In the present study, we investigated experimentally the relative role of tissue geometry on the electrotonic modulation of repolarization. We showed, for the first time, that the effect previously proposed by Cherry and Fenton (2011) was present at the level of the whole heart, both in experiments and simulations. Activation from the left ventricular free wall toward the right ventricle in the rat heart was associated with decreasing APD in a near linear trend with the exception of the border region between left and right ventricles (**Figure 5**). A band, extending from the base to the apex, of prolonged APDs was observed. This observation was replicated in 3D simulations using the rat geometry. Here, a localized region of prolonged APD_{80} was observed throughout the ventricular wall at the intersection of the septum and right ventricular free wall with the left ventricle. Furthermore, this effect significantly altered the intrinsic transmural APD gradient that was implemented in the cellular model (Pandit et al., 2001).

Computational models are a useful tool for investigating the relative role of AP kinetics and tissue properties in the electrotonic modulation of repolarization. In our study we ran additional simulations whereby the AP kinetics of one species was incorporated into the geometry of the other, and vice versa (**Figures 7**, **11**). When using the rat AP and changing the geometry from the rat whole ventricular model to the pig wedge preparation, we observed a pronounced reduction in the steepness of the AT-APD_{80} relationship. However, when using pig AP kinetics in the rat whole ventricular model we found a more pronounced correlation between AT and APD_{80} than when using the pig wedge geometry. We also found that scaling up the rat geometry reduced the steepness of the AT-APD_{80} relationship (**Figure 8**). Reducing the size of the pig geometry increased the steepness of the linear AT-APD_{80} relationship. Furthermore, uniform activation sequences in isotropic simulations were accompanied by tighter coupling of APD_{80} to AT as shown by more pronounced negative slopes of linear regression analysis compared to anisotropic simulations for both, rat and pig (**Figure 11**). The magnitude of the slope for isotropic simulations was still substantially greater in rat than in pig. In addition, the AT-APD_{80} relationship of the transmural plane was found to be steeper than on the epicardium (**Figure 12**). These results are consistent with previous two-dimensional simulation studies that showed that electrotonic APD modulation is strongest at pacing sites, tissue boundaries, and wave collisions sites. Increasing tissue size effectively reduces the contributions of the pacing site and tissue boundaries to the overall AT-APD_{80} relationship, thus leading to less pronounced correlations and slopes. These results clearly demonstrate that geometry and tissue size play an important role in determining spatial gradients of APD_{80} in tissue.

Dispersion of RT is an important determinant of the vulnerability to arrhythmias following a premature activation. In our experiments we found that, due to electrotonic interactions, RT was relatively homogeneous in the paced intact rat heart, but more heterogeneous in the pig ventricle (**Figure 4**). These results suggest that the rat heart would be more resistant against arrhythmias following ectopic activation, than pig ventricles. Electrotonic modulation of repolarization could therefore be a contributing factor in the reduced occurrence of sudden cardiac deaths in murine animal models compared to larger species (Sabir et al., 2008). However, our study has also highlighted structural features that could provide pro-arrhythmic substrates even in the smaller hearts: regions of tissue expansion at the insertion site between left and right ventricles were associated with APD prolongation and increased RT dispersion (Zubair et al., 1994). Therefore, regions of expanding conductive tissues such as ventricular insertion sites, insertion of papillary muscles and trabeculae carneae, could have increased vulnerability to conduction block following premature stimuli. This study provides the first experimental evidence supporting a mechanism previously only demonstrated computationally (Cherry and Fenton, 2011) for arrhythmogenesis underlayed by a structural substrate.

FUTURE DIRECTIONS

The present study has shown the influence of electrotonic effects for differing tissue structures and AP morphologies of the rat and pig ventricles. Future studies will be aimed at investigating in more detail the relative influence of intercellular coupling and membrane resistance in different species. Equally, it would be important to investigate this phenomenon in cardiac diseases.

LIMITATIONS

All optical mapping recordings in the current study were obtained from the epicardium. Transmural electrophysiological heterogeneities are well documented at a cellular level in various species, but to what extent these are modulated by electrotonic currents in tissues remains a topic of debate (Antzelevitch et al., 1998). Fully depth-resolved transmural imaging of APs is currently not feasible, thus making it difficult to directly address this important question. Nevertheless, our computer simulations indicate that electrotonic modulation by the activation sequence is stronger in the transmural direction than epicardially, especially in thin ventricles (see **Figures 5**, **12**), which can be sufficient to overcome intrinsic transmural heterogeneities. These findings are in accordance with previous computational studies (Sampson and Henriquez, 2005; Walton et al., 2010) and corroborate experimental findings on the rabbit left ventricular wedge cut surface (Myles et al., 2010) and in the intact rat heart (Walton et al., 2010). Furthermore, non-uniformities in tissue geometry can greatly affect transmural patterns of repolarization (**Figure 5**). Electrotonic modulation by the activation sequence of transmural repolarization dispersion is therefore likely to be important, even in the large intact mammalian heart.

We used an electro-mechanical uncoupler in the experiments to prevent motion artifacts and reliably measure repolarization optically. Furthermore, all computational simulations ignored cardiac contraction and electro-mechanical coupling. It is well-known that stretch can affect repolarization (Kohl et al., 2011). Activation of the ventricles from an electrode or ectopic source will create heterogeneous stretch patterns during repolarization that are likely to impact on dispersion of repolarization. To what extent stretch will impact on the findings of the current study remains to be investigated, however a tight coupling between activation and repolarization has been reported in several *in vivo* studies (Hanson et al., 2009; Yue et al., 2005).

There are differences in absolute AT between simulations and experimental data in our study.

Although realistic geometries are used, several factors may account for differences in total AT between simulations and experiments: (1) we have used a single geometry for the rat heart and pig wedge obtained from separate DT-MRI experiments. Therefore, variations in tissue size and electrophysiological properties across the various optical mapping experiments are not accounted for in simulations; (2) the simulations are run on the complete tissue sample (whole heart or wedge) whereas optical mapping data is obtained from a limited field-of-view; (3) transmural electrophysiological heterogeneities were included based on available experimental data. However, no other heterogeneities were incorporated in our models (such as base-to-apex gradients or differential connexin expression) due to the lack of established data; (4) retrograde activation through the Purkinje network may contribute to faster activation in experiment vs. simulation. However, our simulations are in excellent qualitative agreement with experimental data in terms of electrotonic modulation of repolarization.

In our simulations we used a monodomain approach without taking the tissue bath into account. However, this bath is known to increase electrotonic load at the tissue boundaries or at tissue heterogeneities such as vessels [see for example (Bishop et al., 2011; Kelly et al., 2013)]. Bath-loading at the tissue boundary is therefore likely to enhance the boundary effects we observe in our monodomain simulations and could play a role in further modulating the transmural APD gradient. The main conclusions of our study remain however valid.

CONCLUSION

In conclusion, our study has highlighted that electrophysiological and structural differences between species and the type of tissue preparations have significant roles in electrotonic modulation of repolarization. AP shape, tissue size and tissue geometry should all be taken into account when investigating dispersion of repolarization in cardiac tissue.

ACKNOWLEDGMENTS

This study was supported in part by grants from the Medical Research Council (G0701776 to Alan P. Benson and G900524 to, Alan P. Benson, Olivier Bernus, and Ed White), the Engineering and Physical Sciences Research Council (EP/F065574/1, Olivier Bernus), the Lefoulon-Delalande Institute (Richard D. Walton), the Marie Curie (IEF-PSCD, Richard D. Walton) and the Agence Nationale de la Recherche (ANR-10-IAHU04 - LIRYC).

REFERENCES

Antzelevitch, C. (2005). Modulation of transmural repolarization. *Ann. N.Y. Acad. Sci.* 1047, 314–323. doi: 10.1196/annals.1341.028

Antzelevitch, C., Shimizu, W., Yan, G. X., and Sicouri, S. (1998). Cellular basis for QT dispersion. *J. Electrocardiol.* 30(Suppl.), 168–175. doi: 10.1016/S0022-0736(98)80070-8

Banville, I., and Gray, R. A. (2002). Effect of action potential duration and conduction velocity restitution and their spatial dispersion on alternans and the stability of arrhythmias. *J. Cardiovasc. Electrophysiol.* 13, 1141–1149. doi: 10.1046/j.1540-8167.2002.01141.x

Benoist, D., Stones, R., Drinkhill, M., Bernus, O., and White, E. (2011). Arrhythmogenic substrate in hearts of rats with monocrotaline-induced pulmonary hypertension and right ventricular hypertrophy. *Am. J. Physiol. Heart Circ. Physiol.* 300, H2230–H2237. doi: 10.1152/ajpheart.01226.2010

Benson, A. P., Al-Owais, M., and Holden, A. V. (2011a). Quantitative prediction of the arrhythmogenic effects of de novo hERG mutations in computational models of human ventricular tissues. *Eur. Biophys. J.* 40, 627–639. doi: 10.1007/s00249-010-0663-2

Benson, A. P., Bernus, O., Dierckx, H., Gilbert, S. H., Greenwood, J. P., Holden, A. V., et al. (2011b). Construction and validation of anisotropic and orthotropic ventricular geometries for quantitative predictive cardiac electrophysiology. *Interface Focus* 1, 101–116. doi: 10.1098/rsfs.2010.0005

Benson, A. P., Aslanidi, O. V., Zhang, H., and Holden, A. V. (2008). The canine virtual ventricular wall: a platform for dissecting pharmacological effects on propagation and arrhythmogenesis. *Prog. Biophys. Mol. Biol.* 96, 187–208. doi: 10.1016/j.pbiomolbio.2007.08.002

Bishop, M. J., Vigmond, E., and Plank, G. (2011). Cardiac bidomain bath-loading effects during arrhythmias: interaction with anatomical heterogeneity. *Biophys. J.* 101, 2871–2881. doi: 10.1016/j.bpj.2011.10.052

Chauhan, V. S., Downar, E., Nanthakumar, K., Parker, J. D., Ross, H. J., Chan, W., et al. (2006). Increased ventricular repolarization heterogeneity in patients with ventricular arrhythmia vulnerability and cardiomyopathy: a human *in vivo* study. *Am. J. Physiol. Heart Circ. Physiol.* 290, H79–H86. doi: 10.1152/ajpheart.00648.2005

Cherry, E. M., and Fenton, F. H. (2011). Effects of boundaries and geometry on the spatial distribution of action potential duration in cardiac tissue. *J. Theor. Biol.* 285, 164–176. doi: 10.1016/j.jtbi.2011.06.039

Faber, G. M., and Rudy, Y. (2000). Action potential and contractility changes in [Na(+)](i) overloaded cardiac myocytes: a simulation study. *Biophys. J.* 78, 2392–2404. doi: 10.1016/S0006-3495(00)76783-X

Franz, M. R., Bargheer, K., Rafflenbeul, W., Haverich, A., and Lichtlen, P. R. (1987). Monophasic action potential mapping in human subjects with normal electrocardiograms: direct evidence for the genesis of the T wave. *Circulation* 75, 379–386. doi: 10.1161/01.CIR.75.2.379

Hanson, B., Sutton, P., Elameri, N., Gray, M., Critchley, H., Gill, J. S., et al. (2009). Interaction of activation-repolarization coupling and restitution properties in humans. *Circ. Arrhythm. Electrophysiol.* 2, 162–170. doi: 10.1161/CIRCEP.108.785352

Kelly, A., Ghouri, I. A., Kemi, O. J., Bishop, M. J., Bernus, O., Fenton, F. H., et al. (2013). Subepicardial action potential characteristics are a function of depth and activation sequence in isolated rabbit hearts. *Circ. Arrhythm. Electrophysiol.* 6, 809–817. doi: 10.1161/CIRCEP.113.000334

Kohl, P., Sachs, F., and Franz, M. R. (2011). *Cardiac Mechano-Electric Coupling and Arrhythmias*. 2nd Edn. New York, NY: Oxford University Press.

Kongstad, O., Yuan, S., Hertervig, E., Holm, M., Grins, E., and Olsson, B. (2002). Global and local dispersion of ventricular repolarization: endocardial monophasic action potential mapping in swine and humans by using an electroanatomical mapping system. *J. Electrocardiol.* 35, 159–167. doi: 10.1054/jelc.2002.31825

Lacroix, D., Extramiana, F., Delfaut, P., Adamantidis, M., Grandmougin, D., Klug, D., et al. (1999). Factors affecting epicardial dispersion of repolarization: a mapping study in the isolated porcine heart. *Cardiovasc. Res.* 41, 563–574. doi: 10.1016/S0008-6363(98)00269-7

Laurita, K. R., Girouard, S. D., and Rosenbaum, D. S. (1996). Modulation of ventricular repolarization by a premature stimulus. Role of epicardial dispersion of repolarization kinetics demonstrated by optical mapping of the intact guinea pig heart. *Circ. Res.* 79, 493–503. doi: 10.1161/01.RES.79.3.493

Laurita, K. R., Girouard, S. D., Rudy, Y., and Rosenbaum, D. S. (1997). Role of passive electrical properties during action potential restitution in intact heart. *Am. J. Physiol.* 273(3 Pt 2), H1205–H1214.

Liang, Y., Kongstad, O., Luo, J., Liao, Q., Holm, M., Olsson, B., et al. (2005). QT dispersion failed to estimate the global dispersion of ventricular repolarization measured using monophasic action potential mapping technique in swine and patients. *J. Electrocardiol.* 38, 19–27. doi: 10.1016/j.jelectrocard.2004.09.012

Macchi, E., Baruffi, S., Rossi, S., Miragoli, M., Bertuzzi, A., Musso, E., et al. (2004). Does cardiac pacing reproduce the mechanism of focal impulse initiation? *J. Electrocardiol.* 37(Suppl.), 135–143. doi: 10.1016/j.jelectrocard.2004.08.038

Myles, R. C., Bernus, O., Burton, F. L., Cobbe, S. M., and Smith, G. L. (2010). Effect of activation sequence on transmural patterns of repolarization and action potential duration in rabbit ventricular myocardium. *Am. J. Physiol. Heart Circ. Physiol.* 299, H1812–H1822. doi: 10.1152/ajpheart.00518.2010

Nerbonne, J. M., and Kass, R. S. (2005). Molecular physiology of cardiac repolarization. *Physiol. Rev.* 85, 1205–1253. doi: 10.1152/physrev.00002.2005

Noujaim, S. F., Pandit, S. V., Berenfeld, O., Vikstrom, K., Cerrone, M., Mironov, S., et al. (2007). Up-regulation of the inward rectifier K+ current (I K1) in the mouse heart accelerates and stabilizes rotors. *J. Physiol.* 578(Pt 1), 315–326.

Osadchii, O. E. (2012). Effects of ventricular pacing protocol on electrical restitution assessments in guinea-pig heart. *Exp. Physiol.* 97, 807–821. doi: 10.1113/expphysiol.2012.065219

Pandit, S. V., Clark, R. B., Giles, W. R., and Demir, S. S. (2001). A mathematical model of action potential heterogeneity in adult rat left ventricular myocytes. *Biophys. J.* 81, 3029–3051. doi: 10.1016/S0006-3495(01)75943-7

Papadakis, N. G., Xing, D., Houston, G. C., Smith, J. M., Smith, M. I., James, M. F., et al. (1999). A study of rotationally invariant and symmetric indices of diffusion anisotropy. *Magn. Reson. Imaging* 17, 881–892. doi: 10.1016/S0730-725X(99)00029-6

Press, W. H., Teukolsky, S. A., Vetterling, W. T., and Flannery, B. P. (2007). *Numerical Recipes: the Art of Scientific Computing, 3rd Edn*. Cambridge: Press Syndicate of the University of Cambridge.

Qu, Z., and Garfinkel, A. (1999). An advanced algorithm for solving partial differential equation in cardiac conduction. *IEEE Trans. Biomed. Eng.* 46, 1166–1168. doi: 10.1109/10.784149

Rossi, S., Baruffi, S., Bertuzzi, A., Miragoli, M., Corradi, D., Maestri, R., et al. (2008). Ventricular activation is impaired in aged rat hearts. *Am. J. Physiol. Heart Circ. Physiol.* 295, H2336–H2347. doi: 10.1152/ajpheart.00517.2008

Sabir, I. N., Usher-Smith, J. A., Huang, C. L., and Grace, A. A. (2008). Risk stratification for sudden cardiac death. *Prog. Biophys. Mol. Biol.* 98, 340–6. doi: 10.1016/j.pbiomolbio.2009.01.013

Sampson, K. J., and Henriquez, C. S. (2005). Electrotonic influences on action potential duration dispersion in small hearts: a simulation study. *Am. J. Physiol. Heart Circ. Physiol.* 289, H350–H360. doi: 10.1152/ajpheart.00507.2004

Vigmond, E. J., Tsoi, V., Yin, Y., Page, P., and Vinet, A. (2009). Estimating atrial action potential duration from electrograms. *IEEE Trans. Biomed. Eng.* 56, 1546–1555. doi: 10.1109/TBME.2009.2014740

Walton, R. D., Benoist, D., Hyatt, C. J., Gilbert, S. H., White, E., and Bernus, O. (2010). Dual excitation wavelength epifluorescence imaging of transmural electrophysiological properties in intact hearts. *Heart Rhythm* **7**, 1843–1849. doi: 10.1016/j.hrthm.2010.08.019

Wan, X., Bryant, S. M., and Hart, G. (2000). The effects of [K+]o on regional differences in electrical characteristics of ventricular myocytes in guinea-pig. *Exp. Physiol.* 85, 769–774. doi: 10.1111/j.1469-445X.2000.02048.x

Wang, Y., and Rudy, Y. (2000). Action potential propagation in inhomogeneous cardiac tissue: safety factor considerations and ionic mechanism. *Am. J. Physiol. Heart Circ. Physiol.* 278, H1019–H1029.

Wasserstrom, J. A., Sharma, R., Kapur, S., Kelly, J. E., Kadish, A. H., Balke, C. W., et al. (2009). Multiple defects in intracellular calcium cycling in whole failing rat heart. *Circ. Heart Fail.* 2, 223–232. doi: 10.1161/CIRCHEARTFAILURE.108.811539

Yuan, S., Kongstad, O., Hertervig, E., Holm, M., Grins, E., and Olsson, B. (2001). Global repolarization sequence of the ventricular endocardium: monophasic action potential mapping in swine and humans. *Pacing Clin. Electrophysiol.* 24, 1479–1488. doi: 10.1046/j.1460-9592.2001.01479.x

Yue, A. M., Betts, T. R., Roberts, P. R., and Morgan, J. M. (2005). Global dynamic coupling of activation and repolarization in the human ventricle. *Circulation* 112, 2592–2601. doi: 10.1161/CIRCULATIONAHA.104.510412

Zubair, I., Pollard, A. E., Spitzer, K. W., and Burgess, M. J. (1994). Effects of activation sequence on the spatial distribution of repolarization properties. *J. Electrocardiol.* 27, 115–127. doi: 10.1016/S0022-0736(05)80094-9

Conflict of Interest Statement: The authors declare that the research was conducted in the absence of any commercial or financial relationships that could be construed as a potential conflict of interest.

Received: 21 June 2013; accepted: 18 September 2013; published online: 08 October 2013.

Citation: Walton RD, Benson AP, Hardy MEL, White E and Bernus O (2013) Electrophysiological and structural determinants of electrotonic modulation of repolarization by the activation sequence. Front. Physiol. ***4****:281. doi: 10.3389/fphys.2013.00281*

This article was submitted to Cardiac Electrophysiology, a section of the journal Frontiers in Physiology.

frontiers in PHYSIOLOGY

ORIGINAL RESEARCH ARTICLE
published: 05 February 2015
doi: 10.3389/fphys.2015.00025

Myocardial electrotonic response to submaximal exercise in dogs with healed myocardial infarctions: evidence for β-adrenoceptor mediated enhanced coupling during exercise testing

***Carlos L. del Rio*[1,2,3]*, Bradley D. Clymer*[2,4] *and George E. Billman*[1,5]*

[1] *Department of Physiology and Cell Biology, The Ohio State University, Columbus, OH, USA*
[2] *Department of Electrical and Computer Engineering, The Ohio State University, Columbus, OH, USA*
[3] *Safety Pharmacology, QTest Labs, Columbus, OH, USA*
[4] *Biomedical Engineering, The Ohio State University, Columbus, OH, USA*
[5] *Davis Heart and Lung Research Institute, The Ohio State University, Columbus, OH, USA*

Edited by:
Ruben Coronel, Academic Medical Center, Netherlands

Reviewed by:
Joris R. De Groot, University of Amsterdam, Netherlands
Jin O-Uchi, Thomas Jefferson University, USA
Marcel Van Der Heyden, University Medical Center, Netherlands

****Correspondence:***
George E. Billman, Department of Physiology and Cell Biology, The Ohio State University, 1645 Neil Avenue, 305 Hamilton Hall, Columbus, OH, USA
e-mail: billman.1@osu.edu

Introduction: Autonomic neural activation during cardiac stress testing is an established risk-stratification tool in post-myocardial infarction (MI) patients. However, autonomic activation can also modulate myocardial electrotonic coupling, a known factor to contribute to the genesis of arrhythmias. The present study tested the hypothesis that exercise-induced autonomic neural activation modulates electrotonic coupling (as measured by myocardial electrical impedance, MEI) in post-MI animals shown to be susceptible or resistant to ventricular fibrillation (VF).

Methods: Dogs ($n = 25$) with healed MI instrumented for MEI measurements were trained to run on a treadmill and classified based on their susceptibility to VF (12 susceptible, 9 resistant). MEI and ECGs were recorded during 6-stage exercise tests (18 min/test; peak: 6.4 km/h @ 16%) performed under control conditions, and following complete β-adrenoceptor (β-AR) blockade (propranolol); MEI was also measured at rest during escalating β-AR stimulation (isoproterenol) or overdrive-pacing.

Results: Exercise progressively increased heart rate (HR) and reduced heart rate variability (HRV). In parallel, MEI decreased gradually (enhanced electrotonic coupling) with exercise; at peak exercise, MEI was reduced by 5.3 ± 0.4% (or -23 ± 1.8Ω, $P < 0.001$). Notably, exercise-mediated electrotonic changes were linearly predicted by the degree of autonomic activation, as indicated by changes in either HR or in HRV ($P < 0.001$). Indeed, β-AR blockade attenuated the MEI response to exercise while direct β-AR stimulation (at rest) triggered MEI decreases comparable to those observed during exercise; ventricular pacing had no significant effects on MEI. Finally, animals prone to VF had a significantly larger MEI response to exercise.

Conclusions: These data suggest that β-AR activation during exercise can acutely enhance electrotonic coupling in the myocardium, particularly in dogs susceptible to ischemia-induced VF.

Keywords: electrotonic coupling, β-adrenoceptor stimulation, exercise, arrhythmic risk, myocardial infarction

INTRODUCTION

Myocardial infarction is a well-established risk factor for sudden cardiac death (SCD) due to malignant arrhythmias (Adabag et al., 2010; Zaman and Kovoor, 2014). However, despite significant advances in the understanding of the physiological substrate(s) mediating/facilitating the onset of arrhythmias, risk stratification for SCD in post-MI patients remains difficult and insufficient (Goldberger et al., 2014; Wellens et al., 2014; Zaman and Kovoor, 2014). Indeed, the majority of SCD episodes occur in patients with either low-/intermediate- or without known risk factors (e.g., Wellens et al., 2014).

In these patients, underlying ionic current abnormalities, particularly those mediating repolarization, either co-exist with and/or are exacerbated by autonomic imbalances favoring enhanced sympathetic drive (e.g., Chen et al., 2007; Pokornı et al., 2011; Wellens et al., 2014). As such, multi-modality stratifications techniques, encompassing electrocardiographic evaluation of repolarization abnormalities during states of autonomic activation, such as exercise, are favored (Goldberger et al., 2014; Wellens et al., 2014). For instance, the assessment of microvolt T-wave alternans (TWA or MTWA) during low-intensity exercise has been shown to predict not only arrhythmic events in post-MI

patients but also arrhythmia-free survival in patients with LV dysfunction (Cantillon et al., 2007; Amit et al., 2010; Verrier et al., 2011; Merchant et al., 2012; Shizuta et al., 2012).

Interestingly, activation of the autonomic nervous system (e.g., during exercise), and its concomitant catecholamine release, may in turn also modulate the passive electrical properties that govern electrotonic interactions in the myocardium. For example, several studies have shown that catecholamines (and increased cAMP levels) enhance junctional coupling in myocytes (e.g., see De Mello, 1996a; Dhein, 2004; Salameh and Dhein, 2011). Notably, electrotonic coupling is a well-established factor modulating both repolarization disturbances and arrhythmic risk, as poorly coupled cells are more likely to exhibit pro-arrhythmic behaviors (e.g., Pastore and Rosenbaum, 2000; De Groot and Coronel, 2004; Saffitz and Kléber, 2012; Wit and Peters, 2012). For instance, enhanced electrotonic coupling has been shown to suppress early after-depolarizations (EADs) (Huelsing et al., 2000; Himel et al., 2013), and reduce transmural dispersion of repolarization (Quan et al., 2007). Similarly, preserved electrotonic interaction has been shown to modulate TWA *in silico,* and more recently, also *in vivo* (Pastore and Rosenbaum, 2000; Watanabe et al., 2001; Cherry and Fenton, 2004; Sato et al., 2006; Kjølbye et al., 2008; Jia et al., 2012). Remarkably, no study to date has investigated concomitant passive electrical (electrotonic) changes during autonomic neural activation *in vivo*.

It was, therefore, the purpose of this study to investigate myocardial electrotonic coupling changes induced by submaximal exercise in the left-ventricle of post-MI animals, as measured by myocardial electrical impedance (MEI). Specifically, the hypothesis that exercise-induced autonomic activation can modulate myocardial electrotonic coupling (i.e., MEI) was tested in animals with healed myocardial infarctions later demonstrated to be either susceptible or resistant to ischemia-induced VF. Briefly, β-adrenoceptor (β-AR) activation during submaximal exercise acutely decreased the electrical impedance of the surviving myocardium, particularly in animals susceptible to VF, consistent with an increased electrotonic coupling.

MATERIALS AND METHODS

The principles governing the care and treatment of animals, as expressed by the American Physiological Society, were followed at all times during this study. In addition, the animal protocols and experimental procedures were approved by The Ohio State University's Institutional Lab Animal Care and Use Committee (ILACUC) at this institution, and adhered to the statutes of the Animal Welfare Act and the guidelines of the Public Health Service.

SURGICAL PREPARATION

The studies were performed using a well-characterized canine model of sudden cardiac death, known to mimic/combine the most prevalent features associated with this disease in the clinic: healed myocardial ischemic injury, acute myocardial ischemia, and cardiac autonomic activation (see Billman, 2006).

Briefly, thirty-five ($n = 35$) heartworm-free purpose bred mixed-breed dogs (weight: 16.1–24.1 kg, 19.0 ± 0.4 kg) were sedated (morphine sulfate 15 mg IM, and thiopental sodium 20 mg/kg IV), and connected to a respirator via an endotracheal cuffed tube. Anesthesia was maintained with inhaled isoflurane (1–1.5%) mixed with oxygen (100%). Under sterile conditions, the chest was opened via a left thoracotomy (fifth intercostal space); the heart was exposed, and suspended with a pericardial cradle. Subsequently, an antero-lateral myocardial infarction (MI) was created by a two-stage ligature of the left anterior descending (LAD) coronary artery. The left circumflex (LCX) coronary artery was dissected free of the surrounding tissue near its origin (under the edge of the left atrial appendage) and was instrumented with a 20 MHz Doppler-flow transducer, and a hydraulic coronary artery occluder; inflation of this balloon would later render a portion of the LCX distribution acutely ischemic (see *Arrhythmia Susceptibility*).

As required for MEI measurements (see below), a bipolar pacing electrode (Medtronic Inc., model Streamline™ 6495) was placed remote to the infarct, in the distal (non-ischemic) distribution of the LCX coronary artery. In a subset of animals ($n = 10$), a second MEI electrode was placed in the healthy (*non-infarcted*) anterior myocardium for pacing purposes (see *Experimental Protocol*). The leads were inserted into the mid-myocardial wall (parallel to the local fiber alignment), and were firmly secured in place with non-absorbable sutures (prolene 2-0). The pericardial cradle was released, the chest closed in layers and evacuated of air restoring the negative intra-thoracic pressure. All leads were tunneled under the skin, exited at the neck, and were carefully bandaged.

EXERCISE TEST PROTOCOL

The animals were allowed to recover for 3–4 weeks, and subsequently, were trained to run on a motor-driven treadmill. A 6-stage submaximal exercise stress-test (SMT), as initially described by Stone (1977), was used to activate the autonomic nervous system. This protocol is summarized in **Figure 1**, and consisted of a 3 min warm-up walking period (4.8 km/h, 0% grade; level L1), followed by running (6.4 km/h) for 15 min with the grade

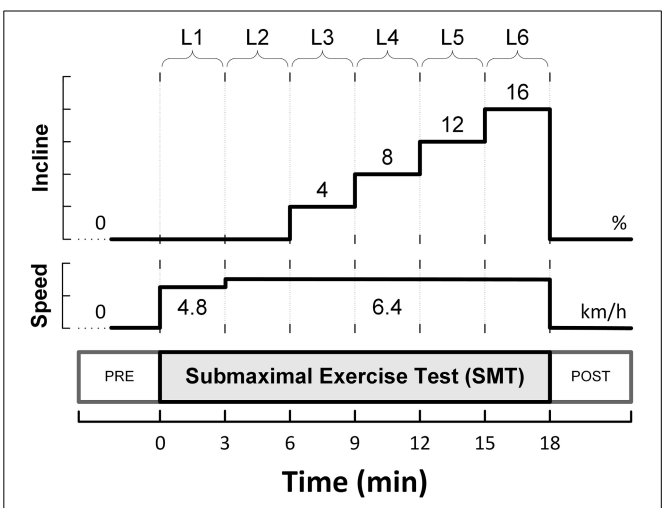

FIGURE 1 | Schematic representation of the six-level submaximal exercise test (SMT).

(incline) increased every 3 min (i.e., 0, 4, 8, 12, and 16%; levels L2-L6).

ARRHYTHMIA SUSCEPTIBILITY

The susceptibility to ischemia-induced ventricular fibrillation was assessed at the end of the study using a standardized protocol, generally referred as the "exercise-plus-ischemia" test (see Billman, 2006). In short, a submaximal exercise bout was performed (as described above) and during the last minute of exercise, the animals were subjected to a brief (2 min) LCX occlusion (i.e., while running at 6.4 km/h, 16%). This combination of exercise plus ischemia, when applied post-MI, yields two stable and well-differentiated populations of animals: one susceptible and the other resistant to ischemia-induced malignant arrhythmias, such as ventricular fibrillation [see Billman (2006) for review]. In this study, 12 animals developed VF (susceptible, S) and 9 did not (resistant, R) during the exercise-plus-ischemia test. Four animals ($n = 4$) could not be classified due to equipment failure (e.g., occluder rupture).

MYOCARDIAL ELECTRICAL IMPEDANCE (MEI)

As has previously been described, a computer controlled circuit developed in this laboratory was used to measure the complex electrical impedance of the myocardium (Howie et al., 2001; Dzwonczyk et al., 2004; Del Rio et al., 2005, 2008a,b). In short, using a bipolar pacing lead (see above) the myocardium was probed with a sub-threshold zero-mean bipolar current, consisting of two rectangular pulse of alternating polarity ($\pm$ 5 μA, 100 μs wide) generated 200 ms apart. The complex MEI spectrum was calculated in the frequency domain, as the ratio (at each frequency) of the current and voltage spectra resulting from the ensemble averages of 10 stimulus pulses and their respective (voltage) responses. The mean modulus of the complex MEI spectrum in the 0.27–5.90 kHz frequency range was examined (Del Rio et al., 2008a).

EXPERIMENTAL PROTOCOL

As described above, thirty-five animals ($n = 35$) were instrumented with MEI electrodes in the remote, non-infarcted myocardium. However, five animals ($n = 5$) experienced lead malfunctions (e.g., dislodgement) either before or at the time of experimentation, and therefore, were excluded from the analysis, while another five animals ($n = 5$) failed to acclimatize to the treadmill exercise protocol. Thus, the studies were performed in 30 animals ($n = 30$), with exercise-data successfully collected and analyzed in 25 dogs ($n = 25$).

First, in order to investigate the time-course of the electrotonic coupling (i.e., MEI) during submaximal exercise, all animals, regardless of arrhythmias susceptibility (9 resistant, 12 susceptible, and 4 unable to be classified), had MEI measurements collected during a submaximal exercise test (SMT) performed approximately 1-month after the LAD ligature (28 $\pm$ 1.7 days post-MI).

On a different day (26 $\pm$ 1.7 days post-MI), a subset of animals (5 resistant, 7 susceptible, and 4 unable to be classified; $n = 16$) performed the submaximal exercise test, but after pretreatment with the β-adrenoceptor antagonist propranolol HCl (1.0 mg/kg IV, Sigma Chemical, St. Louis, MO). Previous studies demonstrated that this dose of propranolol (1) completely abolished the cardiac response to the β-adrenoceptor agonist isoproterenol HCl (1 μg/kg IV) (Collins and Billman, 1989), and (2) did not compromise the exercise capacity during the submaximal exercise test in the presence of a 1-month-old anterior wall myocardial infarction (Brice and Stone, 1986). Propranolol was given intravenously (cephalic vein) as a bolus injection 3 min before the onset of exercise. A partially counter-balanced design was used: some dogs (6/16) were first exercise-tested under the influence of this β-adrenoceptor antagonist, and on a later day, had a control test (i.e., with no drug) performed; whereas in the remaining animals (10/16) the response to the submaximal exercise test (SMT) was first studied under control conditions, and on a subsequent day, following β-adrenoceptor blockade. In all cases, MEI measurements during the exercise tests were taken (continuously) from the distal LCX distribution (remote non-ischemic region) in awake, unsedated, and otherwise unstressed, post-MI animals (in a quiet and dimly lit room).

In order to investigate further the role of exercise-induced autonomic neural activation on myocardial electrotonic coupling (MEI), the total β-adrenoceptor response was quantified at rest in some animals ($n = 10$). Briefly, the dogs were lightly sedated with acepromazine (0.5 mg/kg IM; Ft. Dodge Animal Health, Ft. Dodge, IA), and a (cephalic vein) catheter was percutaneously placed for the administration of isoproterenol HCl (Sigma Chemical, St. Louis, MO); five increasing doses of this β-adrenoceptor agonist were given: 0.005, 0.015, 0.05, 0.15, and 0.5 μg/min/kg. MEI measurements were obtained continuously during isoproterenol infusion and washout. Data are reported (averaged over 30s) when a steady-state response was achieved at each dose, and 2 min after dosing discontinuation.

Finally, the possible confounding effects of exercise-mediated heart rate changes were evaluated in another subset of dogs ($n = 10$) via overdrive left-ventricular pacing at rest. Briefly, with the animal standing on the treadmill (awake and unsedated), an impulse generator (Grass Medical Instruments, model Grass S44, via impulse-isolation unit model SIU105-B) was used to maintain ventricular rates of 180 and 210 beats/min, mimicking those observed during moderate (L2; 6.4 km/h, 0%) and peak exercise (L6; 6.4 km/h, 16%). In these animals, a second bipolar MEI/pacing electrode was placed at the time of instrumentation (see *Surgical Preparation* above); the pacing protocol was repeated from each lead (while MEI was simultaneously recorded from the other, i.e., the non-stimulating electrode), and, as similar impedance responses were obtained, the results for the two sites (leads) were combined. MEI data collected before pacing onset, and after stabilization at each pacing rate, are reported (averaged over at least a 30s interval).

Data analysis

A single-lead bipolar electrocardiogram (ECG) was recorded during each presentation of the submaximal exercise test. The ECG signals were band-pass filtered and digitally sampled (1 kHz)/analyzed (on-line) using a heart rate variability (HRV) monitor (Delta-Biometrics, Inc.; Urbana-Champaign, IL). Briefly, using a previously well-described (Billman and

Hoskins, 1989; Billman and Dujardin, 1990) R-R interval time-series analysis technique, the heart rate (HR) mean and its variability (i.e., HRV) were determined continuously from non-overlapping 30s-segments of the ECG. Two kinds of HRV indices were studied simultaneously: (1) two measures of statistical dispersion, namely the standard deviation (RR_{SD}) and the range ($RR_{RNG;}$ longest—shortest R-R interval) of the R-R intervals within each 30 s analysis-window; and (2) an index estimating the amplitude of the respiratory sinus arrhythmia (R-R interval variability in the 0.24—1.04 Hz frequency range), or vagal tone index (VT). MEI, HR and HRV data are reported (averaged over 30 s) at eight time-points sampled before (one), during (six), and after (one) the bouts of submaximal exercise. Pre- (baseline) and post-exercise (recovery) values were taken 2 min before/after exercise onset/offset (i.e., at $t = -2$ min, and $t = 20$ min, see **Figure 1A**) with the animals standing on the treadmill. Meanwhile, the six exercise data-points were recorded during the last 30s of each stage in the submaximal stress protocol (i.e., L1—L6).

In addition, exercise-induced changes in the ECG morphology as well as on ECG-derived indices of the duration and heterogeneity of ventricular repolarization were evaluated in a subset of animals ($n = 19$). In short, with the aid of pattern-recognition software (ECG Auto; EMKA Technologies, France), fiducial points/intervals were determined and measured offline from two sets of thirty consecutive ECG complexes (beats), one recorded before (i.e., at rest) and the other immediately following a control submaximal exercise test (i.e., within 5 beats of stopping the treadmill). The effects of exercise on the duration of the T-wave's terminal portion (i.e., peak-to-end interval, TPE (Yan and Antzelevitch, 1998; Opthof et al., 2007) and on the QT-interval's length, as well as on the relationship between cardiac electrical systole and diastole (i.e., ratio of QT- and TQ-intervals, QT/TQ) (Fossa et al., 2007; Kijtawornrat et al., 2010) were evaluated; both absolute (QT) and rate-corrected (QTc, via van de Water's formula; Van de Water et al., 1989) QT-intervals are reported. In addition, the standard deviation of the T-wave amplitude within each 30-beat epoch (T_{SD}) was calculated and used as a surrogate-marker of temporal repolarization variability (e.g., T-wave alternans; Nearing and Verrier, 2002).

All data are presented as mean ± standard error of the mean (SEM). Statistical analyses were performed with SigmaStat (Systat Software, Inc., San Jose, CA) and NCSS (NCSS, Inc., Kaysville, UT). The mean time-course of electrotonic coupling (i.e., MEI), and ECG-derived variables during the submaximal exercise tests (SMT) was evaluated using a One-Way (exercise level: baseline, L1–L6, and recovery) analysis of variance (ANOVA) with repeated measures. Intergroup comparisons (i.e., resistant vs. susceptible) were made using a Two-Way (exercise level, and group: susceptible/resistant) ANOVA with repeated measures on one factor (exercise level). Similarly, the responses to exercise, recorded under control conditions (control) and after β-adrenoceptor blockade (beta), were compared using a Two-Way (exercise level, and control/beta tests) ANOVA with repeated measures on both factors. Finally, the statistical significance of any impedance changes induced by either pacing (3 levels: baseline/two rates) and/or by isoproterenol infusion/washout (7 levels: baseline/five doses/recovery) was evaluated using One-Way ANOVA with repeated measures. The sphericity assumption (i.e., homogeneity of the covariance matrix) was verified using the Mauchley's test (NCSS, Inc.). If this assumption was not met, then a non-parametric repeated measurements ANOVA on Ranks (Friedman) test was used. In all cases, if significant *F*-values (or *Q*-values in the non-parametric case) were observed, *post-hoc* pair-wise comparisons were made using the Tukey test.

Linear regression analyses were performed as well in order to study the relationship (interaction) between exercise-induced changes in electrotonic coupling (i.e., ΔMEI) and in two indices of autonomic activation, the heart rate (ΔHR) and the vagal-tone index (ΔVT); the regression data were "centered," i.e., deviations from each animal's mean values (over the whole exercise bout) were studied. The equality of the ΔMEI/ΔHR (and ΔMEI/ΔVT) linear models fitted to the different groups and conditions studied (susceptible vs. resistant, and control vs. β-AR blockade) was tested by multiple linear regression analysis, considering both qualitative (group) and interaction terms (i.e., simultaneously testing the differences in slope and intersect of the regression functions). For all analyses, $P < 0.05$ was considered, a priori, to be statistically significant.

RESULTS

EFFECTS OF EXERCISE

As expected and consistent with previous studies (Billman and Hoskins, 1989; Billman and Dujardin, 1990; Billman, 2006), submaximal treadmill exercise resulted in a progressive acceleration of heart rate and a concomitant decrease in heart rate variability (see **Figure 2** and **Table 1**). At peak exercise (L6; 6.4 km/h, 16%) heart rate increased on average 78 ± 4.3% (HR: from 119 ± 4 at rest to 208 ± 4 bpm at L6, $P < 0.05$), while the cardiac vagal-tone index, for instance, decreased 86 ± 2.3% (VT: from 7.9 ± 0.3 at rest to 1.2 ± 0.2 ln ms^2 at L6, $P < 0.05$). In parallel with these changes indicative of strong cardiac autonomic neural activation, MEI decreased progressively during exercise in all animals studied (see **Figure 2** and **Table 1**), suggesting enhanced electrotonic coupling. For example, at the highest exercise level (i.e., L6) MEI decreased −23 ± 1.8Ω (or 5.3 ± 0.4%) from the pre-exercise (at rest) values (MEI: from 446 ± 16 to 423 ± 16Ω at L6, $P < 0.05$). Moreover, following discontinuation of exercise offset (i.e., recovery), all parameters returned toward the pre-exercise (baseline) values.

Notably, exercise-mediated impedance changes (ΔMEI) were linearly predicted by (i.e., correlated with) the degree of autonomic neural activation, as indicated by either changes in heart rate (ΔHR; slope ΔMEI vs. ΔHR $= -0.249$Ω/bpm; $R^2 = 0.83$, $P < 0.05$), or in vagal tone index (ΔVT; slope ΔMEI vs. ΔVT $= 3.134$ Ω/ln(ms^2); $R^2 = 0.77$, $P < 0.05$) (see **Figure 3** and **Table 1**).

Indeed, pretreatment with the (non-selective) β-AR antagonist propranolol significantly attenuated the MEI response to exercise (e.g., at L6, CTRL: −23 ± 2.5 Ω vs. BB: −11 ± 2.0Ω; $P < 0.05$, $n = 15$) (see **Figure 4**, **Table 2**), markedly reducing the slope of the ΔMEI vs. ΔHR (−0.250 vs. −0.139 Ω/bpm; $R^2 = 0.78$, $P < 0.05$) and the ΔMEI vs. ΔVT relationships (Ω/ln(ms^2); $R^2 = 0.77$, $P < 0.05$). Similarly, as expected, β-AR blockade blunted the exercise-induced heart rate increase (e.g., at L6, CTRL: +47 ± 6

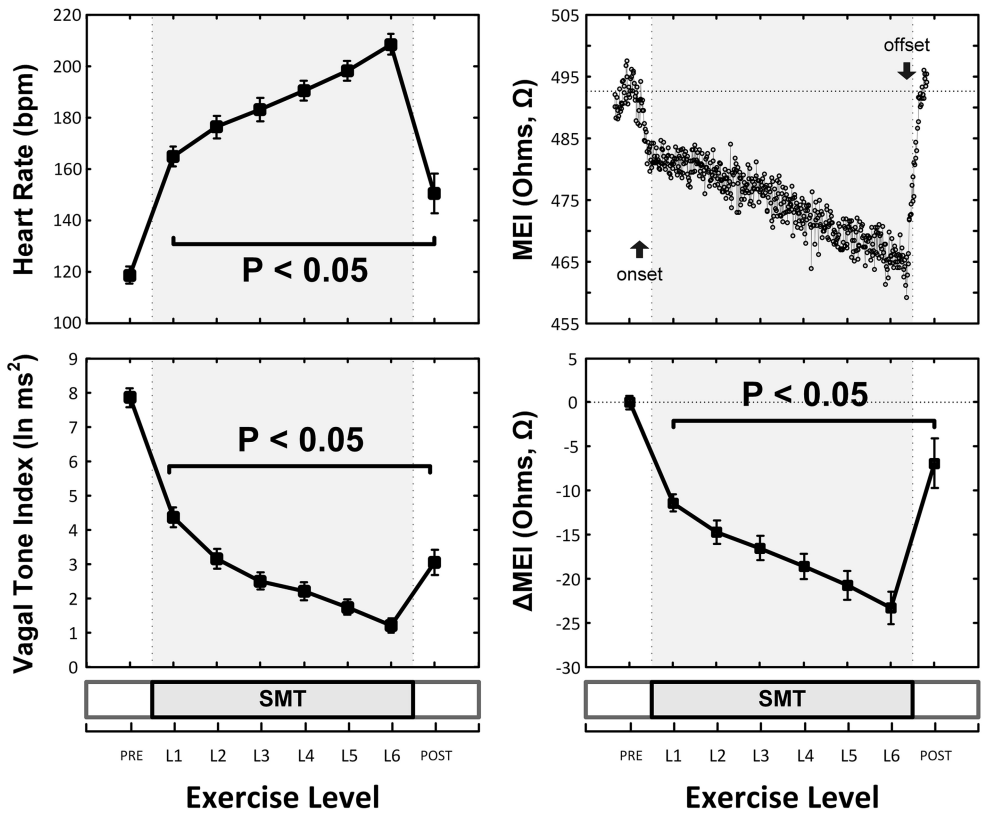

FIGURE 2 | Exercise-Induced changes in the heart-rate (HR, top-left) and ECG-derived vagal-tone index (bottom-left) and well as in the myocardial electrical impedance (MEI, bottom-right with representative response in top-right) of awake-unsedated dogs with healed left-anterior descending (LAD) myocardial infarcts ($n = 25$, except at recovery where $n = 14$).

Table 1 | Myocardial electrical impedance (MEI), heart-rate (HR) and ECG-derived indices of heart rate variability in awake-unsedated dogs with healed left-anterior descending (LAD) myocardial infarcts, both before (baseline) as well as during a submaximal exercise test.

	Baseline	Submaximal exercise test (SMT)			Correlation
Parameter	**0 km/h, 0%**	**6.4 km/h, 0%**	**6.4 km/h, 8%**	**6.4 km/h, 16%**	**vs. ΔMEI**
MEI (Ohms)	446 ± 16	431 ± 16*	427 ± 16*	423 ± 16*	–
Heart rate (bpm)	119 ± 3	176 ± 4*	190 ± 4*	208 ± 4*	(–) $R^2 = 0.83$
Vagal Tone (ln ms^2)	7.9 ± 0.3	3.1 ± 0.3*	2.2 ± 0.3*	1.2 ± 0.2*	(+) $R^2 = 0.77$
RR_{SD} (ms)	71 ± 6	22 ± 2*	14 ± 1*	8 ± 1*	n/s
RR_{RNG} (ms)	329 ± 30	101 ± 8*	63 ± 7*	38 ± 4*	n/s

$P < 0.05$ vs. Baseline.

n/s, not studied.

vs. BB: +30 ± 5 bpm; see **Figure 4**), but accentuated cardiac parasympathetic withdrawal (e.g., lower vagal tone index values were recorded). Moreover, direct β-adrenoceptor stimulation at rest (with isoproterenol infusions) triggered a dose-dependent MEI response (decrease) comparable to that observed during submaximal exercise (see **Figure 5**). On average, at the highest dose-level assayed (i.e., at 0.5 μg/min·kg), isoproterenol decreased MEI by −14 ± 1.7Ω (from 453 ± 40 to 440 ± 45Ω, $P < 0.05$). Thus, when considered together, these data suggest that the acute electrotonic (impedance) changes induced by exercise are predominantly mediated by sympathetic β-adrenoceptor activation.

On the other hand, while both submaximal exercise and direct β-adrenoceptor stimulation (at rest) led to acute MEI reductions, suggestive of favored increased electrotonic coupling, elevations in heart-rate via overdrive left-ventricular pacing had no significant effects on the passive electrical properties of the myocardium (see **Figure 6**). For instance, when resting animals were paced at

210 beats/min (from a basal rate of 123 ± 7 bpm) MEI changed only +2 ± 0.8Ω (from 426 ± 28Ω at baseline to 428 ± 29Ω, $n = 10$; N.S.); meanwhile, when the same subset of animals performed a submaximal exercise test, MEI decreased −20 ± 3.3Ω (from 435 ± 38Ω at rest to 414 ± 38.3Ω at L6, $n = 8$; $P < 0.05$) although heart rate increased similarly (from 124 ± 7 at rest to 213 ± 9 bpm at L6, $P < 0.05$). These data support the conclusion that the effects of exercise on electrotonic coupling (enhancement) are not mediated by its concomitant chronotropic effects (i.e., rate acceleration).

ARRHYTHMIA SUSCEPTIBILITY

Although (as mentioned above), MEI decreased with exercise onset in all animals studied, the degree of reduction was modulated by the underlying arrhythmic susceptibility of each animal: Animals prone to ischemia-induced VF had a significantly larger MEI response to submaximal exercise (see **Figure 7**, **Table 2**). At the peak exercise level (i.e., at L6), for instance, MEI decreased −30 ± 1.6Ω in dogs susceptible to VF (S, $n = 12$) and only −17 ± 2.1Ω in those resistant (R, $n = 9$) ($P < 0.05$), albeit comparable heart rates (e.g., S: 211 ± 5 vs. R: 210 ± 6 bpm at L6, N.S.) and heart rate variability indices (e.g., VT; S: 1.3 ± 0.3 vs. R: 0.7 ± 0.2 ln ms^2 at L6, N.S.) were reached by both groups; these observations suggest an increased impedance responsiveness to exercise-induced autonomic neural activation in dogs prone to arrhythmias.

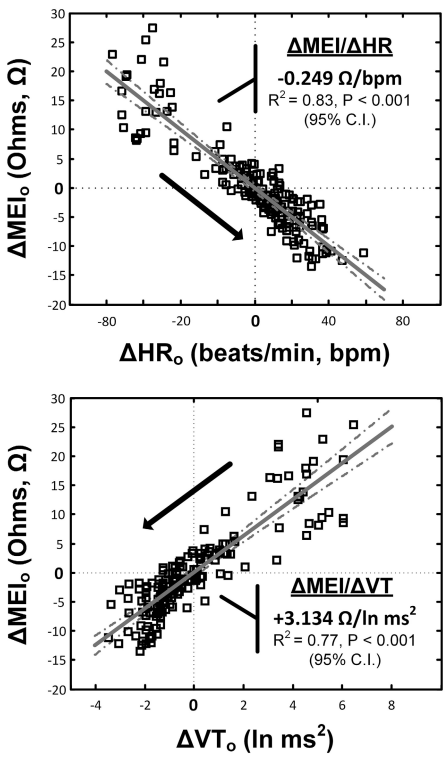

FIGURE 3 | Relationship(s) between the exercise-induced changes in the heart-rate (top) and ECG-derived vagal-tone index (bottom) with the concomitant reductions in myocardial electrical impedance (MEI); relationships were "centered," i.e., deviations from each animal's mean values (over the whole exercise bout) were studied.

In fact, susceptible animals had significantly ($P < 0.001$, see **Table 2**) steeper relationships between the exercise-mediated changes in impedance (ΔMEI) and those recorded for the heart rate (slope of ΔMEI vs. ΔHR; S: −0.295 vs. R: −0.180 Ω/bpm, $R^2 = 0.87$) and/or the vagal tone index (slope of ΔMEI vs. ΔVT; S: 4.11 vs. R: 2.09 Ω/ln ms^2, $R^2 = 0.85$). Notably, such marked intergroup differences were evident even when the slopes of the ΔMEI vs. ΔHR (S: −0.31 ± 0.2 vs. R: −0.18 ± 0.2 Ω/bpm, $P = 0.001$) and/or the ΔMEI vs. ΔVT (S: 4.3 ± 0.27 vs. R: 2.4 ± 0.46 Ω/ln ms^2, $P = 0.002$) relationships were calculated individually for each animal, rather than from the study groups. Moreover, complete β-AR blockade (with propranolol) blunted the exercise-induced impedance differences between animals susceptible (S, $n = 7$) and resistant (R, $n = 5$) to ischemia-induced arrhythmias (during control test; S: −30 ± 2.4 vs. R: −17 ± 2.7 Ω, $P < 0.05$, but after β-AR blockade; S: −16 ± 1.5 vs. R: −10 ± 4.1Ω, N.S.).

ELECTROCARDIOGRAPHIC DATA (RESPONSE TO EXERCISE)

Concomitantly with the above mentioned changes on indices of autonomic neural activation (cardio-acceleration, decreased heart-rate variability), exercise shortened the PR-interval and flattened the T-wave (data not shown) while decreasing indices of ventricular repolarization temporal duration (QTc, TPE) (see **Table 3**). For instance, on average, exercise shortened the rate-corrected QT-interval from 251 ± 4 msc at rest to 229 ± 4 msc ($P < 0.05$), suggesting a faster and/or more homogeneous repolarization. On the other hand, exercise increased the QT/TQ ratio (an index of the steepness of ventricular restitution, Fossa et al., 2007; Kijtawornrat et al., 2010) as well as the standard deviation of the T-wave amplitude (a marker of repolarization variability and/or T-wave "alternans"). Notably, exercise-induced changes on the T-wave amplitude variability were larger in animals susceptible to ischemia-induced VF (from 20.5 ± 3.1 μV at rest to 50.5 ± 9.0 μV post-exercise, $P < 0.05$) than in those resistant such arrhythmias (from 25.8 ± 4.7 μV at rest to 39.2 ± 5.6 μV post-exercise, N.S.); no other significant electrocardiographic differences, either at rest or following exercise, were noted between animals susceptible and resistant to VF.

DISCUSSION

The present study investigated the acute effects of submaximal exercise and its resulting autonomic neural activation on the myocardial electrotonic coupling of dogs with healed myocardial infarctions, as described by changes in the electrical impedance of surviving remote (i.e., non-infarcted) myocardium. This study demonstrated that acute β-adrenoceptor activation (either during bouts of exercise or via a direct pharmacological challenge) acutely increased passive (electrotonic) coupling in the myocardium, with the largest changes noted in those animals that were subsequently shown to be susceptible to malignant ventricular arrhythmias. In short, myocardial impedance was shown to decrease gradually as the level of exercise and autonomic neural activation increased. In contrast, ventricular overdrive pacing (at heart rates matched to those seen with exercise) had no significant effects on MEI.

As noted by Kléber et al. (1987), the gross myocardial electrical impedance measurements used in this study as a surrogate

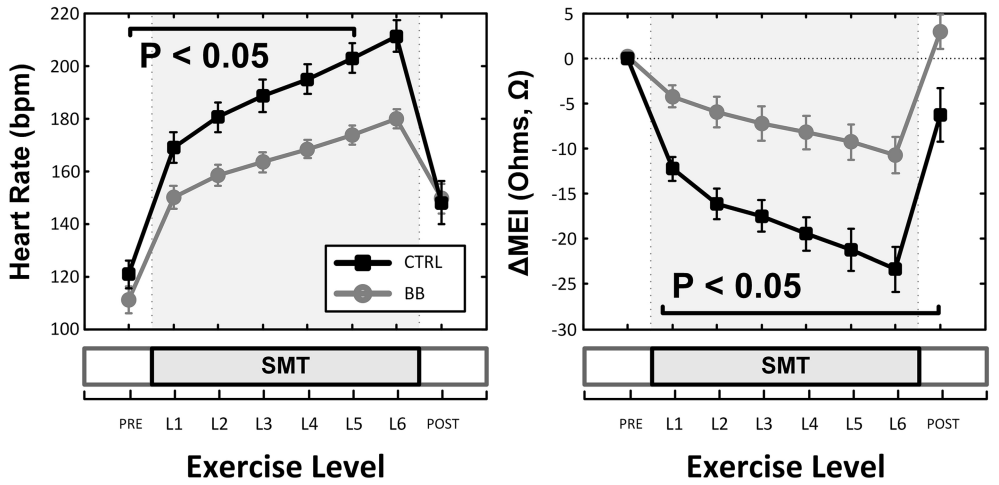

FIGURE 4 | Effects of (non-selective) β-adrenoceptor blockade (+BB, propranolol) in the myocardial electrical impedance (MEI, right), and heart-rate (HR, left) response(s) to exercise; β-adrenoceptor blockade blunted the MEI response to exercise. SMT, submaximal exercise test.

Table 2 | Exercise-induced changes in both the myocardial electrical impedance (MEI) and the heart-rate (HR) of awake-unsedated dogs with healed left-anterior descending (LAD) myocardial infarct; comparative effects of the underlying susceptibility to malignant arrhythmias (S vs. R), and of β-adrenoceptor blockade (+BB).

	Parameter/Sub-Group	Baseline 0 km/h, 0%	SMT (Peak) 6.4 km/h, 16%	Slope (Correlation) vs. ΔMEI
MEI (Ohms)	Susceptible (S, $n = 12$)	454 ± 24	424 ± 24*(-30 ± 1.6)	*n/a*
	Resistant (R, $n = 9$)	439 ± 28	422 ± 26*(-17 ± 2.1)†	
	Control ($n = 16$)	433 ± 22	409 ± 22*(-23 ± 2.5)	*n/a*
	+BB ($n = 16$)	470 ± 26	459 ± 27*(-11 ± 2.0)‡	
Heart Rate (bpm)	Susceptible ($n = 12$)	114 ± 4	211 ± 6*($+97 \pm 5$)	-0.30 ± 0.02
	Resistant ($n = 9$)	124 ± 8	210 ± 6*($+86 \pm 4$)	-0.19 ± 0.03
	Control ($n = 16$)	121 ± 5	211 ± 6*($+91 \pm 5$)	-0.25 ± 0.03
	+BB ($n = 16$)	111 ± 5‡	180 ± 4*($+70 \pm 5$)‡	-0.16 ± 0.03

*$P < 0.05$ vs. Baseline.

†$P < 0.05$ vs. Susceptible.

‡$P < 0.05$ vs. Control.

of electrotonic coupling represent the combined passive electrical properties of the intra-, extra- and inter- (i.e., junctional) cellular pathways. Thus, the observed changes (i.e., decreases) in impedance can be a reflection of both direct changes (increases) in cell-to-cell coupling at the gap-junctions, and/or geometrical effects affecting the myocyte/interstitial space ratios during exercise (Fleischhauer et al., 1995; De Mello, 2010) (see below). Notably, pharmacological interventions that result in stimulation of the β-AR/adenylyl-cyclase/PKA pathway and increase cAMP concentration have been shown to enhance gap junctional coupling in many preparations (e.g., see Manoach et al., 1995; De Mello, 1996a; Dhein, 2004). In agreement with these *in vitro* reports, complete β-AR blockade attenuated the MEI response to exercise while direct β-AR stimulation (at rest with isoproterenol) triggered MEI decreases comparable to those observed during exercise.

Moreover, in the present study, β-AR meditated exercise-induced electrotonic changes were not only demonstrated *in vivo* (conscious animals), but more importantly, the magnitude of these changes were shown to differ between post-MI dogs subsequently shown to be susceptible or resistant to ischemia-induced ventricular fibrillation (VF). In this clinically-relevant scenario, a significantly larger MEI response to exercise was noted in animals prone to malignant arrhythmias (i.e., VF), suggesting increased electrotonic responsiveness to autonomic (β-AR) activation. The VF-susceptible animals have been extensively studied, presenting marked derangements in ionic current (Sridhar et al., 2008; Bonilla et al., 2012), electrotonic coupling (Del Rio et al., 2008b), intracellular calcium homeostasis (Belevych et al., 2009, 2012), and autonomic control (see Billman, 2006). For instance, susceptible dogs have been shown to have a larger degree of electrotonic remodeling post-MI (Del Rio et al., 2008b), presenting

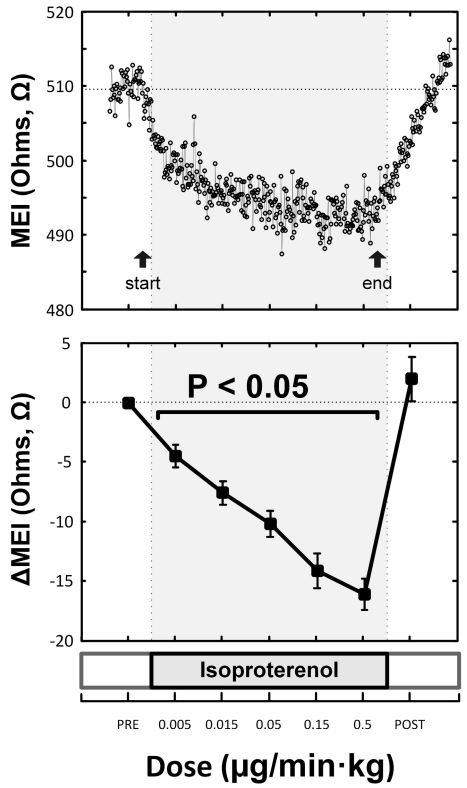

FIGURE 5 | Representative (top) and overall/mean (bottom) myocardial electrical impedance (MEI) response to direct β-adrenoceptor stimulation at rest (via escalating-dose infusion of isoproterenol), showing dose-dependent MEI decrease.

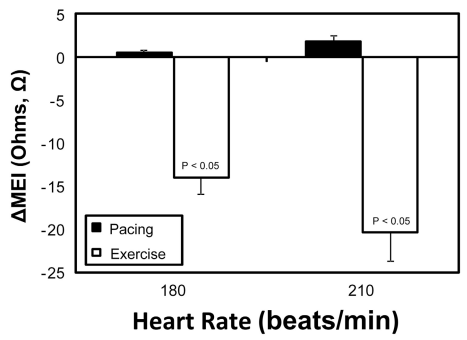

FIGURE 6 | Comparative myocardial electrical impedance (MEI) response to either submaximal exercise (white) or acute rate-matched ventricular pacing (black); only exercise decreased MEI.

moderately (albeit not statistically significant) higher remote MEI values at rest which could favor the observed increased electrotonic responsiveness. Indeed, in this study, animals prone to arrhythmias tended to have slightly higher baseline (i.e., pre-exercise) impedances but reached similar (absolute) values during exercise, suggesting, perhaps, a role of basal electrotonic derangements to their increased passive electrical responses to β-AR activation. Interestingly, the post-MI remodeling (e.g., down-regulation) of junctional proteins mediating electrotonic coupling is a well-established risk factor for malignant arrhythmias (e.g., see Saffitz and Kléber, 2012). On the other hand, susceptible animals also exhibit enhanced cardiac β-AR responsiveness, presenting a dominant functional contribution of the β_2-adrenergic receptors following MI, both *in vivo* and *in vitro* (Billman et al., 1997; Houle et al., 2001). Notably, acute β_2-AR stimulation can increase junctional conductance and protein expression in cardiac myocytes (Xia et al., 2009), likely via the exchange protein directly activated by cAMP (Epac)/Rap1 signaling pathway (Somekawa et al., 2005; Duquesnes et al., 2010; Mostafavi et al., 2014).

It also should be noted that much like patients prone to SCD (Rubart and Zipes, 2005), post-MI VF-susceptible dogs have well-documented abnormalities in myocardial calcium handling, being characterized by leaky and oxydized ryanodine receptors (Belevych et al., 2009) as well as increased calcium (Ca^{2+}) entry and Ca^{2+} transients, particularly during β-AR stimulation (Billman et al., 1997; Altschuld and Billman, 2000; Belevych et al., 2012). Moreover, in these animals, β_2-AR mediated increases in Ca^{2+}-transient amplitudes and Ca^{2+}-entry have been reported (Billman et al., 1997), rendering them exceptionally responsive (i.e., anti-arrhythmic protection) to the pharmacological blockade of L-type current (Billman, 1989). Interestingly, intracellular Ca^{2+} and junctional/electrotonic conductance are tightly coupled. For instance, inhibition of junctional communication can attenuate Ca^{2+} transients and sparks (Li et al., 2012). Meanwhile, pathologically-elevated intracellular Ca^{2+} levels (e.g., during a sustained ischemic insult) have been shown to decrease junctional conductance leading to electrotonic uncoupling (Cascio et al., 1990, 2005; Kléber, 1992; Smith et al., 1995; Owens et al., 1996; García-Dorado et al., 2004; De Groot and Coronel, 2004), likely as a protective mechanism against the spread of calcium overload (i.e., myocytes live and work together but die alone; quote from Engelmann (1875) in Janse et al., 2002). In contrast, moderate (i.e., within physiological levels) intracellular Ca^{2+} changes can enhance junctional coupling (perhaps via Ca^{2+}-activated kinases) (e.g., see Delage and Délèze, 1999). Indeed, Joyner et al. (1996) using a hybrid (both *in vitro and in silico*) paired-myocyte model showed that both β-AR stimulation (with isoproterenol) and direct opening of the L-type Ca^{2+} channels (with Bay K8644), facilitated cell-to-cell coupling and impulse propagation (an effect prevented by the L-type Ca^{2+} channel antagonist nifedipine). Thus, β-AR mediated electrotonic changes can provide mechanistic explanation(s) for the enhanced electrotonic responsiveness observed in the present study, particularly when the fact that complete β-AR blockade abolished the exercise-induced (electrotonic) differences with their VF-resistant counterparts is considered.

CLINICAL IMPLICATIONS

Regardless of the potential mechanism(s), the observed increase in electrotonic coupling during exercise and/or β-adrenergic autonomic activation may have important clinical implications. Notably, enhancements in electrotonic coupling can reduce repolarization heterogeneities thereby blunting or masking intrinsic pro-arrhythmic ionic substrates. Indeed, increased electrotonic

coupling has been shown to suppress early after-depolarizations (EADs) and reduce pro-arrhythmic dispersion of repolarization (e.g., Huelsing et al., 2000; Quan et al., 2007; Himel et al., 2013). Interestingly, Vanoli et al. (1995) showed that adrenergic activation via either left stellate ganglion stimulation (*in vivo*) or isoproterenol administration (*in vitro*) blunted the d-sotalol-mediated prolongation of the action potential duration. Similarly, Järvenpää et al. (2007) reported that post-MI patients susceptible to VF have an impaired capacity of the autonomic nervous system to alter (i.e., prolong) electrocardiographic indices of repolarization. These observations are in agreement with the results of the present study; namely, the observed shortening of both the rate-corrected QT interval and the terminal portion of the T-wave (reflecting spatial repolarization heterogeneities); changes that are consistent with the exercise-mediated increases in myocardial electrotonic coupling.

Finally, substantial evidence supports the role of abnormal repolarization and calcium mishandling during neural autonomic activation in the onset and maintenance of lethal arrhythmias, particularly in the setting of both congenital and acquired (e.g., post-MI) electro-mechanical remodeling. For instance, exercise testing has been shown to amplify the arrhythmic genotype-phenotype relationship in patients with both long-QT syndrome (Takenaka et al., 2003) and catecholaminergic polymorphic ventricular tachycardia (Obeyesekere et al., 2011). However, in a stark contrast, exercise-driven risk stratification of post-MI patients (particularly those with preserved ejection fraction) remains difficult and, at times, counter-intuitive. For instance, in a recent meta-analysis, Chan et al. (2010) showed that abnormal microvolt TWA results were more likely to reflect an increased risk for arrhythmic events only when β-adrenoceptor blocker therapy was not withheld prior to testing. In a similar manner, cardiac pacing elicited not only positive TWA responses in susceptible patients (Hohnloser et al., 1997; Raatikainen et al., 2005), but led to a lower incidence of indeterminate test results when compared to exercise testing (Kraaier et al., 2009). In this study, exercise not only shortened the Tpeak to Tend interval (TPE), an index that has been reported to prolong during pro-arrhythmic stimulation (Johnson et al., 2013), but failed to induce significant TWA differences between susceptible and resistant animals (i.e., S: 50.5 ± 9.0 vs. R: 39.2 ± 5.6 μV, N.S.). Thus, enhanced myocardial electrotonic coupling mediated by exercise-induced β-adrenoceptor activation could mask (e.g., via reductions in repolarization heterogeneities) changes in indices of risk for arrhythmia and could thereby explain the false negative results often obtained by exercise stress testing.

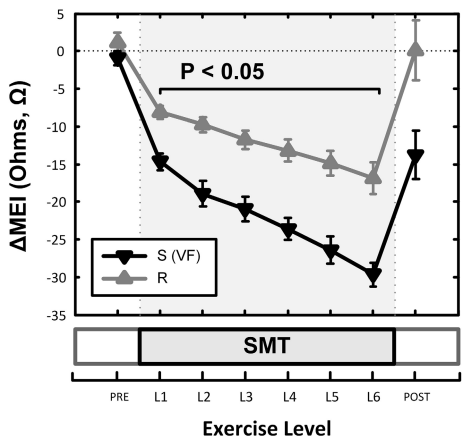

FIGURE 7 | Effects of underlying arrhythmic susceptibility of each animal in the myocardial electrical impedance (MEI) response to exercise; animals prone to ischemia-induced VF (i.e., S; *n* = 12) had a significantly larger MEI response to submaximal exercise, when compared those that were resistant (i.e., R; *n* = 9).

On the other hand, it is also important to note that improved electrotonic coupling has been shown to blunt myocardial ionic heterogeneities (e.g., Huelsing et al., 2000; Quan et al., 2007; Himel et al., 2013), masking and even reducing pro-arrhythmic risk (e.g., via pharmacological gap-junction modulation,; Hennan et al., 2006; Kjølbye et al., 2008). However any improvement in electrotonic coupling that was induced by acute exercise was of insufficient magnitude to prevent the onset of ischemic (coronary artery occlusion) arrhythmias in susceptible animals. Indeed, myocardial ischemia has been shown to depress electrotonic coupling acutely (e.g., Kléber et al., 1987; Cascio et al., 1990; Smith et al., 1995; Del Rio et al., 2005, 2008a). Thus, in the setting of a healed infarction/remodeling (Del Rio et al., 2008b) and exercise-mediated electrotonic enhancements, concomitant regional ischemia likely resulted in marked local passive electrical heterogeneities, which are pro-arrhythmic (e.g., Bishop et al., 2014). Similarly, as noted above, impedance measurements represent the "average" electrotonic properties, (Kléber et al., 1987) of a specific myocardial region. Therefore, the observed MEI decreases are unlikely to reflect a homogenous enhancement

Table 3 | Electrocardiographic response(s) to submaximal exercise.

Time	RR(ms)	PR (ms)	QRS (ms)	QT (ms)	QT_c(msc)	TPE (ms)	QT/TQ (n/u)	T_{SD}(μV)
Baseline	479 ± 19	92 ± 3	66 ± 2	206 ± 5	251 ± 4	51 ± 4	0.79 ± 0.04	25 ± 3
Exercise	329 ± 8	79 ± 3	65 ± 3	170 ± 4	229 ± 4	39 ± 2	1.11 ± 0.06	45 ± 5
P < 0.05†	↓	↓	–	↓	↓	↓	↑	↑

Data collected immediately after the discontinuation of exercise.

†Arrows (↓,↑): P < 0.05 Exercise vs. Baseline (rest).

QTc, van der Water's rate-corrected QT interval; TPE, Tpeak-Tend; QT/TQ, index reflecting the steepness of restitution; TSD, Standard deviation of the T-Wave amplitude.

of electrotonic coupling. Indeed, the heterogeneous distribution of the myocardial autonomic innervation, would favor the onset of "focal" arrhythmias during β-AR stimulation (Myles et al., 2012).

STUDY LIMITATIONS

This study demonstrated that β-adrenoceptor activation mediates exercise-driven changes (increased) in myocardial electrotonic coupling. However, it also should be noted that despite complete β-adrenoceptor blockade, a moderate decrease in MEI was observed during exercise. Several factors, that were not assessed in the present study, may have contributed to the residual (non-β-AR mediated) increases in myocardial electrotonic coupling during exercise.

For instance, during exercise, circulating cathecholamines activate both β- and α-adrenoceptors. Interestingly, sub-chronic α-adrenergic stimulation has been reported to exert PKC-mediated enhancements in connexin43 expression (Salameh et al., 2006). Furthermore, Rojas-Gomez et al. (2008) found that phenylephrine (an α-adrenergic receptor agonist) enhanced Cx43 expression in neonatal rat cardiac myocytes, resulting in enhanced gap-junction conductance. However, it also should be noted that opposite electrotonic (i.e., reductions in junctional conductance) have been reported during acute α-adrenoceptor stimulation (De Mello, 1997; de Boer et al., 2007), albeit these effects may vary in the setting of concomitant β-adrenoceptor stimulation (Salameh et al., 2010). Similarly, the renin-angiotensin system is also acutely activated during exercise, increasing the circulating levels of angiotensin-II, which can modulate the passive electrical properties of the myocardium (De Mello, 1996b, 2014; Sovari et al., 2013).

Also, as noted above, changes in both spatial/geometrical and/or ionic composition of the myocardium can alter its electrotonic properties. For example, Veeraraghavan et al. (2012) recently reported that changes in interstitial volume can modulate both conduction velocity and its dependence on gap-junction conductance. Changes in interstitial and/or myocyte volumes during exercise are likely, particularly given the reported ionic, metabolic, and plasma-volume changes during exercise (Paterson, 1996); interestingly, β-AR activation has been implicated in the volume-regulation (i.e., decrease) of cardiac myocytes (Wang et al., 1997). Thus, β-adrenoceptor mediated changes in myocyte volume could also contribute to the exercise-induced changes MEI reported in the present study.

Similarly, changes in both cell-to-cell coupling (e.g., Burt and Spray, 1988; Saffitz and Yamada, 1998; Salameh and Dhein, 2013) and global indices of myocardial passive electrical properties (e.g., Sasaki et al., 1994; Dekker et al., 1996; Howie et al., 2001) have been linked/associated with alterations in the mechanical properties of the myocardium. Indeed, in isolated myocytes, positive/negative inotropic agents have been shown to enhance/depress (respectively) junctional coupling in parallel with their functional effects (Burt and Spray, 1988; Dhein, 2004). In the present study, both exercise and direct pharmacological β-AR stimulation (with isoproterenol), two well-defined inotropic interventions, decreased MEI, consistent with an enhanced electrotonic coupling. Although neither systemic/cardiac hemodynamics nor mechanics were assessed directly in the present study, previous studies have extensively documented the hemodynamic/functional responses of susceptible/resistant post-MI dogs, both at rest and during exercise (e.g., Billman et al., 1985, 1997; De Ferrari et al., 1993; Avendano and Billman, 1994). For instance, Billman et al. (1985) reported comparable increases in the peak rate of left-ventricular pressure change (i.e., dP/dtmax—an inotropic index) during exercise in both groups of post-MI dogs, with animals prone to arrhythmias showing larger elevations in ventricular filling (end-diastolic) pressures (consistent with the exercise-driven preload changes, Miyazaki et al., 1990) and blunted increases in systolic pressures. Meanwhile, Avendano and Billman (1994) described similar inotropic/hemodynamic changes (i.e., dP/dtmax and systolic pressure increases) following isoproterenol administration (and other interventions that increased cAMP levels) in post-MI dogs and, in contrast to exercise, moderate isoproterenol-mediated end-diastolic pressure reductions were also noted (consistent with pre-load reductions Barnes et al., 1979). Hence, as mechanical stretch can alter intercellular coupling (Salameh and Dhein, 2013), it is possible that exercise-mediated changes in myocardial wall-tension could also play a role in the passive electrical changes that were observed in the present study. Finally, neither myocardial nor core body temperature were measured during exercise in this study. Notably, the resistivity of a medium can decrease as temperature increases (e.g., 2%/°C; Tsai et al., 2002). However, previously unpublished data from our laboratory (Billman GE, and del Rio CL) found that core body temperature not only increased moderately (∼1°C) during exercise, but also, recovered slowly post-exercise (consistent with the limited heat-dissipation of dogs); an observation that contrasts with the rapid restoration of electrotonic coupling following the termination of exercise. Thus, changes in myocardial temperature induced by exercise probably did not contribute to the MEI changes noted in the present study.

In conclusion, the results of the present study demonstrate that β-AR activation during exercise can acutely enhance passive electrical properties (i.e., electrotonic coupling) of the myocardium, particularly in post-MI dogs susceptible to ischemia-induced VF. Increased coupling during β-AR stimulation may have important clinical implications, as it could mask intrinsic (and/or acquired) pro-arrhythmic repolarization abnormalities during states of autonomic activation (e.g., exercise) *in vivo*.

ACKNOWLEDGMENTS

This study was supported in part by a National Heart, Lung, and Blood Institute Grant, HL-68609 (GEB).

REFERENCES

Adabag, A. S., Luepker, R. V., Roger, V. L., and Gersh, B. J. (2010). Sudden cardiac death: epidemiology and risk factors. *Nat. Rev. Cardiol.* 7, 216–225. doi: 10.1038/nrcardio.2010.3

Altschuld, R. A., and Billman, G. E. (2000). Beta(2)-Adrenoceptors and ventricular fibrillation. *Pharmacol. Ther.* 88, 1–14. doi: 10.1016/S0163-7258(00)00075-9

Amit, G., Rosenbaum, D. S., Super, D. M., and Costantini, O. (2010). Microvolt T-wave alternans and electrophysiologic testing predict distinct arrhythmia substrates: implications for identifying patients at risk for sudden cardiac death. *Heart Rhythm* 7, 763–768. doi: 10.1016/j.hrthm.2010.02.012

Avendano, C. E., and Billman, G. E. (1994). Effect of interventions that increase cyclic AMP levels on susceptibility to ventricular fibrillation in unanesthetized dogs. *Eur. J. Pharmacol.* 255, 99–109.

Barnes, G. E., Horwitz, L. D., and Bishop, V. S. (1979). Reliability of the maximum derivatives of left ventricular pressure and internal diameter as indices of the inotropic state of the depressed myocardium. *Cardiovasc. Res.* 13, 652–662.

Belevych, A. E., Terentyev, D., Terentyeva, R., Ho, H. T., Gyorke, I., Bonilla, I. M., et al. (2012). Shortened Ca2+ signaling refractoriness underlies cellular arrhythmogenesis in a postinfarction model of sudden cardiac death. *Circ. Res.* 110, 569–577. doi: 10.1161/CIRCRESAHA.111.260455

Belevych, A. E., Terentyev, D., Viatchenko-Karpinski, S., Terentyeva, R., Sridhar, A., Nishijima, Y., et al. (2009). Redox modification of ryanodine receptors underlies calcium alternans in a canine model of sudden cardiac death. *Cardiovasc. Res.* 84, 387–395. doi: 10.1093/cvr/cvp246

Billman, G. E. (1989). Effect of calcium channel antagonists on susceptibility to sudden cardiac death: protection from ventricular fibrillation. *J. Pharmacol. Exp. Ther.* 248, 1334–1342.

Billman, G. E. (2006). A comprehensive review and analysis of 25 years of data from an *in vivo* canine model of sudden cardiac death: implications for future anti-arrhythmic drug development. *Pharmacol. Ther.* 111, 808–835. doi: 10.1016/j.pharmthera.2006.01.002

Billman, G. E., Castillo, L. C., Hensley, J., Hohl, C. M., and Altschuld, R. A. (1997). Beta2-adrenergic receptor antagonists protect against ventricular fibrillation: *in vivo* and *in vitro* evidence for enhanced sensitivity to beta2-adrenergic stimulation in animals susceptible to sudden death. *Circulation* 96, 1914–1922.

Billman, G. E., and Dujardin, J. P. (1990). Dynamic changes in cardiac vagal tone as measured by time-series analysis. *Am. J. Physiol.* 258(Pt 2), H896–H902.

Billman, G. E., and Hoskins, R. S. (1989). Time-series analysis of heart rate variability during submaximal exercise. Evidence for reduced cardiac vagal tone in animals susceptible to ventricular fibrillation. *Circulation* 80, 146–157.

Billman, G. E., Schwartz, P. J., Gagnol, J. P., and Stone, H. L. (1985). Cardiac response to submaximal exercise in dogs susceptible to sudden cardiac death. *J. Appl. Physiol.* 59, 890–897.

Bishop, M. J., Connolly, A., and Plank, G. (2014). Structural heterogeneity modulates effective refractory period: a mechanism of focal arrhythmia initiation. *PLoS ONE* 9:e109754. doi: 10.1371/journal.pone.0109754

Bonilla, I. M., Belevych, A. E., Sridhar, A., Nishijima, Y., Ho, H. T., He, Q., et al. (2012). Endurance exercise training normalizes repolarization and calcium-handling abnormalities, preventing ventricular fibrillation in a model of sudden cardiac death. *J. Appl. Physiol.* 113, 1772–1783. doi: 10.1152/japplphysiol.00175.2012

Brice, G., and Stone, H. L. (1986). Exercise tolerance and compensatory sympathetic tone during beta-blockade after myocardial infarction. *Med. Sci. Sports Exerc.* 18, 396–401.

Burt, J. M., and Spray, D. C. (1988). Inotropic agents modulate gap junctional conductance between cardiac myocytes. *Am. J. Physiol.* 254(Pt 2), H1206–H1210.

Cantillon, D. J., Stein, K. M., Markowitz, S. M., Mittal, S., Shah, B. K., Morin, D. P., et al. (2007). Predictive value of microvolt T-wave alternans in patients with left ventricular dysfunction. *J. Am. Coll. Cardiol.* 50, 166–173. doi: 10.1016/j.jacc.2007.02.069

Cascio, W. E., Yang, H., Muller-Borer, B. J., and Johnson, T. A. (2005). Ischemia-induced arrhythmia: the role of connexins, gap junctions, and attendant changes in impulse propagation. *J. Electrocardiol.*38, 55–59. doi: 10.1016/j.jelectrocard.2005.06.019

Cascio, W. E., Yan, G. X., and Kléber, A. G. (1990). Passive electrical properties, mechanical activity, and extracellular potassium in arterially perfused and ischemic rabbit ventricular muscle. Effects of calcium entry blockade or hypocalcemia. *Circ. Res.* 66, 1461–1473.

Chan, P. S., Gold, M. R., and Nallamothu, B. K. (2010). Do Beta-blockers impact microvolt T-wave alternans testing in patients at risk for ventricular arrhythmias? a meta-analysis. *J. Cardiovasc. Electrophysiol.* 21, 1009–1014. doi: 10.1111/j.1540-8167.2010.01757.x

Chen, L. S., Zhou, S., Fishbein, M. C., and Chen, P. S. (2007). New perspectives on the role of autonomic nervous system in the genesis of arrhythmias. *J. Cardiovasc. Electrophysiol.* 18, 123–127. doi: 10.1111/j.1540-8167.2006.00590.x

Cherry, E. M., and Fenton, F. H. (2004). Suppression of alternans and conduction blocks despite steep APD restitution: electrotonic, memory, and conduction velocity restitution effects. *Am. J. Physiol. Heart Circ. Physiol.* 286, H2332–H2341. doi: 10.1152/ajpheart.00747.2003

Collins, M. N., and Billman, G. E. (1989). Autonomic response to coronary occlusion in animals susceptible to ventricular fibrillation. *Am. J. Physiol.* 257(Pt 2), H1886–H1894.

de Boer, T. P., van Rijen, H. V., Van der Heyden, M. A., Kok, B., Opthof, T., Vos, M. A., et al. (2007). Beta-, not alpha-adrenergic stimulation enhances conduction velocity in cultures of neonatal cardiomyocytes. *Circ. J.* 71, 973–981. doi: 10.1253/circj.71.973

De Ferrari, G. M., Salvati, P., Grossoni, M., Ukmar, G., Vaga, L., Patrono, C., et al. (1993). Pharmacologic modulation of the autonomic nervous system in the prevention of sudden cardiac death. A study with propranolol, methacholine and oxotremorine in conscious dogs with a healed myocardial infarction. *J. Am. Coll. Cardiol.* 22, 283–290.

De Groot, J. R., and Coronel, R. (2004). Acute ischemia-induced gap junctional uncoupling and arrhythmogenesis. *Cardiovasc. Res.* 62, 323–334. doi: 10.1016/j.cardiores.2004.01.033

Dekker, L. R., Fiolet, J. W., VanBavel, E., Coronel, R., Opthof, T., Spaan, J. A., et al. (1996). Intracellular Ca2+, intercellular electrical coupling, and mechanical activity in ischemic rabbit papillary muscle. Effects of preconditioning and metabolic blockade. *Circ. Res.* 79, 237–246.

Delage, B., and Délèze, J. (1999). Chapter 9: a reexamination of calcium effects on gap junctions in heart myocytes. *Curr. Top Membr.* 49, 189–206.

Del Rio, C. L., Dawson, T. A., Clymer, B. D., Paterson, D. J., and Billman, G. E. (2008a). Effects of acute vagal nerve stimulation on the early passive electrical changes induced by myocardial ischaemia in dogs: heart rate-mediated attenuation. *Exp. Physiol.* 93, 931–944. doi: 10.1113/expphysiol.2007.041558

Del Rio, C. L., McConnell, P. I., Clymer, B. D., Dzwonczyk, R., Michler, R. E., Billman, G. E., et al. (2005). Early time course of myocardial electrical impedance during acute coronary artery occlusion in pigs, dogs, and humans. *J. Appl. Physiol.* 99, 1576–1581. doi: 10.1152/japplphysiol.00830.2004

Del Rio, C. L., McConnell, P. I., Kukielka, M., Dzwonczyk, R., Clymer, B. D., Howie, M. B., et al. (2008b). Electrotonic remodeling following myocardial infarction in dogs susceptible and resistant to sudden cardiac death. *J. Appl. Physiol.* 104, 386–393. doi: 10.1152/japplphysiol.01106.2007

De Mello, W. C. (1996a). Impaired regulation of cell communication by beta-adrenergic receptor activation in the failing heart. *Hypertension* 27, 265–268.

De Mello, W. C. (1996b). Renin-angiotensin system and cell communication in the failing heart. *Hypertension* 27, 1267–1272.

De Mello, W. C. (1997). Influence of alpha-adrenergic-receptor activation on junctional conductance in heart cells: interaction with beta-adrenergic adrenergic agonists. *J. Cardiovasc. Pharmacol.* 29, 273–277.

De Mello, W. C. (2010). Cell swelling impairs dye coupling in adult rat ventricular myocytes. Cell volume as a regulator of cell communication. *Mol. Cell. Biochem.* 343, 107–113. doi: 10.1007/s11010-010-0504-8

De Mello, W. C. (2014). Angiotensin (1-7) re-establishes heart cell communication previously impaired by cell swelling: implications for myocardial ischemia. *Exp. Cell. Res.* 323, 359–365. doi: 10.1016/j.yexcr.2014.03.006

Dhein, S. (2004). Pharmacology of gap junctions in the cardiovascular system. *Cardiovasc. Res.* 62, 287–298. doi: 10.1016/j.cardiores.2004.01.019

Duquesnes, N., Derangeon, M., Métrich, M., Lucas, A., Mateo, P., Li, L., et al. (2010). Epac stimulation induces rapid increases in connexin43 phosphorylation and function without preconditioning effect. *Pflugers Arch.* 460, 731–741. doi: 10.1007/s00424-010-0854-9

Dzwonczyk, R., del Rio, C., Brown, D. A., Michler, R. E., Wolf, R. K., and Howie, M. B. (2004). Myocardial electrical impedance responds to ischemia and reperfusion in humans. *IEEE Trans. Biomed. Eng.* 51, 2206–2209. doi: 10.1109/TBME.2004.834297

Fleischhauer, J., Lehmann, L., and Kléber, A. G. (1995). Electrical resistances of interstitial and microvascular space as determinants of the extracellular electrical field and velocity of propagation in ventricular myocardium. *Circulation* 92, 587–594.

Fossa, A. A., Wisialowski, T., Crimin, K., Wolfgang, E., Couderc, J. P., Hinterseer, M., et al. (2007). Analyses of dynamic beat-to-beat QT-TQ interval (ECG restitution) changes in humans under normal sinus rhythm and prior to an event of torsades de pointes during QT prolongation caused by sotalol. *Ann. Noninvasive. Electrocardiol.* 12, 338–348. doi: 10.1111/j.1542-474X.2007.00183.x

García-Dorado, D., Rodríguez-Sinovas, A., and Ruiz-Meana, M. (2004). Gap junction-mediated spread of cell injury and death during myocardial ischemia-reperfusion. *Cardiovasc. Res.* 61, 386–401. doi: 10.1016/j.cardiores.2003.11.039

Goldberger, J. J., Basu, A., Boineau, R., Buxton, A. E., Cain, M. E., Canty, J. M. Jr., et al. (2014). Risk stratification for sudden cardiac death: a plan for the future. *Circulation* 129, 516–526. doi: 10.1161/CIRCULATIONAHA.113.007149

Hennan, J. K., Swillo, R. E., Morgan, G. A., Keith, J. C. Jr., Schaub, R. G., Smith, R. P., et al. (2006). Rotigaptide (ZP123) prevents spontaneous ventricular arrhythmias and reduces infarct size during myocardial ischemia/reperfusion injury in open-chest dogs. *J. Pharmacol. Exp. Ther.* 317, 236–243. doi: 10.1124/jpet.105.096933

Himel, H. D. 4th., Garny, A., Noble, P. J., Wadgaonkar, R., Savarese, J., Liu, N., et al. (2013). Electrotonic suppression of early afterdepolarizations in the neonatal rat ventricular myocyte monolayer. *J. Physiol.* 591(Pt 21), 5357–5364. doi: 10.1113/jphysiol.2013.262923

Hohnloser, S. H., Klingenheben, T., Zabel, M., Li, Y. G., Albrecht, P., and Cohen, R. J. (1997). T wave alternans during exercise and atrial pacing in humans. *J. Cardiovasc. Electrophysiol.* 8, 987–993.

Houle, M. S., Altschuld, R. A., and Billman, G. E. (2001). Enhanced *in vivo* and *in vitro* contractile responses to beta(2)-adrenergic receptor stimulation in dogs susceptible to lethal arrhythmias. *J. Appl. Physiol.* 91, 1627–1637.

Howie, M. B., Dzwonczyk, R., and McSweeney, T. D. (2001). An evaluation of a new two-electrode myocardial electrical impedance monitor for detecting myocardial ischemia. *Anesth Analg.* 92, 12–18.

Huelsing, D. J., Spitzer, K. W., and Pollard, A. E. (2000). Electrotonic suppression of early afterdepolarizations in isolated rabbit Purkinje myocytes. *Am. J. Physiol. Heart Circ. Physiol.* 279, H250–H259.

Janse, M. J., Tan, H. L., Dekker, L. R. C., and Kléber, A. G. (2002). "Cellular electrical uncoupling during ischemia," in *Heart Cell Coupling and Impulse Propagation in Health and Disease*, eds W. C. de Mello, M. J. Janse (Boston; Dordrecht; London: Kluwer Academic Publishers), 257–282.

Järvenpää, J., Oikarinen, L., Korhonen, P., Väänänen, H., Toivonen, L., and Viitasalo, M. (2007). Changing capacity of electrocardiographic ventricular repolarization in post-myocardial infarction patients with and without nonfatal cardiac arrest. *Am. J. Cardiol.* 99, 295–299. doi: 10.1016/j.amjcard.2006.08.027

Jia, Z., Bien, H., Shiferaw, Y., and Entcheva, E. (2012). Cardiac cellular coupling and the spread of early instabilities in intracellular Ca2+. *Biophys. J.* 102, 1294–1302. doi: 10.1016/j.bpj.2012.02.034

Johnson, D. M., Heijman, J., Bode, E. F., Greensmith, D. J., van der Linde, H., Abi-Gerges, N., et al. (2013). Diastolic spontaneous calcium release from the sarcoplasmic reticulum increases beat-to-beat variability of repolarization in canine ventricular myocytes after β-adrenergic stimulation. *Circ. Res.* 112, 246–256. doi: 10.1161/CIRCRESAHA.112.275735

Joyner, R. W., Kumar, R., Wilders, R., Jongsma, H. J., Verheijck, E. E., Golod, D. A., et al. (1996). Modulating L-type calcium current affects discontinuous cardiac action potential conduction. *Biophys. J.* 71, 237–245.

Kijtawornrat, A., Panyasing, Y., Del Rio, C., and Hamlin, R. L. (2010). Assessment of ECG interval and restitution parameters in the canine model of short QT syndrome. *J. Pharmacol. Toxicol. Methods* 61, 231–237. doi: 10.1016/j.vascn.2010.02.001

Kjølbye, A. L., Dikshteyn, M., Eloff, B. C., Deschênes, I., and Rosenbaum, D. S. (2008). Maintenance of intercellular coupling by the antiarrhythmic peptide rotigaptide suppresses arrhythmogenic discordant alternans. *Am. J. Physiol. Heart Circ. Physiol.* 294, H41–H49. doi: 10.1152/ajpheart.01089.2006

Kléber, A. G., Riegger, C. B., and Janse, M. J. (1987). Electrical uncoupling and increase of extracellular resistance after induction of ischemia in isolated, arterially perfused rabbit papillary muscle. *Circ. Res.* 61, 271–279.

Kléber, G. (1992). The potential role of Ca2+ for electrical cell-to-cell uncoupling and conduction block in myocardial tissue. *Basic Res. Cardiol.* 87, 131–143.

Kraaier, K., Verhorst, P. M., van der Palen, J., van Dessel, P. F., Wilde, A. A., and Scholten, M. F. (2009). Microvolt T-wave alternans during exercise and pacing are not comparable. *Europace* 11, 1375–1380. doi: 10.1093/europace/eup253

Li, C., Meng, Q., Yu, X., Jing, X., Xu, P., and Luo, D. (2012). Regulatory effect of connexin 43 on basal Ca2+ signaling in rat ventricular myocytes. *PLoS ONE* 7:e36165. doi: 10.1371/journal.pone.0036165

Manoach, M., Varon, D., and Erez, M. (1995). The role of catecholamines on intercellular coupling, myocardial cell synchronization and self-ventricular defibrillation. *Mol. Cell Biochem.* 147, 181–185.

Merchant, F. M., Ikeda, T., Pedretti, R. F., Salerno-Uriarte, J. A., Chow, T., Chan, P. S., et al. (2012). Clinical utility of microvolt T-wave alternans testing in identifying patients at high or low risk of sudden cardiac death. *Heart Rhythm.* 9, 1256.e2–1264.e2. doi: 10.1016/j.hrthm.2012.03.014

Miyazaki, S., Guth, B. D., Miura, T., Indolfi, C., Schulz, R., Ross, J., et al. (1990). Changes of left ventricular diastolic function in exercising dogs without and with ischemia. *Circulation* 81, 1058–1070.

Mostafavi, H., Khaksarian, M., Joghataei, M. T., Soleimani, M., Hassanzadeh, G., Eftekhari, S., et al. (2014). Selective β2 adrenergic agonist increases Cx43 and miR-451 expression via cAMP-Epac. *Mol. Med. Rep.* 9, 2405–2410. doi: 10.3892/mmr.2014.2120

Myles, R. C., Wang, L., Kang, C., Bers, D. M., and Ripplinger, C. M. (2012). Local β-adrenergic stimulation overcomes source-sink mismatch to generate focal arrhythmia. *Circ. Res.* 110, 1454–1464. doi: 10.1161/CIRCRESAHA.111.262345

Nearing, B. D., and Verrier, R. L. (2002). Modified moving average analysis of T-wave alternans to predict ventricular fibrillation with high accuracy. *J. Appl. Physiol.* 92, 541–549. doi: 10.1152/japplphysiol.00592.2001

Obeyesekere, M. N., Klein, G. J., Modi, S., Leong-Sit, P., Gula, L. J., Yee, R., et al. (2011). How to perform and interpret provocative testing for the diagnosis of Brugada syndrome, long-QT syndrome, and catecholaminergic polymorphic ventricular tachycardia. *Circ. Arrhythm. Electrophysiol.* 4, 958–964. doi: 10.1161/CIRCEP.111.965947

Opthof, T., Coronel, R., Wilms-Schopman, F. J., Plotnikov, A. N., Shlapakova, I. N., Danilo, P. Jr., et al. (2007). Dispersion of repolarization in canine ventricle and the electrocardiographic T wave: Tp-e interval does not reflect transmural dispersion. *Heart Rhythm.* 4, 341–348. doi: 10.1016/j.hrthm.2006.11.022

Owens, L. M., Fralix, T. A., Murphy, E., Cascio, W. E., and Gettes, L. S. (1996). Correlation of ischemia-induced extracellular and intracellular ion changes to cell-to-cell electrical uncoupling in isolated blood-perfused rabbit hearts. *Circulation* 94, 10–13.

Pastore, J. M., and Rosenbaum, D. S. (2000). Role of structural barriers in the mechanism of alternans-induced reentry. *Circ. Res.* 87, 1157–1163. doi: 10.1161/01.RES.87.12.1157

Paterson, D. J. (1996). Antiarrhythmic mechanisms during exercise. *J. Appl. Physiol.* 80, 1853–1862.

Pokornı J., Stanìk, V., and Vrána, M. (2011). Sudden cardiac death thirty years ago and at present. The role of autonomic disturbances in acute myocardial infarction revisited. *Physiol. Res.* 60, 715–728.

Quan, X. Q., Bai, R., Liu, N., Chen, B. D., and Zhang, C. T. (2007). Increasing gap junction coupling reduces transmural dispersion of repolarization and prevents torsade de pointes in rabbit LQT3 model. *J. Cardiovasc. Electrophysiol.* 18, 1184–1189. doi: 10.1111/j.1540-8167.2007.00923.x

Raatikainen, M. J., Jokinen, V., Virtanen, V., Hartikainen, J., Hedman, A., and Huikuri, H. V. (2005). (CARISMA Investigators). Microvolt T-wave alternans during exercise and pacing in patients with acute myocardial infarction. *Pacing Clin. Electrophysiol.* 28. S193–S197. doi: 10.1111/j.1540-8159.2005.00110.x

Rojas-Gomez, D. M., Schulte, J. S., Mohr, F. W., and Dhein, S. (2008). Alpha-1-adrenoceptor subtype selective regulation of connexin 43 expression in rat cardiomyocytes. *Naunyn. Schmiedebergs Arch. Pharmacol.* 377, 77–85. doi: 10.1007/s00210-007-0244-9

Rubart, M., and Zipes, D. P. (2005). Mechanisms of sudden cardiac death. *J. Clin. Invest.* 115, 2305–2315. doi: 10.1172/JCI26381

Saffitz, J. E., and Kléber, A. G. (2012). Gap junctions, slow conduction, and ventricular tachycardia after myocardial infarction. *J. Am. Coll. Cardiol.* 60, 1111–1113. doi: 10.1016/j.jacc.2012.05.020

Saffitz, J. E., and Yamada, K. A. (1998). Do alterations in intercellular coupling play a role in cardiac contractile dysfunction? *Circulation* 97, 630–632.

Salameh, A., and Dhein, S. (2011). Adrenergic control of cardiac gap junction function and expression. *Naunyn. Schmiedebergs Arch. Pharmacol.* 383, 331–346. doi: 10.1007/s00210-011-0603-4

Salameh, A., and Dhein, S. (2013). Effects of mechanical forces and stretch on intercellular gap junction coupling. *Biochim. Biophys. Acta* 1828, 147–156. doi: 10.1016/j.bbamem.2011.12.030

Salameh, A., Frenzel, C., Boldt, A., Rassler, B., Glawe, I., Schulte, J., et al. (2006). Subchronic alpha- and beta-adrenergic regulation of cardiac gap junction protein expression. *FASEB J.* 20, 365–367. doi: 10.1096/fj.05-4871fje

Salameh, A., Karl, S., Djilali, H., Dhein, S., Janousek, J., and Daehnert, I. (2010). Opposing and synergistic effects of cyclic mechanical stretch and α- or

β-adrenergic stimulation on the cardiac gap junction protein Cx43. *Pharmacol. Res*. 62, 506–513. doi: 10.1016/j.phrs.2010.08.002

Sasaki, E., Conger, J. L., Kadipasaoglu, K. A., Pehlivanoglu, S., and Frazier, O. H. (1994). Simultaneous evaluation of cardiac wall motion and myocardial ischemic injury by measurement of electrical impedance. *ASAIO J.* 40, M826–M829.

Sato, D., Shiferaw, Y., Garfinkel, A., Weiss, J. N., Qu, Z., and Karma, A. (2006). Spatially discordant alternans in cardiac tissue: role of calcium cycling. *Circ. Res*. 99, 520–527. doi: 10.1161/01.RES.0000240542.03986.e7

Shizuta, S., Ando, K., Nobuyoshi, M., Ikeda, T., Yoshino, H., Hiramatsu, S., et al. (2012). (PREVENT-SCD Investigators). Prognostic utility of T-wave alternans in a real-world population of patients with left ventricular dysfunction: the PREVENT-SCD study. *Clin. Res. Cardiol.* 101, 89–99. doi: 10.1007/s00392-011-0368-2

Smith, W. T. IV, Fleet, W. F., Johnson, T. A., Engle, C. L., and Cascio, W. E. (1995). The Ib phase of ventricular arrhythmias in ischemic *in situ* porcine heart is related to changes in cell-to-cell electrical coupling. *Circulation* 92, 3051–3060.

Somekawa, S., Fukuhara, S., Nakaoka, Y., Fujita, H., Saito, Y., and Mochizuki, N. (2005). Enhanced functional gap junction neoformation by protein kinase A-dependent and Epac-dependent signals downstream of cAMP in cardiac myocytes. *Circ. Res*. 97, 655–662. doi: 10.1161/01.RES.0000183880.49270.f9

Sovari, A. A., Rutledge, C. A., Jeong, E. M., Dolmatova, E., Arasu, D., Liu, H., et al. (2013). Mitochondria oxidative stress, connexin43 remodeling, and sudden arrhythmic death. *Circ. Arrhythm. Electrophysiol*. 6, 623–631. doi: 10.1161/CIRCEP.112.976787

Sridhar, A., Nishijima, Y., Terentyev, D., Terentyeva, R., Uelmen, R., Kukielka, M., et al. (2008). Repolarization abnormalities and afterdepolarizations in a canine model of sudden cardiac death. *Am. J. Physiol. Regul. Integr. Comp. Physiol*. 295, R1463–R1472. doi: 10.1152/ajpregu.90583.2008

Stone, H. L. (1977). Cardiac function and exercise training in conscious dogs. *J. Appl. Physiol.* 42, 824–832.

Takenaka, K., Ai, T., Shimizu, W., Kobori, A., Ninomiya, T., Otani, H., et al. (2003). Exercise stress test amplifies genotype-phenotype correlation in the LQT1 and LQT2 forms of the long-QT syndrome. *Circulation* 107, 838–844. doi: 10.1161/01.CIR.0000048142.85076.A2

Tsai, J. Z., Will, J. A., Hubbard-Van Stelle, S., Cao, H., Tungjitkusolmun, S., Choy, Y. B., et al. (2002). Error analysis of tissue resistivity measurement. *IEEE Trans. Biomed. Eng*. 49, 484–494. doi: 10.1109/10.995687

Van de Water, A., Verheyen, J., Xhonneux, R., and Reneman, R. S. (1989). An improved method to correct the QT interval of the electrocardiogram for changes in heart rate. *J. Pharmacol. Methods* 22, 207–117.

Vanoli, E., Priori, S. G., Nakagawa, H., Hirao, K., Napolitano, C., Diehl, L., et al. (1995). Sympathetic activation, ventricular repolarization and Ikr blockade: implications for the antifibrillatory efficacy of potassium channel blocking agents. *J. Am. Coll. Cardiol.* 25, 1609–1614.

Veeraraghavan, R., Salama, M. E., and Poelzing, S. (2012). Interstitial volume modulates the conduction velocity-gap junction relationship. *Am. J. Physiol. Heart Circ. Physiol.* 302, H278–H286. doi: 10.1152/ajpheart.00868.2011

Verrier, R. L., Klingenheben, T., Malik, M., El-Sherif, N., Exner, D. V., Hohnloser, S. H., et al. (2011). Microvolt T-wave alternans physiological basis, methods of measurement, and clinical utility–consensus guideline by international society for holter and noninvasive electrocardiology. *J. Am. Coll. Cardiol*. 58, 1309–1324. doi: 10.1016/j.jacc.2011.06.029

Wang, Z., Mitsuiye, T., Rees, S. A., and Noma, A. (1997). Regulatory volume decrease of cardiac myocytes induced by beta-adrenergic activation of the Cl-channel in guinea pig. *J. Gen. Physiol.* 110, 73–82.

Watanabe, M. A., Fenton, F. H., Evans, S. J., Hastings, H. M., and Karma, A. (2001). Mechanisms for discordant alternans. *J. Cardiovasc. Electrophysiol.* 12, 196–206. doi: 10.1046/j.1540-8167.2001.00196.x

Wellens, H. J., Schwartz, P. J., Lindemans, F. W., Buxton, A. E., Goldberger, J. J., Hohnloser, S. H., et al. (2014). Risk stratification for sudden cardiac death: current status and challenges for the future. *Eur. Heart J*. 35, 1642–1651. doi: 10.1093/eurheartj/ehu176

Wit, A. L., and Peters, N. S. (2012). The role of gap junctions in the arrhythmias of ischemia and infarction. *Heart Rhythm*. 9, 308–311. doi: 10.1016/j.hrthm.2011.09.056

Xia, Y., Gong, K. Z., Xu, M., Zhang, Y. Y., Guo, J. H., Song, Y., et al. (2009). Regulation of gap-junction protein connexin 43 by beta-adrenergic receptor stimulation in rat cardiomyocytes. *Acta Pharmacol. Sin*. 30, 928–934. doi: 10.1038/aps.2009.92

Yan, G. X., and Antzelevitch, C. (1998). Cellular basis for the normal T wave and the electrocardiographic manifestations of the long-QT syndrome. *Circulation* 98, 1928–1936.

Zaman, S., and Kovoor, P. (2014). Sudden cardiac death early after myocardial infarction: pathogenesis, risk stratification, and primary prevention. *Circulation* 129, 2426–2435. doi: 10.1161/CIRCULATIONAHA.113.007497

Conflict of Interest Statement: The authors declare that the research was conducted in the absence of any commercial or financial relationships that could be construed as a potential conflict of interest.

Received: 15 October 2014; paper pending published: 30 October 2014; accepted: 15 January 2015; published online: 05 February 2015.

*Citation: del Rio CL, Clymer BD and Billman GE (2015) Myocardial electrotonic response to submaximal exercise in dogs with healed myocardial infarctions: evidence for β-adrenoceptor mediated enhanced coupling during exercise testing. Front. Physiol. **6**:25. doi: 10.3389/fphys.2015.00025*

This article was submitted to Cardiac Electrophysiology, a section of the journal Frontiers in Physiology.